REGIONAL DIAGENESIS AND ITS RELATION TO FACIES CHANGE IN THE UPPER SILURIAN, LOWER ACACUS FORMATION, HAMADA (GHADAMES) BASIN, NORTHWESTERN LIBYA

OMAR B. ELFIGIH

INFORMATION TO USERS

This manuscript has been reproduced from the microfilm master. UMI films the text directly from the original or copy submitted. Thus, some thesis and dissertation copies are in typewriter face, while others may be from any type of computer printer.

The quality of this reproduction is dependent upon the quality of the copy submitted. Broken or indistinct print, colored or poor quality illustrations and photographs, print bleedthrough, substandard margins, and improper alignment can adversely affect reproduction.

In the unlikely event that the author did not send UMI a complete manuscript and there are missing pages, these will be noted. Also, if unauthorized copyright material had to be removed, a note will indicate the deletion.

Oversize materials (e.g., maps, drawings, charts) are reproduced by sectioning the original, beginning at the upper left-hand corner and continuing from left to right in equal sections with small overlaps.

Photographs included in the original manuscript have been reproduced xerographically in this copy. Higher quality 6" x 9" black and white photographic prints are available for any photographs or illustrations appearing in this copy for an additional charge. Contact UMI directly to order.

ProQuest Information and Learning
300 North Zeeb Road, Ann Arbor, MI 48106-1346 USA
800-521-0600

REGIONAL DIAGENESIS AND ITS RELATION TO FACIES CHANGE IN THE UPPER SILURIAN, LOWER ACACUS FORMATION, HAMADA (GHADAMES) BASIN, NORTHWESTERN LIBYA

BY

OMAR B. ELFIGIH

A thesis submitted to the

School of Graduate Studies

in partial fulfilment of the

requirements for the degree of

Doctor of Philosophy

DEPARTMENT OF EARTH SCIENCES

MEMORIAL UNIVERSITY OF NEWFOUNDLAND

January, 2000

St. John's **Newfoundland**

Canada

ABSTRACT

The Lower Acacus Formation consists of fourteen deltaic packages which change laterally across the Hamada Basin, NW Libya. Southern fluvial-channel sandstones prograded northward into coastal-deltaic sandstones and siltstones, and eventually to offshore-marine sandstones and shales. Each depositional environment in the Lower Acacus Formation produced a characteristic facies with specific compositional characteristics.

Petrographic and petrophysical properties of selected sandstone units within the Lower Acacus Formation indicate that the sandstones have been altered by the diagenetic processes of compaction, authigenesis, and dissolution. Three diagenetic facies are identified from the southern basin flanks to the northern basin centre respectively: (a) ***quartz-cemented facies***, (b) ***carbonate-cemented facies***, and (c) ***clay-cemented facies***. Each of the diagenetic facies contains a characteristic authigenic mineral suite reflecting a specific sequence of alterations which are (a) quartz-overgrowths and iron oxide, (b) carbonate cementation and dissolution, and (c) clay authigenesis respectively.

Isotopic study of selected sandstone units reveals a diagenetic history involving meteoric fluids modified by increasing water/rock interactions and saline (connate) water mixing with burial.

The major types of porosity have a regional distribution related to type of grain

framework, matrix and cement in each depositional facies. Dissolution of carbonate cements and unstable grains was the dominant process to create secondary porosity; such porosity being associated with the proximal deltaic facies. Preserved primary porosity is mainly associated with the fluvial-channel facies. Microporosity and some fracture porosity are the dominant porosity types in the distal deltaic and reworked marine-offshore facies. With continued diagenesis, differential cementation and dissolution redistributed porosity and modified primary porosities in the Lower Acacus Formation.

A multistage model of the leaching of carbonate cements and secondary porosity development is proposed. This includes: (1) a shallow depth (early) diagenetic stage wherein CO_2-charged meteoric waters flushed through channel systems of the fluvial sandstone facies in the southern part of the basin, and (2) a deeper (late) diagenetic stage mainly due to carbonic acid-rich waters expelled from maturing organic-rich Tanezzuft shales into the deltaic sandstone facies in the northern part of the basin.

Early diagenesis recognized in the different sandstones of the Lower Acacus Formation has major impact on the present-day hydrologic system across the Hamada Basin. Present-day hydrologic zones have a distribution which is spatially expanded relative to the Lower Acacus diagenetic zones and indicates the role of fluid flushing and dilution through time.

At the basin-wide scale the relationship between sandstone facies and the distribution of diagenetic elements is an important aspect of the Lower Acacus reservoir character heterogeneity. Recognized diagenetic facies heterogeneity includes: (1) iron-

oxides and interstitial clay coatings associated with quartz-overgrowths in the quartz-cemented facies of fluvial origin, (2) calcite cement patterns in the carbonate-cemented facies of proximal deltaic origin, (3) ferroan-dolomite cement associated with the fine-grained, micaceous, clay-clast-rich sandstones of proximal deltaic origin, and with the reworked marine sandstone units, and (4) authigenic clay (kaolinite) and its effect on permeability throughout the various depositional facies.

Integration of the many data sets results in a basin-wide 3-D geological model which includes four phases of major regional diagenetic changes: ***Phase I*** and ***II*** represent reduction of primary porosity and permeability in fluvial sandstone units. ***Phase III*** led to secondary pore formation and to modification of primary porosity in proximal delta front sandstone units. ***Phase IV*** represents pore-filling in distal delta front siltstones and reworked marine sandstone units.

Improved regional basin analysis and computerized basin modelling must consider and apply the variability expected from a multitude of parameters ranging from primary depositional processes to processes of burial and subsequent modification of formation characteristics. Commonly-applied generalizations regarding diagenesis as determined from individual well studies are inadequate and in many instances perhaps invalid for developing productive regional model. Use of regional diagenetic modelling integrated with depositional facies and basin analysis represents an initial step in predicting regions of maximum enhanced and preserved porosity in the subsurface.

ACKNOWLEDGEMENTS

I would like to express my sincere thanks and appreciation to my supervisor, Dr. John D. Harper. His continuous guidance, encouragement, wisdom, constructive criticism, and insight motivated me to earn my degree. He was helpful, supportive, patient, and available at all times.

I am also thankful to my supervisory committee members, Dr. E. Burden, and Dr. J. Gale for their encouragements throughout the project.

I am grateful to AGOCO management for their generous help for providing me with unlimited access to the core storage facility, Technical Data Library (TDL), and their continuous support throughout this study. Financial support from School of Graduate Studies in Memorial University of Newfoundland is also greatly appreciated.

I am very grateful to Mr. Mickey Abougoush, President and Mr. Richard Gilbert, Finance Manager, Teknica Petroleum Service Ltd, Calgary, for their great assistance and understanding to the latest financial situation of this project.

Special gratitude is expressed to Dr. F. Longstaffe, University of Western Ontario for conducting the oxygen-carbon isotope analyses for this study and his precious suggestions.

I am particularly thankful to Drs. M. Wadleigh and M. Wilson, Earth Sciences Department, Memorial University of Newfoundland, for their fruitful discussions of many issues related to oxygen-carbon isotope analyses and interpretations. Mr. R. Cox is

gratefully acknowledged for his assistance during CL-laboratory work.

I greatly appreciate the help and the guidance of Mrs. Lisa Lee, Biology Department, Memorial University of Newfoundland, during the SEM/EDS work and whose suggestions resulted in material improvement of the presentation of this work.

Deep thanks are also extended to Dr. H. J. Daniels, AGOCO Lab., Benghazi, Libya, for conducting the core-plug porosity/permeability analyses and for his thoughtful discussions.

I am also wish to thank Mr. Moukhtar Ibrahim, AGOCO Lab., Benghazi, Libya, for assisting me on preparing all thin-sections used in this study.

To all who helped me, in whatever capacity in preparing this thesis, I express my sincere thanks and appreciation.

The completion of this study would not have been possible without love and support of my wife **(AISHA)**, my sons **(WAIL, SERAJ & AHMED)**, and my **FAMILY** in Libya. Recognition of their share is beyond expression in words.

TO ALL OF THEM I DEDICATE THIS THESIS.

CONTENTS

PAGE

ABSTRACT ii
ACKNOWLEDGEMENTS v
LIST OF TABLES ix
LIST OF FIGURES x
I- INTRODUCTION 1
I.1- The purpose of the study 1
I.2- Research problems and objectives 4
I.3- Contribution of the study 6
I.4- Approach 7
I.5- Regional geology of the Hamada Basin 9
I.6- Previous work 35
II- METHODS OF STUDY 52
III- SANDSTONE PETROGRAPHY AND ISOTOPIC ANALYSES 60
III.1- Sandstone petrography 60
III.1.1- Thin-section petrography 60
III.1.1.1- Interpretation of thin-section petrography 73
III.1.2- Cathodoluminescent petrography 75
III.1.2.1- Interpretation of cathodoluminescent petrography 77
III.1.3- SEM/EDS analyses of the Lower Acacus Formation 77
III.1.3.1- Interpretation of SEM/EDS analyses 87
III.1.4- X-Ray Diffraction (XRD) analyses 88
III.1.4.1- Interpretation of XRD analyses 100
III.2- Isotopic analyses 102
III.2.1- Oxygen-carbon isotopic compositions in calcite cements 102
III.2.1.1- Interpretation of isotopic composition of calcite cements 106
III.2.1.2- Interpretation of pore water evolution 110
IV- DIAGENETIC FACIES AND THEIR INTERPRETATION (CEMENTS & POROSITY) 118
IV.1- Diagenetic facies 118
IV.2- Diagenetic sequences 128
IV.2.1- Diagenetic sequence in quartz-cemented facies 131
IV.2.2- Diagenetic sequence in carbonate-cemented facies 136
IV.2.3- Diagenetic sequence in clay-cemented facies 140
IV.2.4- Summary of diagenetic sequences 142
IV.3- Porosity evolution, distribution and diagenesis 143
IV.3.1- Porosity and diagenesis in the Lower Acacus Formation 163
IV.3.2- Porosity and oil emplacement 167
IV.3.3- Relationship between porosity types, facies, and depth 168
IV.3.4- Summary of porosity evolution, distribution, and diagenesis 171

V- REGIONAL BASIN HYDROLOGIC ZONES AND THEIR INTERACTIONS WITHIN THE LOWER ACACUS FORMATION 173
V.1- Overview of ground water concepts 173
V.2- Present day hydrologic zones in the Lower Acacus Formation 177
V.3- Post Lower Acacus diagenetic minerals and related fluid zones 184
V.4- Comparison of Lower Acacus fluid zones with those of present-day 186
VI- DIAGENETIC HETEROGENEITY IN RESERVOIR SANDSTONES OF THE LOWER ACACUS FORMATION 190
VI.1- Basin-wide diagenetic facies heterogeneity 190
VI.2- 3-D geological and diagenetic model 201
VI.3- Reservoir potential and diagenesis 204
VII- SUMMARY AND CONCLUSIONS 206
VIII- REFERENCES 212
IX- APPENDICES 235
APPENDIX I- Core-sections and descriptions 235
APPENDIX II- Thin-section photomicrographs (petrography) 268
APPENDIX III- Cathodoluminescent photomicrographs 315
APPENDIX IV- Scanning electron photomicrographs 336
APPENDIX V- Thin-section diagenesis and porosity 349
ENCLOSURES

LIST OF TABLES

PAGE

Table 1. List of wells used in this study from the Hamada Basin, NW Libya..... 54

Table 2. Porosity-permeability data of routine core-plug analysis for sandstone samples from the Lower Acacus Formation in some selected wells, Hamada Basin, NW Libya..... 56

Table 3. Thin-section point counting averages of framework, diagenetic, and porosity components for the various sandstone facies in the Lower Acacus Formation, Hamada Basin, NW Libya..... 61

Table 4. Petrographic and petrophysical data indicating heterogeneity within selected Lower Acacus Sandstone units (A8-A14, Af2-Af7, Ad & Am), Hamada Basin, NW Libya..... 62

Table 5. Percentage of primary and secondary (modified) porosity and present depth of burial in the various facies of the Lower Acacus Formation, Hamada Basin, NW Libya..... 74

Table 6. Oxygen and carbon-isotope compositions of calcite cement, in sandstone units of different facies of the Lower Acacus Formation, Hamada Basin, NW Libya..... 103

Table 7. Formation temperature, formation water salinity, and estimated geothermal gradient from some Drill-Stem Tests (DST) conducted in various formations of some wells in the Hamada Basin, NW Libya..... 109

Table 8. Natural gases recovered during drilling or from Drill-Stem Tests (DST) of some sandstone intervals in wells which penetrated the various Paleozoic Formations of the Hamada Basin, NW Libya..... 152

Table 9. Rock-Eval Pyrolysis for Tanezzuft Shale samples from GG1-NC7A well, Hamada Basin, NW Libya..... 158

Table 10. Relationship between porosity types, porosity line modes, and depth of selected fluvial (Af2-Af7), and deltaic (A8-A14) sandstone units of Lower Acacus Formation, Hamada Basin, NW Libya..... 169

LIST OF FIGURES

PAGE

Figure 1. Location map of the Hamada (Ghadames) Basin, NW Libya..... 2

Figure 2. Flow chart showing physical and compositional characteristics which control the different paths of diagenesis in rocks of different facies..... 3

Figure 3. Surface geology and outcrops distribution of the Hamada Basin, NW Libya..... 10

Figure 4. Geological map of important structural elements of Libya and the Hamada (Ghadames) Basin..... 11

Figure 5. Structure-contour map of the Hamada Basin, northwestern Libya, drawn on top of Precambrian basement..... 12

Figure 6. Regional structural cross-section on top of Lower Cretaceous unconformity, showing present structure of the intracratonic polycyclic Hamada Basin, NW Libya..... 14

Figure 7. Stages of the regional tectonic evolution of the Hamada Basin, NW Libya..... 15

Figure 8. Precambrian-Paleozoic stratigraphic type section for the Hamada Basin, NW Libya..... 19

Figure 9. Schematic stratigraphic and depositional model for the Lower Acacus Formation, Hamada Basin, NW Libya..... 22

Figure 10. Lithofacies of the Lower Acacus Formation and Acacus South, Hamada Basin, NW Libya..... 25

Figure 11A. Schematic construction of depositional environments on top of A8 sandstone unit of Lower Acacus Formation in the Hamada Basin, NW Libya..... 31

Figure 11B. Schematic construction of depositional environments on top of A10 sandstone unit of Lower Acacus Formation in the Hamada Basin, NW Libya..... 32

Figure 11C. Schematic construction of depositional environments on top of A12 sandstone unit of Lower Acacus Formation in the Hamada Basin, NW Libya..... 33

Figure 11D. Schematic construction of depositional environments on top of A14 sandstone unit of Lower Acacus Formation across the Hamada Basin, NW Libya..... 34

Figure 12. Map of the Silurian-Devonian outcrops, Ghat area, southern Libya..... 41

Figure 13. Structural relief of Libya during Early and Late Paleozoic..... 44

Figure 14. Well location map, showing distribution of wells used in this study in the Hamada Basin, NW Libya..... 53

Figure 15. Detrital plot from various facies in the Lower Acacus Formation, Hamada Basin, NW Libya..... 66

Figure 16. Regional distribution of dominant cements in each facies on the level of A8 sandstone unit of Lower Acacus Formation, Hamada Basin, NW Libya..... 68

Figure 17. Regional distribution of dominant cements in each facies on the level of A10 sandstone unit of Lower Acacus Formation, Hamada Basin, NW Libya..... 69

Figure 18. Regional distribution of dominant cements in each facies on the level of A12 sandstone unit of Lower Acacus Formation, Hamada Basin, NW Libya..... 70

Figure 19. Regional distribution of dominant cements in each facies on the level of A14 sandstone unit of Lower Acacus Formation, Hamada Basin, NW Libya..... 71

Figure 20. Typical EDS spectrum of (A) Quartz "quartz-overgrowths" in fluvial sandstone unit (Af3), EE1-NC7A @ 2686 m. (8810 ft.), (B) Quartz "quartz-overgrowths" in fluvial sandstone unit (Af3), EE1-NC7A @ 2687 m. (8812 ft.), (C) Quartz "quartz-overgrowths" in fluvial sandstone unit (Af2), CC1-NC7A @ 2750 m. (9020 ft.)..... 79

Figure 21. Typical EDS spectrum of (A) Hematite "iron-oxides" in fluvial sandstone unit (Af2), CC1-NC7A @ 2749 m. (9017 ft.), (B) Hematite "iron- oxides" in fluvial sandstone unit (Af2), B3-61 @ 2839 m. (9311 ft.), (C) K-feldspar "microcline" in fluvial sandstone unit (Af2), B3-61 @ 2839 m. (9311 ft.)..... 80

Figure 22. Typical EDS spectrum of (A) Calcite cement in fluvial sandstone unit (Af3), EE1-NC7A @ 2686 m. (8810 ft.), (B) Calcite cement "rich in iron" in proximal delta front sandstone unit (A8), C1-NC2 @ 2965 m. (9725 ft.)..... 81

Figure 23. Typical EDS spectrum of (A) Ferroan-dolomite cement in proximal delta front sandstone unit (A14), T1-23 @ 8454', (B) Ferroan-dolomite cement in reworked marine sandstone unit (Am), B3-61 @ 2670 m. (8756 ft.), (C) Ferroan dolomite in fluvial sandstone unit (Af3), EE1-NC7A @ 2687 m. (8812 ft.), (D) Siderite cement in fluvial sandstone unit (Af4), Z1-66 @ 2768 m. (9080 ft.)..... 82

Figure 24. Typical EDS spectrum of (A) Kaolinite cement in fluvial sandstone unit (Af3), A1-NC118 @ 3061 m. (10040 ft.), (B) Kaolinite cement in proximal delta front sandstone unit (A14), T1-23 @ 2577 m. (8454 ft.), (C) Kaolinite cement in distal delta front siltstone unit (Ad), A1-NC2 @ 2382 m. (7814 ft.)..... 83

Figure 25. Typical EDS spectrum of (A) Illite cement in distal delta front siltstone unit (Ad), A1-NC2 @ 2382 m. (7814 ft.), (B) Illite cement in distal delta front siltstone unit (Ad), A1-NC2 @ 2383 m. (7817 ft.), (C) Illite cement in fluvial sandstone unit (Af2), B3-61@ 2839 m. (9311 ft.)..... 84

Figure 26. X-ray diffraction patterns showing bulk minerals identification and clay fraction (mainly kaolinite with traces of illite) associated with the hematitic fluvial sandstone unit (Af3), EE1-NC7A @ 2687m. (8812 ft.)..... 89

Figure 27. X-ray diffraction patterns showing bulk minerals identification and clay fractions (mainly kaolinite) associated with the hematitic fluvial sandstone unit (Af4), Z1-66 @ 2768 m. (9080 ft.)..... 90

Figure 28. X-ray diffraction patterns showing bulk minerals identification and clay fractions (partial kaolinite and illite) associated with the fluvial sandstone unit (Af3), A1-NC118 @ 3061 m. (10040 ft.)..... 91

Figure 29. X-ray diffraction patterns showing bulk minerals identification and clay fraction (mainly kaolinite) associated with the hematitic fluvial sandstone unit (Af2), B3-61 @ 2839 m. (9311 ft.)..... 92

Figure 30. X-ray diffraction patterns showing bulk minerals identification and clay fractions (mainly kaolinite, with traces of illite) associated with the proximal sandstone unit (A14), T1-23 @ 2577 m. (8454 ft.)..... 93

Figure 31. X-ray diffraction patterns showing bulk minerals identification and clay fractions (mainly kaolinite with traces of illite) associated with the proximal delta front sandstone unit (A14), T1-23 @ 2583 m. (8473 ft.)..... 94

Figure 32. X-ray diffraction patterns showing bulk minerals identification and clay fractions (kaolinite and illite) associated with the distal front siltstone unit (Ad), E1-NC2 @ 2780 m. (9117 ft.)..... 95

Figure 33. X-ray diffraction patterns showing bulk minerals identification and clay fractions (kaolinite and illite) associated with the distal delta front siltstone unit (Ad), A1-NC2 @ 2383 m. (7817 ft.)..... 96

Figure 34. X-ray diffraction patterns showing bulk minerals identification and clay fractions (mainly kaolinite with traces of illite) associated with the reworked marine sandstone unit (Am), B3-61 @ 2656 m. (8756 ft.)..... 97

Figure 35. X-ray diffraction patterns showing bulk minerals identification and clay fractions (mainly kaolinite with traces of illite) associated with the reworked marine sandstone unit (Am), Q1-23 @ 2580 m. (8461 ft.)..... 98

Figure 36. Oxygen-versus carbon-isotope compositions of calcite cements in the various sandstone/siltstone units in the deltaic systems (NE-W, S-NNW) of Lower Acacus Formation, Hamada Basin, NW Libya..... 105

Figure 37. Burial history curve and estimated subsurface temperature grids of the Lower Acacus Formation, Hamada Basin, NW Libya..... 111

Figure 38. Oxygen isotope composition of pore water ($\delta^{18}O$‰SMOW) versus crystallization temperature (formation temperature in this case °C) for the Lower Acacus Formation..... 114

Figure 39. Petrographic and petrophysical characteristics of the three diagenetic facies of the Lower Acacus Formation..... 120

Figure 40A. Measured porosity and permeability for each depositional facies of the Lower Acacus Formation based on core-plug analysis..... 121

Figure 40B. Measured porosity and permeability within the diagenetic-cemented facies of the Lower Acacus Formation based on core-plug analysis..... 122

Figure 41. Histogram showing distinct ranges in density values defined by bulk density logs for each diagenetic facies in the Lower Acacus Formation, Hamada Basin, NW Libya..... 123

Figure 42. Gamma-ray log signature (GR) of the fluvial channel sandstone units (Af2, Af3 and Af5) of Lower Acacus Formation, Hamada Basin, NW Libya..... 125

Figure 43. Gamma-ray log signature (GR) of typical proximal delta front sandstone units (A8-A14) of Lower Acacus Formation, Hamada Basin, NW Libya..... 127

Figure 44. Measured porosity (core-plug porosity) versus point-count porosity (thin-section porosity) in clay-cemented facies of Lower Acacus Formation, Hamada Basin, NW Libya..... 129

Figure 45. Spiky Gamma-ray log signature (GR) Of (A) distal delta front, clay-rich siltstones (Ad units), (B) reworked marine sandstones (Am units) of Lower Acacus Formation, Hamada Basin, NW Libya..... 130

Figure 46A. Regional representation of the dominant porosity types in A8 sandstone unit of Lower Acacus Formation, Hamada Basin, NW Libya..... 144

Figure 46B. Regional representation of the dominant porosity types in A10 sandstone unit of Lower Acacus Formation, Hamada Basin, NW Libya..... 145

Figure 46C. Regional representation of the dominant porosity types in A12 sandstone unit of Lower Acacus Formation, Hamada Basin, NW Libya..... 146

Figure 46D. Regional representation of the dominant porosity types in A14 sandstone unit of Lower Acacus Formation, Hamada Basin, NW Libya..... 147

Figure 47. Variation of mole % CO_2 of natural gases recovered during drilling of Acacus and Tanezzuft Formations with depth, Hamada Basin, NW Libya..... 153

Figure 48. Zone correlation of mole % CO_2 in natural gases recovered from Silurian sequence, Hamada Basin, NW Libya..... 154

Figure 49. Distribution of mole % CO_2 in natural gases recovered in some wells during drilling of Lower Acacus Formation, Hamada Basin, NW Libya..... 155

Figure 50A. Structure map on top of the Tanezzuft Shale, Hamada Basin, NW Libya..... 156

Figure 50B. Structure map on top of the Lower Acacus Formation, Hamada Basin, NW Libya..... 157

Figure 51. Comparison of primary and secondary porosity decline in the Upper Silurian Lower Acacus Sandstone units of Acacus delta, Libya, and the Cretaceous Sandstones of Mackenzie delta, Canada..... 170

Figure 52. Schematic representation of ground water flow in different regimes of a large sedimentary basin..... 175

Figure 53. S-N Cross-section showing distribution of salinity readings in some tested sandstone intervals in the Lower Acacus Formation..... 179

Figure 54. Present-day salinity distribution in the Silurian sequence of the Hamada Basin from the southern basin flank to the west-northwestern basin centre..... 180

Figure 55. Present-day salinity distribution in the Silurian sequence of the Hamada Basin from the northeastern basin flank to the west-northwestern basin centre..... 181

Figure 56. Distribution of Lower Acacus present-day waters and ancient diagenetic minerals across the Hamada Basin, NW Libya..... 182

Figure 57. Sandstone quality map based on average log-porosity values of the fluvial reservoir, Af2 unit, in the Lower Acacus Formation, Hamada Basin, NW Libya..... 192

Figure 58. Core-section from the various types of Lower Acacus Sandstone units (A8-A14, Af, Ad & Am) in the Hamada Basin, showing calcite cement occurrences in these units; from continuous-wide (bands) occurrence with relative proximity to shale beds, to scattered occurrences associated with intercalated shale lenses..... 194

Figure 59. Gamma-ray, density, and sonic logs correlation for the proximal deltaic sandstone units (A8-A14) in the Lower Acacus Formation, Hamada Basin, NW Libya..... 196

Figure 60. Permeability versus grain size in the various facies of Lower Acacus Formation characterized by greater than 1% kaolinite of the rock volume... 199

Figure 61. 3-D Regional diagenetic model showing heterogeneity of the Lower Acacus Formation as caused by facies changes, fluid changes, and structural influences, Hamada Basin, NW Libya..... 202

I- INTRODUCTION

I.1- The purpose of the study:

This study investigates regional diagenetic relationships in the Lower Acacus Formation of the Upper Silurian of the Hamada Basin (also known as the Ghadames Basin and used interchangeably by various workers) of northwestern Libya (Fig. 1). Regional studies permit the establishment of context within which local variations and change can be addressed. Diagenesis in a sedimentary basin is the result of regional relationships between fluids, the associated rocks and pathways available for fluid migration (Fig. 2). In order to understand the local diagenetic changes observed in a stratigraphic unit it is necessary to appreciate the regional influences.

Each depositional environment produces a lithofacies with a limited extent, and range of petrophysical characteristics such as grain size and sorting (Visher, 1969; Reed et al., 1975; Anderson et al., 1982), size, shape and grains packing (Peterson and Osmond, 1961), and sedimentary textures and structures associated with the sand body (Friedman, 1961; Moiola and Weiser, 1968). Lithofacies characteristics act as important controls on fluid flow through a sandstone and thereby also indirectly control pore-fluid composition (Potter, 1967; Pettijohn et al., 1972). Detrital mineralogy has also been shown to be process-dependent because each detrital component has its own characteristic size distribution (Blatt et al., 1972; Odom, 1975; Doe et al, 1976). As a result, sorting during transport and deposition will generally produce different detrital assemblages in sediment

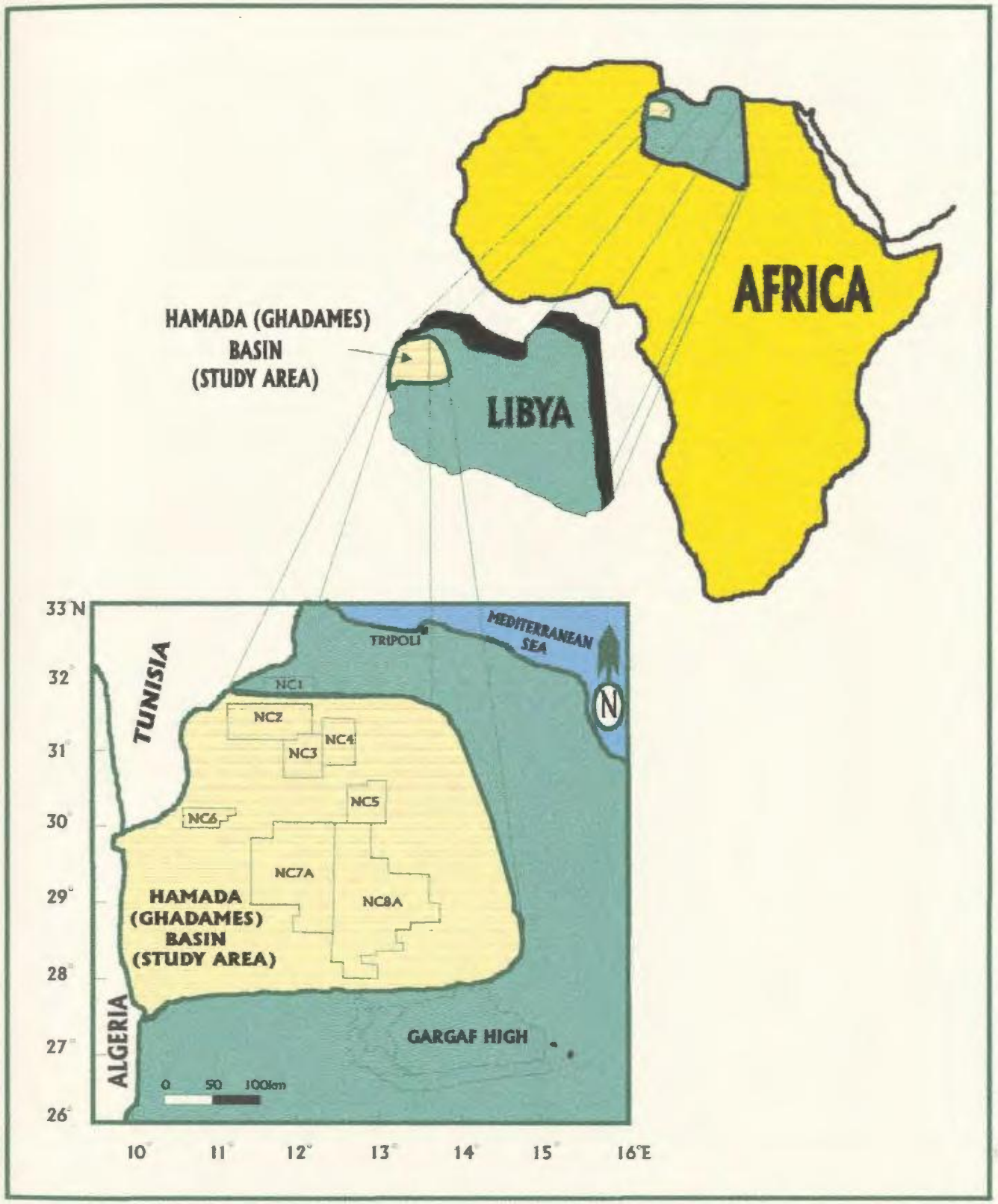

Figure 1. Location map of the Hamada (Ghadames) Basin, NW Libya.
(NC1-NC8A are AGOCO Concessions).

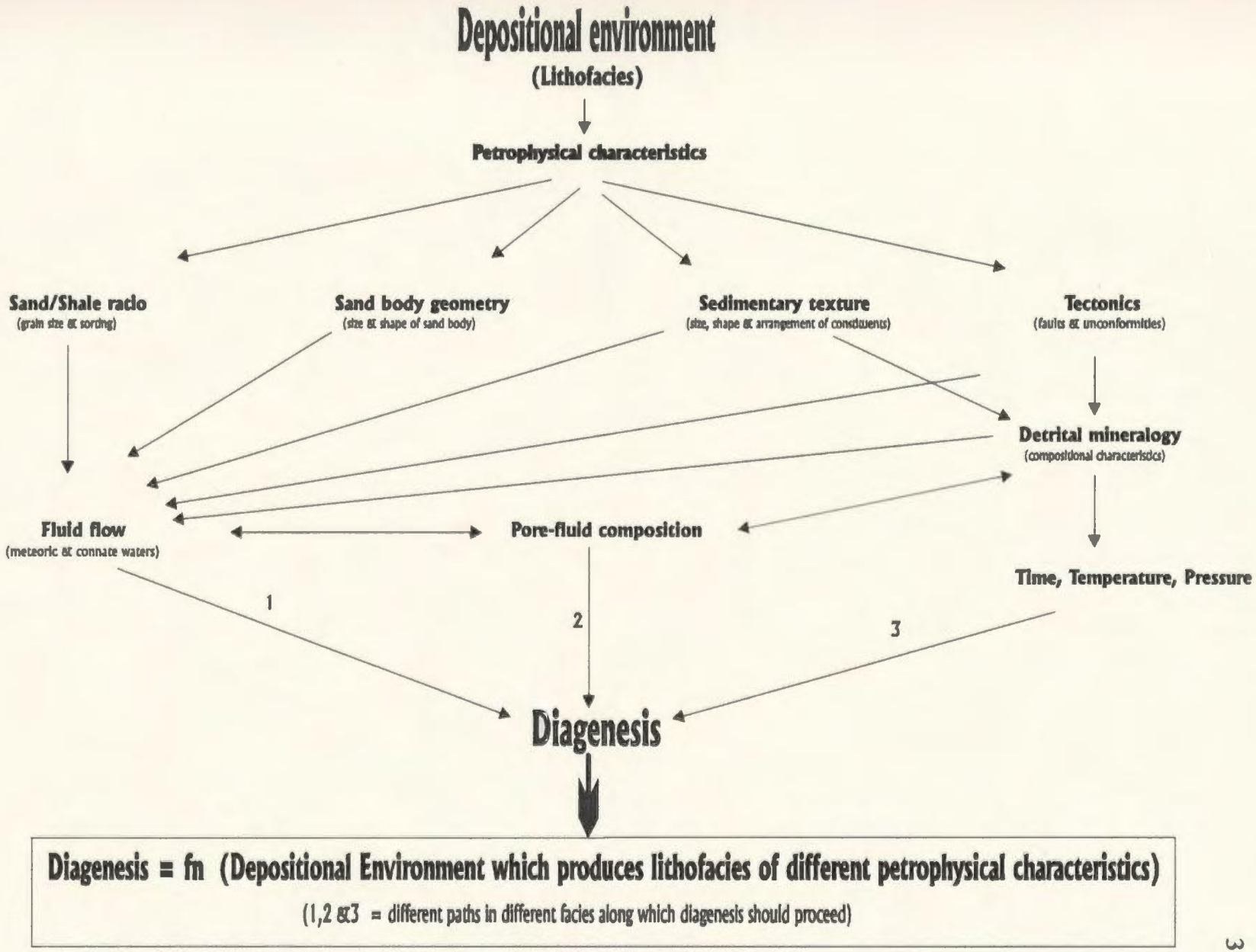

Figure 2. Flow chart showing physical and compositional characteristics which control the different paths of diagenesis in rocks of different facies (modified after Stonecipher et al., 1984).

deposited in environments of different energies (Davies and Ethridge, 1975). Detrital grain composition also affects pore-fluid composition. Therefore, it is likely that because of these differences or heterogeneities in physical and compositional characteristics, diagenesis should proceed along different paths in rocks (diagenetic heterogeneities) of different facies (Taylor, 1978; Blanche and Whitaker, 1978; Stonecipher, 1982).

The Lower Acacus Formation in the Hamada Basin is suitable for such a study because there is a broad distribution of wells in the basin with adequate sampling available to develop a 3-dimensional regional model of relationships based on a multidisciplinary integrated approach to analysis.

I.2- Research problems and objectives:

The term diagenesis refers to the changes that occur in sediments after deposition but before metamorphism (Cook and Egbert, 1983). These changes include compaction, cementation, dissolution, replacement, and alteration. Subsidence of the intracratonic Hamada (Ghadames) Basin both during and after deposition of the Lower Acacus Formation resulted in the Formation being subjected to such processes and thereby permits assessment of such relationships.

There are many reasons for studying the regional diagenesis of the Lower Acacus Formation in this basin.

1: This basin offers the opportunity to compare diagenetic relationships within and between depositional wedges in the Lower Acacus Formation.

2: Diverse facies occur across the basin from north to south.

3: The differences in waters (fluid regime zones) and their mineralogical imprints through diagenetic changes across this basin are detectable only on a regional scale; and are therefore likely to show regional diagenetic variations with changing facies.

4: Regional diagenetic heterogeneity of sandstone reservoirs may have practical significance in exploring for diagenetic traps.

The main problems to be addressed in this regional study of the Lower Acacus Formation in the Hamada Basin are:

1- The nature of the diagenetic system. Comparative study between facies of the structurally high basin flanks to those of the low basin centre will be used to determine the regional diagenetic characteristics of depositional facies, basin fluid movements, basin fluid distribution, and basin tectonic history. This analysis will incorporate the determination and characterization of regional differences in detrital composition, cements and textures.

2- Delineation of hydrologic zones. Lower Acacus sandstones of fluvial origin (Elfigih, 1991) in the southern portion of the Hamada Basin are continental deposits and therefore it is anticipated that they may reveal events of meteoric diagenesis. It is anticipated that the equivalent prograded sandstones of deltaic-coastal origin (Elfigih, 1991) in the middle part of the basin (northward) could reveal events of mixed meteoric and connate water diagenesis and sediment compaction with increasing burial depth. The range of diagenetic processes active in the basinal shale and sandstone facies of prodeltaic-shallow marine origin to the north cannot be readily anticipated. In addition the more complex structural history of the northern portions of the Basin are anticipated to record a range of

diagenesis from meteoric to deep burial processes.

3- Impact of the hydrodynamic (plumbing) system on porosity evolution, types, and distribution. Diagenetic fluids are anticipated to leave their record in the form of dissolution/alteration features and precipitation of different authigenic minerals. Porosity will be either enhanced or destroyed according to the nature of the diagenetic fluid involved in that facies.

4- Identification of regional modifications or variations of the system across the Basin.

The Lower Acacus sandstones are considered to be the primary reservoirs in some areas of the Hamada Basin (eg. Concession NC2). This study will define basin-wide (large-scale) reservoir characterization and heterogeneity as related to the nature of sandstone distribution, and regional and local facies changes within and between specific facies (grain size variations, shale intercalations, and cement types associated with each facies).

5- Creation of a three-dimensional (3-D) diagenetic model for the Basin. Such a model will provide a basis for applying the findings in other basins, and other stratigraphic units.

I.3- Contribution of the study:

This study provides new insights into:

1- Facies changes and basin structure as they relate to regional diagenetic variations observed in the intracratonic Hamada Basin, northwestern Libya, North Africa.

2- The relationship between diagenetic fluids and their records as interpreted through diagenetic sequences observed in the various hydrologic zones of the Lower Acacus

Formation.

3- The effect of diagenesis on porosity of sandstones in an intracratonic basin.

4- Defining the components of a 3-D diagenetic model for the assessment of diagenetic heterogeneity in sandstone reservoirs in this basin and other areas with a similar geologic setting.

I.4- Approach:

This study approaches the datasets from a regional point of view in order to identify trends and patterns in both the geographic and vertical (stratigraphic position) context. The datasets utilized are multidisciplinary, complementary, and diverse. The basic aspects of well logging, core and cutting analysis, and thin-section petrography are supported in complementary fashion by integration of formation salinities, bottom-hole pressures, carbonate analyses, XRD, EDS, and isotopic analyses to characterize the regional aspects and lateral facies variations documented. Such an approach provides significant insight into the character of the unit being investigated and the possible factors which have resulted in the development of that character.

Published literature relative to the Hamada Basin is minimal and that which is available is general in character and dominantly pre-1980 in source of information. Many articles published in the 1980's and 1990's are based on the pre-1980's datasets. Unpublished literature includes works by Libyan oil companies, consulting firms, and international researchers. These reports contain great amounts of multidisciplinary data, some of which is being released in this study. The important point to note is that in spite of

being unpublished these data sets can be made available for future investigators now that they know these data exist.

The approach used in this study is illustrated in the following flow chart:

Stratigraphic Analysis of

Upper Silurian, Lower Acacus Formation

from.....to

⇓ ⇓

Basin Flanks Basin Centre

⇓

Regional Facies Distribution

⇓

Depositional Environments

⇓

Petrography, Cements Distribution & Isotopic Analysis

⇓

Diagenesis & Diagenetic Facies

(Cement & Porosity)

⇓

Regional Basin Hydrologic Zones and their Interactions

within the Lower Acacus Formation

⇓

Diagenetic Heterogeneity in Reservoir Sandstones

of the Lower Acacus Formation

I.5- Regional geology of the Hamada Basin:

I.5.1- Structural setting:

The Hamada (Ghadames) Basin occupies the northwestern part of Libya (Fig. 1), and is characterized morphologically at the surface by a very broad plateau (Hamada El Hamra Plateau) (Fig. 3) with a general elevation of about 601 m. (1970 ft.). The plateau stretches 400 km from the Jabal Nafusa in the north to the Gargaf Arch in the south.

Structurally, the basin is bounded on the north by Gefara Arch, on the south by the Gargaf Arch, to the east by Tripoli-Soda Arch, and to the west by the Tihemboka Arch (Fig. 4). Across the western part of the Gargaf Arch, the Hamada Basin connects with the Murzuk Basin to the south.

The Hamada Basin is dissected by regional normal faults (Fig. 5) (Goudarzi and Smith, 1978; Goudarzi, 1980) having possible wrench components related to the initiation of the Sirte Basin rift (personal communication, Dr. J. D. Harper). General basement structural relationships are depicted in figure 5 which represents the most recent understanding of basement configuration. Faults are generalized and no sense of motion is provided although one might infer movement from the structure depicted. A central northwest trending structural nose splits the Basin into two parts but specific details related to the nose are lacking. A great deal of structural analysis remains to be completed in this Basin in order to have adequate appreciation for the structural history.

Gravity maps for the region are very low resolution, of incomplete coverage, and data acquisition parameters between studies are inconsistent, having been completed by

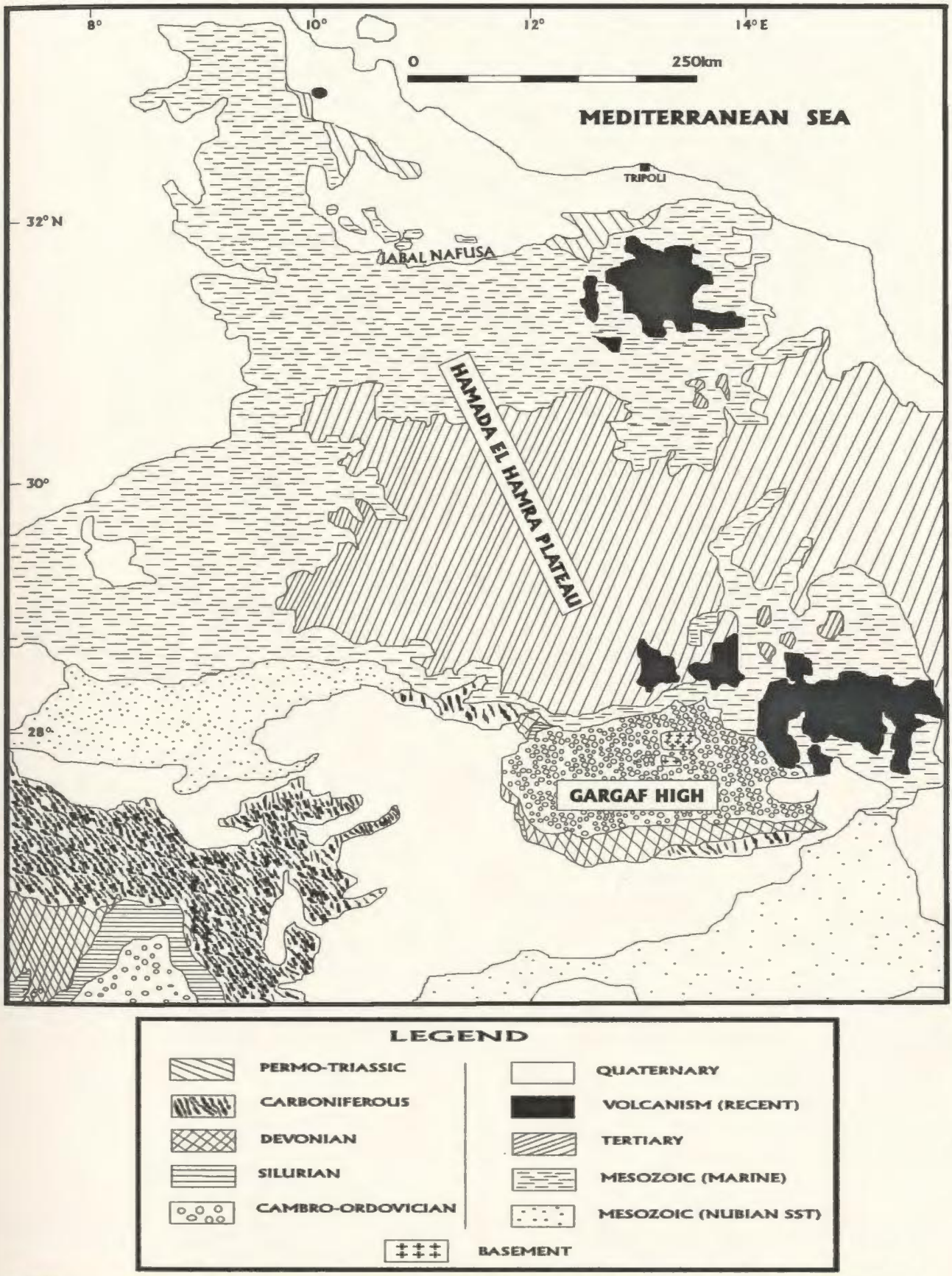

Figure 3. Surface geology and outcrops distribution of the Hamada Basin, NW Libya (modified after Bellini and Massa, 1978).

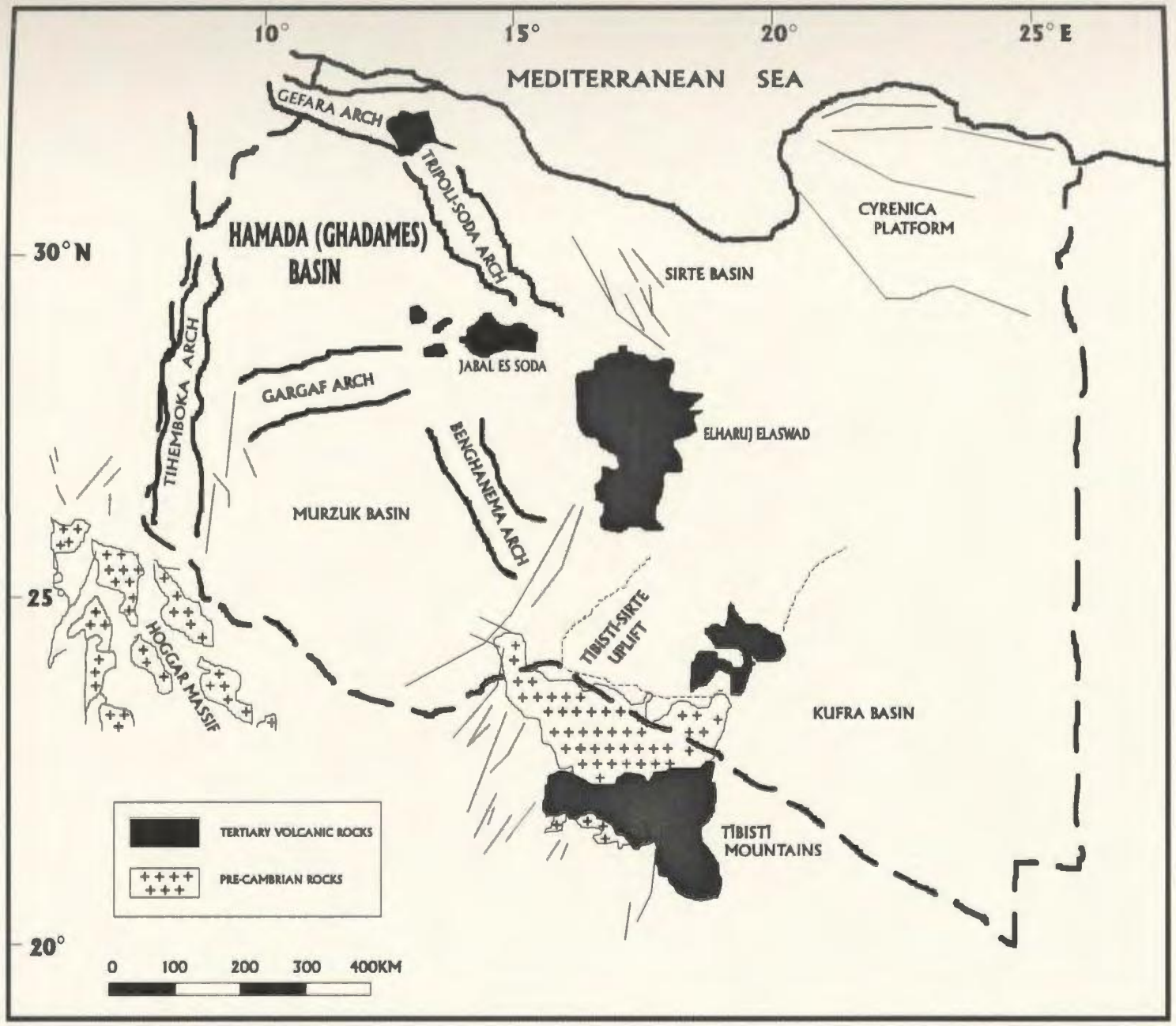

Figure 4. Geological map of important structural elements of Libya and the Hamada (Ghadames) Basin (modified after Said, F. M., 1974; Bellini and Massa, 1978).

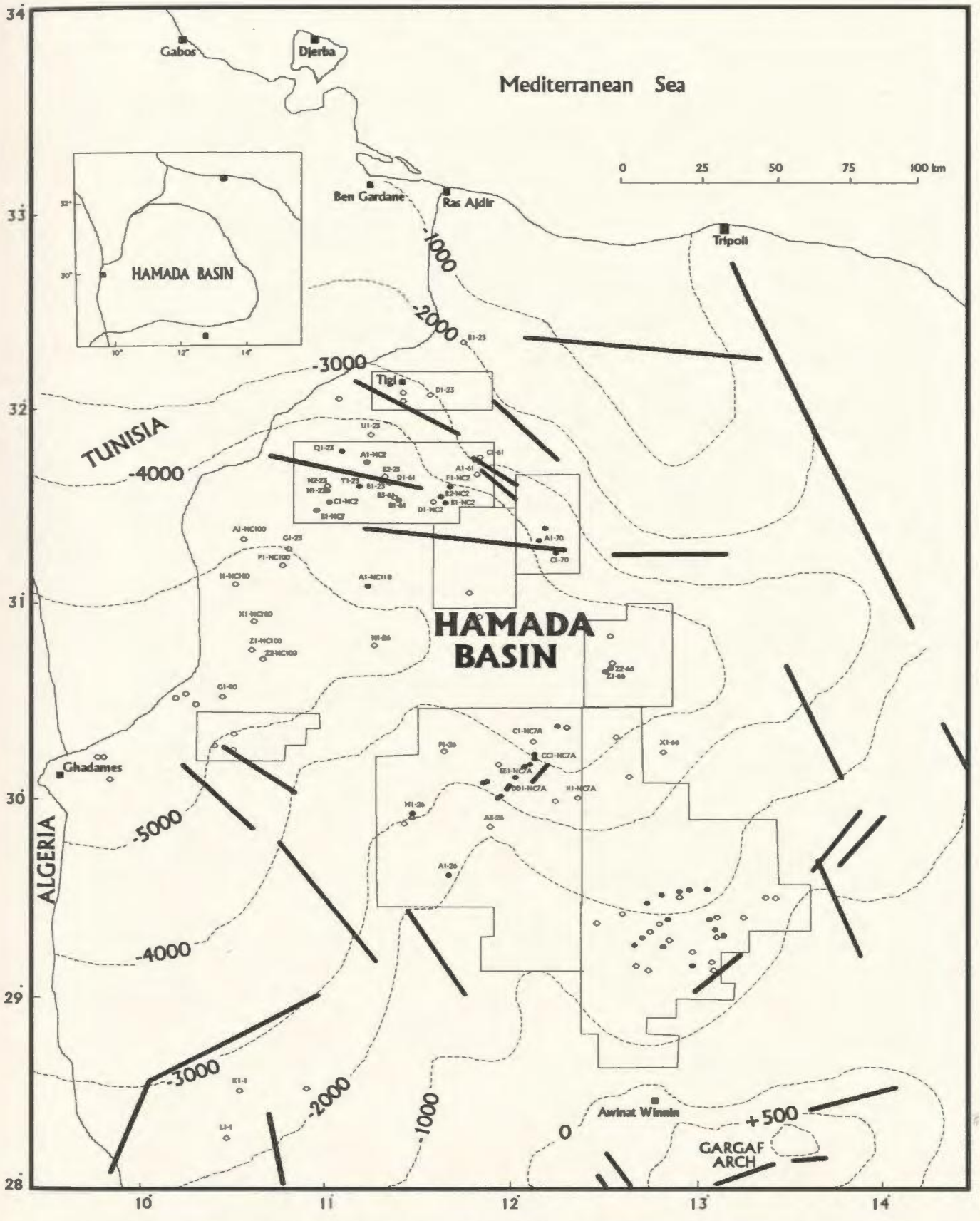

Figure 5. Structure-contour map of the Hamada Basin, northwestern Libya, drawn on top of Precambrian basement (modified after Goudarzi and Smith, 1978; Goudarzi, 1980).

many different companies. In many cases the original data are not even available today for re-evaluation (Essed, 1978).

Tectonic reconstruction of the Hamada Basin:

The Hamada Basin is a typical intracratonic polycyclic basin (Fig. 6). In fact, it is a composite of several different basins superimposed on top of one another, where sediments deposited in each basin during and after tectonic events were influenced by the subsequent regional tectonic framework and structure created by those tectonic events. These tectonic events with their corresponding unconformities form the evolutionary stages in the basin history (Fig. 7).

Using north-south oriented structural cross-sections (figures 7a-e), a tectonic reconstruction of the Hamada Basin based on review of the literature has been attempted to illustrate both the polygenetic history of the Hamada Basin and the potential implications for groundwater movements through time. The major known tectonic breaks or unconformities are chosen as the different cross-section datums through time. The relationship between the tectonic events and the sedimentary fill (sedimentary sequences and facies) clearly indicates the step-by-step evolution of the basin through five (5) regional tectonic stages:

a) Pre-Upper Silurian-Lower Devonian (Caledonian) unconformity stage (Fig. 7a):

During this interval basin subsidence was greatest to the north creating a marginal sag basin (Kingston et al., 1983), at which time continental sediments were being deposited in the south and basinal sediments in the north. Uplifted areas in the south of the

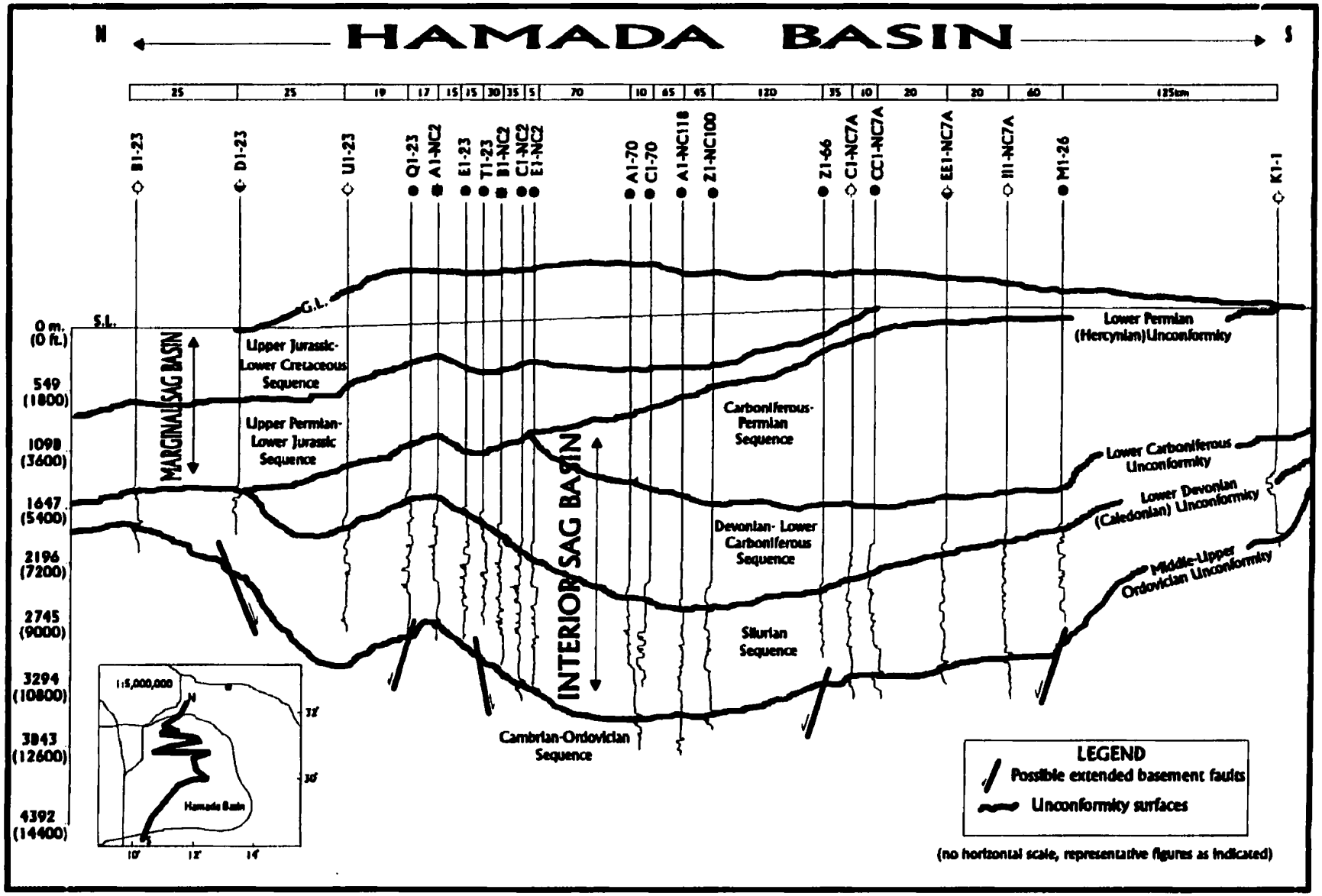

Figure 6. Regional structural cross-section on top of Lower Cretaceous unconformity, showing present structure of the intracratonic polycyclic Hamada Basin, NW Libya.

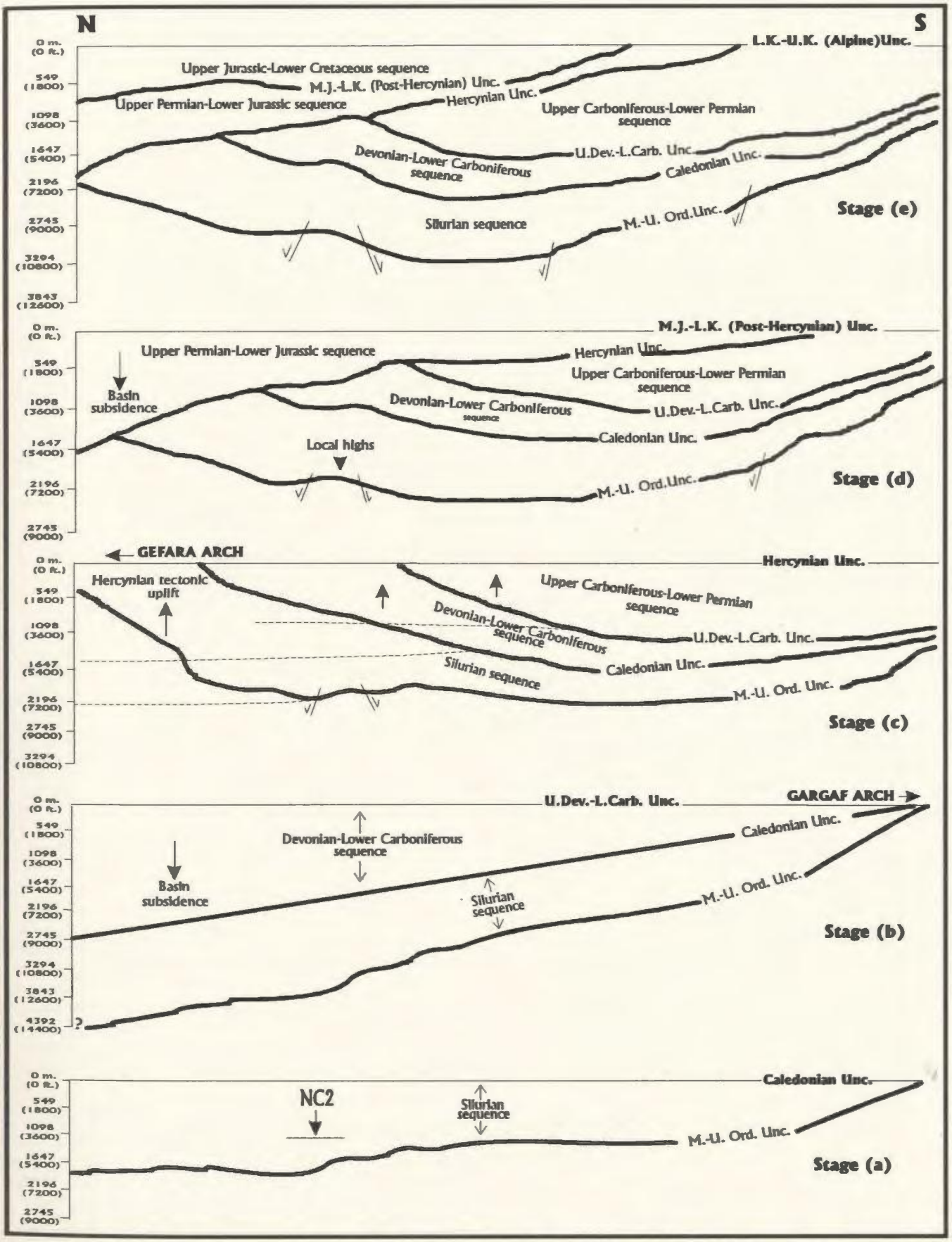

Figure 7. Stages of the regional tectonic evolution of the Hamada Basin, NW Libya, (modified after Exploration Department, N. O. C., 1981; Santa Maria, 1991).

basin such as the Tihemboka Arch and the Hoggar Massif (Santa Maria, 1991; Makhous et al., 1997) implies that meteoric groundwater would be introduced from the south into the Hamada Basin. The paleodepocentre of the basin is in the vicinity of Concession NC2 (Fig. 7a). The basal boundary in this cross-section (and all other stages) has been extrapolated since the boundary under consideration is deeper than most of the drilling in the region.

b) Caledonian Unconformity to the Upper Devonian-Lower Carboniferous unconformity stage:

In this stage (Fig. 7b) renewed subsidence occurred in the north. This subsidence led to the deposition of thick Devonian-Carboniferous sedimentary deposits thickening to the north. From at least Ordovician through to Lower Carboniferous times, the present Gefara Arch to the north did not exist (Goudarzi, 1970; Klitzsch, 1981; Santa Maria, 1991). To the south the presence of the regional Gargaf high is in question. There has been some sense in the literature that the Gargaf Arch may have begun by this time (Klitzsch, 1981).

c) Upper Carboniferous-Lower Permian (Hercynian) unconformity stage:

Figure 7c shows relationships at the end of the Hercynian unconformity. Uplift of the Gefara Arch to the north converted the Hamada Basin into an interior sag basin and provided a new source of clastic sediments from the north as the previous deposits in the area were eroded. Precambrian and/or Lower Paleozoic faults were rejuvenated during this time (BEICIP, 1975; AGOCO internal report, 1988; seismic report-AGOCO, 1989;

Santa Maria, 1991). Recognition of these faults is very clear in the vicinity of Concession NC2 to the north and other areas on the southern flank of the basin (Fig. 5 and unreleased seismic data).

d) Middle Jurassic-Lower Cretaceous (Post-Hercynian) unconformity stage:

During this stage (Fig. 7d) the Gefara Arch collapsed and subsidence dominated the northern portion of the Hamada Basin. Hence, the shape of the newly developed basin once again could be defined as a marginal sag basin (Kingston et al., 1983). Most of its southern flank is located in the Hamada Basin and most of its submerged central part extended to Algeria in the west and northwestern directions. Basement faults extended to at least the Silurian sequence and possibly to the end of the Paleozoic. Local highs developed, especially in the northern flank of the basin. Additional uplift took place in the vicinity of the Gargaf Arch.

e) Lower Cretaceous-Upper Cretaceous (Alpine Orogeny) unconformity stage:

In this stage (Fig. 7e) subsequently the basin continued as a marginal sag basin (Kingston et al., 1983) affected by the Alpine orogeny during Upper Cretaceous, Middle Miocene and Recent times.

Summation of tectonic evolution overview:

This polygenetic developmental history of the Hamada Basin must be kept in mind as one assesses the data for interpretation of the Basin's diagenetic history.

I.5.2- Stratigraphic setting:

The Paleozoic sedimentary record in the Hamada Basin spans from the Cambrian to Carboniferous (Fig. 8) and is characterized by four regional unconformities representing emergent episodes that are related to the fluctuation of sea level across the African cratonic margin. The timing of these unconformities appears to closely correspond to the ages of the Sloss sequences as defined in North America (Sloss, 1974). The apparent correspondence deserves further study and if valid would be as indicated below:

Upper Carboniferous-Lower Permian (Hercynian).....(end of Absaroka)

Upper Devonian-Lower Carboniferous (Acadian).....(end of Kaskaskia)

Upper Silurian-Lower Devonian (Caledonian).....(end of Tippecanoe)

Middle-Upper Ordovician.....(end of Sauk)

It should be noted that North American and European stratigraphic terminology has been applied regularly in Libya because of the numerous foreign researchers studying the geology of the country.

Glacial deposits of late Ordovician to early Silurian age were discovered in the 1960s in north Africa and others have been reported from South America and the Soviet Union (eg. Spjeldnæs, 1961; Bain, 1963; Destombes, 1968). The north African deposits are associated with long glacial grooves in bedrock, well preserved striated pavements, ice-scoured valleys, and sandy tillites occurring over such large areas that it is clear they must result from ice sheet erosion and not merely the action of local upland glaciers (Beuf et al., 1971; Allen 1975; Spjeldnæs, 1981; Selby, 1985).

AGE				FORMATIONS	CHARACTERISTICS	Depositional Cycles and Origin
PALEOZOIC	CARBONIFEROUS	LATE	STEPHANIAN	TIGUENTOURINE	CLYST: red-brown, soft, sticky, slightly calcareous, occ. w/ ANH. layers, SH; red-brown, soft, calc., non-fossl., w/ some SST beds; white, fine, calc., dolomitic in parts.	
			WESTPHALIAN	DEMBABA	LST: white-light brown, silty, fossil.(biocalcarenite), w/ dense SH; grey-green, fissile, occ. silty, w/ some ANH. interb..	
			NAMURIAN	ASSEDJEFAR	SH: grey, thin SLTST interlaminations, calcareous, w/ fine SST, macro/micro fossils.	
		EARLY	VISEAN	MRAR	SST/SH: cyclic alternations; SST; white, fine, micro-cross bed., SH; dark grey, mic., fiss, silty, Pelec., Brach., wood frag.	
			TOURNAISIAN			
	DEVONIAN	LATE	FAMENNIAN	TAHARA	SST/SH: coarsening upward seq., SST. cross bed., skolith., wood frag.	
				AQUINET OUENINE C	SH: grey, fiss., mic., w/ minor SST. fine grained, cross-bedded.	
			FRASNIAN	B	LST: white-light grey, occ.fossil. at the top of the unite, w/alter. bioc. silty-SH, and SST. at the base.	
		MIDDLE	GIVETIAN			
			COUVINIAN	A	SH: grey-dark grey, fissile at the base, overlain by SST; fine-medium grained, coarsening upward sequences at the top.	
		EARLY	EMISIAN	OUAN KASA	SH : v.silty, biot., sandy at the top, LST; white-grey, silty, brach. at the base.	
			SIEGENIAN	TADRART	SST: fine-conglom., kaolinitic, occ. sil./ferr. cement, cross-bedded, w/ wood fragments, Cruziana.	
			GEDINIAN			
	SILURIAN	LATE	LUDLOVIAN	ACACUS UPPER ACACUS	SST: white-light grey, occ. brown, v.fine-fine grained, moderatly-sorted, kaolinitic, occ.w/ferr.SST at the top, inserb. w/SH.	Regressive SST (Fluvial)
				MIDDLE ACACUS	SH: grey-green, firm, subfissile-fissile, flaky, micaceous, w/ thin lenticular SLST. lenses, bioturbated.	Transgressive SH (Shallow marine)
			WENLOCKIAN	LOWER ACACUS	SST: light brown-tan, grey, fine-medium grained, w/coarsening upward sequences, subangular-subrounded, moderatly sorted, cross-laminated at the top, w/some SH alternations, biot., w/Harlania at the top and Cruziana at the base.	Regressive SST (Deltaic)
		EARLY	LLANDOVERIAN	TANEZZUFT	SH: grey-green, fissile, silty, micaceous, w/ graptolites, radiactive at the base, interlaminated w/ SLST, light grey, light green, micaceous.	Transgressive-Regressive SH, SLST (Shallow marine-prodeltaic)
	ORDOVICIAN	LATE	ASHGILLIAN	MEMOUNIAT	SST: white-tan, fine-coarse, cross-bedded, kaolinitic, Tigillites, Scolithos.	Transgressive SST (Shallow marine)
			CARADOCIAN	MELEZ CHOGRANE	SH: green, micaceous, chloritic, interbeds w/ SST, fine-coarse, occ. pebbl-bould, usually straited filling paleovalleys, w/ ferr. oolites at the base, Trilobites and Brachiopods.	Shallow marine-periglacial SH/SST
		EARLY	LLANDEILIAN	HAOUAZ	SST: white, fine-medium grained, occ. argillaceous, arkosic; SLST: bioturbated, Tigillites, Scolithos, Trilobites.	
			LLANVIRNIAN			
			ARENIDIAN SKIDDAVIAN			
			TREMADOCIAN	ACHEBYAT	SST: white, medium-coarse grained, w/ Tigillites, Brachiopods.	
	CAMBRIAN	LATE		HASSAONA	SST: medium-v.coarse grained at the base, kaolinitic at the top, occasionally cross-bedded, fluvial in origin, non-fossiliferous.	
		MIDDLE				
		EARLY		MOURIZIDIE (INFRA-CAMBRIAN)	SST: red, conglomeritic, cross-bedded, with tillites.	
PRE-CAMBRIAN	ALGONKIAN			BASEMENT	Metamorphic and igneous rocks: slate, phyllite, gneisses, schists and granites associated.	

Figure 8. Precambrian-Paleozoic stratigraphic type section for the Hamada Basin, NW Libya

(compiled from: Van Eysinga, 1975; Bellini and Massa, 1980; DeCastro et al, 1991; Elfigih, 1991; Pierobon, 1991; and N.O.C., 1995).

According to Massa and Collomb (1960, 1962) glacial deposits occur over a large area in the central Sahara region, and around the margins of the Hoggar Massif and Tibisti Mountains (Fig. 4). These glacial deposits were documented in the Melez Chograne Formation of Middle-Late Ordovician (Fig. 8) which represents the strong glaciation period in central-north Africa. The end of glacial deposition is recorded in the subsurface by the Memouniat Formation. A thick section of Memouniat sandstones and shales observed in outcrop was deposited in shallow marine, coastal and continental environments (Elfigih, 1991). No glacial criteria have been documented from the subsurface although it is anticipated that future seismic studies will shed light on the subject (per discussion with Dr. John D. Harper).

A period of structural quiescence (post-glacial period) followed by a eustatic rise in sea level (Karasek, 1981; Weerd and Ware, 1994) and basin subsidence resulted in deposition of the Early Silurian marine transgressive shales of the Tanezzuft Formation (Klitzsch, 1981).

The Hoggar Massif to the south (Fig. 4) was the main source of detrital materials during the Early Silurian (Bishop, 1985; Makhous et al., 1997). Sediment source areas include the Tihemboka and Gargaf Arches which were uplifted due to epirogenic movements in middle-Late Silurian through Early Devonian time (unpublished AGOCO {Arabian Gulf Oil Company} internal report, Makhous et al., 1997). These resulted in deposition of the regressive sand-rich fluvio-deltaic Upper Silurian Lower Acacus Formation (Elfigih, 1991).

The Lower Acacus Member of the Acacus Formation:

The Lower Acacus Member (informal term) of the Acacus Formation (Fig. 8) is generally referred to throughout the literature either as the Lower Acacus Sandstone or most commonly as the Lower Acacus Formation. This convention of using the term "Lower Acacus Formation" will be adhered to in this study. Many informal approaches to stratigraphic unit terminology are used in Libya, thereby creating the necessity to know the terms in order to locate and utilize available data.

In detail, the Lower Acacus Formation consists of sandstones and shales of Upper Silurian (Ludlovian) age deposited in a fluvio-deltaic system (Elfigih, 1991) that prograded northwards into the western flank of the intracratonic Hamada (Ghadames) Basin. Figure 9 and enclosures 1 and 2 based on well log correlation illustrate both the intraformational and basin stratigraphic relationships of the Lower Acacus Formation.

The Lower Acacus Formation is overlain by the Middle Acacus Shale with transgressive contact in the north (Fig. 9). In the south the Lower Acacus Formation is overlain by the Acacus South Formation. The Acacus South Formation is laterally equivalent to the Lower Acacus Formation to the north. The basal contact of the Lower Acacus Formation is transitional and diachronous with the underlying Tanezzuft Formation. The convention in the region is to apply the term "Tanezzuft Shale" (eg. Klitzsch, 1966 to 1981) to the Tanezzuft Formation.

For correlation purposes attention is drawn here to the radioactive-rich shale zone at the base of the Tanezzuft (Enclosures. 3 and 4). This zone is clearly evident on the well

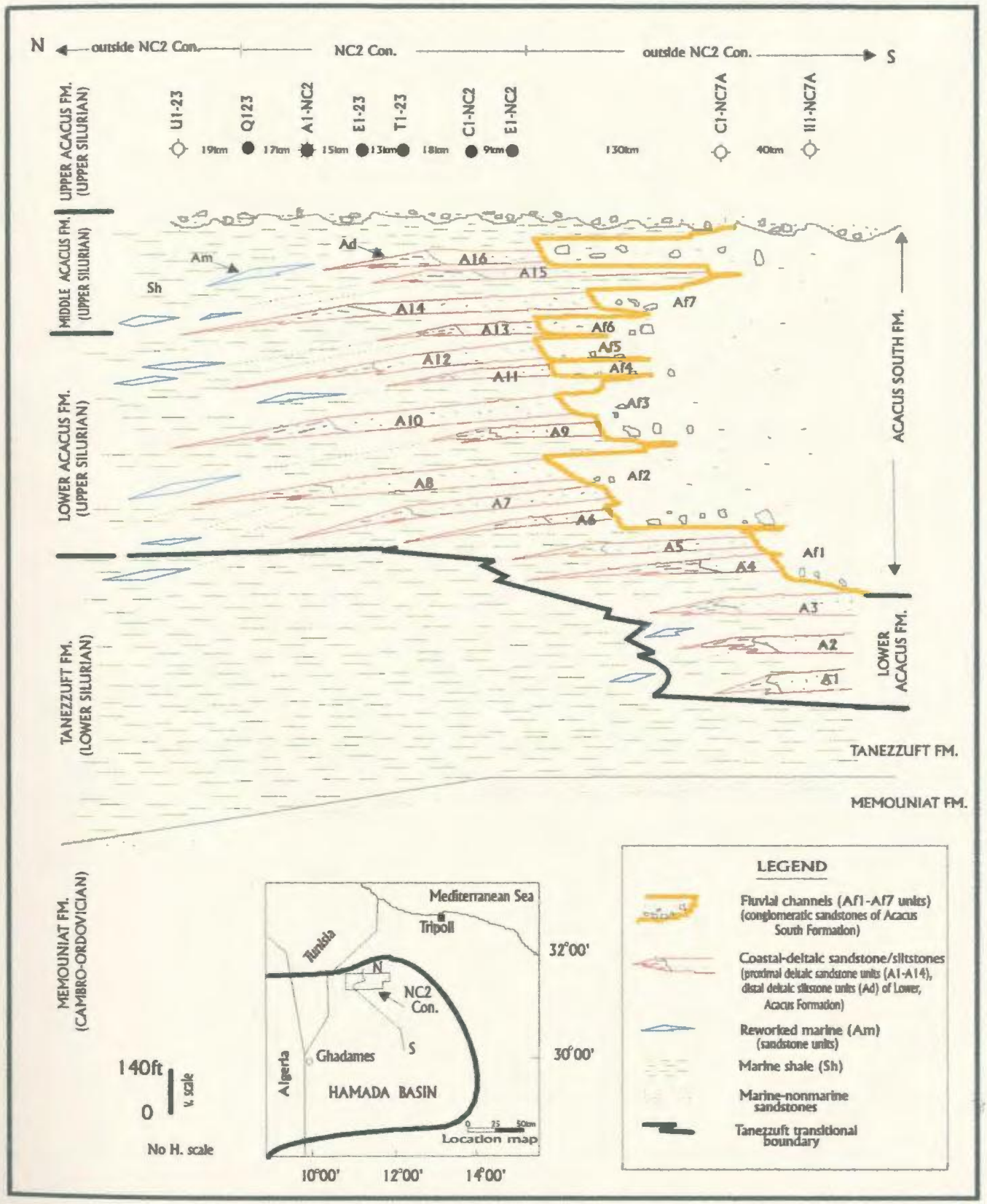

Figure 9. Schematic stratigraphic and depositional model for the Lower Acacus Formation, Hamada Basin, NW Libya (after Elfigih, 1991).

logs throughout the region. This shale unit overlies the sandstones of the Upper Ordovician Memouniat Formation. The top of the Memouniat sandstones is also a useful interval for correlation purposes.

The Lower Acacus Formation can be subdivided into 14 coarsening-upward coastal deltaic units (A1 - A14) (Fig. 9) which are laterally equivalent to 7 fining upward fluvial units (Af1 - Af7). Facies represented in these rocks include: fluvial sandstones, proximal delta front sandstones/siltstones, distal delta front bioturbated silty-sandstones, and prodeltaic silt/shales and reworked marine sandstones. Where it is possible to identify distal subfacies of the coastal-deltaic facies these distal occurrences are identified by the designation "Ad" for their corresponding facies units. These units pass northward into reworked marine sandstones "Am" and Acacus/Tanezzuft shales. Each of the 14 depositional units are separated by transgressive marine shales which die out laterally to the south where the basinal and coastal sediments have been replaced by fluvial environments. These 14 units represent 14 deltaic lobes deposited during basin subsidence (Elfigih, 1991).

The stratigraphic framework of the Lower Acacus Formation reveals the following (from Elfigih, 1991):

"Individual sandstone units begin with marine shales representing a transgressive phase and terminate with a regressive deltaic sandstone/siltstone phase (progradational units). This latter phase is overlain by less persistent, thin, reworked marine sands representing the destructional phase. Thus, each of the sandstone units make up major

progradational sequences bounded by local or regional time-stratigraphic markers.

Major river systems occur to the south of the study area. These systems flowed northward.

The largest delta lobes prograded 45-50 km northward in the Concession NC2. The resulting vertical accumulation of sandstone/siltsone in each deltaic lobe averaged 14 m. (45ft)."

The stratigraphic relationship between the Lower Acacus deltaic sandstones and the Tanezzuft marine shales is diachronous.

Lithofacies of the Lower Acacus Formation and Acacus South Formation:

The following description of the Lower Acacus Formation and the Acacus South Formation lithofacies is derived from Elfigih (1991).

"Five lithofacies types (1 to 5) (Fig. 10) are recognized within the Lower Acacus/Acacus South Formations across the Hamada Basin. These lithofacies are based on particular associations of rock types, sedimentary structures, and electric log patterns. They are presented below in depositional sequence from basinal marine to deltaic to fluvial lithofacies:

1- Dark grey, greenish black, finely laminated, occasionally bioturbated shale (marine shale; "Sh". units).

2- Bioturbated silty sandstone (distal delta front, marginal; "Ad" units).

3- Horizontal to low-angle cross-laminated to indistinct laminated, fine to medium grained sandstone (proximal delta front; "A1-A14" units)...

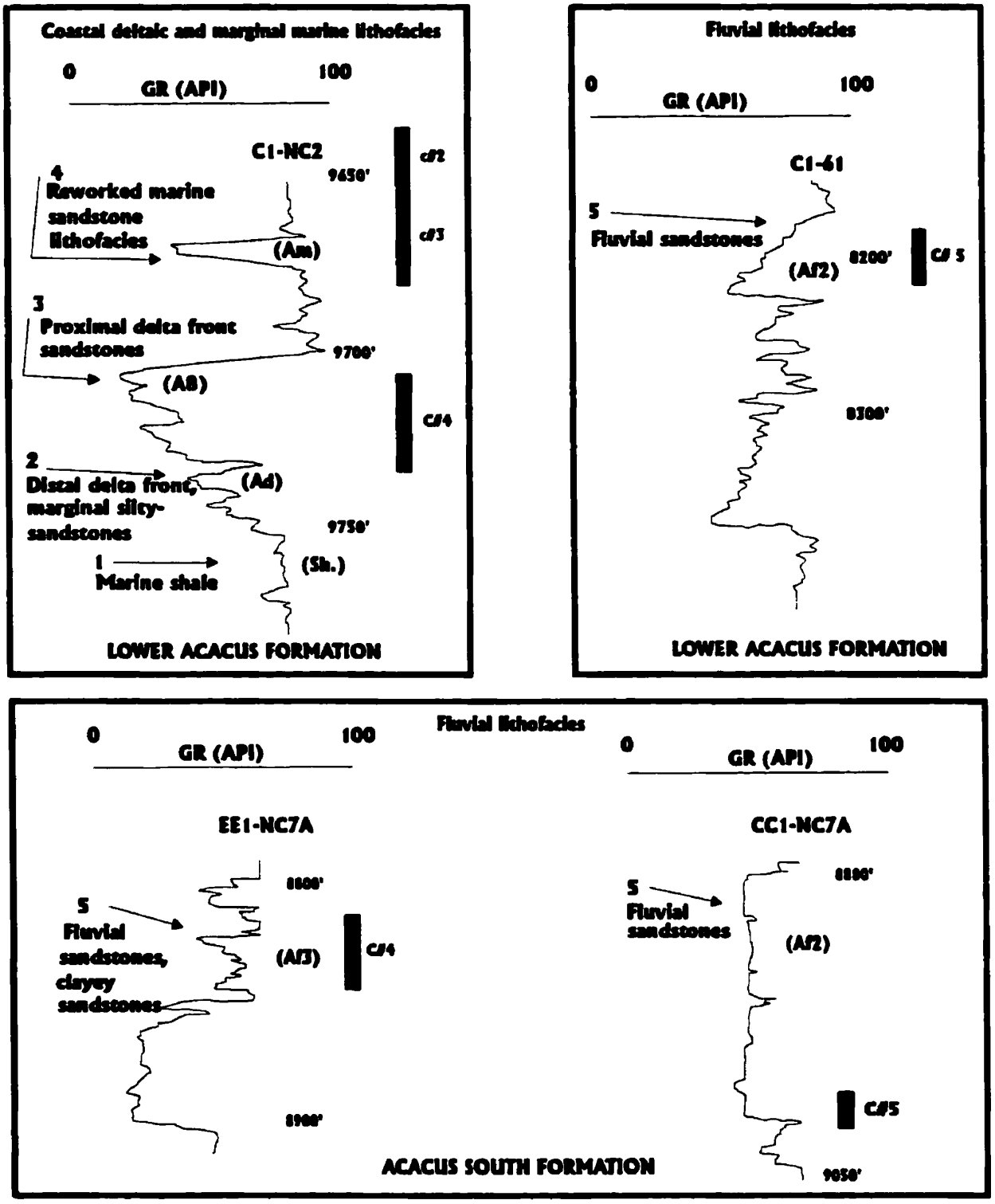

Figure 10. Lithofacies of the Lower Acacus Formation and the Acacus South Formation, Hamada Basin, NW Libya. (See text for more details about lithofacies (1 to 5), and units (Sh., Ad, A8, Am, Af2-Af5)). Note the units of depth are as recorded on the well logs. Black bars = core intervals.

4- Glauconitic, calcareous, wavy-laminated, very fine to fine grained sandstone (reworked marine sandstone; "Am" units).

5- Low-angle cross-laminated to parallel laminated medium to fine- grained sandstone which occasionally silty to clayey, bioturbated and contains carbonaceous matter at the top and of general fining upward sequence (fluvial sandstone; "Af1-Af7" units).

Lithofacies description:

1- Finely laminated-biouturbated shale (Sh. units):

This facies consists mainly of thick sequences of dark grey, greenish black shales which are occasionally micaceous, with rippled lenticular finely laminated silty sandstone lenses which are approximately 0.02 to 0.30 m. (0.05-1 ft.) thick. Where burrowing has not obscured the laminae the sandstones are occasionally finely laminated. Some soft sediment deformation features are locally preserved and tend to be silty at the top of the section. This lithofacies becomes more highly bioturbated and burrowed at the base...

2- Bioturbated silty sandstone ("Ad" units):

Occurring gradationally at the top of the marine shale with a thickness of 0.6 to 2.1 m. (2 to 7 ft.), this lithofacies consists of very silty sandstone which is occasionally very fine grained, dark grey, grayish cream in colour, usually bioturbated and burrowed with very distorted structure as in well C1-NC2 at 2941 m. (9648 ft.), well E1-NC2 at 2901 m. (9515 ft.), and well A1-NC2 at 2386.1 m. (7826.5 ft.). The sediment tends to be calcareous and contains a high percentage of clay matrix (10%-15%). There are

occasional minor contorted laminations, especially in well C1-NC2 at 2114 m. and 2942 m. (6933 ft. and 9651 ft.). In well T1-23 at 2582 m. (8468 ft.) these contortions may be due to differential loading. This lithofacies has a generally gradational contact with the upper fine to medium relatively clean sandstone...

3- Horizontal to cross-laminated sandstone (A1-A14 units):

Overlying the bioturbated silty sandstones are calcareous sandstones which occasionally contain some carbonaceous debris and clay clasts. This sandstone consists of moderately to well sorted, subangular to rounded grains. The sandstones of this lithofacies are texturally mature and show an upward decrease in matrix.

Sedimentary structures include horizontal parallel to indistintive laminations or low-angle cross-laminations at top of the unit suggesting a relatively high energy lithofacies. Most core sections of sandstone units of this lithofacies have vertical burrows of "Skolithos trace fossils" which indicate high energy environment (Chamberlain, 1978)...

The vertical sequence of the above lithofacies (1 to 3) shows a difference in texture and an increase of sedimentary structures upward; from laminated to bioturbated shale (lithofacies No. 1), to bioturbated silty sandstone (lithofacies No. 2), to fine to medium grained sandstone with horizontal to cross-laminations (lithofacies No. 3). This suggests a transitional relationship from prodelta-marine shale (1) to delta-front and coastal siltstones and sandstones (2 and 3)...

4- Glauconitic, calcareous, wavy laminated sandstone (Am units):

These sandstones are less extensive than lithofacies 2 and 3, with thicknesses ranging from 0.61 to 6.1 m. (2 to 20 ft.). They occasionally demonstrate either general fining-upward or coarsening-upward log signatures. They usually occur as sand lenses (or stringers) of spiky well-log character as can be seen clearly in well Q1-23 from 2494 to 2498 m. (8180 to 8193 ft.), and from 2274 to 2277 m. (7459 to 7470 ft.).

These sand lenses are composed of very fine to fine-grained sandstone, silty at the base, glauconitic (similar sandstones have been described by Hubert et al., 1972). The tops of analogous stringers were either "...shallow or deep and reworked by waves and current action..." (Turner and Conger, 1981). Such processes were responsible for the relatively quartz-rich sandstone. Both wave and current action could have produced the common thin wavy laminations to low angle cross laminations. Rarely there is bioturbation.

In general, these marine sand bodies are most prominent in the northern part of the Concession NC2 in well A1-NC2, well Q1-23, and well U1-23 (Enclosures 1 to 3 in Elfigih, 1991). The less extensive nature of these sand sandstone lenses and their locations in front of each deltaic sandstone/siltstone package attests to a destructional phase origin for these sandstones. They may have been formed by intermittent wave or current activity...

5- Low angle cross laminated to parallel laminated , carbonaceous medium (occasionally coarse) to fine-grained complex sandstones (Af1-Af7 units):

The presence of channel system deposits is emphasized by isolated, thick, less continuous sandstone bodies of fining-upward or blocky serrated GR-log nature (Fig. 10).

They are observed to occur especially in well B1-61 from 2787 to 2838 m. (9140 to 9310 ft.), in well B3-61 from 2828 to 2877 m. (9275 to 9437 ft.) and in well C1-61 from 2480 to 2550 m. (8135 to 8365 ft.) (Enclosures 2 and 3 in Elfigih, 1991)...

The lowest sequence of these sandstone units was not cored. Only the uppermost fluvial channel was recovered in well B3-61 and in well C1-61. Based on log interpretation, the fluvial channels rest abruptly on the marine shale and cut through the deltaic sandstone units...

The sediment of this lithofacies is generally massive, unbedded with some low-angle cross-lamination and horizontal lamination. It represents a relatively clean sublithofacies which is medium to coarse-grained sandstone at base to fining-upward from light-grey whitish gray fine-grained sandstone to dark gray, silty sandstone with carbonaceous matters and clay matrix... This interval represents the low energy sublithofacies of channel-filling deposits which occur during a late stage of deposition as the channels are filled and abandoned...

Small fining-upward and coarsening-upward cycles are repeated along the cored interval at different levels in the channel sandstones. These cycles are interbedded with dark gray, carbonaceous shale...

This lithofacies represents fluvial channel deposits which prograded northward and cut the delta facies, leaving a strong imprint of superimposed fluvial character on the sandstone facies complex".

Facies relationships in the Lower Acacus Formation across the Hamada Basin:

Reconstruction of the paleogeographic relationships of facies in four of the units (A8, A10,A12, A14) (Figs. 11A-D) across the Hamada Basin was undertaken for this present study by utilizing well-log correlation (Enclosures 3 and 4) and depositional environmental interpretation based on core description (Appendix I). Figures 11A-D illustrate the various depositional facies for the Lower Acacus Formation (and its equivalent the Acacus South Formation to the south). From south to north, the Hamada Basin can be divided into a fluvial continental facies zone (mainly represented by the Acacus South Formation to the south), a coastal-deltaic facies zone and an offshore-marine facies zone (mainly represented by the Lower Acacus Formation to the north). These depositional zones are separated by facies boundaries whose extension in areas of minimal data is arbitrary.

Lower Acacus Formation sandstone heterogeneity is expressed in the changes of sedimentary textures and structures and in the differences in composition between facies as depositional environments changed.

Anomalous Paleozoic freshwater-bearing formations occur below oil zones in some localities in the Hamada Basin. These waters are attributed to northward migration from stratigraphically lower water-bearing formations (Cambrian-L.Devonian) (Enclosures 1 and 2) which occupy a higher structural position towards the Gargaf Arch to the south (Hammuda, 1980; Pallas, 1980).

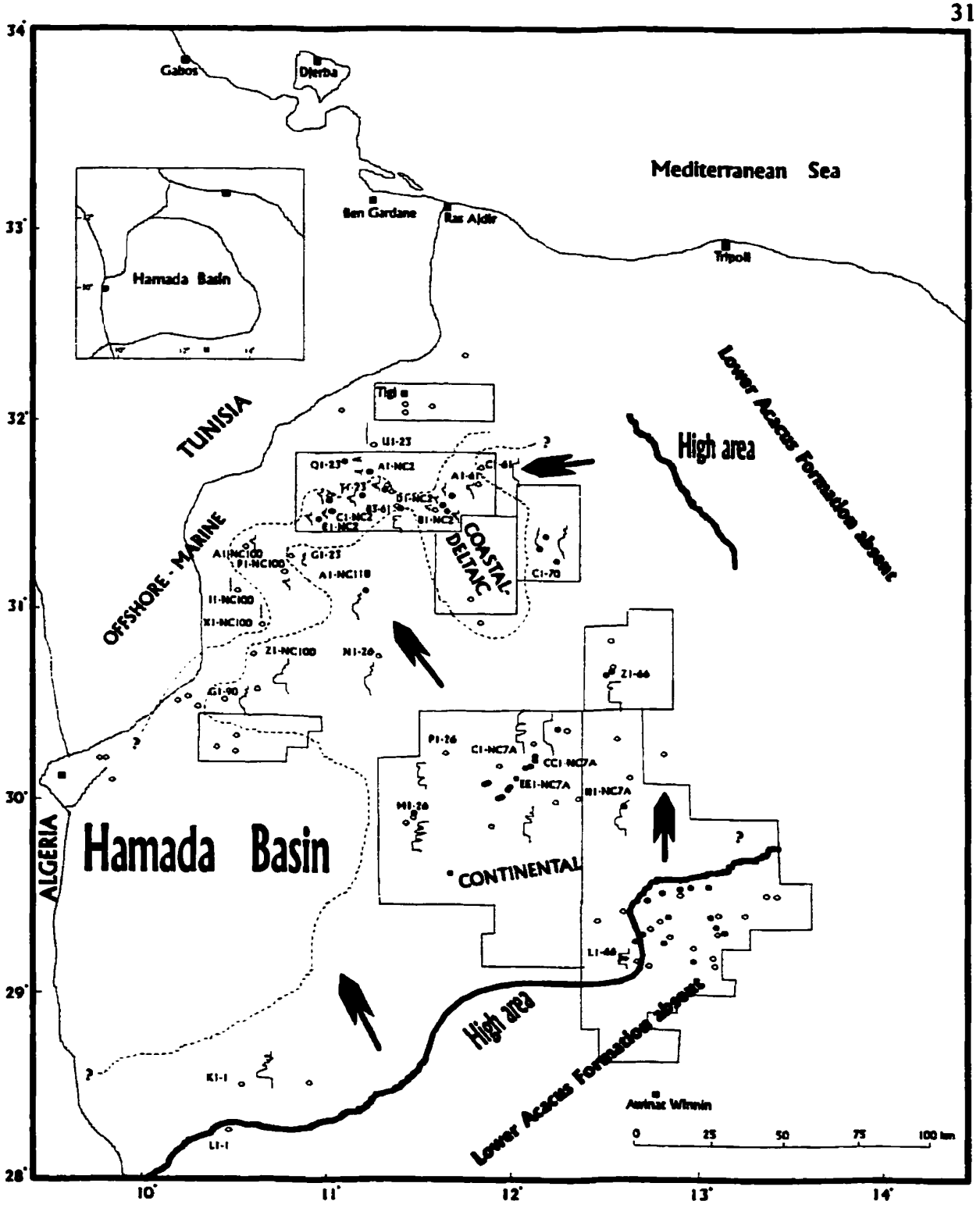

Figure 11A. Schematic construction of depositional environments on top of A8 sandstone unit of Lower Acacus Formation in the Hamada Basin, NW Libya.

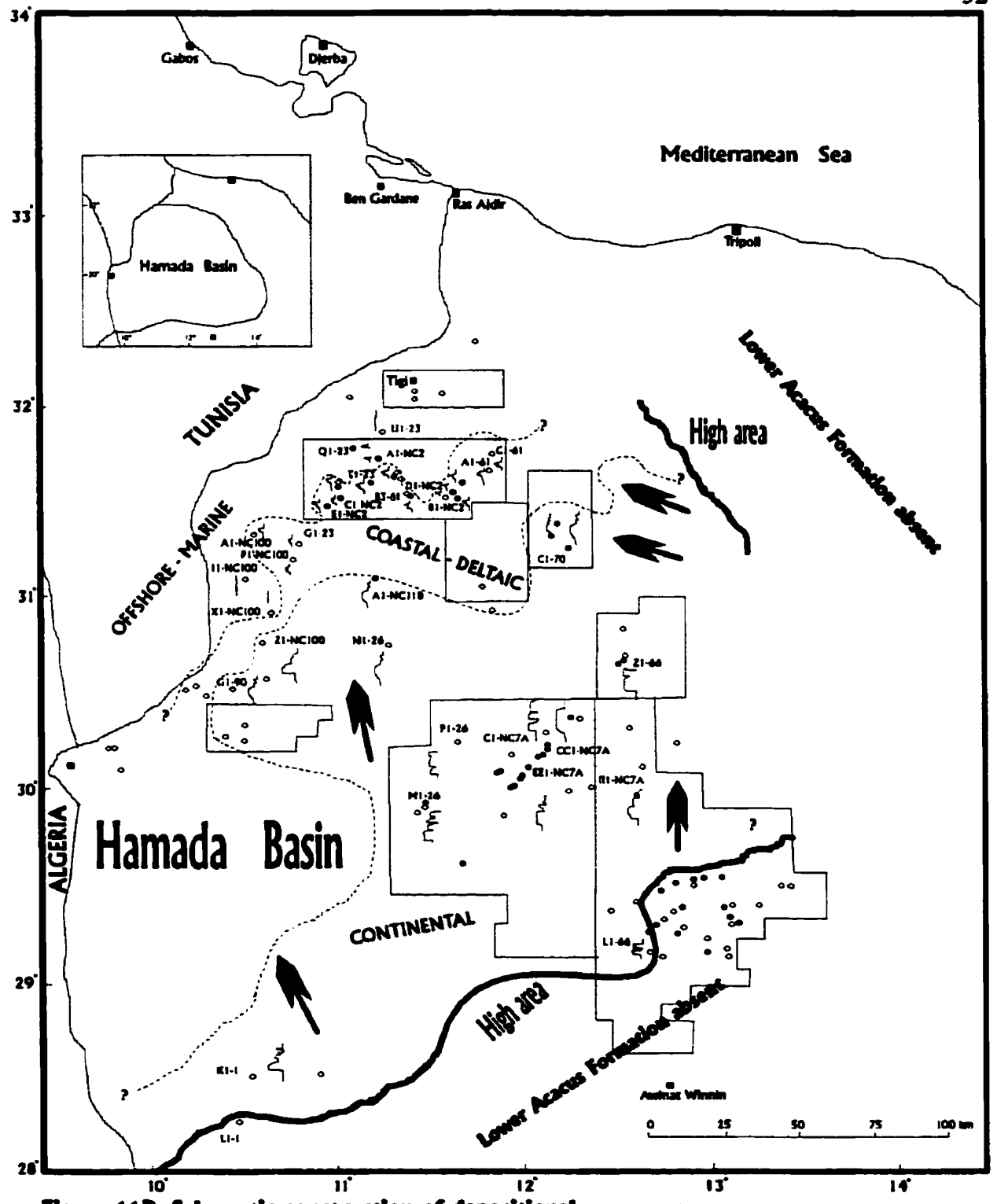

Figure 11B. Schematic construction of depositional environments on top of A10 sandstone unit of Lower Acacus Formation in the Hamada Basin, NW Libya.

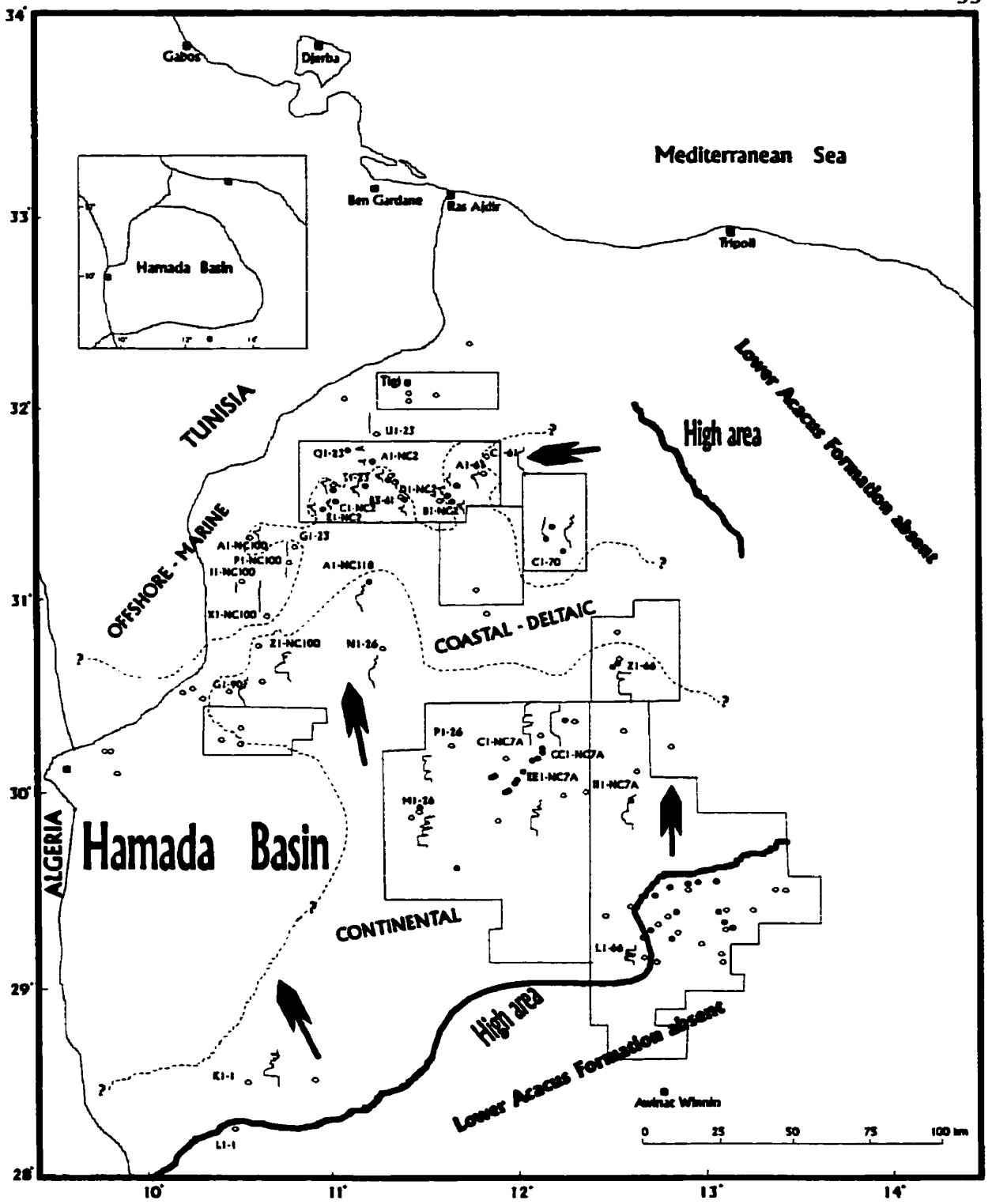

Figure 11C. Schematic construction of depositional environments on top of A12 sandstone unit of Lower Acacus Formation in the Hamada Basin, NW Libya

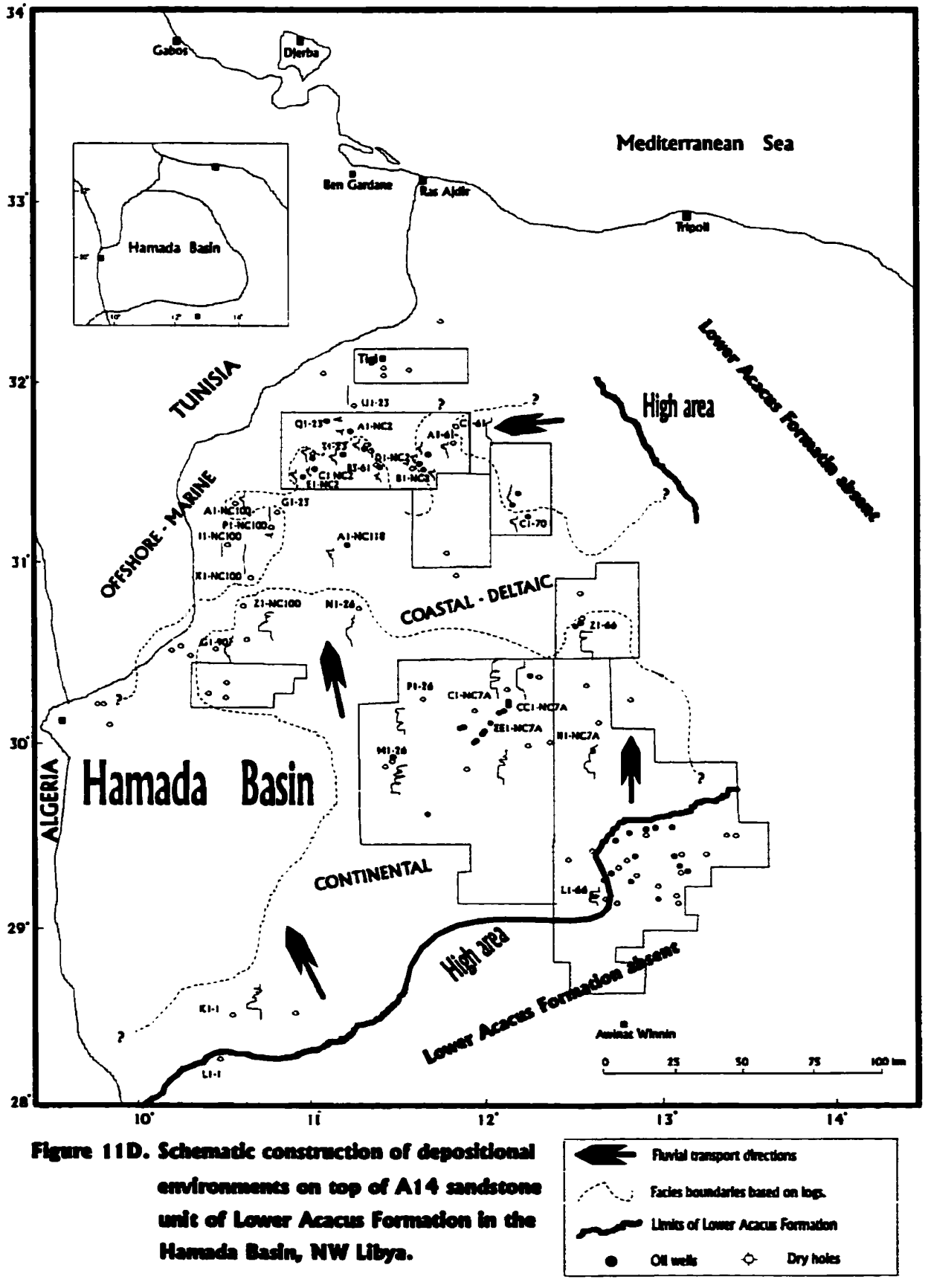

Figure 11D. Schematic construction of depositional environments on top of A14 sandstone unit of Lower Acacus Formation in the Hamada Basin, NW Libya.

I.6- Previous work:

I.6.1- Regional diagenesis:

Regional diagenetic studies are uncommon (Levandowski et al., 1984; Fox et al., 1975; Fuchtbauer, 1979; Breyer, 1983; Hoholick et al., 1984; Loomis and Crossey, 1996). Hence, relatively little is known on a basinwide scale about regional sandstone diagenesis, and how composition, cements and porosity types vary regionally with facies and depth. The role of basement structure and the situations whereby such structure can have an impact on diagenesis are poorly understood.

The source of the components of chemical diagenesis in sandstones is a major question in the understanding and predicting reservoir quality in sandstones. These components include silica, organic and inorganic acids and various cations (K^{+}, Ca^{++}, Na^{+}, Fe^{+}, Mg^{++}, Al^{+++}, etc.). However, the relative importance of localized sandstones and interbedded shales versus stratigraphically distant rocks as sources for diagenetic components is controversial; in part because data are either local or sparse (e.g. Johnson, 1920; Fothergill, 1955; Siever, 1962; Towe, 1962; Fuchtbauer, 1967, 1974; Land and Dutton, 1978; Boles and Franks, 1979; Krystinik, 1981; Milliken et al., 1981; Moncure et al., 1984; Land et al., 1987). Local diagenetic trends near sandstone/shale contacts for the Frio Formation, Texas, have been studied by Sullivan and McBride (1991) to evaluate heterogeneity of diagenetic processes on a local scale.

The concept of secondary porosity development in sandstones, and porosity caused primarily by dissolution has gained considerable attention. Basic contributions were

made by Chepikov et al. (1959) who recognized that upon the introduction of hydrocarbons into a porous system all mineral-forming processes come to a halt in the oil column but new minerals continue to form in the water column. Chepikov et al. (1961) suggested that the arrival of oil in the reservoir leads to dissolution of cements and causes an improvement in reservoir properties.

Yermolova and Orlova (1961) noted that high porosity in sandstones can be produced at considerable depths. The main process in the studied cases was removal of authigenic minerals that acted as earlier cement. Savkevich (1969) was the first to illustrate that porosity could actually increase with depth owing to the dissolution of early cements. Later workers (Loucks et al., 1977; Schmidt and McDonald, 1977, 1979a; McBride, 1977; Hayes, 1979) reached similar conclusions and produced graphic curves for the distribution of porosity with depth.

Porosity, diagenesis and productive capability of sandstone reservoirs were studied by Pittman (1979) who concluded that more cores will be needed in the future for petrographic study because available logs often cannot discriminate between important differences in pore geometry. Lynch (1996) has indicated that fluid flow is an important factor influencing the diagenesis of sandstones of the Frio Formation, Texas. Porous and permeable rocks were considered to be the preferred sites for precipitation of diagenetic minerals because of higher potential flow volumes. Therefore sandstones that were originally the most porous and permeable were modified by diagenesis more than their originally less permeable neighbours.

The role of dissolved CO_2 in creating secondary porosity was discussed by Schmidt and McDonald (1979a), Bray and Foster (1980), and by Al-Shaieb and Shelton (1981). Dissolved CO_2 lowers the pH of pore fluids thus providing an acidic solvent for carbonate and other minerals. Any CO_2 in the gas phase creates a gas-drive mechanism for the migration of hydrocarbons into reservoir rock. This gas-drive process was favoured as the process by which acidic pore fluids may have migrated into the sandstones of the Spindle Field, Colorado to dissolve calcite (Porter and Weimer, 1982). Also Laserse et al. (1983), Loucks, Dodge, and Galloway (1984), Franks and Forster (1984), and Bjørlykke (1984) also emphasized the importance of dissolved CO_2 in leaching sandstone constituents. However, Surdam, Boese, and Crossey (1984) indicated that organic acids generated from maturing horizons are the main contributors to secondary porosity at great depths. Bjørlykke (1979) and Markert et al. (1984) reported that meteoric subsurface water can be a very important mechanism for developing secondary porosity.

Al-Shaieb and Walker (1986) studied the evolution of secondary porosity in Pennsylvanian Morrow Sandstones, Anadarko Basin, Oklahoma, and defined diagenetic complexity as a function of depositional environments, burial, and thermal history of the basin. They did not relate the diagenetic changes to basinal facies changes. Moreover, they interpreted diagenetic history as a function of depth only.

Wescott (1983) discussed the diagenesis of the deltaic complex of Cotton Valley Sandstone (Upper Jurassic), East Texas, and indicated that probably only a limited volume of this potential reservoir rock was subaerially exposed or subjected to freshwater

flushing. However, much of the middle portion of Cotton Valley sequence was deposited in a lower coastal plain, nonmarine environment, characterized by: (1) fluvial and distributary channels and crevasse splays, (2) abandoned channels , and (3) interdistributary lakes (Bailey, 1983). Sediments deposited in these settings certainly were affected by fresh water during their depositional and post-depositional history. As mentioned by Coleman (1985), the greatest effect of freshwater exposure would have been the introduction of clays into clean sandstones by percolating phreatic waters.

The pervasive distribution of authigenic kaolinite in fluvial, shallow marine and deltaic sandstones suggests that exposure to meteoric water is a prerequisite for kaolinite to form at the expense of dissolved feldspar and mica (Hurst and Irwin, 1982; Bjørlykke, 1984; Bjørlykke and Brendsdal, 1986; Bath et al., 1987).

Saigal et al. (1992) studied the diagenetic processes involved in the Flumar reservoir sandstones, central North Sea and concluded that these sandstones show little evidence of leaching of feldspar or carbonate cement and contain almost no diagenetic kaolinite. This is probably due to their depositional environment (marine shelf - basin). These sandstones apparently were not significantly exposed to meteoric water.

Loomis and Crossey (1996) studied diagenesis in the cyclic, regressive siliciclastic sequence of Point Lookout Sandstone, San Juan Basin, Colorado, and concluded that the distribution of key diagenetic features is controlled by: (1) depositional facies and (2) the position of the sandstone within the overall cyclical sequence of the Point Lookout Sandstone. Their outcrop study covered an area of only 4 km^2 . Vertical changes of a

diagenetic sequence were identified but lateral relationships as facies changed were not reported. The paragenetic sequence is reported to be fairly consistent throughout the studied sections.

Petrographic documentation and discussion of the general diagenetic patterns observed in the Potiguar and Reconcavo Rift Basins, Brazil, were presented by (De Ros, 1986; Anjos et al., 1990; Moraes and De Ros, 1990; Moraes, 1991; Moraes and Surdam, 1993). Moraes and Surdam (1993) suggested that similar pathways exist in diagenetic evolution and they generalized a diagenetic sequence for all facies. Tang et al. (1997) studied diagenesis and reservoir potential of the Permian-Triassic fluvial/lacustrine sandstones in Southern Junggar Basin, Northwestern China, and stated that the diversity of authigenic minerals is related to the interplay of several factors including depositional environment, pore-water chemistry, detrital composition, and burial depth. They provide a generalized diagenetic sequence for the whole sandstone sequences. In their study facies were not identified as a primary control on diagenetic changes.

Maps related to regional variation of cements and porosity types across a basin have great significance in exploration for new deep reservoirs associated with diagenetic traps. Such information also can be used to minimize well formation damage. Such regional maps are uncommon (Todd, 1963; Levandowski et al., 1973; Fox et al. 1975; Breyer, 1983).

I.6.2- Previous local studies in the Hamada Basin:

The following discussion summarizes the findings of earlier workers in the Hamada

Basin. Much of this work was done prior to the mid-1970s even though the papers may have been published at much later dates. These early studies were based on field work in support of oil exploration. Very few subsurface data were available to corroborate their findings at the time these workers collected their data. However the following discussions will provide some context within which this present regional study of the Hamada Basin can be viewed. There is little doubt that a great deal of new research is needed to improve understanding of the geological history of this Basin and of Libya itself.

I.6.2a) Stratigraphic nomenclature:

The term Acacus Formation was introduced by Desio (1936) after the Jabal Acacus in the Ghat area (Banerjee, 1980), southmost Libya (Fig. 12). Desio (1936) referred to outcrops in the area of Wadi Tanezzuft where Klitzsch (1966-1970) described the type section (Fig. 12). Massa and Jaeger (1971) proposed to replace the term Acacus Formation by Interbedded Sandy-Shale Formation and the term Tanezzuft Shale by Principle Shale Formation. The older terms are commonly used in Libya; therefore it is not likely that the later ones will replace them.

The lower boundary of the Acacus Formation with the Tanezzuft Formation is gradational (Bellini and Massa, 1980) (Fig. 8). The upper boundary with the overlying Tadrart Sandstone is erosive and discordant (Banerjee, 1980).

According to BEICIP (1973), an international commercial consulting firm, the Acacus Formation can be divided into three main parts: Acacus "A", Acacus "B", and Acacus "C" or Lower Acacus, Middle Acacus, and Upper Acacus, respectively. This

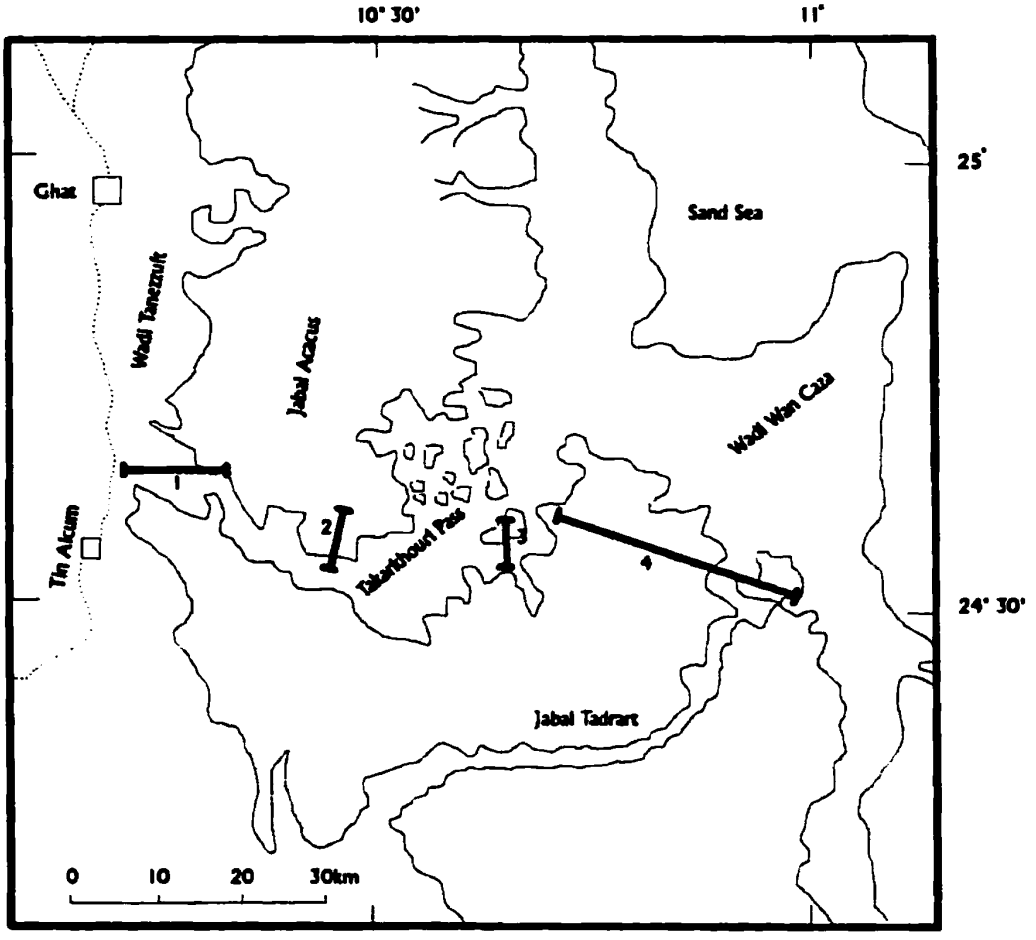

Figure 12. Map showing the type localities of the Silurian-Devonian outcrops, Ghat area, southern Libya.
Section (1) - Tanezzuft Formation outcrop.
Section (2) - Lower Acacus Formation outcrop.
Section (3) - Upper Acacus Formation outcrop.
Section (4) - Top Acacus Formation and Tadrart Formation outcrop.
(after Klitzsch, 1969).
(Note: Jabal Acacus is the type locality of exposed Acacus Formation in the Hamada Basin, which extends to about 25°38'N.)

division and nomenclature of the Acacus Formation was based on lithological differences between the three mentioned parts.

In accordance with BEICIP (1973), this present study refers to the Lower Acacus Formation or Acacus "A" interval which is confined between the Middle Acacus Shale or Acacus "B" Shale above and the Tanezzuft Shale beneath. In the southern part of the Hamada Basin the Acacus South Formation (an informal unit) is overlain by the Tadrart Formation and underlain by the Lower Acacus Formation. Subsequent data (well-log correlation) indicate that the Acacus South Formation represents the lateral equivalents of the Upper Acacus and Middle Acacus formations (Fig. 8).

I.6.2b) Stratigraphy and sedimentology:

According to Klitzsch (1969) in the Jabal Acacus area (Fig. 12) the approximate exposed section of the Acacus Formation is about 360 m. (1182 ft.) of white, grey and brown, mainly fine-grained, thin to thick- bedded sandstones, with clean sandstone near the top and shale interbeds in the lower part. Goudarzi (1970), reported that the Acacus Formation west of Jabal Al Haruj al Aswad consists chiefly of sandstone with minor siltstone interbeds. Klitzsch (1981) estimated the maximum thickness of the Acacus Formation to be 465m. (1525 ft.) in the north Dor-El Gussa area (16° 30'E) at the eastern edge of Murzuk Basin, extending along Jabal Acacus to about 25° 38'N (Fig. 12).

Bishop (1975), summarized the general geology of Tunisia and the adjacent parts of Libya and Algeria, integrating subsurface and outcrop data in an attempt to define good stratigraphic correlation and to define the parameters which control various hydrocarbon

productive trends. He also reported that the Paleozoic rocks are largely clastic sediments of both marine and continental origin with thick Infracambrian sediments deposited during an early Paleozoic transgression which began in Morocco and spread generally eastward, reaching its maximum areal extent over western Libya in the Silurian.

Bellini and Massa (1980) investigated the relationship between the Tanezzuft Formation and the Acacus Formation in the Ghadames Basin (Hamada Basin). They related the diachronism of the Silurian sequences to the progradation of sandy Acacus units from south to north over the graptolitic Tanezzuft Shale. They indicated that "...the distinction between Tanezzuft and Acacus formations is not clear-cut, the passage from one to another always being gradual and progressive". In the Sirte Basin, Cambrian and Ordovician rocks directly underlie sediments of Mesozoic age.

On the basis of a best-facies-fit-correlation approach, Elfigih (1991) demonstrated that the Lower Acacus Formation consists regionally of at least 14 progradational units which change laterally in a progradational fashion from south to north in the Basin.

I.6.2c) Structural geology:

Klitzsch (1971) addressed the structural development of parts of North Africa since the Cambrian, and identified the main structural elements during the Lower Paleozoic-Devonian in Libya (Fig. 13). The bounding arches for the Basin (Fig. 4) formed during the Hercynian Orogeny (Bellini and Massa, 1978) after development of the Paleozoic structures.

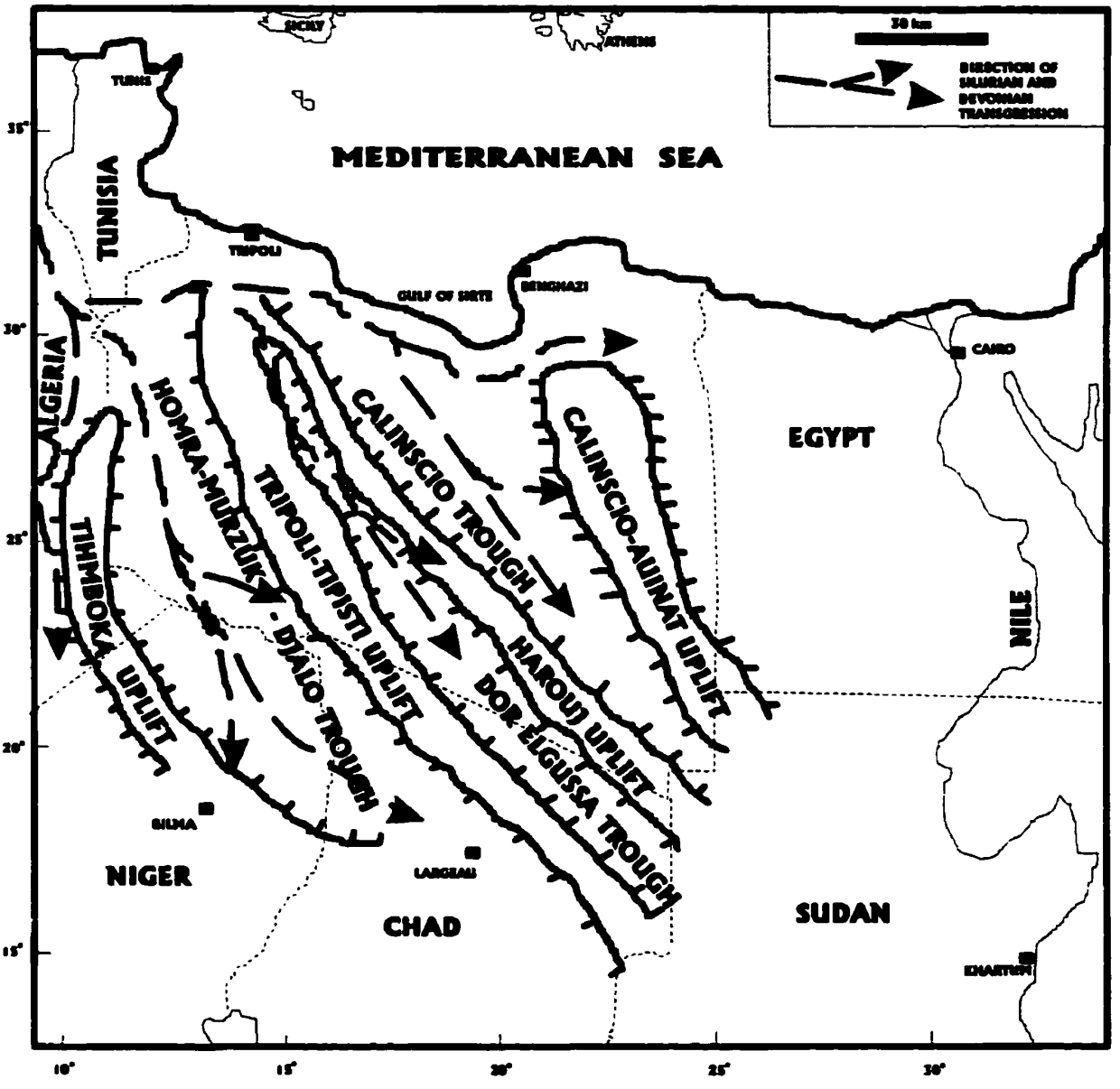

Figure 13. Structural relief of Libya during Early and Late Paleozoic (after Klitzsch, 1971).

Conant and Goudarzi (1967) summarised the stratigraphic and tectonic framework of Libya especially as it relates to the search for petroleum. Oil and gas have been found in sandstones of Ordovician, Silurian, Devonian, Carboniferous and Triassic ages. Most of the producing sandstones were believed to occur in anticlines, although several unconformities within the section were considered potentially to have created stratigraphic traps. It was reported that compressional folds are almost wholly absent but uplift, subsidence, block faulting, and tilting have occurred and angular unconformities and disconformities are common. The major diastrophic disturbances of sedimentation were considered to be the Caledonian and Hercynian orogenies, as well as disturbances during Late Cretaceous and the Oligocene through Miocene to Recent times.

Bishop (1975) studied the geology of Tunisia and adjacent parts of Algeria and Libya. He reported that the Caledonian tectonic movements produced structural alignments and important regressions, but general uplift resulting from the Hercynian orogeny caused the major withdrawal of the sea.

Van Houten (1980) summarized the Late Jurassic and Early Cretaceous regressive sedimentary events in northeastern Africa. He interpreted these events to have resulted from differential uplift and regression of broad uplands coupled with subsidence of three large intracratonic basins (Ghadames, Murzuk, and Kufra Basins) and of the pericratonic margin (Sirte Basin) where horsts and grabens developed.

Weerd and Ware (1994) suggested that the Ghadames, Kufra, Murzuk and Illizi Basins were the result of Hercynian (Late Paleozoic) tectonic movements. Prior to the

Hercynian orogeny the North African craton was one large and flat depositional basin with little regional deformation. Uplift, deformation and deep erosion during the Hercynian orogeny removed large parts of the Paleozoic section in most areas. Subsequently a Jurassic-Cretaceous basin (the Triassic Basin, and its eastern continuation the Ghadames Basin) became established on the eroded remains of the Paleozoic Basin.

I.6.2d) Paleontology and paleoecology:

Bonnefous (1963) published details of some exploration wells in southern Tunisia close to the Libyan border. These wells partly or totally penetrated the Silurian sequence. This publication also includes long lists of fauna (mainly graptolites) in shales of Llandovery and Wenlock age that are overlain by several hundred metres of Ludlow age sediments (including sandstones in the upper part of the Acacus Formation). Bonnefous reported that radioactive tracer beds occurred within the Llandovery and at the top of the Wenlock shale. These radioactive beds are the equivalent of the basal Tanezzuft high radioactive shale zone evident on well-logs (Enclosures 3 and 4).

Klitzsch (1966) reported that the Acacus Formation is of Middle to Upper Llandoverian age based on graptolitic associations found at its base. The presence of a rich abundance of the ichnofossil Harlania suggested to Klisch that the Formation extends into the Wenlockian.

Seilacher (1969) studied trace fossil distributions in Paleozoic sandstones of Libya and compared them with those found in Paleozoic sandstones of Jordan. He assigned the thicker-bedded sandstones at the top of the Acacus sequence to the Skolithos facies,

representing upper shoreface environments, whereas the Cruziana facies occurs in thin bedded sand/shale intercalations and represents lower shoreface environments.

Massa and Jaeger (1971) are the only authors to have published details of the stratigraphy of Silurian sediments of the Hamada Basin, including a well-defined fauna and flora. They reached conclusions similar to those of Bonnefous (1963):

"...above the relatively thin strata of Ludlow age shale occur the intercalated sandstones and siltstones within the upper part of the sequence which defines the Acacus Formation. The uppermost 200 m. (656 ft.) of the Silurian strata are characterised by increasing amounts of spores and plants (Cooksoniacae) and by the absence of graptolites, while fragments of other marine fossils still continue to be present (Tentaculites, ostracodes, crinoids, orthoceratids, and others)" (p. 319). Increasing continental influence was documented towards the end of Ludlovian sedimentation, being the result of Caledonian movements.

Klitzsch (1981) reported that the Tanezzuft shale contains mainly planktonic and nektonic fossils (graptolites, orthoceratids, and small bivalves). Trace fossils typical of a shallow water environment are frequent in the Acacus Sandstones (Tigillites sp., Cruziana sp., and especially Harlania sp.). Thus the Tanezzuft shale was interpreted to represent sediments deposited during transgression and in basinal areas far from the coast, whereas the Acacus sandstones generally were deposited during the regression of the Silurian sea, and near its shoreline.

Tekbali and Wood (1991) analysed core samples from the Tanezzuft and Acacus

Formations in the Bani Walid section for spores, chitinozoans and acritarchs. Their preliminary analysis identified several relatively advanced spore species indicative of an upper Silurian-Lower Devonian age (e.g. Cymbosporites ssp., vermiculata, etc.). Acritarchs, and chitinozoans constitute more than 70% of the lower section of Lower Silurian age, but decrease in diversity and abundance in relation to spores.

I.6.2e) Petrography and diagenesis:

Petrography and diagenesis of the Acacus Formation in the Hamada Basin has received little study. Daniels (1989) studied the petrography of sidewall cores from the Memouniat, Tanezzuft and Acacus Formations in the Hamada area in well II1-NC7A (Fig. 11A). By means of thin-section analysis he determined that the major framework constituents of the Acacus were quartz, with chlorite, clays, chloritized muscovite, and ferruginous volcanic grains. All constituents are pervasively cemented with an iron oxide which Daniels (1989) reports to be of hematitic-goethitic composition. This iron oxide also has partly replaced some framework grains.

Elfigih (1991) studied the petrography of the Lower Acacus Formation in Concession NC2 and concluded that these sandstones are moderately sorted sublitharenites, with complex mineralogy.

I.6.2f) Geochemistry:

The Tanezzuft Shale is the main hydrocarbon source rock for the known hydrocarbon accumulations in the Silurian sandstone reservoirs of the Hamada Basin (BEICIP, 1972-75; Ghori, 1985). Regionally the Tanezzuft shales and their equivalents

are known throughout the subsurface across North Africa from Egypt (Klitzsch, 1981) to Morocco (Destombes et al., 1985), southward into Coastal Ghana, and eastward into Jordan (Keegan et al., 1990), and into central Saudi Arabia (Jones and Stump, 1999).

BEICIP (1972-1975) investigated the geochemistry and burial history of the source rocks in the Hamada Basin, and outlined the influence of the structural evolution of the basin on hydrocarbon migration and entrapment.

Ghori (1982) identified the hydrocarbon potential of source rock and maturation levels in different parts of the Basin. Ghori (1985) studied the thermal maturity of the Tanezzuft shale source rock in well GG1-NC7A (Fig. 11A). He recommended that this type of study should be extended to other wells across the Hamada Basin.

A basin evolution model by Makhous et al. (1997) was applied to evaluate hydrocarbon generation and migration histories in the general Saharan Basin including the Ghadames Basin (Libya), and the Illizi and Oued el Mya Basins (Algeria). The authors reported that thermal gradients in the Ghadames and Illizi Basins are greater than those in the Oued el Mya Basin. This difference is attributed to differences in sedimentation and subsidence rates and to less Hercynian erosion.

I.6.2g) Basin evaluation:

After years of hydrocarbon prospecting by different oil companies in different areas in the Hamada Basin the understanding of the structural complexities and entrapment of oil has advanced slowly. Play concepts of drilling drape structures overlying Cambro-Ordovician paleohighs and of considering the reservoirs to be blanket sandstones

occurring across the basin does not reflect existing tectono-stratigraphic sequences in terms of natural sedimentary cycles and facies changes.

In 1972 to 1975 BEICIP undertook an exploration study and evaluation of the Hamada Basin. Their report covered the stratigraphy of the geological formations and the history and entrapment of oil.

A number of regional studies investigated potential play types and addressed new regional evaluations of the basin. Hammuda (1978) summarized the results of a geological study conducted as part of an evaluation for recoverable reserve estimates for the National Oil Corporation (NOC). He concluded that Al Hamada al Hamra area (Hamada Basin area) had more traps than had been discovered to that time. Seismic information revealed that some oil traps could be attributed to draping, arching or extensive faulting but little was revealed about truncated beds due to cutoffs or pinch-outs. Hammuda also concluded that the fresh water below the oil zones in sandstones in the northern part of the Hamada Basin are sourced from the Lower Paleozoic (Cambrian-Lower Devonian) freshwater-bearing formations to the south in a structurally higher position.

Echikh and Sulieman (1982) completed a preliminary geological study and petroleum evaluation of the Ghadames Basin (an internal N.O.C. report). No new original work was contributed.

Shah et al. (1988) studied geological factors controlling the oil and gas deposits of the Hamada Basin and made recommendations for their future exploration. He postulated

exploration models involving drape structures over paleohighs and hydrodynamic and facies changes in monoclinal settings.

Santa Maria (1991) completed a regional study on the Hamada Basin. The main purpose of this study was to evaluate the hydrocarbon potential of the Ghadames Basin as it related to the distribution and characteristics of oil and gas. One of the principal objectives was to establish a reliable stratigraphic framework for the main sedimentary cycles in the total geological section, for exploration purposes. To this study he appended recommendations regarding expectations for the hydrocarbon potential of the Basin.

Cridland (1991) completed a seismic stratigraphic evaluation of Concession NC2 in which he integrated his seismic interpretations with existing geological studies of the Lower Acacus Formation. Play types for Lower Acacus sandstone reservoirs were also identified in this study.

Teknica Exploitation Group (1995) initiated an exploitation study of hydrocarbon pools of Lower Acacus sandstones in selected wells in the west half of Concession NC2, and recommended these sandstones for their good reservoir quality and their hydrocarbon potential in the area.

Summation:

As the preceding review illustrates, detailed studies within the Hamada Basin are few, of older vintage, and often from unpublished reports. However the data associated with these studies is invaluable and awareness of the existence of the studies is critical for future research.

II- METHODS OF STUDY

Fifty petroleum exploration wells which penetrated the Lower Acacus Formation have been used in this study (Fig. 14, Table 1). Well data in Libya are reported in Imperial units. In order to maintain compatibility and integrity the original Imperial units are retained. Where appropriate, units are converted to the Metric System.

A total of 528 m. (1486 ft.) of core-sections from different deltaic units of Lower Acacus Formation were available from sixteen (16) wells (out of the 25 detailed studied wells) (Fig. 14). Interpretation of depositional environments for the various Lower Acacus sandstones was based mainly on the examination of cores and their integration with wireline-logs and thin-section data (Appendix I).

Point counts (300/slide) of 139 thin-sections were taken from cores to characterize the detrital composition and texture, determine the extent, nature and sequences of diagenetic alteration, and delineate the magnitude of secondary porosity development (Appendices II, V). Cements and authigenic clays were differentiated from detrital grains and reported as bulk rock percentages.

Cutting samples (56 thin-sections) were studied from uncored sandstone units in some selected wells in order to identify and confirm the existence of these units and to seek their extensions between correlated wells (Fig. 14).

Thin-sections were stained with potassium ferricyanide and alizarin red-S for

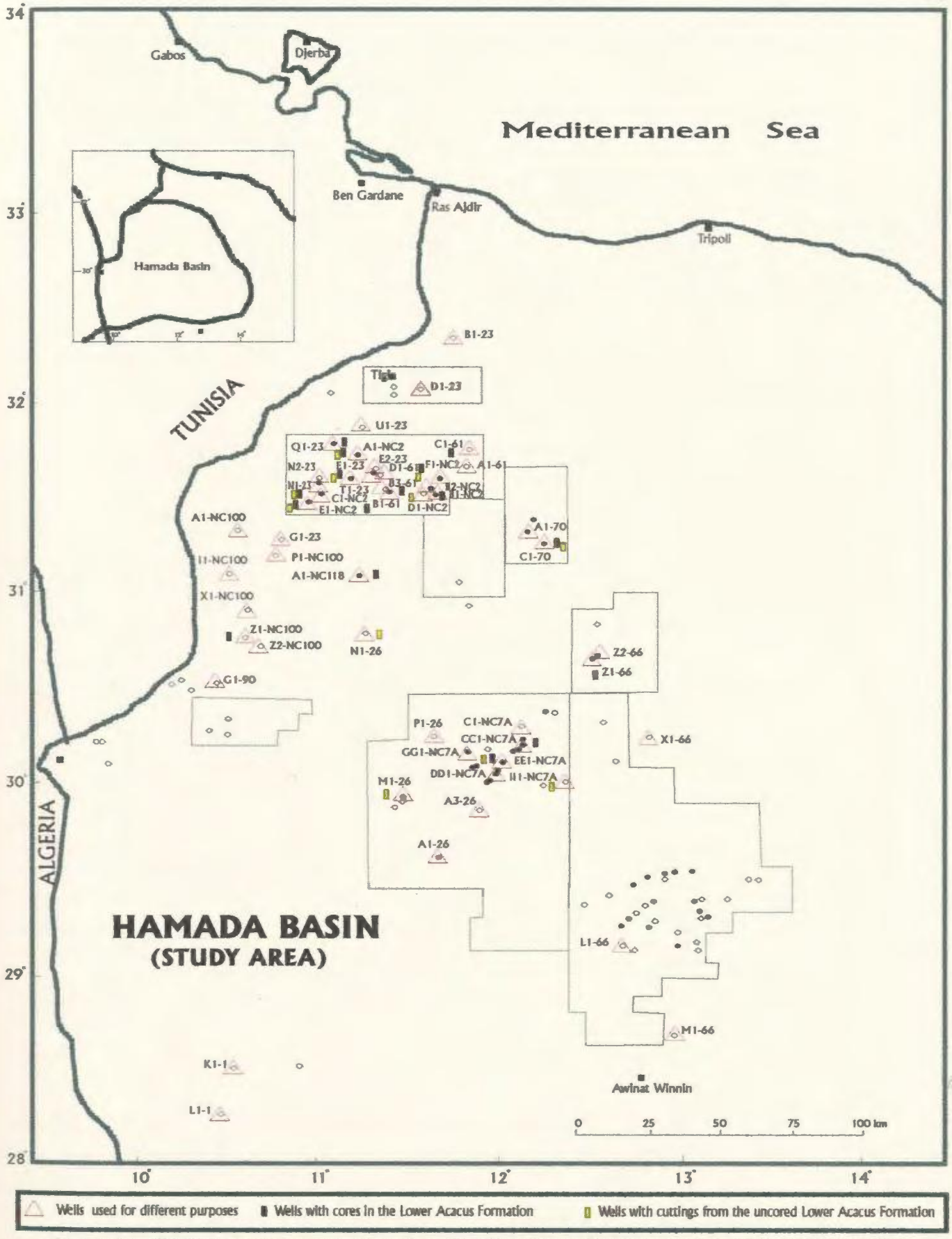

Figure 14. Well location map, showing distribution of wells used in this study in the Hamada Basin, NW Libya.

Table 1. List of wells used in this study from the Hamada Basin, NW Libya. (*See figure 14 for well locations).

Well #	Well Name	Well Location *
1	A1-NC2	NC2
2	B1-NC2	NC2
3	B2-NC2	NC2
4	C1-NC2	NC2
5	D1-NC2	NC2
6	E1-NC2	NC2
7	F1-NC2	NC2
8	A1-61	NC2
9	B1-61	NC2
10	B3-61	NC2
11	C1-61	NC2
12	D1-61	NC2
13	E1-23	NC2
14	E2-23	NC2
15	N1-23	NC2
16	N2-23	NC2
17	T1-23	NC2
18	Q1-23	NC2
19	U1-23	N. NC2
20	B1-23	N. NC2
21	D1-23	N. NC2
22	A1-70	NC4
23	C1-70	NC4
24	Z1-66	NC5
25	Z2-66	NC5
26	G1-23	SW. NC2
27	A1-NC100	SW. NC2
28	I1-NC100	SW. NC2
29	P1-NC100	S. NC2
30	X1-NC100	SW. NC2
31	G1-90	N. NC6
32	Z1-NC100	N. NC6
33	Z2-NC100	N. NC6
34	A1-NC118	W. NC3
35	C1-NC7A	NC7A
36	CC1-NC7A	NC7A
37	DD1-NC7A	NC7A
38	EE1-NC7A	NC7A
39	GG1-NC7A	NC7A
40	II1-NC7A	NC7A
41	A1-26	NC7A
42	A3-26	NC7A
43	M1-26	NC7A
44	N1-26	NC118 (NW NC7A)
45	P1-26	NC7A
46	K1-1	SW.NC7A
47	L1-1	SW.NC7A
48	L1-66	NC8A
49	M1-66	NC8A
50	X1-66	E.NC8A

carbonates (Dickson, 1965). Grain size was determined by measurement (100grains/slide) of the long axis of the sand and silt-size framework grains. In addition to cores, a detailed geophysical log suite was collected at all wells, allowing better correlation and analysis of reservoir quality in different levels in the Lower Acacus Sandstones.

Routine core-porosity-permeability analyses were conducted by AGOCO Core Laboratory, Benghazi, Libya, on 65 core-plugs of 5 cm. (2 in.) diameter at 0.3 m. to 1 m. (1 ft. to 3 ft.) selected intervals throughout the studied cores. Core-plug measurements consisted of core-plug helium porosity (ϕ_c), and air permeability (vertical K_v, horizontal K_h) performed at net effective stress 5516 kPa. (800 psi) and at 27580 kPa. (4000 psi) overburden pressure, and grain density measurements (Table 2). Well-log responses (neutron, density, and sonic logs) were also used in several intervals to better compare porosity, permeability and cement distribution.

In addition to standard petrographic analysis, cement distribution and textural alteration caused by the diagenetic development of secondary porosity, the nature of grain to grain contacts, and diagenetic quartz overgrowth were investigated by cathodoluminescence (CL) petrography (Appendix III). The CL study was conducted in the CL-Laboratory at Memorial University of Newfoundland and was carried-out using a Nuclide Luminoscope CL-unit, with doubly magnified objectives, giving a maximum magnification of 640x at long working distances. Operating conditions varied but accelerating voltage was between 10-15 kV with a beam current of 0.1-2 mA. The sample chamber had a 50-75 millitorr helium atmosphere.

Table 2. Porosity-Permeability data of routine core-plug analysis for sandstone samples from the Lower Acacus Formation in some selected wells, Hamada Basin, NW Libya. (AGOCO Lab., 1995).

Well Name	Depth (ft)	Permeability[1] (md)		Core-plug porosity (%)[2]	Grain density
		K_v	K_h	$\emptyset c$	(gm/cm³)
A1-NC2	7814	1	2	12	2.33
	7817	2.8	3	15	2.34
C1-NC2	9630	25	25	16	2.63
	9645	-	-	26	2.66
	9703	245	250	18	2.65
	9725	3010	3133	14	2.70
E1-NC2	9105	762	829	21.5	2.65
	9111	401	418	14.8	2.33
	9115	30	31	19.7	2.35
	9117	29	36	13	2.62
	9122	3	4	13	2.62
	9125	1842	2302	25.6	2.70
	9140	-	2442	27	2.68
	9143	-	4	13.3	2.69
	9512	11	11	16	2.68
Q1-23	7461	244	252	17	2.65
	7470	45	45	16	2.65
	8180	6.7	8.5	14.5	2.62
	8190	11	12	14	2.65
	8461	-	3	19.6	2.64
	8481	6.4	12	14	2.64
	8485	47	47	14.5	2.65
T1-23	8454	30790	30879	30.5	2.66
	8473	1252	1254	22	2.69
B1-61	8420	1924	2820	18	2.66
	8422	-	3010	19	2.67
	8442	-	7	10	2.66
	8462	2301	2331	21	2.67
	8479	2003	2015	16	2.66
	8484	1325	2609	16.5	2.67
	8490	3	5	16	2.33
B3-61	8756	697	703	28.3	2.67
	8764	58	58	15.4	2.68
	8893	109	113	16	2.65
	8908	-	-	15.2	2.66
	8929	242	278	15.4	2.67
	8950	-	58	14	2.67
	8969	-	102	14	2.65
	8974	9	11	14	2.62
	9311	73	90	25	2.56
	9328	88	94	24	2.55
	9345	7	7	23	2.60
	9360	-	-	18.3	2.60
C1-61	7522	13	13	22.9	2.53
	7525	9127	18384	18.7	2.53
	8199	1854	1856	32	2.55
	8209	-	-	27	2.56

Cont.....

Cont....Table 2.

Well Name	Depth (ft)	Permeability[1] (md)		Core-plug porosity (%)[2]	Grain density (gm/cm³)
		K_v	K_h	Øc	
D1-61	8236	120	247	17.5	2.65
	8240	157	268	16	2.69
	8314	112	228	13	2.37
	8319	175	234	14	2.36
	8420	-	263	-	2.66
	8420	-	-	-	2.65
	8845	-	-	13.5	2.66
	8866	201	320	14.6	2.67
	8872	-	-	13.5	2.36
Z1-66	9080	513	952	22	2.50
	9081	1420	2833	23	2.50
	9130	1234	2467	18	2.51
	9140	-	2488	23.5	2.51
C1-70	7913	314	721	19	2.65
Z1-NC100	11680	-	2829	17	2.54
A1-NC118	10040	1320	2656	23	2.55
	10115	5.6	18	6	2.56
CC1-NC7A	9017	86	250	21.5	2.52
	9020	92	288	22	2.50
EE1-NC7A	8810	2328	4992	26	2.50
	8812	2334	5202	27	2.45

[1] K_v = Vertical permeability, K_h = Horizontal permeability

[2] $Ø_c$ = Core-plug Helium porosity

Note: K_v : K_h is always approximately 1:1 or 1: 2 in some cases.

Porosity-Permeability data for all sandstone samples of Lower Acacus Formation were updated in September 1995.

(All measurements are in the units of the wells studied. Where both Metric and Imperial units are utilized they are provided).

CL-photomicrographs were taken using 1-2 minute exposures on high speed Kodak Ektachrome film (ASA 400). Approximately 35 color photomicrographs of Lower Acacus sandstone thin sections were taken. Two photographs were taken for each (1.5 x 0.75mm) field to be analysed, one under transmitted polarized light and the other under CL. When compared, the two photos define the position of detrital-grain overgrowth boundaries, or associated cement type. Observation of diagenetic minerals from selected thin-sections in the Lower Acacus Formation through a technique that combines CL with light microscopy will be discussed below (CL results and their application to petrographic observations were reported according to Potosky, 1970; Marshall, 1978; and Wilson and Sibley, 1978).

A total of 20 carbon-coated sandstone samples from different facies in the Lower Acacus Formation were examined by scanning electron microscopy (SEM) (Appendix IV) coupled with energy dispersive spectroscopy (EDS) to assess pore-space morphologies and identify cement types, clay mineralogy, and the diagenetic attributes associated with each studied facies across the Hamada Basin. SEM/EDS techniques were used in this study to support and help to confirm morphological details and gross mineralogical composition identified in thin-section petrography. The techniques permitting these identifications were developed by various authors (Borst and Gregg, 1969; Weinbrandt and Fatt, 1969; Pittman, 1972; Kieke and Hartmann, 1973; Kaldi et al. 1978; Krinsley and McCoy, 1978; Le Ribault, 1978; Mycielska-Dowgiallo, 1978; Werle and Schneider, 1978; and Imam, 1986).

X-ray diffraction (XRD) analyses for bulk sample mineralogical identification associated with the different facies in the Lower Acacus Formation were conducted in the XRD-Laboratory at Memorial University of Newfoundland by using a Rigaku Ru-200 diffractometer equipped with a graphite monochromator and rotating copper anode. Ten samples were collected from sandstone/shale intervals of different facies in the Lower Acacus Formation. Samples were crushed to 5-10μm and smeared on a glass slide using acetone. The X-rays were generated at 40 kV and 70 mA. Analyses were made at a scan rate of 5° 2θ/min. The XRD analyses were conducted only for the purpose of bulk mineralogical identification complementary to the other analysis techniques used in this study and to confirm regional mineralogical variation identified in thin-section petrography as facies changed from fluvial, deltaic to marginal marine origin across the Basin.

Stable isotope mass spectrometry analyses were carried-out for this study on 30 samples from different facies of the Lower Acacus Formation in order to demonstrate regional variations.. The analyses were conducted by Dr. Fred Longstaffe-University of Western Ontario, Canada, and were used to determine oxygen and carbon isotopic compositions of the authigenic calcite cement associated with these facies. Oxygen and carbon isotopic compositions were calculated using an orthophosphoric acid (H_3PO_4) - carbon dioxide (CO_2) fractionation factor of 1.01025 at 25°C for calcite. The oxygen and carbon isotope data are reported in normal δ notation relative to SMOW for oxygen and PDB for carbon.

III- SANDSTONE PETROGRAPHY AND ISOTOPIC ANALYSES

III.1- Sandstone petrography:

III.1.1- Thin-section petrography: (See Appendix II- Plates 1-23)

III.1.1a) Detrital composition:

The framework grain composition (Tables 3), and the percentage amounts frame work, diagenetic (authigenic cement types) and porosity components (Table 4) of samples in the four facies (fluvial sandstone facies "Af2-Af7", proximal deltaic sandstone facies "A1-A14", distal deltaic sandstone/siltstone facies "Ad", and reworked marine sandstone facies "Am") are described as follows:

Quartz:

Quartz grains range from a low of 77% in distal deltaic siltstones to 91% in medium to coarse fluvial sandstones with an average of 86%. Quartz grains show straight (non-undulose) to undulose extinction (Appendix II- Plates 1A-3A).

Quartz-overgrowths are interfaced with each other and are readily visible (Appendix II- Plate 1A) because of the euhedral termination of the quartz-overgrowths and abundant inclusions trapped on their boundaries with the detrital quartz grains.

Monocrystalline quartz is the most abundant mineral in these sandstones. Mean quartz grain size in individual sandstone units ranges from 0.15mm to 0.37mm for the

Table 3. Thin-section point counting averages of framework, diagenetic, and porosity components for the various sandstone facies in the Lower Acacus Formation, Hamada Basin, NW Libya.

Facies	Framework Composition (%) [a]					Average Composition			Range of grain size (mm)	Authigenic Cement Types (%) [b]					T.S.Ø [c] (%)
	Q.	F.	L.	Micas & Others	Mx.	Q	F	L		Si/O	I	C	D	Cly	
Fluvial (n= 24)	91	4	2	1	2	93	4	3	0.25 - 0.70	12	7	6	-	2	16
Proximal Deltaic (n= 67)	88	1	8	2	1	89	1	10	0.15 - 0.37	4	-	14	5	3	12
Distal Deltaic (n=32)	77	tr.	8	4	11	86	tr.	12	0.04 - 0.1	2	-	9	2	11	4
Reworked Marine (n=16)	84	3	6	2	5	88	3	8	0.15 - 0.20	4	-	11	7	3	10

[a] Q = Quartz, F = Feldspar, L = Lithic Fragments, Micas & Others = Micas and other labile grains, Mx = Matrix.

[b] Si/O = Silica and Quartz overgrowth, I = Iron-oxides, C = Calcite, D = Dolomite, Cly = Clay. (All authigenic cements are in percent of bulk rock).

[c] T.S. ϕ = Thin-Section Porosity

(n = Number of samples, * = 300 Points Per Section).

Table 4. Petrographic and petrophysical data indicating diagenetic heterogeneity within selected Lower Acacus Sandstone units (A8-A14, Af2-Af7, Ad, and Am), Hamada Basin, NW Libya.

1 Lower Acacus Sandstone Units	Well Name	Depth		2 Facies Type	Distinctive Cement	3 Quartz O.%	4 Carbonate (%)		5 Clay (%)			6 Grain Size (mm)	7 Thin-Section Porosity (%)		8 Measured Porosity (%)	9 Permeability (md)
		ft.	m.				C	D	I	K	IL.		fr.	Sec.		
A14	B1-61	8420	2567	Prz.delt.frt.	Carbonate	2	14	6	-	2	-	0.30	-	14	18	2820
		8422	2568	,,	,,	3	15	4	-	1	-	0.37	-	15	19	3010
		8462	2579	,,	,,	2	14	4	-	2	1	0.26	-	17	21	2331
		8479	2585	,,	,,	4	13	4	-	3	1	0.25	-	12	16	2015
		8484	2586	,,	,,	4	15	5	-	2	-	0.33	-	12	16.5	2609
Ad		8490	2588	Dis.delt.frt.	Clay	0	9	2	-	13	5	0.55	-	6	16	5
	D1-61	8236	2510	Prz.delt.frt.	Carbonate	2	16	6	-	3	-	0.25	-	13	17.5	247
		8240	2512	,,	,,	2	15	5	-	2	-	0.26	-	12	16	368
Ad		8314	2534	Dis.delt.frt.	Clay	3	10	2	-	10	2	0.09	-	6	13	228
		8319	2536	,,	,,	tr	7	0	-	8	2	0.10	-	4	14	234
	A1-NC2	7814	2382	,,	,,	3	9	1	-	11	2	0.08	-	1	12	-
		7817	2383	,,	,,	2	8	1	-	9	4	0.04	-	0	13	2.8
A14	E1-NC2	9105	2775	Prz.delt.frt.	Carbonate	4	15	5	-	1	-	0.26	-	14	21.5	829
Ad		9111	2777	Dis.delt.frt.	Clay	2	1	1	-	10	1	0.11	-	2	14.8	418
		9115	2779	,,	,,	0	1	0	-	11	2	0.90	-	1.5	9.7	31
		9117	2780	,,	,,	0	1	1	-	10	3	0.10	-	2	13	36
A14		9125	2780	Prz.delt.frt.	Carbonate	3	14	4	-	2	-	0.26	-	16	25.6	2302
		9131	2784	,,	,,	3	15	5	-	1	-	0.25	-	15	22	2381
		9140	2786	,,	,,	3	15	4	-	1	-	0.28	-	18	27	2442
	T1-23	8454	2577	,,	,,	3	18	3	-	5	1	0.37	-	20	30.5	30879
		8473	2582	,,	,,	2	14	5	-	4	-	0.24	-	17	22	1254
A12	B1-NC2	8542	2605	,,	,,	4	17	5	-	1	-	0.34	-	16	26	18340
		8546	2606	,,	,,	3	15	4	-	2	-	0.32	-	15	26	15722
		8550	2608	,,	,,	2	14	4	-	3	-	0.30	-	14	25	15630
		8555	2608	,,	,,	3	15	3	-	3	-	0.29	-	13	24.3	12487
	E1-NC2	9512	2900	,,	,,	3	16	5	-	2	-	0.15	-	13	16.5	11
	E1-NC2	9513	2900	,,	,,	2	15	6	-	-	tr.	0.15	-	11	12	-
	B3-61	8893	2711	,,	,,	2	15	3	-	1	-	0.23	-	13	16	113
		8969	2734	,,	,,	2	14	4	-	2	-	0.20	-	11	14	102
	C1-70	7913	2413	,,	,,	4	18	5	-	4	-	0.27	-	15	19	721
A10	B1-NC2	8638	2633	,,	,,	2	14	6	-	2	-	0.27	-	12	15.2	729
	C1-61	7795	2376	,,	,,	1	14	2	2	3	tr	0.23	-	9	12.6	-
	D1-61	8845	2696	,,	,,	2	15	4	-	4	-	0.22	-	12	13.5	-
		8866	2703	,,	,,	2	14	4	-	2	-	0.26	-	11	14.6	320
Ad		8872	2704	Dis.delt.frt.	Clay	1	9	0	-	14	2	0.10	-	3	13.5	-
A8	C1-NC2	9703	2958	Prz.delt.frt.	Carbonate	2	13	4	-	6	1	0.24	-	10	18	250
		9725	2965	,,	,,	2	16	2	-	2	-	0.30	-	7.5	14	3133

Cont.....

Cont.... Table 4.

[1] Lower Aptian Sandstone Units	Well Name	Depth		[2] Facies Type	Distinctive Cement	[3] Quartz O.%	[4] Carbonate (%)		[5] Clay (%)			[6] Grain Size (mm)	[7] Thin-Section Porosity (%)		[8] Measured Porosity (%)	[9] Permeability (md)
		ft.	m.				C	D	I	K	IL		Pr.	Sec.		
Af2	B3-61	9311	2839	Fluv.	Quartz	13	1	2	7	3	2	0.45	14	4	25	90
		9328	2843	,,	,,	14	5	1	2	1	-	0.46	12	1	24	94
		9345	2849	,,	,,	15	6	2	5	-	1	0.25	12	2	23	7
Af7	C1-61	7100	2165	,,	,,	13	2	-	2	-	-	0.30	22	-	-	-
Af5		7522	2168	,,	,,	11	3	-	tr	-	-	0.30	16	-	-	-
		7522	2293	,,	,,	13	8	4	3	4	-	0.25	18	5	22.9	13
		7525	2294	,,	,,	11	6	2	2	1	-	0.60	16	3	18.7	18384
Af2		8199	2499	,,	,,	12	10	1	3	-	-	0.38	28	2	32	1856
		8209	2503	,,	,,	13	8	tr	4	-	tr	0.37	20	4	27	-
Af3	A1-NC118	10040	3061	,,	,,	11	4	-	3	8	-	0.37	13	5	23	2656
		10115	3084	,,	,,	17	2	-	tr	1	-	0.37	3	-	6	18
Af3	Z1-NC100	11680	3561	,,	,,	11	5	tr	3	-	-	0.38	11	2	17	2829
Af4	Z1-66	9080	2768	,,	,,	13	5	tr	5	2	-	0.47	15	2	22	952
		9081	2768.5	,,	,,	13	4	1	6	1	-	0.50	15	4	23	2833
Af3		9130	2784	,,	,,	12	3	1	4	-	-	0.46	13	4	23.5	2467
		9140	2785	,,	,,	12	4	2	6	-	-	0.48	12	2	18	2488
Af2	CC1-NC7A	9017	2749	,,	,,	15	2	1	12	3	-	0.48	12	5	21.5	250
		9020	2750	,,	,,	14	2	tr	9	3	-	0.64	10	8	22	288
Af3	EE1-NC7A	8810	2686	,,	,,	15	3	1	5	1	1	0.48	16	2	26	4992
		8812	2687	,,	,,	13	2	1	6	3	tr	0.50	14	2	27	5202
Am	Q1-23	7461	2275	Rewmar.	Carbonate	2	15	4	-	3	-	0.20	-	12	17	252
		7471	2277	,,	,,	2	14	4	-	4	-	0.16	-	11	16	45
		8180	2494	,,	,,	3	16	5	-	7	-	0.15	-	9	14.5	8.5
		8190	2497	,,	,,	2	14	5	-	2	-	0.15	-	10	14	12
		8461	2580	,,	,,	3	18	6	-	8	-	0.15	-	8	19.6	3
		8481	2586	,,	,,	4	16	4	-	2	-	0.16	-	9	14	12
		8485	2586	,,	,,	2	14	5	-	2	-	0.18	-	9	14.5	47
	B1-61	8442	2574	,,	,,	-	13	3	-	5	-	0.14	-	8	10	7
	B3-61	8756	2669	,,	,,	-	12	3	-	4	1	0.16	-	13	28.3	703
		8758	2670	,,	,,	-	10	2	-	6	-	0.16	-	10	15	63
		8950	2728	,,	,,	-	15	3	-	4	1	0.16	-	10	14	58

[1] A8-A14 = Lower Aptian deltaic sandstone/siltstone units, Af = Lower Aptian fluvial sandstone unit, Am = Lower Aptian reworked marine sandstone unit.

[2] Prx.delt.frt. = Proximal delta front sandstone facies, Dis.delt.frt. = Distal delta front siltstone facies, Fluv. = Fluvial sandstone facies, Rewmar. = Reworked marine sandstone facies.

[3] Quartz O. = Quartz-overgrowths

[4] C = Calcite, D = Dolomite

[5] I = Iron-oxides, K = Kaolinite, IL = Illite.

[6] Grain size = Grain size from thin-sections point counting.

[7] Pr. = Primary porosity from thin-sections, Sec. = Secondary porosity from thin-sections.

[8] Measured porosity = Measured porosity from core-plugs.

[9] Permeability = Measured horizontal permeability from core-plugs

(Most thin-section data were obtained from core samples, occasionally if cores were not available cutting samples may be used).

A8-A14 proximal deltaic sandstone units, from 0.04mm to 0.11mm for the distal deltaic siltstone/sandstone units, from 0.25 to 0.70mm for the fluvial sandstone units, and from 0.15 to 0.20mm for the reworked marine sandstone units (Table 3).

Feldspars:

Feldspars are volumetrically a minor constituent of the detrital grains, being an average of 2% (Table 3) (range from 0-4%) of total framework constituents, (Table 4). Feldspar grains mostly exhibit gridiron structures with occasional albite twinning (Appendix II- Plates 3B, 4A). Alkali and plagioclase feldspars commonly decrease from the fluvial sandstones to the distal deltaic siltstones although in some samples the feldspar grains appear fresh and unaltered.

Rock fragments (Lithics):

Rock fragments or lithics represent the other dominant detrital constituents . They range from 2% to 8% (averaging 5%) of the detrital grain population and demonstrate an overall increase in percentages from the southern fluvial facies northward towards the deltaic facies. Lithics are fragments of igneous, metamorphic, and sedimentary rocks.

Igneous and metamorphic rock fragments are volumetrically minor components, representing only 1-2% of total detrital constituents. *Igneous rock fragments* were identified by their glassy appearance (may be of volcanic origin) combined with the presence of either opaque granules or some crystal laths which may be an alteration product (Appendix II- Plate 4B). *Metamorphic rock fragments* consist of medium sized grains of occasionally elongated and stretched micro-polycrystalline quartz grains, or of a

foliated appearance (Appendix II- Plate 5A,B). *Sedimentary rocks fragments* are represented by *clay or shale clasts*, and some *detrital dolomite grains* and comprise 1-6% of total detrital composition. *Clay clasts* (2-4mm) are occasionally light brown to light green (Appendix II- Plates 6A,B), and show some deformation between the rigid quartz grains. *Detrital dolomite fragments* are few and where present are 2-6mm in size, rhombic to blocky in shape, with light-dull grey to cloudy colour, and show no response to stain (Appendix II- Plate 7A). *Other accessory minerals* represent 1-4% of the total detrital composition and comprise an average of 2.5%. The accessory minerals identified include, muscovite, glauconite, trace chlorite, trace chamosite, and trace zircon (Appendix II- Plates 7B, 8A,B, 9A,B, 10A).

Most sandstone samples can be classified as sublitharenites (Fig. 15), a few are quartzarenites and litharenites; where the average compositions are Q_{93} F_4 L_3 for the fluvial sandstones, Q_{89} F_1 L_{10} for the proximal deltaic sandstones, Q_{86} F_{tr} L_{12} for the distal deltaic sandstones/siltstones, and Q_{88} F_3 L_8 for the reworked marine sandstones (Table 3).

Table 4 shows detailed petrographic and petrophysical variations observed in thin-sections from the various Lower Acacus sandstone units of different facies. These petrographic variations include:

III.1.1b) Cement types:

The predominant cement is carbonate which includes patchy-poikilotopic calcite (0.5-15mm in diameter), of irregular forms and patchy dolomite pore-filling and grain-replacive rhombs associated with proximal deltaic and reworked marine sandstone facies

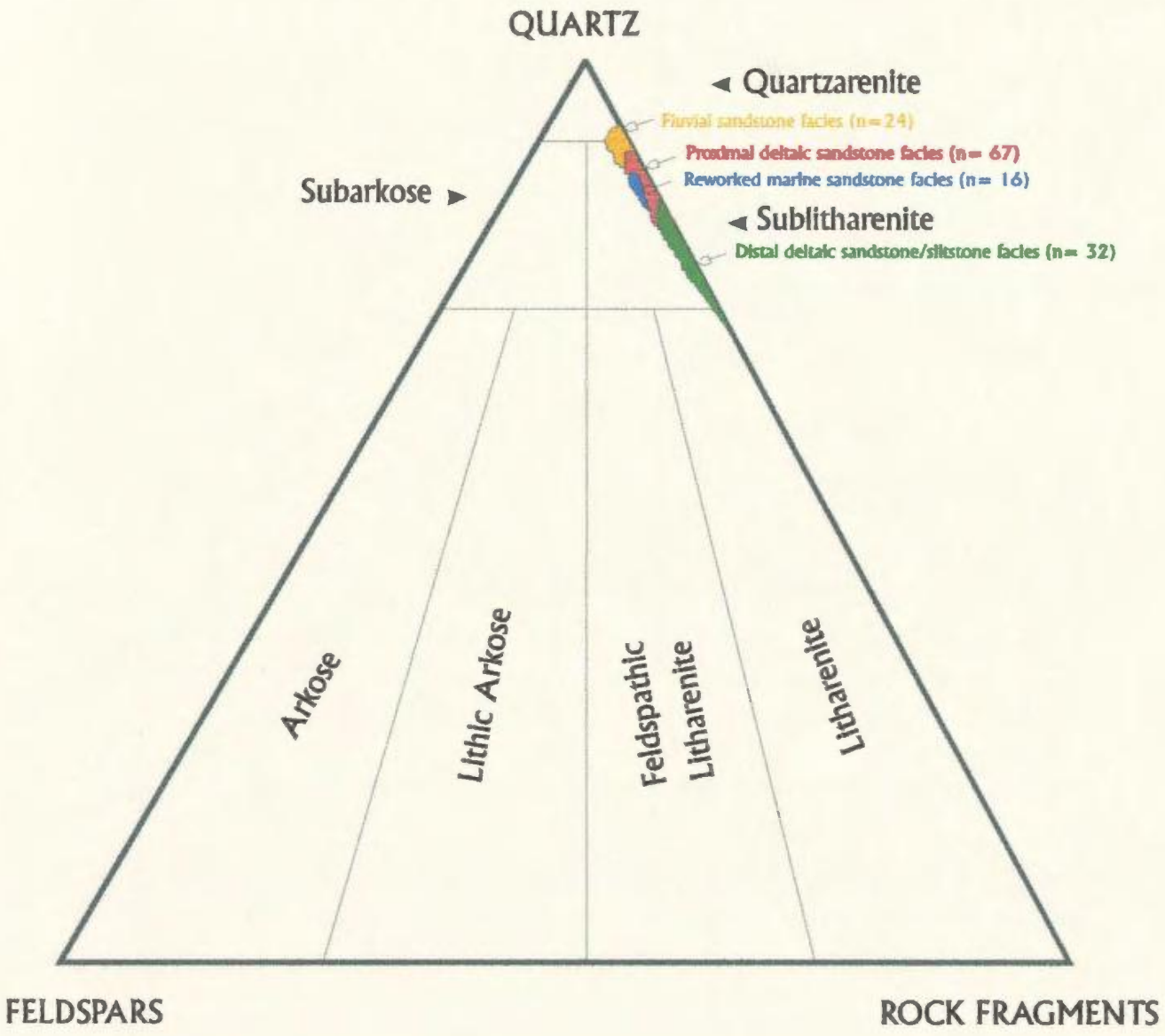

Figure 15. Detrital plot from various facies in the Lower Acacus Formation, Hamada Basin, NW Libya. (n= number of samples in each facies, QFR classification of sandstones after Folk, 1980).

(Appendix II- Plates 10B, 11A,B). Total carbonate cements range from 2 to 13% and average 8% (Tables 3 and 4). Patchy carbonate (calcite/dolomite) cements range from 2 to 10%, and average about 6%. Trace amounts of siderite can be seen partially filling primary porosity in the fluvial sandstones (Appendix II- Plates 12A,B and 13A,B).

Quartz-overgrowth cement through grain-to-grain contacts characterize the clean fluvial sandstones in wells (CC1-NC7A and Z1-66) located in the southern end of the Hamada Basin. Total silicate cements range from 2 to 12% (an average of 7%) (Appendix II- Plates 13A,B).

Authigenic clay cements range from 1 to 18% and average 9.5% which mostly (1-14%) consists of pore-filling and replacive kaolinite (Appendix II- Plates 14A,B, 15A), and some (tr.-5%) grain-coating illitic clay (Appendix II- Plates 16A,B, 17A,B).

Other authigenic minerals, include iron-oxide coating (rimming quartz grains, Appendix II- Plates 18A,B) which range from 0 to 7% and average 3.5% (Tables 3 and 4).

The zones of basinward transition between main cement types in the Lower Acacus sandstone units (A8-A14) may be 15-35km or wider. Present sampling is inadequate to define fully the transition from one dominant cement type to another in each unit (Figs. 16-19). It is for this reason that the data from the available core-sections, drill cuttings and wireline-logs were integrated to define better those cement transition zones. The main contribution of these maps is to provide relative proportions of cements in each

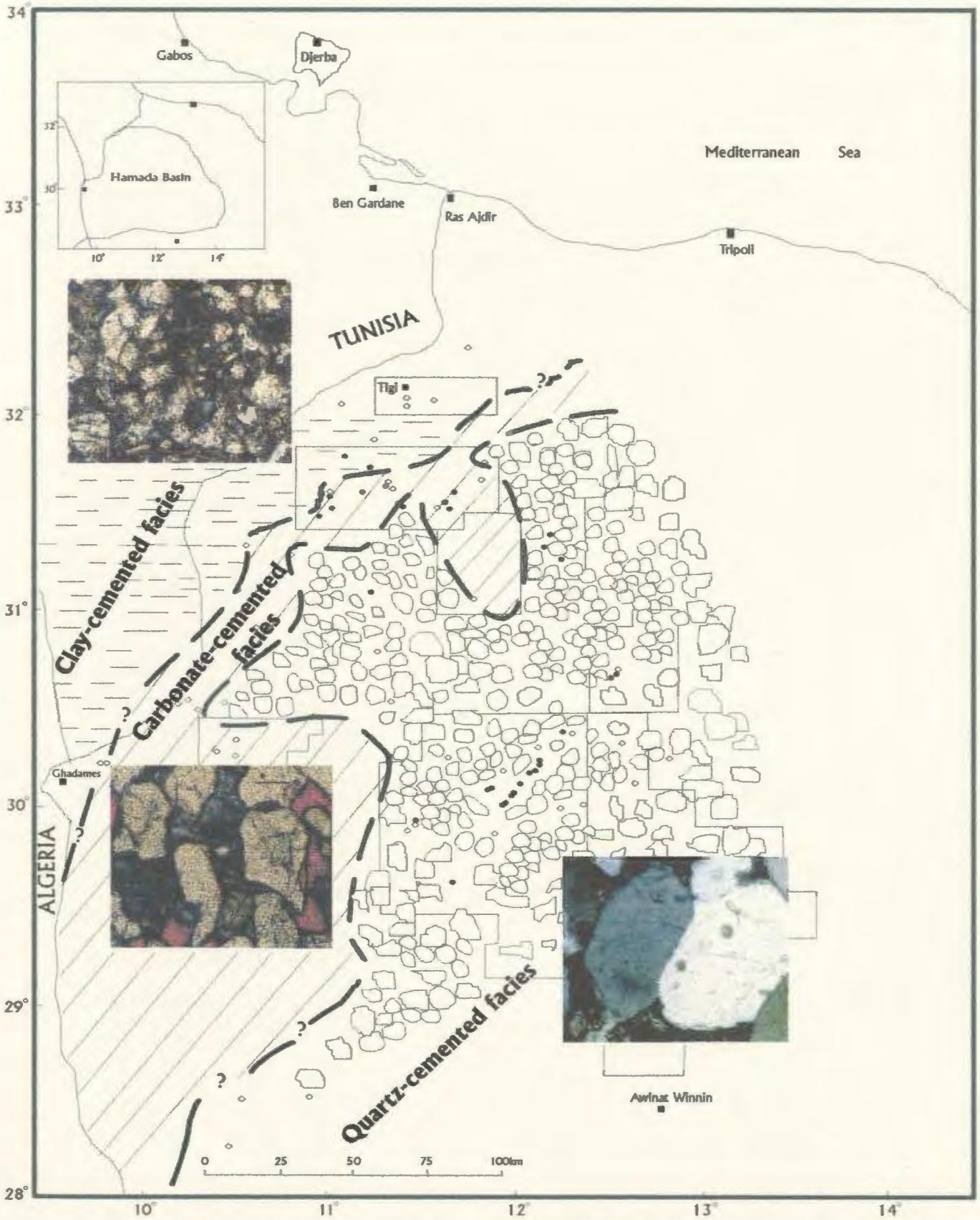

Figure 16. Regional distribution of dominant cements in each facies on the level of A8 sandstone unit of Lower Acacus Formation, Hamada Basin, NW Libya.

(Cement boundaries are based on cement types observed in petrographic thin-sections of A8 sandstone unit of Lower Acacus Formation at each well location).

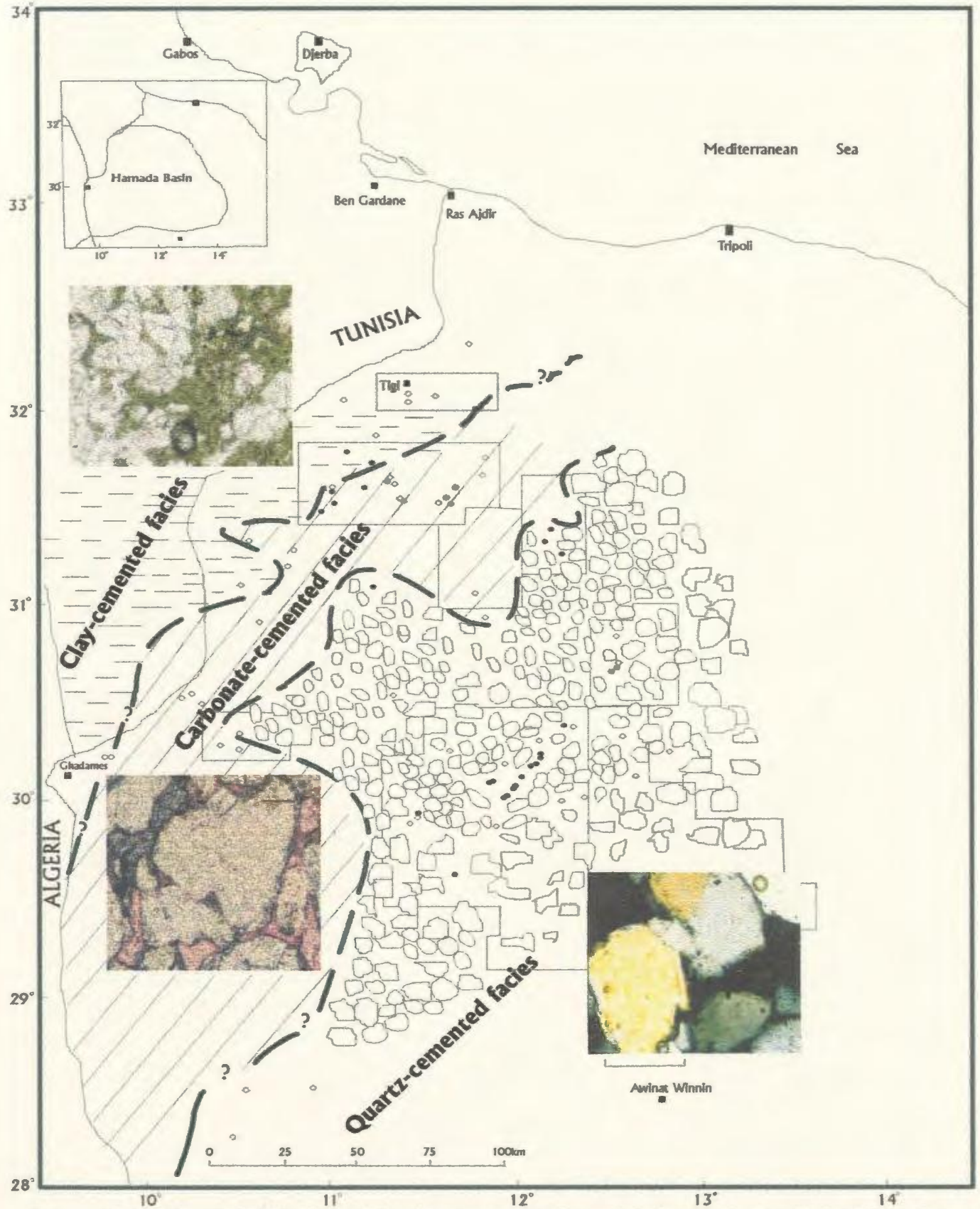

Figure 17. Regional distribution of dominant cements in each facies on the level of A10 sandstone unit of Lower Acacus Formation, Hamada Basin, NW Libya.

(Cement boundaries are based on cement types observed in petrographic thin-sections of A10 sandstone unit of Lower Acacus Formation at each well location).

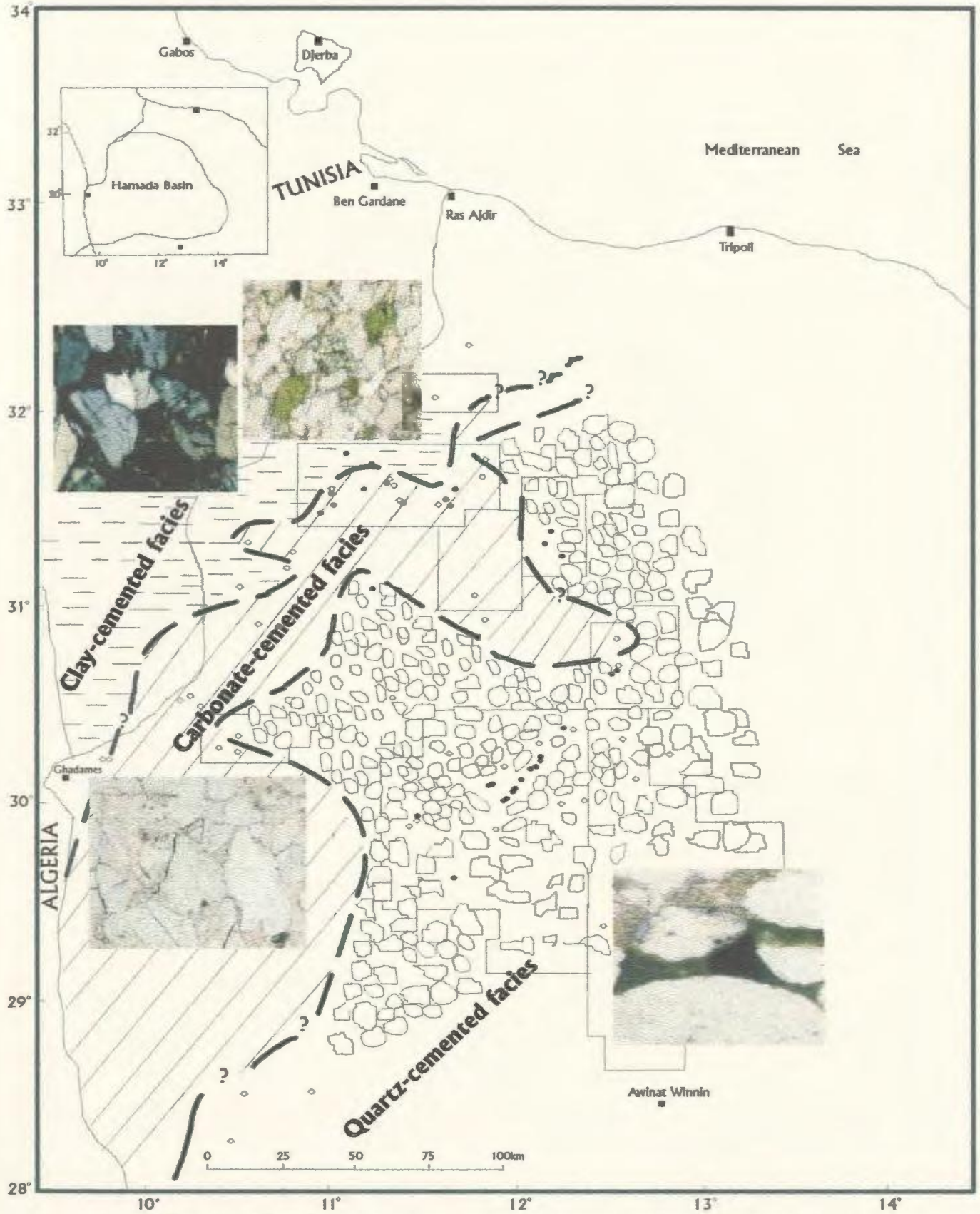

Figure 18. Regional distribution of dominant cements in each facies on the level of A12 sandstone unit of Lower Acacus Formation, Hamada Basin, NW Libya.

(Cement boundaries are based on cement types observed in petrographic thin-sections of A12 sandstone unit of Lower Acacus Formation at each well location)

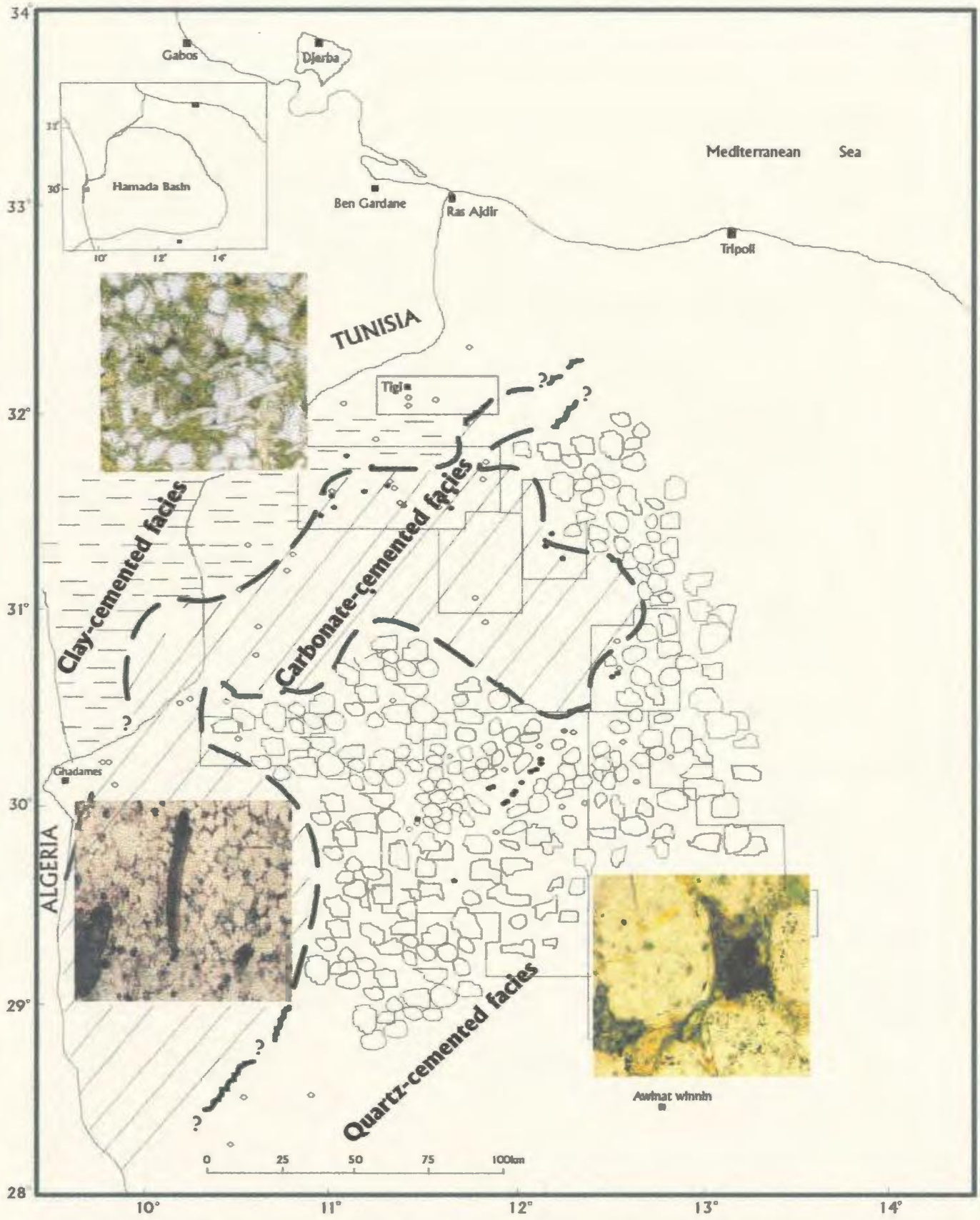

Figure 19. Regional distribution of dominant cements in each facies on the level of A14 sandstone unit of Lower Acacus Formation, Hamada Basin, NW Libya.

(Cement boundaries are based on cement types observed in petrographic thin-sections of A14 sandstone unit of the Lower Acacus Formation at each well location).

facies which can help to guide successful prediction for diagenetic alteration and reservoir quality: for example, which cements are soluble, or oxidizable, or precipitated, or even movable by introduced fluids.

III.1.1c) Authigenic clay and clay matrix in each facies:

In the quartzarenites of the fluvial sandstones, the clay matrix when present may intermix with interstitial iron oxide coating and rim most of the quartz grains (Appendix II-Plate 19A). However, authigenic clay is occasionally present in the quartzarenite-sublitharenites of fluvial sandstones as kaolinite-filling, partially preserved primary porosity (Appendix II- Plates 20A,B), with some traces of illite. In the sublitharenites of the proximal deltaic and reworked marine sandstones, clays of kaolinitic origin partially fill secondary porosity (dissolutional porosity) (Appendix II- Plate 21A). The litharenites or lithic-rich sandstone and siltstone samples associated with the distal deltaic facies contain abundant clay laminations (Appendix II- Plate 2B), rock fragments and minor feldspar grains.

III.1.1d) Total porosity ranges and types in each facies:

Total porosity (measured porosity) of the Lower Acacus Formation ranges from a low of 9.7% (in distal delta front siltstone facies) to a high of 32% (in fluvial sandstone facies) and averages 20.8% (Table 4). This average includes 11.8% intergranular secondary porosity from dissolution of carbonate cements, 5% intragranular secondary porosity in partially dissolved feldspar grains forming oversized and elongate pores, and 4% intergranular primary porosity enclosed between non-corroded quartz grains especially

in the fluvial sandstone facies of Lower Acacus Formation. Table 5 shows the percentage of primary and secondary (modified) porosity observed in thin-sections of various facies of Lower Acacus Formation (porosity will be discussed in detail under porosity evolution, distribution, and diagenesis).

III.1.1.1- ***Interpretation*** of thin-section petrography:

According to petrographic observation of the various facies in the Lower Acacus Formation the decrease in quartz percentages from basin flank to basin centre samples is interpreted to be due to decreasing current velocity responsible for the deposition of very fine-silty sandstones and clay matrix basinward. The majority of quartz grains in the various samples of the Lower Acacus Formation show straight (non-undulose) to undulose extinction suggesting a granitic source terrane (eg. Padki and Fox, 1989). However, a few quartz grains are composed of some foliated and stretched micro-polycrystalline quartz which may imply that metamorphic rocks were minor contributors to the sediments.

Feldspars decrease from basin flank (in the fluvial facies) to basin centre (in the deltaic-marine facies) (Table 3) and like quartz show basinward decreasing grain size indicating lower current velocity. So too, feldspar alteration to clay minerals is always associated with samples from distal deltaic siltstones.

Clay clasts show some deformation where surrounded by rigid quartz grains. As a result the clay clasts may be crushed and could be major contributors to clay-matrix either in the fluvial sandstones or downsection in the deltaic sandstones and siltstones.

Table 5 . Percentage of primary and secondary (modified) porosity and present depth of burial in the various facies of the Lower Acacus Formation, Hamada Basin, NW Libya.

Well Name	Depth		Facies	Primary Porosity (%)	Secondary Porosity (%)				Remarks
	ft.	m.			Dissolution of cements "overlined, elongate"	Dissolution of grains "partial diss. of fld.grains"	Molds "total diss. of grains"	Fractures	
A1-NC118	10040	3061	Fluv.	75	20	5	-	-	
	10115	3083	,,	65	25	8	2	-	
C1-61	7100	2165	,,	80	18	2	-	-	
	7522	2293	,,	60	20	20	-	-	
	7525	2294	,,	55	20	25	-	-	
	7795	2376	,,	50	40	9	1	-	
	8199	2499	,,	50	40	10	-	-	
CC1-NC7A	9017	2749	,,	90	7	1	2	-	
	9020	2750	,,	88	10	1	1	-	
EE1-NC7A	8810	2686	,,	80	19	1	-	-	
	8812	2687	,,	80	20	-	-	-	
Z1-66	9081	2768.5	,,	85	10	5	-	-	
	9130	2784	,,	75	20	5	-	-	
Z1-NC100	11680	3561	,,	88	11	1	-	-	
B1-61	8420	2567	Prx.Delt.Frt.	10	60	25	5	-	
	8484	2586	,,	7	4	-	-	-	Highly compacted Qz.ss.
B3-61	8893	2711	,,	-	55	20	20	5	
	8969	2734	,,	-	60	20	20	-	
C1-NC2	9645	2941	,,	-	70	30	-	-	
	9703	2958	,,	-	90	10	-	-	
E1-NC2	9131	2784	,,	-	5	-	-	-	Highly compacted Qz.ss.
T1-23	8454	2577	,,	10	5	-	-	-	,,
Q1-23	8180	2494	Rem.Mar.	-	95	5	-	10	
	8461	2580	,,	-	30	5	-	10	Kaol. rich ss., w/frac.qz.gr.
	8485	2586	,,	-	80	2	-	18	,,
A1-NC2	7817	2383	Dis.Delt.Frt.	-	30	5	-	15	,,

The low percentages of calcite cement in the fluvial sandstone samples (Table 4) may suggest that either calcite was not deposited or was incompletely cemented (partial calcite cement) due to meteoric water flushing in these sandstones. If calcite cement did exist in these samples it would have post-dated quartz-overgrowth. However, poikilotopic calcite cement is dominant in samples from the proximal deltaic sandstones which strongly indicates that the fluid became oversaturated with respect to calcite basinward.

A portion of clay matrix in the fluvial sandstone samples was probably derived from clay infiltration through minor fractures and associated unconformities related to pedogenic (soil formation + unconformity) processes during periods of emergence of the southern flank of the Hamada Basin. Some of the clay matrix in the distal deltaic samples is believed to be related to crushed lithic fragments (labile grains, and shale laminations) which deformed during compaction, partially filling fractures (Appendix II- Plates 22A,B, 23A,B).

III.1.2- Cathodoluminescence petrography: (See Appendix III- Plates 24-33)

Cathodoluminescence (CL) is useful in distinguishing detrital grains from authigenic overgrowths (Sippel, 1968), particularly in sandstones.

CL study of the Lower Acacus sandstones established that there is generally one major generation of quartz overgrowth, which shows a uniformly dull-light brown luminescence and a range in thickness (within a thin-section) from less than 50 (0.05mm) to 250μm (0.25mm) (Appendix III- Plates 24A, 25A). Quartz-overgrowths on adjoining grains often interlock and thus surrounding pores. Fracturing of individual quartz grains

contributes significantly to mechanical compaction (Stone and Siever, 1996). Such fracturing is observed in a few examined samples (Appendix III- Plates 26A,B, 27A). Many of the fractured quartz grains are subsequently healed by quartz cement of brown-yellowish luminescence. Grain fracturing/healing has been documented in CL studies of many other sandstones (Sippel, 1968; Sibely and Blatt, 1976; Dickinson and Milliken, 1993; Dunn, 1993).

Detrital feldspar grains present in some samples display a bright-blue CL (Appendix III- Plate 28A,B).

Calcite cement ranges in occurrence from widespread sparry crystals to scattered patches. The cement, often in contact with corroded quartz grains, displays golden, bright-orange to dark-orange CL and is unzoned (while occasionally appears to be dark-brown in some stained samples). Calcite cement shows some leaching at places as evidenced by scattered bright-orange CL surrounding pore-spaces (Appendix III- Plate 29A,B).

The relative abundance of authigenic kaolinite cement in the clay-cemented facies or the quartz-cemented facies is clearly revealed by CL-microscopy where kaolinite cement shows royal-blue CL (Appendix III- Plate 30A,B). The presence of other clay or iron-oxide coatings in some sandstones of fluvial origin, appears to be non-luminescent (Appendix III- Plates 31A,B, 32A,B).

Traces of detrital zircon found in association with the fluvial sandstone facies in wells C1-61 and A1-NC118 were identified by their bright golden yellow CL (Appendix III- Plates 26A, 33A).

III.1.2.1- ***Interpretation*** of cathodoluminescence petrography:

Detrital quartz grains of light grey-light blue luminescence are subrounded to rounded in most fluvial sandstone samples. Subsequent authigenic quartz-overgrowth, generally showing dull-light brown luminescence, has obliterated most porosity and it gives the appearance of interlocked and compacted fabric when CL is not used (plane light). The major difference in luminescence between detrital quartz grains and authigenic quartz-overgrowths is that the overgrowths may contain different trace elements and thus contrast sharply with detrital grains.

Most samples have only a few fractured/healed grains; therefore, the contribution of this process to mechanical compaction is not significant except in a few samples from wells characterized by some diagenetic compaction as in A1-NC2, and C1-61.

CL photographs of calcite cement in some samples reveal that the nonluminescent character can be attributed to increased iron contents in the calcite structure.

The non-luminescent appearance of iron-oxides blocking pore-spaces in some fluvial sandstone samples suggests that iron-oxides may inhibit luminescence from surrounding minerals.

III.1.3- SEM/EDS analyses of the Lower Acacus Formation: (See Appendix IV- Plates 34-39)

The observed data through CL application and normal light microscopy are supplemented by scanning electron microscope (SEM) imaging.

SEM photographs (Appendix IV) of the different cements and other associated

minerals, supported by EDS spot-mode analyses in the various facies of Lower Acacus Formation, are presented in Figures 20 to 25.

1- Quartz-overgrowths:

Quartz is the most common, pore-reducing cement within fluvial sandstones. In these medium to coarse grained sandstones, quartz-overgrowths are large euhedrally terminated crystals (Appendix IV- Plate 34A) occasionally characterized by pitted and rough texture (Appendix IV- Plate 34B) and surrounding micropore spaces. Primary pores are characterized by uncorroded boundaries of quartz grains and have triangular shape between the numerous crystal coalescing in these facies (Appendix IV- Plates 34C,D, 35A). EDS analysis confirms the presence of quartz and indicates its mineralogy (Figs. 20A-C)

2- Authigenic hematite (iron-oxide/clay matrix coating) cement:

The most commonly observed grain coating in quartz-supported sandstones of fluvial origin is authigenic hematite. Coarsely crystalline authigenic hematite (Appendix IV- Plate 35B) occurs as aggregates of platy crystals similar in appearance to kaolinite. EDS beam spot-mode analysis show high Fe-spectra (Figs. 21A,B) which confirms the hematite occurrence and is consistent with the earlier identifications by thin-section petrography.

3- Detrital feldspar crystals:

Long platy crystals of feldspar with markedly smooth parallel crystal faces were detected only in the medium to coarse grained sandstones of fluvial origin in

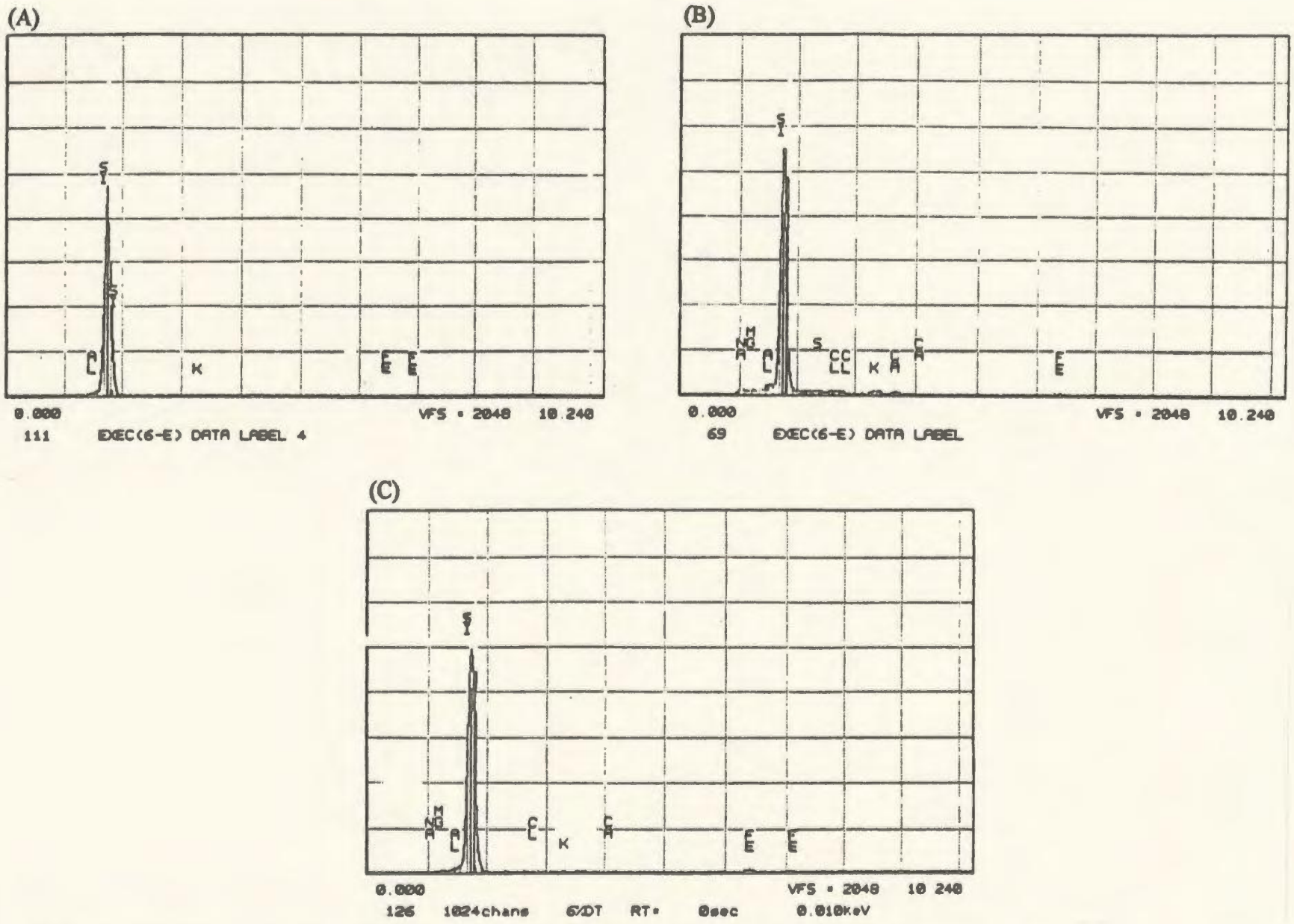

Figure 20. Typical EDS spectrum of (A) ***Quartz "quartz-overgrowths"*** in fluvial sandstone unit (Af3), EE1-NC7A @ 2686 m. (8810 ft.), (B) ***Quartz "quartz-overgrowths"*** in fluvial sandstone unit (Af3), EE1-NC7A @ 2687 m. (8812 ft.), (C) ***Quartz "quartz-overgrowths"***, in fluvial sandstone unit (Af2) CC1-NC7A @ 2750 m. (9020 ft.).

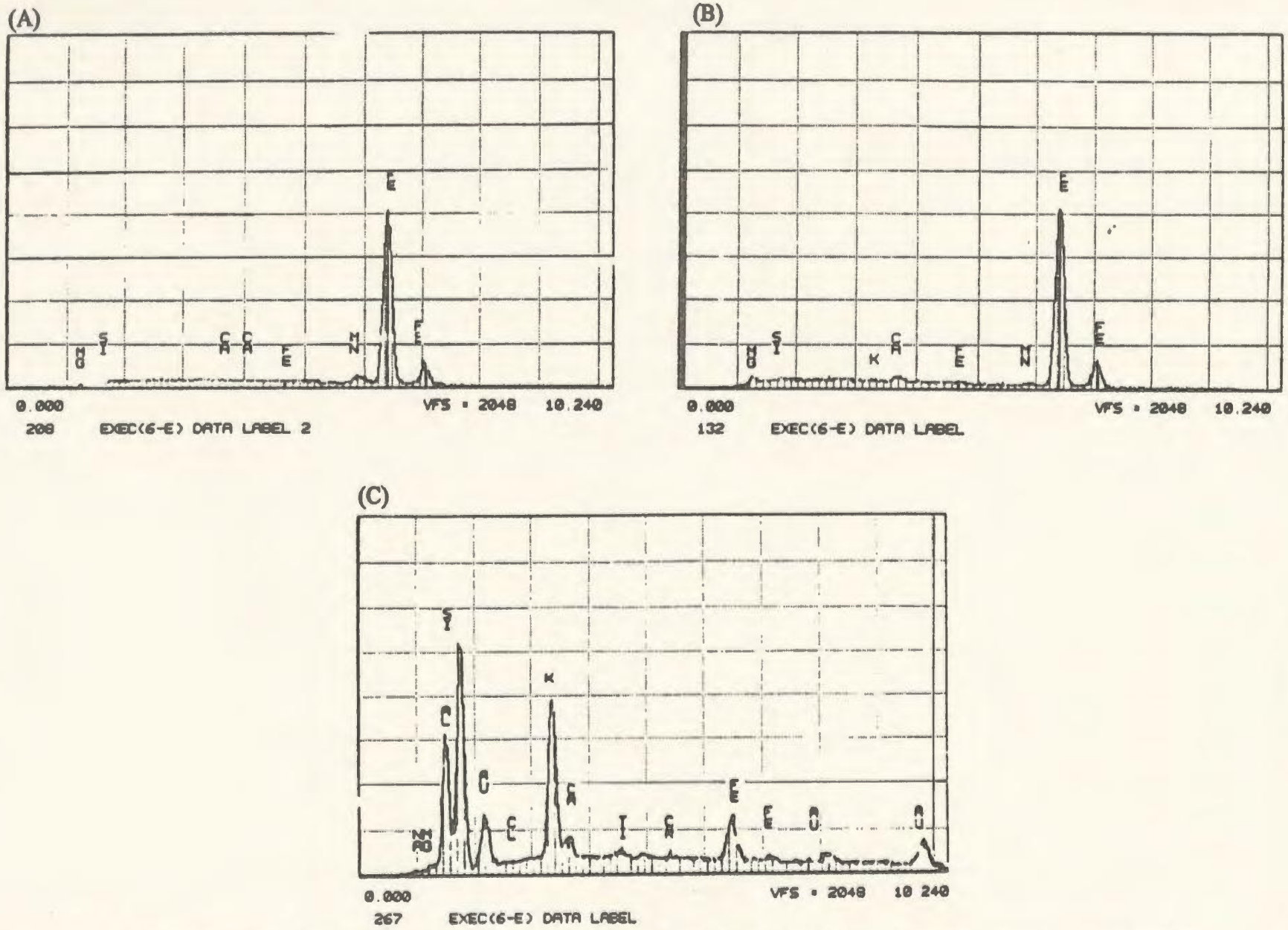

Figure 21. Typical spectrum of (A) ***Hematite "iron-oxides"*** in fluvial sandstone unit (Af2), CC1-NC7A @ 2749 m. (9017 ft.), (B) ***Hematite*** "iron-oxides " in fluvial sandstone unit (Af2) B3-61 @ 2839 m. (9311 ft.), (C) ***K-feldspar "microcline"*** in fluvial sandstone unit (Af2), B3-61 @ 2839 m. (9311 ft.).

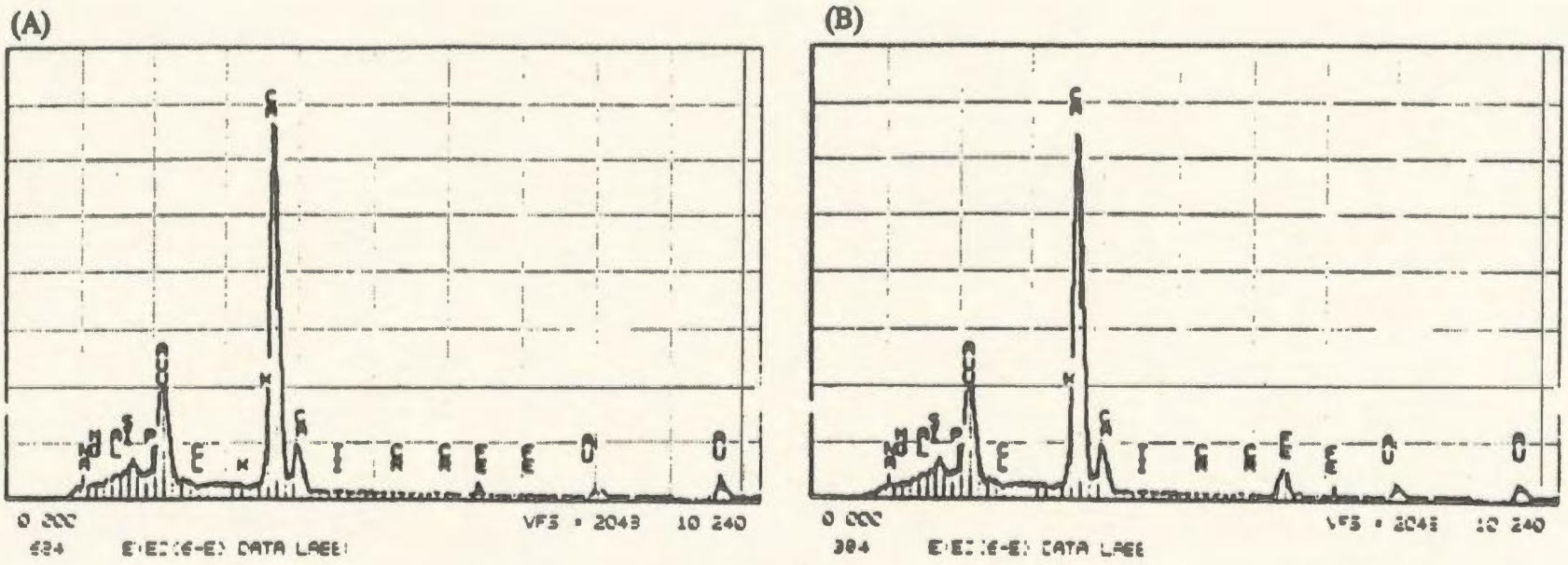

Figure 22. Typical EDS spectrum of (A) ***Calcite cement*** in fluvial sandstone unit (Af3), EE1-NC7A @ 2687 m. (8812 ft.), (B) ***Calcite cement"rich in iron"*** in proximal delta front sandstone unit (A8), C1-NC2 @ 2965 m. (9725 ft.).

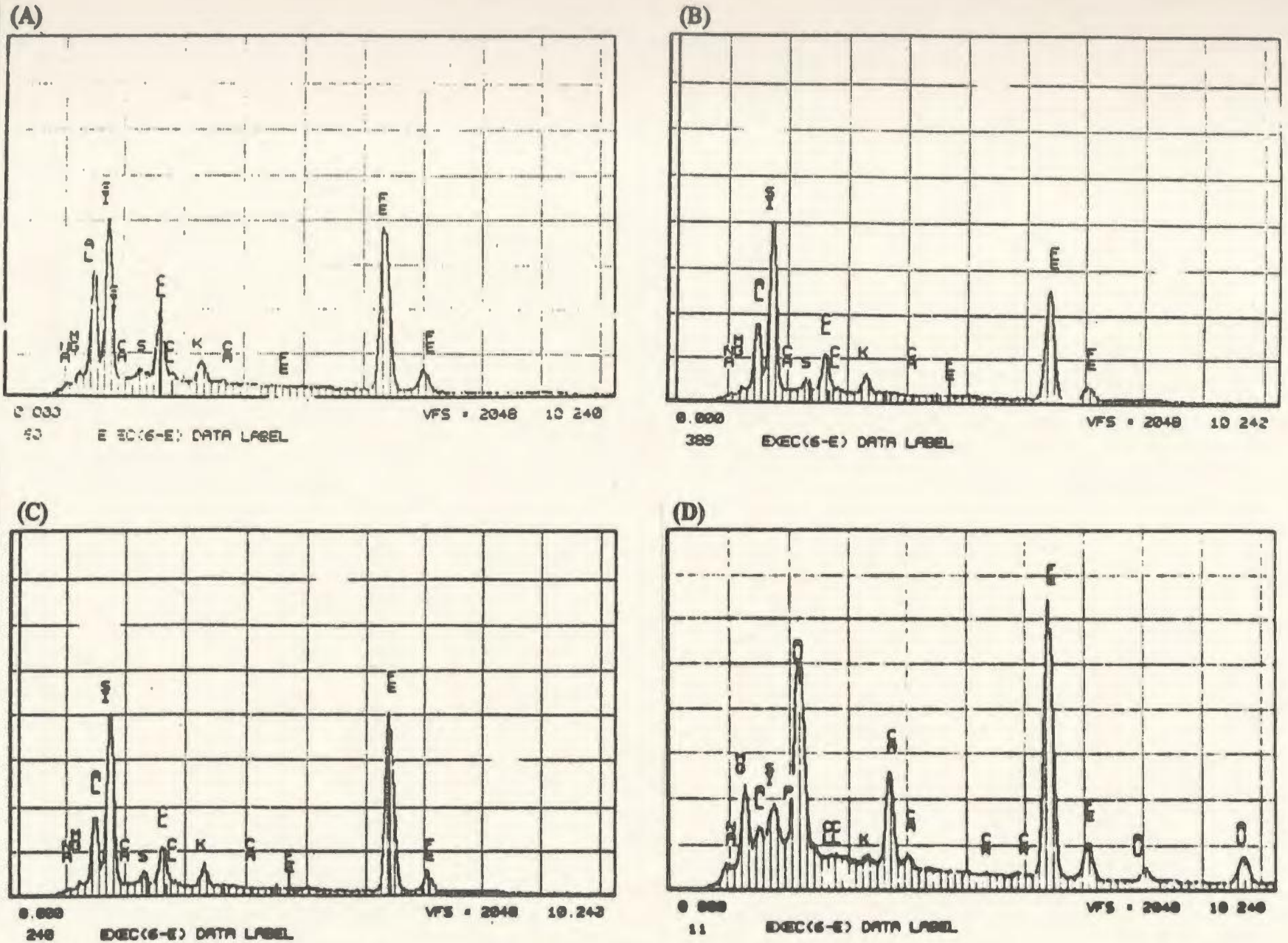

Figure 23. Typical EDS spectrum of (A) ***Ferroan dolomite cement*** in proximal delta front sandstone unit (A14), T1-23 @ 2577 m. (8454 ft.), (B) ***Ferroan dolomite cement*** in reworked marine sandstone unit (Am), B3-61 @ 2670 m. (8756 ft.), (C) ***Ferroan dolomite cement*** in fluvial sandstone unit (Af3), EE1-NC7A @ 2687 m. (8812 ft.), (D) ***Siderite cement*** in fluvial sandstone unit (Af4), Z1-66 @ 2768 m. (9080 ft.).

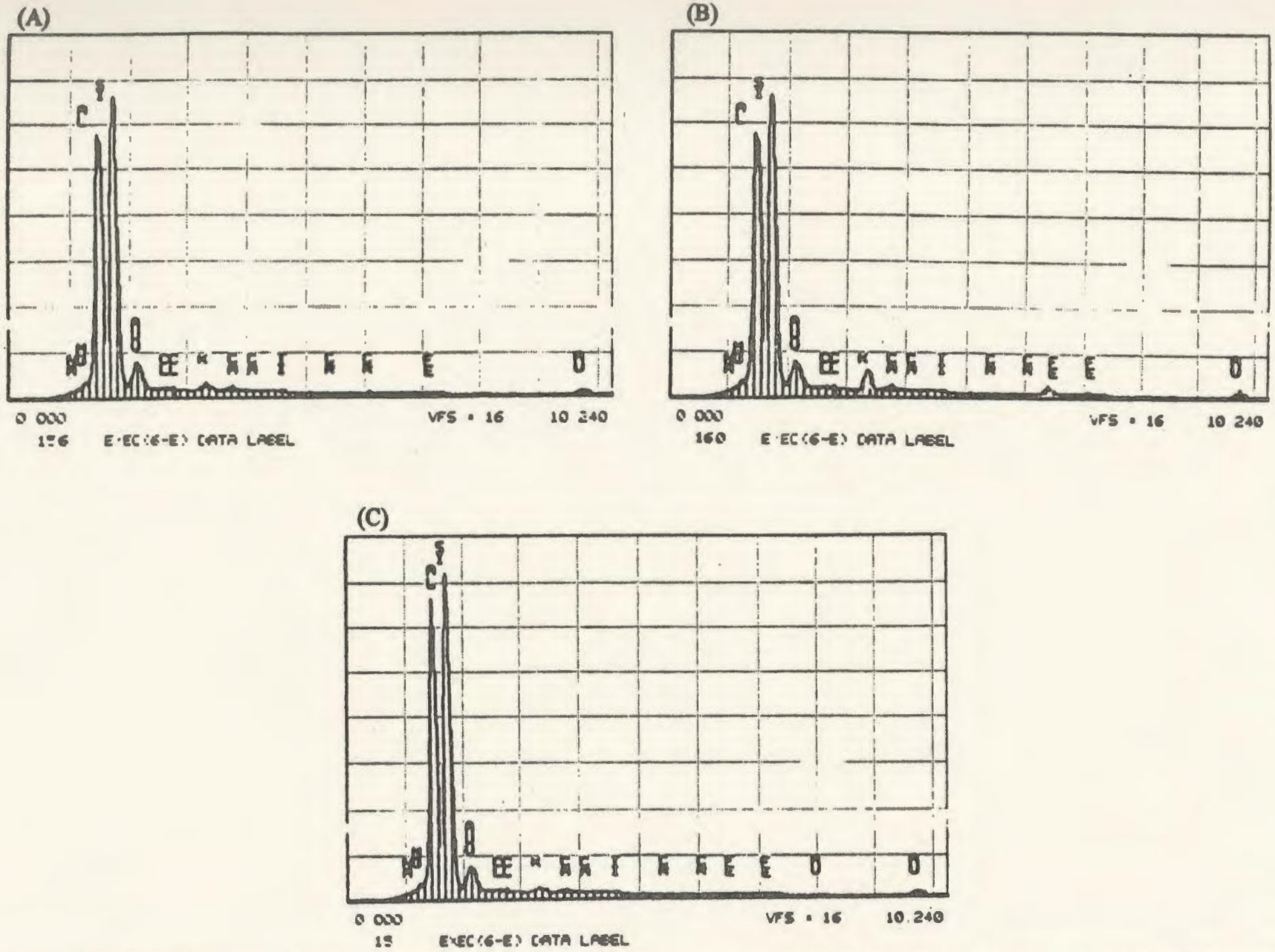

Figure 24. Typical EDS spectrum of (A) ***Kaolinite cement*** in fluvial sandstone unit (Af3), A1-NC118 @ 3061 m. (10040 ft.), (B) ***Kaolinite cement*** in proximal delta front sandstone unit (A14), T1-23 @ 2577 m. (8454 ft.), (C) ***Kaolinite cement*** in distal delta front siltstone unit (Ad), A1-NC2 @ 2382 m. (7814 ft.).

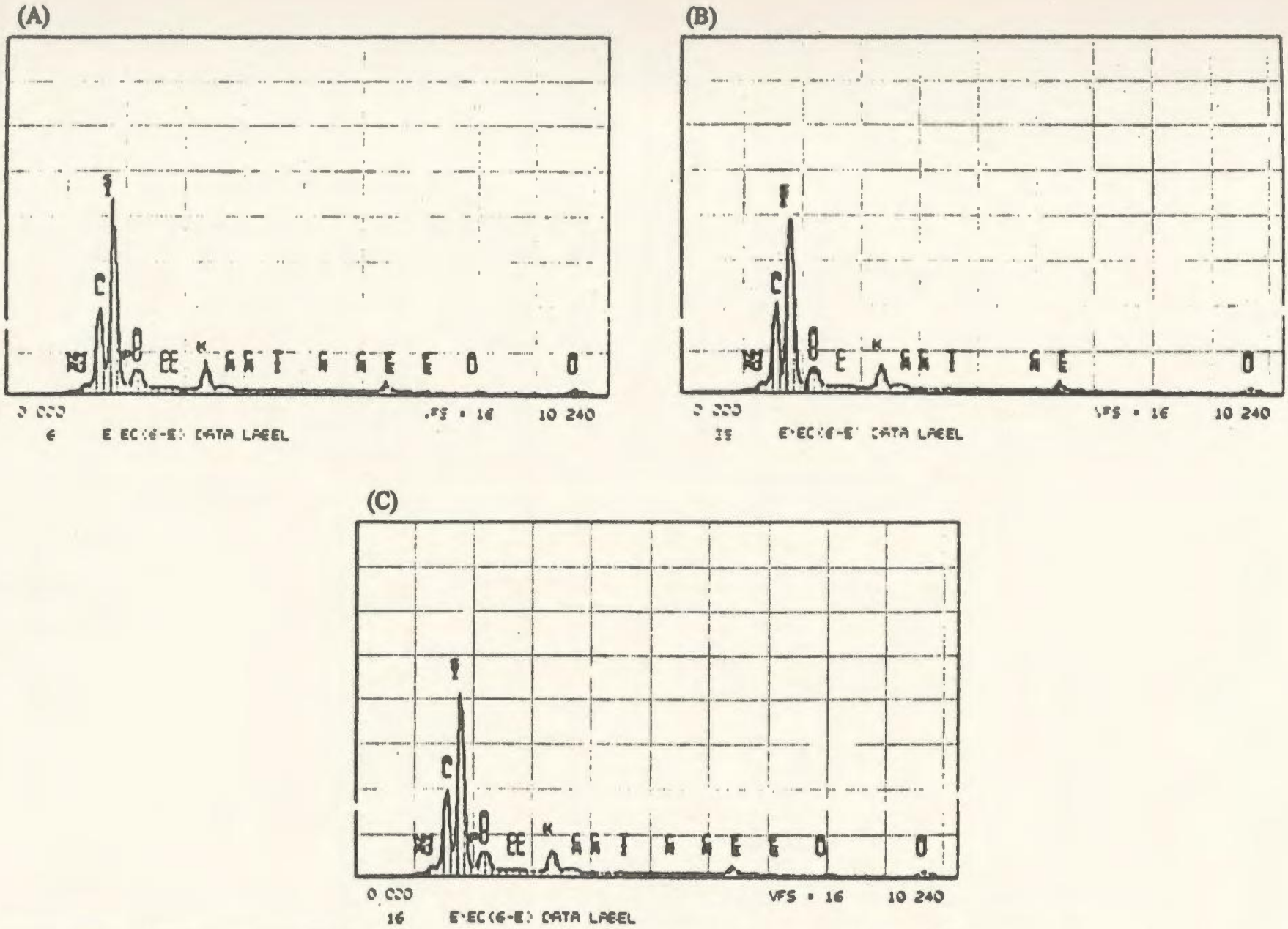

Figure 25. Typical EDS spectrum of (A) ***Illite cement*** in distal delta front siltstone unit (Ad) unit (Af3), A1-NC2 @ 2382 m. (7814 ft.), (B) ***Illite cement*** in distal delta front siltstone unit (Ad), A1-NC2 @ 2383 m. (7817 ft.), (C) ***Illite cement*** in fluvial sandstone unit (Af2), B1-61 @ 2839 m. (9311 ft.).

well B3-61 @ (2838 m.) 9311 ft. (Appendix IV- Plate 35C). Beam spot-mode analysis confirms the K-feldspar mineralogy (Fig. 21C).

4- Carbonate (calcite, dolomite, and some siderite) cements:

Carbonate cements (calcite, dolomite, and siderite) were determined in the SEM samples supported by EDS analyses of the various facies in the Lower Acacus Formation (Figs. 22, 23).

4.a Calcite cement:

Partial calcite cement was detected in some fluvial sandstone samples (Appendix IV- Plate 36A,B) and showing some calcite crystal filling intergranular primary pore-spaces between quartz grains. Pervasive-continuous poikilotopic calcite cement is dominant in the proximal deltaic sandstone facies (Appendix IV- Plate 36C), occasionally demonstrating dissolution porosity (Appendix IV- Plate 36D). EDS beam spot- mode analyses of these samples indicated overall high percentage of calcite (Fig. 22A,B).

4.b Ferroan dolomite cement:

Patchy ferroan dolomite rhombs, both pore-filling and grain-replacive, were observed in the sandstones and silty sandstones of proximal deltaic and reworked marine sandstone facies (Appendix IV- Plate 37A,B) with minor fractions in the fluvial sandstone facies (Appendix IV- Plate 37C). EDS indicates the dolomite is iron-rich (Fig. 23A-C).

4.c Siderite cement:

Trace amounts of siderite cement formed clusters of rhombic crystals (Appendix IV- Plate 37D) around quartz grains observed in the fluvial sandstone of well Z1-66 @

(2768 m.) 9080 ft. (EDS analyses presented in Fig. 23D confirmed the mineralogy of siderite).

5- Authigenic kaolinite cement:

Authigenic kaolinite cement is observed in the medium to coarse grained fluvial sandstones (Appendix IV- Plate 38A, Fig. 24A) and occasionally in the fine-grained proximal deltaic sandstones. This cement occurs as kaolinite booklets partially filling pore-spaces (Appendix IV- Plate 38B, Fig. 24B). Pore-filling kaolinite cement is associated with both the reworked marine sandstones and the silty distal deltaic facies. The kaolinite cement either surrounds or fills microporosity (Appendix IV- Plate 38C,D). EDS analysis (Fig. 24C) confirms the kaolinite cement presence in these facies.

6- Authigenic illite cement:

Authigenic illite cement was found to be most commonly associated with the very shaly-silty sandstones of distal deltaic facies. It forms either as cluster aggregates that have grown on top of or across euhedral kaolinite booklets (Appendix IV- Plate 38D), or as densely packed and well crystallized flakes on top of quartz grains (Appendix IV- Plate 39A). Authigenic illite cement is less frequently observed in the medium to coarse grained sandstone samples. However, where present it forms as micro-plates or blades surrounding and lining large pores (Appendix IV- Plate 39B,C).

Trace amounts of Titanium, sodium, chlorine, magnesium, and iron were ubiquitous in EDS spot-mode analyses of the samples from the sandstones of fluvial to deltaic in origin.

III.1.3.1- *Interpretation* of SEM/EDS analyses:

Large smooth euhedral quartz-overgrowths along with numerous smaller quartz-overgrowths which have the appearance of pitted to rough texture on detrital quartz were identified in some fluvial sandstone samples (Appendix IV- Plates 34A-D, 35A), and are interpreted to have formed simultaneously at different places in these samples.

Coarse, platy crystalline authigenic hematite (Appendix IV- Plate 35B) identified in fluvial sandstone samples is indicative of oxidizing conditions.

The presence of minor amounts of siderite cement in the carbonaceous fluvial sandstones of well Z1-66 @ 2768 m. (9080 ft.) indicates an inadequate supply of oxygenated water and the establishment of reducing conditions.

EDS analyses (Figs. 23A-C) suggest that dolomite cement associated with samples from the proximal deltaic and reworked marine sandstones is iron-rich. This points to a diagenetic environment wherein these sandstones typically favour reduced mineral phases rich in iron.

SEM photographs (Appendix IV- Plates 38A,B) indicate that authigenic kaolinite cement booklets are partially filling pore-spaces (primary porosity and dissolution surfaces) in samples from fluvial and proximal deltaic sandstones which probably do not significantly affect fluid flow in these sandstones. However kaolinite cement is very effective in reducing porosity in the distal siltstone samples (Appendix IV- Plates 38C,D) as booklets are stacked and welded together.

Authigenic illite micro-plates (Appendix IV- Plate 38D) are found to be associated

with and to have grown on top of kaolinite booklets in the distal siltstone samples. This textural evidence indicates that illite was precipitated after kaolinite. On the other hand, the presence of authigenic illite which formed aggregates of platy and bladed morphology (Appendix IV- Plates 39B,C) lining pores in fluvial sandstones suggests that it is recrystallized an authigenic clay that was introduced as cutans (laminar clay coats partially cover sand grains (Brewer, 1964; Wescott, 1983; Coleman, 1985)) when meteoric water infiltrated the fluvial sandstones before intensive compaction. Platy illite seems to have inhibited development of quartz-overgrowth in some cases. In these sandstones (fluvial origin) quartz-overgrowths are developed best where authigenic clay cements are absent.

III.1.4- X-Ray Diffraction (XRD) analyses:

Figures 26 to 35 are arranged in sequential order from the southern Hamada Basin fluvial sandstones to the northern basinal siltstones and shales to create a cross-section illustrating characteristic XRD patterns for the bulk mineralogical components in the examined samples. It is necessary to note that XRD application in this study was only for the purpose of regional minerals identification and distribution as facies changed from the basin flanks to the basin centre, and as an integration tool complementary to the thin-section petrographic results.

Quartz is present in all samples. A sharp peak of high intensity was detected at 26.6° 2θ, 3.35Å, and another small peak at 20.9° 2θ, 4.2Å whereas the intensity of both peaks was observed to decrease basinward. Some amounts of iron oxides are present in samples of fluvial origin (Figs. 26-29). Strong peaks of iron-oxides were detected at 33.2°

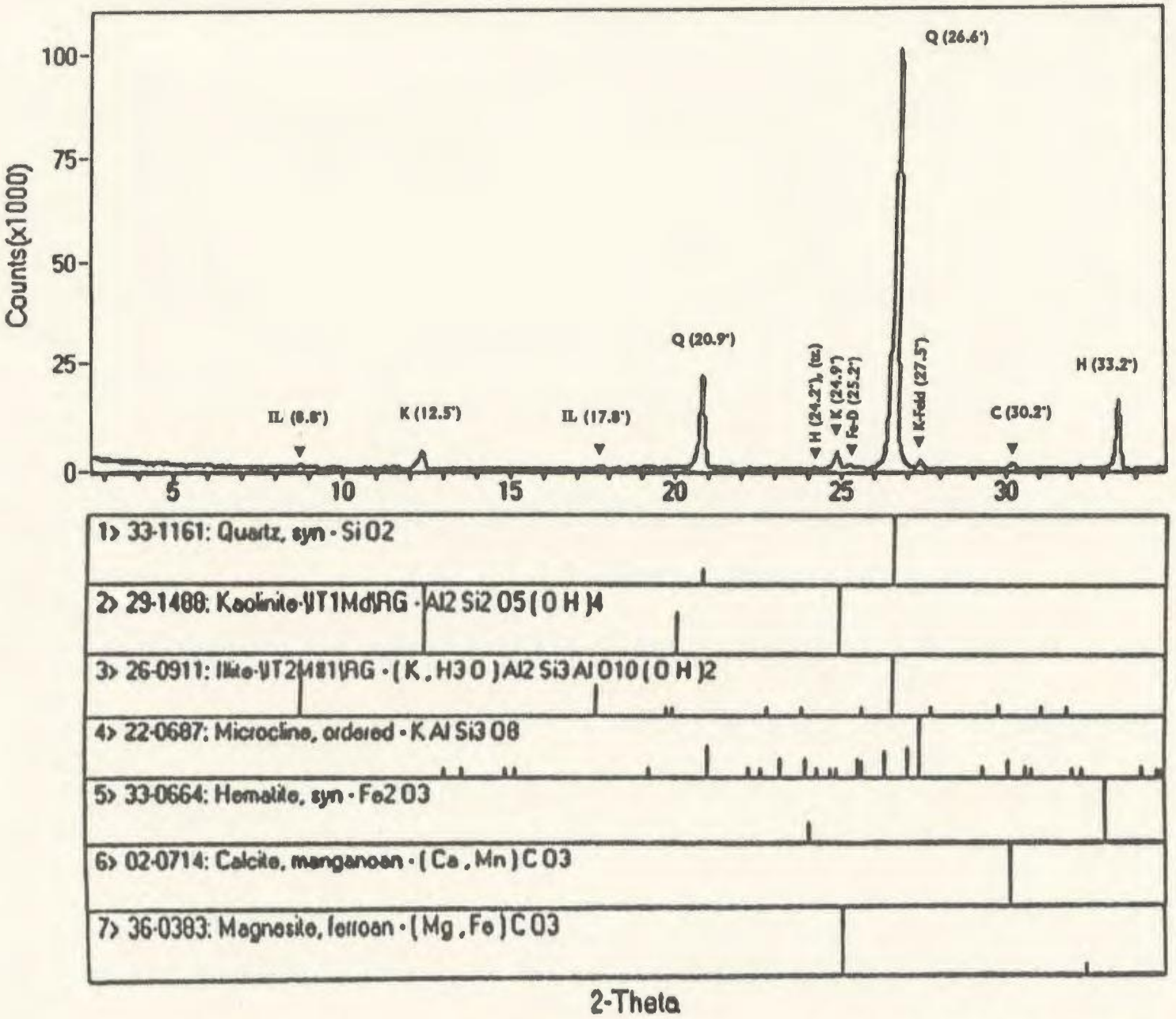

Figure 26. X-ray diffraction patterns showing bulk minerals identification and clay fraction (mainly kaolinite with traces of illite) associated with the hematitic ***fluvial sandstone unit (Af3)***, EE1-NC7A @ 2687 m. (8812 ft.).

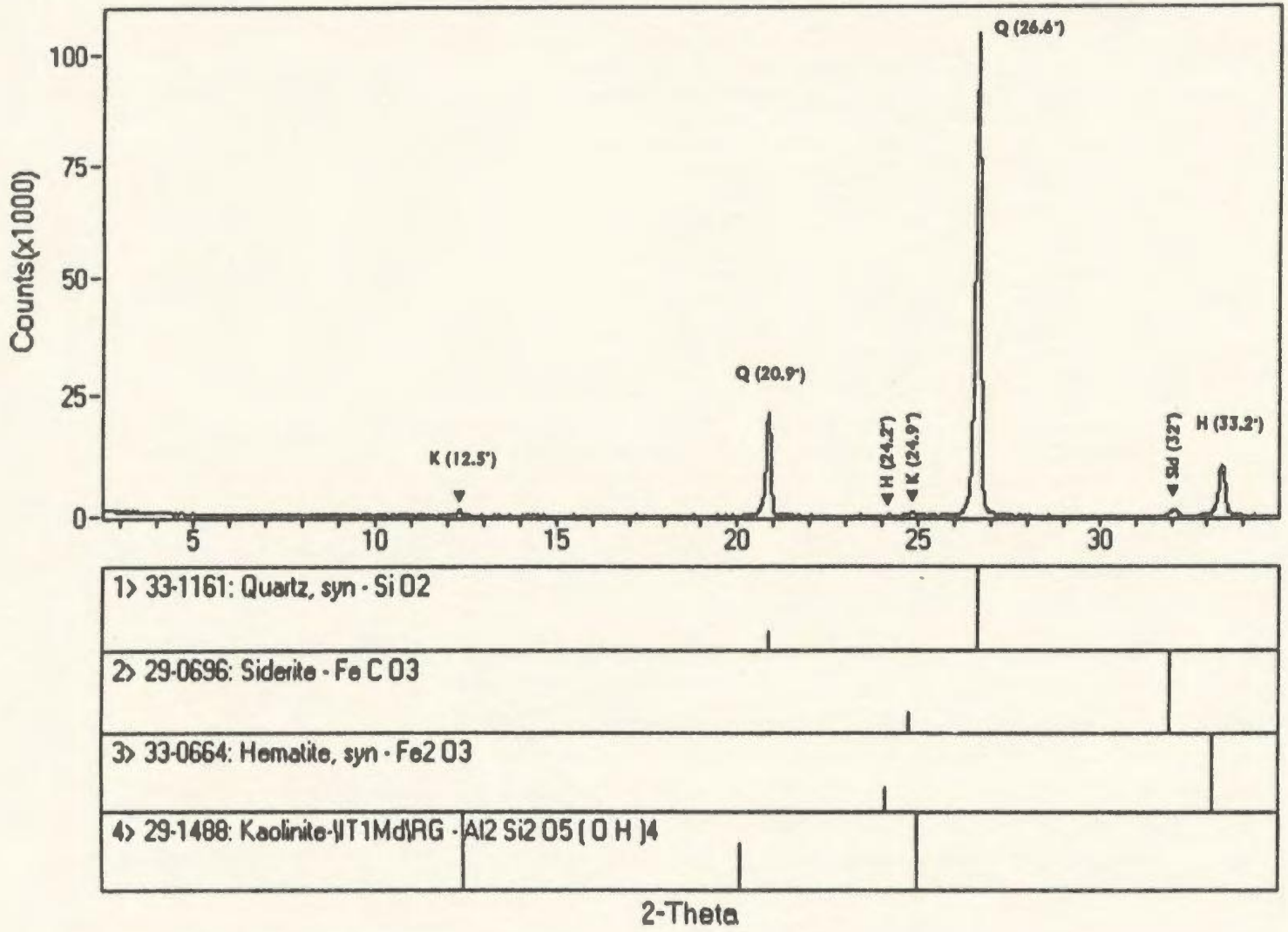

Figure 27. X-ray diffraction patterns showing bulk minerals identification and clay fraction (mainly kaolinite) associated with the hematitic ***fluvial sandstone unit (Af4)***, Z1-66 @ 2768 m. (9080 ft.). Note traces of siderite are also present.

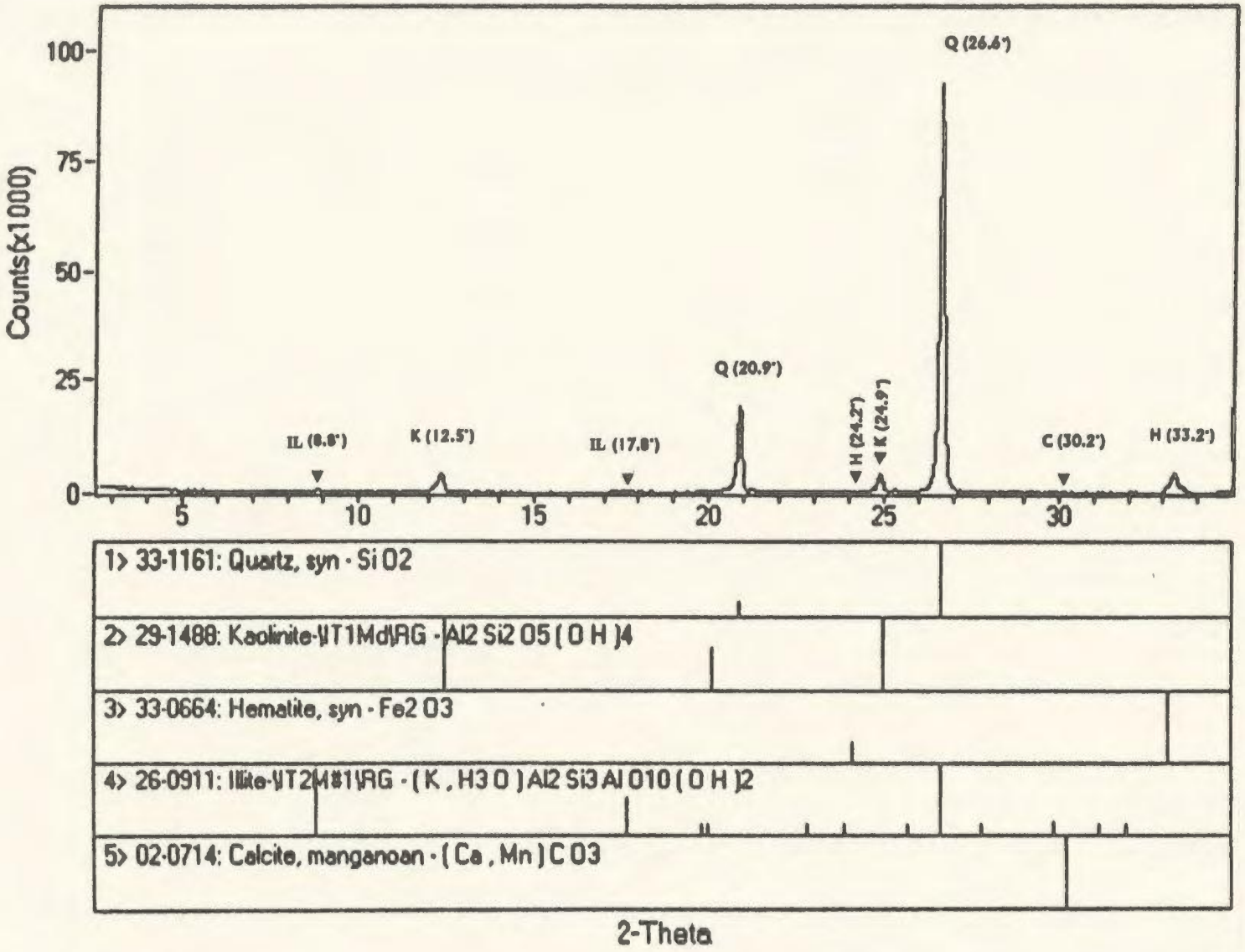

Figure 28. X-ray diffraction patterns showing bulk minerals identification and clay fraction (partial kaolinite and illite) associated with the ***fluvial sandstone unit (Af3)***, A1-NC118 @ 3061 m. (10040 ft.). Note hematite with calcite cement are also present in this sample.

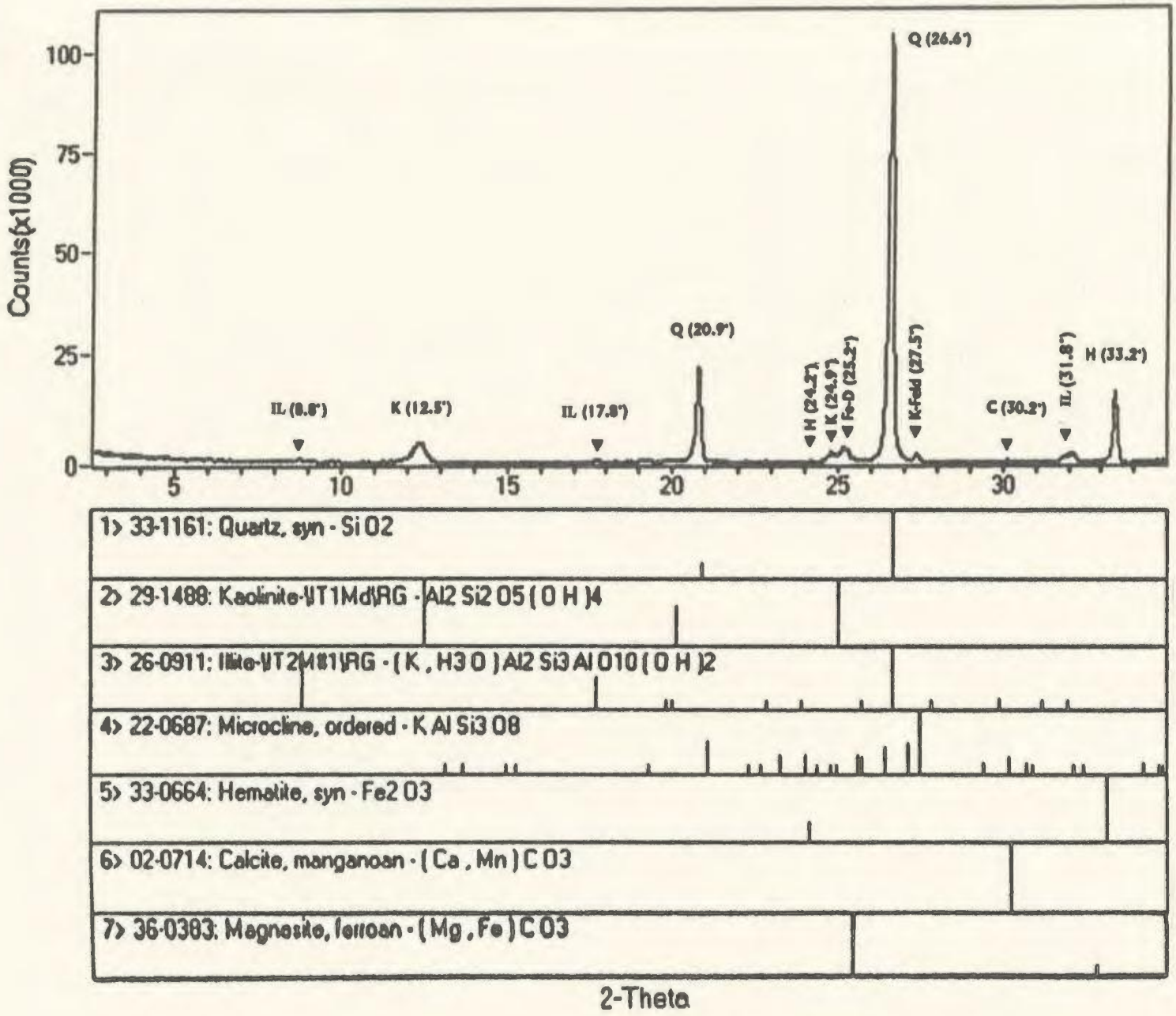

Figure 29. X-ray diffraction patterns showing bulk minerals identification and clay fraction (mainly kaolinite) associated with the hematitic ***fluvial sandstone unit (Af2)***, B3-61 @ 2839 m. (9311 ft.).

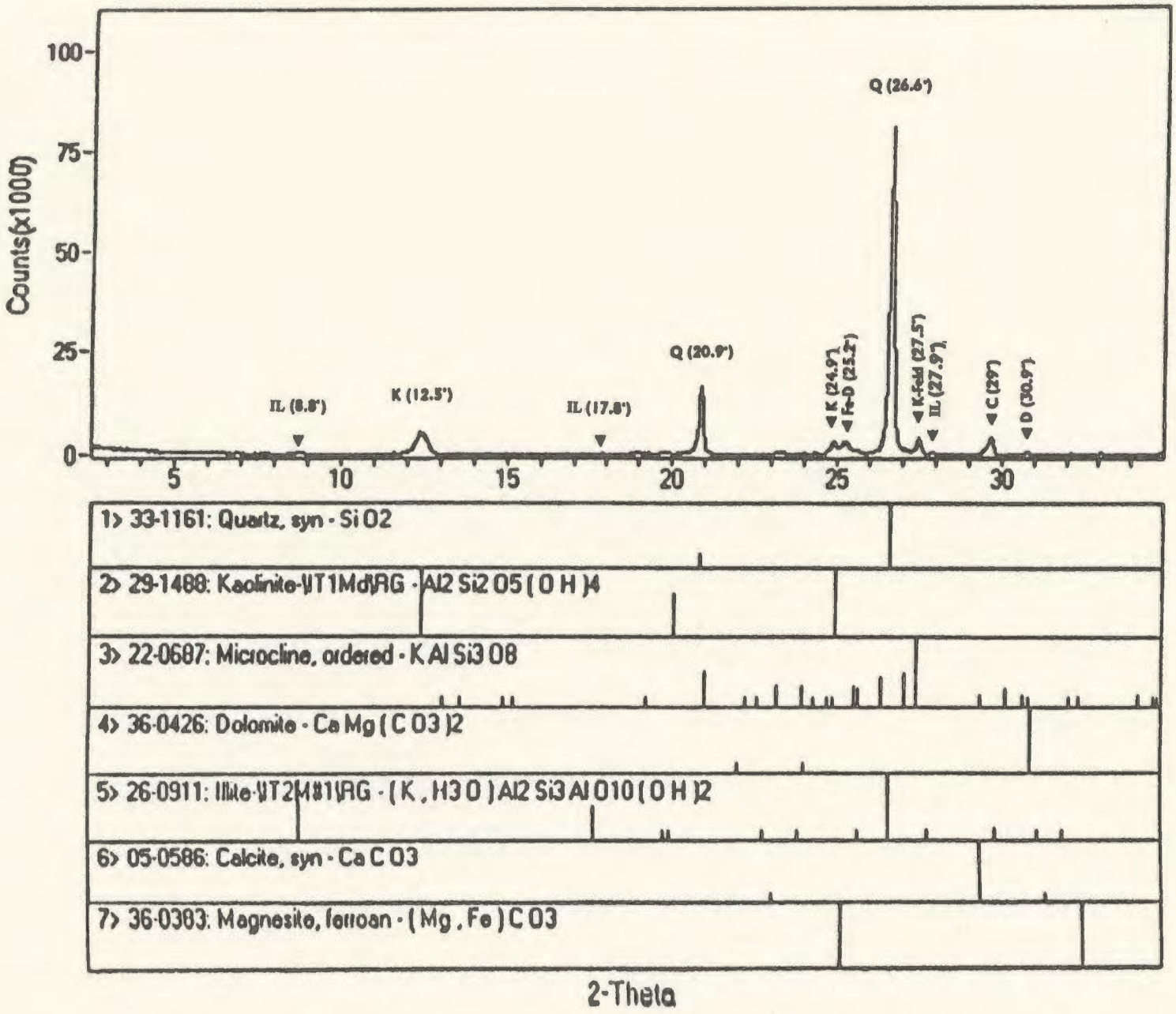

Figure 30. X-ray diffraction patterns showing bulk minerals identification and clay fraction (mainly kaolinite with traces of illite) associated with the ***proximal delta front sandstone unit (A14)***, T1-23 @ 2577 m. (8454 ft.). Note calcite, dolomite, and ferroan dolomite cements are present along with some feldspar.

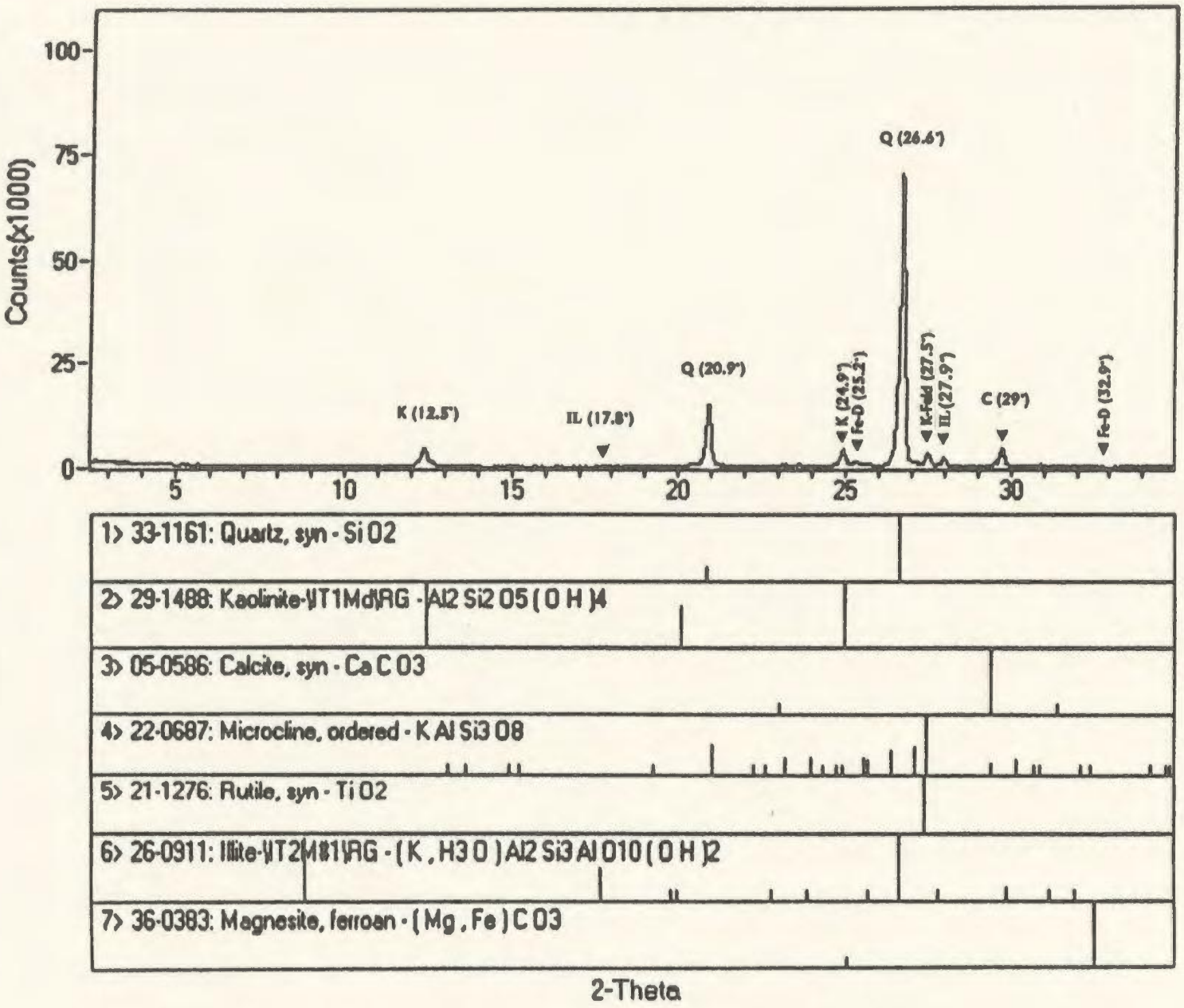

Figure 31. X-ray diffraction patterns showing bulk minerals identification and clay fraction (kaolinite and illite) associated with the ***proximal delta front sandstone unit (A14)***, T1-23 @ 2583 m. (8473 ft.). Note the presence of some ferroan dolomite cement in this sample.

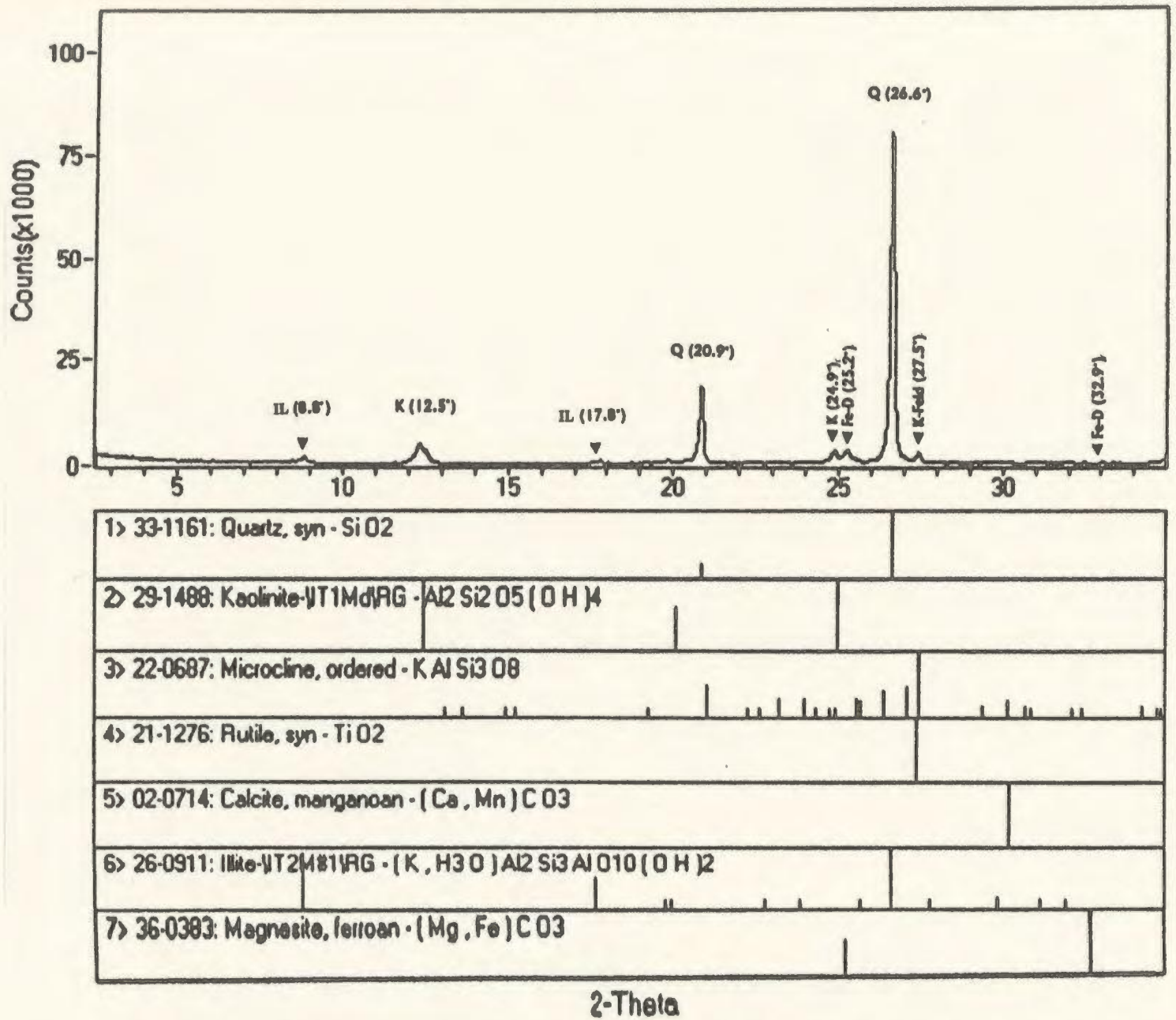

Figure 32. X-ray diffraction patterns showing bulk minerals identification and clay fraction (kaolinite and illite) associated with the ***distal delta front siltstone unit (Ad)***, E1-NC2 @ 2780 m. (9117 ft.).

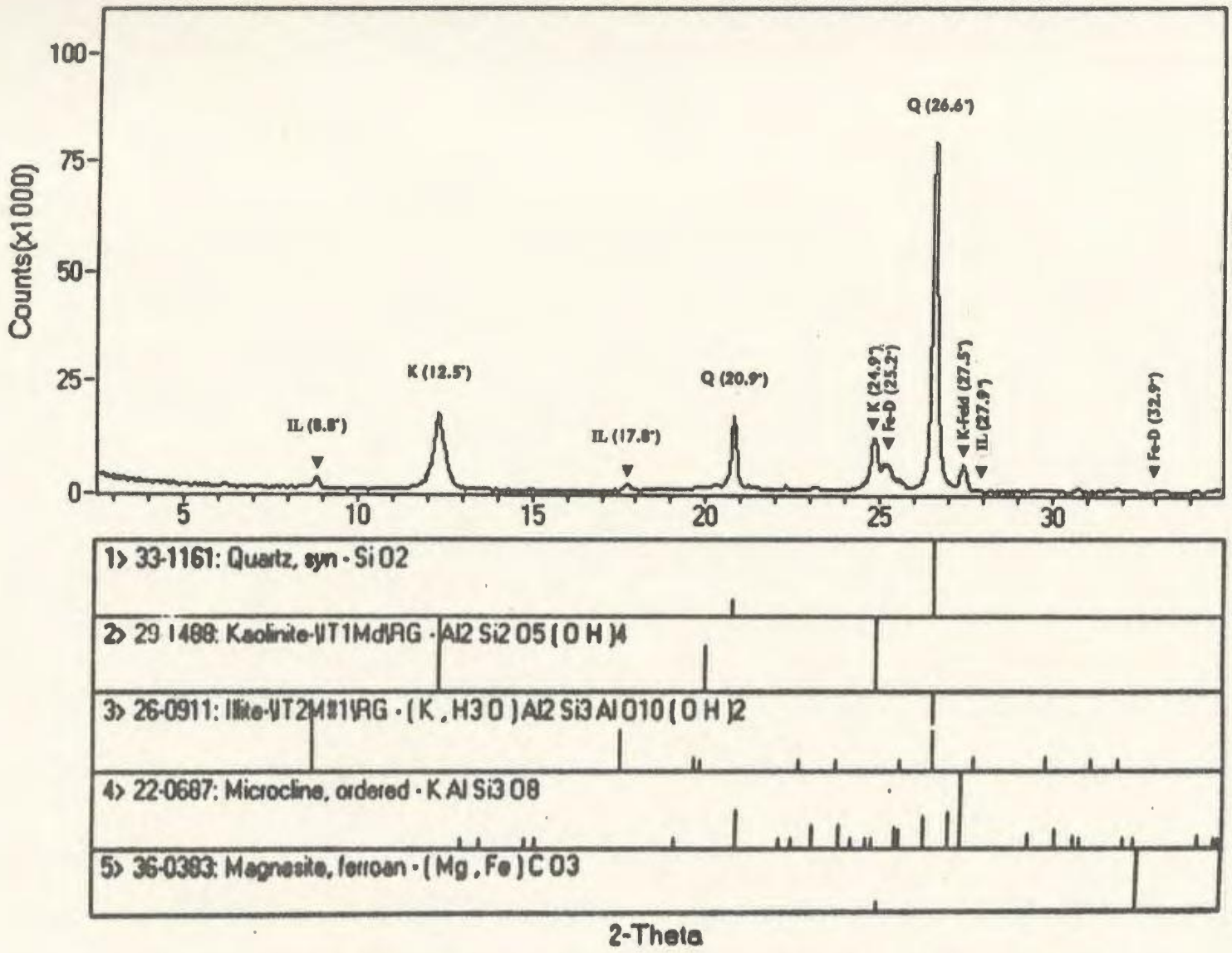

Figure 33. X-ray diffraction patterns showing bulk minerals identification and clay fraction (kaolinite and illite) associated with the ***distal delta front siltstone unit (Ad)***, A1-NC2 @ 2383 m. (7817 ft.).

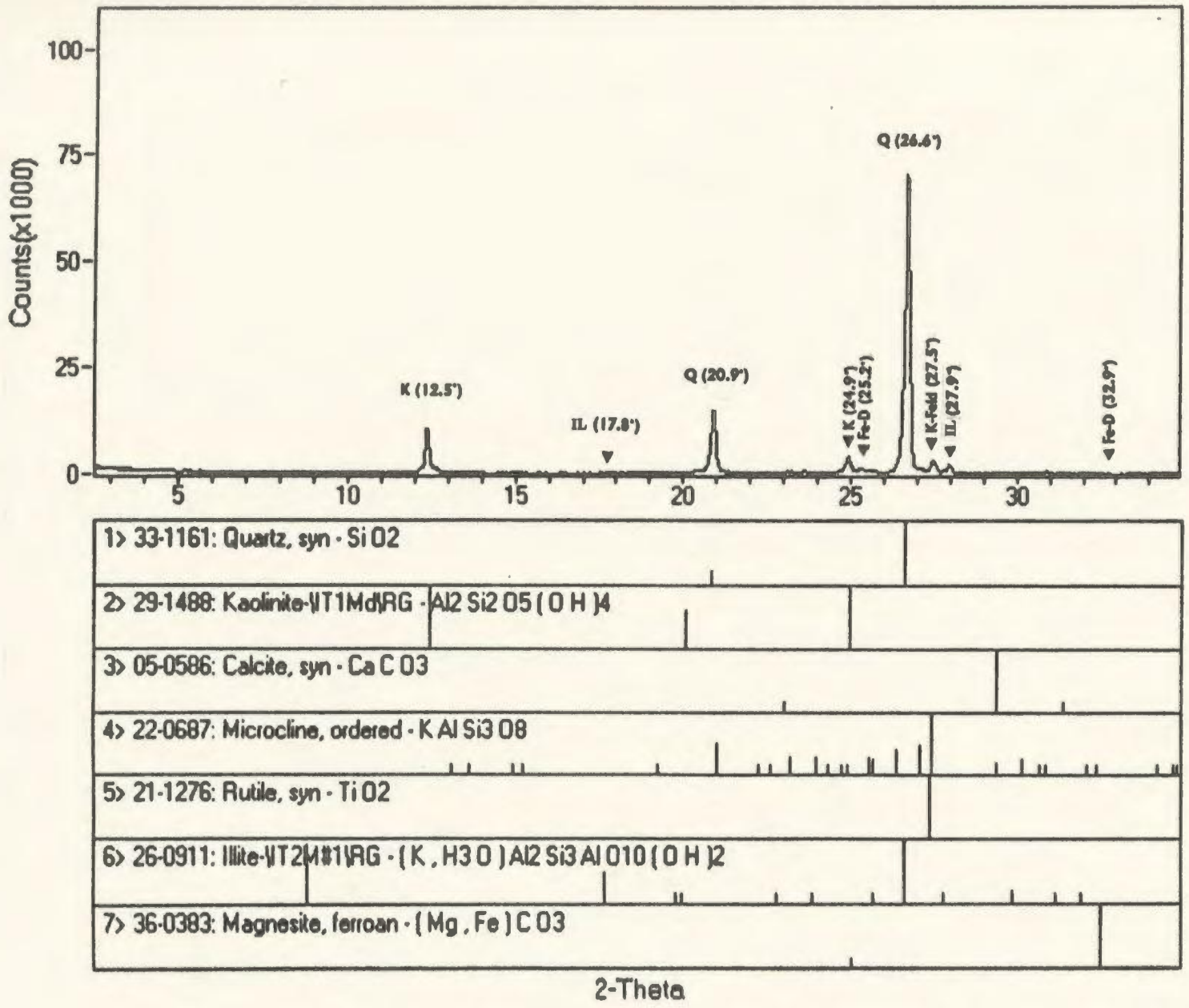

Figure 34. X-ray diffraction patterns showing bulk minerals identification and clay fraction (mainly kaolinite with traces of illite) associated with the ***reworked marine sandstone unit (Am)***, B3-61 @ 2670 m. (8756 ft.). Note the presence of some ferroan dolomite cement in this sample.

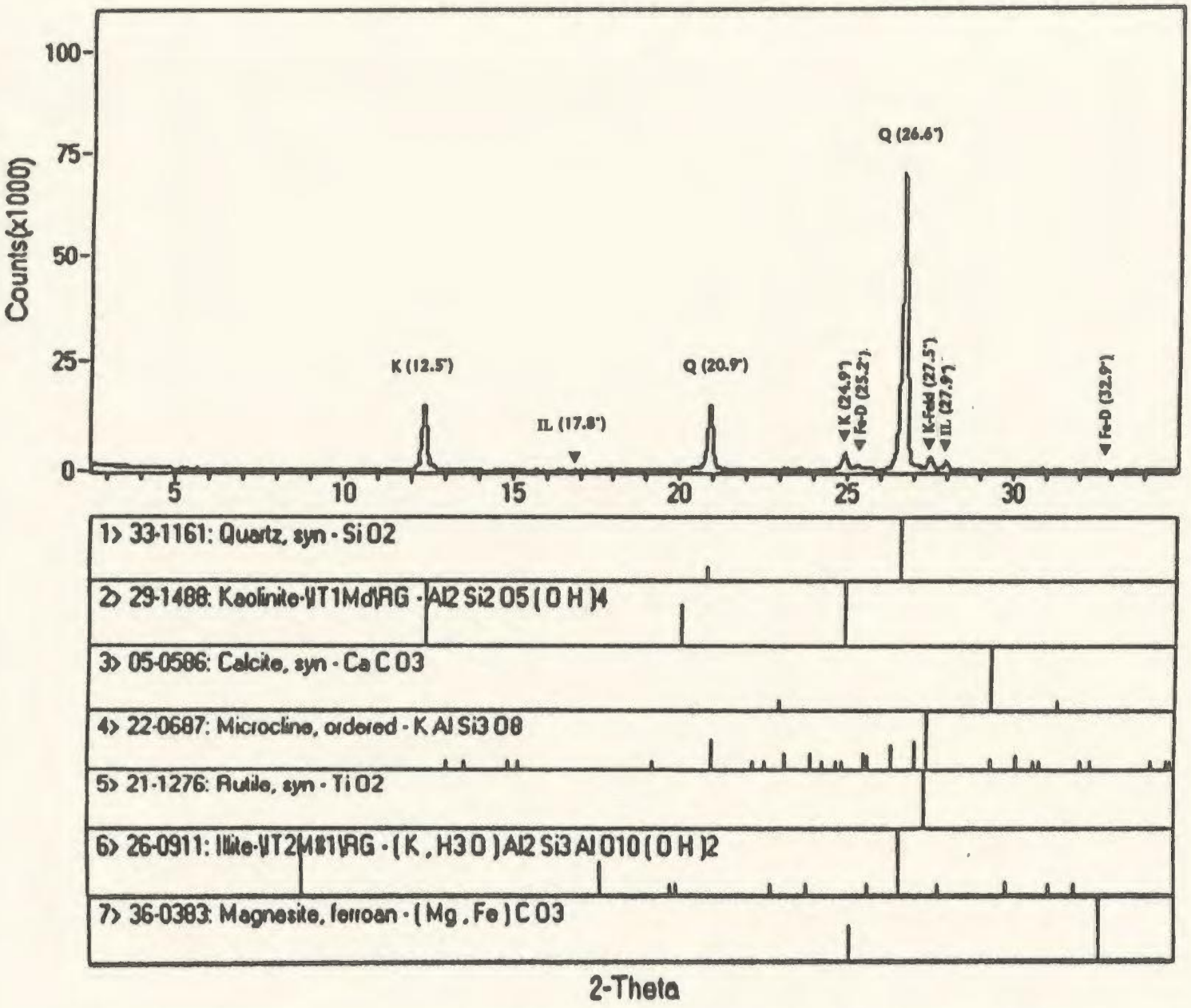

Figure 35. X-ray diffraction patterns showing bulk minerals identification and clay fraction (mainly kaolinite with traces of illite) associated with the ***reworked marine sandstone unit (Am)***, Q1-23 @ 2580 m. (8461 ft.). Note ferroan dolomite cement is present in this sample.

2θ, 2.69Å. Additional peaks of weak reflection occur at 24.2° 2θ, 3.67Å, especially in wells EE1-NC7A, Z1-66 and B3-61. Minor amounts of K-feldspar (microcline) with small peaks at 27.5° 2θ, 3.24Å occur in most samples.

K-feldspar peaks appear to be more pronounced in deltaic and reworked marine silststones and sandstones (Figs. 30-35).

Carbonate cements of different chemical compositions have been also detected. Calcite ($CaCO_3$) shows some reflection at 29° 2θ, 3.04Å, in proximal deltaic sandstones (Figs. 30, 31), whereas minor amounts of manganoan calcite (Ca,Mn) CO_3 were detected at 30°2θ, 2.95Å in the fluvial sandstones of wells EE1-NC7A, and A1-NC118 (Figs. 26, 28). Dolomite (Ca Mg $(CO_3)_2$) shows some peaks at 30.9° 2θ, 2.89Å, in the deltaic sandstone facies in well T1-23 (Figs. 30, 31). Magnesite-ferroan carbonate (Mg,Fe)CO_3 shows a weak peak at 25.2° 2θ, 2.54Å in fluvial sandstones of well EE1-NC7A (Fig. 26), and small peaks in the deltaic and reworked marine sandstones (Figs. 30-35). Another weak reflection may can be seen at 32.9° 2θ, 2.7Å (Figs. 31-35). Trace amounts of siderite were identified by a small peak at 32° 2θ, 2.79Å in well Z1-66 at 2768 m. (9080 ft.) (Fig. 27).

Kaolinite cement is the most common clay component in most samples (Figs. 26-35). Strong kaolinite peaks were detected at 12.5° 2θ, 7.08Å, and 24.9° 2θ, 3.57Å. Their intensities increased in samples of distal deltaic and reworked marine origin (Figs. 33-35).

Illite cement is not common throughout the basin . Trace amounts of illite cement can be observed in the clay matrix-rich fluvial sandstones of wells EE1-NC7A, A1-NC118

and B3-61 (Figs. 26, 28, 29), being recorded as small to weak reflections between 8.6-8.8° 2θ, 10.2-10Å, 17.8° 2θ, 4.9Å, and at 31.8° 2θ, 2.8Å. Lesser amounts of illite were found to be associated with the very shaly-siltstones of distal deltaic facies of wells E1-NC2, and A1-NC2 (Figs. 32, 33).

III.1.4.1- ***Interpretation*** of XRD-analyses:

X-ray patterns of bulk samples mineralogical identification indicate that quartz is the dominant mineral in the studied sandstone samples of fluvial origin. In the fluvial sandstones high intensity peaks of diffraction occur (Figs. 26-29) whereas the intensity decreases regionally in sandstone/siltstone samples of deltaic and offshore marine origin which are rich in clay minerals relatively. This confirms the thin-section observations.

Small amounts of hematite with strong peak at 33.2° 2θ, 2.69Å in the fluvial sandstones in wells EE1-NC7A, Z1-66, A1-NC118, and B3-61 may have been derived largely from the alteration of ferriferous minerals in the vadose and phreatic zones shortly after deposition. The iron released during alteration was subsequently oxidized.

The general decrease in K-feldspars from south to north in the Basin is indicated by low intensity peaks in all samples. It is interpreted here that the feldspars are a likely source of K for the formation of illite, especially in distal deltaic siltstone samples (Figs. 32, 33).

The diagenetic manganoan calcite ((Ca, Mn) (CO_3)) cement associated with the fluvial sandstone samples (Figs. 26, 28 & 29) probably indicates deposition from and equilibrium with meteoric water. Such water, in general, contains more Mn^{2+} than sea

water (Bathurst, 1983).

The low intensity peaks for ferroan-dolomite in the quartz-cemented sandstones (fluvial sandstones) (Figs. 26, 29) is lower than in the carbonate and clay cemented sandstones (deltaic-marine sandstones) (Figs. 30-35) and coincides with a change in depositional environment from fluvial to deltaic to basin. This accounts for the increase observed in total iron.

A minor amount of siderite in fluvial sandstone samples (well Z1-66 (Fig. 27)) is interpreted to have formed at the expense of partial calcite cement present in this sandstone. The concentration of siderite was limited by the availability of Fe^{++}which may have come from silicates such as biotite, pyroxene, olivine etc. during shallow diagenesis. Many workers have observed similar relationships (Selley, 1982; Bjørlykke, 1983; Dutton et al., 1996).

X-ray diffraction confirms the petrographic identifications made and indicates that the general increase of kaolinite and illite cements from fluvial to deltaic samples is strongly facies controlled.

Summation:

The results of the XRD analyses corroborate the findings from thin sections which indicate lateral mineralogic changes from the basin flanks (fluvial sandstones) north to the basin centre (basinal shales). In similar fashion there are significant regional changes in the intensities of diffraction peaks for the mineral suites from south to north.

III.2- Isotopic analyses:

III.2.1- Oxygen-carbon isotopic compositions in calcite cements:

On the basis of petrographical studies, 30 samples from the various facies of the Lower Acacus Formation were chosen for oxygen and carbon isotope study of calcite cement (Table 6). These samples were taken from different sandstones and siltstones units in different facies of different origin; from fluvial (Af2-Af7 units) to proximal deltaic (A1-A14 units) to distal deltaic (Ad units) to reworked marine (Am units) throughout the Hamada Basin. The analyses show the following relationships:

Calcite is one of the dominant cements in the Lower Acacus Formation, ranging from 1% to 18% of the rock (Table 4). Calcite was not always pure; occasionally magnesite, manganoan, and iron-rich ferroan calcites are present in some samples, as indicated by XRD analyses.

Two types of calcite cement have been distinguished based on texture and manner of occurrence in thin-sections:

1) Patchy calcite cement is a cement with a patchy texture of irregular scattered forms, low in

iron, usually manganoan-calcite, partially **filling primary porosity** between quartz grains. These calcites are a mixture of both bright and dull luminescence, unzoned. Patchy calcite cement occurs in the southerly shallower portions of the Basin characterized by fluvial, iron oxide-rich sandstones. (Appendix II- Plate 12A,B, Appendix III- Plates 29A, 30B, Figs 22A, 26, 29).

Table 6. Oxygen and carbon-isotope compositions of calcite cement, in sandstone units of different facies of the Lower Acacus Formation, Hamada Basin, NW Libya.

Lower Acacus Units*	Well	Depth (ft)	Rock type**	Calcite cement type	δ18O (‰)		δ13C (‰) (PDB)
					(SMOW)	(PDB)	
Af3	EE1-NC7A	8810	fgst.	Shallow	20.4	-10.1	-10.1
Af3	"	8812	vfgst.-slst.	"	20.8	-9.8	-11.5
Af7	CC1-NC7A	7840	vfgst.-slst.	"	16.4	-14.2	-12.9
Af2	"	9020	mgst.	"	20.3	-10.2	-12.9
Af2	B3-61	9345	fgst.	"	20.5	-10.1	-9.7
Af4	Z1-66	9081	fgst.	"	18.7	-11.7	-12.0
Af3	"	9130	fgst.	"	20.1	-10.4	+7.6
Af3	A1-NC118	10040	fgst.	"	17.7	-12.7	-10.7
Af3	Z1-NC100	11480	fgst.	"	20.9	-9.7	-9.6
Af7	C1-61	7110	mgst.	"	20.9	-9.7	-8.1
Af5	"	7525	mgst.	"	25.5	-5.1	-5.3
Af2	"	8199	vfgst.	"	16.1	-14.3	-12.9
A8	C1-Nc2	9703	mgst.	Deep	19.7	-10.8	-13.1
	"	9725	mgst.	"	19.3	-11.2	-12.4
A10	D1-61	8845	mgst.	"	15.6	-14.8	-15.1
	"	8866	mgst.	"	14.1	-16.2	-20.4
A12	B1-NC2	8542	mgst.	"	24.5	-6.1	-17.2
	"	8555	mgst.	"	21.71	-8.9	-18.0
	C1-70	7913	fgst.	"	18.3	-12.2	-9.5
	B3-61	8893	mgst.	"	18.4	-12.2	-19.9
	"	8969	"	"	23.9	-6.7	-19.2
A14	T1-23	8454	fgst.	"	15.4	-14.9	-20.7
	"	8473	vfgst.	"	19.8	-10.6	-18.4
	C1-NC2	8855	fgst.	"	20.6	-10.0	-12.4
	E1-NC2	9105	mgst.	"	19.3	-11.2	-12.9
Ad	A1-NC2	7814	slst.	"	15.6	-14.8	-3.8
	"	7817	slst.	"	15.3	-15.2	-11.1
Am	Q1-23	7461	fgst.	"	15.1	-15.3	-15.8
	"	7471	fgst.	"	14.9	-15.5	-16.0
	"	8180	fgst.	"	14.8	-15.6	-16.4
	"	8485	vfgst.	"	17.5	-13.0	-18.5

* Af2-Af7 = Lower Acacus fluvial sandstone units, A8-A14 = Lower Acacus proximal delta front sandstone units, Ad = Lower Acacus distal delta front siltstone units, Am = Lower Acacus reworked marine sandstone units.

** slst. = siltstone, vfgst. = very fine-grained sandstone, fgs. = fine-grained sandstone, mgst. = medium-grained sandstone.

Note: All measurements are in the units of the wells studied. Where both Metric and Imperial units are utilized they are provided

(Samples were analysed by Dr. Longstaffe at the request of Ellgh, November 1998).

2) ***Patchy-Poikilotopic calcite cement*** has patchy to piokilotopic texture (0.5-15mm in diameter) with scattered to occasionally continuous and homogeneous distribution (Appendix II- Plates 10B, 11A). These calcites have dull-yellow luminescence, are unzoned, and are associated with magnesium and ferroan carbonate. This cement is found to be **filling mainly secondary porosity** and occasionally replacing feldspars. Patchy-poikilotopic calcite cement occurs in the northerly deeper parts of the Basin characterized by the deltaic and basinal facies (A8-A14 units) (Appendix II- Plates 10B, 11A,B, Appendix III- Plate 29B, Figs 22B, 30, 31).

The transition between these cement-type regions is broad and gradational. Well densities are inadequate at this point to make specific statements regarding the details of the transitions. For the purposes of the regional discussion the patchy calcite cement will be termed the ***Shallow calcite cement.*** The patchy-poikilotopic cement will be termed the ***Deep calcite cement.***

A plot (Table 6; Figure 36) of oxygen isotope ($\delta^{18}O$ ‰) versus carbon isotope composition ($\delta^{13}C$‰) of calcite cement illustrates the variations encountered in the different facies of the Lower Acacus Formation. For the fluvial sandstone facies (Af2-Af7), shallow calcites have $\delta^{18}O$ and $\delta^{13}C$ values ranging from +16.1 to +22.6‰ SMOW, and -12.9 to +7.6‰ PDB, respectively. On the other hand the deep calcite cements associated with proximal deltaic sandstone units (A8-A14) are characterized by relatively lower $\delta^{18}O$ values (+14.1 to +19.8‰ SMOW), and have highly negative $\delta^{13}C$ values

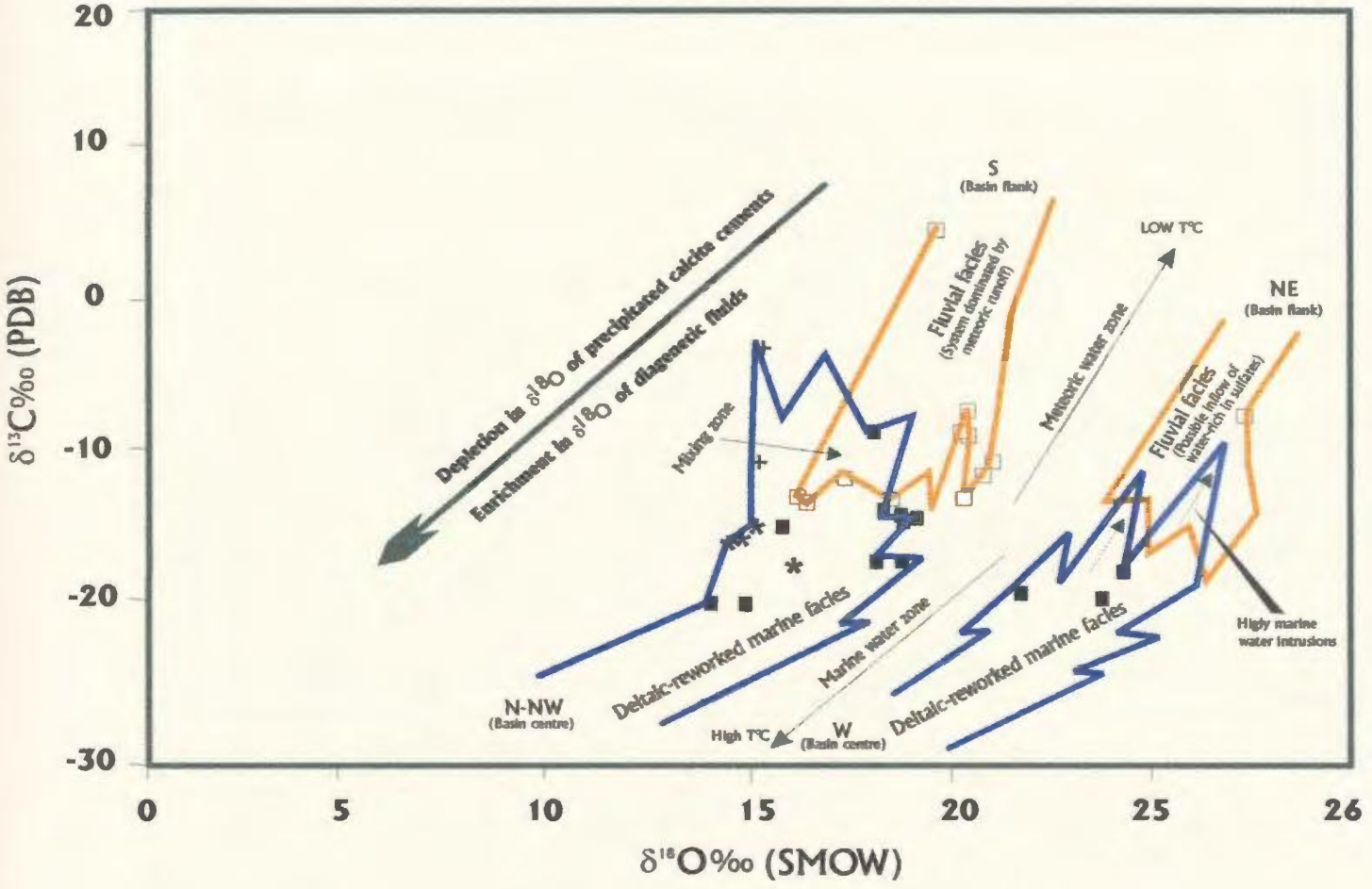

□ Shallow calcite cement in the fluvial sandstone units (Af2-Af7)

■ Deep calcite cement in the proximal delta front sandstone units (A8-A14)

\+ Deep calcite cement in the distal delta front siltstone units (Ad)

* Deep calcite cement in the reworked marine sandstone units (Am)

Figure 36. Oxygen-versus carbon-isotope compositions of calcite cements in the various sandstone/siltstone units in the two deltaic systems (NE-W, S-NNW) of Lower Acacus Formation, Hamada Basin, NW Libya.

In all units the δ18O values decrease with burial either locally on the level of each unit, or regionally from basin flank to basin centre. The δ13C values show contrasting trends, for shallow calcite associated with fluvial sandstone units (Af) increasing from low to high values, and for deep calcite associated with proximal deltaic-reworked marine sandstone units (A8-A14, Am) decreasing from high to low values. However, some highly negative δ13C values can be seen associated with distal delta front siltstone units (Ad) (Note: For units identification and their locations in the tested wells see Table 6, Figs. 9, 11A-D, Appendix I, and Enclosures 3 and 4).

(-20.7 to -9.5‰ PDB).

Cement in the reworked marine sandstone units (Am) ($\delta^{18}O$ = +14.8 to +17.5‰ SMOW, and $\delta^{13}C$ = -18.5 to -15.6‰ PDB) is of the deep calcite variety and is similar to the majority of deep the calcite cements of deltaic origin (Fig. 36).

Distal deltaic units (Ad) have poikilotopic cement textures and record isotopic compositions ($\delta^{18}O$ = +15.3 to +15.6‰ SMOW, and $\delta^{13}C$ = -11.1 to -3.5‰ PDB) similar to the majority of deep calcite cements of deltaic origin (Fig. 36), with some highly negative $\delta^{13}C$ values (-11.1 to -3.5‰ PDB).

III.2.1.1 ***Interpretation*** of isotopic composition of calcite cements:

In fluvial sandstone units (Af2-Af7) the $\delta^{18}O$ values are consistent with precipitation of the shallow calcite cement from meteoric water at low temperature (e.g. Ayalon and Longstaffe, 1995; Tang et al., 1997). The lighter negative $\delta^{13}C$ nature of this calcite suggests an involvement of organically derived CO_2. The probable source of such CO_2 is the oxidation of organic matter from the overlying soil during shallow diagenesis; local meteoric recharge to these fluvial sandstones occurs by percolation through the associated soil zone (overbank deposits) (e.g. Schwartz and Muehlenbachs, 1979). According to Bottinga (1968) and Friedman and O'Neil (1977) the CO_2-calcite fractionation for carbon at low temperatures (soil temperatures from +5°C to +20°C) is about -13‰ to -11‰ PDB. Such fractionation would equate to calcite carbon isotopic ($\delta^{13}C$) values in the range (-12.9 to -5.3‰ PDB; Table 6) recorded for the fluvial sandstones (Af2-Af7). The single high positive $\delta^{13}C$ value recorded (+7.6‰ PDB) (Table

6, Fig. 36) would be consistent with conditions in fluvial facies with associated carbonaceous materials altered by shallow microbial degradation (e.g. Curtis et al., 1986; Longstaffe et al., 1992 ; Longstaffe, 1994). The relative similarities of the oxygen isotope compositions for the shallow calcite cements throughout the fluvial sandstone units suggests that the water in these sandstones were fairly uniform in composition and would be consistent with a fresh water origin.

The lower $\delta^{18}O$ values of the deep calcite cements associated with the deltaic sandstone units (A8-A14) are compatable with these cements being crystallized from formation waters having a composition similar to sea water (e.g. Ayalon and Longstaffe, 1995). Such values may also have resulted from increasing temperature and water-rock interaction as burial diagenesis progressed (e.g. Longstaffe, 1994). The negative $\delta^{13}C$ values probably record the increasing importance with depth of bicarbonate production by thermal decarboxylation (e.g. Tang et al., 1997).

It is important to note that it is difficult to determine the timing (early or late) of the patchy to homogeneously distributed, nonzoned shallow and deep calcite cements. However the data suggest that both the shallow and the deep calcite cements were formed synchronously. The shallow cements were being precipitated in the fluvial sandstones from meteoric waters and the deep calcite cements were being precipitated in the deltaic sandstones as the waters flowed down-basin becoming progressively more saline and reducing (Fig. 36).

Considerations for depth and temperature of precipitation of calcite cements:

The Hamada Basin (western Libya) during the Lower Acacus Formation time (Wenlockian) was at about Latitude 30°- 40°S (Cramer, 1971; Scotese et al., 1979). Thus an assumption of 20°C average surface temperature is reasonable. The present-day average geothermal gradient in the Hamada Basin is approximately 30°C/km. This gradient is based on average bottom-hole temperatures (BHTs) recorded from drillstem tests (DSTs) in 22 wells (Table 7) and compares well with studies in neighbouring sedimentary basins (Tissot and Welte, 1978; Makhous et al., 1997)). Average BHTs of approximately 110°C would equate to precipitation at a depth of about 3 km for the deep calcite cements associated with the deltaic sandstone facies. This interpreted depth is within the depths typical of decarboxylation zone of $\delta^{13}C$ values from -20 to -10‰ PDB suggested by Curtis (1978), and Dutton et al. (1996).

The isotopic similarity of deep calcite cements encountered in the proximal deltaic (A8-A14) and marine sandstone units (Am) suggests that these units contain the same generation of cement precipitated from subsurface brines evolved from sea water. The relatively deep calcite cement associated with the deltaic and reworked marine sandstone units may indicate that connate water mix was involved. The relatively low $\delta^{18}O$ values at well locations such as at C1-NC2 and T1-23 (Table 6, Fig. 36) are consistent with the introduction of meteoric waters during burial diagenesis. Such mixing of meteoric and evolved sea water are typical of many oil and gas pools in the Alberta Basin (Longstaffe, 1984).

Table 7 . Formation temperature, formation water salinity, and estimated geothermal gradient recovered from some Drill-Stem Tests (DST) conducted in various formations of some wells in the Hamada Basin, NW Libya.

Well Name	Depth (ft)	Formation *	Formation Temperature (°F)	Water Salinity (ppm Cl')	Estimated Geothermal Gradient (T°C/km) **	Remarks
A1-NC2	7809	L.Acacus	189	95,000	30	(-) means data not available.
	9904	Tanezzuft	236	-	26	(about 1.6°F/100ft), assuming annual mean surface temperature is about 20°C.
B1-NC2	8541	L.Acacus	233	42,000	37	Anomalous formation water salinity in deltaic ss.
C1-NC2	8855	L.Acacus	236	-	24	
	9720	L.Acacus	240	34,000	24	Anomalous formation water salinity in deltaic ss.
	9962	L.Acacus	194	-	17	(about 1.2°F/100ft)
D1-NC2	6700	Ouan Kasa	160	-	34	
	11180	Memouniat	190	-	26	
E1-NC2	8880	M. Acacus	-	148,000	-	
	9879	L. Acacus	-	120.000	-	
	9970	L. Acacus	-	130,000	-	
	9988	L. Acacus	-	51,000	17	
G1-23	10255	L. Acacus	-	236,000	-	
Q1-23	8146	L. Acacus	236	37,000	26	Anomalous formation water salinity in deltaic ss.
U1-23	7085	L. Acacus	-	37,000	-	
	7710	L. Acacus	-	42,000	-	
B1-61	8460	L. Acacus	-	278,000	-	
	8808	L. Acacus	-	258,000	-	
	8818	L. Acacus	-	290,000	-	
C1-61	7110	L. Acacus	119	35,000	47	
	7525	L. Acacus	119	42,000	47	
	8200	L. Acacus	-	46,000	-	
B3-61	8969	L. Acacus	236	230,000	26	
L1-66	4608	A. South	-	28,000	-	
Z1-66	8141	M. Acacus	155	6000	18	Anomalous formation water salinity in Middle Acacus ss.
	9042	L. Acacus	-	114,000	-	
	9145	L. Acacus	178	166,000	15	
A1-70	8818	L. Acacus	235	160,000	26	
	8881	L. Acacus	235	70,000	26	
X1-NC100	11316	L. Acacus	-	281,000	-	
Z1-NC100	11392	L. Acacus	-	180,000	-	
A1-NC118	10354	L. Acacus	-	161,000	-	(PH.value is 4, Lab.analysis)
	10400	L. Acacus	-	110,000	-	(PH.value is 6.5, Lab. analysis)
C1-NC7A	10700	Memouniat	222	-	35	
CC1-NC7A	7655	A. South	140	18,000	15	
	8170	A. South	-	18,000	-	
	10918	Memouniat	210	-	18	
DD1-NC7A	7802	A. South	-	20,000	-	
	7850	A. South	-	100,000	-	
	8788	A. South	138	-	11	
EE1-NC7A	8805	A. South	-	13,000	-	
H1-NC7A	8007	A. South	-	10,000	-	
	8300	A. South	-	11,000	-	
	8322	A. South	-	11,000	-	
	8742	A. South	-	13,000	-	
	8808	A. South	-	15,000	-	
	10900	Memouniat	180	-	13	

* Ouan Kasa= Ouan Kasa Fm., A. South= Acacus South Fm., M. Acacus= Middle Acacus Fm., L. Acacus= Lower Acacus Fm., Tanezzuft= Tanezzuft Fm., Memouniat = Memouniat Fm.

** Estimated average geothermal gradient for the Hamada Basin is 30 C/km.

(Data from Halliburton DST reports and charts, after TDL-AGOCO, Benghazi, 1961-1986. Note: All measurements are in the units of the wells studied. Where Metric and Imperial units are utilized they are provided).

According to observations by Longstaffe (1983, 1989) and Lundegard and Land (1986), marine carbonate rocks normally have $\delta^{13}C$ compositions of about 0 ± 4‰ PDB as do cements derived by dissolution of pre-existing carbonate. The distal deltaic samples (Ad) have $\delta^{13}C$ of -3.5‰ PDB, and therefore are consistent with an origin whereby dissolved marine carbonate was precipitated in these samples.

III.2.1.2- ***Interpretation*** of pore water evolution:

Geological, petrographic and isotopic data are combined to interpret changes in oxygen isotope composition of pore water in each facies of the Lower Acacus Formation.

Independent constraints on temperature during diagenesis of the Lower Acacus Formation were used to assess the evolution of $\delta^{18}O$ of the diagenetic waters. These constraints are: (1) the minimum surface temperature at which certain diagenetic processes may have occurred (e.g. iron-oxide coating), (2) the possible changes in subsurface temperatures where shallow and deep calcite cements have developed, and their representation on a burial curve supported by a presumed subsurface temperature grid based on recorded field temperatures (bottom-hole temperatures) (Fig. 37).

A hypothetical burial history curve (Fig. 37) for the Lower Acacus Formation was constructed using field temperatures (Table 7), formation tops (from well-logs, Enclosures 3, 4), and stratigraphic data for the other shallower datums or formations (based on full depth, surface to TD). This burial curve was constructed using Lopatin's techniques as described by Waples (1985), using a present-day average Lower Acacus Formation depth of about 2805 m. (9200 ft), and an average geothermal gradient 30°C/km.. Accuracy of

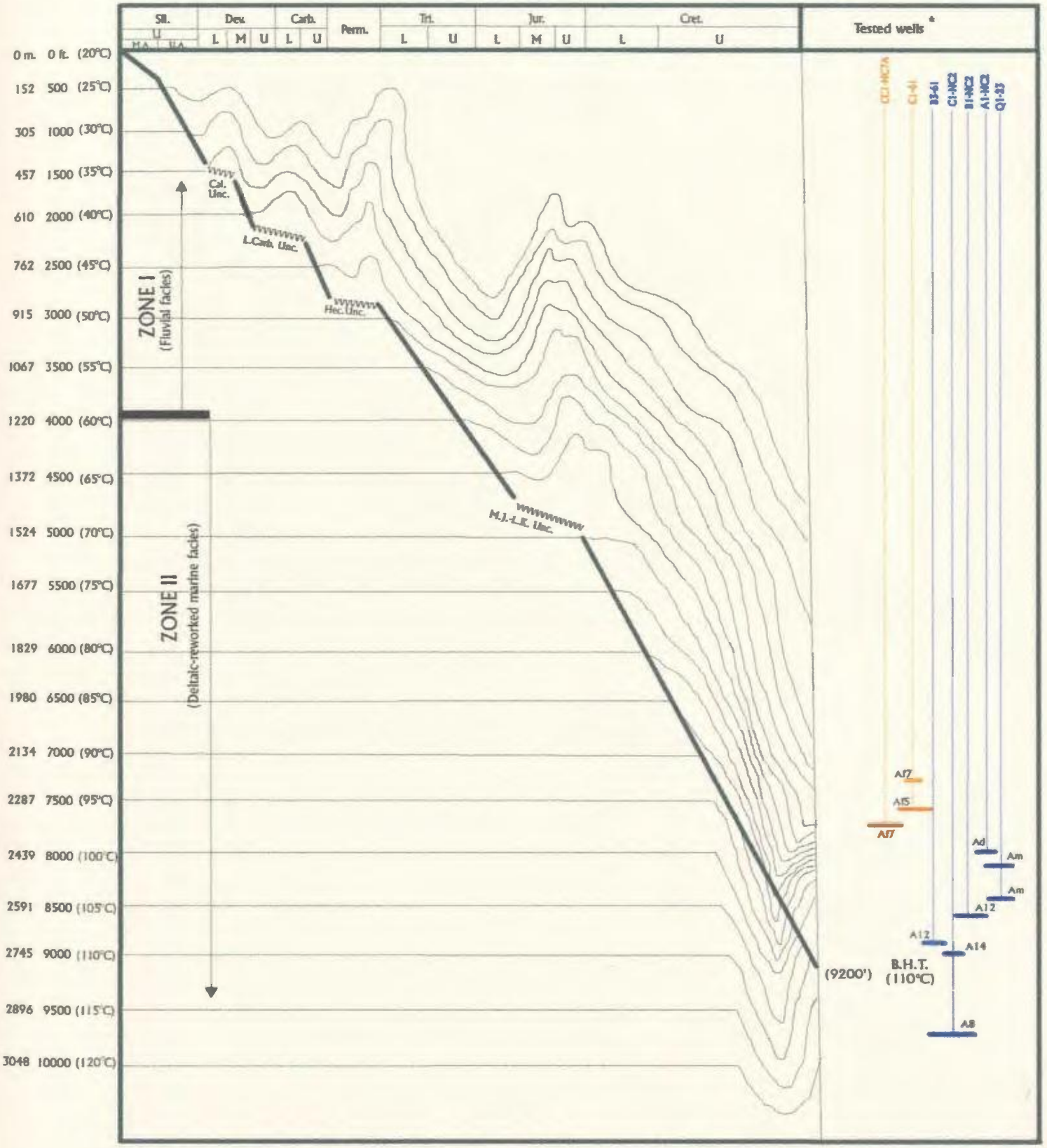

Figure 37. Hypothetical burial history curve and estimated subsurface temperature grids of the Lower Acacus Formation, Hamada Basin, NW Libya. Note shallow and deep calcite cements are identified by temperature-contour zones (I & II) as they assumed to be changed with facies and depth.

* Wells are used to test their oxygen isotope values with corresponding formation temperature.

the time-temperature diagram (Fig. 37) is subject to the uncertainties inherent in establishing both the paleogeothermal gradient of the Lower Acacus Formation in the Hamada Basin and determining the amount of erosion that occurred at all unconformities in the figure. This is a useful exercise however for it establishes a context within which regional interpretations can be assessed.

By using the recorded bottom-hole temperatures (BHT) of the various Lower Acacus units in some wells (Table 7), isotherm contours are no longer parallel because the geothermal gradient changed through time. Sinking of the isotherms (low-temperature gradient) may be due to climate cooling and/or rapid sediment accumulation. Subsequent elevation of isotherms (high-temperature gradient) may be due to surface warming associated with erosional unconformities (Waples, 1985; Makhous et al., 1997) or to tectonic-related activities.

The minimum temperature of the shallow calcite cements associated with the fluvial sandstones is chosen to be between 35°C and 60°C ((the inferred temperatures of the onset of shallow burial diagenesis and the precipitated calcite in equilibrium with meteoric pore waters) (Dutton and Land, 1985; Al-Aasm and Azmy, 1996)) based on the assumption that these sandstones were infiltrated by meteoric water from the shallow basin flanks (see burial history curve Fig. 37). The maximum temperature of precipitation of the deep calcite cements is assumed to be between 60°C to +110°C in accordance with the finding of Pusey (1973) and Dorobek (1987). Based on these assumptions the diagenetic changes of calcite cements in zone I and zone II of the deltaic systems are indicted on the

burial curve.

In the Hamada Basin both the present-day and ancient geothermal gradients can be considered to be approximately 30°C/km because Hercynian erosion of the Late Paleozoic sediments in the northern part of the Hamada Basin (Ghadames Basin) was of the order of 457-610 m. (1500-2000 ft.) (BEICIP, 1973; Bishop, 1975; Makhous et al., 1997). Such a thickness would not cause any major subsurface temperature change since the basin regained its sagging shape during the post-Hercynian and accomodated more sediment. No major tectonic uplifts or subsidences nor magmatic activities have been documented since deposition of the Lower Acacus Formation. It is assumed therefore that the observed formation temperature changes with depth could be compatible with the crystallization temperature for these calcite cements across the Basin. The application of burial depth and its attendant temperature which played a more important role in calcite precipitation and diagenesis was also discussed by Milliken et al. (1998).

In order to model pore water evolution of the Lower Acacus section, standard relationship curves for oxygen isotope composition of pore water ($\delta^{18}O_{water}$‰ SMOW) versus crystallization temperature (°C) (assumed to be represented by burial-temperature in this case), and calcite cement composition as shown by contours ($\delta^{18}O_{calcite}$‰ PDB) (Fig. 38) have been used (based on Friedman and O'Neil, 1977) . The possible bottom-hole formation temperatures and calcite cement $\delta^{18}O_{calcite}$‰ (PDB) values for each examined sample have been applied to determine the approximate corresponding pore water isotopic composition $\delta^{18}O_{water}$‰ (SMOW) (Fig. 38).

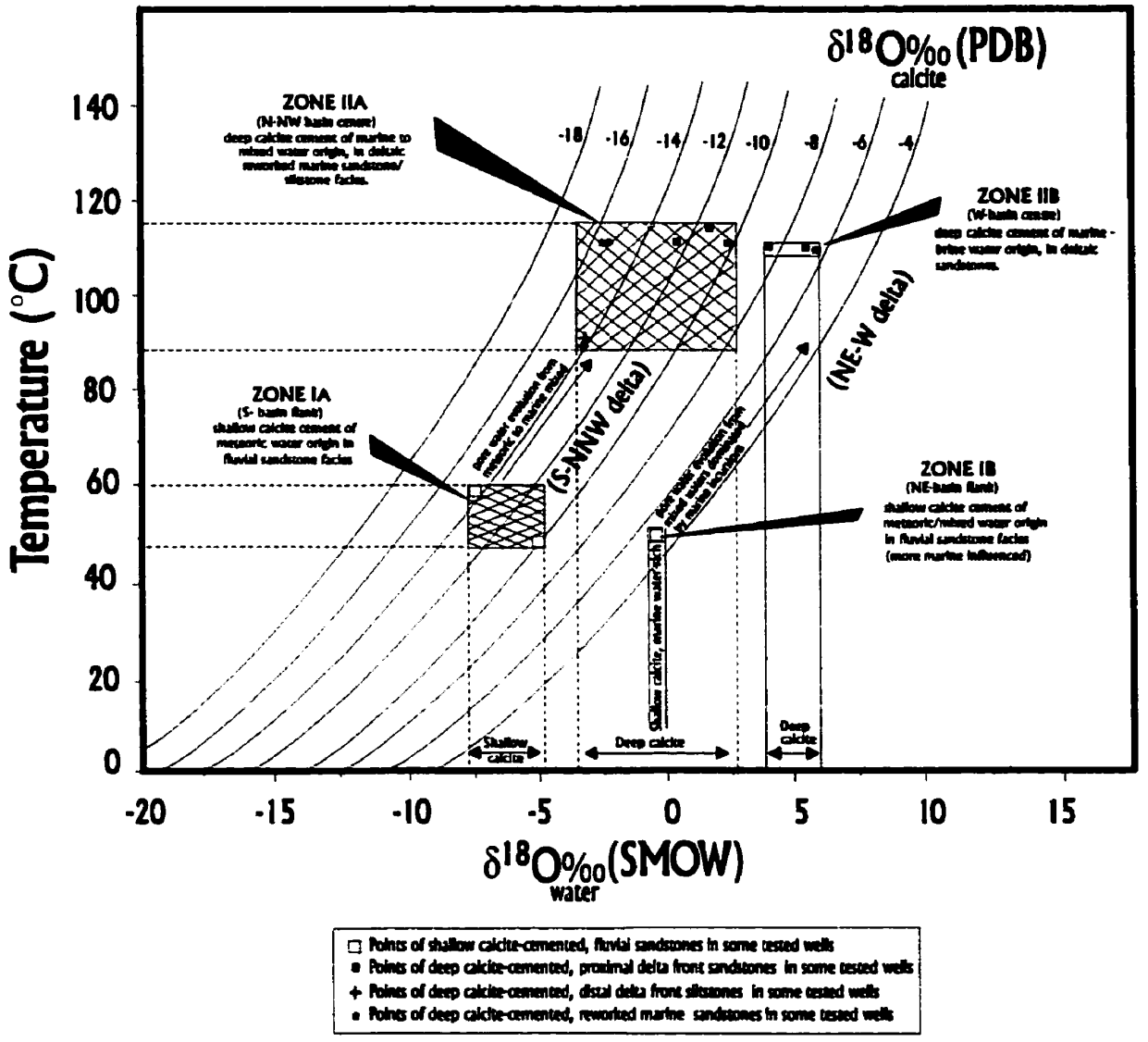

Figure 38. Oxygen isotope composition of pore water ($\delta^{18}O$‰ SMOW) vs. crystallization temperature (formation temperature in this case °C) for the Lower Acacus Formation. Isotopic composition of calcite cements is shown as contours ($\delta^{18}O$‰ PDB). The standard equation relating temperature (T), $\delta^{18}O_{water}$, and $\delta^{18}O_{calcite}$ is $(\delta^{18}O_{calcite} - \delta^{18}O_{water} = 2.78 \frac{10^6}{T^2} - 2.89)$ (Friedman and O'Neil, 1977).

Zone IA (S-basin flank) represents shallow calcite cement precipitated from meteoric water at shallow depth in fluvial sandstone facies; Zone IIA (N-NW basin centre) represents deep calcite cement precipitated from inferred marine to mixed waters at burial depth in deltaic and reworked marine sandstone/siltstone facies; Zone IB (NE basin flank) represents shallow calcite cement precipitated originally from meteoric water but highly influenced with marine water in fluvial sandstone facies; Zone IIB (W basin centre) represents deep calcite cement precipitated from marine -brine water in deltaic sandstone facies.

Note the overall diagenetic trend from Zone I (basin flanks) to Zone II (basin centre) reveals depletion of $\delta^{18}O$ of precipitated calcite cements, enrichment in $\delta^{18}O$ of diagenetic fluids, and an increase of temperature with burial.

Regional variation of isotopic trends:

Two different diagenetic events with distinctive changes in $\delta^{18}O$ pore water were detected in the two deltaic systems present in the region (S-NNW and NE-W) (Fig. 36 and 38),

(see also Enclosures 3 and 4). The S-NNW delta prograded from the south to north-northwest. The NE-W delta prograded from the northeast to west (Figs. 36, 38). The two deltaic systems were sourced from two different directions (S and NE) respectively (Fig. 36).

In Figure 38, zone IA (S-basin flank) represents shallow calcite cement from the fluvial sandstone facies. The $\delta^{18}O_{calcite}$ values between -9.6 and -14.2‰ PDB, were initiated at low temperatures (BHT) of about 48°C to 55°C (Fig. 37, in wells C1-61 (Af7), and CC1-NC7A (Af7)). $\delta^{18}O_{water}$ pore water values range between -8‰ to -5‰ SMOW. Such values suggest that these shallow calcite cements were deposited from meteoric water at low temperatures.

On the other hand, zone IIA (NNW-basin centre, Fig. 38) being subject to increasing depths, burial temperatures and compaction, is characterized by deep calcite cements associated with deltaic and reworked marine sandstone/siltstone facies. These cements are depleted in $\delta^{18}O_{calcite}$ values between -15.6 to -10.8‰ PDB, with slight enrichment in $\delta^{18}O_{water}$ of diagenetic pore water values between -3 to +2.5‰ SMOW, and an increase in temperature ranging from 89°C to 116°C (Fig. 37, in wells A1-NC2 (Ad), Q1-23 (Am), and C1-NC2 (A8, A14)). These data suggest the involvement of marine

(connate mixed) waters for the deposition of this deep calcite cement in these facies.

Zone IB (NE-basin flank, Fig. 38) represents shallow calcite cements from fluvial sandstones facies (well C1-61, unit A5) having $\delta^{18}O_{calcite}$ values of -5.1‰ PDB. These cements are assumed to have initiated at low temperatures of about 48°C to 50°C (Fig. 37) based on the logic used previously. Pore water values range from -1‰ to 0‰ SMOW which suggest that these shallow calcite cements formed from meteoric waters highly influenced by marine mixed water incursions at various times in their history. Isotopic values of shallow calcite cements of this zone (zone IB, NE-basin flank, Fig. 38) are still within the range of daily variation of soil temperatures at the present-day surface and shallow subsurfaceconditions (e.g. Parton, 1984; Kemp et al., 1992). Moreover, the carbon isotope values of these calcite cements in the NE-channel sandstones of well C1-61 (Af5 unit) are approximately -5.3‰ PDB. This would be compatible with an inorganic source related to meteoric water depleted in $\delta^{13}C$ relative to sea water (e.g. Veizer, 1992; Amthor and Okkerman, 1998). In zone IIB (W- basin centre of deltaic origin, Fig. 38), with increasing depth and formation temperature increases from 104°C to 110°C, the deep calcite cements in the deltaic sandstone units (A12) in wells B1-NC2 and B3-61 became enriched in $\delta\ ^{18}O_{calcite}$ (values being between -6.1 to -8.9‰ PDB). There was slight enrichment in $\delta^{18}O_{water}$ of diagenetic pore water (values between +4 to +6‰ SMOW) in the wells B1-NC2 and B3-61 respectively (Fig. 37).

In this NE-W-delta, highly negative $\delta^{13}C$ values (-17.2 to -19.2) (Fig. 36) suggest the increasing importance with depth of bicarbonate production by thermal

decarboxylation. The overall low $\delta^{18}O_{calcite}$ values of calcite cement (-8.9‰ to -6.1‰ PDB) in these deltaic sandstones in turn provide additional evidence for the involvement of hot basinal (brines) waters (e.g Souza et al., 1995). Another point regarding the enrichment in $\delta^{18}O_{water}$ in the NE-W delta is that this enrichment (heavy $\delta^{18}O$) may can represent the flow of groundwaters rich in sulfates from the stratigraphically shallower, highly faulted Lower to Middle Jurassic anhydritic section downward into the basin sequences (Enclosure 2).

In both delta systems, the diagenetic pore-water trends and the relative enrichment in $\delta^{18}O$ from fluvial (basin flanks) to deltaic (basin centre) sandstone units may also have been caused by increasing water-rock interaction as meteoric water percolated down into the basin during burial. Such percolation eventually may have caused the enrichment of the diagenetic water with heavy oxygen (^{18}O) relative to the light isotopic oxygen (^{16}O) (this also was suggested by Land and Prezbindowski, 1981; Al-Aasm et al., 1993).

Summation:

Integration of the various data sets in accordance with the identified assumptions have made it possible to speculate on the nature of the groundwaters and their movements in the Hamada Basin. The result of such modelling suggests that waters of meteoric to connate mixed origin could have caused all of the diagenesis in the sandstones of the Lower Acacus Formation.

IV- DIAGENETIC FACIES AND THEIR INTERPRETATION (CEMENTS & POROSITY)

Examination of 89 epoxyed thin-sections (Appendices II, V) and 20 scanning electron microscope (SEM) samples from 22 core-sections in the various sandstone units of Lower Acacus Formation (Appendix IV) shows that these reservoir sandstones are altered by a number of diagenetic events that affected the porosity and permeability both favourably and adversely at various times.

To aid in understanding the relationship between diagenetic zones, porosity and permeability, and to correlate diagenesis, porosity and permeability to log response, the sandstones of the Lower Acacus Formation have been divided into 3 diagenetic facies; quartz-cemented facies, carbonate-cemented facies, and clay-cemented facies. Each facies has distinct petrographic, diagenetic and petrophysical characteristics (Tables 3, 4) that can be used to describe diagenetic heterogeneity in the subsurface. These diagenetic facies are for the selected A8, A10, A12, A14, Af2-Af7, and Am sandstone units of Lower Acacus Formation. These units are laterally extensive, heavily cored, well pronounced and traceable in well-logs.

IV.1 Diagenetic facies:

IV.1.1 Quartz-cemented facies:

The ***quartz-cemented facies*** is described as any sandstone interval that contains

greater than 5% quartz-overgrowths and less than 13% calcite cement (Table 4). This diagenetic facies is represented by the Lower Acacus sandstone units of fluvial origin (Af2-Af7) situated in the southern part of the Hamada Basin in wells CC1-NC7A, EE1-NC7A, and Z1-66, and in the eastern part of the NC2 Concession in wells A1-61, and C1-61 (Figs. 11A-D). These sandstones were the sediment source channels to the prograded deltaic units (A8-A14) in the northern part of the basin (Elfigih, 1991). Quartz-overgrowths average 13%, calcite averages 6%, and dolomite cement averages 2.4% or less (Figs. 39A,B,C). Clay cement is poorly developed and in total averages only 9% (Fig. 39D). However, iron-oxide rims associated with interstitial clays average 5%, kaolinite averages 4%, and illite averages less than 1%. Detrital grain size averages 0.47mm, the coarsest grained sandstones in the Lower Acacus reservoirs (Fig. 39E).

Thin-section determinations of primary porosity between rigid uncorroded quartz grains averages 16% (Fig. 39F) whereas secondary porosity is very poorly developed by partial dissolution of calcite cement at some places and averages only 3%.

Measured porosity from core plugs in these sandstones averages 23% (Figs. 39G, 40A,B). The high degree of sorting, medium to coarse grain size, and low matrix content in some sandstones in this facies resulted in an initially high permeability, averaging 1726md (Figs. 39H, 40A,B). Derived average density from Formation Density Log (FDL) is 2.50g/cm^3 for this facies (Figs. 39I, 41).

Sandstones of the quartz-cemented facies are often found in the channel sequences characterized by a variety of channel form log signatures such as blocky shaped gamma-

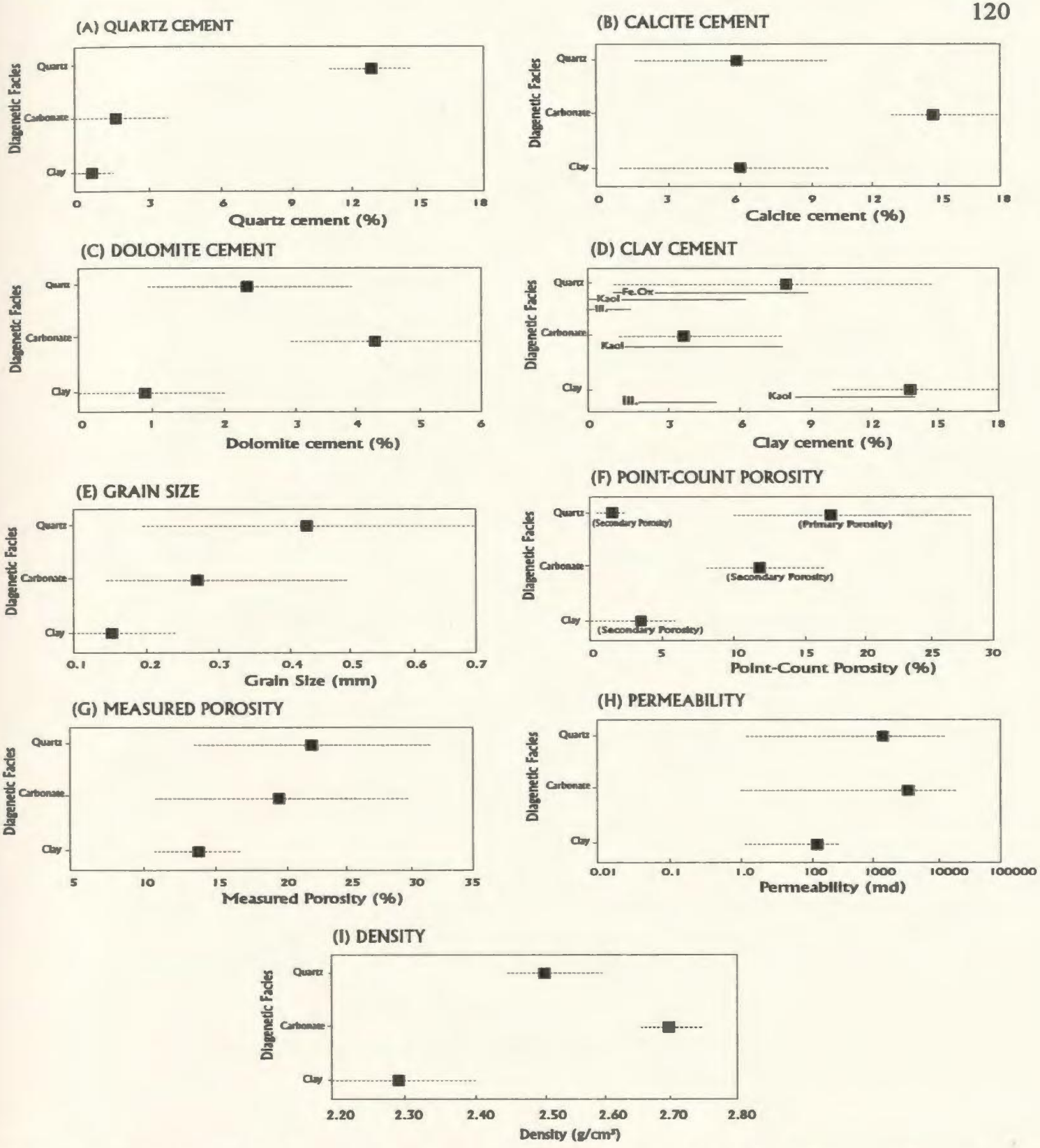

Figure 39. Petrographic and petrophysical characteristics of the three identified diagenetic facies of the Lower Acacus Formation. Plots show the mean value (squares) for the major petrographic and petrophysical characteristic values (dashed lines) that define each diagenetic facies. Note possible diagenetic clay minerals are identified at each level of the diagenetic facies. Also, note that sandstones of the calcite-cemented facies have distinct secondary porosity and density distributions compared to sandstones of the quartz- and clay-cemented facies.

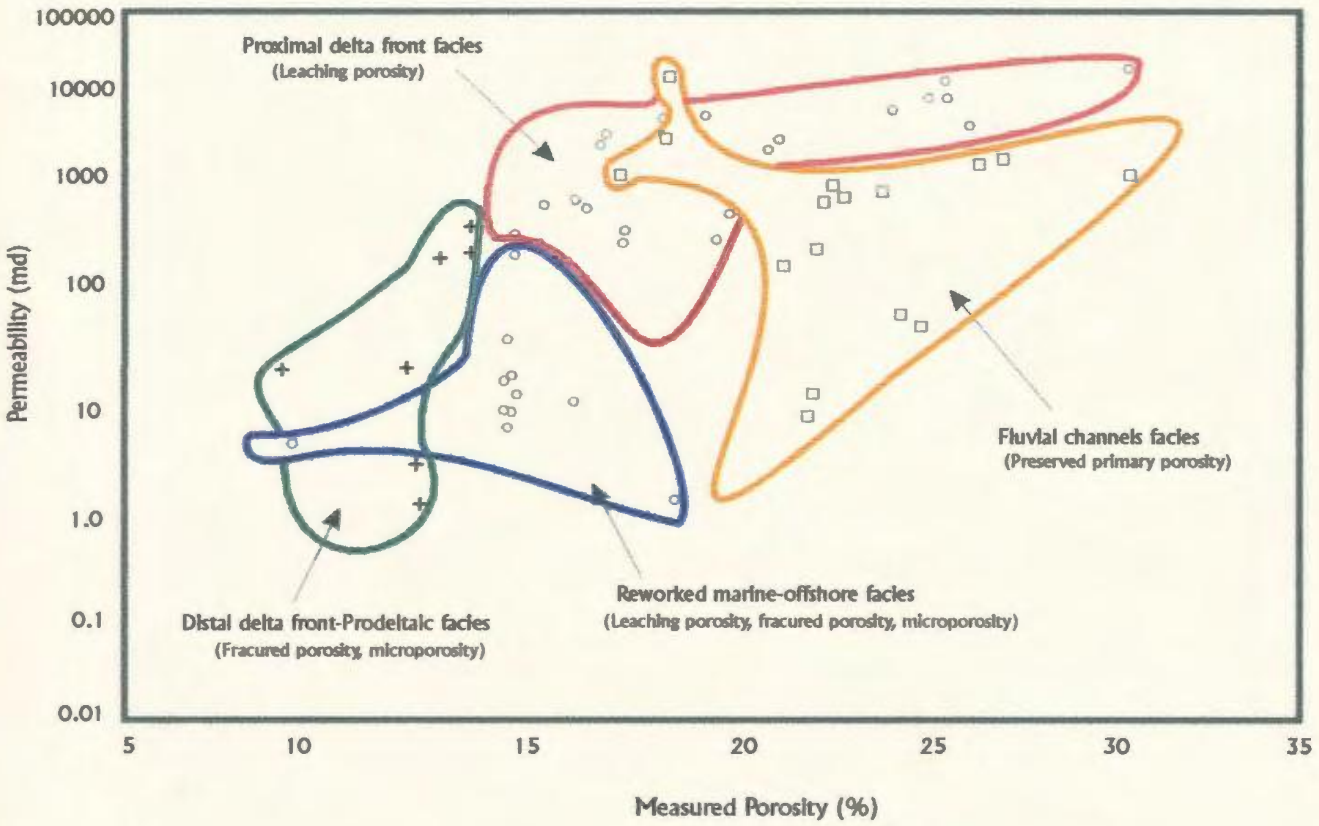

Figure 40A. Measured porosity and permeability for each depositional facies of the Lower Acacus Formation based on core-plug analysis. Note each depositional facies creates distinct fields characterized by distinct porosity type. The best porosity and permeability readings are associated with proximal delta front and fluvial channel facies.

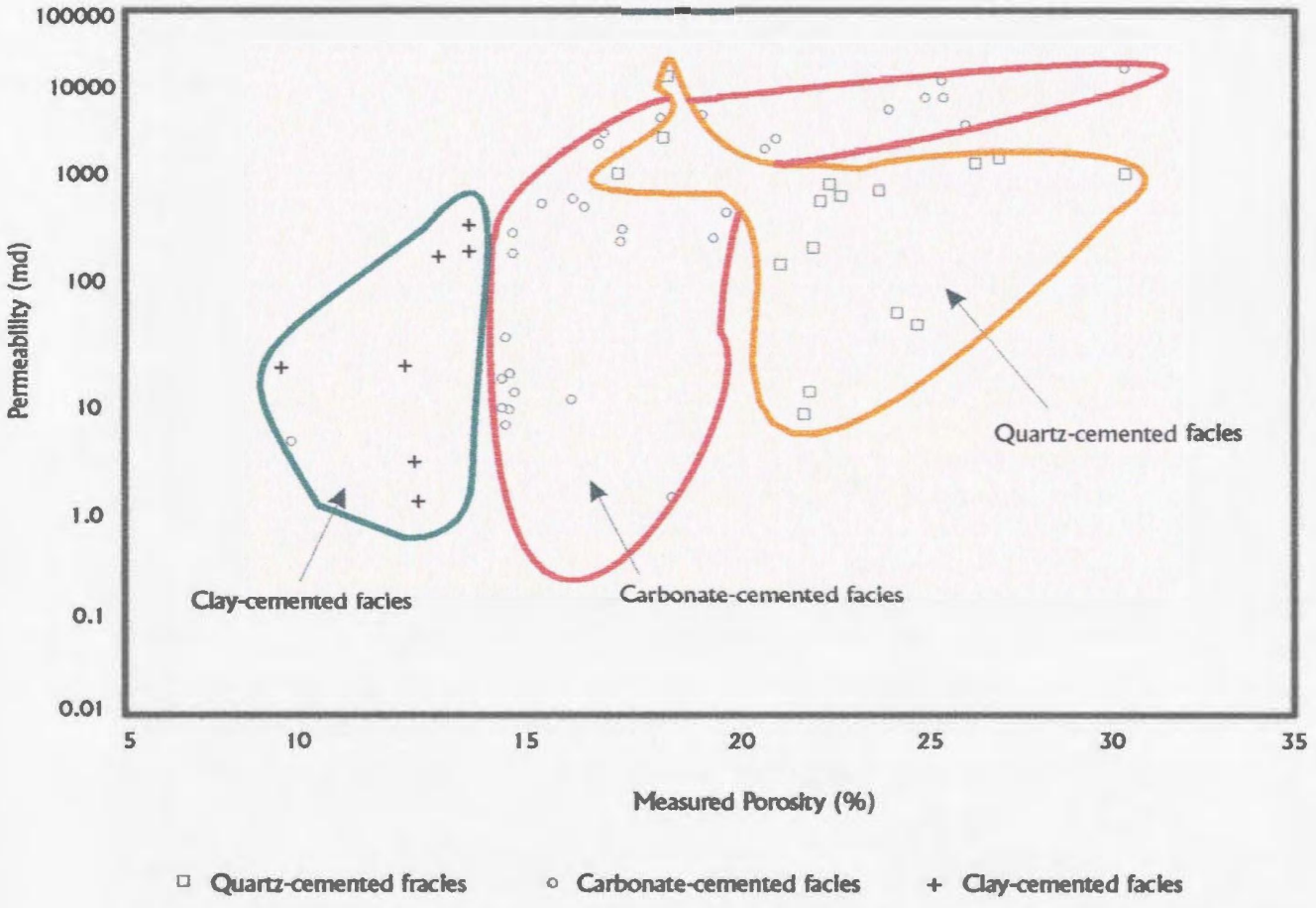

Figure 40B. Measured porosity and permeability within the diagenetic facies of the Lower Acacus Formation based on core-plug analysis. Note each diagenetic facies creates a distinct field, indicating that the type of cement in each facies can accurately predict porosity and permeability.

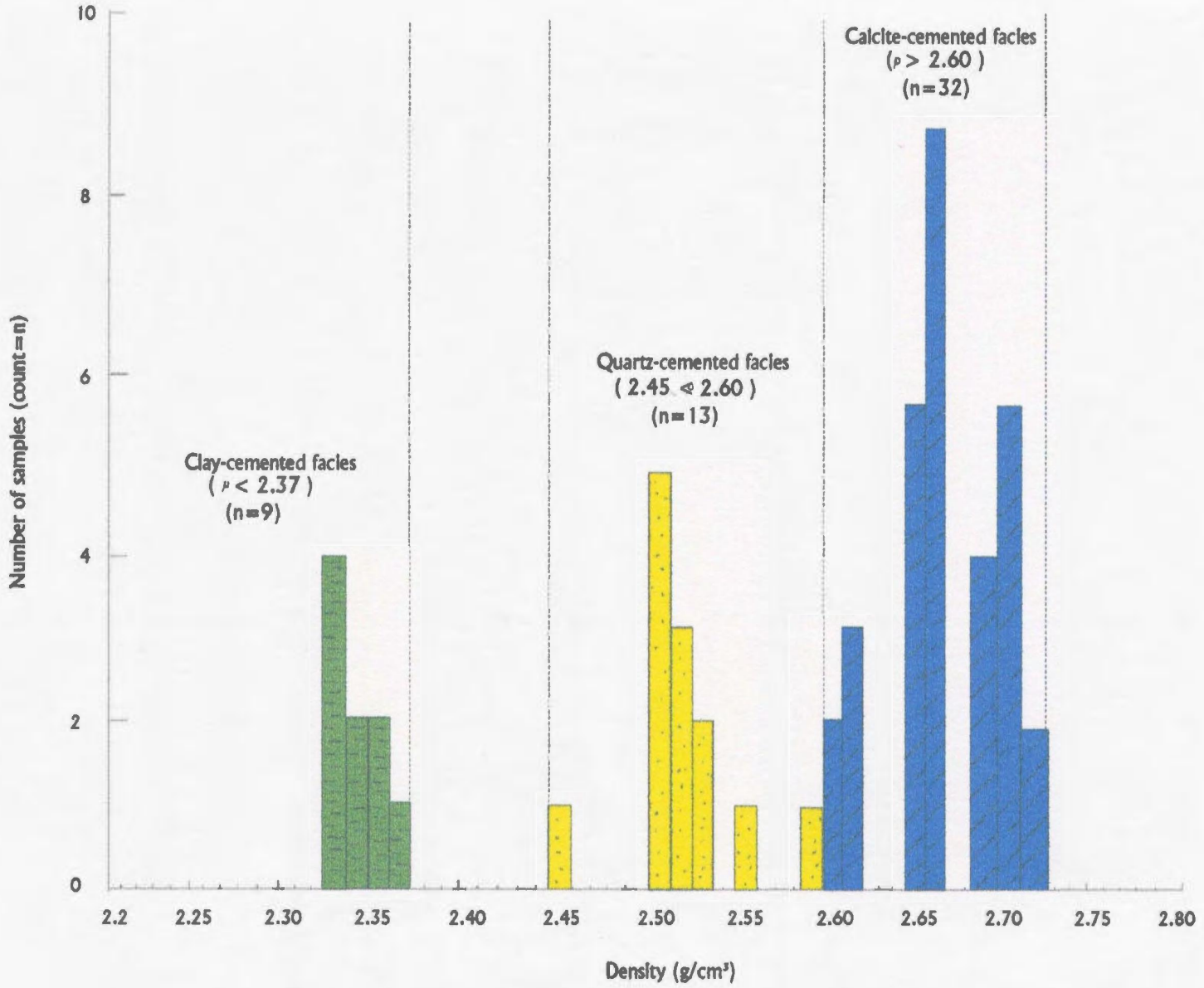

Figure 41. Histogram showing distinct ranges in density values defined by bulk density logs for each diagenetic facies in the Lower Acacus Formation, Hamada Basin, NW Libya.

Ray Log (GR) signature (Fig. 42A), or vertical stacked blocky Gamma-Ray Log (GR) signatures (Fig. 42B), or at the basal portion bottom of fining-upward sequences of smooth to serrated bell Gamma-Ray Log (GR) signatures (Fig. 42C), or at the base of stacked fining-upward sequences of successive channels of serrated bell GR-log signatures (Fig. 42D, E), or in upward coarsening sands of funnel shaped GR-log signatures which cap the fining-upward sequence of a major channel sequence (Fig. 42F).

IV.1.2 Carbonate-cemented facies:

The ***carbonate-cemented facies*** is described as any sandstone interval that contains less than 5% quarz-overgrowths and greater than or equal to 13% calcite cement, and greater than or equal to 3% dolomite cement (Table 4).

Quartz-overgrowths are rare in these sandstones (A8-A14; prograded deltaic sandstone units, and Am reworked marine sandstone units), averaging 2% of the total rock volume (Fig. 39A), whereas calcite cement is well developed, averaging 14% (Fig. 39B), and dolomite cement averages 4.3% (Fig. 39C). The total carbonate cement in this facies averages 18.3% of the total rock volume. Clay cement is poorly developed and averages only 3.5% (Fig. 39D). Grain size averages 0.145mm (Fig. 39E). Secondary porosity is common in this facies as carbonate cements (calcite, dolomite) were partially or totally leached and also by the dissolution of some unstable feldspar grains and rock fragments, averaging 12% (Fig. 39F). Measured porosity from core plugs averages 18% (Figs. 39G, 40A,B), and permeability averages 4181md (Figs. 39H, 40A,B). This is probably the highest average permeability of all of the diagenetic facies. The average log-

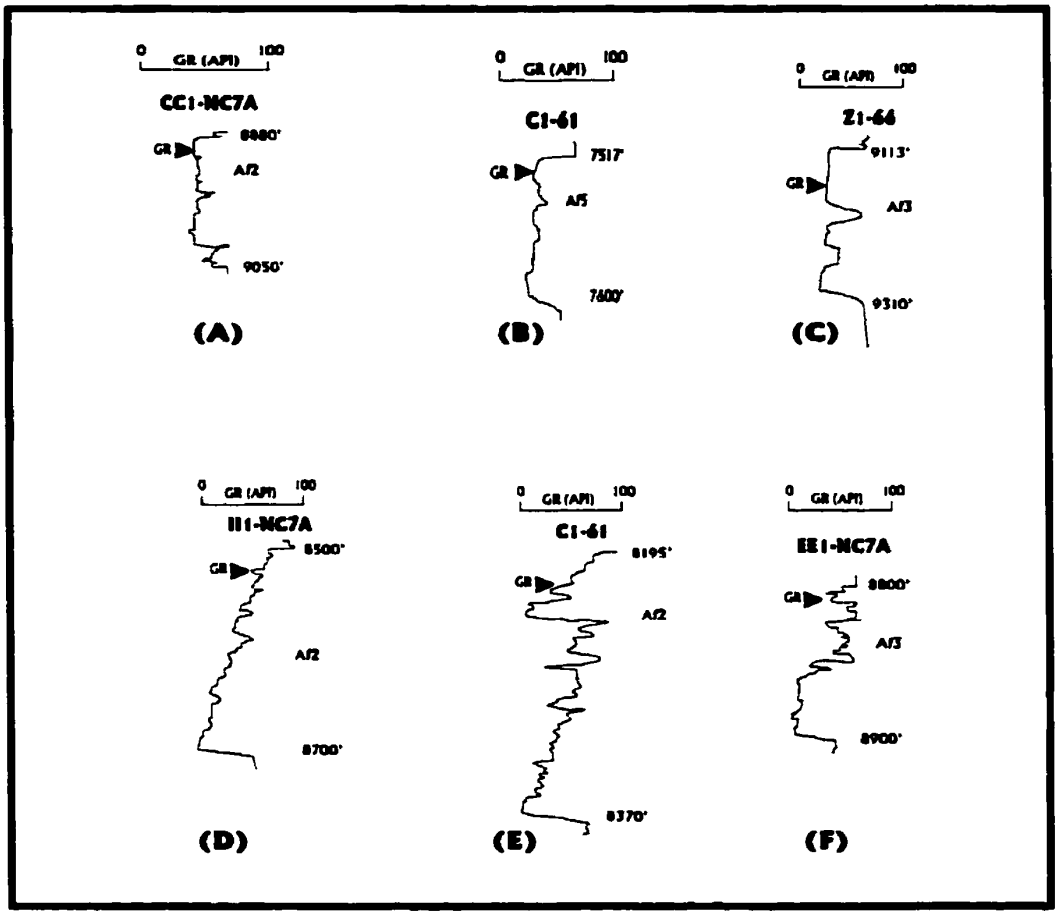

Figure 42. Gamma-ray log signature (GR) of the fluvial channel sandstone units: (A,B) quartz-cemented sandstone units (Af2, Af5) in wells CC1-NC7A and C1--61 respectively of blocky GR-log signature, (C) quartz-cemented sandstone unit (Af3) in well Z1-66 of vertical repeated blocky GR-log signature, (D) Quartz-cemented sandstone unit (Af2) in well II1-NC7A of fining-upward sequence of serrated, bell GR-log signature, (E) quartz-cemented sandstone (Af2) unit in well C1-61 at the bottom of stacked , successive channels of serrated bell Gr-log signature, (F) quartz-cemented sandstone unit (Af3) in well EE1-NC7A of fining-upward sequence capped by coarse-grained, bar-like feature sandstone. (Note: All measurements are in the units of the wells studied. Where both Metric and Imperial units are utilized they are provided).

bulk density of this facies is about 2.70g/cm^3 (Figs. 39I, 41).

This carbonate-cemented facies is often associated with the coarsening-upward sequences of deltaic origin (proximal delta front facies) characterized by smooth-serrated funnel shaped GR-log signatures (Fig. 43).

IV.1.3 Clay-cemented facies:

Sandstones that fall into the ***clay-cemented facies*** (clay-rich sediments) are described as having greater than or equal to 10% clay (Table 4). Quartz-overgrowths, calcite, and dolomite cements are not well developed in these sandstone intervals, averaging only 2%, 9%, and 2%, respectively (Fig. 39A-C). Clay cement averages 11% (Fig. 39D). Grain size in this facies averages 0.055mm (silt size) (Fig. 39E). Secondary porosity is quite variable within clay-rich sandstones associated with the distal deltaic facies in the northern part of the study area. When all clay-cemented samples are combined, secondary porosity averages 4% (Fig. 39F). However leaching secondary porosity ranges from 0% to 8%. This variability led to the heterogeneity of the authigenic phases formed in these sandstones including early authigenic calcite, dolomite, and kaolinite that precipitated within the pore-filling matrix. Measured porosity from core plugs in wells A1-NC2 @ 2382 m. (7814 ft.), 2382.2 m. (7817 ft.); E1-NC2 @ 2779 m. (9115 ft.), 2781 m. (9122 ft.); and B1-61 @ 2588 m. (8490 ft.) averages 14% (Figs. 39G, 40A,B).

Much of the porosity within clay-cemented sandstones is microporosity (Elfigih, 1991) that developed mainly within the kaolinite cement (Appendix II- Plates 22A,B.

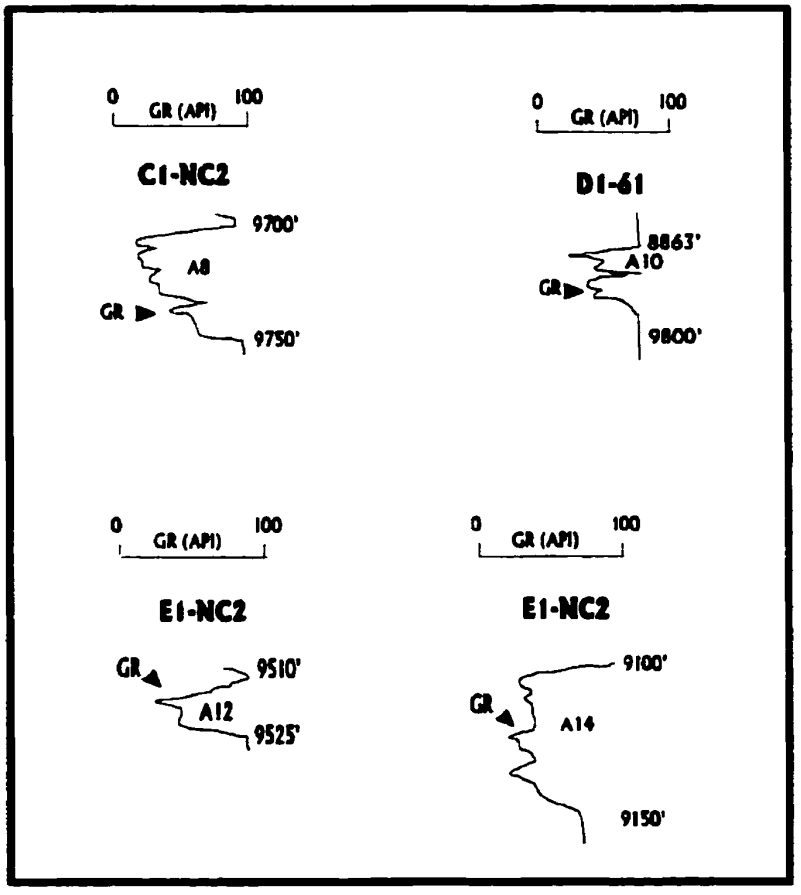

Figure 43. Gamma-ray log signature (GR) of typical proximal delta front sandstone units (A8-A14) of Lower Acacus Formation, Hamada Basin, NW Libya.
(Note: All measurements are in the units of the wells studied. Where both Metric and Imperial units are utilized they are provided).

Appendix IV- 38D). In figure 44, a measured porosity of 11% equates to a thin-section porosity of approximately 0%. This indicates the presence of significant microporosity in the clay-rich sandstones, and in particular when associated with kaolinite cement. However, the high microporosity measurement within partially clay-cemented reworked marine sandstone facies (19.6% in well Q1-23 @ 2580 m. (8461ft.), Appendix IV- Plate 38C) is not representative of effective porosity (no interconnected pore-spaces), which leads to the lower corresponding average permeability (3md) in this well (Table 4) due to the abundance of clay minerals. The average permeability for this facies is about 100md (Figs. 39H, 40A,B). The average log-density is about 2.30g/cm^3 (Figs. 39I, 41); a density which represents dispersed clay in the pore-spaces and which markedly reduces the permeability of the formation (Schlumberger, 1972). This clay-cemented facies, which is often found in distal delta front siltstones, is characterized by a spiky GR-log signature (Fig. 45A), or occasionally either a fining or coarsening upward, spiky GR-log signature (Fig. 45B) in the reworked marine sandstones.

Based on the density data and corresponding petrographic analyses (Figs 39, 41), the carbonate (calcite)-cemented facies and quartz-cemented facies are the dominant diagenetic facies within the reservoir intervals of the Lower Acacus Formation.

IV.2 Diagenetic sequences:

Due to the compositional, textural, and diagenetic fluid differences which characterize the various diagenetic facies (quartz-cemented facies, carbonate-cemented facies, and clay-cemented facies) from basin flanks to basin centre, it was necessary to

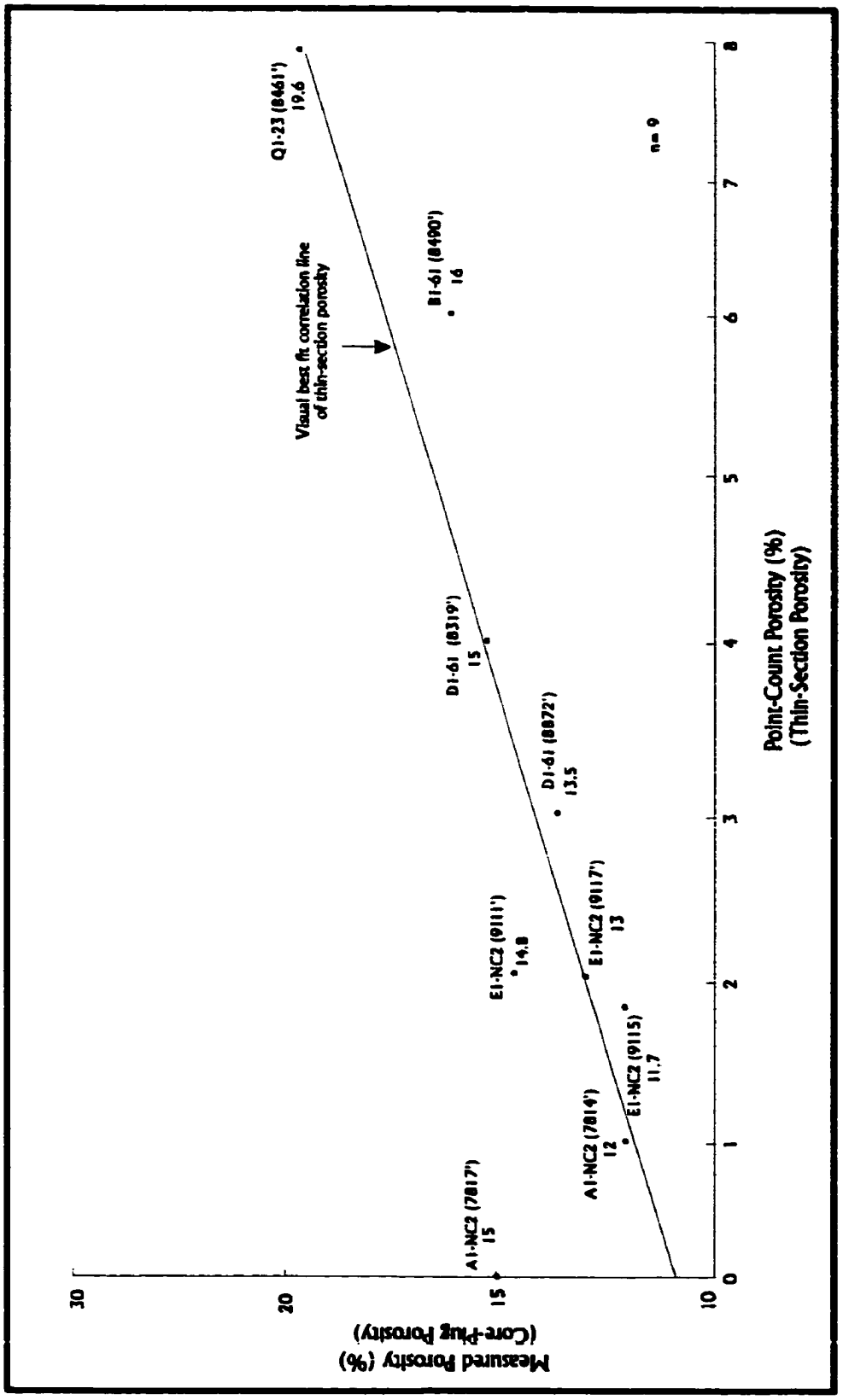

Figure 44. Measured porosity (core-plug porosity) versus point-count porosity (thin-section porosity) in clay-cemented facies. At 0% thin-section secondary porosity, the measured porosity is about 11% indicating microporosity associated with this facies . (n = number of samples).

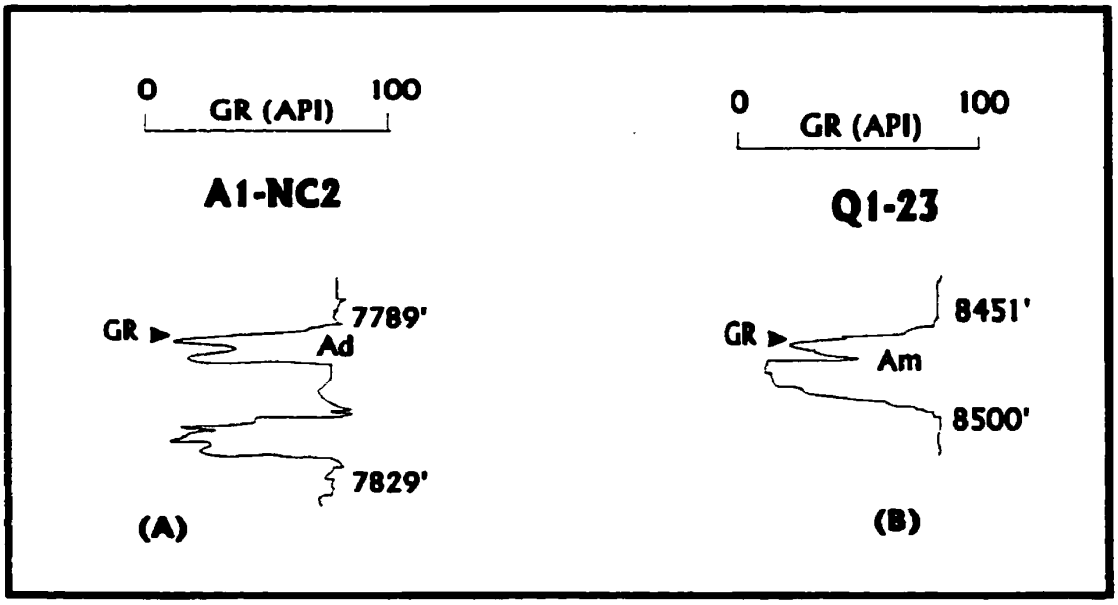

Figure 45. Spiky Gamma-ray log signature (GR) of (A) distal delta front, clay-rich siltstones (Ad units), (B) reworked marine sandstones (Am units) of Lower Acacus Formation, Hamada Basin, NW Libya.
(Note: All measurements are in the units of the wells studied. Where both Metric and Imperial units are utilized they are provided).

describe their diagenetic histories separately. However, interrelationships between the identified diagenetic sequences have to be addressed in order to develop a better history match between the different diagenetic facies.

The diagenetic sequences (Enclosure 5) for the diagenetic facies are described below:

IV.2.1 Diagenetic sequence in the quartz-cemented facies ***(Reduction of primary porosity sequence:***

The steps in the diagenetic sequence which occurred in this quartz-cemented facies are as follows:

Step 1- Iron oxides/clay matrix coatings:

The diagenetic sequence of the quartz-cemented facies (Enclosure 5) is depicted from wells dominated by fluvial sandstone units either on the southern flank of the basin (EE1-NC7A, CC1-NC7A, Z1-66, Z1-NC100, and A1-NC118), or in the eastern part of the study area (B3-61, and C1-61).

The first major step in this sequence after the deposition of quartz-rich, coarse-grained fluvial sandstones was the early precipitation of iron-oxide and clay-rich coatings directly onto the detrital quartz grain surfaces. This precipitation was due to mechanical infiltration and downward percolating oxidizing fresh water flowing through these clean sandstones. Many workers have observed similar relationships (Walker (1976), Walker et al. (1978), Rossel (1982), Seemann (1982), McBride et al. (1987), Cowan (1989), Matlack et al. (1989), and Tang et al. (1997). The occurrence of iron-oxide in the

interstitial clay matrix is quite variable throughout Lower Acacus sandstones of fluvial origin. Where iron-oxide rims are thin or poorly developed, quartz-overgrowths occur (Appendix V- Plates 40A, B). In plates 40A and 41A (Appendix V), zones of iron-oxide coating fill the bottom of primary pores, preventing silica-rich fluid from nucleating on detrital quartz grains, whereas quartz-overgrowths are grown on the top edge of the pores (pendant crystals overgrowth). This textural relationship suggests growth of crystals in fluid filled pores. Thus, quartz-overgrowths are absent in some parts of samples but abundant in others. Formation of iron-oxide coatings and quartz-overgrowths appears to be approximately synchronous in the same sample. Conceivably, the quartz-overgrowths are a later diagenetic event following incomplete development of iron-oxide rims with the increase of compaction.

Step 2- Mechanical compaction:

Grain-to-grain contact relationships as seen by petrographic and CL microscopy (Appendix II- Plates 8A,B, and Appendix III- Plates 24A,B) suggest stages of quartz grain compaction, rearrangement, and crushing of labile grains and clay clasts.

Step 3- Quartz-overgrowths:

The presence of abundant syntaxial quartz-overgrowths (Appendix II- Plates 1A, 12B, 13A) is the distinguishing characteristic in the quartz-cemented facies of fluvial origin. The mosaic of euhedral crystal faces of interlocking overgrowths is used to infer relatively early precipitation of these quartz-overgrowths while primary pore-spaces were open. There was only one quartz-overgrowth generation in this facies as suggested by the

commonly dull brown CL colours for the quartz-overgrowths (Appendix III- Plates 24A,B, 25A). The early precipitation of quartz-overgrowths exerted the most control on the shape and overall geometry of pore-spaces characterizing this facies.

In some samples pressure-solution can be observed at quartz-to quartz grain contacts (Appendix III- Plates 24A, 29A). This pressure solution appears to have occurred after the precipitation of quartz-overgrowths.

Step 4- Shallow calcite cement:

Shallow calcite cement post-dates quartz-overgrowth in most cases as it surrounds most quartz grains. The recognition of corroded quartz grains (Appendix V- Plates 42A,B) and replacement of framework grains characterized by floating remnants also suggests early cement. Early calcite cement in these fluvial sandstones was also evident by loose grain packing with intergranular primary porosity filled partially with calcite cement (Appendix V-Plate 44A,B). Petrographic observation accessional indicates that early calcite cement and iron-oxide coating may overlap in time (Appendix V- Plates 42A, 43A). This observation makes the timing of the two diagenetic components penecontemporaneous with each other to the point the relationship is occasionally (in same sample) difficult to determine.

Step 5- Shallow calcite cement dissolution:

The lack of pervasive quartz overgrowths and calcite cement in the fluvial sandstone facies set the stage whereby fluid migration pathways remained open to permit later acidic fluids to efficiently contact the framework grains and leach them (Appendix V-

Plates 42A,B, 43B).

Step 6- Feldspar grains dissolution:

Following the partial dissolution of early calcite cement as the rock was invaded by acidic water either by downward percolating rain water, channelized ground-water flowing through otherwise clean sandstones in this facies, or from other local sources such as the surrounding shale lenses, relatively unstable detrital grains such as feldspar (Appendix V- Plate 45A,B) were partially dissolved.

Step 7- Partial kaolinite cement:

Following emplacement of syntaxial quartz-overgrowths, partial calcite cement dissolution, and the feldspar grain dissolution, authigenic kaolinite cement partially precipitated in some of the remnant primary pore-spaces in this facies (Appendix II- Plate 15A, Appendix III- Plates 24A, 30B, and Appendix IV- Plate 38A). Kaolinitic cement also precipitated in small pore-spaces created by the partial dissolution of some feldspar grains (Appendix III- Plate 26A). EDS analyses indicate the presence of kaolinite cement in this facies (Fig. 24A).

Step 8- Partial illite cement:

Scanning electron photography revealed the presence of minor amounts of authigenic illite cement in this quartz-cemented facies (Appendix II- Plate 16A,B, and Appendix IV- Plate 39B,C). Illite plates or flames can be seen to have grown either on top of some remaining kaolinite booklets, or to have been directly precipitated on top of rigid quartz grains, as well as having lined pore-spaces, thereby inhibiting any further

quartz-overgrowths, and partially plugging pore-spaces.

Step 9- Iron oxides coating dissolution:

Hematitic coatings around quartz grains in deeper samples were partially removed at the end of this sequence (Appendix V- Plate 46A) by reducing fluids (less hydrated ion fluids) which bleaching the sandstones at some places and creating some modified primary porosity (secondary porosity). McBride et al. (1987) discussed a similar example of inferred dissolution of hematitic grain coatings from the fluvial Norphlet Formation of Mississippi.

Step 10- Minor partial siderite cement:

Trace amounts of siderite cement were found in this facies only in well Z1-66 @ 2768 m. (9080 ft.) as aggregates of rhombic crystals filling partially pore-spaces (Appendix II- Plate 12B; Appendix IV- Plate 37D, and Fig. 21C). The presence of this minor amount of siderite at the end of this diagenetic sequence indicates that this fluvial sandstone was bathed (locally) for sometime in alkaline pore fluids in which less hydrated Fe^{++} ions were contributed partially from dissolution of iron-oxides in the previous step with relative increase in temperature.

Step 11- Minor ferroan-dolomite cement:

Ferroan-dolomite as indicated by EDS analysis (Fig. 23C, Appendix IV- Plate 37C) in this quartz-cemented facies appears to be a minor late cement in the sequence. Dolomite occurs as rhombic crystals rooted in grain surfaces, or as cements which partially fill remaining pore-spaces in the samples (Appendix II- Plate 18A, and Appendix

V- Plate 46B). Ferroan dolomite at some depth in this facies is probably formed at the expense of early dissolved calcite cement. Its concentration is limited in part by the availability of Fe^{++} and Mg^{++} in solution which may have come from either the dissolution of early silicates in the sequence or partially from the previous step of hematite dissolution, thereby terminating the diagenetic sequence in this facies.

IV.2.2 Diagenetic sequence in the carbonate-cemented facies ***(Pore forming and modification sequence)***:

The diagenetic sequence of the carbonate-cemented facies (Enclosure 5) was recognized in wells (B1-NC2, D1-61, E1-NC2, C1-NC2, T1-23, and Q1-23) and penetrated into the various deltaic sandstone units (A8-A14), and the reworked marine sandstone units (Am).

On the basis of diagenetic evidence observed in this facies, all sandstone units are carbonate-cemented, but they can be locally different in forms of auxiliary diagenetic minerals. The occurrence of these mineralogical components was contingent upon different fluid reactions from one location to another. Therefore, each sandstone unit can have its own diagenetic sequence as the observed diagenetic events may be very pronounced in one unit but not so in others. The steps in the diagenetic sequence which occurred in this carbonate-cemented facies are as follows:

Step 1- Mechanical compaction:

In the carbonate-cemented facies of the proximal deltaic sandstones and the reworked marine sandstones, brittle grains such as quartz typically display evidence of

fracture (Plates 4B, 5B). This facies also contains a relatively large amount of deformed labile grains including clay clasts, mica, and some detrital chlorite grains (Appendix II- Plates 6A,B, 7B, 8B). Deformed grains often form matrix hashes around quartz grains (Appendix II- Plate 7B). These sandstones were cemented early by quartz and later by carbonate cements which inhibited and or arrested compaction and contact between quartz grains in early stage of their burial.

Step 2- Minor quartz-overgrowths:

The precipitation of quartz-overgrowths in quartz-rich samples (A14 in T1-23, and A12 in E1-NC2) was the earliest significant event in this facies. Before these quartz-overgrowths could become spatially extensive however, the fluid chemistry had to change (mixed water zone). It was oversaturated with respect to carbonate, and calcite cement began to precipitate instead of quartz.

Step 3- Deep calcite cement:

Deep calcite cement is the most common authigenic mineral in the central, proximal deltaic sandstone units (A8-A14), and the reworked marine sandstone units (Am). It is present in scattered fashion as pore-filling cement but also partially replaces quartz grains. Since these sandstone units were intercalated with shales with scattered marine shell fragments, pressure-solution of these skeletal grains in the shale was a source of carbonate for the calcite cement which formed within these units. Textural relationships represented by the well-packed grains in the calcite-cemented samples of these sandstone units suggest that this step of cementation followed quartz-overgrowths and these grains

were cemented by calcite after appreciable compaction (Appendix II- Plates 10B, 11B). EDS analyses (Fig. 22B) show that this calcite cement contains trace amounts of iron.

Step 4- Ferroan-dolomite cement:

With increased basin temperature, late calcite cement was followed by partial ferroan-dolomite cement, especially at the top of some sandstone units. Ferroan-dolomite cement occurs as partially rimming quartz grains, or as pore-filling euhedral rhombs replacing calcite cement (Appendix II- Plates 11B, and Appendix V- Plate 47A).

Step 5- Fracturing:

Various fluids (with oxygen isotopic ($\delta^{18}O$) values between 14.1-24.5‰, Table 6) moved through the Lower Acacus sandstone units of the deltaic origin by means of minor/major fractures associated with uplift of the northern part of the basin during the Hercynian orogeny. Fractures in both quartz grains and cements were recognized in this facies in various wells (B1-NC2, C1-61, A1-NC2, Q1-23, and B3-61) which were partially filled with authigenic clays (Appendix II- Plate 23A,B, and Appendix V- Plates 61A,B, 62A,B).

Step 6- Dissolution of carbonate cements:

Following this fracturing, the formation water was diluted by mixed meteoric and acidic waters (mixed waters). Dissolution of carbonate cements (calcite/dolomite) took place, thereby enhancing the existing porosity (modified porosity) (Appendix V- Plates 51A,B, 56A,B, 60A,B).

Step 7- Dissolution of feldspar grains:

The diluted mixed waters in the deltaic sandstone units also promoted the partial or total dissolution of unstable feldspar grains at some locations (A8 unit in C1-NC2, and A12 unit in B3-61) enhancing the secondary porosity in these units (Appendix V- Plates 45A,B, 52A,B, 53A,B, 54A,B, 55A).

Step 8- Partial kaolinite cement:

In this step, dissolution of unstable feldspar grains resulted in re-precipitation as authigenic kaolinite cement (Appendix III- Plate 28B). The pore-spaces in this facies have been partially filled by this authigenic cement (Appendix IV- Plate 38B, Fig. 22B). Subsequently, secondary pores developed as the kaolinite cement was partially dissolved; especially in the reworked marine sandstone units (Am) in well Q1-23, where it can be seen that the development of microporosity was associated with kaolinite cement. This microporosity is often filled with oil droplets (Appendix II- Plate 14B, and Appendix IV- Plate 38C).

Step 9- Oil migration:

Oil occurs at the top of nearly every sandstone unit of this facies (proximal delta front sandstones and reworked marine sandstones). This oil apparently was emplaced in pore-spaces that originated by the leaching of carbonate cements, and by dissolution of some grains (Appendix V- Plate 63B), and in microporosity associated with partially kaolinized units (Appendix II- Plate 14B, and Appendix V- Plate 64A,B). Therefore, oil migration to the reservoir pore-spaces of the carbonate-cemented facies of deltaic origin

inhibited further cementation.

IV.2.3 Diagenetic sequence in the clay-cemented facies *(Pore filling sequence)*:

The clay-cemented facies is represented by samples from the distal deltaic siltstones ("Ad" units in wells D1-61, A1-NC2, and E1-NC2) (Appendix I, Appendix II- Plates 21B, 22A,B) deposited in low-energy conditions in deeper parts of the basin. Authigenic clay cements have greatly reduced the porosity and permeability of the siltstone units in this facies. These siltstone units had much lower initial permeability than the sandstones of fluvial and proximal deltaic origin, and underwent less pore-fluid movement which inhibited the early nucleation of quartz-overgrowths.

The diagenetic sequence characterizing this facies is quite different than the diagenetic sequences of the quartz and carbonate cemented facies. The diagenetic differences in this facies were controlled by original composition and texture of the units, their fluid types, and their basinal stratigraphic position. The steps in the diagenetic sequence which occurred in this clay-cemented facies are as follows:

Step 1- Partial deep calcite cement:

Basinal fluids became oversaturated with respect to carbonate as the fluids percolated down through the distal deltaic siltstones. The very-fine quartz grains and clay-rich materials are selectively cemented partially by calcite cement.

Step 2- Fracturing:

Local fractures which are not diagenetic in origin were encountered in this facies, especially in well A1-NC2 (Appendix II- Plate 23A,B). These fractures may contribute

locally to connecting isolated residual pore-spaces to permit some fluid movement through the unit. This fluid movement did not last as these fractures were plugged partially by authigenic clay cements during the later steps of this sequence.

Step 3- Dissolution of calcite cement:

In many instances calcite cement has been dissolved leaving tiny pores which subsequently were filled partially or totally with authigenic kaolinite cement (Appendix II- Plate 21B).

Step 4- Total kaolinite cement:

Authigenic kaolinite cement observed in this facies apparently precipitated and blocked pores created by dissolution of calcite cement, unstable grains, and some mixed clay laminations (Appendix II- Plate 22A,B). SEM photograph (Appendix IV- Plate 38D) shows exactly the development of kaolinite booklets which totally filled microporosity. EDS analyses and XRD-analysis (Figs. 24C, 32, 33) suggested the kaolinite mineralogy and its presence in this facies.

Step 5- Partial illite cement:

Some of the kaolinite cement and matrix materials along with possible leaching of potassium feldspar which increased the K^+ concentration in the pore water were apparently responsible for the formation of partial illite cement which recrystallized across and on top of kaolinite booklets (Appendix II- Plates 21B, 22A),

$$[\underset{\text{Kaolinite}}{3Al_2Si_2O_5(OH)_4} + \underset{\text{in solution}}{2K^+} \rightarrow \underset{\text{Illite ppt.}}{2KAl_3Si_3O_{10}(OH)_2} + 2H^+ + 3H_2O].$$

Late illite cement in these distal deltaic siltstone units (Appendix IV- Plate 38D),

indicates that illite precipitated after kaolinite.

Step 6- Minor ferroan-dolomite cement:

As temperature increased with depth to >90°C, residual iron ions from dissolved clays were mobilized due to mixing with acidic water available in this facies. In addition, the environment of this facies at high temperature was typically reducing, favouring formation of mineral phases that contain reduced iron such as ferroan-dolomite which would become stable, partially filling the tiny pore-spaces.

$$[\underset{\text{dolo.cement}}{CaMg(CO_3)_2} + \underset{\text{in solution}}{Fe^{++}} \rightarrow \underset{\text{ferr.dolo.ppt.}}{MgFe(CO_3)_2} + \underset{\text{in solution}}{Ca^{++}}].$$

XRD-analysis (Fig. 32) indicates the presence of high iron peaks in this facies.

Based on the identified mineralogical components in the clay-cemented facies, their reactions with the existing fluids, and the observed diagenetic sequences of events, the ferroan-dolomite cement is interpreted to have formed at the end of this sequence.

IV.2.4- *Summary* of diagenetic sequences:

In the study area the diagenetic sequences in the quartz-cemented and clay-cemented facies were influenced primarily by these initial sandstone compositions and textures determined by depositional environment. The diagenetic sequences of the carbonate-cemented facies were determined primarily by the stratigraphic position of these sandstone wedges adjacent to the calcareous shale interbeds, and by local fractures which permitted inter- and intraformational fluid movements leading to porosity enhancement.

IV.3 Porosity evolution, distribution and diagenesis:

Primary porosity (i.e initial porosity at the time of deposition) usually persists after burial until complete pore filling by either mechanical compaction or cementation. Secondary porosity develops as a result of modification of primary porosity caused by dissolution of cements and framework with the addition of porosity associated with fractures and grain cracks (Schmidt and McDonald, 1979).

The major types of porosities in the Lower Acacus Formation have a regional distribution (Figs. 40A, 46A-D) related to the grain framework and cement types in each depositional environment of the Lower Acacus Formation in the Hamada Basin.

Secondary porosity evolution in sandstones has been the focus of many investigations of the past decade, with several mechanisms of secondary porosity evolution and development being proposed. Schmidt and McDonald (1979); Al-Shaieb and Shelton (1981); Larese et al. (1984); Loucks, Dodge, and Galloway (1984); and Franks and Forsester (1984) emphasized the role of CO_2 in leaching of both detrital and autigenic sandstone constituents and the formation of CO_2 resulted from decarboxylation of organic acids during thermal maturation. However Surdam et al. (1984) suggested that the generation of organic acids during the maturation of kerogen in source rock shales is the main process to generate secondary porosity at depth. Bjorlykke (1979) and Markert and Al-Shaieb (1984) demonstrated that meteoric and groundwater (subsurface water) leaching of rock constituents are an important mechanism in secondary porosity development in sandstone reservoirs.

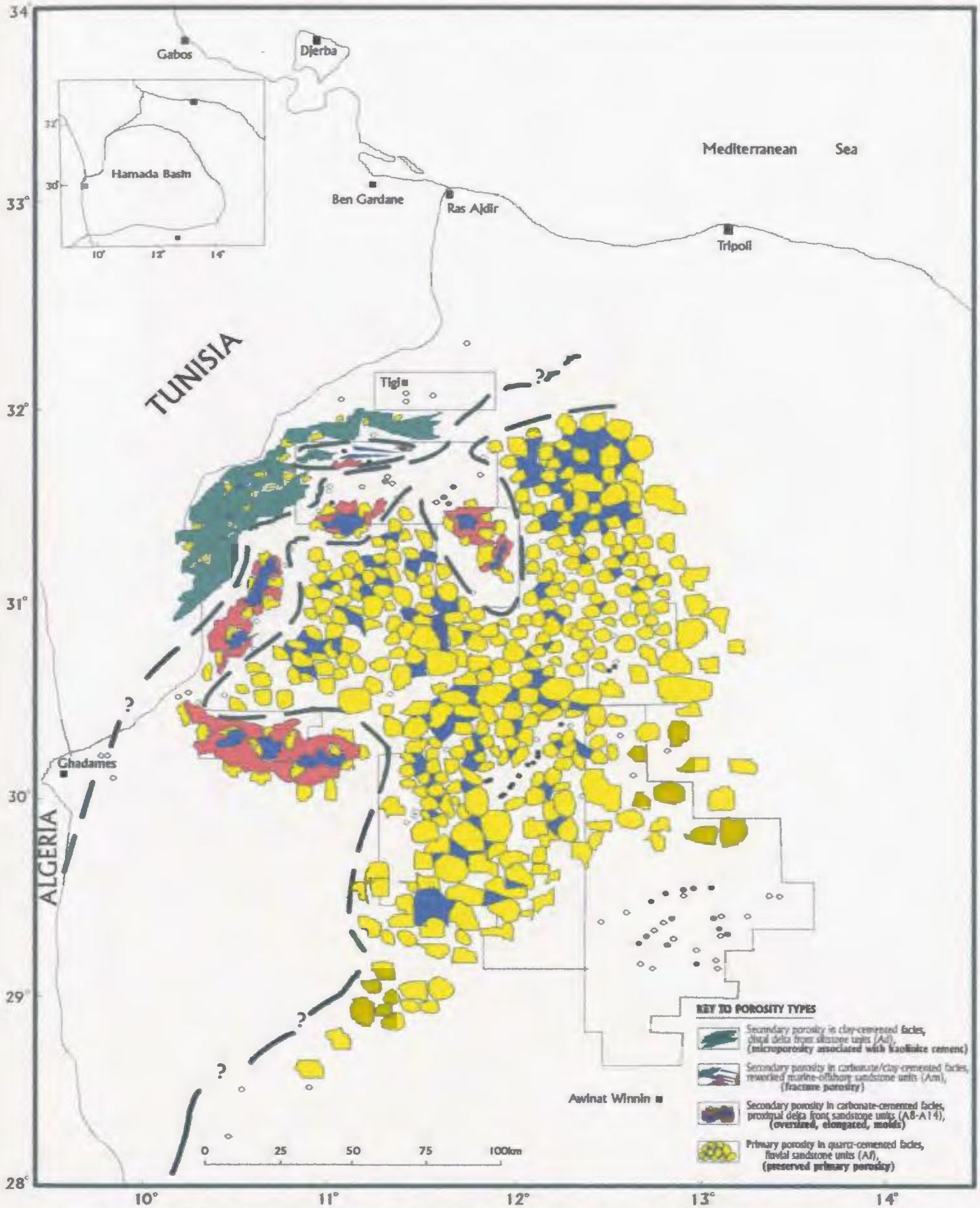

Figure 46A. Regional representation of the dominant porosity types in A8 sandstone unit of Lower Acacus Formation, Hamada Basin, NW Libya.

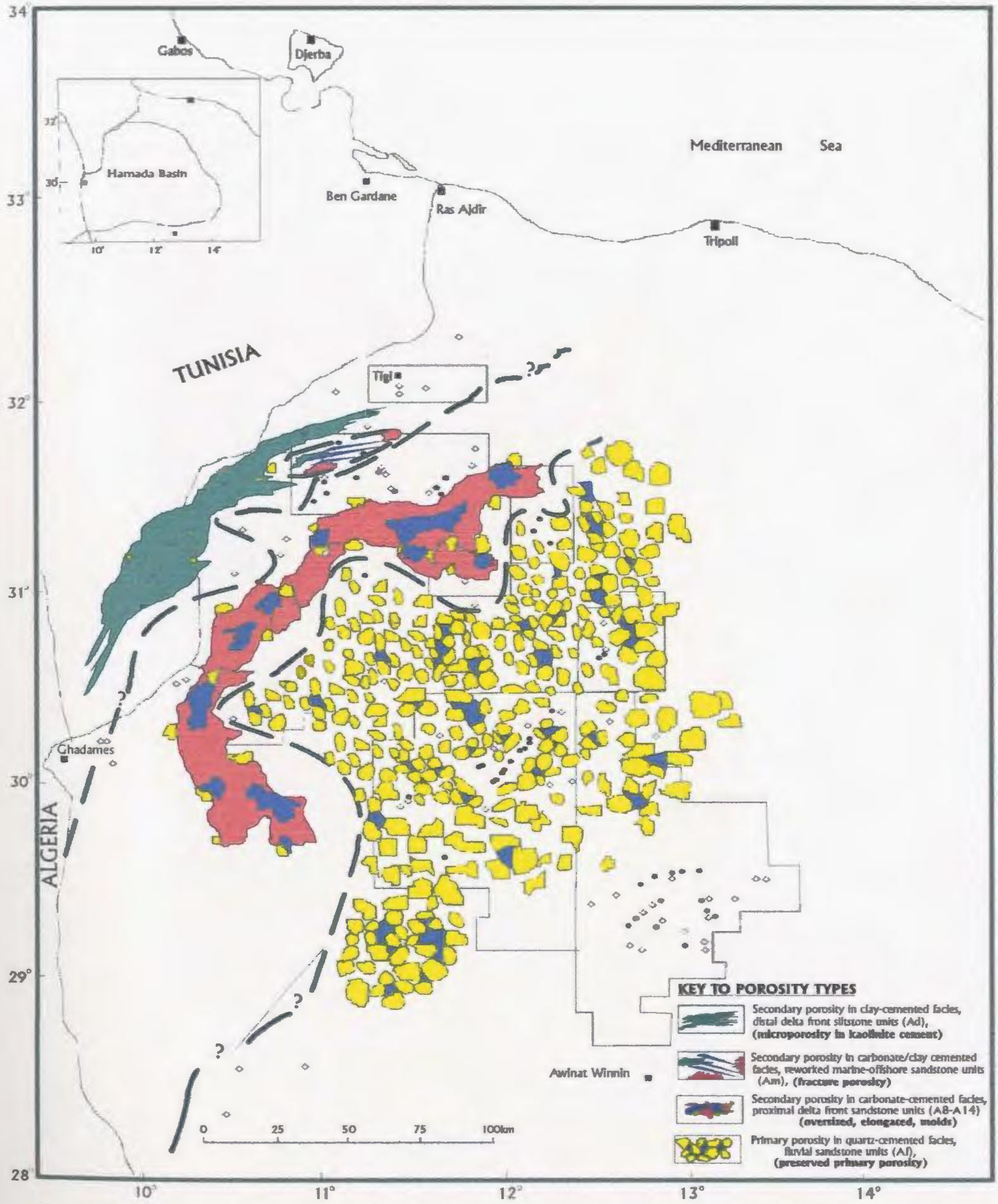

Figure 46B. Regional representation of the dominant porosity types in A10 sandstone of Lower Acacus Formation, Hamada Basin, NW Libya.

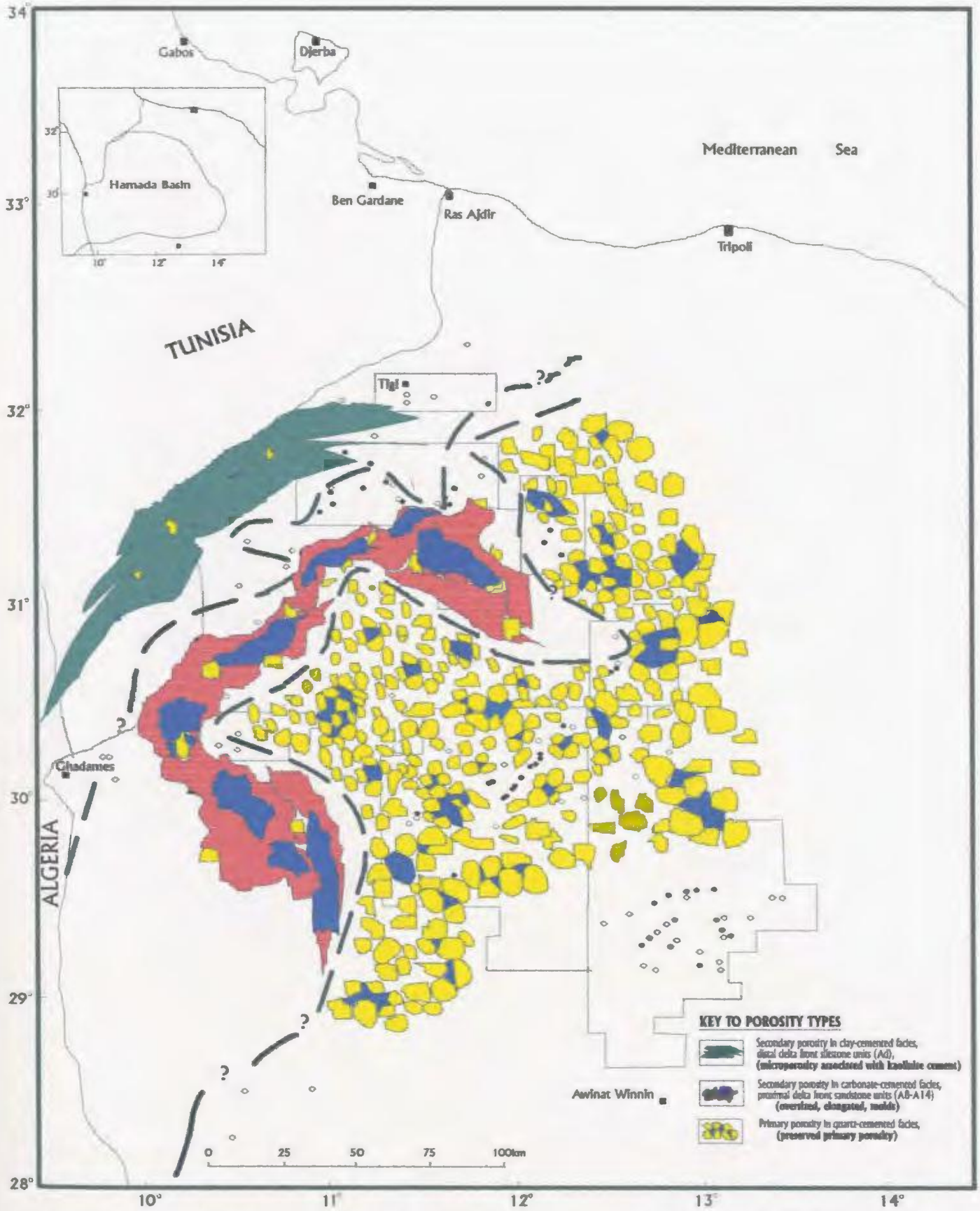

Figure 46C. Regional representation of the dominant porosity types in A12 sandstone unit of Lower Acacus Formation, Hamada Basin, NW Libya.

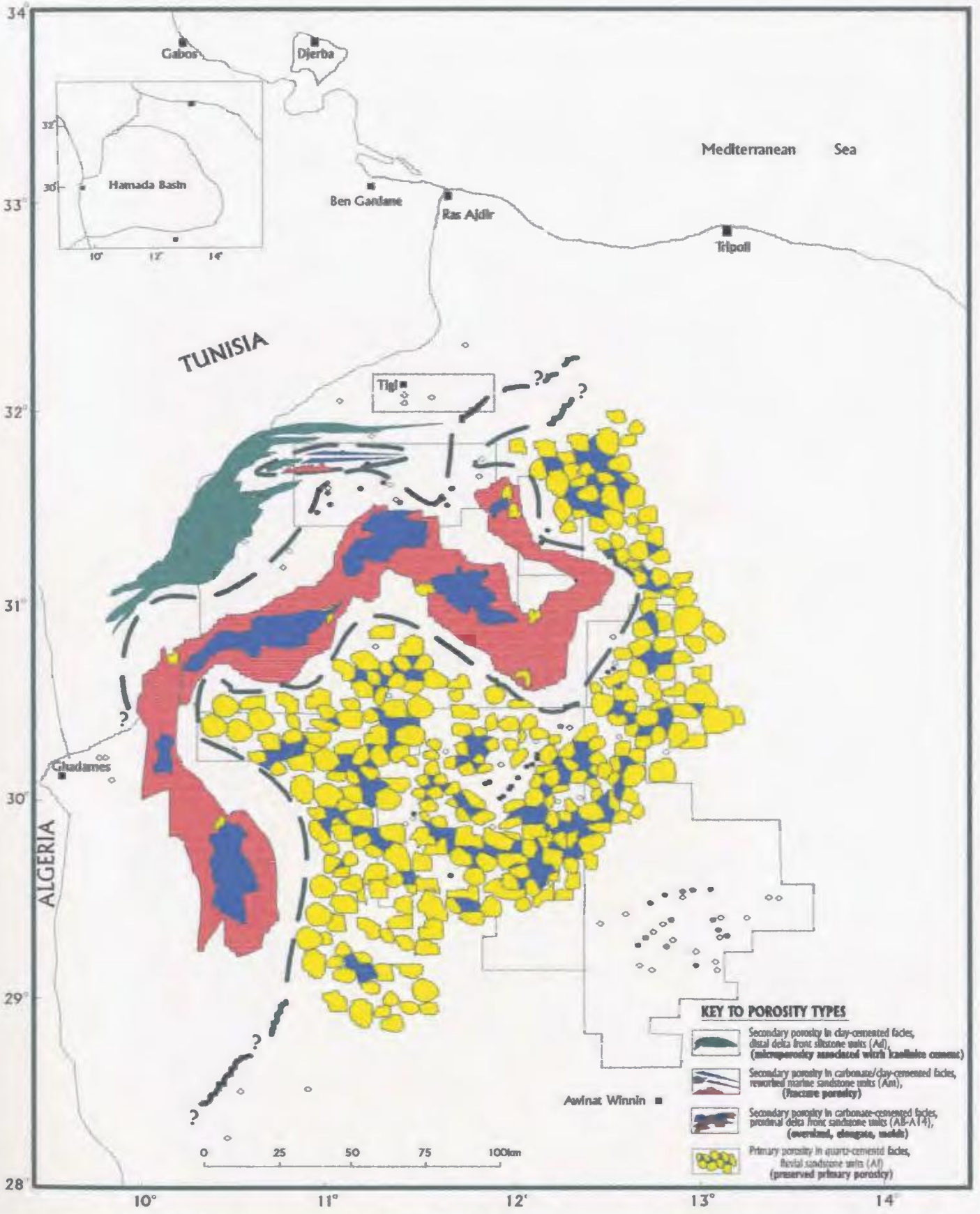

Figure 46D. Regional representation of the dominant porosity types in A14 sandstone unit of Lower Acacus Formation, Hamada Basin, NW Libya.

Two important parameters were examined to produce a comprehensive model for the evolution and development of secondary porosity in the Lower Acacus Formation in the deeper part of the Hamada Basin:

1- the type of lithologies and textures of sandstones in each facies of the Lower Acacus Formation, and

2- the nature of the leaching fluid associated with each facies.

Petrographic observation suggests that porosity enhancement is due mainly to total or partial dissolution of calcite/dolomite cements, and/or total or partial removal of unstable framework components from the general rock fabric. The unstable framework components include detrital feldspars and skeletal materials or detrital clay clasts.

The Lower Acacus Formation exhibits various types of lithologies; from quartz supported sandstones of fluvial origin, to sandstones/siltstones of proximal-distal deltaic origin, and to reworked sandstones of marine origin (Figs. 9-11A-D, Enclosures 3, 4). These lithologies consist of a wide variety of sand types, including quartzarenites, sublitharenites, and occasionally litharenites (Fig. 15). These sandstone/siltstone lithologies, when they come in contact with meteoric water would have been affected by:

a) the relative amount of dissolved cements (calcite, dolomite), and metastable framework grains (feldspars, skeletal materials, and clay clasts), and

b) the textural parameters such as grain size, sorting, and packing which mainly affect the initial porosity.

The development of secondary porosity or enhancement of initial porosity was

accomplished by the reaction of leaching fluids with unstable rock constituents (either cements or grains). The most significant property of the fluid is the acidity or the availability of H^+ ions for reaction, supplied by:

- organic acids and carbonic acid (Carothers et al., 1978; Surdam, Boese and Crossey, 1984)
- mainly carbonic acid that formed by decarboxylation of organic acids (Takenouchi and Kennedy, 1965; Schmidt and McDonald, 1979a; Shanmugam, 1985; Al-Shaieb and Walker, 1986).
- possible hydrogen sulfide (H_2S) associated with hydrocarbon zones and other sulfur-bearing materials at high temperature (>200°C) (Andreev et al., 1968). This would not have been applicable to the Hamada Silurian source rock (Tanezzuft shale) because the temperature of the Saharan Silurian Shale source rock in the Hamada (Ghadames) Basin was between 136°C and 146°C (R_0 = 1.082-1.267%) (Makhous et al., 1997).
- fluid flow through unconformity surfaces (Krynine, 1947; Hancock and Tylor, 1978; Sommer, 1978; Bjoriykke, 1982).

Because carbonates dissolve readily in acidic solutions, the pH of interstitial fluids is an important control on solution and precipitation (eg. Curtis, 1978; Schmidt and McDonald, 1979; Longman, 1981; Moore and Druckman, 1981; Morse, 1983; Boggs, 1987; and Prothero and Schwab, 1996). Most natural waters associated with carbonates are slightly basic so it takes some "unusual" event such as shale dewatering or high CO_2

content to create acidic conditions in which H^+ ions will be released (Longman, 1981). Solution pH is linked in turn to the partial pressure of dissolved carbon dioxide in the water, as illustrated by the following reactions (Boggs, 1987):

$$CO_2 + H_2O \rightleftharpoons H_2CO_3 \text{ (carbonic acid)} \quad \text{(I)}$$

$$H_2CO_3 \rightleftharpoons H^+ + HCO_3^- \text{ (bicarbonate ion)} \quad \text{(II)}$$

$$HCO_3 \rightleftharpoons H^+ + CO_3^{2-} \text{ (carbonate ion)} \quad \text{(III)}$$

These reactions show that the dissolved carbon dioxide in water and the formation of carbonic acid (I), then dissociation of carbonic acid to hydrogen ions and bicarbonate ions (II), and further dissociation of bicarbonate ions to hydrogen ions and carbonate ions (III) and release of free hydrogen ions, thus lowering the pH of the solution. If calcite cement in sandstones is allowed to react with a carbonic acid solution, this calcite cement will readily dissolve, hence, secondary dissolution porosity will be developed. This reaction can be summarized as:

$$H_2CO_3 + CaCO_3 \text{ (calcite cement)} \rightleftharpoons Ca^{2+} + 2HCO_3^-$$

With this preceding discussion as background one can focus on the possible source of H^+ ions (acidic leaching fluid) at the level of the Lower Acacus Formation. No data on organic acid concentration have been reported from subsurface fluids recovered through Drill-Stem Tests (DST) in the Lower Acacus Formation. However, it is reasonable to assume that organic acids formed during thermal maturation of the Tanezzuft shale as the Hamada Basin subsided and under a sediment thickness of approximately +1524 m. (+5000 ft.) overburden during pre-Hercynian time (Ghori, 1982).

The composition of natural gases recovered as recorded on gas-chromatograph during drilling of the Lower Acacus Formation has been reported in DST results, and on mud-logs against the tested intervals (Table 8). Data concerning the abundance and recovery of CO_2 in the natural gases and from Rock-Eval pyrolysis of samples from the Tanezzuft shale were obtained from BEICIP (1972-1975) and Ghori (1982).

Figure 47 illustrates the relationship between depth and mole % CO_2 of the approximate amount of recovered CO_2 from natural gases associated with the drilling of Acacus sandstone units in wells in the Hamada Basin. The content of CO_2 in recovered natural gases tends to increase with depth. In addition, the data show two major clusters or groups of wells representing relatively low CO_2% in natural gases in the basin margin area, and CO_2% increasing basin-ward. The same relationship is demonstrated by CO_2 zone correlation (Fig. 48) across the Hamada Basin. It is interesting to note the similarity between mole % CO_2 distribution (Fig. 49) and the configuration of the basin (Figs. 50A,B). Rock-Eval pyrolysis data (Table 9) for well GG1-NC7 (Ghori, 1985) in which there is an increase of T_{max} values (Thermal maturation index) with S_3 (amount of carbon dioxide formed by thermal breakdown of kerogen in the shales of Tanezzuft Formation) with depth suggests a genetic relationship between CO_2 gas and Tanezzuft shale. This additional source of CO_2 in the deeper part of the Hamada Basin may reflect degassing of the Cambro-Ordovician Memouniat Formation in wells A1-NC2 and B2-NC2.

Takenouchi et al. (1965), Hunt (1979), Galloway et al. (1982), and Bjørlykke, (1984) show that the solubility of CO_2 in water is dependent on the temperature, pressure

Table 8 . Natural gases recovered either during drilling or from Drill-Stem Tests (DST) of some sandstone intervals in wells which penetrated the various Paleozoic Formations of the Hamada Basin, NW Libya.

Well Name	Interval (ft)	Formation	Total Gas units (During drilling)	Gas-type	R e m a r k s
A1-NC2	8232-8340	Lower Acacus	30-70	C1-C4	(100 total gas units is equivalent to 2% methane-in-air)
	8604-8690	"	80-100	"	traces of gas in sampler PT#2 @ 8614-8644'.
	8770-9808	Tanezzuft	50-80	"	
	10040-10090	Memouniat	10-20	C4	In sample chamber PT#1, rec.6.8cu.ft of gas @ 320psi.
B1-NC2	8272-8319	Lower Acacus	20-50	C1-C4	
	8810-8940	"	50-80	"	
B2-NC2	8210-8250	"	80-100	"	
	8910-8990	"	20-30	"	
	10365-10460	Memouniat	80-100	"	
C1-NC2	8825-9010	Middle-Lower Acacus	20-50	"	In sample chamber DST#1, rec.2.11cu.ft of gas @ 10psi.
	9472-9590	Lower Acacus	40-80	"	In sample chamber PT#1, rec.4.11cu.ft of gas @ 250psi.
	10590-10640	Tanezzuft	10-40	"	
E1-NC2	9110-9140	Lower Acacus	20-50	"	In sample chamber DST#1, rec.0.15cu.ft of gas @ 5psi.
	9550-9580	"	80-100	"	In sample chamber PT#4, rec.1.70cu.ft of gas @ 10psi.
	9950-9972	"	50-80	"	In sample chamber PT#1 rec.0.25cu.ft of gas @ 15psi
F1-NC2	7910-8022	Middle-Lower Acacus	20-50	C4	(0.0015 psi/ft.)
	8035-8095	Lower Acacus	30-60	C1-C4	
	8520-8550	"	10-30	C4	
	8850-8892	"	80-90	C1-C4	
	8980-9070	Lower Acacus-Tanezzuft	80-100	"	
B3-61	9335-9450	"	2-4	C4	
C1-70	7920-7945	Lower Acacus	100	C1-C4	In sample chamber PT#3, rec.0.20cu.ft og gas @ 20psi
	8080-8110	"	80	C4	(0.002 psi/ft.).
A1-NC118	10040-10058	"	3-8	C1-C4	during preliminary build-up.
	10196-10250	"	1-7	"	
	10354-10374	"	1-7	"	
	10400-10438	"	1-3	"	
DD1-NC7A	5855-6100	Tahara	2	C4	
	6220-6400	Aouinat Ouenine C-8	2	"	
	6675-6900	Aouinat Ouenine A-Ouan Kasa	4	C1-C4	
	6905-7322	"	2	C4	
	7340-7410	Tadrart	4-8	C1-C4	
	7805-7870	Acacus South	2	C4	
	8735-8760	"	0.5-1	"	In sample chamber rec.0.15cu.ft of gas @ 10psi.
EE1-NC7A	8875-8950	"	80-100	C1-C4	

(Note: All measurements are in the units of the wells studied. Where both Metric and Imperial units are utilized they are provided. 1 psi = 6.895 kPa.).

(Data as reported in well-mud-logs, and chromatograph charts, TDL-AGOCO, Benghazi, Libya, 1961-1986).

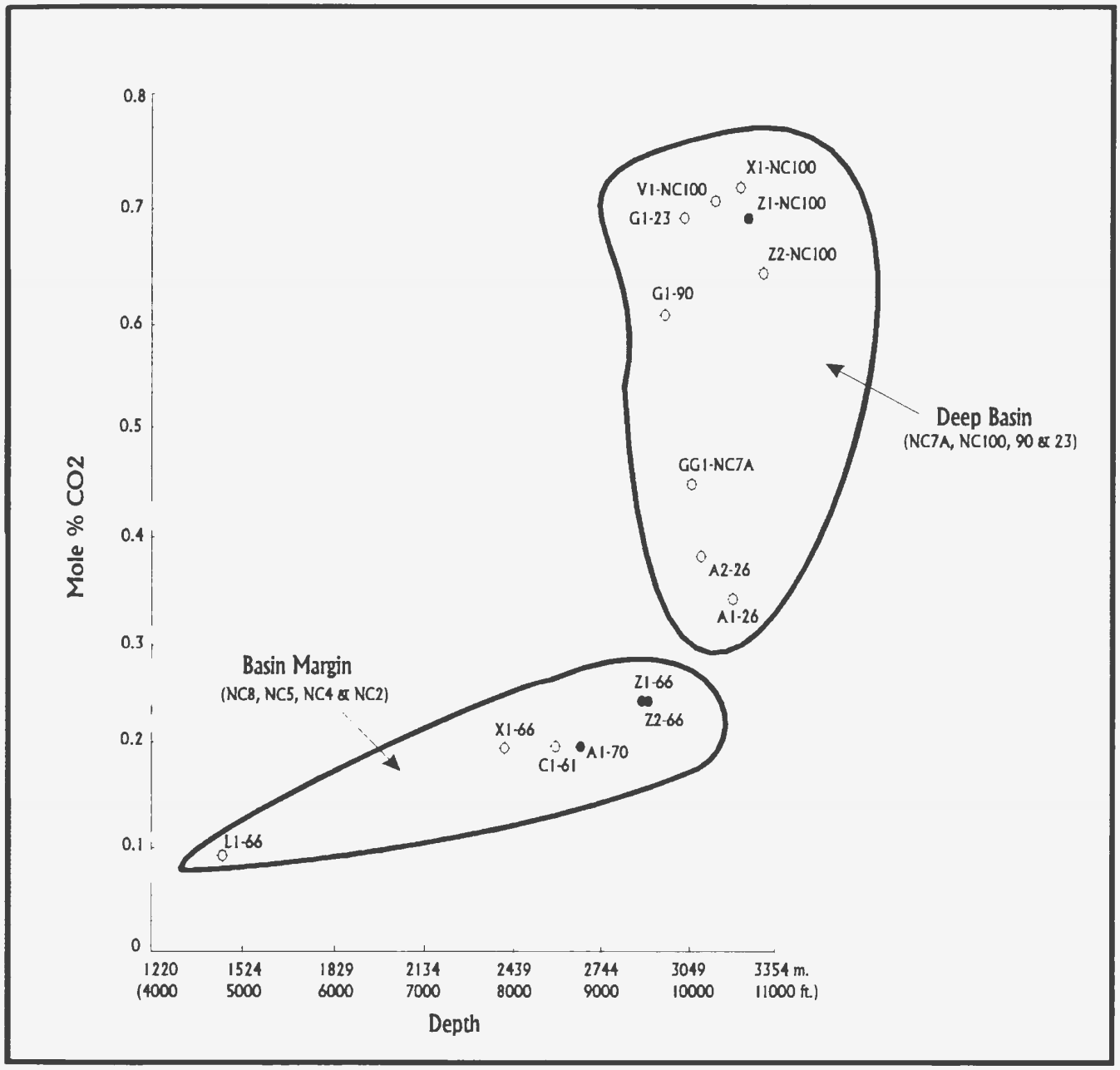

Figure 47. Variation of mole % CO2 of natural gases recovered during drilling of Acacus and Tanezzuft Formations with depth, Hamada Basin, NW Libya. (See figure 12 for well locations).

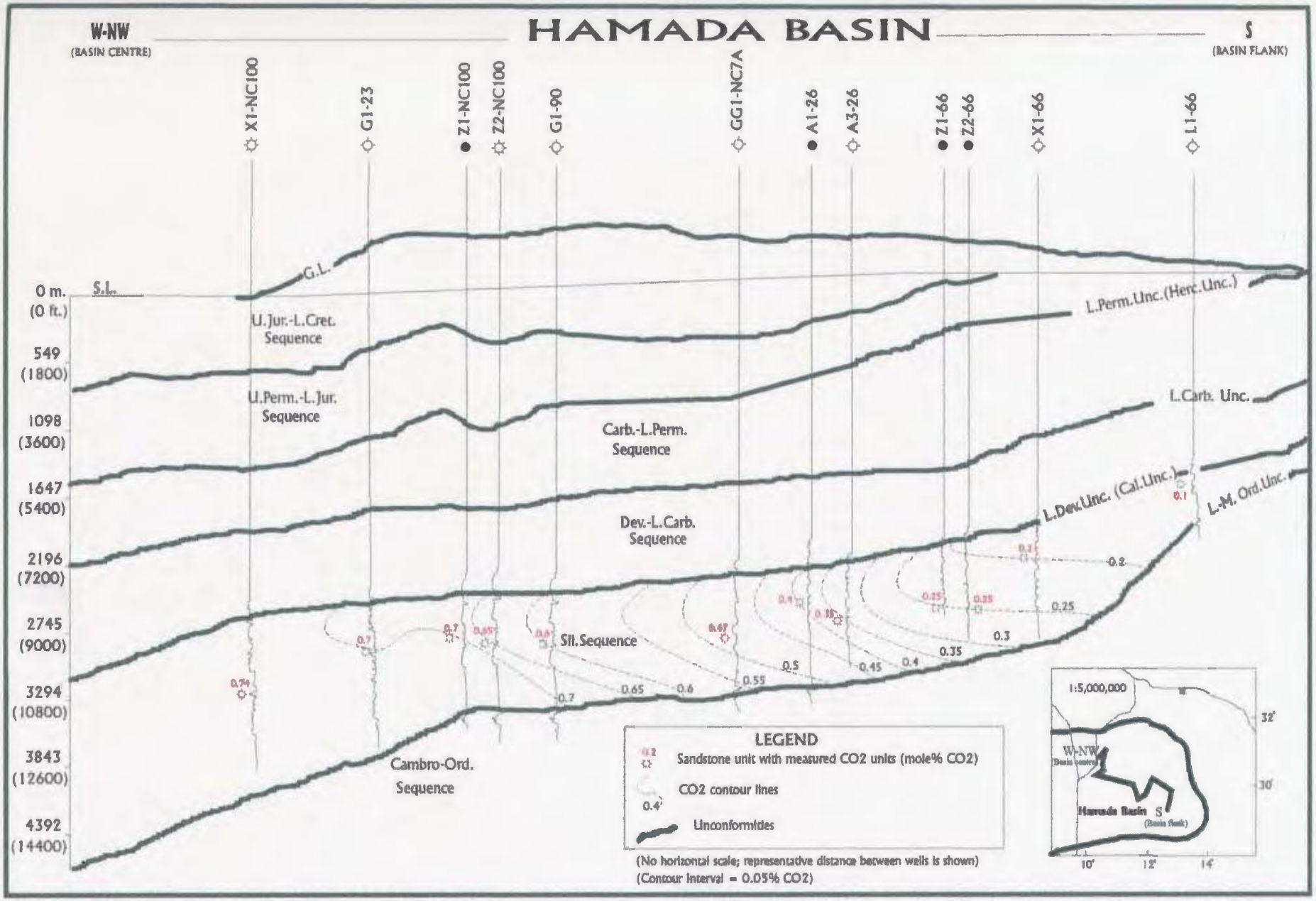

Figure 48. Zone correlation of mole% CO2 in natural gases recovered from Silurian sequence, Hamada Basin, NW Libya. Note decrease of CO2 concentration towards the basin flank as a function of fresh water penetration (see map 49 for location of wells and cross-section, and map 53 for comparison).

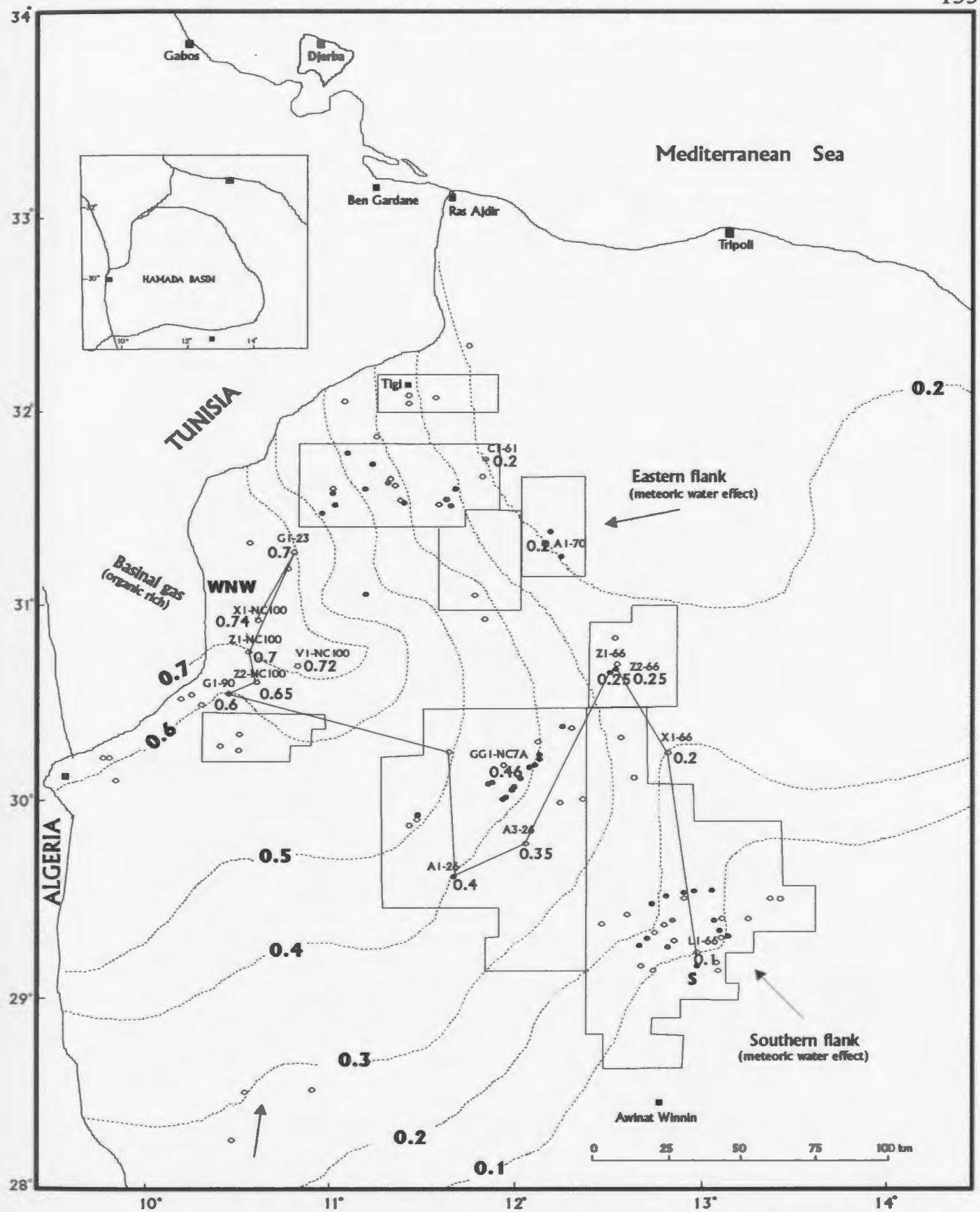

Figure 49. Distribution of mole% CO2 in natural gas recovered in some wells during drilling of Lower Acacus Formation, Hamada Basin, NW Libya. (Data source from Ghori (1982, 1985), some DST reports, and Chromatograph-mud log descriptions). (See Figure 48 for details of zone correlation of mole % CO2 along the line S-WNW). along the line S-WNW).

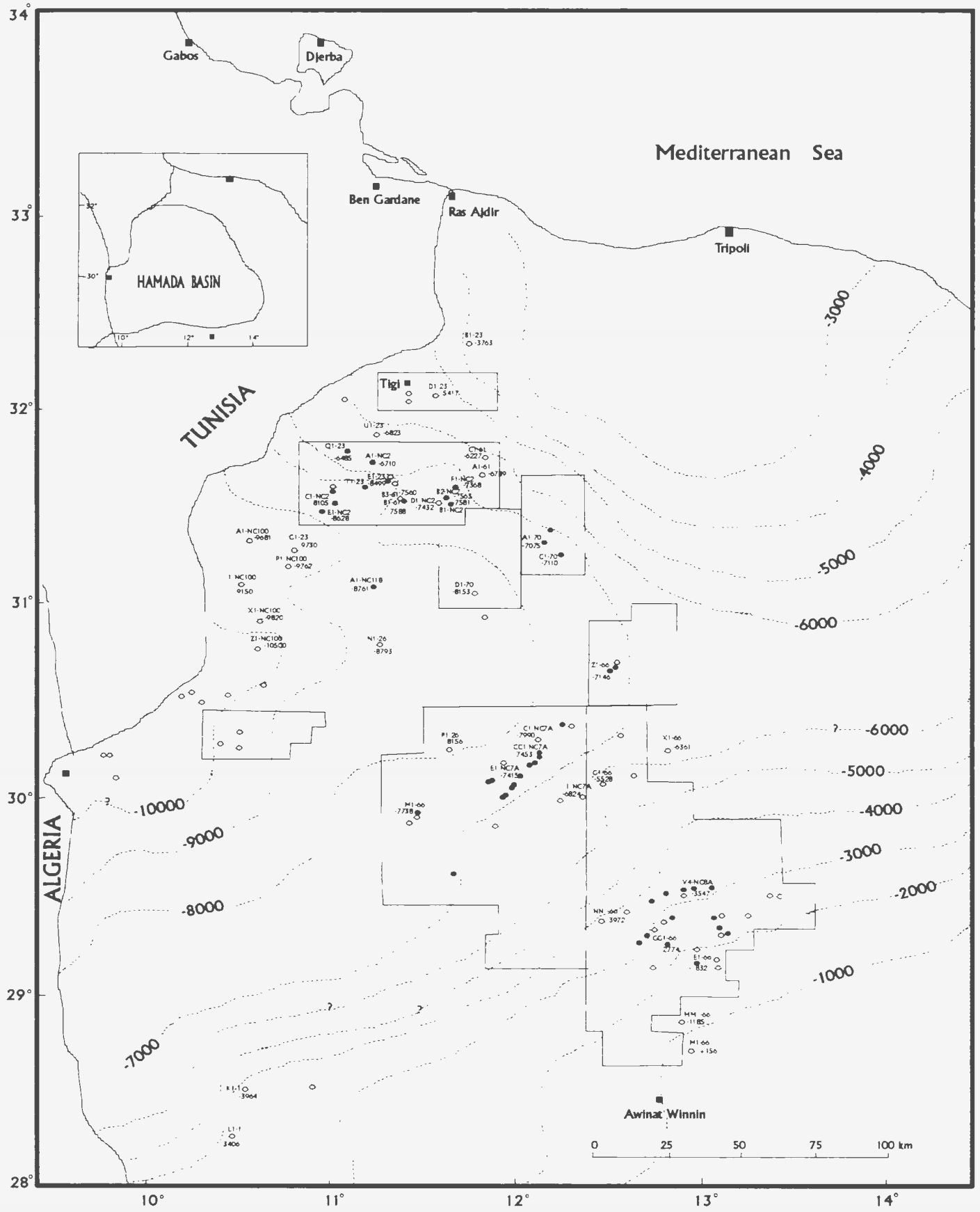

Figure 50A. Structure map on top of the Tanezzuft Shale, Hamada Basin, NW Libya. (Data based on drilled wells. Contours are in feet in order to equate with the units of the well logs).

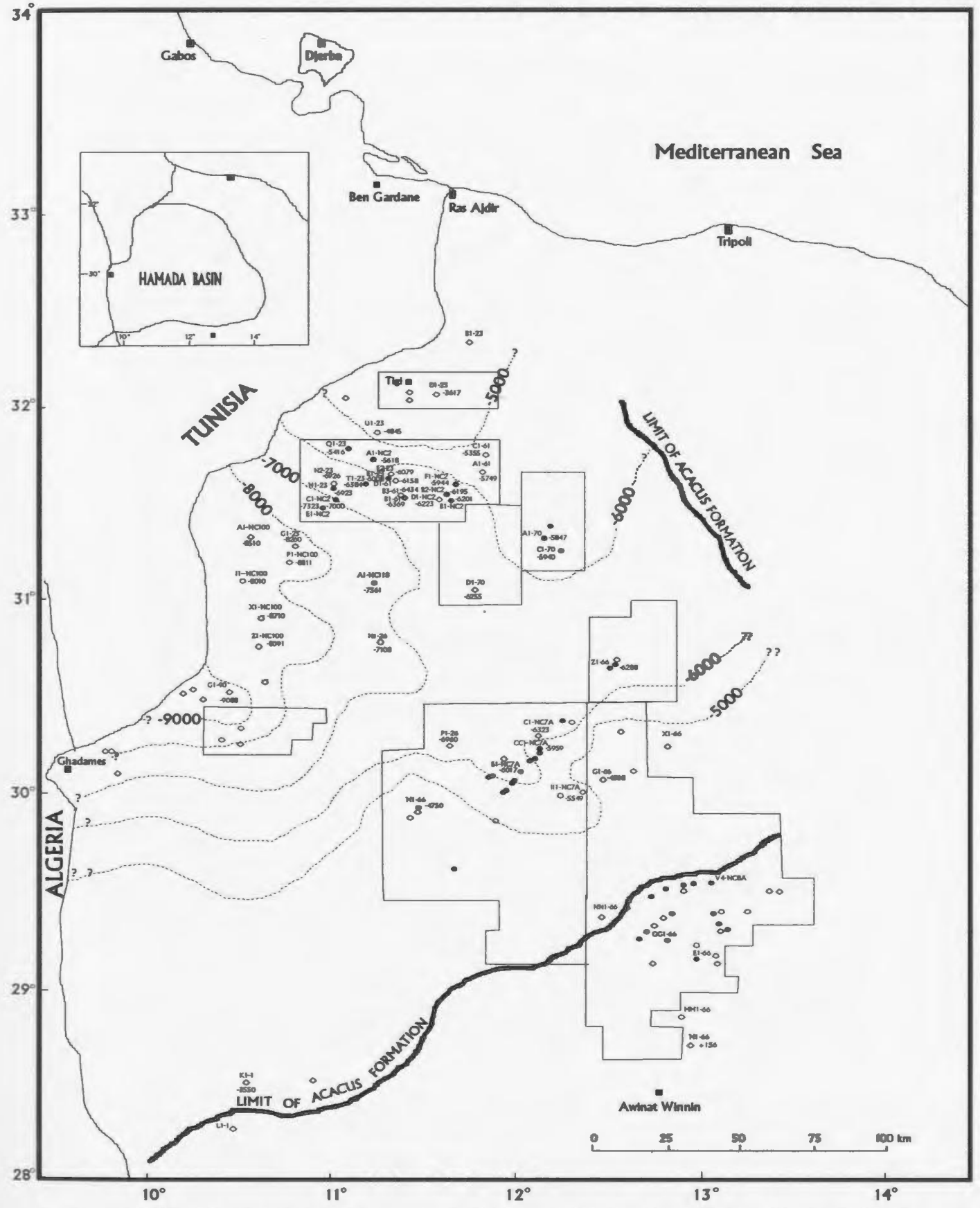

Figure 50B . Structure map on top of the Lower Acacus Formation, Hamada Basin, Nw Libya. (Data based on drilled wells. Contours are in feet in order to equate with the units of the well logs).

Table 9. Rock-Eval Pyrolysis analysis for Tanezzuft shale samples from GG1-NC7A well, Hamada Basin, NW Libya. (Data after Ghori, 1985).

S.No.	Depth in feet From	To	[a] Tmax (°C)	[b] S1 (mg/g)	[c] S2 (mg/g)	[d] S3 (mg/g)	[e] S1/S1+S2	[f] S2/S3	[g] TOC (%)	[h] S2/ TOC
1	10080	10090	430	0.18	0.46	0.46	0.28	1.00	0.45	102
2	10120	10130	435	0.09	0.52	0.68	0.15	0.76	0.41	126
3	10140	10150	431	0.15	0.66	0.56	0.19	1.17	0.41	160
4	10170	10180	440	0.22	0.97	0.28	0.19	3.46	0.62	156
5	10200	10210	442	0.13	0.89	0.72	0.13	1.23	0.60	148
6	10230	10240	438	0.20	1.09	0.87	0.16	1.25	0.79	137
7	10260	10270	436	0.28	1.22	0.66	0.19	1.84	0.71	171
8	10300	10310	442	0.41	1.21	0.53	0.25	2.28	0.83	145
9	10330	10340	443	0.52	1.89	0.93	0.22	2.03	1.51	125
10	10360	10370	445	0.73	1.76	1.02	0.29	1.73	2.18	80
11	10390	10400	420	0.57	1.21	1.50	0.32	0.80	2.97	40
12	10420	10430	440	0.68	1.85	1.19	0.27	1.55	2.34	79
13	10450	10460	431	0.55	1.46	1.19	0.27	1.22	1.89	77
14	10480	10490	421	0.54	1.16	1.12	0.32	1.03	1.69	68
15	10510	10520	427	0.50	1.07	0.82	0.32	1.30	1.46	73
16	10540	10550	440	0.39	1.10	0.68	0.26	1.61	1.47	74
17	10570	10580	447	0.33	1.02	0.76	0.25	1.34	1.34	76
18	10600	10610	429	0.43	0.99	0.72	0.30	1.37	1.38	71
19	10630	10640	422	0.62	1.14	1.04	0.35	1.09	2.55	44
20	10660	10670	432	0.63	1.20	0.84	0.35	1.42	2.41	49
21	10690	10700	451	1.10	2.86	1.07	0.28	2.67	5.76	49
22	10720	10730	456	1.69	4.33	1.06	0.28	4.08	9.86	43
23	10760	10770	453	0.83	3.13	1.66	0.21	1.88	6.59	47

[a] Tmax = Thermal maturation index, in this case Tmax= 430-460 (R_o.eq. 0.5-1).

[b] S1 = Amount of free hydrocarbon already generated in the rock (volatile hydrocarbon).

[c] S2 = Amount of hydrocarbon formed by breakdown of kerogen due to heating through pyrolysis (>250° C-500° C).

[d] S3 = Amount of molecular-mass of Co2 released by thermal breakdown of kerogen, which is related to the amount of oxygen in the kerogen.

[e] S1/S1+S2 = Production index ratio.

[f] S2/S3 Expected petroleum generated ratio.

[g] TOC = Total-organic-carbon contents, or source richness, in weight percent of dry rock.

[h] S2/TOC = Kerogen type (either gas prone or oil prone).

(Note: All measurements are in the units of the wells studied. Where both Metric and Imperial units are utilized they are provided).

and salinity. Based on bottom-hole formation temperature and water salinity measurements in some intervals in the Lower Acacus Formation (Table 7), and gas-data provided by DST results in various Paleozoic Formations (Table 8), a normal pressure regime with an average gradient of 0.4 kPa/m (0.02psi/ft) (ranging from a low of 0.04 kPa/m and a high 0.67 kPa/m (0.002 psi/ft - 0.03 psi/ft)) exists in the Acacus and Memouniat Formations respectively.

According to Takenouchi et al. (1965), Tissot and Welte (1978), Hunt (1979), and Al-Shaieb (1986), the solubility of CO_2 is between 100°C and 150°C for fresh to saline water. Since Lower Acacus formation water is basically a meteoric-connate water mix and occasionally is brine water (Table 7), it is reasonable to assume that the solubility of CO_2 either in the Lower Acacus Formation waters or in waters expelled from surrounding shale dewatering during compaction and maturation (pore water or connate water) at normal formation pressure may account for 1%-2% weight of dissolved CO_2 , which is sufficient to dissolve calcite cement. According to Hunt (1979) 1 m^3 of expelled formation water will dissolve about 30 m^3 of CO_2 at formation pressure ranging between 137.9 kPa-2206.8 kPa (20 psi-320psi), at 100°C.

Fluid flow through erosional unconformity surfaces as related to the creation of secondary porosity was first suggested by Krynine (1947) who noted that carbonate cement in sandstone reservoirs undergoes dissolution during uplift and weathering. In the North Sea feldspar dissolution in Jurassic sandstones has been explained by the circulation of meteoric waters related to the Cimmerian uplifts (Sommer, 1978; Hencock et al., 1978;

Bjørlykke, 1982). In the Lower Acacus Formation dissolution of mineral constituents, chiefly feldspars has been attributed to large-scale removal of ions such as K^{+}, Ca^{++}, Fe^{++}, and Mg^{++} as well as Si^{4+} during fresh-water circulation. This large-scale ion removal and water circulation coincides with basin uplift episodes and partial Lower Acacus Formation weathering during the pre-Hercynian. Along the numerous outcrops of the Acacus Formation in the south of Ghat area (Fig. 12) the sandstones are a ferruginous dark-brown to red-brown colour indicating a period of subaerial exposure and erosion at the top of the Acacus Formation / base of the Tadrart Formation (Klitzsch, 1970, 1981). However in the northern part of the study area, when uplift reactivated the Gefara Arch, meteoric water migrated and its circulation opened up the reservoir by increasing secondary (dissolution) porosity. This dissolution is partially evidenced by the recovery of meteoric water under the unconformity of 34,000 ppm Cl^{-} in well C1-NC2 @ 2963-2966 m. (9720-9730 ft.), and of 37,000 ppm Cl^{-} in well Q1-23 @ 2484-2500 m. (8146-8199 ft.). However percolating meteoric waters gradually lose their capacity to generate secondary porosity as they move down toward the basin centres because these waters approach saturation with respect to dissolved constituents.

Partial dissolution of calcite cement

$$[CaCO_3 + H_2CO_3 \rightharpoonup 2HCO_3^{-} + Ca^{++}]$$

and breakdown of feldspars during exposure to CO_2 charged waters related to unconformity and fractures

$$[2KAlSi_3O_8 + 2H_2CO_3 + 9H_2O \rightarrow Al_2Si_2O_5(OH)_4 + 2K^+ + 4H_4SiO_4 + 2HCO_3^-]$$

k-feldspar carb.acid Kaolinite in solution silicic acid in solution

is a major cause in some areas for creating secondary porosity in reservoir sandstones (Shanmugam, 1985). The breakdown of K-feldspar explains the common association of kaolinite with unconformities and/or fractures. This relationship is very pronounced in the northern part of the study area, especially in wells Q1-23, D1-61, A1-NC2 where K-feldspar grains were commonly exposed to chemical attack, and were the main contributor to the formation of kaolinite cement in these wells (Appendix II- Plates 14A, 21B, 22A). Similar relationships have been observed by many workers (Al-Gailani, 1981; Hurts and Irwin, 1982; Bjørlykke, 1984; Franks and Forester, 1984; Loucks et al., 1984; Bjørlykke and Brendsdal, 1986 Bath et al., 1987; Brown et al., 1989; Franklin and Tieh, 1989).

In summary, in a slowly subsiding intracratonic basin such as the Hamada Basin, the contribution of H^+ ions to the leaching fluids can be derived from several sources. Carbonate-mineral dissolution was caused by CO_2 released from maturing shales of the Tanezzuft Formation, and through CO_2-charged waters related to unconformity surfaces. Since the production of H^+ ion sources is not restricted to a single maturation stage during the subsidence history of the basin or the uplifting events coincident with unconformities, a multistage model of porosity development heterogeneity is proposed in the Lower Acacus Formation:

Stage I: CO_2-charged meteoric waters originated in topographically high areas, gaining access to the Formation through its eroded margins, and flowed toward basinal low areas. This is especially in the fluvial sandstone facies (southern part of the basin in

the vicinity of Gargaf and Hoggar high areas) during shallow diagenesis, and in deltaic sandstone facies (northern part of the basin from the vicinity of Gefara uplift) (Enclosures 1, 2)

Stage II- Mainly carbonic acid was released from maturing organic matter. The maximum development of secondary porosity in the Lower Acacus Formation was directly related to the amount of H^+ ions produced in the leaching fluids during each stage. Leaching required an initial porosity and permeability in the sandstones to secure fluid movement throughout the system.

Petrographic data (Appendix V- Plates 42A,B, 43B) suggest that the early cementation was not pervasive. If early cementation by carbonate or quartz-overgrowth had completely occluded the pore system, fluids would have had a difficult time subsequently contacting the sandstone units efficiently enough to modify pore-spaces and create secondary porosity. The porosity enhancement resulting from the leaching fluids must have represented an enhancement and redistribution of primary porosity in the Lower Acacus Formation. Total shut-down of the porosity system by cements did not occur because leaching requires that initial permeability in sandstones is preserved as either connected primary porosity or fractures through which the plumbing system can act easily.

Primary porosity is most clearly recognized where small pore-spaces are angular in shape resulting from the close proximity of adjacent overgrowths on quartz grains bounding the pore in the quartz-supported sandstones of fluvial origin (Appendix V- Plates 48A,B, 49A,B). In this case we can consider the pore-spaces to represent remnant

primary porosity.

When overgrowth edges or quartz grains are irregular, corrosion is implied and may represent one or both of the following cases: 1) secondary enlargement of primary pore-spaces by a leaching solution with partial or no prior calcite cementation, as in the fluvial sandstones facies where calcite cement is either incomplete or absent, and 2) cement dissolution and re-opening of calcite-cemented primary pore-spaces with additional enlargement as in the proximal delta front sandstone facies.

IV.3.1 Porosity and diagenesis in the Lower Acacus Formation:

Primary intergranular porosity in the Lower Acacus Formation is mainly associated with the fluvial sandstone facies. This porosity was partially reduced during early diagenesis as a result of silica precipitation as quartz-overgrowths, occlusion by clay and iron oxides coatings (especially in wells in the southern portion of the basin), and by partial shallow carbonate (calcite/dolomite) cements (Appendix V- Plates 40A,B, 41A, 42A,B). The relationship between these different cement types and porosity appears to be approximately time synchronous (Appendix V- Plate 50A).

Secondary porosity is mainly associated with the proximal delta front sandstone facies of the Lower Acacus Formation. The genetic classification of secondary porosity proposed by Schmidt and McDonald (1979a,b) reflects diagenetic processes (dissolution of calcite cement, dissolution of dolomite cement, dissolution of feldspar grains, and fractures). The predominant types of secondary porosity observed in the Lower Acacus Formation include mainly partial to total dissolution of calcite/dolomite cements, and

unstable grains. Dissolution of calcite cement is reflected by corroded quartz boundaries (carbonate cement exhibits a corrosive relationship with adjacent quartz grains). The resultant porosity is referred to as oversized, elongated intergranular porosity (Appendix V- Plates 51A,B, 56A,B, 57A,B, 59A,B, 60A,B) .

Approximately 70% of the thin-sections examined contained calcite which was sourced mainly from pressure-solution of the intercalated skeletal marine shale between different deltaic sandstone wedges. The dissolution of calcite cement in these sandstones is a predominant source for secondary porosity developed in the Lower Acacus Formation. In 20% of the examined thin-sections the partial to total dissolution of unstable grains, such as K-feldspar resulted in the formation of enlarged, oversized, moldic pores (Appendix V- Plates 52A,B-55A,B, 58A,B) making this type of dissolution a significant process in the origin of secondary porosity.

The distal and proximal deltaic and the reworked marine facies in the northern portion of the Hamada Basin (Concession NC2) are characterized by fracture porosity (Appendix II- Plate 23A,B, and Appendix V- Plates 61A,B, 62A,B). The fractures cut both cement and framework quartz grains, and are either open or partially filled with clay matrix, carbonate cements or hydrocarbons. These fractures are related to structural features (basement faulting) in the vicinity of these regions, although the data are insufficient to fully document this conclusion. The locations of the three wells from which the appendix figures have been taken are in the transition zone between the proximal delta front facies and the distal (prodeltaic) facies (Elfigih, 1991). These locations coincide with

the area where the Precambrian basement (Fig. 5) is documented to be faulted (in the vicinity of Concession NC2) (Figs. 5-7 and 11A-D). This faulted area appears to mark the edge of the transition zone .

The presence of oil staining (Appendix V- Plate 62A,B) along fracture walls indicates that the fractures predate drilling and did not originate during coring or sample processing. Incipient clay cementation along fractures (Appendix V- Plates 61A,B, 62A,B) also can be used as evidence of original fracturing.

Secondary porosity may also be reduced by authigenic kaolinite. Kaolinite occurs as a volumetrically significant phase of authigenic clay cement only in wells A1-NC2 and Q1-23 in the distal deltaic siltstone and reworked marine sandstone units respectively. In contrast low percentages of secondary porosity occur in the fluvial sandstone units (Table 4). Fine kaolinite crystal aggregates partially fill secondary pores (Appendix II- Plates 21A, 22A,B, Appendix IV- Plate 38C,D, and Appendix V- Plate 64A,B), and may have the highest potential for reducing reservoir quality in the distal deltaic siltstone and reworked marine sandstone facies.

Kaolinite distribution in the proximal deltaic sandstone facies cannot be related to proximity to shale (compaction, and expelled water) because sandstone samples immediately adjacent to the shale contacts (A14 unit @ 2567 m. (8420 ft.) in B1-61, and @ 2577 m. (8454 ft.) in T1-23, A12 unit @ 2604 m. (8542 ft.) in B1-NC2, and @ 2900 m. (9512 ft.) in E1-NC2) contained the least amount of these authigenic clays (Table 4). Kaolinite cement therefore was either derived from feldspar breakdown in these

sandstones, or a relatively open system with respect to aluminum was probably responsible for the increased solubility and mobility of the element at these locations. The data suggest that significant quantities of acidic fluids must have entered the system from the structurally active Gefara high area in the northern part of the Hamada Basin. A combination of vertically and laterally migrating acidic fluids flowed from deeper portions of the Basin via fractures which cut basement and younger rocks (Goudarzi and Smith, 1978; Goudarzi, 1980). Al/Si rich fluids established the condition for calcite dissolution, enlargement of pore spaces and eventual precipitation of kaolinite. Moreover, partial distribution of authigenic kaolinite in the fluvial, deltaic and reworked marine facies from the Lower Acacus Formation suggests that exposure to meteoric water is a prerequisite for kaolinite to form at the expense of dissolving feldspar (Appendix II- Plates 14A,B, 21B, 22A). Kaolinite appears during the late steps of diagenesis. In support of this interpretation is the fact that poikilotopic calcite (large crystals) incorporate no kaolinite deposits. Pore-filling authigenic kaolinite is present only after dissolution of calcite cement and the formation of secondary porosity.

Therefore authigenic kaolinite is a late diagenetic mineral which occurs in minor amounts in both shallow and deeper parts of the Hamada Basin where occasionally it is readily replaced by illite; especially in clay-rich sandstones. Illite occurs as replacement of kaolinite in the distal deltaic clay-cemented facies (Appendix II- Plate 22A, and Appendix IV- Plate 38D). It is conceivable that clay matrix recrystallization occurred before and after secondary porosity development.

IV.3.2 Porosity and oil emplacement:

Oil was observed in the proximal deltaic sandstone facies and reworked marine sandstone facies (units A8-A14 and Am) (Appendix V- Plate 63A,B) to occupy secondary porosity that had resulted from dissolution of calcite cement and the leaching of unstable grains. Occasional hydrocarbon droplets were encountered in the microporosity associated with kaolinite cement in the reworked marine sandstones. Such droplets were observed in well Q1-23, unit Am (Appendix II- Plate 14A,B, and Appendix V- Plate 64A,B). Clay growth was inhibited by the oil emplacement predating the kaolinite cement.

No residual hydrocarbon has been observed in the clay-cemented siltstones of distal deltaic facies. SEM photomicrographs of samples in this facies (well A1-NC2, Appendix IV- Plates 38D, 39A) show either authigenic illite flames that have grown on top of euhedral kaolinite booklets or a meshwork of plates that do not show any significant dissolutional pore-spaces where oil staining would be observed. Hence, the placement of authigenic illite cement occurred after precipitation of kaolinite in the diagenetic sequence of this facies is observed (Enclosure 5).

It is interpreted therefore that because oil droplets were occupying microporosity associated with kaolinite cement in the reworked marine sandstones (Am) petroleum emplacement must have occurred after dissolution of calcite cement, after porosity enlargement and modification in the carbonate-cemented facies of proximal deltaic origin (units A8-A14) and after kaolinite cement precipitation.

The relative timing of hydrocarbon emplacement in the clay-cemented siltstone

facies is uncertain.

IV.3.3 Relationship between porosity types, facies and depth:

Although it is well established that reduction of sandstone porosity occurs with depth of burial (Taylor, 1950; Weller, 1959; Maxwell, 1964; Fuchtbauer, 1967, 1974; Rieke and Chilinorian, 1974; Selley, 1978; Thomas and Oliver, 1979; Magara, 1980, Selley, 1982, 1998), the manner in which this reduction occurs is not fully understood. The origin of secondary porosity in different sedimentary basins is also controversial (Schmidt and MacDonald, 1979; Loucks et al., 1984; Immam and Shaw, 1987).

Selley (1978) suggested that porosity decreases linearly with depth of burial, whereas Thomas and Oliver (1979) suggested a nonlinear relationship. When primary and secondary porosities in the Hamada Basin are plotted against depth, two groups of porosities are recognized; each characterizing a specific facies with changing depth (Fig. 51). Primary porosity occurs in the fluvial sandstone units (Af2-Af7) at relatively shallow depth. Secondary porosity is usually associated with the deltaic sandstone units (A8-A14), at greater depths. Also there is a decrease in porosity from each fluvial channel(s) to its equivalent deltaic unit(s). In figure 51 the generalized depth-porosity plot of Lower Acacus Formation shows a porosity offset (inflection) between fluvial channel units (Af2-Af7) characterized by primary porosity and their equivalent deltaic units (A8-A14) characterized by secondary porosity.

An attempt was made to analyse the relation between porosity slope lines, depth and porosity types in each facies (Table 10, Fig. 51). Slope lines connecting points of

Table 10. Relationship between porosity types, porosity line mode, and depth of selected fluvial (Af2-Af7), and deltaic (A8-A14) sandstone units of Lower Acacus Formation, Hamada Basin, NW Libya.

Well name	Depth (ft)	Unit [1]	Porosity type [2]	Type of curve	Slope of line	Average thin-section porosity [3]		Compactional diagenesis [4]
						Pr. P.	Sec. P.	
C1-61	7522-7525	Af7	Pr.	Linear	Steep	17		+
C1-61	8199-8209	Af5	"	"	Gentle	24		-
EE1-NC7A	8810-8812	Af3	"	"	Steep	16		+
CC1-NC7A	9017-9020	Af2	"	"	Gentle	11		-
Z1-66	9080-9140	Af3	"	"	"	14		+
B3-61	9311-9345	Af2	"	"	Steep	13		+
D1-61	8236-8319	A14	Sec.	Linear	Gentle		12	-
B1-61	8420-8490	A14	"	"	Steep		14	+
T1-23	8454- 8473	A14	"	"	Steep		18	+
B1-NC2	8542-8555	A12	"	"	"		15	+
B3-61	8893-8969	A12	"	"	"		12	+
E1-NC2	9510-9575	A12	"	"	"		12	+
D1-61	8845-8872	A10	"	"	Gentle		10	-
C1-NC2	9703-9725	A8	"	"	Steep		9	+

[1] Af= Lower Acacus fluvial sandstone units, A8-A14= Lower Acacus deltaic sandstone units.

[2] Pr.= Primary porosity associated with fluvial sandstone units, Sec.= Secondary porosity associated with deltaic sandstone units.

[3] Pr. P.= Average primary preserved porosity associated with fluvial sandstone units, Sec. P.= Average secondary dissolution porosity associated with deltaic sandstone units.

[4] + = High compaction facies (steep slope line), - = Low compaction facies (gentle slope line).

(Note: All measurements are in the units of the wells studied. Where both Metric and Imperial units are utilized they are provided).

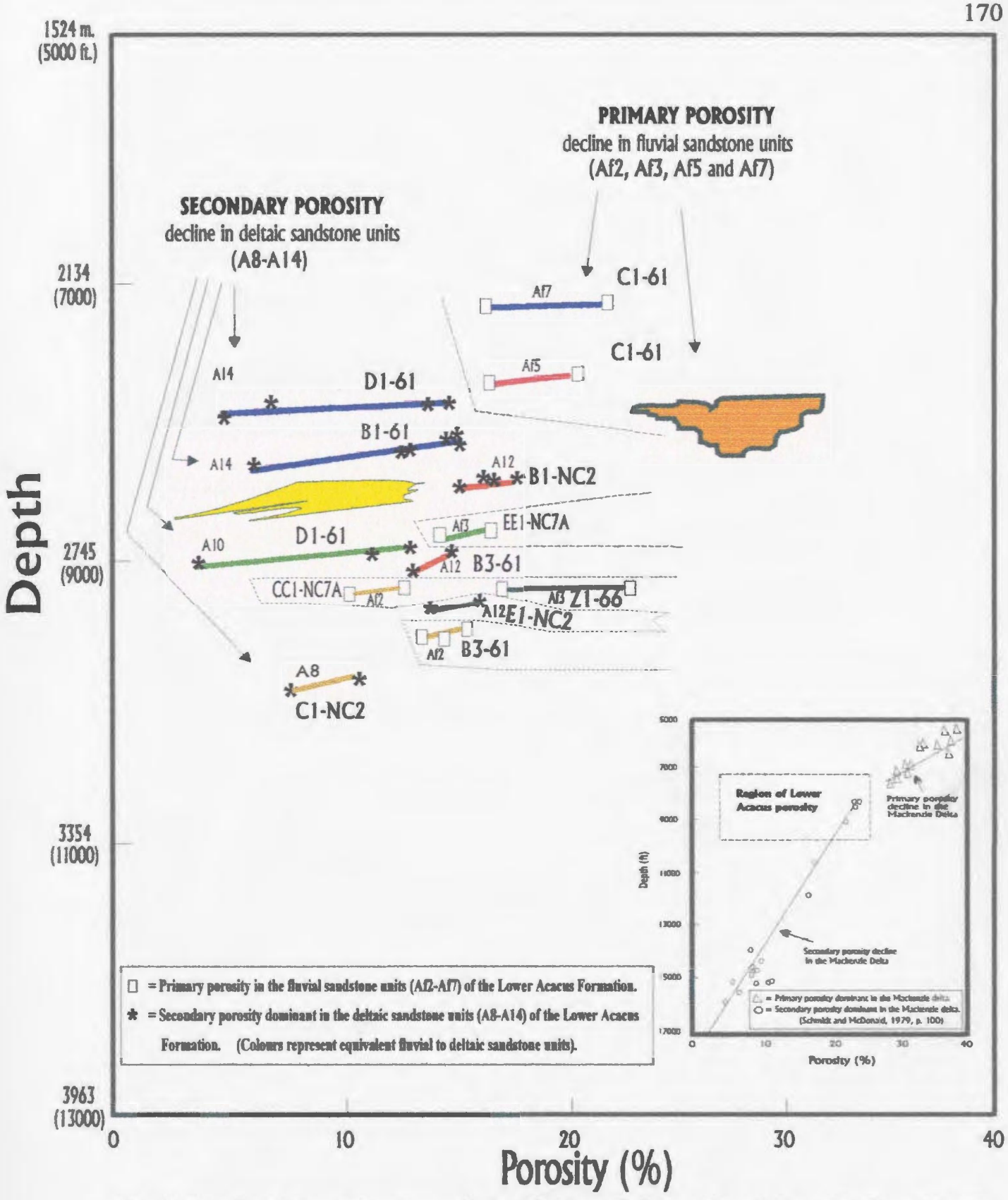

Figure 51. Comparison of primary and secondary porosity decline in the upper Silurian Lower Acacus Sandstone units of Acacus delta, Libya, and the Cretaceous Sandstones of Mackenzie delta, Canada (adapted from Schmidt and McDonald, 1979, p.100).

Note that, the offset points between porosity types of different deltaic units (A8-A14) of Lower Acacus Formation and their equivalent channel feeders (Af2-Af7) is indicated a general porosity decrease which is not only a function of depth but also is strongly facies controlled. (See Fig. 9 and Enclosures 3 and 4 for location of Lower Acacus Formation units).

either primary or secondary porosity for each sandstone unit of either fluvial or deltaic in origin were observed to have linear mode (Table 10, Fig. 51). The best-fit porosity lines are characterized by gentle or steep slope. This steepness of slope is a function of maximum overburden stress or sediment compaction (eg. Rieke and Chilingarian, 1974). Comparison of these porosity slope lines suggests that there is a decrease in porosity represented by the offset relationship of porosity values from each fluvial channel(s) to its equivalent deltaic unit(s). These results define a pattern of primary and secondary porosity of the Lower Acacus Formation in the Acacus delta (Fig. 51) which is comparable to those reported by Schmidt and McDonald (1979a) in quartzarenites of the Cretaceous Mackenzie delta.

IV.3.4 *Summary* of porosity evolution, distribution and diagenesis:

In the most porous and permeable deeply buried Lower Acacus facies (e.g. delta front sandstone facies) porosities are dominantly intergranular. These porosities are interpreted to be original pore-spaces preserved during burial and later modified by cement leaching.

Porosity preservation in the deep Lower Acacus Formation was not the result of any single diagenetic event, but was due to a combination of suitable conditions that overlapped in time and space. These conditions are:

a) the early formation of iron-oxide/clay matrix rims which inhibited quartz-overgrowth in the fluvial sandstones at shallower depths and during the early step of diagenesis,

b) open pathways through which later fluids (meteoric waters) could efficiently move

down and contact the sandstones at deeper parts of the basin,

c) CO_2 producing reactions either mixed with meteoric water or coming from maturing fractured horizons at depth which inhibited carbonate cementation and enhanced secondary porosity,

d) the migration of hydrocarbon to the reservoir pore-spaces which inhibited cementation in the

carbonate-cement leached sandstones of proximal deltaic origin.

The decrease in porosity between the fluvial channel units and their equivalent deltaic units was not only a function of depth but it also represented differences in the time and amount of diagenetic compaction and the leaching of cements and framework grains. Such porosity decrease was therefore strongly facies controlled, especially in the deltaic sandstone units (A8-A14).

V- REGIONAL BASIN HYDROLOGIC ZONES AND THEIR INTERACTIONS WITHIN THE LOWER ACACUS FORMATION

V.1- Overview of ground water concepts:

Analysis and description of modern basin hydrology and extant geochemistry provides a view only of the present diagenetic environment. Diagenetic relationships we observe in the Lower Acacus Formation are the result of earlier fluid regimes. The main objective of this chapter is to bring together general observations about the hydrology of sedimentary basins in order to create the framework in which the observed sandstone diagenesis can be explained. The diagenetic changes in the Lower Acacus Formation offer a major step in understanding and predicting the diagenetic alterations of these sandstones across the Hamada Basin.

Groundwater is the main constituent of the hydrologic framework of a sedimentary basin. The term groundwater in this thesis includes all subsurface waters moving within several different regimes (e.g. Bogomolov et al., 1978; Kissin, 1978; and Galloway, 1984). Topographic relief is the dominant force for groundwater flow in continental land masses, both in the shallow and deep subsurface (Toth, 1962; Freeze and Witherspoon, 1967; Galloway, 1984; Garven, 1995). Additional factors related to groundwater flow and water-rock interaction include landscape evolution (Dunne, 1990), diagenesis of sediments

(Wood and Hewett, 1984), formation of evaporites (Hardie, 1991), migration and entrapment of petroleum (Hubbert, 1953; Toth, 1980), generation of overpressures (Bredehoef and Hanshaw, 1968; Sharp and Domenico, 1976), and basin heat flow (Smith and Chapman, 1983; Smith et al., 1990; Deming et al., 1992). Groundwater flow can be studied at various scales, ranging from the smallest mineral grain boundary to the largest aquifer formation (Garven, 1995). This present review however focuses specifically on the large-scale hydrologic regimes that extend laterally for hundreds of kilometres across the subsurface of a sedimentary basin. The relative position of these subsurface waters, their different regimes, and anticipated flow directions in a large sedimentary basin are illustrated in Figure 52.

The meteoric regime encompasses the shallow portions of the basin fill (Bogomolov et al., 1978; Kissin, 1978; Galloway and Hobday, 1983; and Galloway, 1984). Meteoric water, recharging by infiltration of precipitation and surface waters, moves down the topographic gradient in the direction of decreasing gravitational energy, and discharges vertically at a constant hydrologic base level commonly represented by a sea or lake where the shoreline is a typical major discharge area of meteoric waters (Fig. 52). The meteoric environment can be defined in most general terms by the vadose zone, and the phreatic zone (James and Choquette, 1990). Because of the differences in degree of water mixing in vadose and phreatic zones the expected meteoric diagenesis in these two zones should be different (Longman, 1980).

The relative rates of sediment alteration, cementation, and dissolution in the

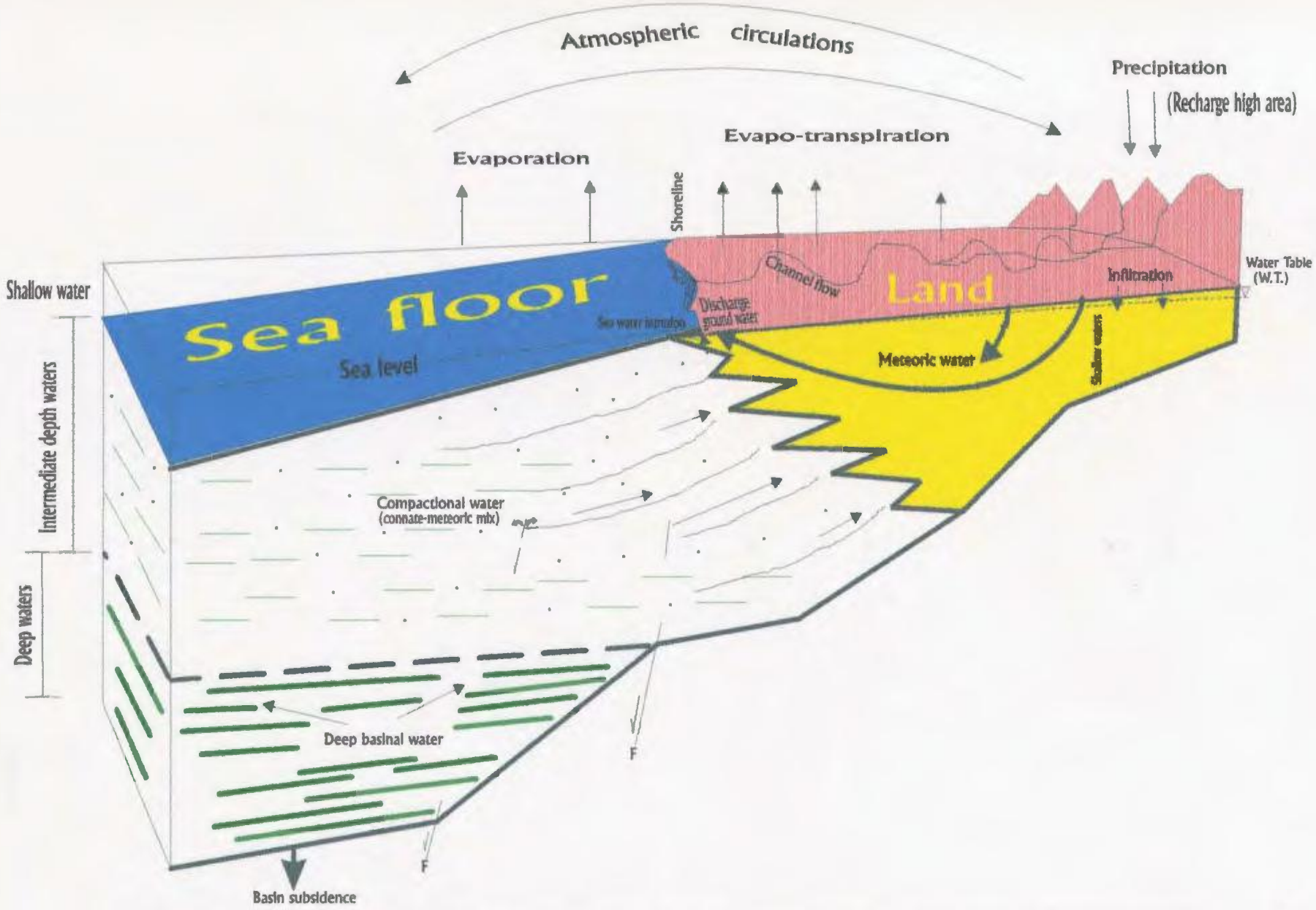

Figure 52. Schematic representation of ground water flow in different regimes of a large sedimentary basin (modified after, Galloway and Hobday, 1983; Galloway, 1984).

vadose and phreatic zones have been studied in Pleistocene carbonates (Land, 1970; Steinen and Matthews, 1973; Plummer et al., 1975). These general results can be used to approximate conditions and define possible diagenetic alterations (iron-oxide rimming, carbonate cement precipitation and dissolution) that can be related to vadose or phreatic processes in the Lower Acacus Formation.

The compaction regime is defined by upward moving pore-waters which are expelled under pressure from a compacting sediment pile (Fig. 52; Galloway,1984). These waters of intermediate depth may include either connate or meteoric waters buried below the zone of active meteoric circulation. In cases where water is confined within a sediment pile, unable to be expelled, fluid pressure increases with depth.

The deep regime occurs in the deepest portion of the basin-fill where temperature and pressure are greatest, and significant volumes of water are released by dehydration reactions of clay minerals and other hydrous minerals (Fig. 52). Fluid movement in this regime is usually generated by mineral-bound water or is due to release of pressured hydrocarbons in response to lithostatic loading (Galloway, 1984).

These regimes can be recognized by their imprints on rocks. Therefore, the diagenetic alteration pattern observed in any rock is a summation of the effects of all the different pore fluids that have flowed through that rock during burial, in combination with attendant physical and geochemical conditions (Harrison and Tempel, 1993). In cases where basin filling is stopped due to tectonic uplift, periodic erosional levelling of part of the basin or cessation of subsidence the pressure-driven water flow of the compactional

and deep basinal waters will be terminated. Any additional meteoric water recharged through the uplifted areas enters the basin and flows downdip where the sediment fill will be flushed by meteoric waters (Hitchon, 1969a, 1969b).

V.2- Present day hydrologic zones in the Lower Acacus Formation:

The Hamada Basin of northwestern Libya has been the subject of regional hydrologic studies (Dubay, 1978; Hammuda, 1978; Pallas, 1978; and Sinha, 1978). The main groundwater system is characterized by flow to the north through the various Paleozoic sandstones in the Basin (Memouniat, Acacus South, and Tadrart Formations) (Enclosures 1, 2) which crop out in the southern part of the basin (Pallas, 1980). The origin of this water is poorly understood but can be attributed in part to local recharge of the Paleozoic aquifer during exceptional rainfalls of high intensity and short duration (Dubay, 1980), and to the inflow of water from the Gargaf high area. This present study contributes to our understanding of present-day hydrologic zones and also defines possible major ancient diagenetic zones in the Lower Acacus Formation.

The ***present day*** fluid regime zones in Lower Acacus Formation aquifers are described below in terms of: (a) a shallow-updip meteoric zone, and (b) an intermediate-deep mixed (meteoric/connate) water zone (Enclosure 2).

Active portions of the present shallow-updip meteoric zone occur essentially within Acacus South Formation fluvial channels which have experienced meteoric flow throughout their depositional history, as indicated by the $\delta^{18}O$ values of the shallow calcite cement associated with the fluvial sandstone units (Af2-Af7; Figs. 36, 38; Table 6). The

present waters of the Lower Acacus Formation in the Hamada Basin show a gradual increase from fresh waters updip to saline waters downdip (Table 7, Figs. 53-55). In Figure 53 tongues of meteoric water are clearly seen in both the southern and northern flanks of the basin. Figures 54 and 55 illustrate the present-day regional salinity increase from basin flanks to basin centre. Figure 54 identifies fresh water/saline water interactions as reflected by the interdigitating salinity contours along a gentle slope and over a significant distance from south to north. This salinity distribution is consistent with the CO_2 zones illustrated in Figure 48. CO_2 also increases from basin flanks (high area) to basin centre . On the other hand Figure 55 shows relatively steep relief salinity increases from NE to SW towards the basin centre and over a shorter distance compared to those relationships observed in the S to NW transient of Figure 54.

In general, fresh-water penetration is controlled by downdip changes in aquifer permeability or may be affected by minor faults which contribute to improved connectivity along the fault plane (Fig. 56).

Compaction and pore-space reduction occur rapidly upon earliest burial to a few hundreds of metres (Galloway, 1984). During the first kilometre of burial shale releases much of its interstitial water (Chilingarian, 1983; Galloway, 1984). Water lost during burial of thick sand/shale sequences in the intermediate-deep mixed zone (Fig. 56) could typify Lower Acacus delta-front and prodeltaic facies. In the Lower Acacus Formation the depth dominated by the compactional water zone (regime) is defined by low salinity contours at 1829-2439 m. (6000-8000 ft.) from south to north (Figs. 53,54) and from east

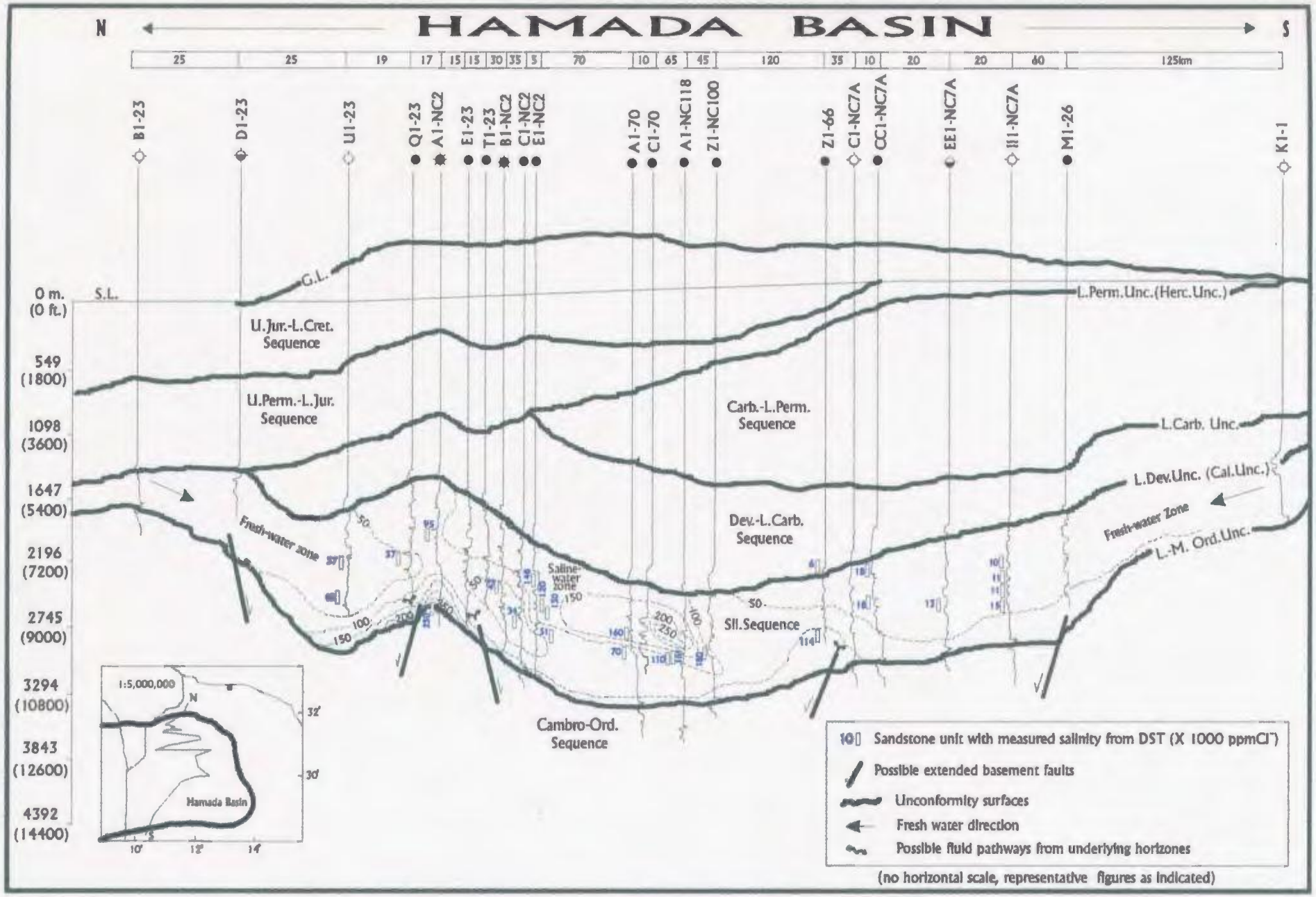

Figure 53. S-N Cross-section showing distribution of salinity readings in tested intervals in the Lower Acacus Formation. In the cross-section, fluvial meteoric water (freshwater) tongues from north and south of the Hamada Basin are shown to extend into the deeper part of the basin which is charaterized by more saline water. Note: areas of inclined, and closely spaced salinity contours coincide with fault zones.

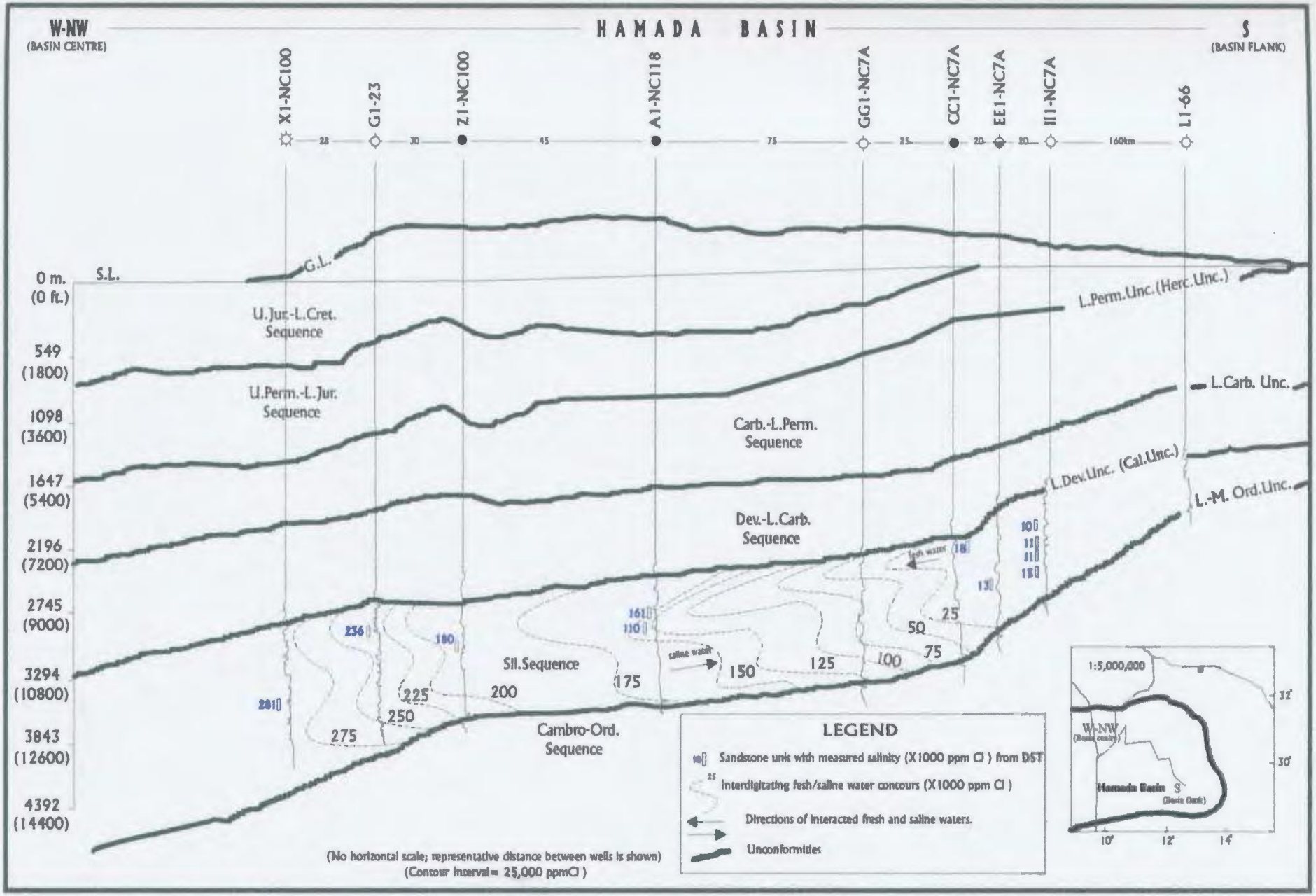

Figure 54. Present-day salinity distribution in the Silurian sequence of the Hamada Basin from the southern basin flank to the west-northwestern basin centre. Note the interdigitating fresh water (south) and saline water (west-northwest) contours indicated by arrows which suggest fluid zones interaction.

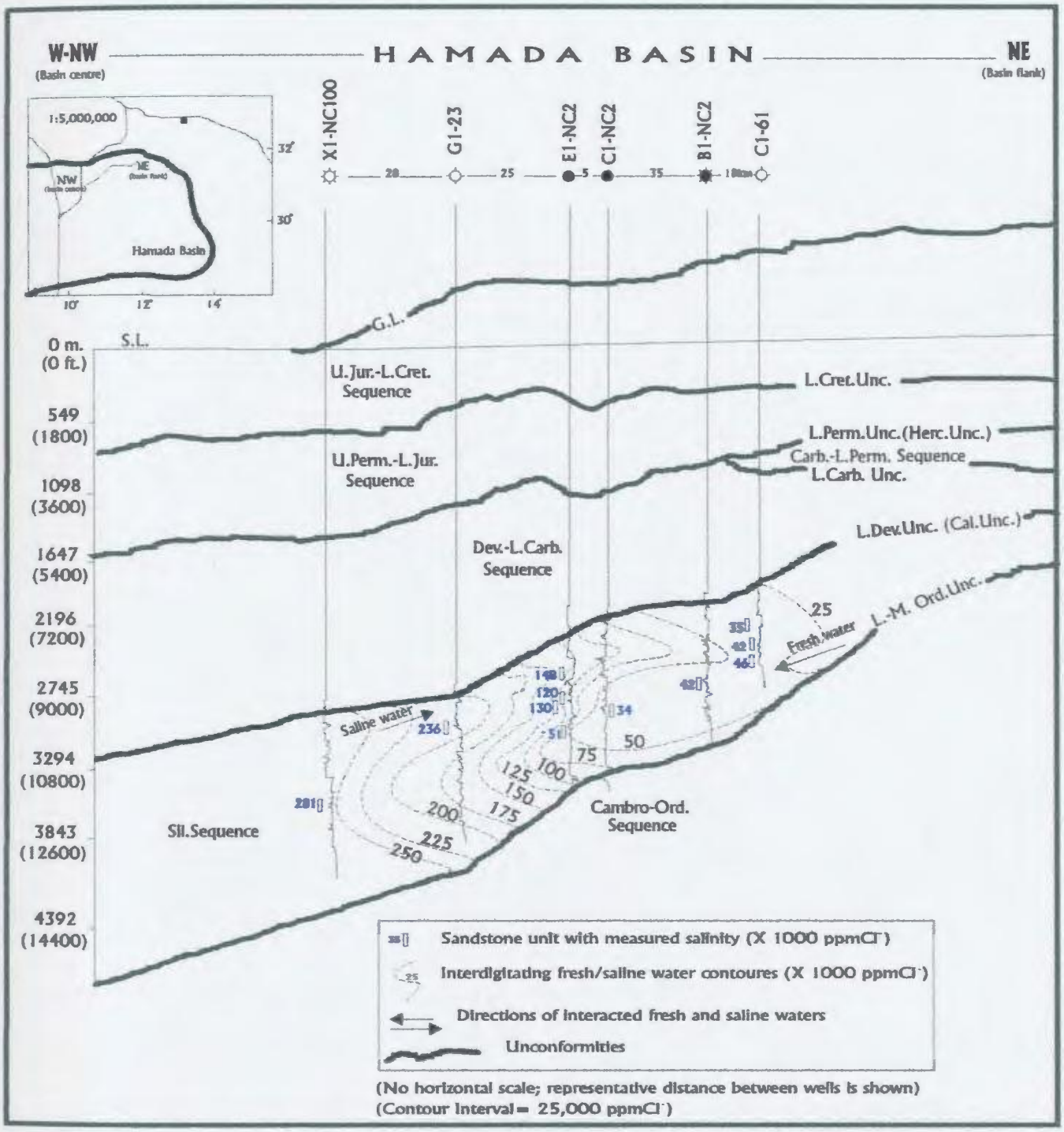

Figure 55. Present-day salinity distribution in the Silurian sequence of the Hamada Basin from the northeastern basin flank to the west-northwestern basin centre. Note fresh water pushin down dip, and saline water intruded at top. This is mainly due to the steep slope, short distance of traverse, and its proximity to shoreline in this locality.

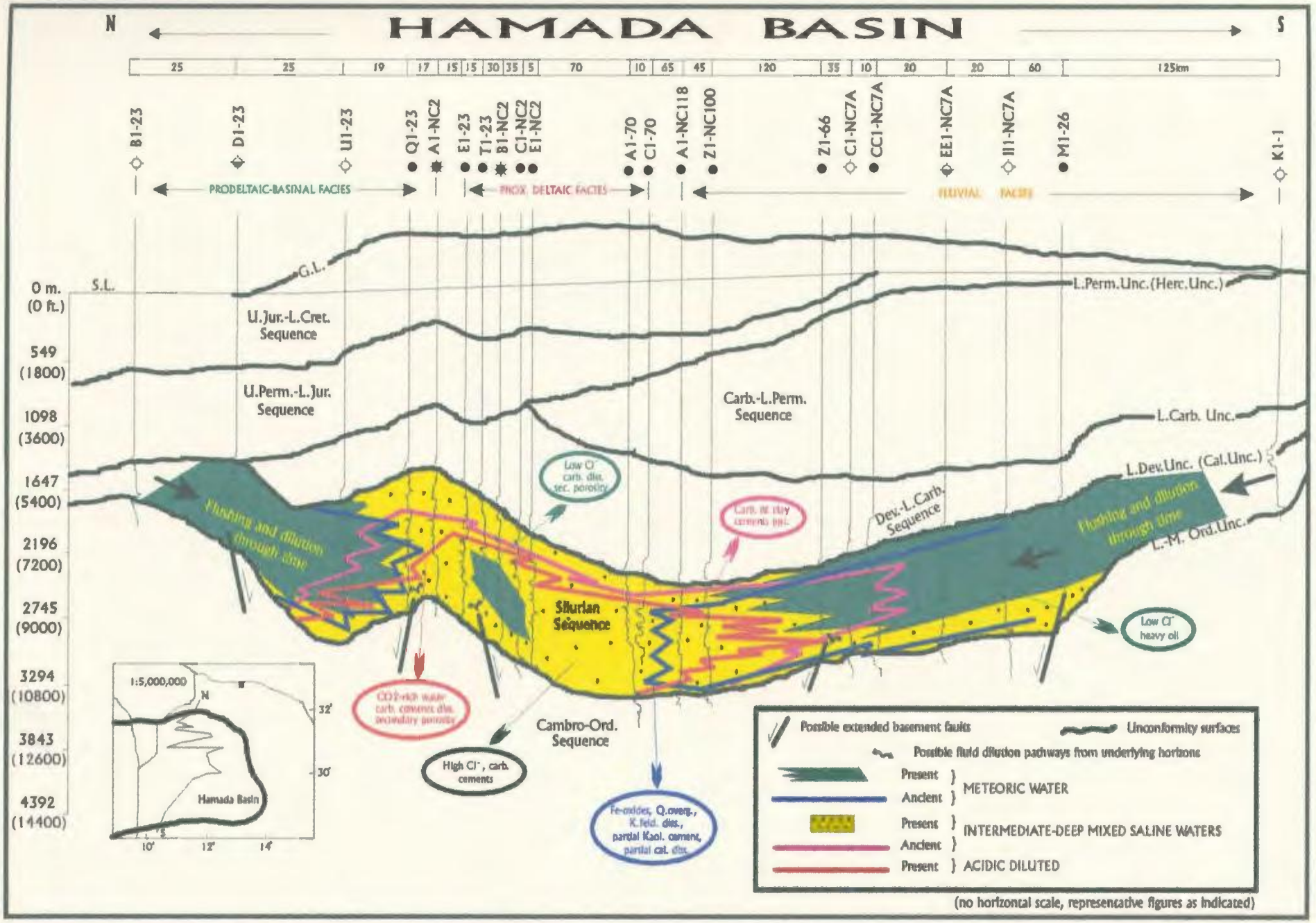

Figure 56. Distribution of Lower Acacus present day waters and ancient diagenetic minerals across the Hamada Basin, NW Libya.

to west (Fig. 55), and at the top of the faulted marine Tanezzuft shale at 2439-3049 m. (8000-10000 ft.) Deming and Nunn (1991), Cathles (1993) reported that the circulation of meteoric water quickly sweeps solutes in sedimentary basins. This replacement of saline intermediate-deep mixed water by dilute fresh-water can be seen in the vicinity of wells E1-NC2, C1-NC2, B1-NC2, T1-23, and E1-23 (Fig. 53) (at depths from 2195 m. (7200 ft.) to 3049 m. (10000 ft.)). The remnant saline basinal water (>100,000 ppm Cl^-) in the vicinity of wells A1-NC2 and Q1-23 characterizes areas bypassed by meteoric water flushing. At depths greater than 3049 m. (10000 ft.) the waters are characterized by slightly saline brines which are carbon-dioxide rich and contain abundant natural hydrocarbon gases (wells B2-NC2 @ 3160-3189 m. (10365-10460 ft.); C1-NC2@ 3229-3244 m. (10590-10640 ft.); and A1-NC118 @ 3061-3182 m. (10040-10438 ft.) (Tables 7, 9). The recovery of low pH water (between 4 and 6.5) in well A1-NC118 @ 3157-3171 m. (10354-10400 ft.) and consequently intensive acidic water corrosion of the sandstones in the vicinity of wells B1-NC2 and C1-NC2, by the dissolution of carbonate cements, enhanced secondary porosity to an average of 18% (Table 4). Moreover, due to considerable CO_2 content together with other gases, the waters from Devonian and Cambro-Ordovician Sandstones are highly corrosive and characterized by low pH 6.6 (Dubay, 1978). This may suggest that some of the Cambro-Ordovician corrosive (acidic) and pressured fresh water had escaped up-section through fractures, diluting the Lower Acacus waters at these locations (Figs. 53, 56).

V. 3- Post Lower Acacus diagenetic minerals and related fluid zones:

Diagenetic minerals and events dominant in the fluvial sediments in the southern part of the Hamada Basin (Fig. 56; blue line = ancient meteoric water zone) include quartz-overgrowths, iron-oxides, kaolinite, early leached feldspars and rock fragments, and formation of heavy oil in well Z1-66 in Concession NC5.

Acidic meteoric water is characterized by low pH due mainly to dissolved CO_2. Such water is initially under-saturated with respect to most minerals (Selley, 1982; Bjørlykke, 1983). Dynamic circulation of meteoric water in the subsurface can increase the concentration of dissolved solids in those waters. Since the solubility of quartz is low at low temperature and low pH, acidic meteoric water can reach saturation very quickly with respect to quartz (Bjørlykke, 1983). Quartz-cement precipitation has occurred in fluvial sandstone units in the southern part of the Hamada Basin under similar conditions. On the other hand this acidic meteoric water is strong enough to leach feldspars. The dissolution of feldspars will proceed only if the diagenetic fluid is renewed by waters under-saturated with respect to feldspars.

As a result of this extensive dissolution, kaolinite cement can be precipitated at the expense of dissolved K-feldspars. Also partial dissolution of calcite cements will take place as long as the diagenetic water in these units is acidic. XRD analyses in the fluvial sandstone units (Figs. 26, 28, 29) show some Mn-rich calcite, less Fe-rich calcite and dolomite, and a concentration of iron which may have contributed to the formation of hematite in these fluvial units. Such mineralogies can be attributed to the low

concentration of these elements in the diagenetic fluid or may reflect an oxidizing condition in which meteoric water was involved (e.g. Dixon et al., 1989; Johnson et al., 1990; Sullivan; McBride, 1991; and Al-Aasm and Azmy, 1996).

The diagenetic water in the intermediate-deep zone consists of either saline water (marine water), or mixed saline and freshwater (connate water) or diluted saline water (Fig. 56). Subsurface diagenetic processes including compaction , cement leaching, and some clay authigenesis were identified and discussed earlier from thin-section petrography of the deltaic sediments (Ch. III). The observed diagenetic minerals in these sediments include calcite, ferroan-dolomite, kaolinite and illite cements. These minerals indicate that these deltaic sandstones were bathed in mildly alkaline (pH 7 - 10) pore fluids. As meteoric water percolated down through the sandstones the fluid-rock interactions would have been increased. As a result, the fluids would have become saturated with respect to carbonate anions (CO_3^{2-}) resulting in precipitation of carbonate cements during burial from marine (saline) water.

Cations such as Mg^{++} and Fe^{++} when associated with modern shallow meteoric water are strongly hydrated and cannot mix with carbonate at low temperatures (Bjørlykke, 1983). With increasing temperatures, these ions become less hydrated and mix with carbonate in alkaline fluids (resulted from fluid-rock interactions). The deep carbonate cements associated with the proximal, distal deltaic, and reworked marine sandstone/siltstone facies are commonly iron and magnesium-rich (Figs. 30-35). Ferroan-dolomite cement was formed at the expense of calcite and dolomite cements. This

concentration of iron and magnesium is a good indicator of the availability of the Fe^{++} and Mg^{++} in those diagenetic fluids associated with the intermediate-deep mixed water zone. Illite as a late diagenetic cement rich in Al was also observed in the distal deltaic siltstones facies (Figs. 32, 33, and Enclosure 5). This mineral may record an increase in the pH of the diagenetic fluids in the intermediate-deep mixed water zone. These diagenetic mineral indicators have defined indirectly the extension of the ancient intermediate-deep mixed water zone (Fig. 56) associated with the Lower Acacus deltaic wedges. These wedges were later affected by fractures which acted as conduits for acidic diluted fluids which escaped from underlying horizons and exerted critical control on the reservoir quality of those horizons.

This investigation shows that the regional changes in the observed diagenetic minerals resulted from ancient fluid zones whose distributions were controlled by flow from high topography along the basin flanks in addition to compaction/structure processes in the basin centre. These distributions coincide with the observed diagenetic sequences in the various facies of Lower Acacus Formation.

V. 4- Comparison of Lower Acacus fluid zones with those of present-day:

The fluid regime zones for both the ancient Acacus sandstones and their present-day distribution (Fig. 56) reflect aspects of the hydrologic evolution of the Lower Acacus Formation in the Basin. The regional hydrologic pathways within the Lower Acacus Formation depend on the original depositional environment. With ongoing deposition , some of the sediments appear to have been flushed by meteoric water down-basin. (Fig.

56; blue line). With continued burial, deltaic sands and clay-rich sequences seaward of the ancient fluvial flushed meteoric water zone were dominated mainly by marine connate water (Fig. 56; purple line) and were occasionally enriched by acidic and diluted marine water (Fig. 56; red line). As deposition, sediment loading and water influx continued, meteoric water penetration increasingly dominated the Basin from both its southern and northern ends, and the basinal marine waters (Fig. 56; yellow stippled area) were diluted by present-day meteoric water (Fig. 56; green line). As these hydrologic zones evolved through time, the boundaries between them (Fig. 56) define the nature of their mixing and show complex interaction zones which are the focus of diagenetic alteration.

In summary, investigation of the Lower Acacus Formation deltaic wedges in the Hamada Basin (Fig. 56) reveals the continuing presence of meteoric and intermediate-deep marine water zones. The distribution and paragenesis of diagenetic features such as iron-oxide coating, quartz-overgrowths, K-feldspar dissolution, carbonate precipitation, replacement and dissolution, clay minerals authigenesis provide an indirect indication of the ancient fluids (either meteoric or marine) in each facies. In addition, data from wells such as formation water salinity, formation temperature, mole% CO_2 distribution, and some heavy oil occurrences provide information on present day active meteoric water. Interaction between these fluid zones in the Lower Acacus Formation from post-depositional to present-day time can be summarized as follows:

1- Ancient meteoric water occurred primarily within the fluvial sandstone facies (in the north and south of the Hamada Basin). These subsurface shallow deposits have

experienced meteoric water flow throughout their depositional history as indicated by diagenetic features which include the formation of oxidized iron rims (vadose-phreatic zones), quartz-overgrowths, and partial calcite and kaolinite cements (phreatic zone).

2- Ancient marine water intrusions were evidenced by total calcite cementation in the deltaic facies and partial calcite and ferroan dolomite cements in the fluvial facies.

3- There is indirect evidence for considerable mixing and interaction of intermediate-marine water (connate water) in some Lower Acacus Formation and acidic water from deeper horizons (Tanezzuft and Memouniat Formations) which caused intensive leaching of carbonate cements and enhancement of secondary porosity at depths greater than 2439 m. (8000 ft.). Hence upward fluid migration is indirectly indicated by the presence of major faults which extend to the Lower Acacus reservoirs especially in the vicinity of wells E1-23, A1-CN2, and Q1-23 (Fig. 56). Fault zones as interpreted in Figure 56 to be characterized by vertical fluid migration appear to have acted as main conduits for the discharge of fluids from deeper into shallower groundwater zones. The result of this interaction is a mixing zone which became the site for new diagenetic alterations.

4- Flushing of present-day meteoric water is evidenced by low-chlorinity waters (compared with the high chlorinity marine water down the basin) which extended as much as 1524-2439 m. (5000-8000 ft.) associated mainly with the fluvial facies in the southern part of the Hamada Basin. Other present-day meteoric water flushing has been encountered in the northern part of the basin as evidenced by low-chlorine waters

and some kaolinite cements associated with prodeltaic-basinal facies (Figs. 53, 56) in the vicinity of wells Q1-23 and U1-23. However, present-day meteoric water of low-chlorinity can also be seen as an isolated contour (Figs. 53, 56) in the vicinity of wells B1-NC2, and C1-NC2. This may indicate local dilution of acidic and saline water. The updip formation of heavy oil in the vicinity of well Z1-66 suggests that crude oil alteration by anaerobic bacteria was aided by meteoric water washing and flushing in the fluvial system.

5- In Figure 56 early diagenesis (post Lower Acacus time) as recognized in the different facies of the Lower Acacus Formation has had an impact on the present-day hydrologic system across the Hamada Basin. The present-day meteoric zone has a distribution which is expanded relative to the ancient Lower Acacus diagenetic zone distributions. Cements deposited in the marine (connate) phreatic zone are at present in meteoric vadose and phreatic zones, thereby providing an illustration of the role of flushing and dilution through time.

VI- DIAGENETIC HETEROGENEITY IN RESERVOIR SANDSTONES OF THE LOWER ACACUS FORMATION

Studies of sandstone diagenesis have commonly been restricted to a particular hydrocarbon field, or even to a single producing zone. Heterogeneity of the distribution of diagenetic properties has been previously reported (Lasseter et al., 1986; Moraes and Bruhn, 1988; Anjos et al., 1990; Moraes and De Ros, 1990) but no attempt has been made to integrate such observations with depositional facies changes or tectonic factors.

Diagenetic heterogeneity in the Lower Acacus Formation is studied in two stages. The first stage delineates the diagenetic elements, their heterogeneity between facies at the basin-wide scale, and their controls and effects that are common to many reservoirs. The second stage describes large-scale differences in facies architecture, and diagenetic and reservoir properties characterizing these units (eg: grain sizes, cements, isotopes, permeability, and structure). The combined analysis permits the development of a 3-D regional geological and diagenetic model that is of general applicability.

VI.1 Basin-wide diagenetic facies heterogeneity:

In the sandstone reservoirs of the Lower Acacus Formation, iron-oxide/clay matrix coating, calcite/dolomite, and authigenic clays are the diagenetic elements that have significant impact on heterogeneity of this formation.

As a result of iron-oxide rims, which may occur intermixed with an interstitial clay-

matrix, the euhedral quartz-overgrowths within the clean quartzarenite fluvial sandstones occurred separate from the rimmed quartz grains. The coating of iron-oxides and infiltration of clay matrix in this facies occurred during subaerial exposure due to the seepages of these iron-oxide-mud rich waters through the surface sediments (e.g. Walker, 1976; Moraeo and DeRos, 1990; and Malice and Mazzullo, 1996). This process was particularly effective in the medium-coarse grained fluvial sandstones where deeply penetrating water favoured the deposition of greater clay-loads. However, this process was not effective in the fine-medium grained fluvial sandstones (Table 4). Such grain-size variation is probably the reason for the relative enrichment in iron-oxide and clay coating observed in the fluvial coarse-grained sandstones.

At the local scale the heterogeneity in sandstone porosity is well pronounced between adjacent wells in different channel sequences. Vertically stacked channels of blocky GR-log signature (Fig. 57) are characterized by medium-coarse grained sandstones of low average porosity values (8%-12%). The well-developed permeabilities of these sands led to greater infiltration of iron-oxide-clay matrix bearing waters. In contrast, fine-medium grained channel sands at the bottom of complete fining upward channel sequences of bell-shaped GR-log signature (Fig. 57) have better-than-average porosity values (13%-22%) since the silty-very fine sandstones at the top of each sequence prevented iron-oxide-clay matrix water-rich percolation down sequence.

Figure 57 illustrates the distribution of average porosities in Lower Acacus

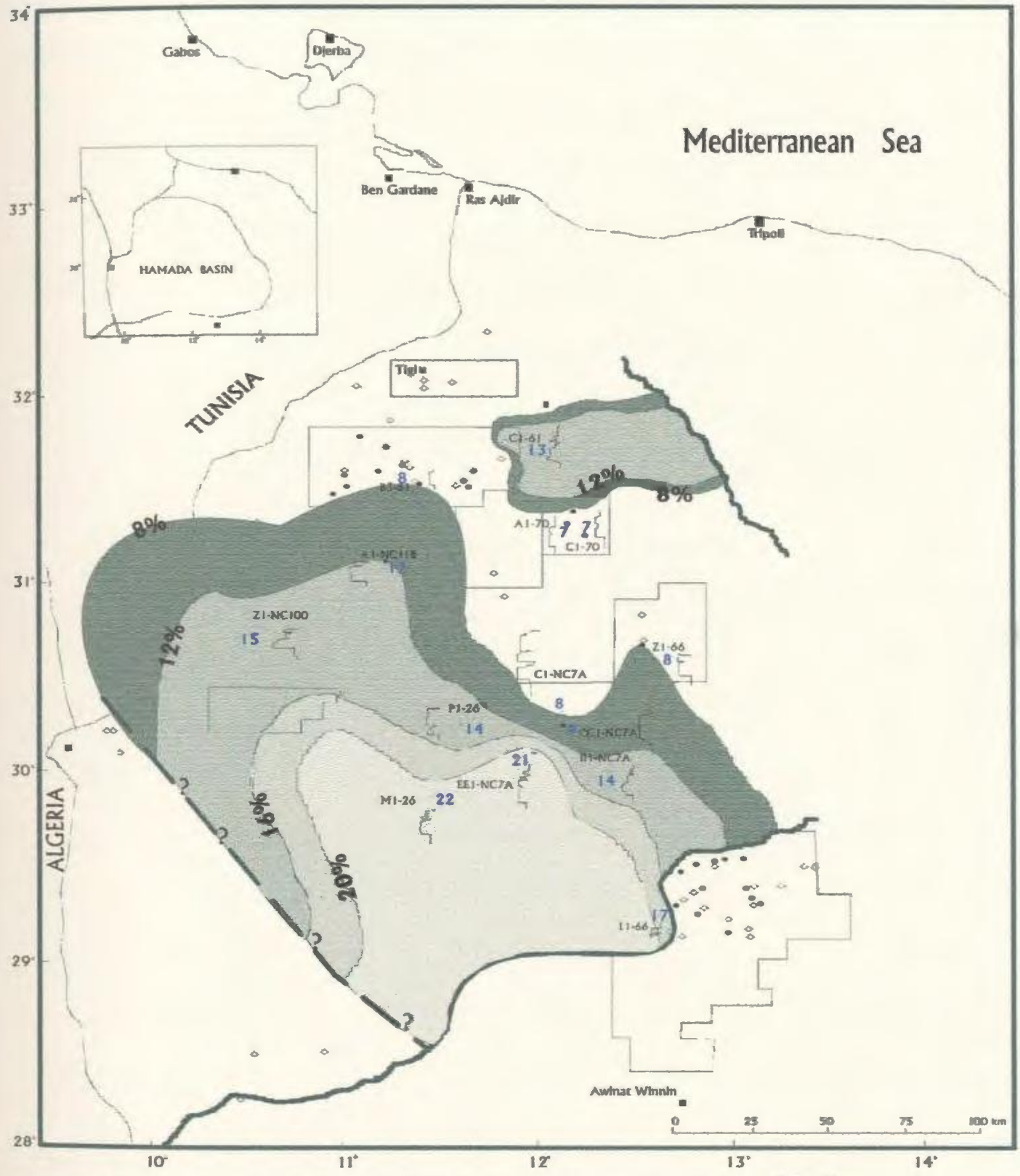

Figure 57. Sandstone quality map based on average log-porosity values of the fluvial reservoirs, Af2 unit, in the Lower Acacus Formation, Hamada Basin, NW Libya. Note the GR-log signature at each well accompanied with porosity values. (Contour interval= 4%).
(Average log-porosity values were derived from SONIC, CNL & FDL logs).

Map Key:

- Very-good (> 20%)
- Good (16% < < 20%)
- Fair (Regular) (12% < < 16%)
- Poor (< 12%)

reservoir quality fluvial (Af2) sandstones across the Basin. These data have been derived from porosity logs (compensated neutron log = CNLϕ; formation density log = FDLϕ; sonic log = Sonic ϕ). Factors such as primary depositional channel switching, paleo-fluvial channel widths, or the stacking architecture of fluvial sandstones contributed to reservoir partitioning of buried channel sandstones over short distances between wells. As a result the significant variations in sandstone quality reflect changes in percolated clay contents between channels. Figure 57 also shows an elongated trend of paleochannels in the eastern and southern portions of the Basin. These paleochannels provided the pathways for clays to infiltrate the sediments.

In order to assess the distribution of calcite on a regional basis both drill-core and gamma-ray logs were used to identify sandy zones. Density and neutron logs were used to identify matrix densities and porous zones. This determination was carried out both at the single well scale and by means of regional correlation to address the degree of continuity of each pattern within the proximal delta front sandstone reservoirs (A8-A14). It is in these sandstones that the most abundant carbonate-cemented zones occur (Fig. 58; Tables 3, 4).

Calcite distribution is characterized by the occurrence of either continuous wide bands having close proximity to shale beds or scattered occurrences associated mainly with intercalated shale lenses within the unit. The heterogeneity of calcite patterns between wells in a single correlatable unit is evident. The scattered calcite-cemented facies is the dominant diagenetic facies within the proximal delta front sandstone reservoir

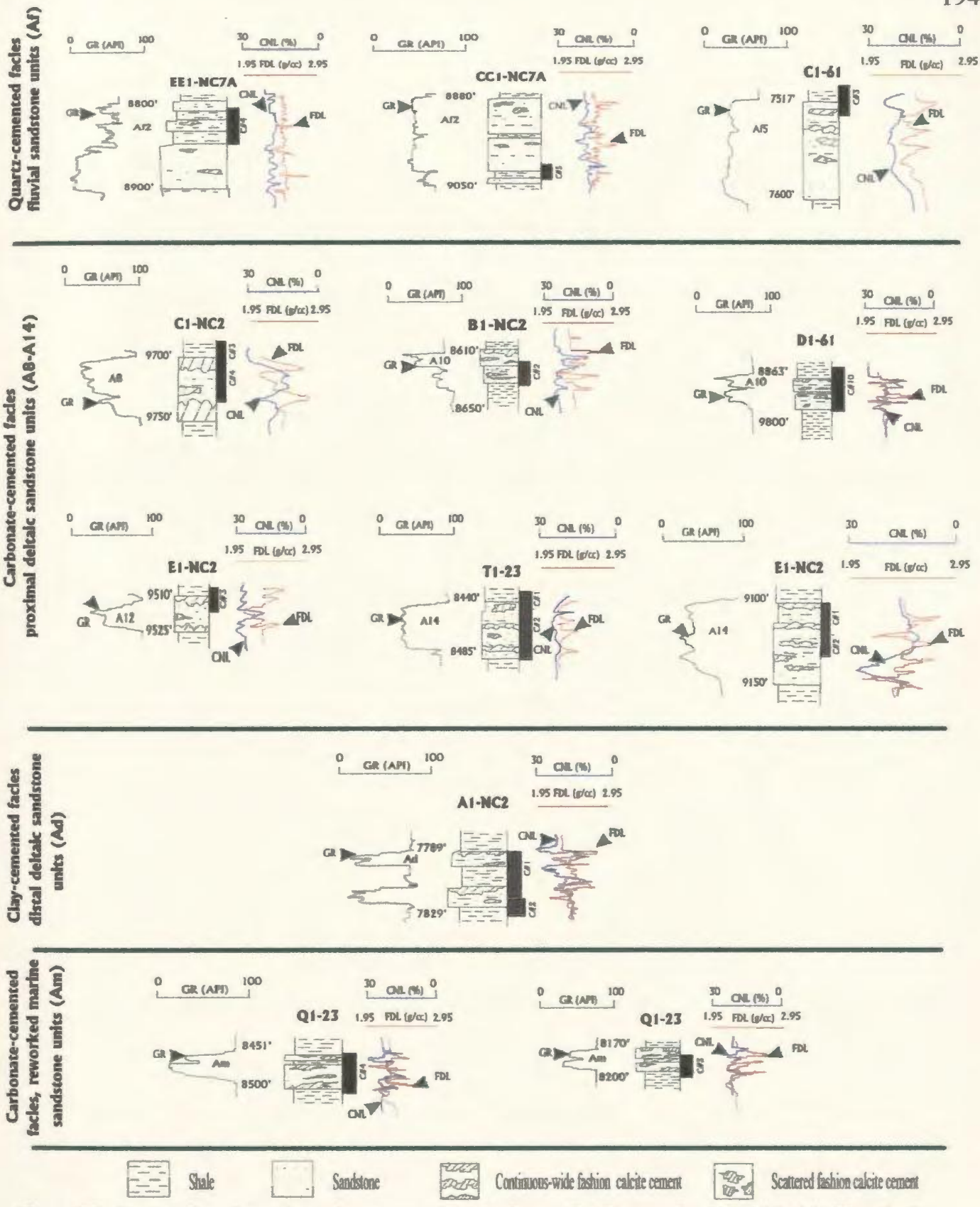

Figure 58. Core-sections from the various types of Lower Acacus Sandstone units (A8-A14, Af, Ad & Am) in the Hamada Basin, showing calcite cement occurrences in these units; from continuous-wide (bands) occurrence with relative proximity to shale beds, to scattered occurrences associated with intercalated shale lenses. GR = Gamma-ray log, FDL = Formation density log, CNL = Compensated neutron log, Black bars = Core intervals. (Note: The units of depth are as recorded on the well logs).

interval (Fig. 59). Sandstone bodies in these intervals are wedged-shaped and shingle against one another with resultant disruption of continuity by clay intercalations. The calcite cement occurrences and their fashion of distribution associated with each sandstone unit have different implications for reservoir properties and evaluation. Where the distribution of calcite cement is as continuous wide bands of poikilotopic texture the reservoir quality is mostly dependent on sandstone continuity and thickness. Such is not the case for the very-thin, scattered sandstone lenses. These lenses tend to be tight as a result of total calcite cementation (tight zones have been reported in several wells including A1-NC2, C1-NC2, and E1-NC2). In contrast the scattered (patchy) occurrences of calcite cement bear no relation with or proximity to the wide continuous shale beds. Instead the patches are closely related to either the intercalated calcareous shale lenses which extend only a few metres between the wells or to basin-wide facies changes.

Similar relationships have been described by Sullivan and McBride (1991) as being most common in the sandstones of the Frio Formation, Texas, and by Moraes and Surdam (1993) in the Lower Cretaceous deltaic and turbiditic sandstones of the onshore Potiguan and Reconcavo rift basins in northeastern Brazil. The common presence of scattered calcite cement in these very thin units indicates that they can be either of good reservoir quality, as it is the case of the hydrocarbon-bearing deltaic reservoirs in Concession NC2, or tight between closely-spaced wells. In addition, similar relationships can occur within a single well where adjacent sands can be either porous or tight.

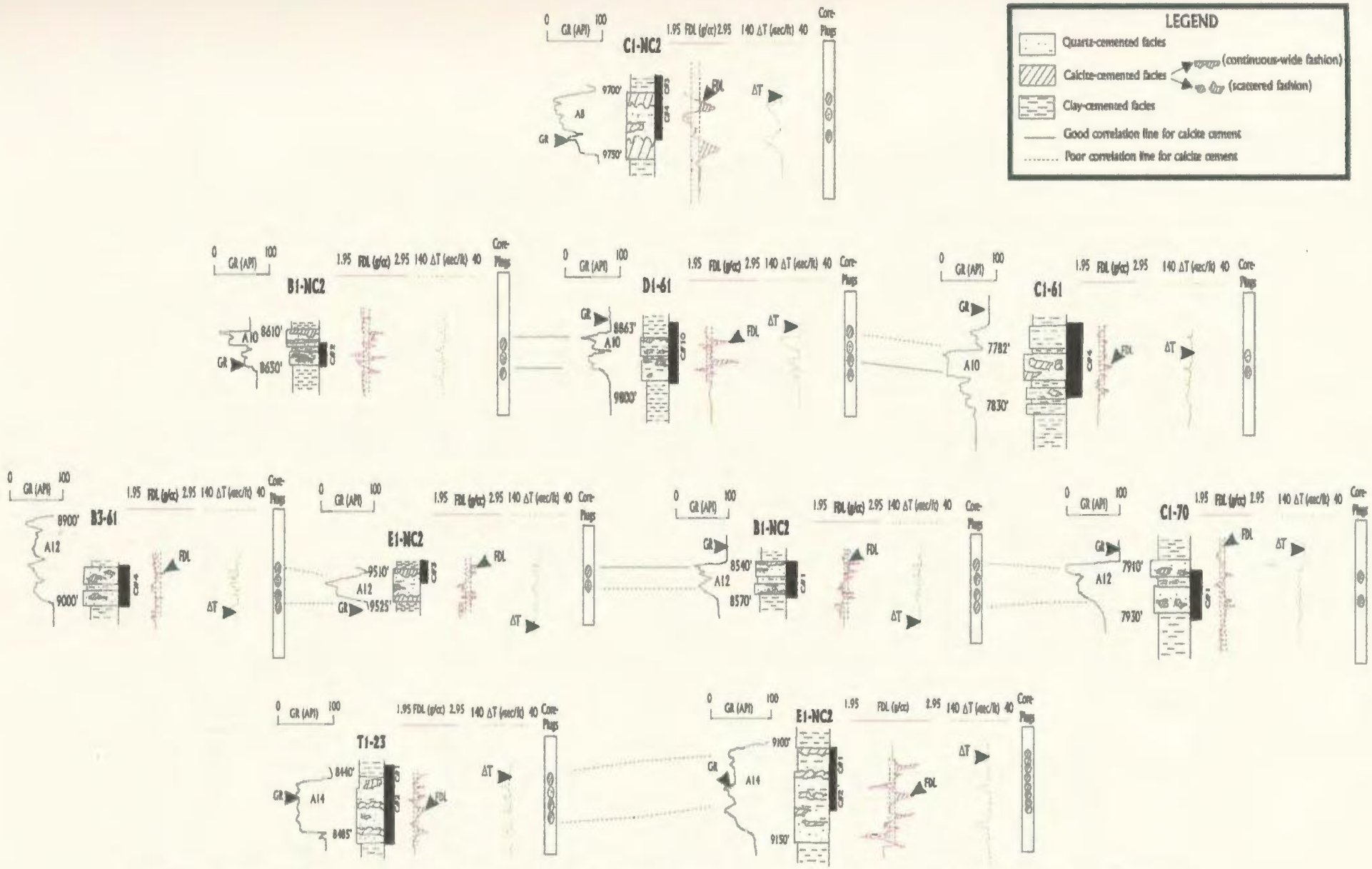

Figure 59. Gamma-ray, Density, and Sonic Logs correlation for the proximal deltaic sandstone units (A8-A14) in the Lower Acacus Formation. Dashed vertical line on the density log shows the predominant diagenetic cement types and their proportion at each cored interval in the sandstone units. Sonic log is showing the relative porous zones associated with each cemented interval. Gamma-ray log was used to define sandstone/siltstone and mudstone intervals. This correlation coincides or corresponds well with thin-section data from core-plugs (circles define diagenetic facies patterns) as it shows calcite cement heterogeneity between units. The sandstone unit (A8) in well C1-NC2 shows poikilotopic calcite cement. (Black bars = Core intervals). Note: The units of depth are as recorded on the well logs.

Fine-grained authigenic ferroan dolomite is associated with calcite, mud clasts and micas in the calcite-cemented facies, and of small patches associated with pore-filling clay minerals in the clay-cemented facies.

The association with calcite is apparently simple calcite replacement (e.g. Tucker and Wright, 1990; Moraes and Surdam, 1993; Boggs, 1995). In this case, dolomite will show the same occurrence and distribution as calcite (as in wells B3-61 @ 2670 m. (8756 ft.), C1-NC2 @ 2941 m., 2958 m. (9645 ft., 9703 ft.), and T1-23 @ 2583 m. (8473 ft.). In general, the replacement of calcite by dolomite does not affect reservoir quality. In other cases, as in wells D1-61 @ 2705 m. (8872 ft.) and Q1-23 @ 2275 m. (7461 ft.), the association of dolomite with mud clasts, micas and glauconite in fine-grained deltaic sandstones involves very minor replacement and then extensive precipitation of dolomite in pore-spaces.

Deltaic reservoirs in the northern part of the Hamada Basin were most affected by dolomite. Moreover, these stratified or cross-laminated sandstones display permeability contrasts between adjacent sandstone units since the dolomite plugs pore-spaces along the laminations. The effect of dolomite on the permeability of the Lower Acacus reservoirs was evaluated by comparing core plug permeability readings (Tables 2, 3) with petrographic and petrophysical data. Permeability contrasts are evident between deltaic sandstone units in wells C1-NC2 @ 2958-2965 m. (9703-9725 ft.), and T1-23 @ 2577 m. (8454 ft.), 2588 m. (8473 ft.). In well C1-NC2 at 2958 m. (9703 ft.) the A8 unit is a fine-grained, cross-laminated sandstone of the proximal deltaic facies. Calcite cement is about

13%, whereas dolomite (4%) is associated with some kaolinite and micas, and horizontal permeabilities of 250 md. At 2965 m. (9725 ft.) in a similar unit of few cross-laminations, and of only 2% dolomite, with less clay minerals association, the horizontal permeability was evaluated to be of 3133 md. Similarly in well T1-23 in unit A14 at 2577 m. (8454 ft.), in fine-grained, cross to parallel laminated sandstones of the proximal deltaic facies containing 3% dolomite and low clay minerals and micas, the horizontal permeability was computed to be of 30879 md.. The same unit at 2583 m. (8473 ft.) being characterized by fine-grained, more cross-laminations, and relatively higher clay and dolomite percentages (4% and 5%) respectively, displays low permeabilities of about 1254 md. In contrast, dolomite is not as abundant in coarse-grained, cross-bedded fluvial sandstones as it is in deltaic sandstones (Tables 2, 3, 4). In those sandstones, even with the presence of dolomite, the effect on permeability is less intense (CC1-NC7A @ 2749 m. (9017 ft.), 2750 m. (9020 ft.), EE1-NC7A @ 2686 m. (8810 ft.), 2686.5 m. (8812 ft.), and Z1-66 @ 2768 m. (9080 ft.), 2768.5 m. (9081ft.).

Authigenic clays (kaolinite and illite) formed as late diagenetic rims on grains and filling secondary porosity (Appx. IV- Plates 38A-D, 39A-C) (Table 4) in minor percentages. These rims probably contributed to permeability reduction in the sandstone reservoirs of Lower Acacus Formation. The influence of clay (kaolinite) on permeability depends on grain size, especially in deltaic sandstones. Based on both thin-section (grain size) and petrophysical data (permeability) from selected sandstone units in different facies of the Lower Acacus Formation, the data indicate (Figure 60) that sandstones having

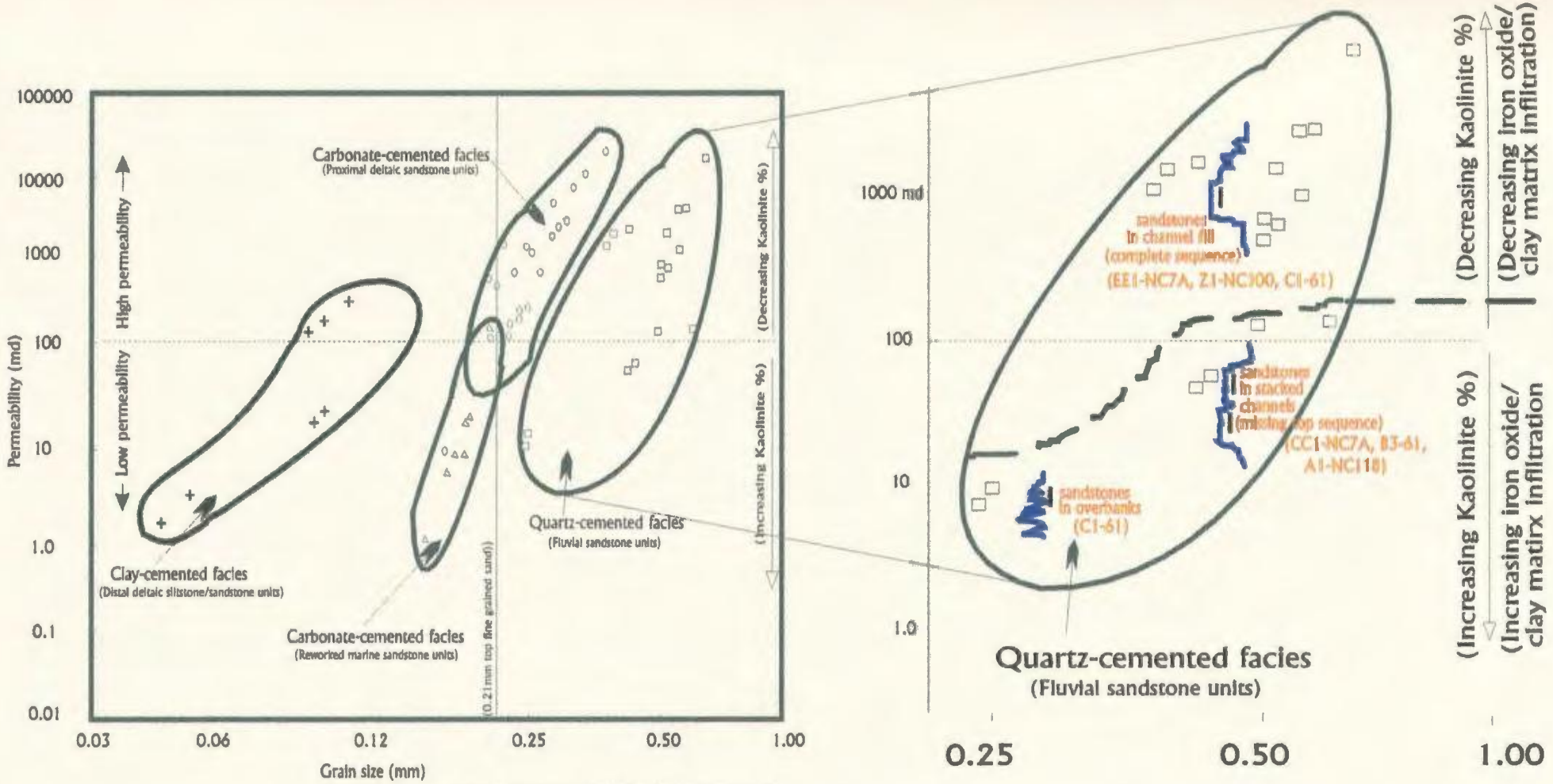

□ Quartz-cemented facies in fluvial sandstone units
(min.grain size 0.25mm, max.grain size 0.70mm, mean grain size 0.47mm, min. permeability 7md, max.permeability 18384md, mean permeability 9195md).

○ Carbonate-cemented facies in proximal deltaic sandstone units
(min.grain size 0.15mm, max.grain size 0.37mm, mean grain size 0.25mm, min. permeability 11md, max.permeability 30879md, mean permeability 15445md).

△ Carbonate-cemented facies in reworked marine sandstone units
(min.grain size 0.15mm, max.grain size 0.20mm, mean grain size 0.17mm, min.permeability 3md, max.permeability 252md, mean permeability 127md).

\+ Clay-cemented facies in distal deltaic siltstone/sandstone units
(min.grain size 0.04mm, max.grain size 0.11mm, mean grain size 0.07mm, min.permeability 2.8md, max.permeability 418md, mean permeability 210md).

| Location of samples from different fluvial sandstones

Figure 60. Permeability versus grain size in the various facies of Lower Acacus Formation characterized by greater than 1% kaolinite of the rock volume. Note the low permeabilities are found to be associated with deltaic-reworked marine sandstones/siltstones of mean grain size (determined in thin-sections) less than 0.21mm (top fine grained sand). Also note permeability reduction in fluvial sandstones from various facies associations (overbanks, channel fill) is not only a function of increasing kaolinite cement but also increasing percentages of iron oxides and clay matrix infiltrated into these sandstones. Hence this demonstrates local diagenetic heterogeneity between channel and overbank sandstone units of the same well or in adjacent wells.

kaolinite as the main diagenetic clay (>1% of the rock volume) display a significant reduction in permeability in rocks with an average grain size less than 0.21mm (top fine grained sand). This was evidenced in distal deltaic and reworked marine siltstones and sandstones and some very argillaceous proximal deltaic units (Fig. 60).

Permeability reduction in the fluvial sandstone units is not only a function of increasing kaolinite cement but also of increasing percentages of iron oxides and clay matrix infiltrated into these sandstones. This clay infiltration generated strong permeability contrasts between channel and overbank sandstones within the same well and within short distances between adjacent wells (Fig. 60). The permeability changes affected fluid movement and thereby the resultant diagenetic character differences between the two sandstone types.

Permeability distribution in deltaic sandstones is a function of the architecture of the various depositional elements. Fluvial and coastal depositional environments mix in the proximal parts of deltas whereas the transition to offshore distal units occurs over large areas and is much more uniform. In proximal deltaic areas permeabilities vary significantly over short distances normal to the depositional axes and tend to be more readily correlatable parallel to the depositional axes. These relationships are well documented in the northern part of the Hamada Basin (Figs. 11A-D). Grain sizes commonly range from fine to medium sands (0.15-0.37mm) in the proximal part of a lobe, and from silty to very-fine sands (0.04-0.11mm) in the distal part. Where kaolinite is present in both areas, it had little effect on permeabilities in the fine-medium grained sandstones of the proximal deltaic

facies but resulted in significant permeability reduction in the silty-very fine-grained sandstones of the distal deltaic and reworked marine sandstone facies (wells A1-NC2, Q1-23) (Fig. 60). The transition is fairly abrupt suggesting there may be some threshhold for the entrapment or movement of fines within the connected pores.

VI.2- 3-D geological and diagenetic model:

Integration of the data and interpretations of regional facies distribution, petrographic observation and cement types distribution, and isotopic composition in each facies of the Lower Acacus Sandstones permits development of a basin-wide 3-D geological model (Fig. 61). Such a model is essential to achieve regional understanding of diagenetic changes across the Hamada Basin.

The model developed in this study suggests that all relatively shallow, patchy calcite-cemented zones formed synchronously from meteoric waters that became progressively more reducing and saline as they flowed downdip to enter the deltaic sandstones to mix with saline connate waters.

The exercise of building this full-basin 3-D model of the Lower Acacus Formation suggests that facies changes associated with important diagenetic variations can successfully be included as deterministic elements. For example, in the fluvial sandstone units iron oxides and clay matrix will be the dominant diagenetic elements in the overbank-flood plain facies, while quartz-overgrowths will occur in sandstones of channel-fill deposits or facies. These factual diagenetic differences in this fluvial sandstone example are directly related to facies changes.

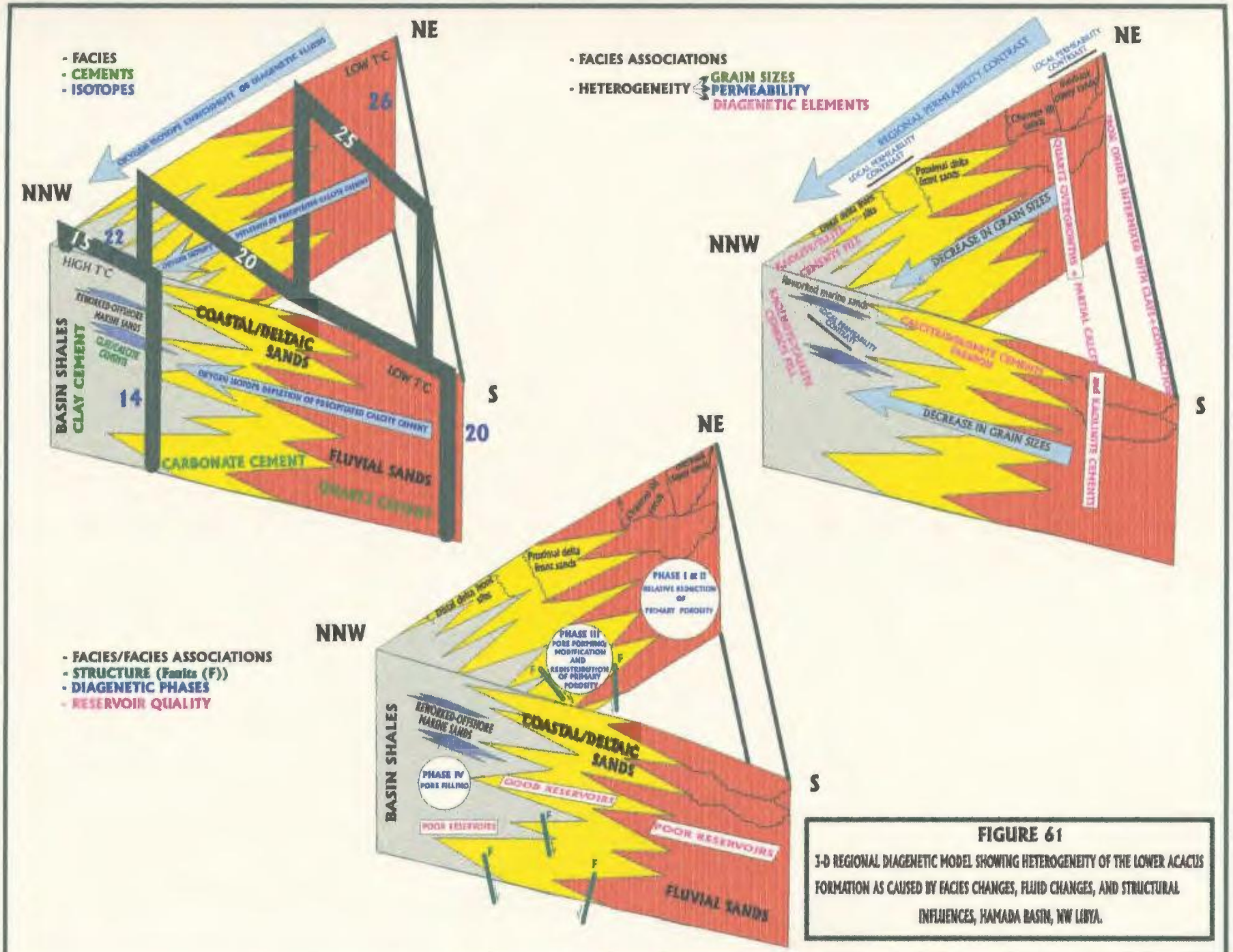

FIGURE 61

3-D REGIONAL DIAGENETIC MODEL SHOWING HETEROGENEITY OF THE LOWER ACACUS FORMATION AS CAUSED BY FACIES CHANGES, FLUID CHANGES, AND STRUCTURAL INFLUENCES, HAMADA BASIN, NW LIBYA.

In light of the diagenetic sequences characterized in each facies of the Lower Acacus Formation (Enclosure 5) this 3-D representation of a diagenetic model concludes that there have occurred **four phases** of major diagenetic changes in the facies and their facies associations across the Hamada Basin. **Phase I** represents the reduction of primary porosity and permeability in fluvial sandstone units by an early stage of iron-oxide coatings and intermixed clay matrix percolation concurrent with compaction in the overbank deposits. **Phase II** represents further reduction of porosity and permeability by partial quartz-overgrowths and shallow calcite and kaolinite cements in the channel fill sandstones. Hence, Phases I & II are related to each other and their sequence can be predicted (from channel fill at the base to flood plain-overbank deposits at the top). **Phase III** is development of pore-forming secondary porosity with associated redistribution and modification of primary porosity through concurrent calcite cement leaching and the dissolution of unstable grains as was common in the proximal delta front sandstone units. **Phase IV** is characterized by total pore-filling in distal delta front siltstones and partial pore-filling in the reworked marine sandstones as a consequence of the formation of kaolinite and illite cements.

From these diagenetic phases we can recognize that Phase I & II have a predictable sequential relationship with each other. They indicate that fluid mixing decreases down-section with an associated increase of quartz-overgrowths, partial calcite, and some kaolinite cements. On the other hand Phases III & IV do not show any sequential relationship to Phases I & II. Each of III & IV do record isolated diagenetic

events relative to their own depositional facies setting. Therefore the lack of any predictable sequential relationship of pore-forming and pore-filling events is a reflection of regional heterogeneity of facies changes. This facies-diagenesis model of the Lower Acacus Formation implies poorer and much more heterogeneous reservoir quality than any earlier 2-D model across the Hamada Basin.

VI.3- Reservoir potential and diagenesis:

Although fresh water may have influenced cementation in the fluvial sandstones it also had a pronounced effect on the leaching of carbonate cement and the modification of porosity in the dominant facies of proximal delta front origin. The best reservoirs of the Lower Acacus sandstones are in the northern portion of the Hamada Basin in the vicinity of NC2, NC3 and NC4 concessions where proximal deltaic sandstones (top part of the deltaic sequence or unit) can be encountered either directly below the Middle Acacus Shale for unit A14 or underlying the intercalated marine transgressive shales separating the different levels of Lower Acacus Formation for the rest of the units (A8-A12). These proximal sandstones developed their diagenetic signatures in concert with Phase III pore-forming diagenesis. Associated extensional faults in the area may have enhanced sandstone quality by improved the plumbing system for oil to migrate into the the reservoirs.

In the southern and eastern portions of the Hamada Basin the initially coarse-grained, well sorted sandstones characterized by channel sequences were altered to non-reservoirs by post-diagenetic events (Phase I & II). Although these deposits locally may form gas reservoirs (wells C1-NC7A, EE1-NC7A), in most cases they are water-wet as

these rocks were subaerially exposed or subjected to freshwater flushing.

As mentioned earlier in Chapters IV and VI the greatest effects of freshwater exposure on these sediments would have been the introduction of iron-oxides and clay matrix to these clean sandstones by means of percolating meteoric waters. The iron-oxides and clay matrix coatings inhibited the development of syntaxial quartz-overgrowths and also served as nucleation sites for later authigenic clay pore-fillings. These coatings would have occurred mainly during the shallow (early) diagenetic history of the fluvial sandstones which would equate with Phase I & II (Figure 61; Enclosure 5).

In the most northern and northwestern part of the Hamada Basin where facies are dominated by the distal delta front siltstones and reworked marine sandstones the reservoirs in general are of poor quality due to total pore-filling by kaolinite/illite cements (Phase IV). If oil occurred in the reworked marine sandstones it would have to fill low-permeability microporosity associated with kaolinite cement. In the reworked marine sandstones reservoir quality may have been enhanced locally by fractured porosity.

Early exploration rationales in the Hamada Basin focussed on anticlinal structures as exploration targets. Lower Acacus Formation reservoirs exist in reality as stratigraphic traps associated in some instances with structural highs. These stratigraphic traps result from sand pinch-outs (lateral facies changes), porosity changes and diagenetic traps occurring on a regional scale and can be attributed to either the formation or the removal of authigenic cements.

VII- SUMMARY AND CONCLUSIONS

Regional relationships among facies changes, diagenetic sequences, and structural history of the Lower Acacus Formation in the Hamada Basin lay the basis for approaches to the analysis of regional diagenesis and for establishment of parameters for basin modelling. Relationships established in this study are as follows:

1- The Lower Acacus Formation of the Hamada Basin has been a good choice for analysis of regional diagenesis and its relation to facies changes because the lateral changes from southern fluvial-channel sandstones northward to coastal-deltaic sandstones and siltstones, and eventually to offshore-marine sandstones and shales permit comparisons of contemporaneous units having diverse and widespread lithologies.

2- Petrographic and petrophysical data delineate three diagenetic facies in the Lower Acacus Formation from the basin flank to the basin centre respectively: (A) ***the quartz-cemented facies***, (B) ***the carbonate-cemented facies***, and (C) ***the clay-cemented facies***. Knowledge of such lateral diagenetic variation is important when establishing regional parameters for basin modelling.

3- Each diagenetic facies contains a characteristic authigenic mineral assemblage reflecting a specific sequence of diagenetic alteration. This finding establishes the need to describe diagenetic histories in the context of the facies architecture in a basin. Analysis of a single well or composites of wells as has been common in the past is

inadequate to characterize basin relationships.

4- The course of diagenesis varies spatially within the Lower Acacus Formation because variations in primary composition , texture and physical properties are related to depositional facies. Variations of textural parameters such as grain size, sorting and packing for each facies control both local permeability distributions and the regional plumbing system. These permeability distributions control fluid movements within a stratigraphic unit and thereby influence the type, amount and character of cements to be formed in the individual facies.

5- Isotopic compositions of calcite cements in the Lower Acacus Formation reflect different regional paleo-fluid regimes (eg. meteoric to mixed water). Relatively shallow depth ***Zone I*** patchy calcite-cements are associated with sandstone units of fluvial origin. These cements formed from enriched $\delta^{18}O$ meteoric waters at low temperature. Deeper depth ***Zone II*** poikilotopic calcite-cements formed from waters depleted in $\delta^{18}O$ that became progressively hotter, more reducing and saline as they flowed downdip to mix with the saline waters in sandstone/siltstone units of deltaic and prodeltaic origin.

6- Porosity types should be anticipated to have a regional distribution related to type of grain framework, matrix and cement in each depositional facies.

7- Dissolution of authigenic carbonate cements and unstable grains is a major factor responsible for the creation of secondary porosities associated with the proximal deltaic sandstone units (A8-A14) of the Lower Acacus Formation.

8- A multistage model of secondary porosity development involving creation of both modified and enlarged pores is proposed for Lower Acacus sandstone units and includes: (1) access to the subsurface formation by CO_2-charged meteoric waters via fluvial channel systems exposed during uplift and erosion along the southern margins of the basin. Later uplift of the northern margin of the basin led to late diagenesis as a result of meteoric water invasion into deltaic and prodeltaic sandstones; (2) expulsion of deep carbonic acid-rich connate waters to overlying proximal delta front sandstone units via fractures from maturing organic-rich Tanezzuft shales during late diagenesis (pore-forming phase).

9- Porosity preservation in the deep Lower Acacus sandstones is not the result of any single diagenetic event, but is due to a combination of suitable conditions that overlapped in time and space. These conditions include: a) the early formation of iron-oxide/clay matrix rims which inhibited quartz-overgrowth and preserved primary porosity in the fluvial sandstones at shallow depths during the early stage of diagenesis; b) maintenance of open pathways through which later fluids could effectively flow to contact the deltaic sandstones in deeper parts of the basin; c) production of CO_2-rich fluids which either mixed with meteoric water or which originated from maturing fractured horizons at depth. The resultant carbonic acid inhibited carbonate cementation and enhanced secondary porosity, especially in the proximal deltaic sandstone facies; d) the migration of hydrocarbons to the reservoir pore-spaces which inhibited further cementation in sandstones of proximal deltaic origin.

10- Early diagenetic modifications in the Lower Acacus Formation have had major impact on the present-day hydrologic system across the Hamada Basin. Present-day hydrologic zones have a distribution which is expanded relative to the defined Lower Acacus diagenetic zones and demonstrate the role of fluid flushing and dilution through time.

11- On the basin-wide scale the relationship between sandstone facies and the distribution of the diagenetic elements is an important aspect for addressing Lower Acacus diagenetic heterogeneity. This diagenetic heterogeneity includes: (1) ***iron-oxides and interstitial clay coating*** associated with quartz-overgrowth in the quartz-cemented facies of fluvial origin. Sandstone quality in this facies is controlled mainly by either the width of paleo-fluid channels and the development of fine-grained overbank deposits topping the sequence or by the architecture of stacking of the fluvial channel fills; (2) ***calcite cements*** with both poikilotopic and scattered patchy textures in the carbonate-cemented facies of proximal deltaic origin. These patterns show no correlation between wells within the same unit. In deltaic units scattered patchy calcite cement is dominant and is associated with intercalated shale lenses. (3) ***ferroan dolomite cement***, which occurs mainly in both the fine-grained, cross-laminated, micaceous, clay clast-rich sandstones of the proximal delta front units and the reworked marine sandstone units has a local effect on the permeability of these units; (4) ***authigenic kaolinite cement*** significantly reduces the permeability of siltstones in the clay-cemented facies of distal delta front origin and in

carbonate/kaolinite cemented facies of the reworked marine sandstone units. This cement had little effect on the reduction of permeability in either the medium-coarse grained fluvial sandstone units or the fine-medium grained proximal delta front sandstone units.

12- Development of a basin-wide 3-D geological model is essential to achieve regional understanding of diagenetic change and for realistic reservoir representation and prediction. Basin modelling benefits from a multidisciplinary approach involving the integration of regional facies, cements distribution, petrographic and isotopic observations, and diagenetic sequence definition as has been utilized in this analysis of the Lower Acacus Formation.

13- Four phases of diagenesis have been identified: **Phase I** represents the relative reduction of preserved primary porosity and permeability in fluvial sandstone units by early stage iron-oxide coatings and intermixed clay matrix in association with compaction in the overbank deposits. **Phase II** represents reduction of primary porosity and permeability by partial quartz-overgrowths, and shallow calcite and kaolinite cements in the channel fill sandstones. Elsewhere down-basin, progressively greater calcite cementation took place. **Phase III** is a secondary porosity pore-forming phase which led to redistribution of porosity and modification of primary porosity through the leaching of calcite cement and dissolution of unstable grains. This pore-forming phase occurred mainly in the proximal delta front sandstone units. **Phase IV** resulted in total pore-filling by kaolinite and illite cements in siltstones of

distal delta front origin, and partial pore-filling in sandstones of reworked marine origin.

14- Lower Acacus Formation reservoirs are stratigraphic traps associated in some cases with structural highs. Stratigraphic traps result from regional sand pinch-outs, porosity changes, and authigenic cement removal or formation (Phases III, IV). Anticlinal structures in the Hamada Basin are only of minor importance. Reservoir sandstones are highly affected by regional facies changes and diagenetic-phase variations across the basin. Future discoveries must depend upon recognizing combined regional depositional and diagenetic variations in addition to tectonic trends in the subsurface.

15- Improved regional basin analysis and computerized basin modelling must consider and apply the variability which can be expected from a multitude of parameters ranging from primary depositional processes to processes of burial and subsequent diagenetic modification of the formation. Commonly-applied generalizations regarding diagenesis as determined from individual well studies are inadequate and in many instances perhaps invalid for effective models to be developed.

VIII- REFERENCES

Al-Aasm, I. S., I. Muir, and S. Morad, 1993, Diagenetic conditions of fibrous calcite vein formation in black shales: petrographic, chemical and isotopic evidence: Bulletin of Canadian Petroleum Geologists, v. 41, p.46-56.

Al-Gailani, M. B., 1981, Authigenic mineralization at unconformities: implication for reservoir characteristics: Sedimentary Geology, v. 29, p. 89-115.

Allen, P., 1975, Ordovician glacials of the central Sahara: In Wright, A. E. And F. Moseley (eds.), Ice ages, ancient and modern, Geol. Jour. Spec. Issue No. 6, Seel House Press, Liverpool, p. 275-286.

Al-Shaieb, Z., and J. W. Shelton, 1981, Migration of hydrocarbons and secondary porosity in sandstones: AAPG Bulletin, v. 65, no. 11, p. 2433-2436.

Al-Shaieb, Z., and P. Walker, 1986, Evolution of secondary porosity in Pennsylvanian Morrow Sandstones, Anadarko Basin, Oklahoma: In Spencer and Mast (eds), Geology of tight gas reservoirs, AAPG Studies in Geology, no. 24, p.45-67.

Amthor, J. E., and Okkerman J., 1998, Influence of early diagenesis on reservoir quality of Rotliegende Sandstones, Northern Netherlands: AAPG Bulletin, v. 82, no. 12, p. 2246-2264.

Anderson, J. B., C. Wolfteich, R. Wright, and M. L. Cole, 1982, Determination of depositional environments of sand bodies using vertical grain-size progressions: Gulf Coast Association of Geological Societies Transactions, v. 32, p. 565-577.

Andreev, P. F., et al., 1968, Transformation of petroleum in nature: London, Pegamon Press Inc., 466p.

Anjos, S. M. C., C. L. Sombra, L. F. De Ros, R. S. Souza, E. V. Santos, and R. Waick, 1990, Ptterens and processes of diagenesis in Cretaceous rift sequence of Potiguar Basin, northeastern Brazil (abs.): AAPG Bulletin, v. 74, p. 599.

Ayalon, A., and F. J. Longstaffe, 1995, Stable isotope evidence for the origin of diagenetic carbonate minerals from the Lower Jurassic Inmar Formation, southern Israel: The Journal of the International Association of Sedimentologists, v. 42, no. 1, p. 147-160.

Arabian Gulf Oil Company (AGOCO), 1995, Exploitation evaluation study, fields in the west half of Concession NC2, Teknica Exploitation Group, AGOCO-Benghazi, 95p.

Bailey, J. W., 1983, Stratigraphy, environments of deposition, and petrography of the Cotton Valley Terryville Formation in eastern Texas: M. A. Thesis, University of Texas, Austin, Texas, 229p.

Bain, G. W., 1963, Climatic zones throughout the ages: In Munyan, A. C. (ed.), Polar wandering and continental drift, SEPM Special Publication No. 10, p. 100-130.

Banerjee, S., 1980, Stratigraphic lexicon of Libya, Department of Geological Researches and Mining, Bulletin no. 13, Industrial Research Centre, Tripoli, Libya, 300p.

Bath, A. H., A. E. Milodowski, and B. Spiro, 1987, Diagenesis of carbonate cements in Permo-Triassic Sandstones in the Wessex and East Yorkshire-Lancashire Basins, UK: a stable isotope study, In J. D. Marshall (ed.), Diagenesis of sedimentary sequences: Geological Society Special Publication 36, p. 173-190.

Bathurst, R. G. C., 1983, Early Diagenesis of carbonate sediments: In Pakrker, A., and B. W. Sellood (eds.), Sediment Diagenesis, NATO ASI Series, p. 349-377.

BEICIP, 1973, Evaluation and geological study of the western part of Libya (Ghadames Basin), final report, N. O. C., Libya, 197p.

Bellini E., and D. Massa, 1980, A stratigraphic contribution to the Paleozoic of the southern basins of Libya, In Salem M. J., and M. T. Busrewil (eds.), Symposium on the Geology of Libya, second edition, v. I, Tripoli, Libya, p. 3-56.

Bishop, W. F., 1975, Geology of Tunisia and adjacent parts of Algeria and Libya, AAPG Bulletin, v. 59, no. 3, p. 413-450.

Beuf, S., Biju-Duva, B., chaparal, O. de., Rognon, R., Gariel, O., and Bennacef, A. J., 1981, Les greś du Paléozoique inférieur au Sahara-sédimentation et discontinuites, évolution structurale d'un Craton, Institut Francais Pétrole Science et Technique du Pétrol, 18, 464p.

Bjørlykke, K., 1979, Discussion, cementation of sandstones: Journal of sedimentary Petrology, v. 49, p. 1358-1359.

Bjørlykke, K., 1982, Formation of secondary porosity in sandstones: how important is it and what are controlling factors? (abs.): AAPG Bulletin, v. 66, p. 549-550.

Bjørlykke, K., 1983, Diagenetic reactions in sandstones: In Parker, A. And B. W. Sellwood (eds.), Sediments Diagenesis, NATO ASI Series, p. 169-213.

Bjørlykke, K., 1984, Formation of secondary porosity: how important is it?, In McDonald, D. A., and Surdam R. C. (eds.), Clastic Diagenesis, AAPG Memoir 37, p. 277.

Bjørlykke, K., and A. Brendsdal, 1986, Diagenesis of Brent Sandstone in the Statfjord Field, In Gautier, D. L. (ed.), Role of organic matter in sediment diagenesis: SEPM Special Publication No. 38, p. 157-167.

Blanche, J. B., and J. H. M. Whitaker, 1978, Diagenesis of part of the Brent Sand Formation (Middle Jurassic) of the northern North Sea Basin: Quarterly Journal of the Geological Society of London, v. 135, p. 73-82.

Blatt, H., G. Middleton, and R. Murray, 1972, Origin of sedimentary rocks: Englewood Cliffs, NJ, Prentice-Hall, Inc., 634p.

Boles, J. R., and S. G. Franks, 1979, Clay diagenesis in Wilcox sandstones of southwest Texas: implications of smectite diagenesis on sandstone cementation: Journal of Sedimentary Petrology, v. 49, p. 55-70.

Boggs, S. Jr., 1995, Diagenesis (part five): In Principles of sedimentology and stratigraphy, second edition, Merrill Publishing Company, p. 265-301.

Bogomolov, Y. G., A. V. Kudelsky, and N. N. Lapshin, 1978, Hydrology of large sedimentary basins, in Hydrology of great sedimentary basins: Publication of the International Association of Scientific Hydrology, no. 120, p. 117-122.

Bonnefous, J., 1963, Synthese stratigraphique sur le Gothlandien des sondages du Sud tunisien: Inst. Francais Petrole Rev., v. 18, no. 10, p. 123-133.

Borst, R. L., and R. Q. Gregg, 1969, Authigenic mineral growth as revealed by the scanning electron microscope: Journal of sedimentary Petrology, v. 39, p. 1596-1597.

Bottinga, Y., 1968, Calculation of fractionation factors for carbon and oxygen exchange in the system calcite-carbon dioxide-water: Journal of Physical Chemistry, v. 72, p. 800-808.

Bredehoeft, J. D., and B. B. Hanshaw, 1968, On the maintenance of anomalous fluid pressures, 1, Thick sedimentary sequences: Geological Society of America Bulletin, v. 79, p. 1097-1106.

Brewer, R., 1964, Fabric and mineral analysis of soil: New York, John Wiley and Sons, 470p.

Breyer, J. A., 1983, Sandstone petrology: a survey for the exploration and production geologist, Mountain Geologist, v. 20, p. 15-40.

Brown, D. M., K. D. McAlpine, and R. W. Yole, 1989, Sedimentology and sandstone diagenesis of Hibernia Formation in Hibernia Oil Field, Grand Banks of Newfoundland: AAPG Bulletin, v. 73, no.5, p. 557-575.

Cathles, L. M., 1993, A discussion of flow mechanisms responsible for alteration and mineralization in the Cambrian Aquifers of the Ouachita-Arkoma Basin-Ozark System: In Horbury and Robinson (eds.), Diagenesis and basin development, AAPG Studies in Geology, no. 36, Chapter 8, p. 99-112.

Carothers, W. W., and Y. K. Kharaka, 1978, Aliphatic acid anions in oil-field waters-implications for origin of natural gas: AAPG Bulletin, v. 62, p. 2441-2453.

Chamberlain, C. K., 1978, Recognition of trace fossils in cores: In Basan, P. B. (ed.), Trace fossil concept, SEPM, Short Course, No. 5, Oklahoma City, P. 119-166.

Chepikov, K. P., Y. P. Yermolova, and N. A. Orlova, 1959, Epigenetic minerals as indicators of the time of entry of petroleum into commercial sandy reservoirs: Doklady of Academy of Sciences of the USSR, Earth Science Sections, v. 125, p. 288-289 (in English).

Chepikov, K. P., Y. P. Yermolova, and N. A. Orlova, 1961, Corrosion of quartz grains and examples of the possible effect of oil on the reservoir properties of sandy rocks: Doklady of Academy of Sciences of the USSR, Earth Science Sections, v. 140, p. 1111-1113 (in English).

Chilingarian, G. V., 1983, Compactional diagenesis: In Parker A., and B. W. Sellwood (eds.), Sediment Diagenesis, Series C: Mathematical and Physical Sciences , v. 115, p. 57-167.

Coleman, J. L., Jr., 1985, Diagenesis of Cotton Valley sandstone (Upper Jurassic), east Texas: implications for tight gas formation pay identification: discussion: AAPG Bulletin, v. 69, no. 5, p. 813-818.

Collomb, G. R., 1962, Etude géologique du jebel Fazzan et de sa bordure Paléozoïque, Notes, Mém. Comp. Fr. Pétrole, 1, 26p.

Conant L. C., and G. H. Goudarzi, (1967), Stratigraphic and tectonic framework of Libya, AAPG Bulletin, v. 51, no. 5, p. 719-730.

Cook, H. E., and R. M. Egbert, 1983, Diagenesis of deep-sea carbonate: In Larsen and Chillingar (eds.), Developments in sedimentology (25B), Diagenesis in sediments and sedimentary rocks, no. 2, p. 213-288.

Cowan, G., 1989, Diagenesis of Upper Carboniferous sandstones: Southern North Sea Basin: In Whateley and Pickering (eds.), Deltas sites and traps for fossil fuels, Geological Society Special Publication no. 41, p. 57-73.

Cramer, F. H., 1971, A palynostratigraphic model for Atlanic Pangea during Silurian time, In Colloque Ordovician-Silurian, Mémoires Du Bureau de Recherches Géologiques et Miniéres (B. R. G. M.), No. 73, p.229-235.

Cridland, R., 1991, Seismic stratigraphic evaluation of NC2 Concession (Ghadames Basin), AGOCO, Benghazi, 78p.

Curtis, C. D., 1978, possible links between sandstone diagenesis and depth-related geochemical reactions occurring in enclosing mudstones: Jour. Geol. Soc. London, v. 135, p. 107-117.

Curtis, C. D., M. L. Coleman and L. G. Love, 1986, Pore water evolution during sediment burial from isotopic and mineral chemistry of calcite, dolomite and siderite concretions. Geochim. Gosmochim. Acta., 50, p.2321-2334.

Daniels H. J., 1989, Petrographic analysis of sidewall cores from Memouniat, Tanezzuft, and Acacus Formation in Hamada Area, NW Libya (with emphasis on the Bir Tlacsin Limestone), AGOCO, Benghazi, 10p.

Davis, D. K., and F. G. Ethridge, 1975, Sandstone composition and depositional environment: AAPG Bulletin, v. 59, p. 239-264.

De Castro, J. C., J. C. D. Favera, and M. El-Jadi, 1991, Tempestite facies, Murzuq Basin, Great Socialist People's Libyan Arab Jamahiriya: Their recognition and stratigraphic implications, In Salem, and Belaid (eds.), The Geology of Libya, v. V, p.1757-1765.

Deming, D., and J. A. Nunn, 1991, Numerical simulations of brine migration by topographically driven recharge: Journal of Geophysical Research, v. 96, no. B2, p. 2485-2499.

Deming D., J. H. Sass, A. H. Lachenbruch, and R. F. De Rito, 1992, Heat flow and subsurface temperature as evidence for basin-scale ground-water flow, North Slope of Alaska: Geol. Soc. Am. Bulletin, v. 104, p. 528-542.

Desio, A., 1936, Riassunto sulla costituzione geologica del Fazzan, Boll. Soc. Geol. Ital., 55, 349-356.

Destombes, J., 1968, Sur la nature glaciaire des sédiments du 2 me Bani, Ashgill Supérieur de l'Anti-Atlas (Maroc), Compte rendu de l'Academie des Sciences, 267, p. 684-689.

De Ros, L. F., 1986, Petrologia et caracteristics de reservatorio da Formação Sergi (Jurãssico) no campo de Sesmaria, Bacia do recõncavo, Brasil: Ciência Têcnica & Petrôleo, v. 19, 107p.

Destombes, J., H. Holland, and S. Willefert, 1985, Lower Paleozoic rocks of Morocco, In C. H. Holland (ed.), Lower Paleozoic of the Middle East, eastern and southern Africa and Antarctica: Lower Paleozoic Rocks of the World, v. 3, New York, John Wiley, 331p.

Dickinson, W. W., and K. L. Milliken, 1993, Sandstone compaction by interrelated brittle deformation and pressure solution, Etjo Sandstone, Namibia: Geological Society of America Abstracts with Programs, v. 25, p. A-65.

Dixon, S. A., D. M. Summers, and R. C. Surdam, 1989, Diagenesis and preservation of porosity in Norphlet Formation (Upper Jurassic), Southern Alabama, AAPG Bulletin, v. 73, no. 6, p. 707-728.

Doe, T. W., R. H. Dott, Jr., and I. E. Odom, 1976, Nature of feldspar grain size relations in some quartz-rich sandstones: Journal of Sedimentary Petrology, v. 46, p. 862-870.

Dorobek, S. L., 1987, Petrography, geochemistry, and origin of burial diagenetic facies, Siluro-Devonian Helderberg Group (Carbonate Rocks), Central Appalachians, AAPG Bulletin, v. 71, no. 5, p. 492-514.

Dubay, L. 1980, Ground water in Wādī ash Shāṭi', Fazzān- A case history of resource development: In Salem, and Busrewil (eds.), The Geology of Libya, v. II, p. 611-627.

Dunn, T. L., 1993, Early quartz grain fracturing and annealing: an important brittle deformation mechanism of early compaction in first cycle orogenic sandstones, revealed by scanning electron cathode luminescence microscopy (abs.): Geological Society of America Abstracts with programs, v. 25, p. A-335.

Dunne, T., 1990, Hydrology, mechanics, and geomorphic implications of erosion by subsurface flow, in Ground water Geomorphology: In Higgins, and Coats (eds.), The Role of Subsurface Water in Earth-Surface Processes and Landforms, Geol, Soc. Am. Spec. Pap., v. 252, no. 1, p. 1-28.

Dutton, S. P., L. S. Land, 1985, Meteoric burial diagenesis of Pennsylvanian Arkosic Sandstones, southwestern Anadarko Basin, Texas, AAPG Bulletin, v. 69, no. 1, p. 22-38.

Dutton, S. P., H. S. Hamlin, R. L. Folk, and S. J. Clift, 1996, Early siderite cementation as a control on reservoir quality in submarine fan sandstones, Sonora Canyon gas play, Val Verde Basin, Texas, SEPM Special Publication No. 55, p. 115-127.

Echikh, A., and A. S. Suleiman, 1982, Preliminary geological study and petroleum evaluation of Ghadames Basin, N. O. C., internal N. O. C. report.

Elfigih, O. B., 1991, The sedimentology and reservoir characteristics of the Lower Acacus Formation, NC2 Concession, Hamada Basin, NW Libya, M.Sc. thesis, Memorial University of Newfoundland, St'John's, Newfoundland, Canada, 569p.

Essed, A., 1978, Gravity map of Libya from Master research: personal copy provided to Dr. J. D. Harper, 1986.

Franks, S., and R. Forester, 1984, Relationships among secondary porosity, pore-fluid chemistry and carbon dioxide, Texas Gulf Coast, in Clastic Diagenesis: AAPG Memoir 37, p. 63-79.

Franklin, S. P., and T. T. Tieh, 1989, Petrography, diagenesis, and reservoir properties of the Dakota Sandstone of West Lindrith Field, Rio Arriba County, New Mexico: In Coalson, E. B. (ed.), Petrogenesis and petrophysics of selected sandstone reservoirs of the Rocky Mountain Region, The Rocky Mountain Association of Geologists, Denver, Colorado, p. 117-244.

Folk, R. L., 1980, Petrology of sedimentary rocks: Austin, Texas, Hemphill, 182p.

Fothergill, C. A., 1955, The cementation of oil reservoir sands and its origin: Proceedings of the 4th World Petroleum Congress, p. 301-314.

Fox, J. E., P. W. Lambert, R. F. Mast, and N. W. Nuss, 1975, Maps showing porosity variations and geothermal gradients of the upper part of the Tensleep Sandstone and equivalents, Bighorn, Wind River and Great Green River Basins, Wyoming: U. S. Geological Survey Open-File Report, 75/280, 8p.

Freeze R. A., P. A. Witherspoon, 1967, Theoretical analysis of regional groundwater flow: 2, Effect of water-table configuration and subsurface permeability variation, Water Resour. Res. 3, p. 623-643.

Friedman, G. M., 1961, Distinction between dune, beach, and river sands from their textural characteristics: Journal of Sedimentary Petrology, v. 31, p. 514-529.

Friedman, I., and J. R. O'Neil, 1977, Compilation of stable isotope fractionation factors of geochemical interest, In M. Fleischer (ed.), Data of geochemistry, sixth edition: U. S. Geological Survey Profissional paper 440-KK, 12p.

Füchtbauer, H., 1967, Influence of different types of diagenesis on sandstone porosity: 7th World Petroleum Congress Proceedings, v. 2, p. 353-369.

Füchtbauer, H., 1974, Sediments and sedimentary rocks 1, sedimentary petrology, part II: New York, John Wiely and Sons, 464p.

Füchtbauer, H. 1979, Die Sandsteindiagenese im Spiegel der neueren Literatur: Geologische Rundschau, v. 68, p. 1125-1151.

Galloway, W. E., D. K. Hobday, and K. Magara, 1982, Frio Formation of the Texas Gulf Coast Plain-depositional systems, strctural framework, and hydrocarbon distribution: AAPG Bulletin, v. 66, p. 649-688.

Galloway, W. E., and D. K. Hobday, 1983, Terrigenous clastic depositional systems: application to petroleum, coal, and uranium exploration: New York, Springer-Verlag.

Galloway, W. E., 1984, Hydrologic regimes of sandstone diagenesis, In McDonald D. A., and Surdam R. C. (eds.), Clastic diagenesis, AAPG Memoir 37, p. 3-13.

Garven, G., 1995, Continental-scale groundwater flow and geologic processes, Annu. Rev. Earth Planet. Sci., 23, p. 89-117.

Ghori, K. A. R., 1982, Suggestions for future geochemical studies in the Ghadames Basin, AGOCO, Benghazi, 26p.

Ghori, K. A. R., 1985, Petroleum geochemical evaluation of Tanezzuft Shale Formation, GG1-NC7A, AGOCO, Benghazi, 10p.

Goudarzi, G. H., 1970, Geology and mineral resources of Libya-A reconnaissance. U. S. Geol. Surv. Prof. Pap., 660, 104p.

Goudarzi, G. H., and J. P. Smith, 1978, preliminary structure contour map of the Libyan Arab Republic and adjacent areas; 1:2000 000. U. S. Geol. Surv. Misc. Geol. Invest., map I-350C.

Goudarzi, G. H., 1980, Structure-Libya, in Salem, M., and Busrewil, M. (eds.), The Geology of Libya, v. III, p. 879-892.

Hammuda, O. S., 1980, Geologic factors controlling fluid trapping and anomalous freshwater occurrence in the Tadrart Sandstone, Al Hamādah al Hamrā' Area, Ghadāmis Basin, In Salem, M., and Busrewil, M. (eds.), The Geology of Libya v. II, p.501-507.

Hancock, N. J., and A. M. Taylor, 1978, Clay mineral diagenesis and oil migration in the Middle Jurassic Brent Sand Formation: Journal of the Geological Society of London, v. 135, p. 69-72.

Hardie, L. A., 1991, On the significance of evaporites, Annu. Rev. Earth Planet. Sci. 19, p. 131-168.

Harrison, W. J., and R. N. Tempel, 1993, Diagenetic pathways in sedimentary basins, In Horbury, A. D., and Robinson, A. G. (eds.), Diagenesis and basin development, AAPG Studies in Geology, no. 36, p.69-86.

Hayes, J. B., 1979, Sandstone diagenesis-the hole truth (abs.): SEPM Special Publication No. 26, p. 127-139.

Hitchon, B., 1969a, Fluid flow in the western Canada sedimentary basin, 1, Effect of topography: Water Resources Research, v. 5, p. 186-195.

Hitchon, B., 1969b, Fluid flow in western Canada sedimentary basin, 2, Effect of geology: Water Resources Research, v. 5, p. 460-469.

Hoholick, J. D., T. Metarko, and P. E. Potter, 1984, Regional variations of porosity and cement: St. Peter and Mount Simon Sandstones in Illinois Basin: AAPG Bulletin, v. 68, p. 753-764.

Hubbert, M. K., 1953, Entrapment of petroleum under hydrodynamic conditions, AAPG Bulletin, v. 37, p. 1954-2026.

Hubert, J. F., J. G. Butera, and R. F. Rice, (1972), Sedimentology of Upper Cretaceous Cody-Parkman delta, southwestern Power River Basin, Wyoming, Geological Society of America Bulletin, v. 83, p. 1649-1670.

Hunt, J. M., 1979, Petroleum geochemistry and geology: San Francisco, W. H. Freeman, 617p.

Hurst, A. R., and H. Irwin (1982), Geological modelling of clay diagenesis in sandstones, Clay Miner., 17, p. 5-22.

Imam, M. D., 1986, Scanning electron microscopy study of the quartz overgrowths within Neogene Sandstones of the Bengal Basin, Bangladesh: Journal of the Geological Society of India, v. 28, p. 407-413.

Imam M. D., and H. F. Shaw, 1987, Diagenetic controls on the reservoir properties of gas bearing Neogene Surma Group Sandstone in the Bengal Basin, Bangladesh, Marine and petrol. Geol., 4, p. 103-111.

Johnson, R. H., 1920, The cementation process in sandstones: AAPG Bulletin, v. 4, p. 33-35.

Johnson, S. Y., C. J. Schenk, D. L. Anders, and M. L. Tuttle, 1990, Sedimentology and petroleum occurrence, Schoolhouse Member, Maroon Formation (Lower Permian), Northwestern Colorado, AAPG Bulletin, v. 74, no. 2, p. 135-150.

Jones, P. J., T. E. Stump, 1999, Depositional and tectonic setting of the Lower Silurian Hydrocarbon source rock facies, central Saudi Arabia, AAPG Bulletin, v. 82. no. 2, p. 314-332.

Kaldi, J., D. H. Krinsley, and D. Lawson, 1978, Experimentally produced aeolian surface textures on quartz sand grains from various environments, In Whally, W. B. (ed.), Scanning electron microscopy in the study of sediments, a symposium, p. 261-274.

Karasek, M. M., 1981, Structural and stratigraphic analysis of the Paleozoic Murzuk and Ghadames Basins, western Libya, Ph.D. thesis, University of South Carolina, 146p.

Keegan, J. B., S. M. Rasul, and Y. Shayeen, 1990, Palynostratigraphy of the Lower Paleozoic, Cambrian to Silurian, sediments of the Hashemite Kingdom of Jordan: Review of Paleobotany and Palynology, v. 66, p. 167-180.

Kieke, E. M., and D. J. Hartmann, 1973, Scanning electron microscopy application to formation evaluation: Gulf Coast Assoc. Geol. Socs., Trans., v. 23, p. 60-67.

Kingston, D. R., C. P. Dishroon, and P. A. Williams, 1983, Global basin classification system, AAPG Bulletin, v. 67, no. 12, p. 2175-2193.

Kingston, D. R., C. P. Dishroon, and p. A. Williams, 1983, Hydrocarbon plays and global basin classification, AAPG Bulletin, v. 67, no. 12, p. 2194-2198.

Kissin, I. G., 1978, The principle distinctive features of the hydrodynamic regime of intensive earth crust downwarping areas, in Hydrogeology of great sedimentary basins: Publication of the International Association of Scientific Hydrology, no. 120, p. 178-185.

Klitzsch, E., 1966, Comments on the geology of the central parts of southern Libya and northern Chad, In Williams, J. J. (ed.), South-Central Libya and Northern Chad, Petrol. Explor. Soc. Libya, 8th annu.Field Conf., p. 1-17.

Klitzsch, E., 1970, Die Strukturgeschichte der zentralsahara: neue erkenntnisse zum bau und zur paläogeographie eines tafellandes, Geol. Rundsch., 59, 459-527.

Klitzsch, E., 1971, The structural development of parts of North Africa since Cambrian time, in Gray, C. (ed.), Symposium on the Geology of Libya, Faculty of Science, Tripoli University, Libya, p. 253-262.

Klitzsch, E., 1981, Lower Paleozoic rocks of Libya, Egypt, and Sudan, In Holland C. H. (ed.), Lower Paleozoic of the Middle East, eastern and southern Africa, and Antarctica, p. 131-161.

Krinsely, D. H., and F. McCoy, 1978, Aeolian quartz sand and silt, in Whally, W. B. (ed.), Scanning electron microscopy in the study of sediments, a symposium, p. 249-260.

Krynine, P. D., 1947, Petrologic aspects of prospecting for deep oil horizons in Pennsylvania: Proceedings of the 11th Technical Conference on Petroleum Production , Pennsylvania State College, University Park, Penssylvania, p. 81-95.

Krystinik, L. F., 1981, Pore-filling cements- products of shale dewatering in the Upper Miocene Stevens Sandstone, Elk Hills, Kern County, Ca. (abs.), Pacific Petroleum Geologists Newsletter, p. 3-5.

Land, L. S., and S. P. Dutton, 1978, Cementation of Pennsylvanian deltaic sandstone-isotopic data: Journal of Sedimentary Petrology, v. 48, p. 1167-1176.

Land, L. S., and D. R. Prezbindowski, 1981, origin and evolution of saline formation water, lower Cretaceous carbonates, south-central Texas, U. S. A: Journal of Hydrology, v. 54, p. 51-74.

Land, L. S., K. L. Milliken, and E. F. McBride, 1987, Diagenetic evolution of Cenozoic sandstones, Gulf of Mexico sedimentary basin: Sedimentary Geology, v. 50, p. 195-225.

Larese, R. E., N. L. Haskell, D. R. Prebindowski, and D. Beju, 1984, Porosity development in selected Jurassic sandstones from Norwegian and North Sea, Norway- an overview, In Graham and Trotman (eds.), Petroleum Geology of the North European Margin, Norw., Pet. Soc., p. 81-95.

Lasseter, T. J., J. R. Waggoner, and L. W. Lake, 1986, Reservoir heterogeneities and their influence on ultimate recovery: In Lake, L. W., and Carrol, H. B., Jr. (eds.), Reservoir characterization, Orlando, Florida, Academic Press, p. 487-544.

Le Ribault, L., 1978, The exoscopy of quartz sand grains, in Whalley, W. B. (ed.), Scanning electron microscopy in the study of sediments, a symposium, p.319-328.

Levandovski, D. W., M. E. Kaley, S. R. Silverman, and R. G. Smalley, 1973, Cementation in Lyons Sandstone and its role in oil accumulation, Denver Basin, Colorado: AAPG Bulletin, v. 57, p. 2217-2244.

Longman, M. W., 1981, Carbonate diagenesis as a control on stratigraphic traps (with examples from the Williston Basin), AAPG Education Course Note Series No. 21, p. 60-117

Longstaffe, F. J., 1983, Stable isotope studies of diagenesis in clastic rocks: Geoscience Canada, v. 10, p. 43-58.

Longstaffe, F. J., 1989, Stable isotopes as traces in clastic diagenesis, In Hutcheon, I. E. (ed.), Burial Diagenesis, Miner. Ass. Canada Short Course, 15, p. 201-277.

Longstaffe, F. J., 1984, The role of meteoric water in diagenesis of shallow sandstones: Stable isotope studies of the Milk River aquifer and gas pool, southeastern Alberta, In McDonald, D. A. And R. C. Surdam (eds.), Clastic Diagenesis, AAPG Memoir 37, p. 81-98.

Longstaffe, F. J., M. A. Racki, and A. Ayalon, 1992, Stable isotope studies of diagenesis in berthierine-bearing oil sands, Clearwater Formation, northeastern Alberta, In Kharaka, Y. K., and Maest, A. S. (eds.), Proceedings of the 7th international Symposium on Water-Rock Interaction, Park City, Utah: A.A. Balkerma Publications, p. 955-958.

Longstaffe, F. J., 1994, Stable isotopic constraints on sandstone diagenesis in the Western Canada sedimentary basin, In Parker, A., and Sellwood, B W. (eds.), Quantitative diagenesis: recent developments and applications to reservoir geology: Dordrecht, Kluwer Academic publishers, p. 223-274.

Loomis, J. L., and L. J. Crossey, 1996, Diagenesis in a cyclic, regressive siliciclastic sequence: The Point Lookout Sandstone, San Juan Basin, Colorado, in SEPM Special Publication No. 55, p.23-36.

Loucks, R. G., D. G. Bebout, and W. E. Galloway, 1977, Relationship of porosity formation and preservation to sandstone consolidation history-Gulf Coast Lower Tertiary Frio Formation: Gulf oast Aossciation of Geological Societies Tranactions, v. 27, p. 109-120.

Loucks, R. G., M. M. Dodge, and W. E. Galloway, 1984, Regional control on diagenesis and reservoir quality in Lower Tertiary sandstones along the Texas Gulf Coast, In McDonald D. A., and Surdam, R. C. (eds.), Clastic Diagenesis: AAPG Memoir 37, p. 15-46.

Lundegard, P. D., and L. S. Land, 1986, Carbon dioxide and organic acids: their role in porosity enhancement and cementation, Paleogene of the Texas Gulf Coast, In Gautier, D. L. (ed.), Roles of Organic Matter in Sediment Diagenesis, SEPM Special publication No. 38, Tulsa, p. 129-146.

Lynch, F. L., 1996, Mineral/water interaction, fluid flow, and Frio Sandstone diagenesis: Evidence from the rocks, AAPG Bulletin, v. 80, no. 4, p. 486-504.

Magara, K., 1980, Comparison of porosity-depth relationships of shale and sandstone: Journal of Petroleum Geology, v. 3, p. 175-185.

Makhous M., Y. Galushkin, and N. Lopatin, 1997, Burial History and kinetic modelling for hydrocarbon generation, Part II: Applying the Galo model to Saharan Basins, AAPG Bulletin, v. 81, no. 10, p. 1679-1699.

Malicsc, A., and J. Mazzullo, 1996, Early diagenesis and paleosoil features of ancient desert sediments: examples from the Permian Basin, SEPM Special publication No. 55, p. 151-161.

Markert, J. C., and Z. Al-Shaieb, 1984, Diagenesis and evolution of secondary porosity in Upper Minnelusa Sandstones, Power River Basin, Wyoming, In McDonald, D. A., and Surdam, R. C. (eds.), Clastic Diagenesis, AAPG Memoir 37, p. 367-389.

Marshall, D. J., 1978, Suggested standars for the reporting of cathodoluminescence results: Journal of Sedimentary Petrology, v. 48, p. 651-653.

Massa, D., and G. R. Collomb, 1960, Observation nouvelles sur la région d'Aouinet ouenine et du Djebel Fazzan (Libye). Proc. 21st Int. Geol. Congr. (Norden), 12, p. 65-73.

Massa, D., and H. Jaeger, 1971, Données stratigraphiques sur le Silurien de l'Ouest de la Libya, In Brest (ed.), Colloque Ordovicien-Silurien, Bur. Rech. Geol. Min. Bull., 73, p. 313-321.

Matlack, K. S., D. W. Housekenecht, and K. R. Applin, 1989, Emplacement of clay into sand by infiltration: Journal of Sedimentary Petrology, v. 59, p. 77-87.

Maxwell, J., C., 1964, Influence of depth, temperature, and geologic age on porosity of quartzose sandstone: AAPG Bulletin, v. 48, p. 697-709.

McBride, E. F., 1977, Secondary porosity-importance in sandstone reservoirs in Texas: Transactions of the Gulf Coast Association of Geological Societies, v. 27, p. 121-122.

McBride, E. F., L. S. Land, and L. E. Mack, 1987, Diagenesis of eolian and fluvial feldspathic sandstones, Nophlet Formation (Upper Jurassic), Rankin County, Mississippi, and Mobile County, Alabama, AAPG Bulletin, v. 71, no. 9, p. 1019-1034.

Milliken, K. L., L. S. Land, and R. G. Loucks, 1981, History of burial diagenesis determined from isotopic geochemistry, Frio Formation, Brazoria County, Texas, AAPG Bulletin, v. 65, p. 1397-1413.

Milliken, K. L., E. F. McBride, W. Cavazza, U. Cibin, D. Fontana, M. D. Picard, and G. G. Zuffa, 1998, Geochemical history of calcite precipitation in Tertiary sandstones, northern Apennines, Italy: In Sadoon Morad (ed.), Carbonate Cementation in Sandstones, Distribution Patterns and Geochemical Evolution, Special Publication No. 26 of the International Association of Sedimentologists, Blackwell Science, p.213-239.

Moiola, R. J., and D. Weiser, 1968, Textural parameters: an evaluation: Journal of Sedimentary Petrology, v. 38, p. 45-53.

Moore, C. H., and Y. Druckman, 1981, Burial diagenesis and porosity evolution, Upper Jurassic Smackover, Arkansas and Louisiana: AAPG Bulletin, v. 65, p. 597-628.

Moncure, G. K., R. W. Lahann, and R. M. Siebert, 1984, Origin of secondary porosity and cement distribution in a sandstone shale sequence from Frio Formation (Oligocene), In McDonald, D. A., and Surdam, R. C. (eds.), Clastic Diagenesis, AAPG Memoir 37, p. 151-161.

Moraes, M. A. S., and C. H. L. Bruhn, 1988, Brazilian turbidite reservoirs: heterogeneity study from outcrops to subsurfsce (abs.), AAPG Bulletin, v. 72, p. 225.

Moraes, M. A. S., and L. F. De Ros, 1990, Infiltrated clays in fluvial Jurassic sandstones of Recôncavo Basin, northeaster Brazil: Journal of Sedimentary Petrology, v. 60, p. 809-819.

Moraes, M. A. S., 1991, Diagenesis and microscopic heterogeneity in lacustrine deltaic and turbiditic sandstone reservoirs (Lower Cretaceous), Potiguar Basin, Brazil: AAPG Bulletin, v. 75, p. 1758-1771.

Moraes, M. A. S., and R. C. Surdam, 1993, Diagenetic heterogeneity and reservoir quality: fluvial, deltaic, and turbiditic sandstone reservoirs, Potiguar and Recôncavo Rift Basins, Brazil, AAPG Bulletin, v. 77, no. 7, p. 1142-1158.

Morse, J. W., 1983, The kinetics of calcium carbonate dissolution and precipitation:In Reeder, R. J. (ed.), Carbonates: Mineralogy and Chemistry, Review in Mineralogy, Mineralogical Society of America, v. 11, p. 227-262.

Mycielska-Dowgiallo, E., 1978, A scanning electron microscope study of quartz grain surface textures from boulder clays of north and central Poland, In Whalley, W. B. (ed.), Scanning electron microscopy in the study of sediments, a symposium, p. 243-248.

National Oil Corporation (N. O. C.)- Libya, 1981, Regional structural cross-section illustrating concepts of stratigraphic and structural relations in the Hamada Basin, NW Libya, N. O. C. Exploration Department, Tripoli.

National Oil Corporation (N. O. C.)- Libya, 1995, Regional Geological study (structure and geomorphology) of northwestern Libya, Jordi, H. A., and Lonfant, F. (eds.), map showing morphology of northwestern Libya, N. O. C., Tripoli.

Odom, I, E., 1975, Feldspar grain-size relations in Cambrian arenites, Upper Mississippi Valley: Journal of Sedimentary Petrology, v. 45, p. 636-650.

Padki, D. C., and J. E. Fox, 1989, Petrography and petrophysics of the Upper Cretaceous Terner sandy members of the Carlile Shale at Todd Field, Power River Basin, Wyoming, In Coalsom, Kaplan, Keighin, Oglesby, and Robinson, (eds.), Petrogenesis and petrophysics of selected sandstone reservoirs of the Rocky Mountain Region, Denver, Colorado, p. 235-244.

Pallas, P., 1980, Water resources of the Socialist People's Libyan Arab Jamahiriya, In Salem, M., and Busrewil, M. (eds.), The Geology of Libya, v. II, p. 539-594.

Peterson, J. A., and J. C. Osmond, 1961, Geometry of sandstone bodies: Tulsa, AAPG Bulletin, v. 31, p. 514-529.

Pettijohn, F. J., P. E. Potter, and R. Siever, 1972, Sand and sandstone: New York, Springer-Verlag, 618p.

Pierobon, E. S. T., 1991, Contribution to the stratigraphy of the Murzuq Basin, SW Libya, In Salem, A., and Belaid, M. (eds.), The Geology of Libya, v. V, p. 1767-1783.

Pittman, E. D., 1972, Diagenesis of quartz in sandstones as revealed by scanning electron microscopy: Journal of Sedimentary Petrology, v. 42, p. 507-519.

Pittman, E. D., 1979, Porosity, diagenesis, and productive capability of sandstone reservoirs, In Scholle, P. A., and Schluger, P. R. (eds.), Aspects of diagenesis SPEM Special Publication No. 26, p. 159-173.

Porter, K. W., and R. J. Weimer, 1982, Diagenetic sequence related to structural history and petroleum accumulation: Spindle Field, Colorado, AAPG Bulletin, v. 66, no. 12, p. 2543-2560.

Potosky, R. A., 1970, Application of cathodoluminescence to petrographic studies: The Compass, v. 47, p. 63-69.

Potter, P. E., 1967, Sand bodies and sedimentary environments: a review: AAPG Bulletin, v. 51, p. 337-365.

Prothero, D. R., and F. Schwab, 1996, Siliciclastic diagenesis: In An introduction to sedimentary rocks and stratigraphy, Sedimentary Geology, Chapter 7, Freeman and Company, p. 121-135.

Prothero, D. R., and F. Schwab, 1996, Carbonate rocks: In An introduction to sedimentary rocks and stratigraphy, Sedimentary Geology, Chapter 11, Freeman and Company, p. 232-253.

Pusey, W. C., III, 1973, Paleotemperatures in the Gulf Coast using the ESR-kerogen method: Gulf Coast Association of Geological Societies Transactions, v. 23, p. 195-202.

Reed, W. E., R. Lefever, and G. J. Moir, 1975, Depositional environment interpretation from settling vel. (psi) distributions: Geological Society of America Bulletin, v. 86. P. 1321-1328.

Riecke, H. H., III, and G.V. Chilingarian (eds.), 1974, Compaction of argillaceous sediments: Elsevier, New York, 424p.

Rossel, N. C., 1982, Clay mineral diagenesis in Rotliegend aeolian sandstones of the southern North Sea: Clay Minerals, v. 17, p. 69-77.

Said, F. M., 1974, Sedimentary history of the Paleozoic rocks of the Ghadames Basin in Libyan Arab Republic, M.Sc. thesis, University of South Carolina, 39p.

Saigal, G. C., K. Bjørlykke, and S. Larter, 1992, The effects of oil emplacement on diagenetic processes-examples from the Flumar Reservoir Sandstones, central North Sea, AAPG Bulletin, v. 76, no. 7, p. 1024-1033.

Santa Maria, F. S., 1991, Ghadames Basin regional study, analysis and evaluation, AGOCO internal report, Benghazi, p. 158.

Savkevich, S. S., 1969, Variation in sandstone porosity in lithogenesis (as related to the prediction of secondary porous oil and gas reservoirs): Doklady of the Academy of Sceinces of the USSR, Earth Science Sections, v. 184, p. 161-163 (in English).

Schlumberger, 1972, Log interpretation manual/principles, v. I, Houston, Schlumberger Well Services, Inc., 113p.

Schmidt, V., D. A. McDonald, and R. L. Platt, 1977, Pore geometry and reservoir aspects of secondary porosity in sandstones, Bulletin of Canadian Petroleum Geology, v. 25, no. 2, p. 271-290.

Schmidt, V., and D. A. McDonald, 1979a, The role of secondary porosity in sandstones, in Scholle, P. A., and Schluger, P. R. (eds.), Aspects of diagenesis: SEPM Special Publication No. 26, p. 175-207.

Schmidt, V. And D. A. McDonald, 1979b, Texture and recognition of secondary porosity in sandstones, In Scholle, P. A., and Schluger, P. R. (eds.), Aspects of diagenesis: SEPM Special Publication 26, p. 209-225.

Schwartz, F. W., and K. Muehlenbachs, 1979, Isotope and ion geochemistry of groundwater in the Milk River aquifer, Alberta: Water Resources Research, v. 15, p. 259-268.

Scotese, C. R., R. K. Bambach, C. Barton, R. Van der Voo, and A. Ziegler, 1979, Paleozoic base maps : Journal of Geology, v. 87, p. 217-227.

Seemann, U., 1982, Depositional facies, diagenetic clay minerals and reservoir quality of Rotliegend sediments in the southern Permian Basin (North Sea): a review: Clay Minerals, v. 17, p. 55-67.

Seilacher, A., 1969, Sedimentary rhythms and trace fossils in Paleozoic sandstones of Libya, In Kanes, W. H. (ed.) Geology Archaeology and prehistory of the southwestern Fazzan-Libya, Petroleum Exploration Society of Libya, 11th Annu. Field Conf., p. 117-123.

Selby, M. J., 1985, Earth's changing surface, An introduction to geomorphology, Ice ages, chapter 16, Clarendon Press. Oxford, p. 468-512.

Selley, R. C., 1978, Porosity gradients in the North Sea oil-bearing sandstones: Geological Society of London Journal, v. 135, p. 119-132.

Selley, R. C. (ed.), 1982, Particles and pores: In An introduction to sedimentology, second edition, Academic Press, Ch. 2, p. 7-44.

Selley, R. C. (ed.), 1982, Allochthonous sediments: In An Introduction to sedimentology, second edition, Academic Press, Ch. 4, p. 62-111.

Selley, R. C. (ed.), 1998, The Reservoir, in Elements of Petroleum Geology, second edition, Academic Press, p. 239-306.

Shah, H. A., O. B. Elfigih, and A. Shahlool, 1988, Geological factors controlling the oil and gas deposits of Hamada Basin and recommendations for their future exploration, AGOCO internal report, Benghazi, 34p.

Shanmugam, G., 1985, Significance of secondary porosity in interpreting sandstone composition, AAPG Bulletin, v. 69, no. 3, p. 378-384.

Sharp, J. M. Jr., and P. A. Domenico, 1976, Energy transport in thick sequences of compacting sediment, Geol. Soc. Am. Bull. 87. P. 390-400.

Sibley, D. F., and H. Blatt, 1976, Intergranular pressure solution and cementation of the Tuscarora orthoquartzite: Journal of Sedimentary Petrology, v. 46, p. 881-896.

Siever, R., 1962, Silica solubility, 0-200°C and the diagenesis of siliceous sediments: Journal of Geology, v. 79, p. 127-151.

Sinha, S. C., 1980, On the application of geophysical logging in the assessment of groundwater potential in Al Hamādah al Hamrā' Basin, in Salem, M., and Busrewil, M. (eds.), The Geology of Libya, v. II, p. 643-658.

Sippel, R. F., 1968, Sandstone petrology, evidence from luminescence petrography: Journal of Sedimentary Petrology, v. 38, p. 530-554.

Sloss, L. L., and R. C. Speed, 1974, Relationships of cratonic and continental-margin tectonic episodes, SEPM Special Publication No. 22, p. 98-119.

Smith, L., and D. S. Chapman, 1983, On the thermal effects of groundwater flow, 1, Regional scale systems, Journal of Geophys. Res. 88, p. 593-608.

Smith, L., C. Forster, and J. Evans, 1990, Interaction of fault zones, fluid flow, and heat transfer at the basin scale, In Neuman, S.P., and Neretnieks, I. (eds.), Hydrogeology of Low Permeability Environments, Int. Assoc. Hydrogeol. Spec. Symp., 28th Int. Geol. Congress, Washington, 2, p. 41-67, Hannover, Germany: H. Heise.

Spjeldnæs, N., 1961, Ordovician climatic zones, Norsk. Geol. Tidsskr., 41, p. 45-77.

Spjeldnæs, N., 1981, Lower Paleozoic palaeoclimatology: In Holland, C. H. (ed.), Lower Paleozoic of the Middle East, Eastern and Southern Africa and Antarctica, John Wiley & Sons, Chinchester, New York, Brisbane, Toronto.

Sommer, F., 1978, Diagenesis of Jurassic sandstones in the Viking graben: Journal of the Geological Society of London, v. 135, p. 63-67.

Souza, R. S., L. F. De Ros, and S. Morad, 1995, Dolomite diagenesis and porosity preservation in lithic reservoirs: Carmópolis Member, Sergipe-Alagoas Basin, Northeastern Brazil, AAPG Bulletin, v. 79, no. 5, p. 725-748.

Stone, W. N., and R. Siever, 1996, Quantifying compaction , pressure solution and quartz cementation in moderately-and deeply-buried quartoze sandstones from the Greater Green River Basin, Wyoming, SEPM Special Publication No. 55, p. 129-150.

Stonecipher, S. A., 1982, Diagenetic/stratigraphic modeling: A tool for understanding porosity/permeability profiles: Abstracts of the 11th International Association of Sedimentologists Congress, Hamilton, ON., p. 120.

Stonecipher, S. A., R. D. Winn, Jr., and M. G. Bishop, 1984, Diagenesis of the Frontier Formation, Moxa Arch: A function of sandstone geometry, texture, and composition, and fluid flux, In McDonald, D.A., and Surdam, R. C. (eds.), Clastic Diagenesis, Part 3-Applications of clastic diagenesis in exploration and production, AAPG Memoir 37, p. 289-316.

Sullivan, K. B., and E. F. McBride, 1991, Diagenesis of sandstones at shale contacts and diagenetic heterogeneity, Frio Formation, Texas: AAPG Bulletin, v. 75, p. 121-138.

Surdam, R. C., S. W. Boese, and L. J. Crossey, 1984, The chemistry of secondary porosity, In McDonald, D. A., and Surdam, R. C. (eds.), Clastic Diagenesis, AAPG Memoir 37, p. 127-151.

Takbali, A. O., and G. D. Wood, 1991, Silurian spores, Acritarchs and Chitinozoans from the Bani Walid Borehole of Ghadames Basin, NW Libya, In Salem, M., Hammuda, O., and Eliagoubi, B. (eds.), The Geology of Libya, v. IV, p. 1243-1274.

TakenouchI, S., and G. C. Kennedy, 1965, The solubility of carbon dioxide in NaCl solutions at high temperatures and pressures: American Journal of Science, v. 263, p. 445-454.

Tang, Z., J. Parnell, and F. J. Longstaffe, 1997, Diagenesis and reservoir potential of Permian-Triassic fluvial/lacustrine sandstones in the southern Junggar Basin, nothwestern China, AAPG, v. 81, no. 11, p. 1843-1865.

Tayler, J. M., 1950, Pore space reduction in sandstones: AAPG Bulletin, v. 34, p. 701-716.

Thomas, M. B., and T. A. Oliver, 1979, Depth-porosity relationships in the Viking and Cardium Formations of central Alberta: Canadian Society of petroleum Geologists Bulletin, v. 27, p. 209-228.

Tissot, B. P., and D. H. Welte, 1978, Petroleum formation and occurrence, First edition, Springer-Verlag, Berlin, 538p.

Todd, T. W., 1963, Post-depositional history of Tensleep Sandstone (Pennsylvanian), Big Horn Basin, Wyoming: AAPG Bulletin, v. 43, p. 273-310.

Toth, J., 1962, A theory of groundwater motion in small drainage basins in central Alberta, Journal of Geophys. Res. 67, p. 4375-4387.

Toth, J. 1980, Cross formational gravity flow of groundwater: A mechanism of the transport and accumulation of Petroleum, In Roert, W. H., and Cordell, R. J., Problems of Petroleum migration, AAPG Studies in Geology No. 10, p. 121-167.

Towe, K. M., 1962, Diagenesis of clay minerals as a possible source of silica cementation in sedimentary rocks: Journal of Sedimentary Petrology, v. 32, p. 26-38.

Tucker, M. E., and V. P. Wright (eds.), 1990, Diagenetic processes, products, and environments (Chapter 7), and Dolomites and dolomitization models (Chapter 8), In Carbonate Sedimentology, Blackwell Scientific Publications, p. 314-396.

Turner, J. R. and S. J. Conger, 1981, Environment of deposition and reservoir properties of the Woodbine Sandstone at Kurten Field, Brazos County, Texas, Gulf Coast Association of Geological Society Transactions, v. 31, p. 213-223.

Van Eysinga, F. W. B., 1975, Geological Time Table (Global), third edition, Elsevier, Amsterdam.

Van Houten, F. B., 1980, Latest Jurassic-Early Cretaceous regressive facies, northeast Africa craton: AAPG Bulletin, v. 64, p. 857-867.

Visher, G. S., 1969, Grain-size distributions and depositional processes: Journal of Sedimentary Petrology, v. 39, p. 1074-1106.

Walker, T. R., 1976, Diagenetic origin of continental red beds, In Falke, H. (ed.), The continental Permian in west, central and south Europe: Dordrecht, Reidel, p. 240-282.

Walker, T. R., B. Waugh, and A. J. Crone, 1978, Diagenesis in first cycle desert alluvium of Cenozoic age, southwestern United States and northwestern Mexico: Geological Society of America Bulletin, v. 89, p. 19-32.

Waples, D. W., 1985, Geochemistry in Petroleum Exploration, In Klein, G. deVries (series ed.), Geological Sciences Series, International Humen Resources Development Corporation, Boston, 232p.

Weerd, A. A., and P. L. G., Ware, 1994, A review of the East Algerian Sahara oil and gas province (Triassic, Ghadames and Illizi Basins), First Break, v. 12, no. 7, p. 363-373.

Weinbranddt, R. M., and F. Irving, 1969, A scanning electron microscope study of the pore structure of sandstone: Journal of Petroleum Technology, v. 21, p. 543-548.

Weller, J. M., 1959, Compaction of sediments: AAPG Bulletin, v. 43, p. 273-310.

Werle, B., and H. E. Schneider, 1978, Scanning electron microscope observations of diagenesis in the Triassic sandstones of the Saar Area, West Germany, In Whalley, W. B. (ed.), Scanning electron microscopy in the study of sediments, a symposium, p. 355-362.

Wescott, W. A., 1983, Diagenesis of the Cotton Valley sandstone (upper Jurassic), east Texas: implications for tight gas formation pay identification: AAPG Bulletin, v. 67, p. 1002-1013.

White, D. A., 1980, Assessing oil and gas plays in facies cycles wedges, AAPG Bulletin, v. 64, no. 8, p. 1158-1178.

Wood, J. R., and T. A. Hewett , 1984, Reservoir diagenesis and convective fluid flow, In McDonald, D A., and Surdam, R. C. (eds.), Clastic Diagenesis, AAPG Memoir 37, p. 3-13.

Yermolova, Y. P., and N. A., Orlova, 1962, Variation in porosity of sandy rocks with depth: Doklady of the Academy of Sciences of the USSR, Earth Science Sections, v. 144, p. 55-56 (in English).

IX-APPENDICES

APPENDIX I
CORE-SECTIONS AND DESCRIPTIONS

Well: EE1-NC7A **Formation: Acacus South** **Core #: 4** **Interval: 8805'-8832'**

Area: Concession NC7A, Hamada Basin, NW Libya

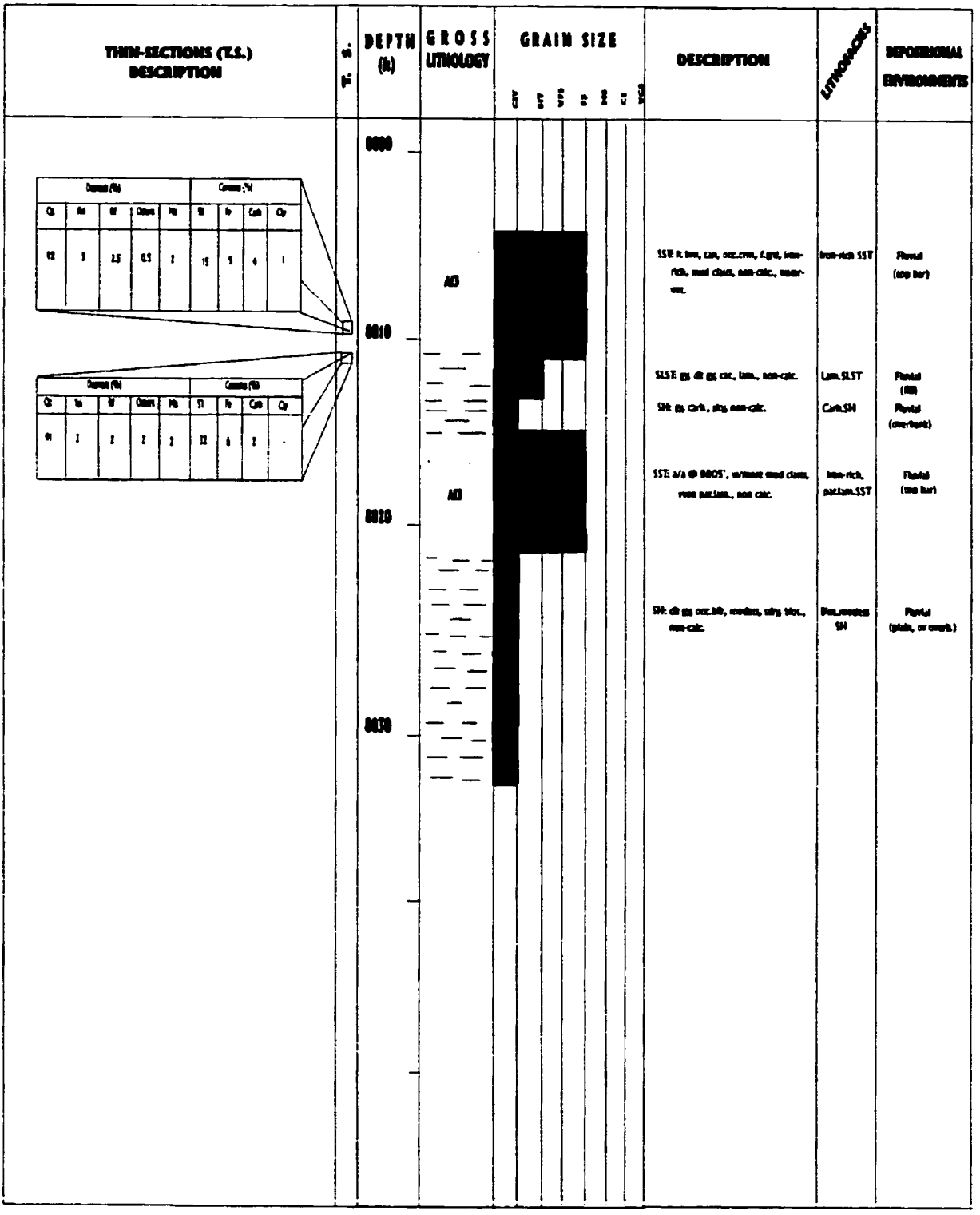

Remarks: @ 8810', 8812', qz supported ss., qz overgrowth, iron oxides coating occur intermixed with interstitial cly matrix, primary intergr. porosity.

Well: CC1-NC7A **Formation: Acacus South** **Core #: 5** **Interval: 9016'-9033'**

Area: Concession NC7A, Hamada Basin, NW Libya

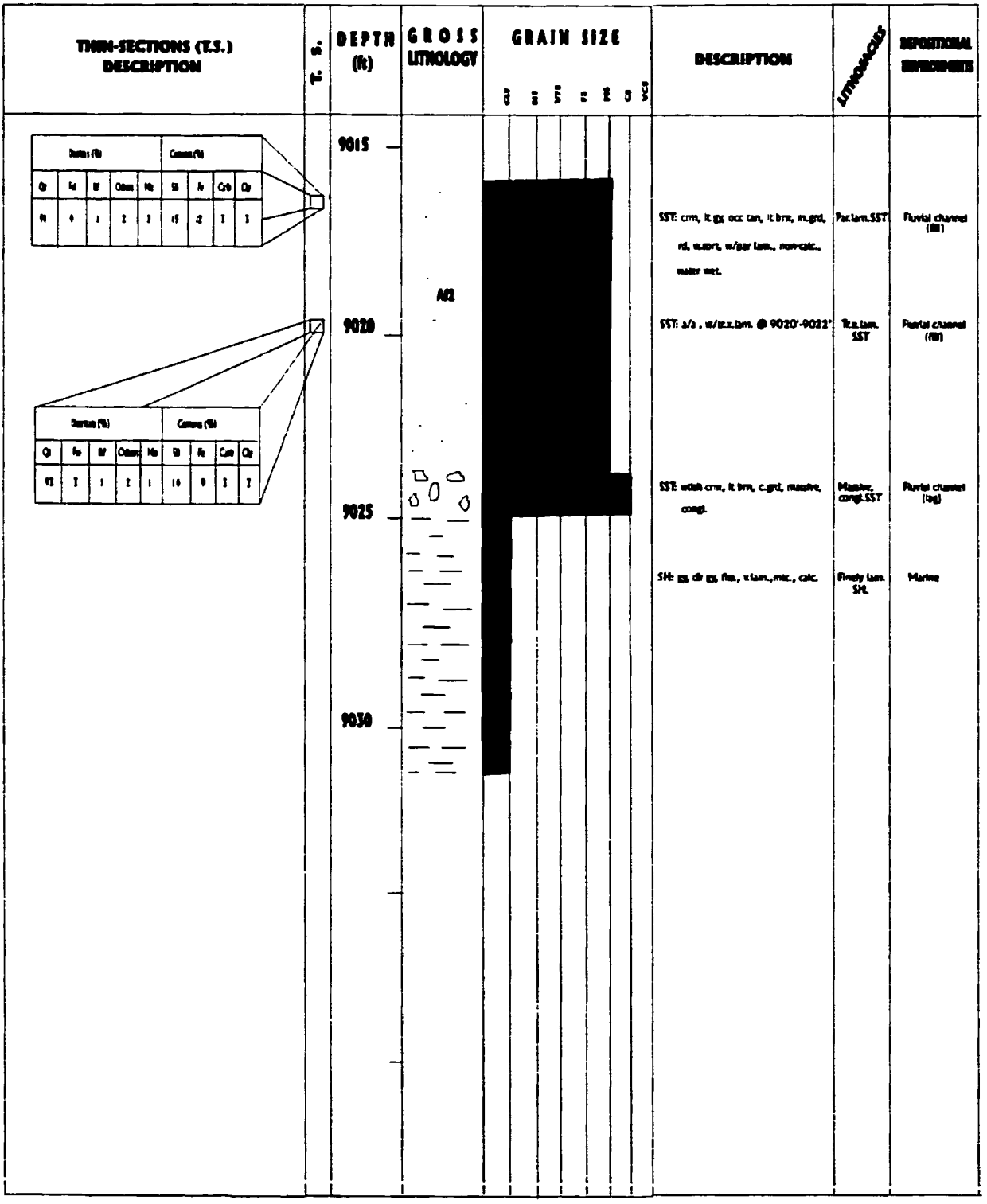

Remarks: @ 9017', 9020', qz cmt, w/ partial iron coating occur intermixed with interstitial clay matrix., intergran. porosity (primary).

Well: Z1-66 **Formation: Lower Acacus** **Core #: 7** **Interval: 9080'-9100'**

Area: Concession NC5, Hamada Basin, NW Libya

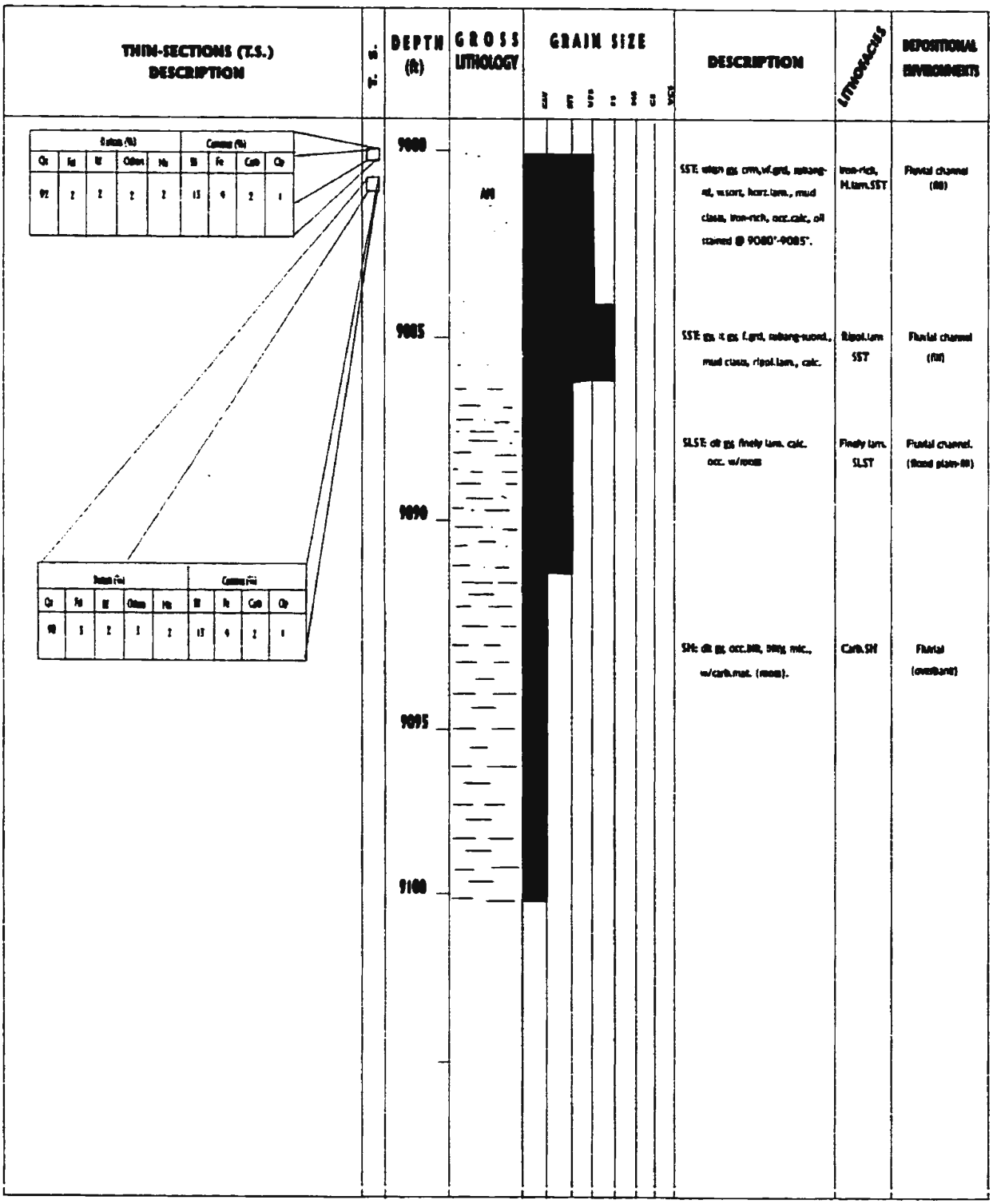

Remarks: @ 9080' at 9081, Qz supported ss. (w/qz.overgr.), w/partial cal.cmt, w/ iron oxides coating, commonly interspersed with clays @ 9081, and fine qz grains and other detrital grains, intergran.primary porosity. Iron oxides coating is apparently mainly derived from the breakdown of unstable iron-bearing heavy minerals.

Well: Z1-66 **Formation: Lower Acacus** **Core #: 8** **Interval: 9110'-9160'**

Area: Concession NC5, Hamada Basin, NW Libya

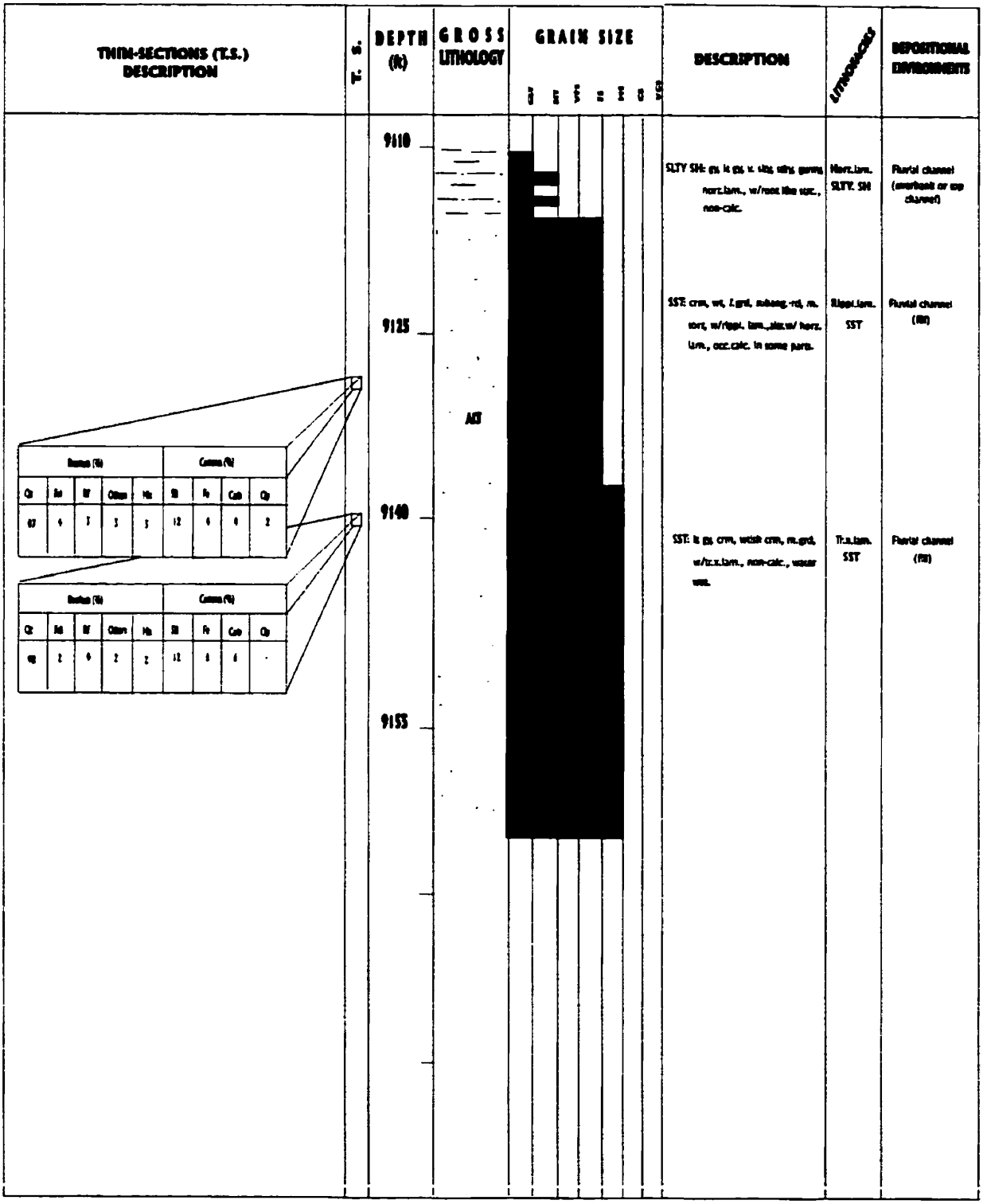

Remarks: @ 9130', 9140' Qz.supported ss., lots of overgro., partial cal. and cly cmts in parts.

Well: A1-NC118 **Formation: Lower Acacus** **Core #: 1** **Interval: 10016'-10048'**

Area: Concession NC118, Hamada Basin, NW Libya

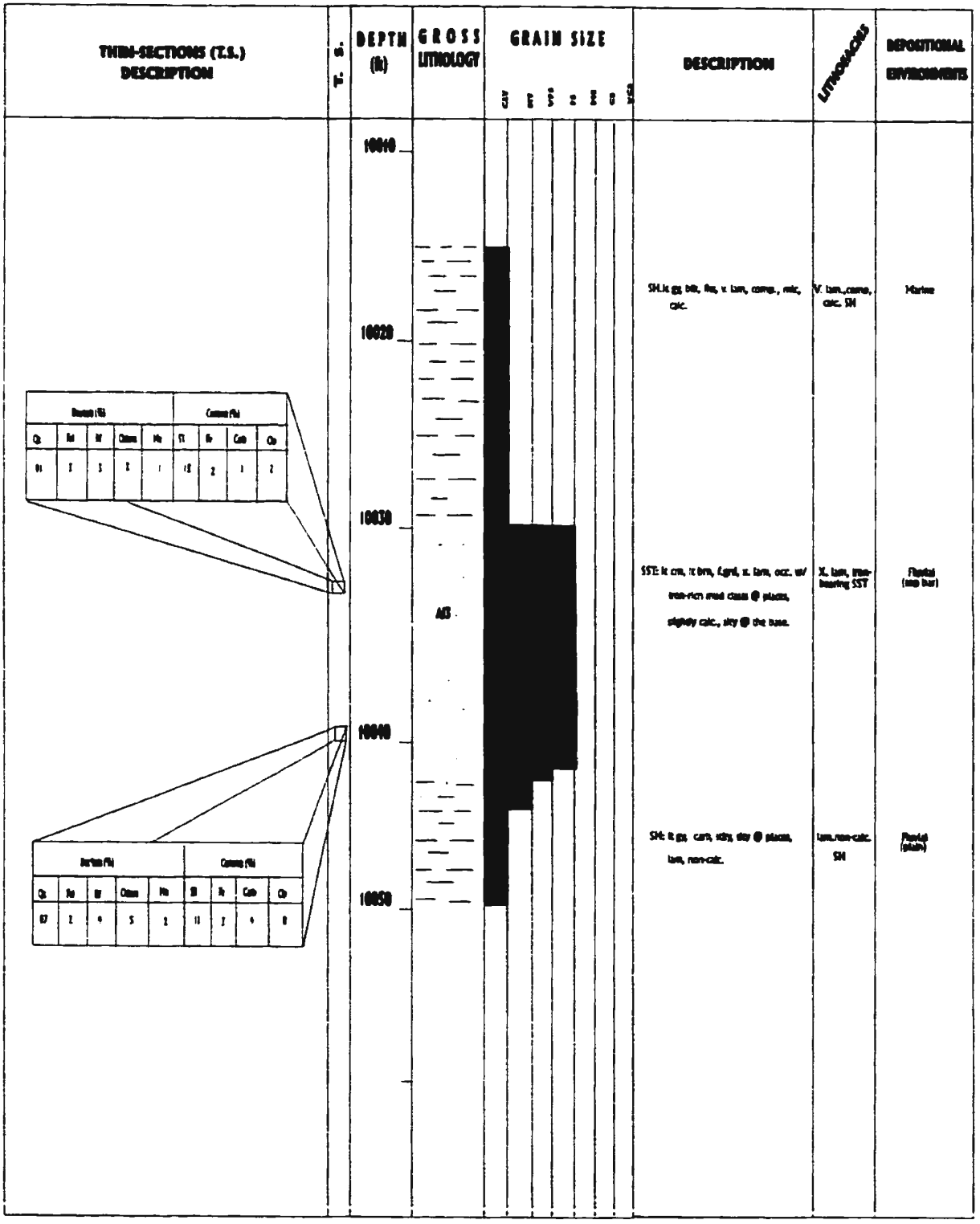

Remarks: @ 10033', 10040', Qz dominated ss, qz.overgr, partial cal.cmt, also some cly cmt (kaol.), and iron coating at places.

Well: A1-NC118 **Formation: Lower Acacus** **Core #: 2** **Interval: 10095'-10125'**

Area: Concession NC118, Hamada Basin, NW Libya

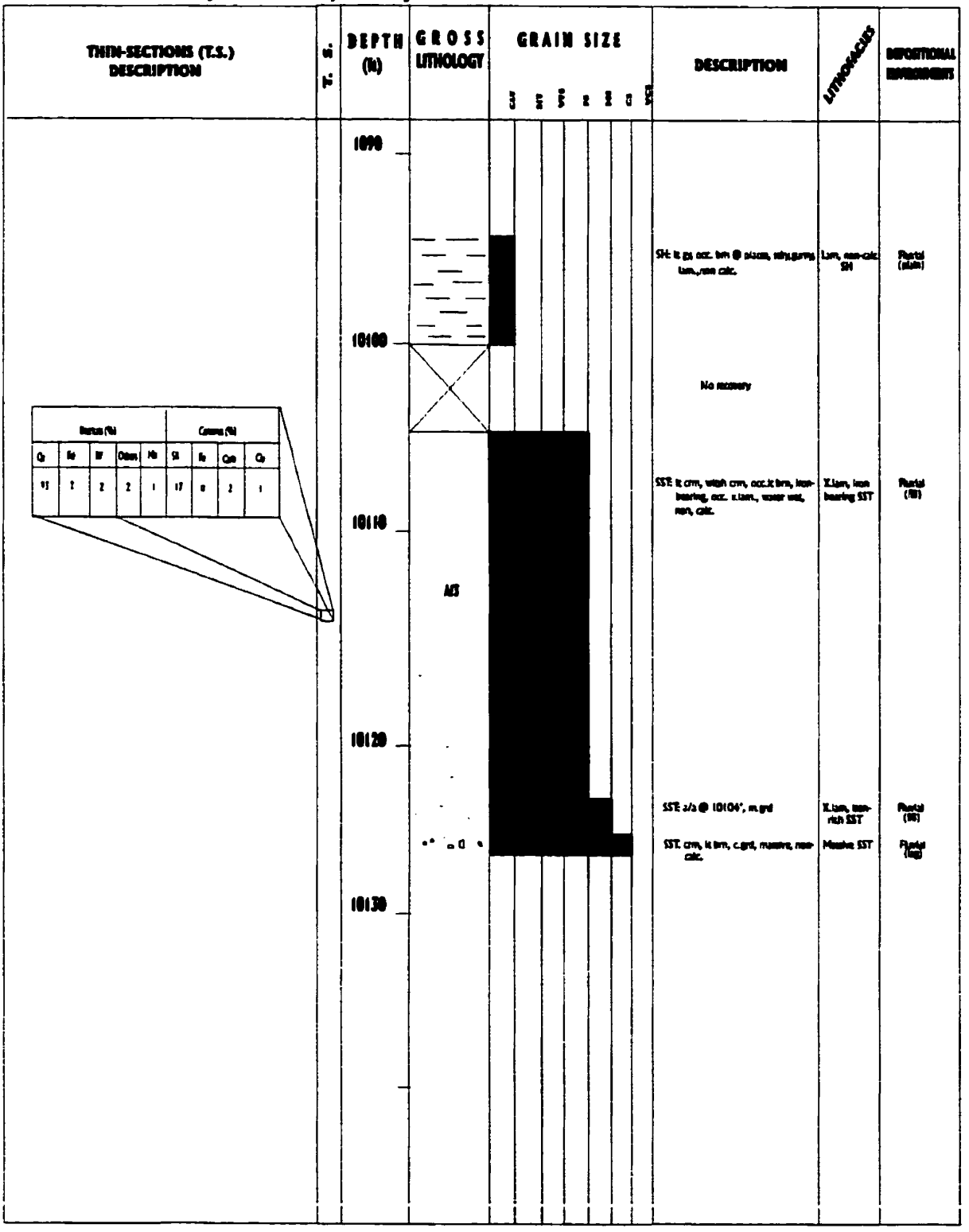

Remarks:, @ 10115', ill sor., poor packing, sil.cmt ss., occ.w/cly cmt, iron coating @ places, fel., interg.primary porosity.

Well: Z1-NC100 **Formation: Lower Acacus** **Core #: 1** **Interval: 11680'-11706'**

Area: Concession NC100, Hamada Basin, NW Libya

THIN-SECTIONS (T.S.) DESCRIPTION	T.S.	DEPTH (ft)	GROSS LITHOLOGY	GRAIN SIZE	DESCRIPTION	LITHOFACIES	DEPOSITIONAL ENVIRONMENT
Detrital (%): Qz 87, Fd 4, Rf 2, Others 3, Mx 1; Cement (%): Si 11, Fe 1, Calc 2, Clay 5		11680	AB		SST: fr brn,tan, crse, f.grd, subang-rd, w.sort, mud clasts, par.lam, iron rich, oil st. @ 11680'-11686'	Iron-rich, par.lam. SST	Fluvial (top bar)
		11690			SLST: fr brn, gy, bioc. occ.w mud lam w/some roots, mud clasts	Bioc.,root. SLST	Fluvial (overbank)
			AB		SST: a/a @ 11680', par.lam., occ. m/m. oil st., silty @base.	Par.lam. SST	Fluvial (mid bar)
		11700			SH: dk gy, carb., silty, pyrite, roots, non-calc.	Carb.SH.	Fluvial (plain)
		11710					

Remarks: AB unit in this well may be equivalent to Af in other nearby wells to the south. @ 11680', qz supported, iron oxides coating/ and some cly mx present.

Well: C1-70 **Formation: Lower Acacus** **Core #: 1** **Interval: 7910'-7930'**

Area: Concession NC4, Hamada Basin, NW Libya

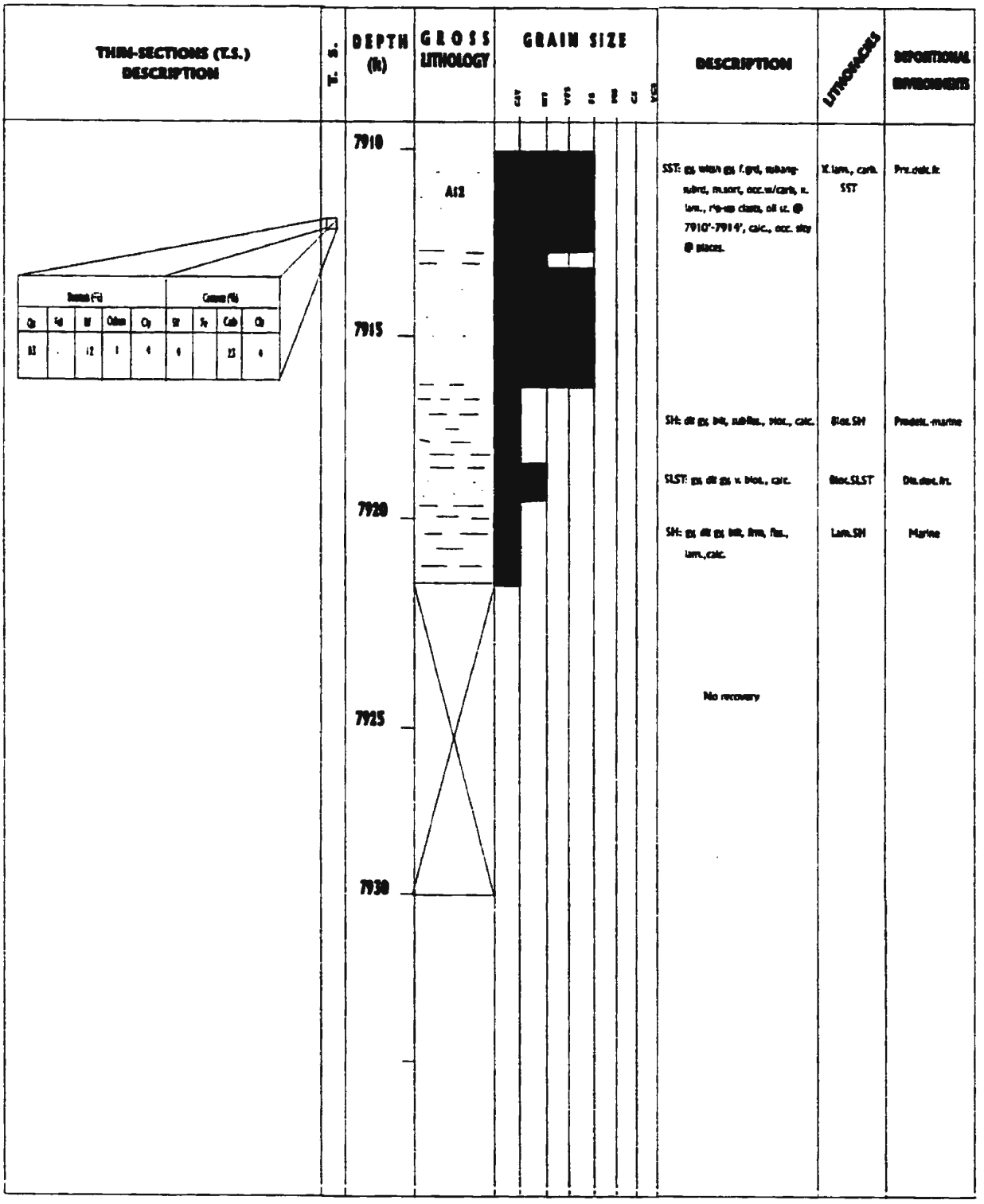

Remarks: @ 7913', cal.cmt ss., w/cly lam.

Well: B1-61 **Formation: Lower Acacus** **Core #: 3** **Interval: 8420'-8459'**

Area: Concession NC2, Hamada Basin, NW Libya

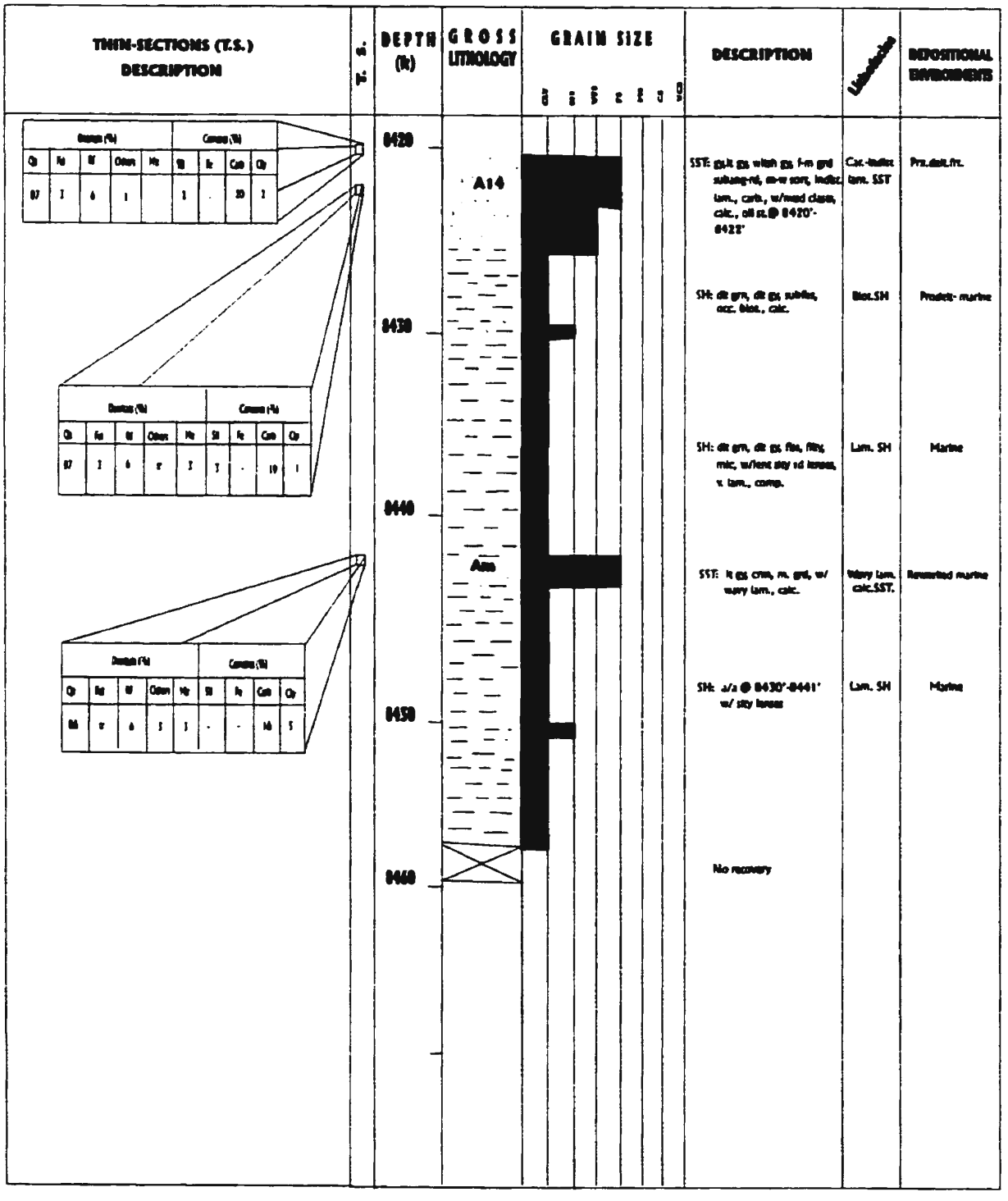

Remarks: @ 8429', Qz overgrowth is very common, partially cal.cmt, cal.diss.w/elongated and oversized porosity, igneous and/or met.R.F. also present

@ 8422', cly mx rich sublitharenite(immature), w/kaolinite cmt.

@ 8442', sublitharenite, w/randomly oriented microstructures, fractured corroded Qz grains, partially cal./dolo cmts, w/ hyd.filling pore spaces.

Well: B1-61 **Formation: Lower Acacus** **Core #: 4** **Interval: 8459'-8518'**

Area: Concession NC2, Hamada Basin, NW Libya

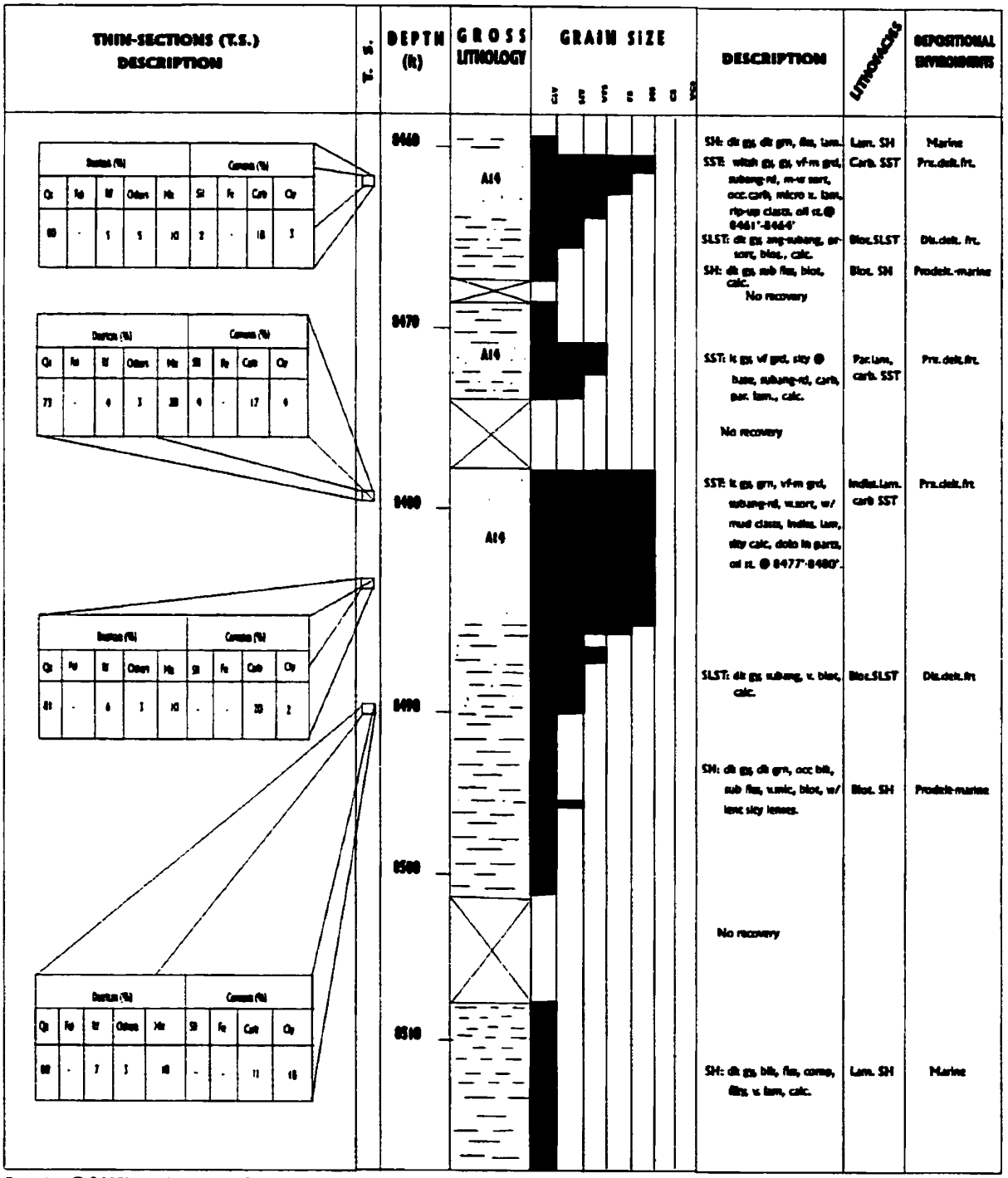

Remarks:, @ 8462', unoriented mica flakes, disturbed cly lamin, may suggests disturbance events such as uplift, faulting, Kaolinite cmt is also present...).
@ 8479', clay mx in subang-subrd ss is anomalous, certainly these v.f.materials were not deposited by the same current of the rock, but may be infiltrated in later stages through unconf.surfaces or microfractures or are diagenetic in origin where this is possible because of the presence of some chlorite plates and also part of it are the bushes of labile grains between rigid Qz grains (formation of pseudomatrix, and kaolinite cmt). Oversized, elongated pore spaces are also present.
@ 8484', this is the middle of the unit away from sd/sh contact where not much dolo.cmt, partially calc. cmt, but of sil. cmt. Loss of Qz overgrowths (concavo-convex-straight grain contacts), sec. por. between corr. Qz grains due to mainly cal.cmt diss.
@ 8490', very argill. cly mx rich, occ. kaolinite cmt str., w/poor porosity.

Well: B3-61 **Formation: Lower Acacus** **Core #: 2** **Interval: 8736'-8796'**

Area: Concession NC2, Hamada Basin, NW Libya

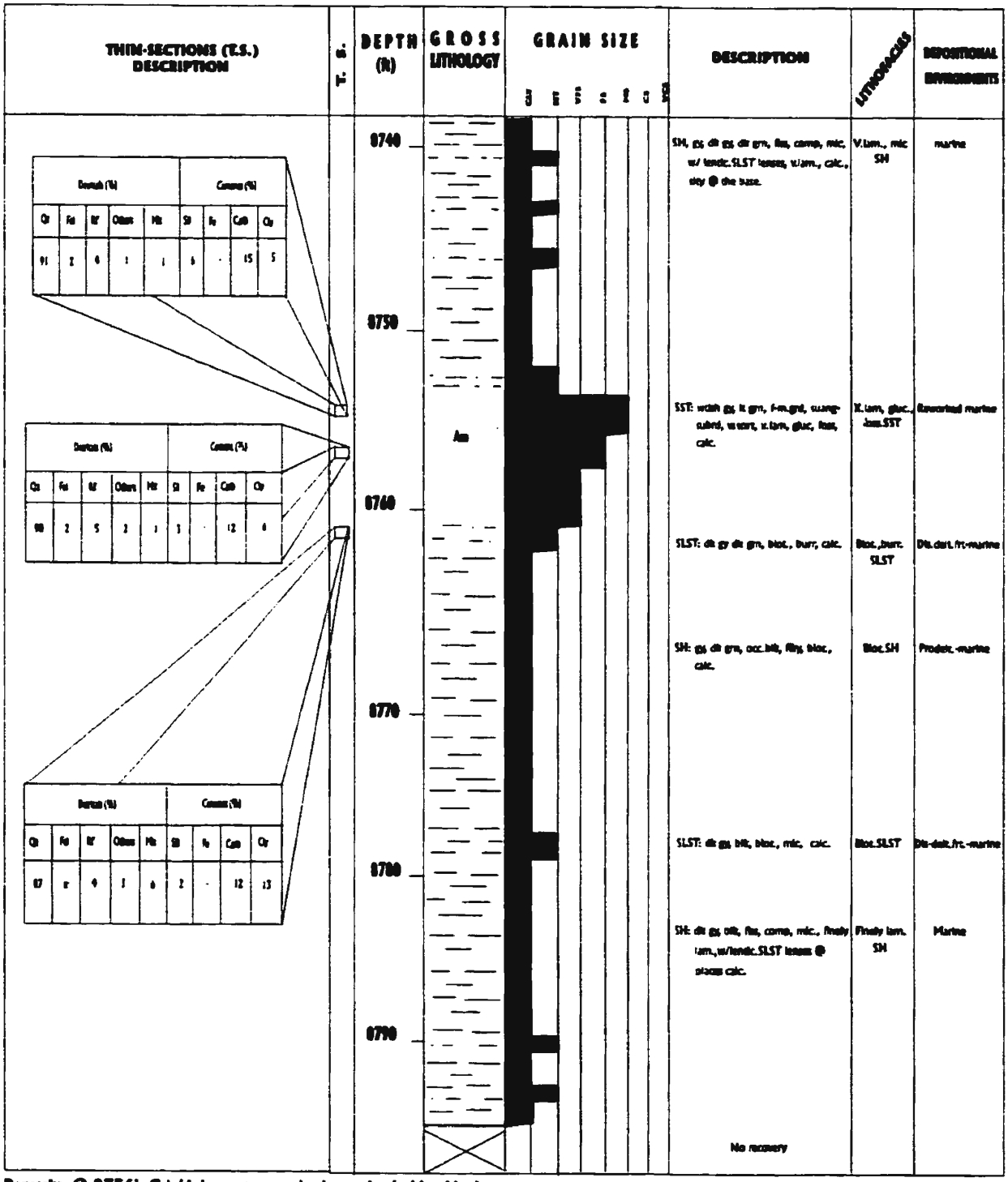

Remarks: @ 8756', Cal./dolo. cmts, oversized porosity (cal.leaching).

@ 8758', Qz.arenite, f-m grd, cal.cmt partly dolo.cmt, the presence of streatched grains of R.F. and elongated chert grains indicates a mixed metamorphic and sedimentary sources, burrows and foss. frag. are also present.

@ 8764', interb. of sh/ss, cly mx rich sand, w/kaolinite cmt in parts.

Well: B3-61 **Formation: Lower Acacus** **Core #: 3** **Interval: 8885'-8945'**
Area: Concession NC2, Hamada Basin, NW Libya

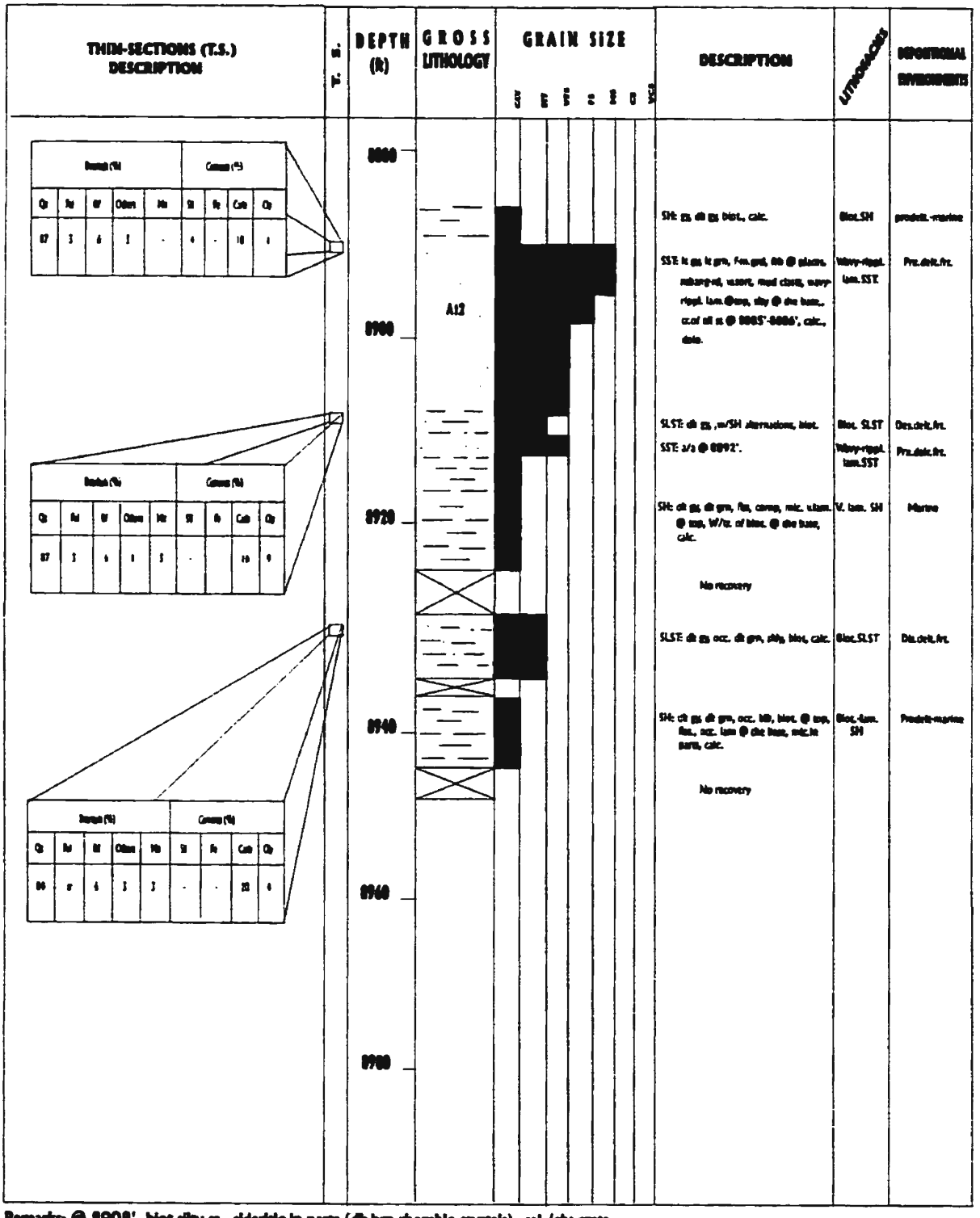

Remarks: @ 8908', blot.silty ss., sideritic in parts (dk brn rhombic crystals), cal./cly cmts.

@ 8893', v.frac.qz grains, fel.plag., cal./dolo. cmts., large/elong. sec porosity.

@ 8929', blot.silty ss., cham. grains, sh.clasts are generally soft and are deformed by blot. or embayed by adjacent qz grains, moreover, the individual crystals are not oriented.

APPENDIX I

Well: B3-61 **Formation: Lower Acacus** **Core #: 4** **Interval: 8945'-8998'**

Area: Concession NC2, Hamada Basin, NW Libya

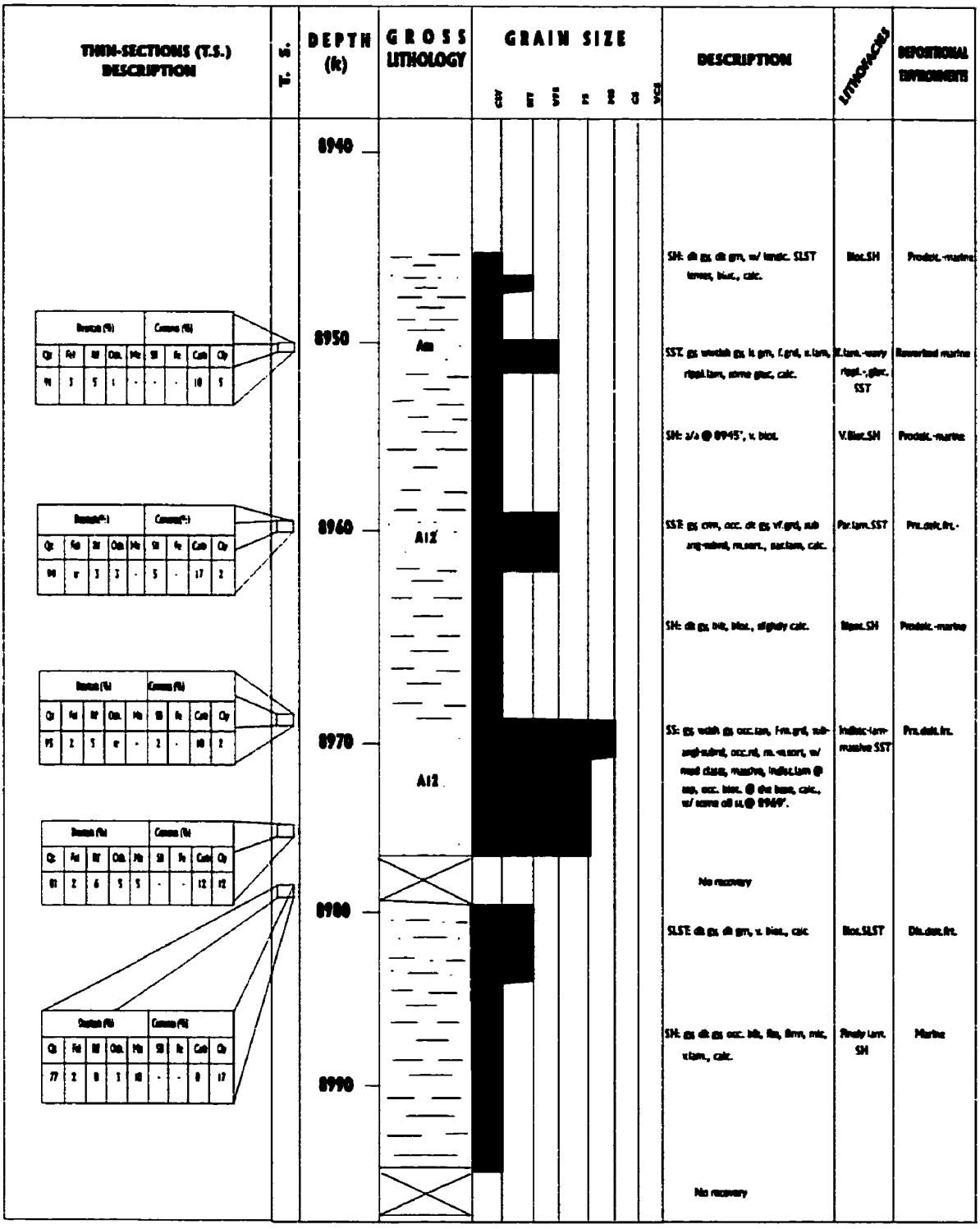

Remarks: @ 8950', sublitharenite w/deformed mica, cal.cmt, tr. of gluc. partially kaol.cmt.
@ 8960', silty-v.f.lami.ss., show evidence of compaction and microfracturing. Microfractures occ.filled w/hyd.
@ 8969', well supported, mature sublithar., occ.w/fract.qz grains, w/inclusions (vermiculides), stright-undulous ext., cal./dolo.cmts, w/altered Rf, v. corroded Qz grains.
@ 8974', relatively cly rich sublithar., w/partially cal.cmt, pores are filled by auth.kaolinite
@ 8979', v.argill, blot.silty ss., cal.cmt occ.sid.cmt w/dk rhombic crystal aggregates.

Well: B3-61 **Formation: Lower Acacus** **Core #: 5** **Interval: 9310'-9365'**

Area: Concession NC2, Hamada Basin, NW Libya

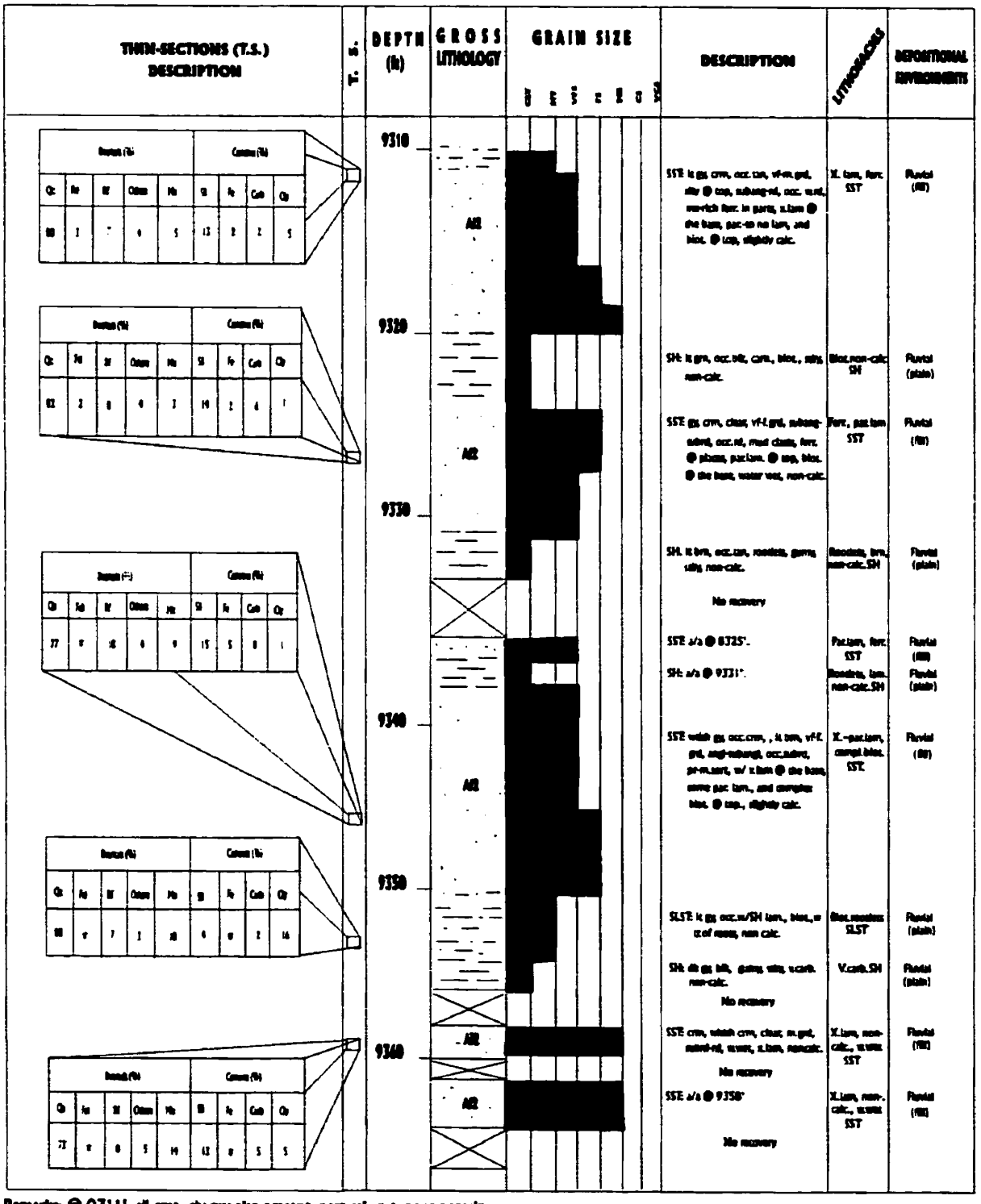

Remarks: @ 9311', sil.cmt, cly mx also present, part.cal.cmt, poor porosity

@ 9328', a/a @ 9311'.

@ 9345', micaceous, cly clast rich sublitharenite, cal.cmt., comm. sil cmt at point contacts, cly clast of blk-brn rims may be of authigenic origin

@ 9353', v.biot. silty ss., rich in mx poor porosity.

@ 9360', cal.cmt rich ss., plug off pore spaces by compacted labile grains (mic., chlo.)

Well: C1-61 **Formation: Lower Acacus** **Core #: 3** **Interval: 7507'-7555'**
Area: Concession NC2, Hamada Basin, NW Libya

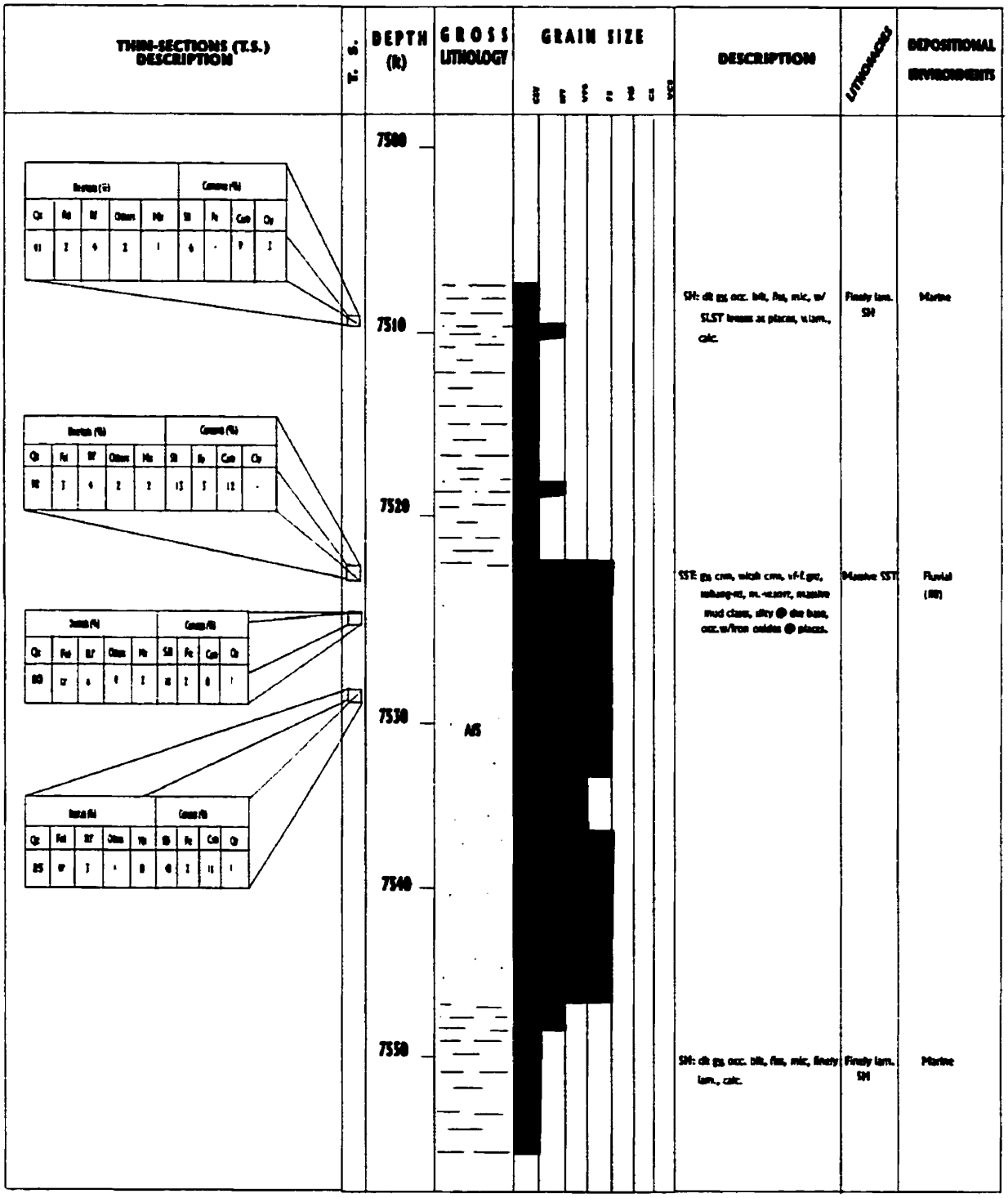

Remarks: @ 7510', Quartzarenite with less packing (early cal.cmt).
@ 7522', ss. w/qtzovergrowth, partially cal./dolo.cmts, hyd.bearing ss.
@ 7525', qtzovergrowth w/ partial cal.cmt ss.
@ 7529', interbedded argill.ss and clay laminations (cly rich ss., low porosity).

Well: C1-61 **Formation: Lower Acacus** **Core #: 4** **Interval: 7770'-7828'**

Area: Concession NC2, Hamada Basin, NW Libya

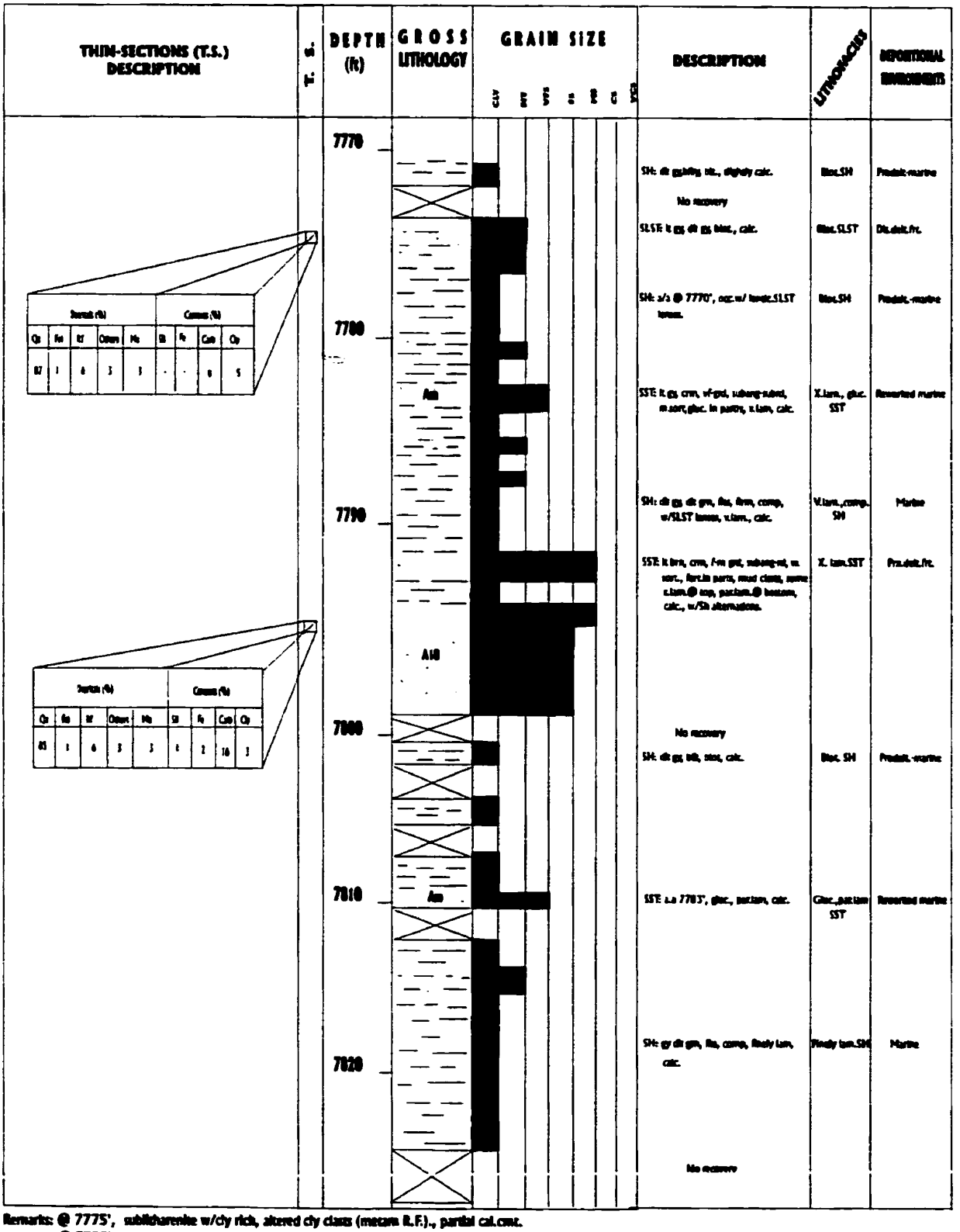

Remarks: @ 7775', subfeldarenite w/cly rich, altered cly clasts (metam R.F.), partial cal.cmt.

@ 7795', complex cementation of ss.; Qz overgrowth was followed by complete porosity occlusion dominatly by cal/dolo cmts. Subsequent partial dis. of cal/dolo cmts yielded sec. porosity which was filled later by diagenetic hematite. Sample as good example for dis. of unstable ferrigenous grains which are the main source of diagenetic iron cement.

Well: C1-61 **Formation: Lower Acacus** **Core #: 5** **Interval: 8180'-8212'**

Area: Concession NC2, Hamada Basin, NW Libya

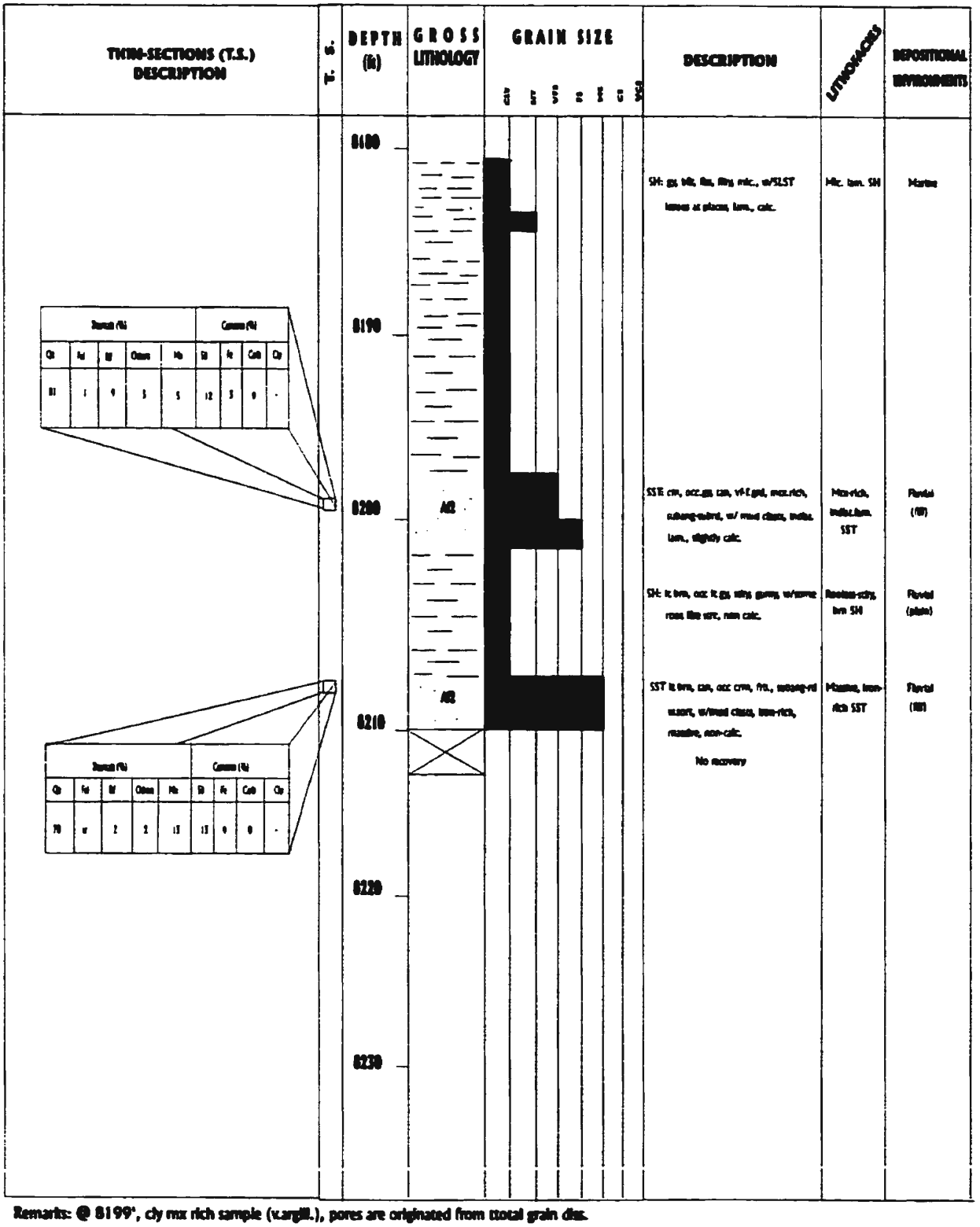

Remarks: @ 8199', cly mx rich sample (v.argill.), pores are originated from ttotal grain diss.

@ 8208', subllitharenite, cal.cmt, w/dolo.floating grains in pores, oversized pore spaces are common (grain molds), occ.w/iron lite grains (authig.).

APPENDIX I

Well: D1-61 **Formation: Lower Acacus** **Core #: 3** **Interval: 8230'-8290'**

Area: Concession NC2, Hamada Basin, NW Libya

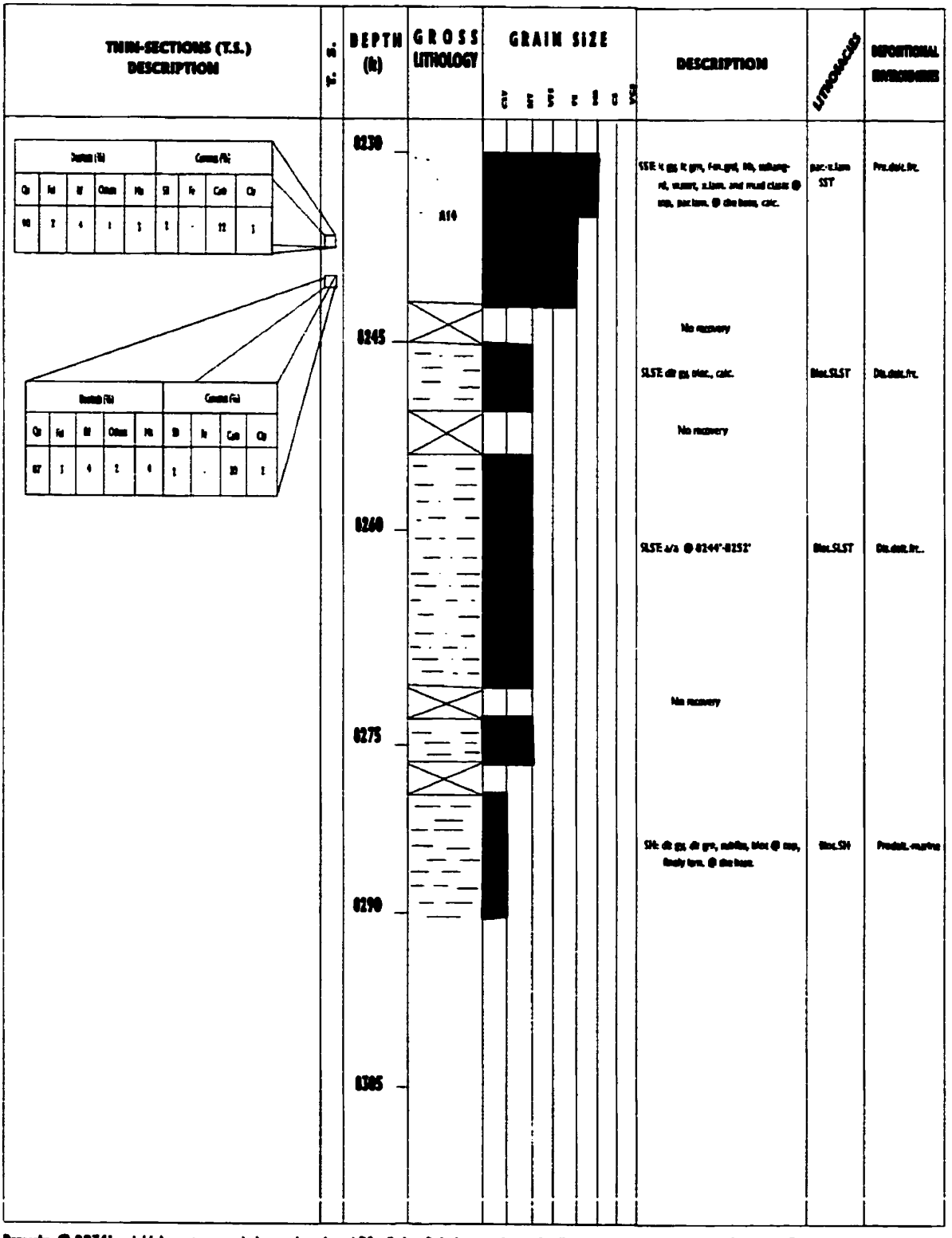

Remarks: @ 8236', cal./dolo.cmts, corroded qz grains, altered Rf.w/lacks of plagio.crystals, partial dis. cal.cmt creating sec.pores filled with floating grains, w/ organic fill.
@ 8240', increasing cly mx and bioc.. Clay mx is anomalous in subrd-rounded texture but that may be suggesting these clay materials of diagnetic origin.

well: D1-61 Formation: Lower Acacus Core #: 4 Interval: 8290'-8340'

Area: Concession NC2, Hamada Basin, NW Libya

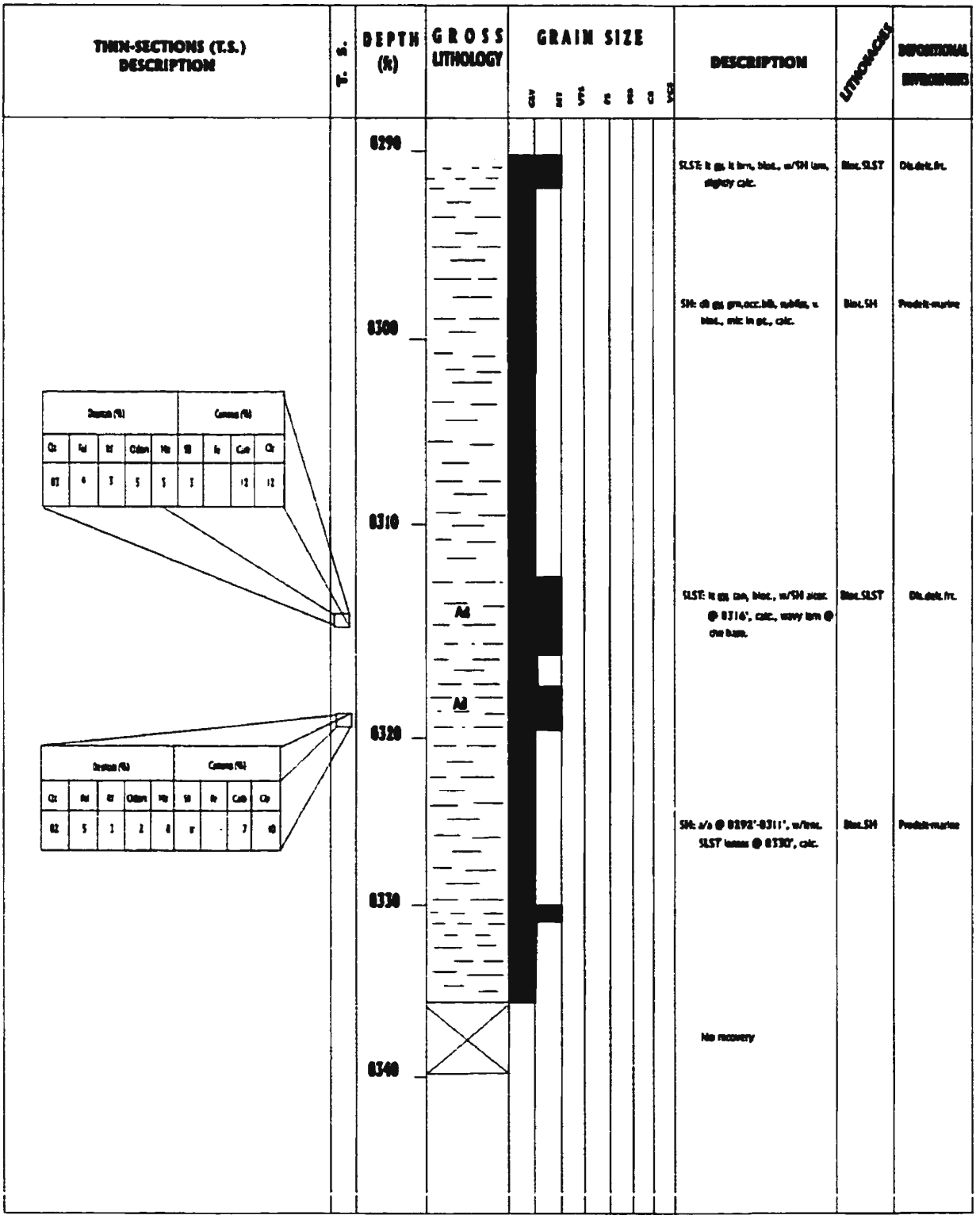

Remarks: @ 8314', biot.silty ss., domin.cal.cmt, occ.cly cmt , chert also present.

@ 8319', rich cly mx siltstone, but of relatively high porosity because of the late unstable grains dissolution .

Well: D1-61 **Formation: Lower Acacus** **Core #: 10** **Interval: 8845'-8895'**
Area: Concession NC2, Hamada Basin, NW Libya

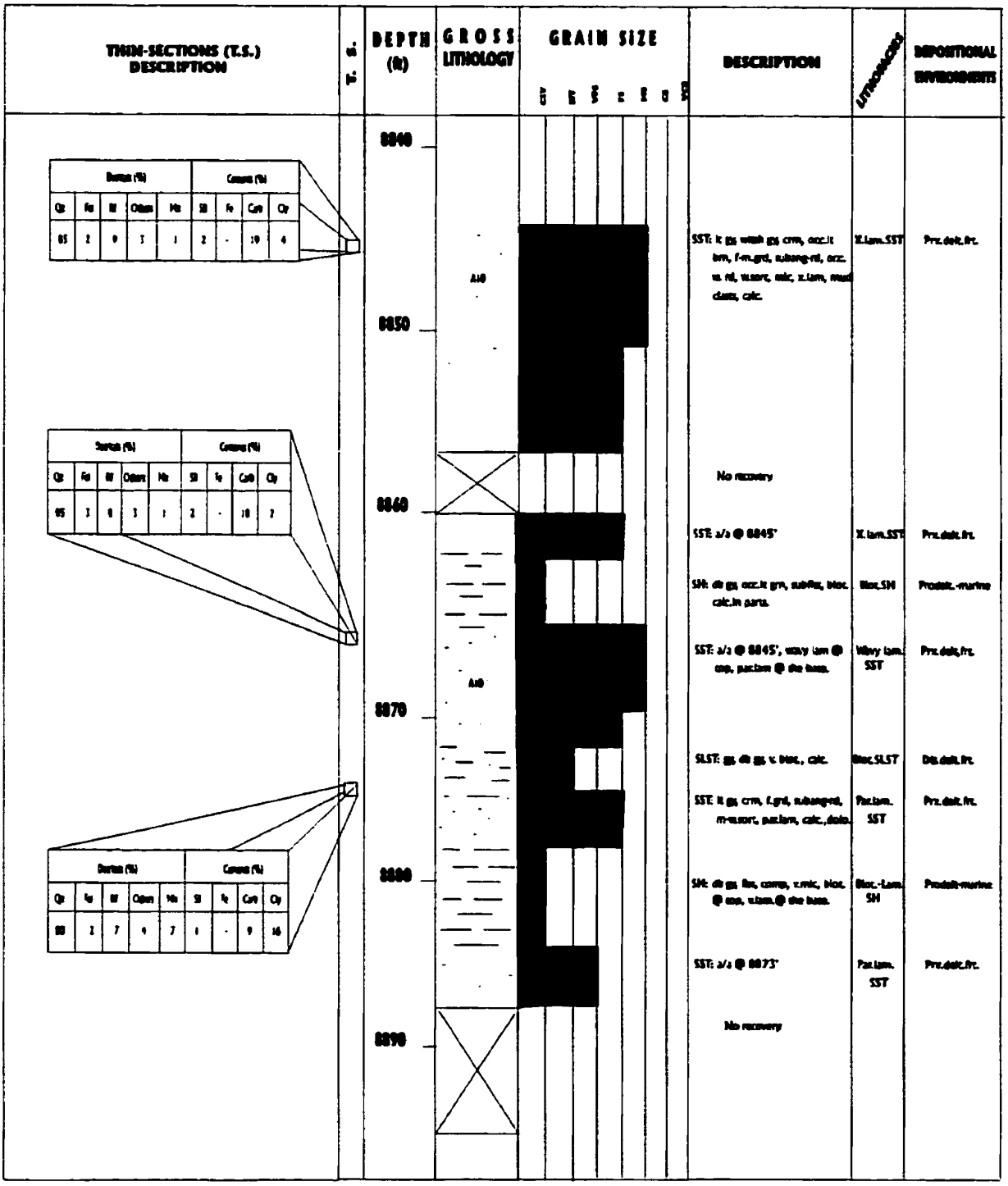

Remarks: @ 8845', sublithar., w/patchy cal/dolo.cmts, chlor., clay clasts, some fel.polysynthetic tw.

@ 8866', cal/dolo cmt ss., w/ cly clasts, feld., and intergran porosity of floating grains and corroded grains edges?grains diss.).

@ 8872', silty-v.f.ss., lamin., biot., w/muscu.show orientation along bedding planes ?as may prohibits v.permeability), mica also show evidence of compaction, mica/labile Rf. plug pore-spaces.

Well: B1-NC2 **Formation: Lower Acacus** **Core #: 1** **Interval: 8541'-8561'**
Area: Concession NC2, Hamada Basin, NW Libya

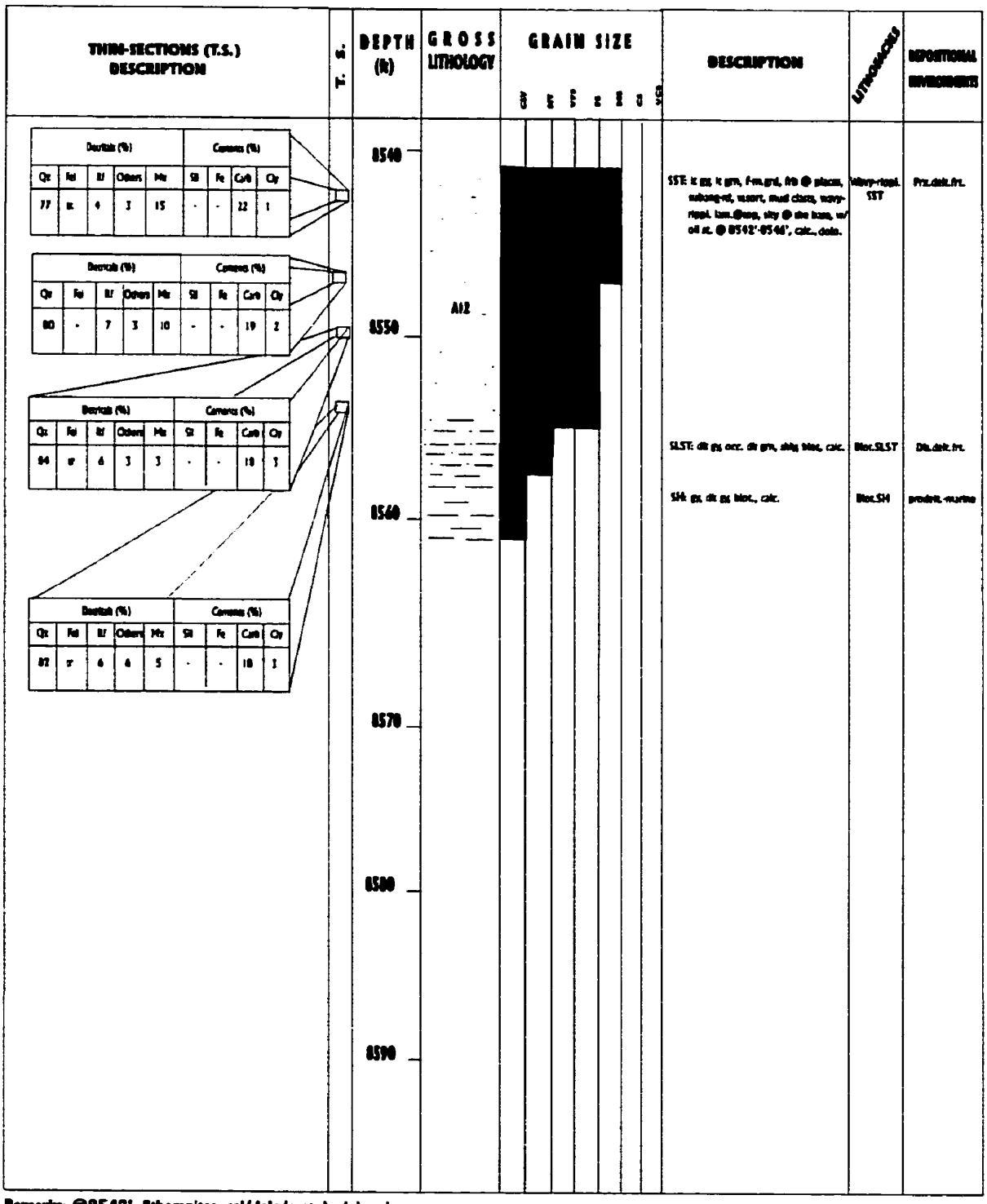

Remarks: @8542', litharenites, cal/dolo/cmt, hydr.bearing ss.
@ 8546', litharenites, mx-rich, mic., cal.cmt.
@ 8550', litharenites-sublitharenites, mx.,calc., sec.enlarged porosity.
@ 8555', litharenites, w/interbed.siltstones and shale lam., cal.cmt, relatively of low porosity.

Well: B1-NC2 **Formation: Lower Acacus** **Core #: 2** **Interval: 8637'-8650'**
Area: Concession NC2, Hamada Basin, NW Libya

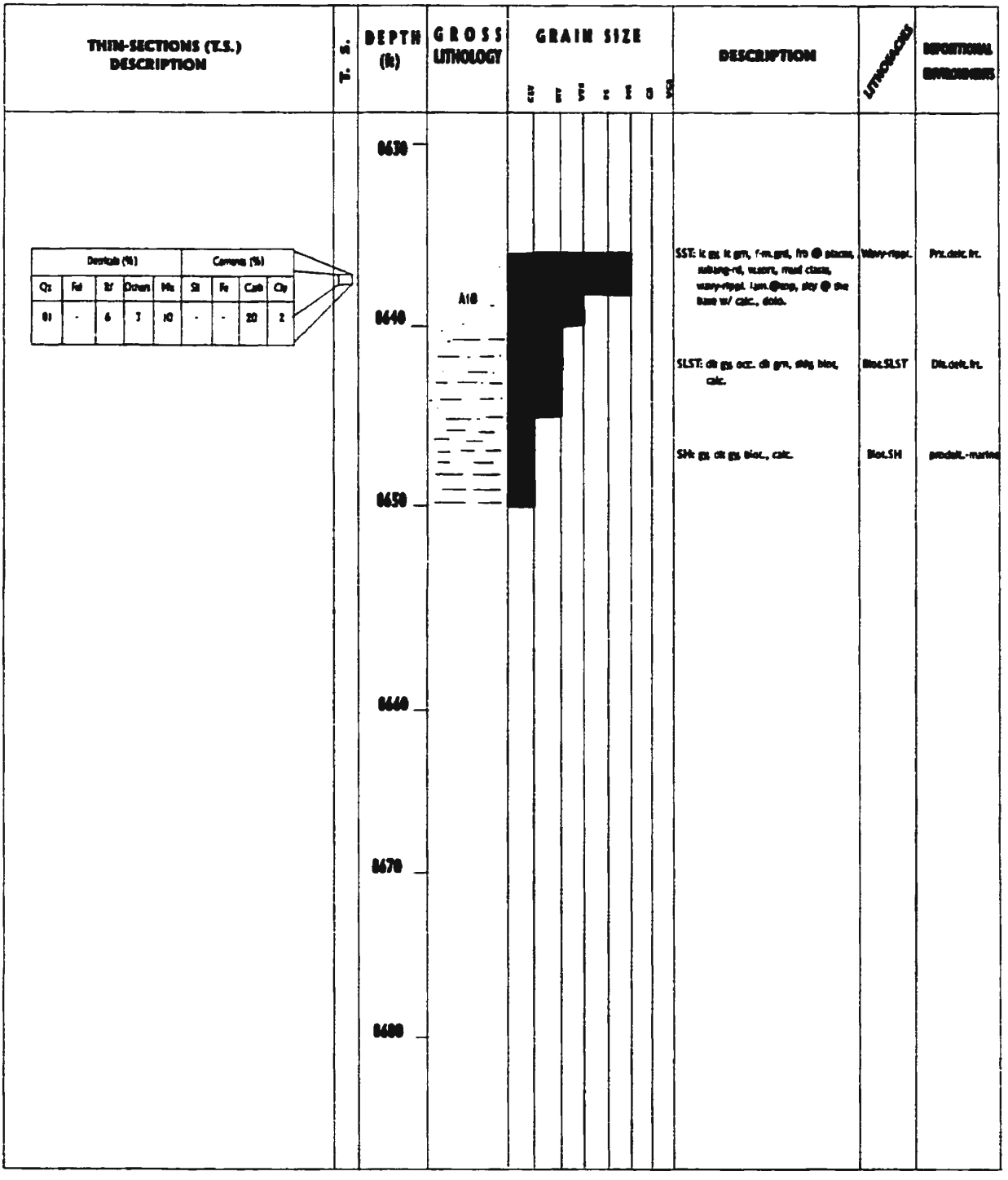

Remarks: @ 8637', litharenites, cal./dolo.cmt, mx-rich, mic, w/rf, w/kaol.cmt @ places, low sec.porosity, low permeability .

Well: C1-NC2 **Formation: Lower Acacus** **Core #: 1 & 2** **Interval: 9621'-9642' 9642'-9672'**

Area: Concession NC2, Hamada Basin, NW Libya

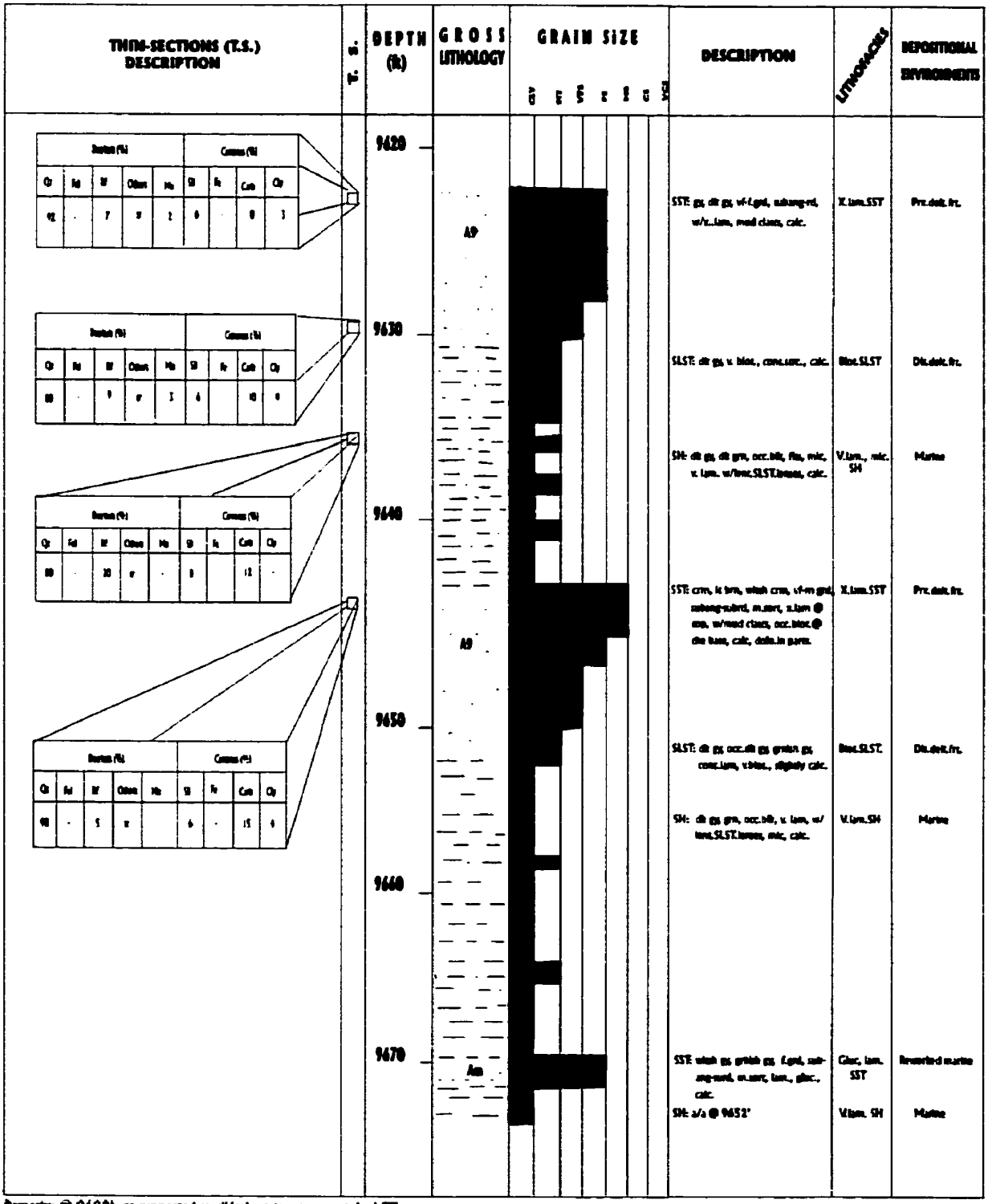

Remarks: @ 9622', qz supported ss, sil/cal. cmts are present, hyd.filling pores.
@ 9630', blot.qz.supp.ss., w/q.overgrowth, patchy dolo.cmt,. argill.in partsw/ heterogeneous texture resulted from extensive blot. In general from 9622'-9630' may be inferred that sediments were transported directly to its depositional site without an extensive period of reworking under shoreline condition, that might have been increased the percentages of monoquartz crystals, but partially was reworked by organisms as quite env. was eached. Also more hyd.in pores @ 9622', while no hyd. @ 9630' that mainly because of clay bedding and laminations and extensive blot. have inhibited continuity of pore spaces.
@ 9645', sublitharenite, rich in organic mat., v.rounded frag., w/dolo.cmt at top of sample, sil.cmt at rest of sample at grain to grain contacts.

Well: C1-NC2 **Formation: Lower Acacus** **Core #: 4** **Interval: 9702'-9732'**
Area: Concession NC2, Hamada Basin, NW Libya

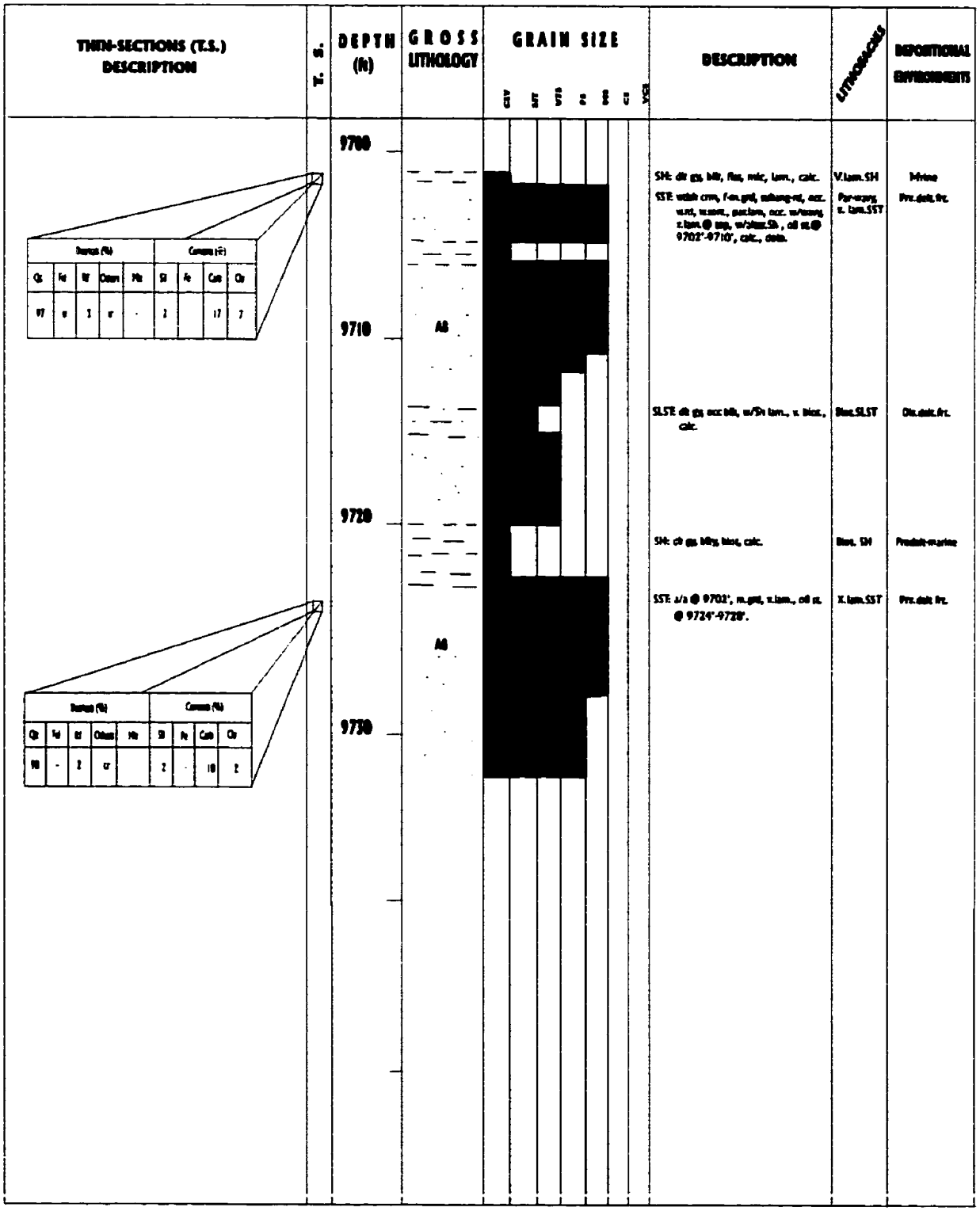

Remarks: @9703', qz.arenite, cal, and patchy dolo.cmt @ top of the sample, sil. cmt @ grain to grain contacts in the rest of the sample. @ 9725', cal/dolo.cmt and rarely sil.cmt.

APPENDIX I

Well: E1-NC2 **Formation: Lower Acacus** **Core #: 1&2** **Interval: 9105'-9126'**
Area: Concession NC2, Hamada Basin, NW Libya **9126'-9146'**

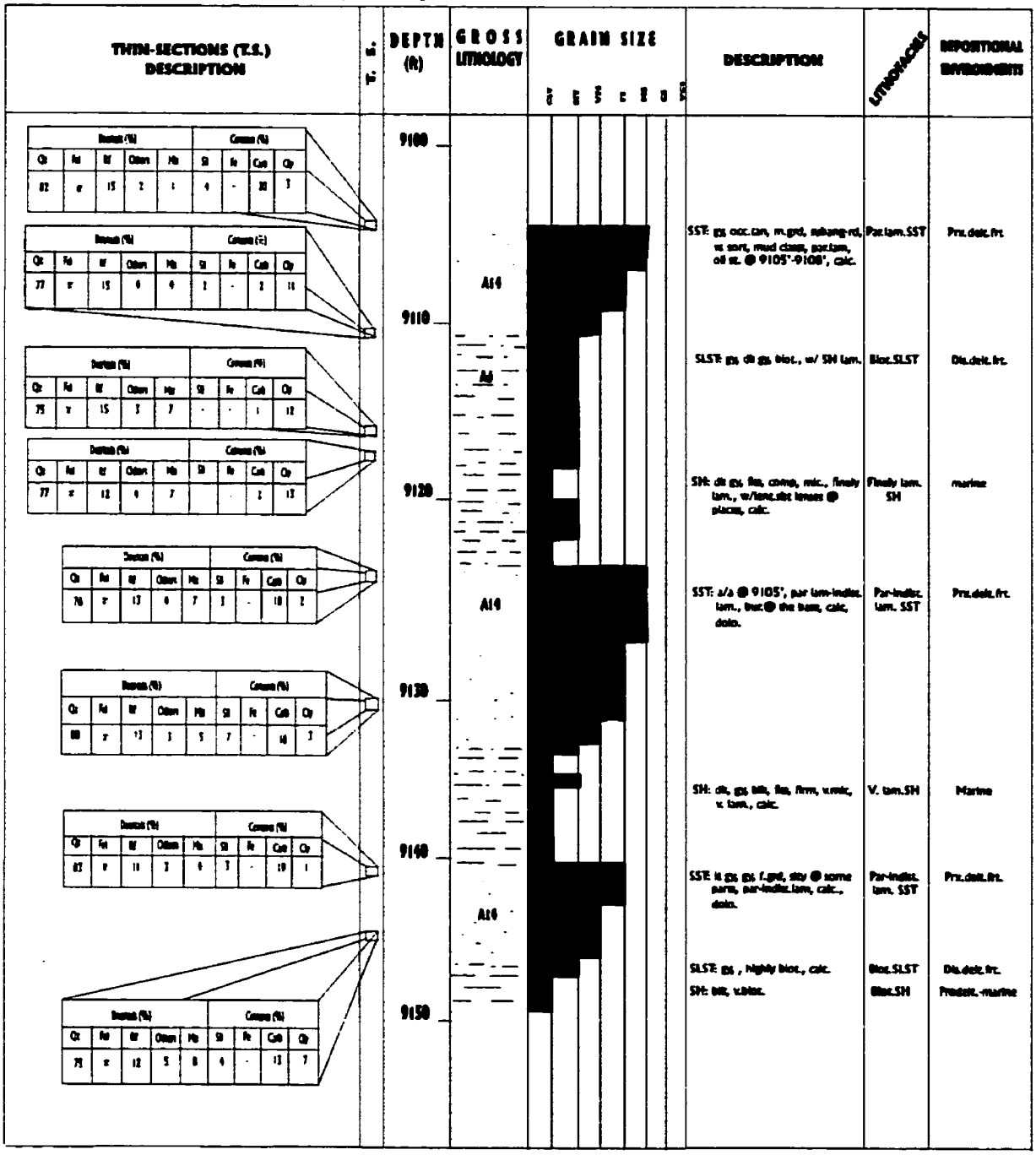

Remarks: @ 9105', organic grains (woody mat., w/ common Qz cement, patchy calc. cmt @ places. The organics interrupting the texture of the normal lamination. They may be of river transported materials showing pronounced roundness by transportation.

@ 9111', clay matrix coating Qz grains.

@ 9115, well cal.cmt rocks of low porosity

@ 9122', f-silty ss, clay supported, bioturbated, w/ mica flakes show some deformation. @ 9131', cal., dolo. cmt, with silica cmt identified by dusty v.thin rim between grains @ 9141'-43', interb. ss/sh, fel.grains suffer abrasions during their trasportation and/or due to grain dis, partially cal. cmt.

Well: E1-NC2 **Formation: Lower Acacus** **Core #: 3** **Interval: 9509'-9524'**
Area: Concession NC2, Hamada Basin, NW Libya

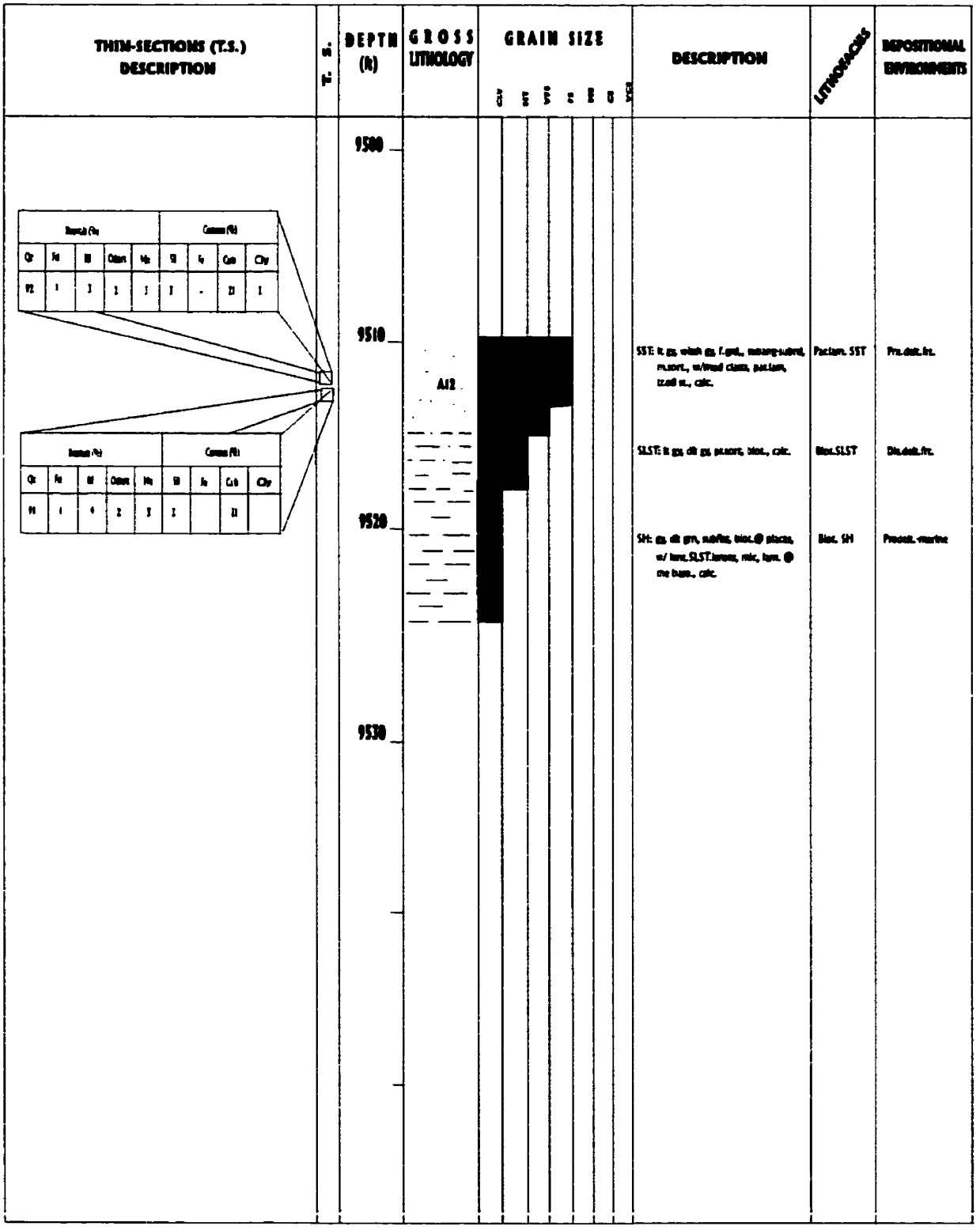

Remarks: @ 9512', 9513' Qz arent., mainly cal., w/ patchy dolo. cmt..

Well: T1-23 **Formation: Lower Acacus** **Core#: 1** **Interval: 8435'-8458'**

Area: Concession NC2, Hamada Basin, NW Libya

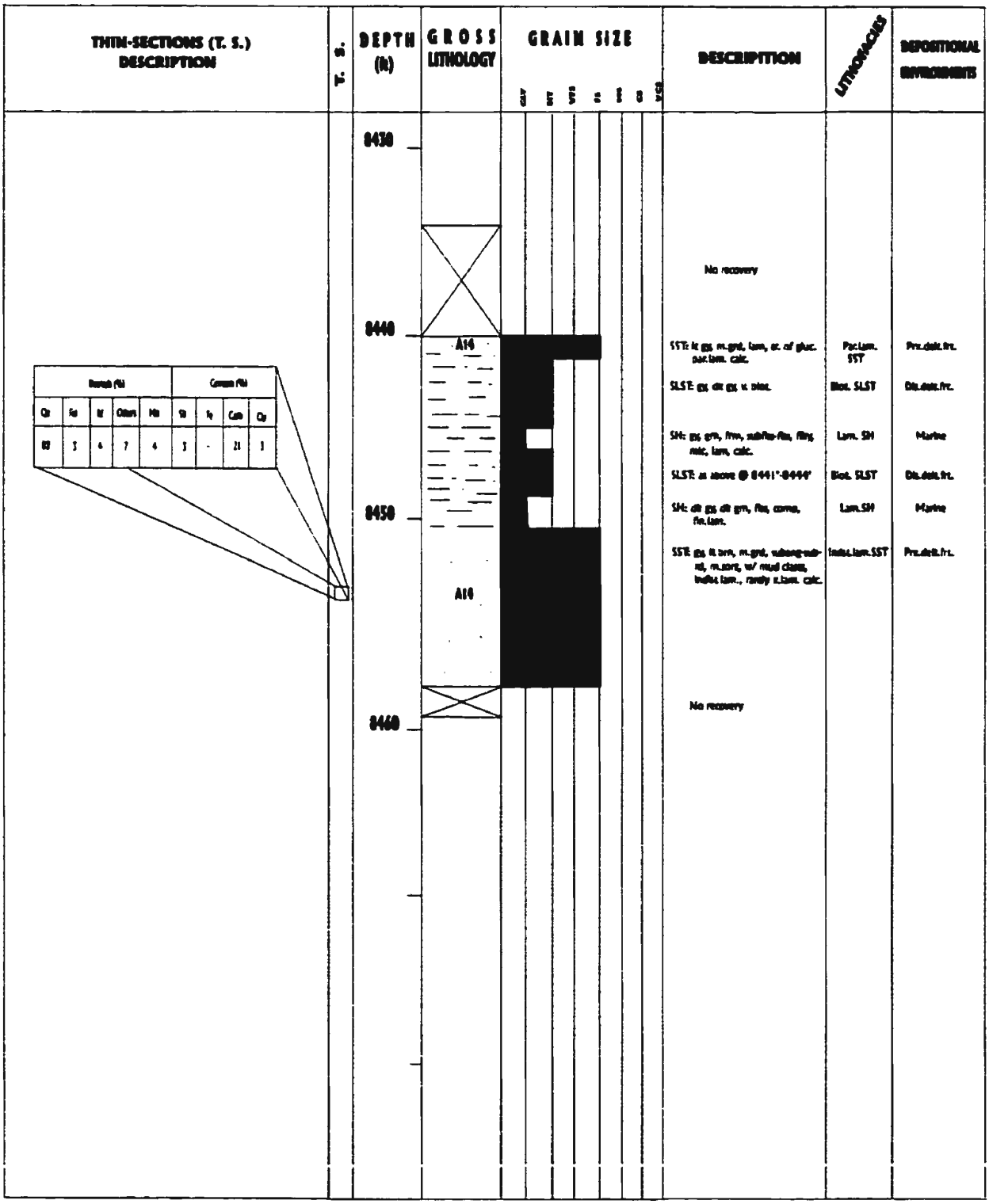

Remarks: Qz supported ss., w/ Qz overgrowth, dominant partial cal./dolo.cmts, occasionally w/compacted cly clasts.

Well: T1-23 **Formation: Lower Acacus** **Core#: 2** **Interval: 8458'-8502'**

Area: Concession NC2, Hamada Basin, NW Libya

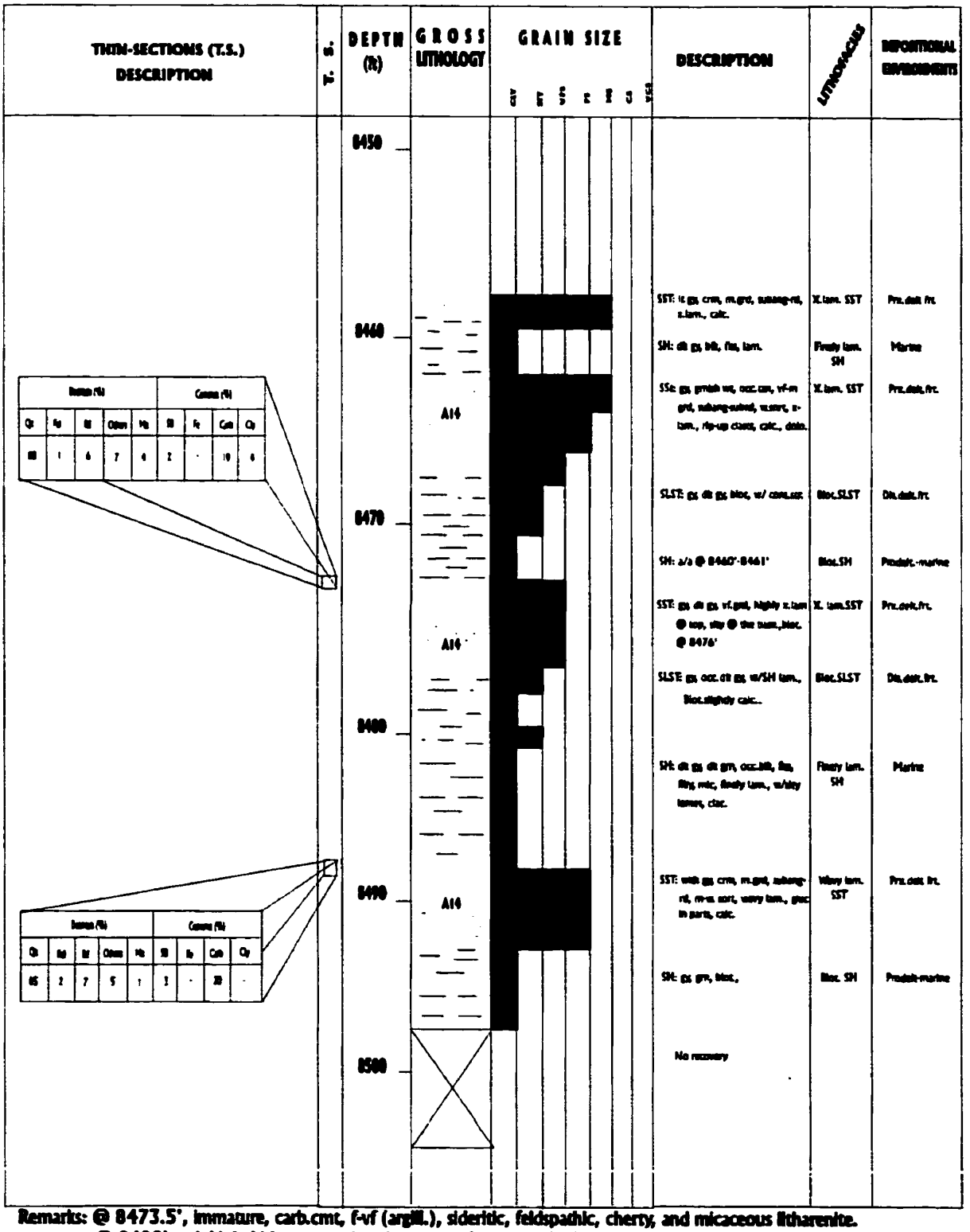

Remarks: @ 8473.5', immature, carb.cmt, f-vf (argill.), sideritic, feldspathic, cherty, and micaceous litharenite.
@ 8489', cal./dolo/sid.cmt ss., glauc.in parts, w/compacted mica, chlorite, also detrital dol. grains are present.

Well: A1-NC2 **Formation: Lower Acacus** **Core#: 2 & 3** **Interval: 7789'-7819' &**

Area: Concession NC2, Hamada Basin, NW Libya **7819'-7829'**

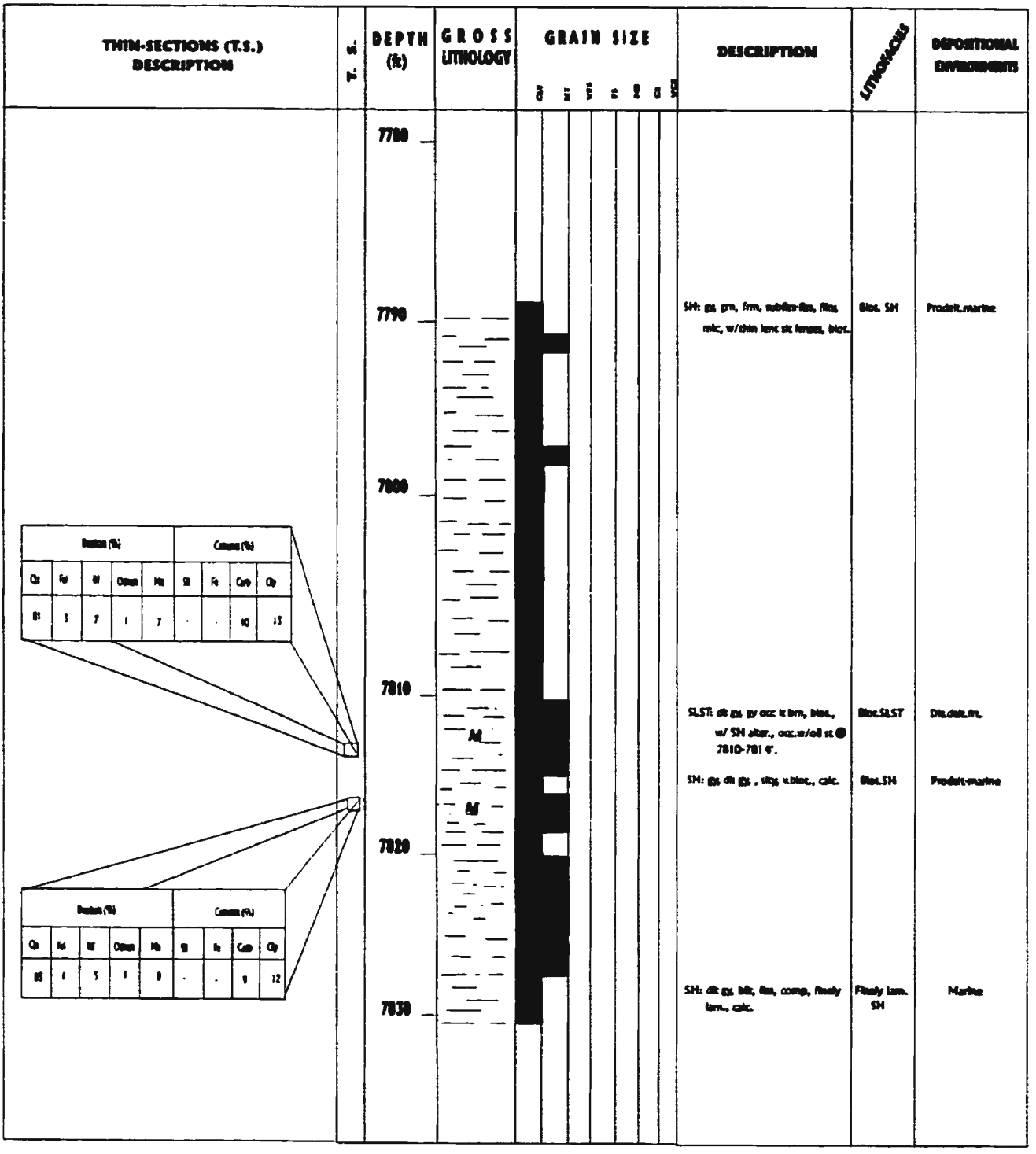

Remarks: @ 7814', Sublitharenites w/ fel. < 5%, detrital dolo.rhombs are common, pores filled w/ hydrocarbons.
@ 7817', most matrix materials were introduced probably by bioturbation of sandy-clay interbeds (laminae).

Well: Q1-23 **Formation: Lower Acacus** **Core #: 1 & 2** **Interval: 7440'-7470'**
7470'-7485'

Area: Concession NC2, Hamada Basin, NW Libya

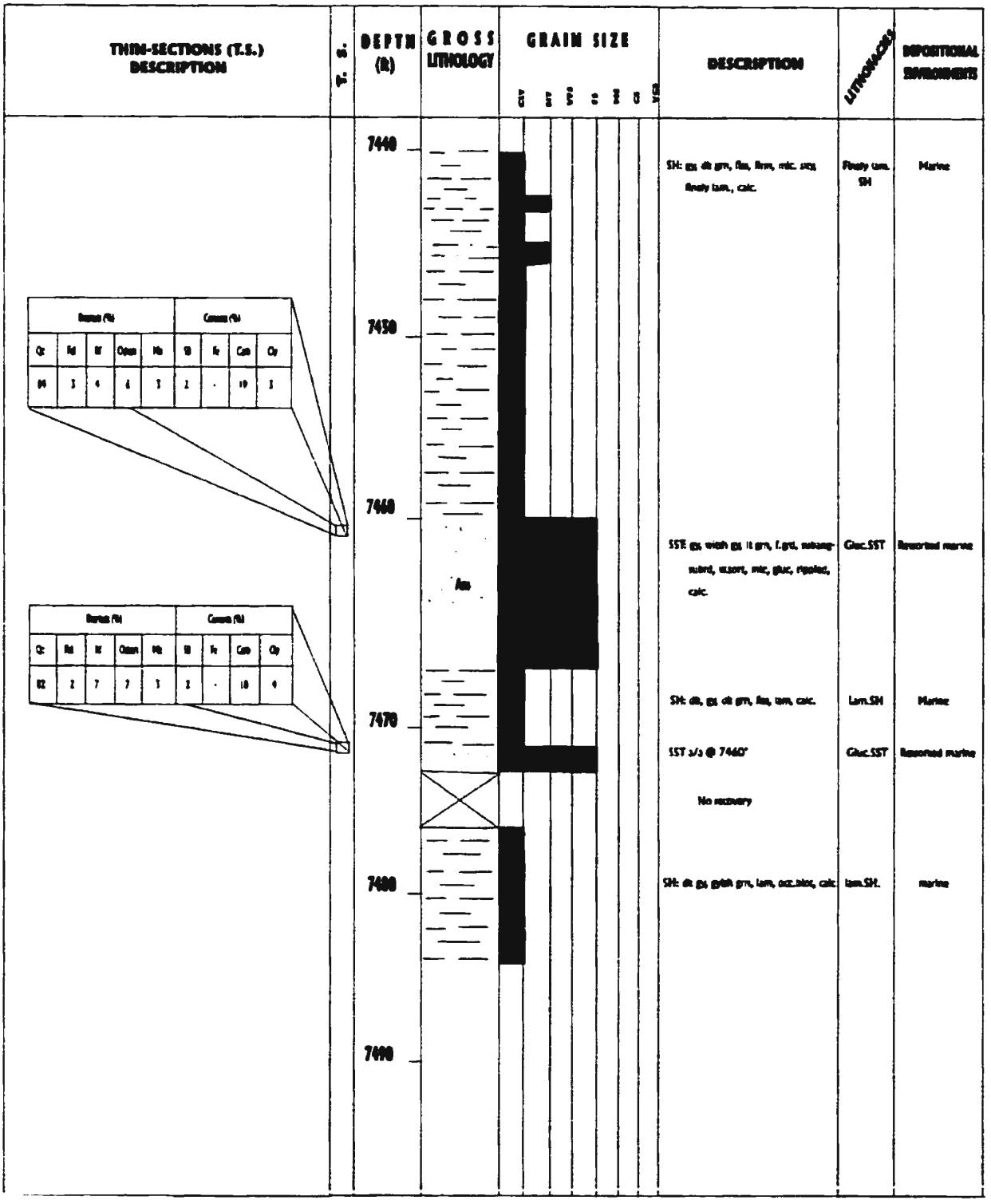

Remarks: @ 7461', Qz arenite, glauc. ss, w/ diagenetic chlorite result possibly from alteration of clay minerals.
@ 7471', feldspathic-glauc.qzarenites, mainly w/cal.cmt, dolo.cmt in parts, sil. cmt is present through grain to grain contact.

Well: Q1-23 **Formation: Lower Acacus** **Core #: 3** **Interval: 8170'-8200'**

Area: Concession NC2, Hamada Basin, NW Libya

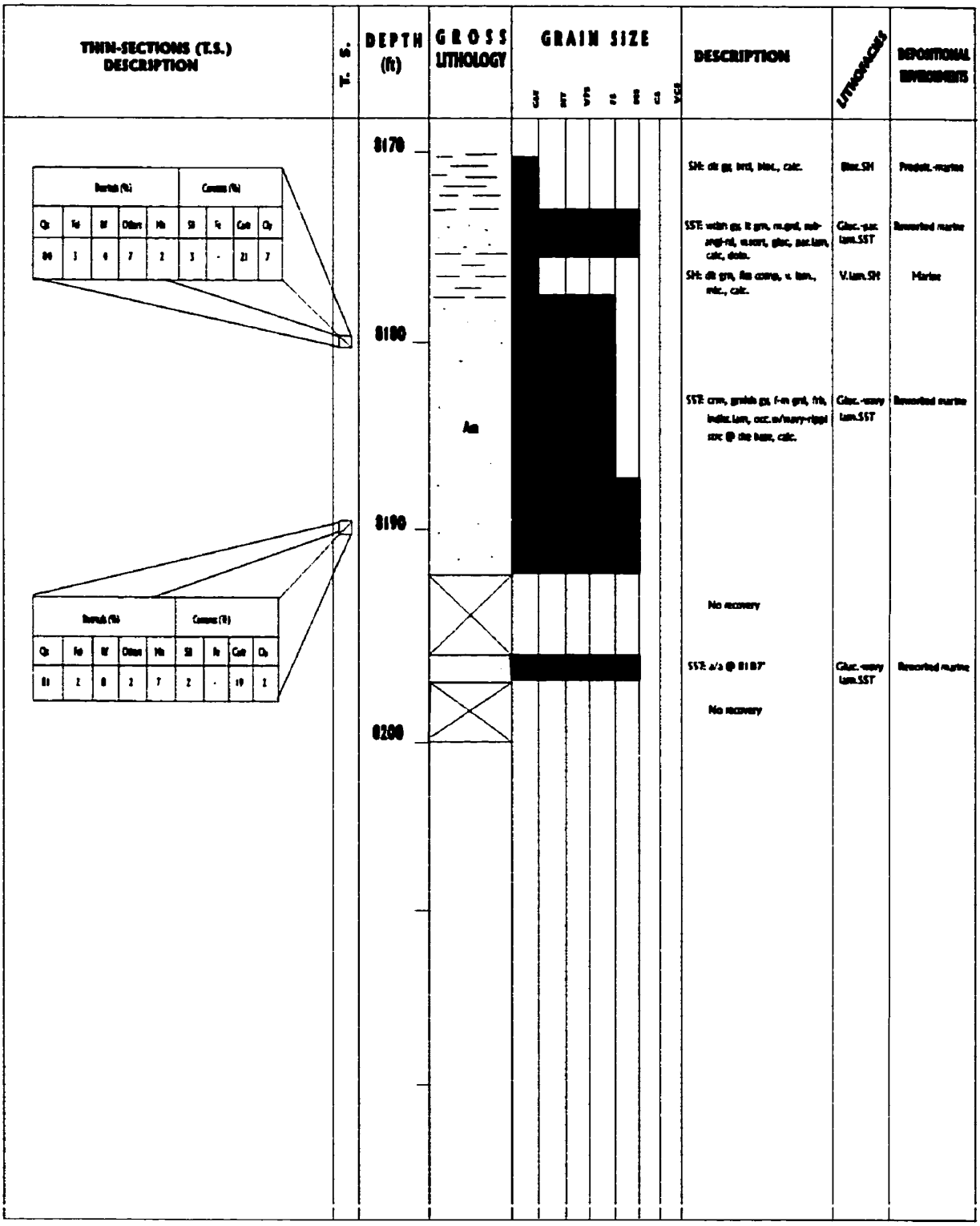

Remarks: @ 8180', highly fractured qz grains, also deformation of labile grains between qz grains. The rather loose packing may be indicative of early cal. cmt. which preserved normal compaction. Sample also shows good microfractures which may enhanced permeability.

@ 8190', Qz grains are corroded either due to metamorphism or effected by cal.cmt surrounding. Strained Qz grains, meta.rock frag., and minor flaky minerals like chlorite which may suggest metamorphism.

Well: Q1-23 **Formation: Lower Acacus** **Core #: 4** **Interval: 8461'-8497'**

Area: Concession NC2, Hamada Basin, NW Libya

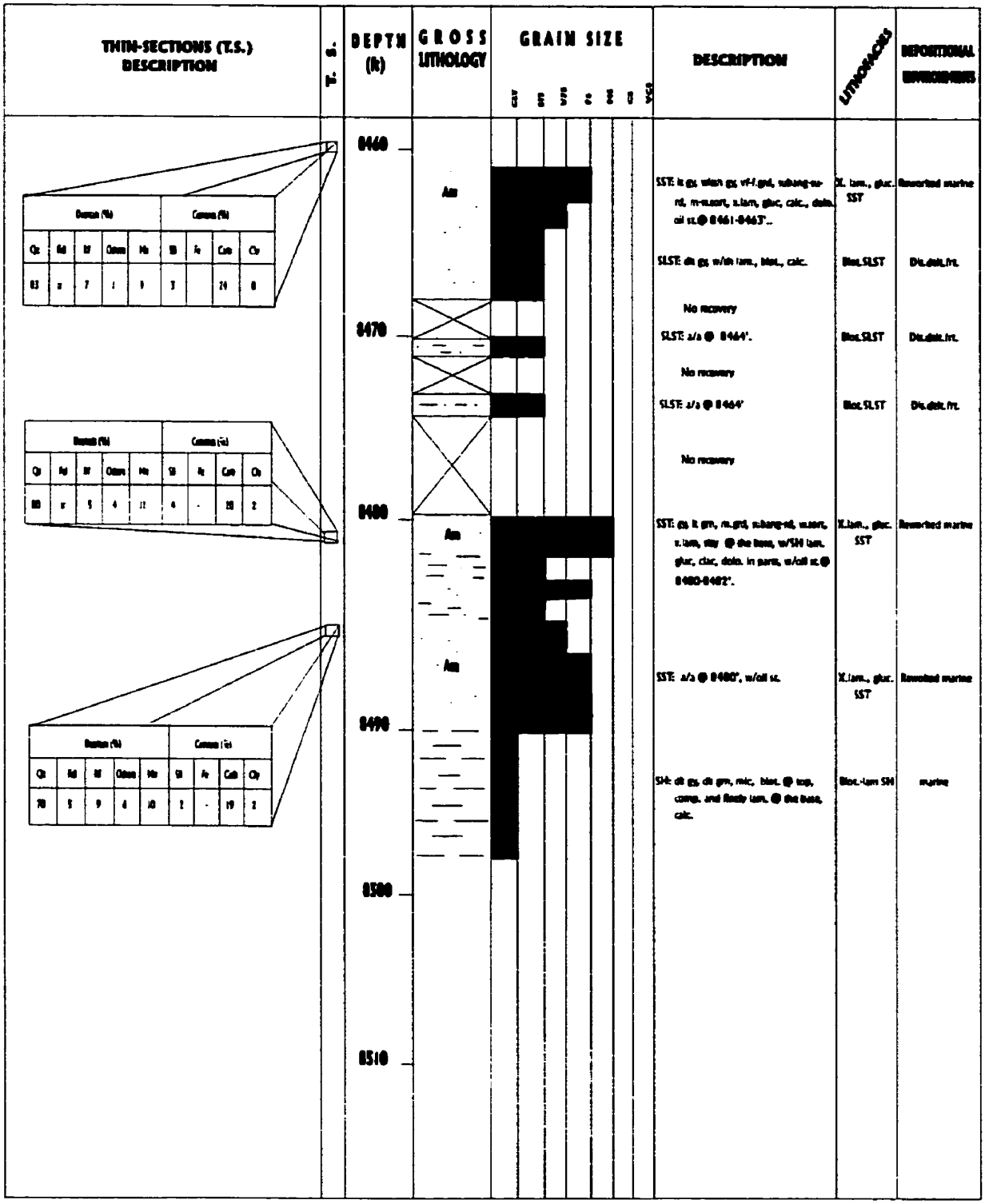

Remarks: @ 8461', subilth., w/cly cmt (kaolinite) , microporosity associated with cly mx as indicated by oil drpts in cly mtx. The association of partially cal. cmt. w/kaolinite cmt. around floating quartz grainsimplies that dissolution of cal. cmt provided some space in which kaolinite precipitated.

@ 8481' carb.cmt, compacted, glauconitic ss., w/less porosity because of cly rich cmt.

@ 8485', Qz dominated, fel., kaolinitic, chloritic ss. (interb. cly/ss.), carb.cmt..

APPENDIX II
THIN-SECTION PHOTOMICROGRAPHS (PETROGRAPHY)

APPENDIX II

THIN-SECTION PHOTOMICROGRAPHS: PLATE 1

A- Medium-coarse, rounded-subrounded quartz grains, quartzarenites-sublitharenites, show single quartz crystals (Q) with straight extinction taken with crossed polar (XPL) and subhedral quartz-overgrowths termination (O). The matrix between the grains contains opaque iron-oxides (I) and some calcite cement (C). Fluvial sandstones, well EE1-NC7A @ 2686 m. (8810 ft.). Scale bar= 0.1mm.

(XPL)

B- Fine-medium, subangular-subrounded quartz grains (Q) with single crystals show straight extinction on crossed polars (XPL), and of sharp, straight, uncorroded boundaries (arrows). Fluvial sandstones, well A1-NC118 @ 3061 m. (10040 ft.). Scale bar= 0.1mm.

(XPL)

APPENDIX II
THIN-SECTION PHOTOMICROGRAPHS: PLATE 1

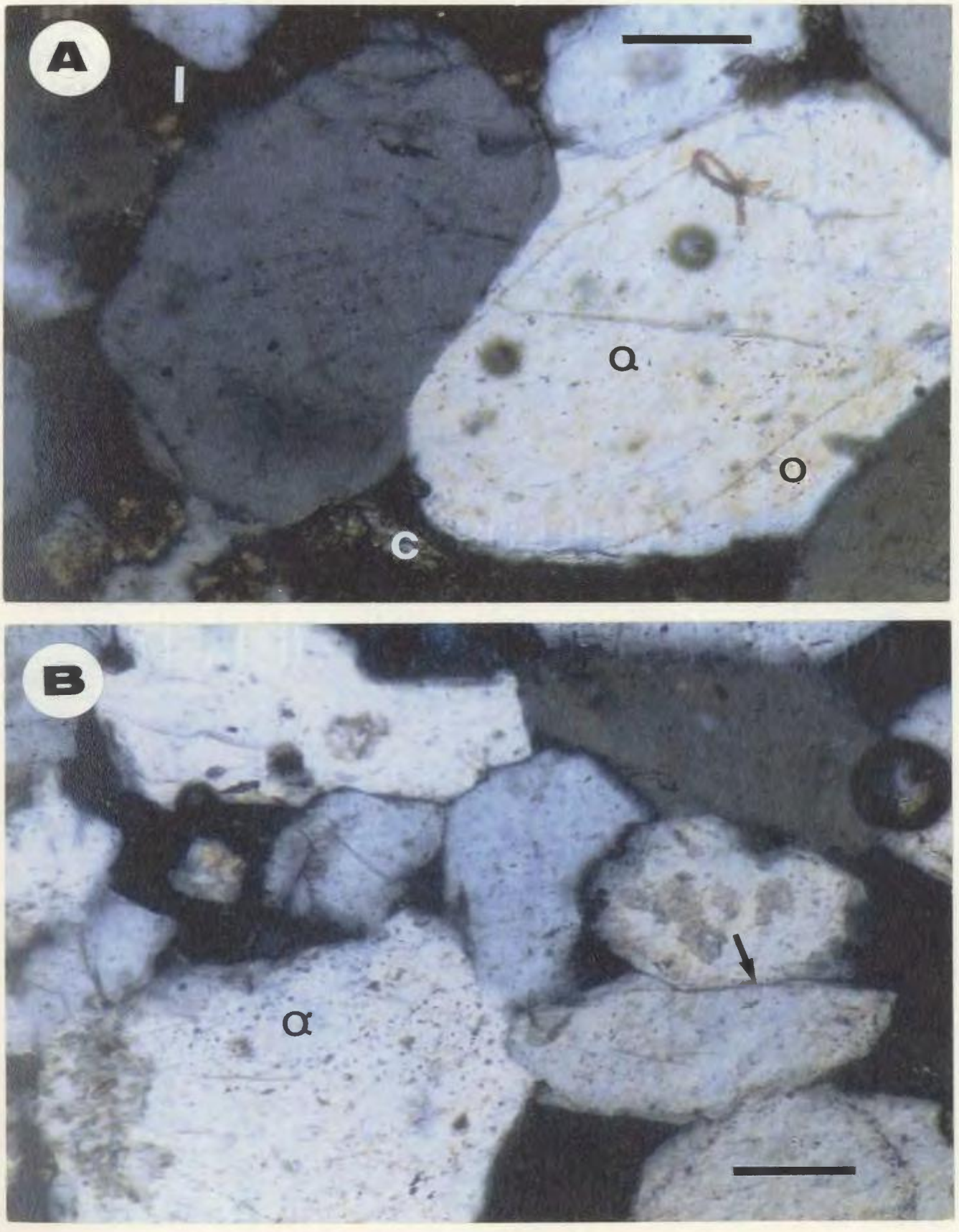

APPENDIX II

THIN-SECTION PHOTOMICROGRAPHS : PLATE 2

A- Fine-medium quartz grains (Q), with straight extinction. The matrix between quartz grains contains calcite cement (C) which shows high-order pink and greenish pink interference colours. Proximal delta front sandstones, well C1-NC2 @ 2965 m. (9725ft.). Scale bar= 0.1mm.

(XPL)

B- Interbedded very fine quartz grains (Q) and silty-clayey laminations (Cly), very common in the distal delta front siltstone facies, well E1-NC2 @ 2780 m. (9117 ft). Scale bar= 0.07mm.

(XPL)

APPENDIX II
THIN-SECTION PHOTOMICROGRAPHS: PLATE 2

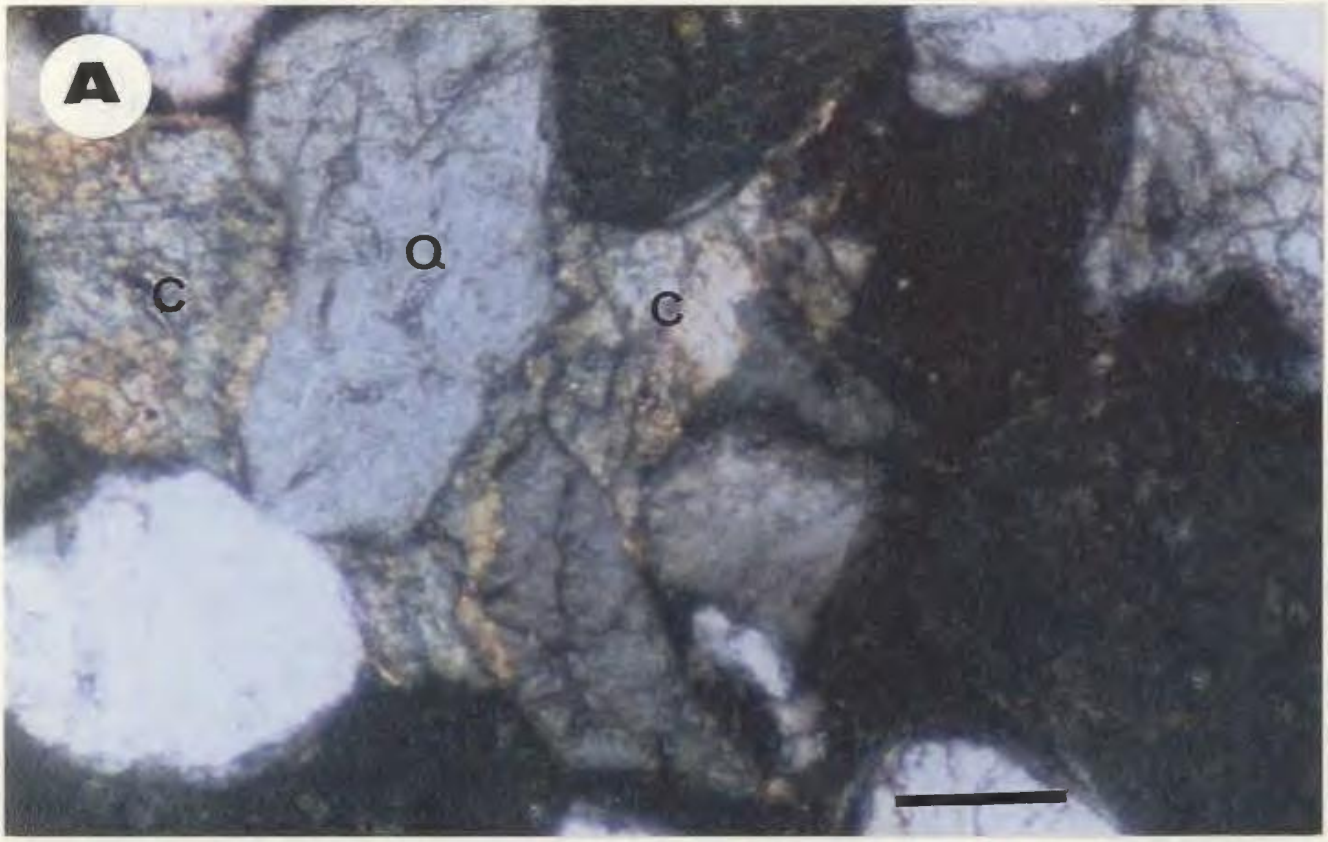

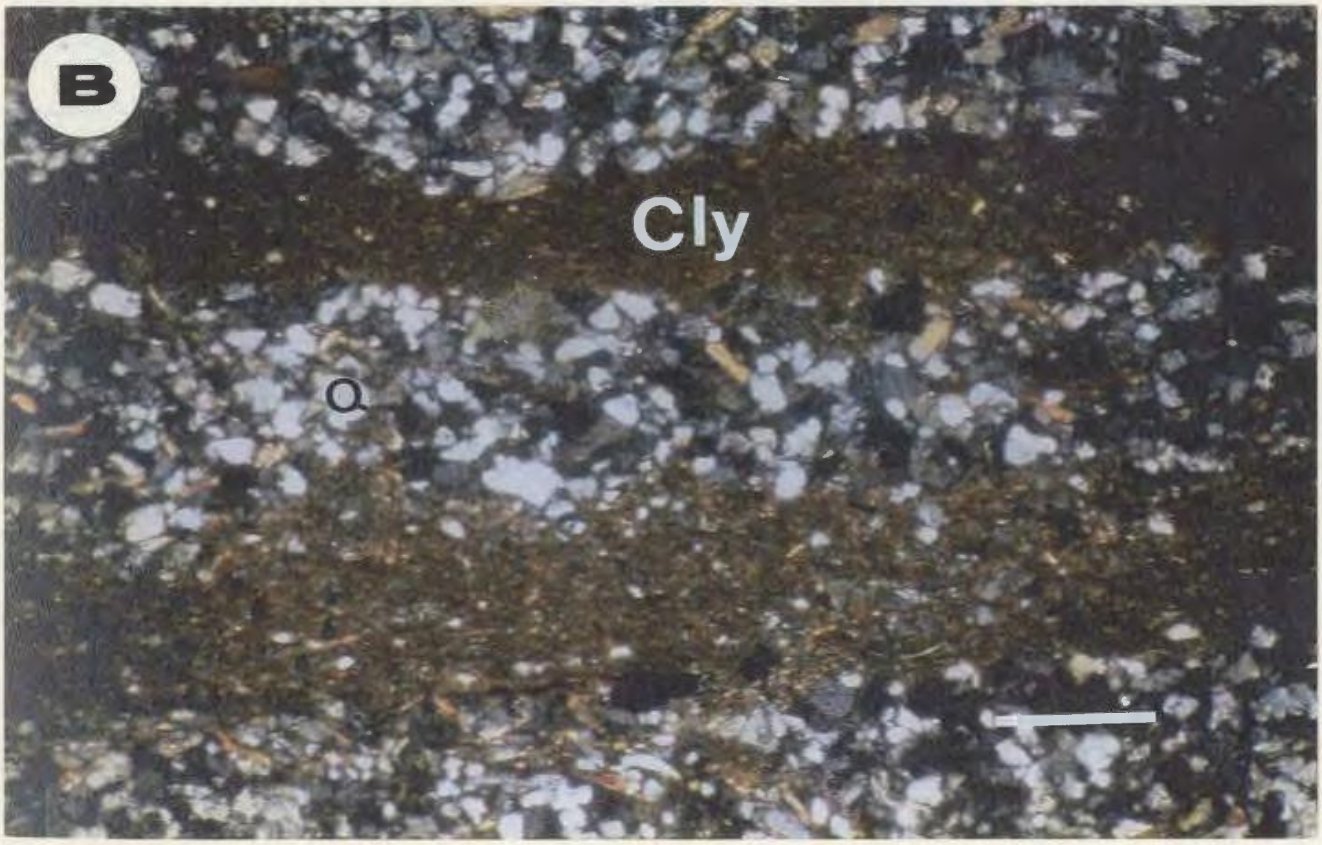

APPENDIX II

THIN-SECTION PHOTOMICROGRAPHS: PLATE 3

A- Fine quartz grains (Q), usually subangular, single crystals of straight extinction, glauconitic (G), with corroded quartz grains boundaries (arrow), and of calcite cement (C). Black areas are pores (P) resulted from partial dissolution of calcite cement in this facies. Reworked marine sandstones, well Q1-23, @ 2275 m. (7461 ft.). Scale bar= 0.1mm.

(XPL)

B- Fine-medium quartz grains (Q), subangular-subrounded in feldspar-rich sandstone. Plagioclase feldspar (PF) shows albite twinning, whereas possible microcline feldspar (MF) shows grid twinning. Proximal delta front facies, well D1-61 @ 2697 m. (8845 ft). Scale bar= 0.1mm.

(XPL)

APPENDIX II
THIN-SECTION PHOTOMICROGRAPHS: PLATE 3

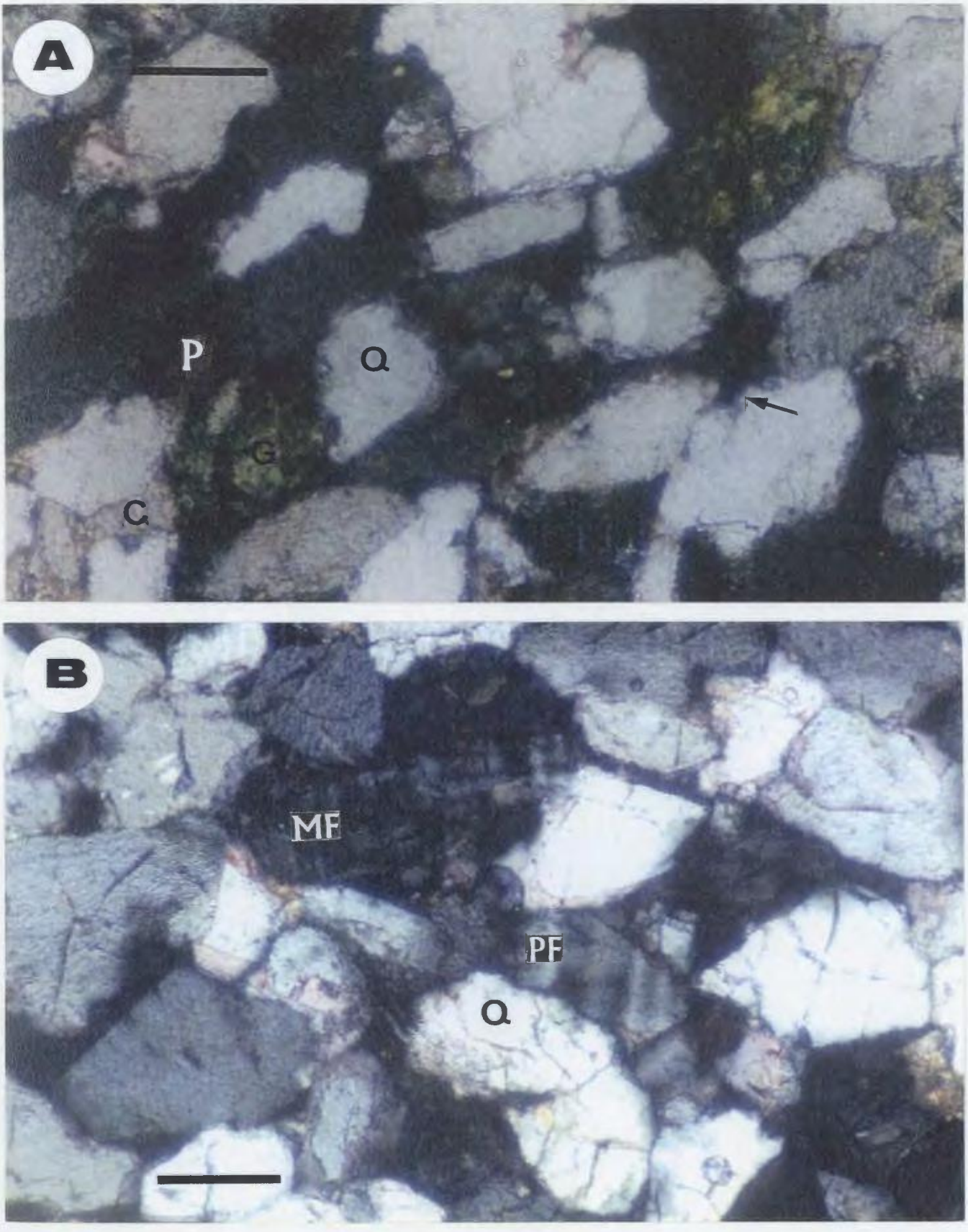

APPENDIX II

THIN-SECTION PHOTOMICROGRAPHS: PLATE 4

A- Shows a large plagioclase feldspar (PF) grain which is easily identified by the albite twinning in the photograph with polars crossed (XPL). Medium-coarse grained fluvial sandstone, well EE1-NC7A @ 2686 m. (8810 ft.). Scale bar= 0.1mm.

(XPL)

B- Fine-medium grained sandstone, sublitharenite, showing possible volcanic rock fragment (VRF) of glassy, dense isotopic appearance (texture), combined with presence of some crystal laths which may be of alteration products, also metamorphic rock fragment (MRF) can also be seen which characterized by much more foliated texture. Note the very fractured (healed fractures) quartz grains (Q) surrounded by calcite cement (C). Proximal delta front sandstone, well B3-61 @ 2734 m. (8969 ft.). Scale bar= 0.1mm.

(XPL)

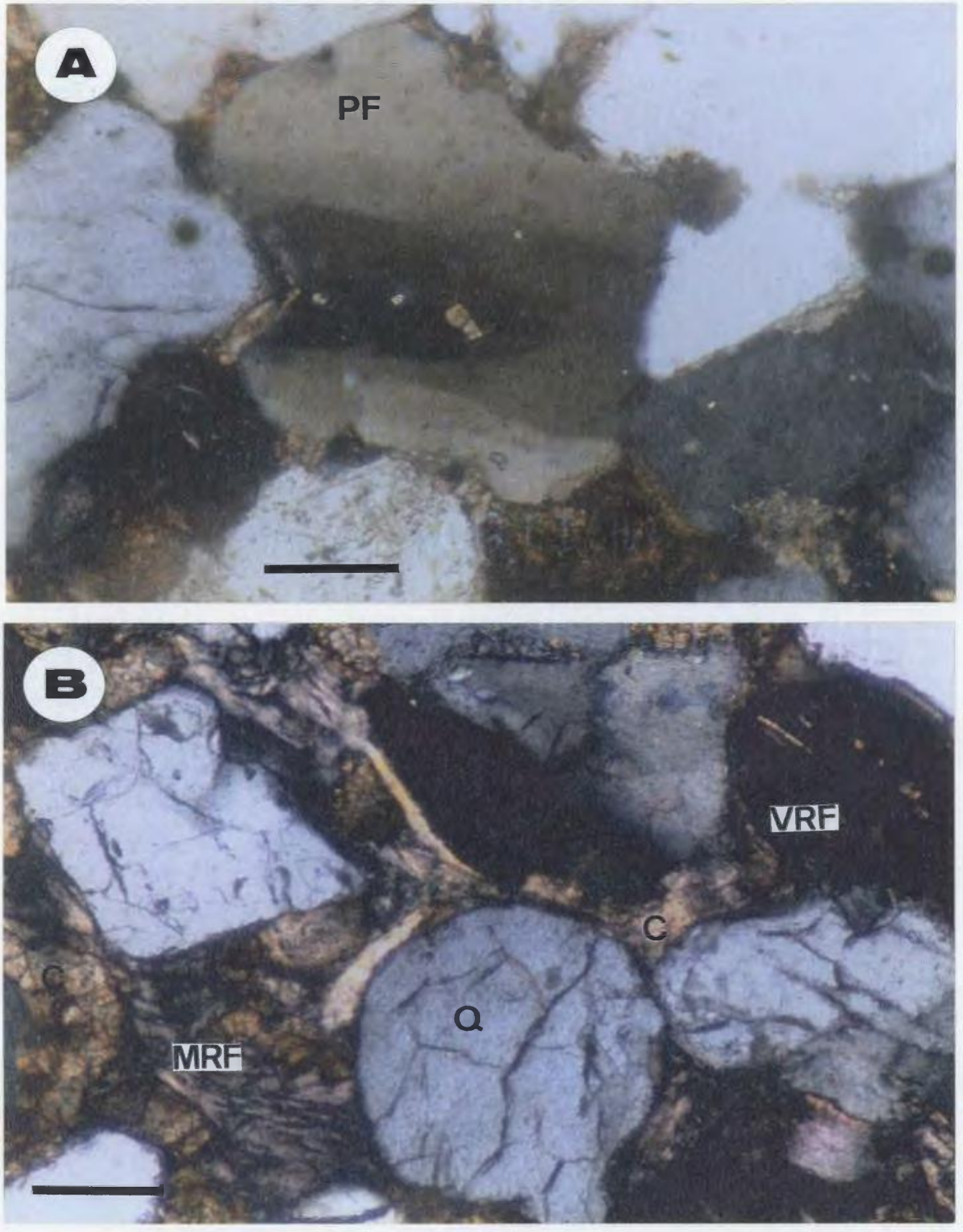
A
PF
B
VRF
C
C
Q
MRF

APPENDIX II

THIN-SECTION PHOTOMICROGRAPHS: PLATE 5

A- Shows a composite, stretched, elongated, and oriented polycrystalline quartz grains (PQ) enclosed between monocrystalline quartz grains (Q). The individual crystal in polycrystalline quartz shows undulose extinction as a result of strain of possible metamorphic origin. Distal delta front siltstone, well D1-61 @ 2567 m. (8420 ft.). Scale bar= 0.03mm.

(XPL)

B- Shows possible altered rock fragment (RF) composed of very fine micaceous crystalline matrix may be of volcanic or metamorphic origin. Note the highly fractured quartz grains (Q) which surrounded by calcite cement (C) of high order pink interference colours, also note pores (P) appear black in crossed polars (XPL) which are formed as a result of partial dissolution of calcite cement in this unit. Proximal delta front sandstone, well B3-61 @ 2734 m. (8969 ft.). Scale bar= 0.1mm.

(XPL)

APPENDIX II
THIN-SECTION PHOTOMICROGRAPHS: PLATE 5

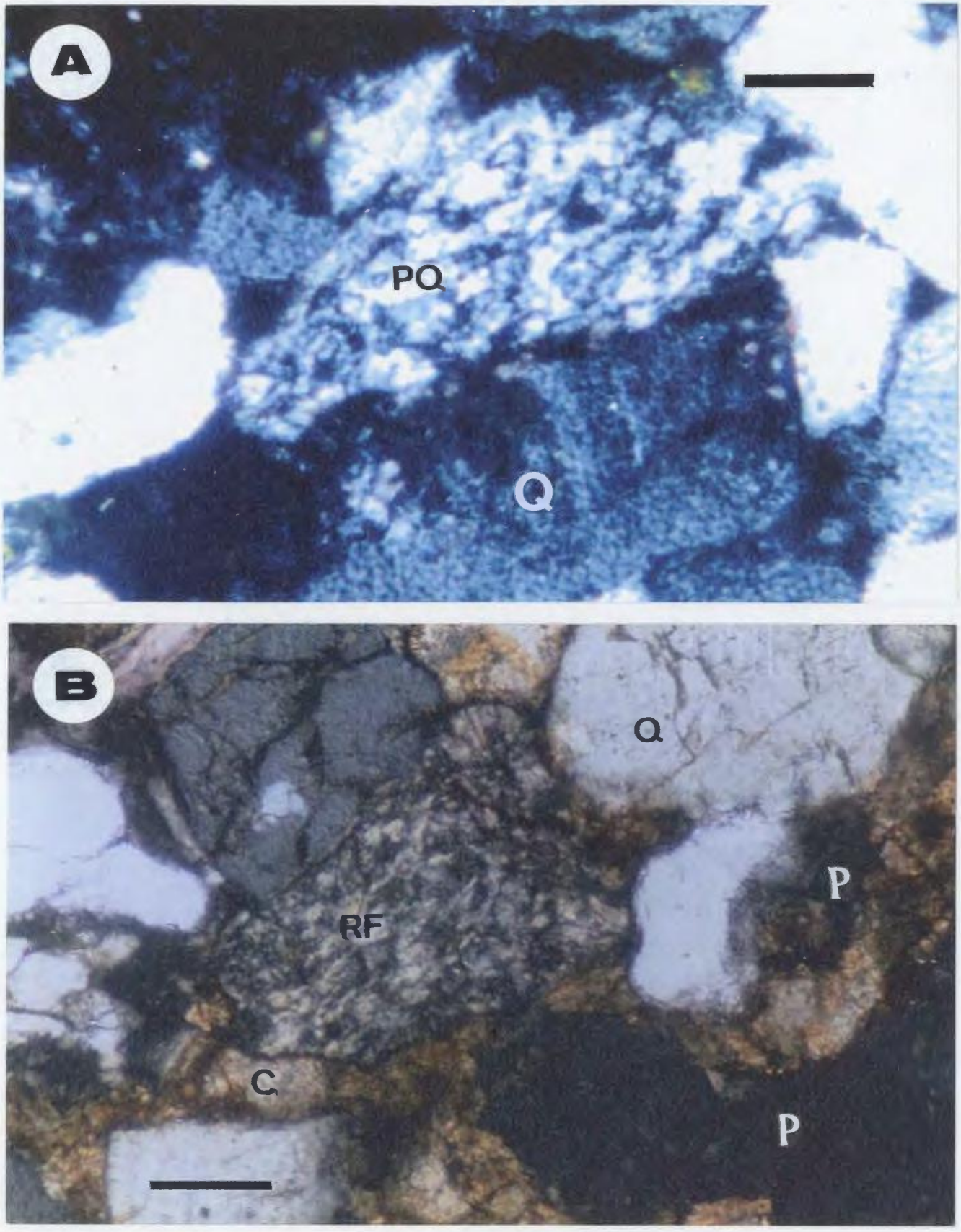

APPENDIX II

THIN-SECTION PHOTOMICROGRAPHS: PLATE 6

A- Fine-medium grained, sublitharenite showing individual clay clasts (Cly C.) of dark grey colour and of finely crystalline texture enclosed between rigid quartz grains (Q), and exhibits some compaction. Proximal delta front sandstone, well T1-23 @ 2577 m. (8454 ft.). Scale bar= 0.1mm.

(XPL)

B- Same as previous photo but with plane-polarized light (PPL).

THIN-SECTION PHOTOMICROGRAPHS: PLATE 6

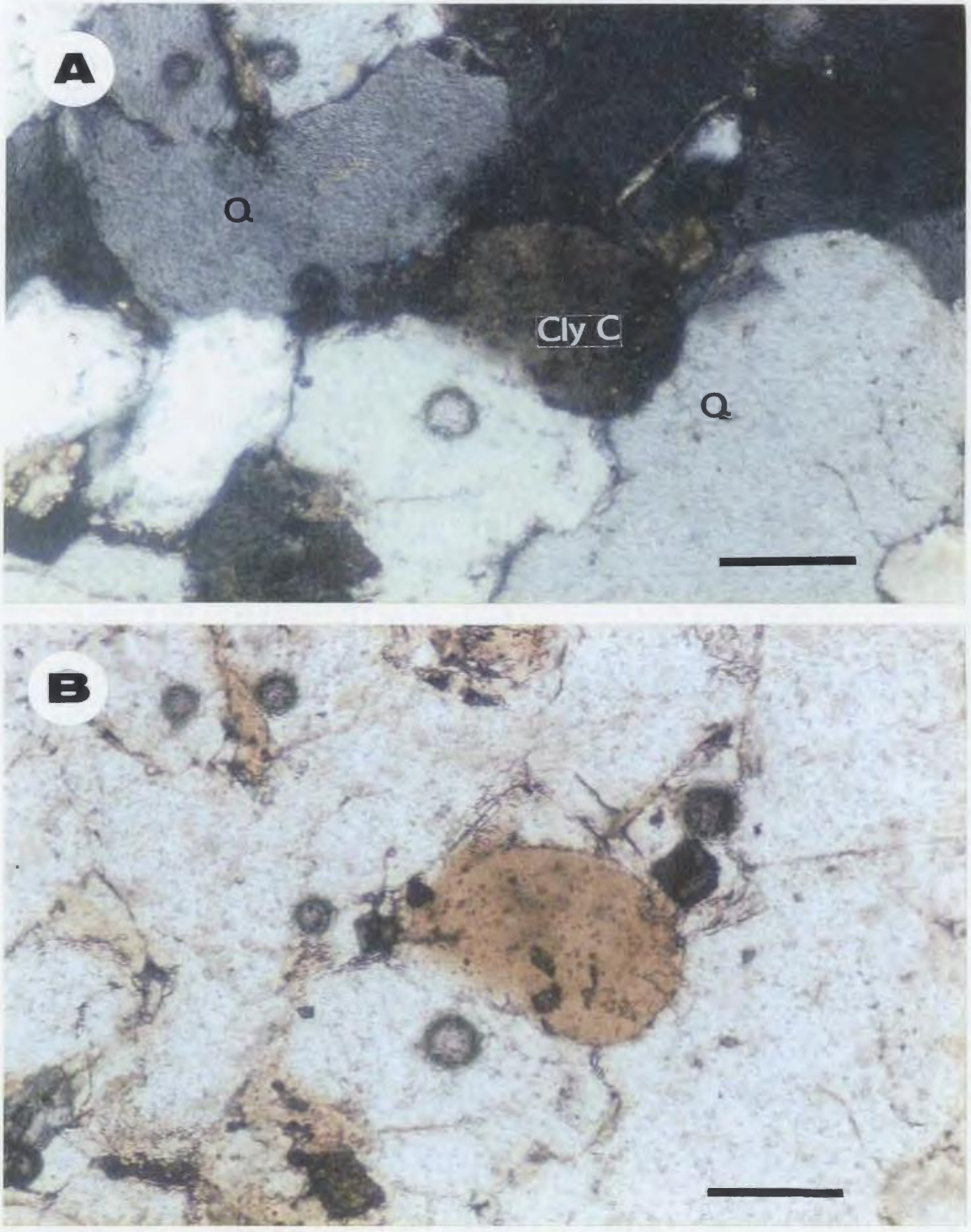

APPENDIX II

THIN-SECTION PHOTOMICROGRAPHS PLATE: 7

A- Fine-medium grained sandstone, sublitharenite showing detrital dolomite grains (D) identified by their rhombic shape and their lack of response to stain. Note moldic porosity (P) Proximal delta front sandstone, well B3-61 @ 2734 m. (8969 ft.). Scale bar= 0.1mm.

(PPL)

B- Detrital mica muscovite (MS) characterized by bright yellow-blue birefringence colours, also show some deformation between the rigid quartz grains (Q). Sublitharenite of proximal delta front sandstone, well D1-61 @ 2705 m. (8872 ft.). Scale bar= 0.1mm.

(XPL)

THIN-SECTION PHOTOMICROGRAPHS: PLATE 7

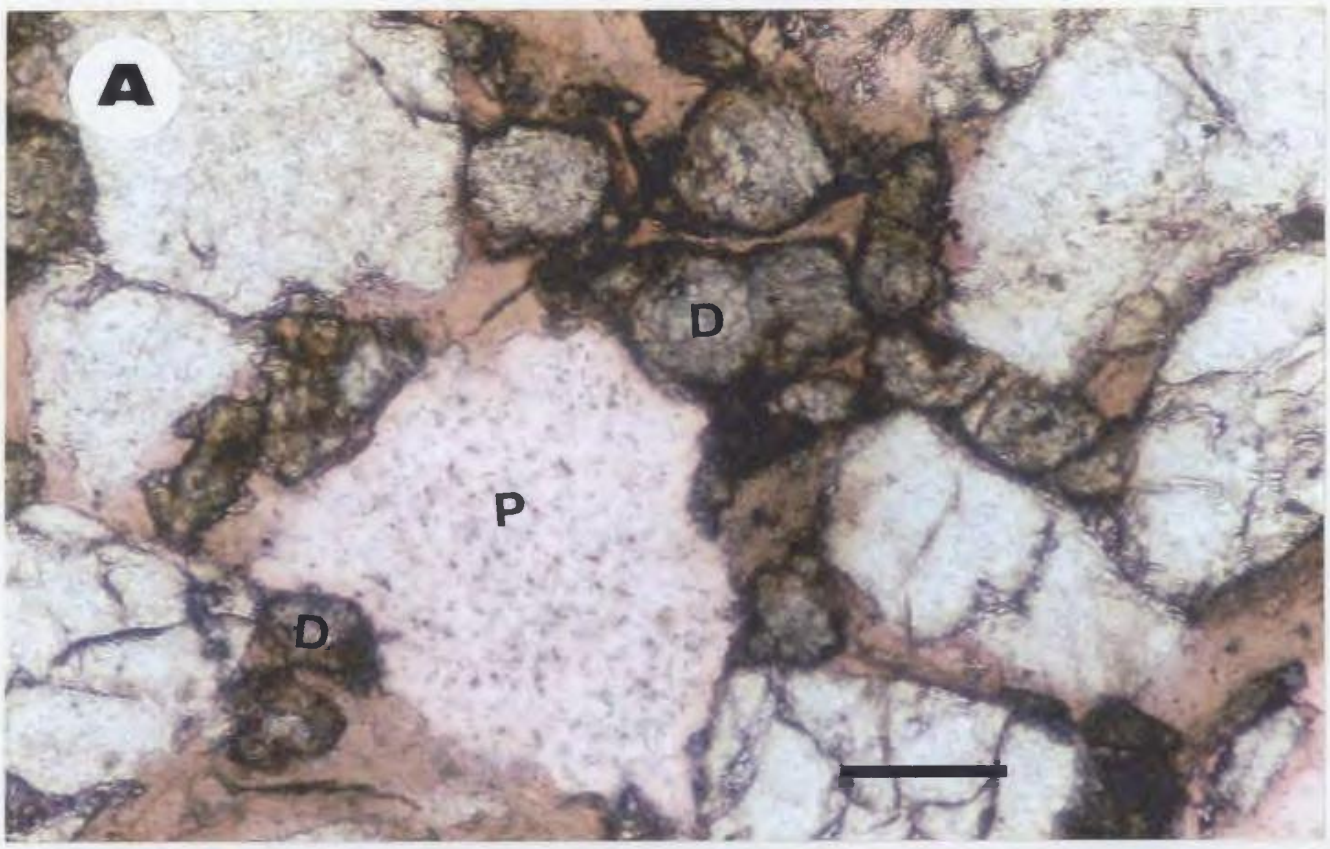

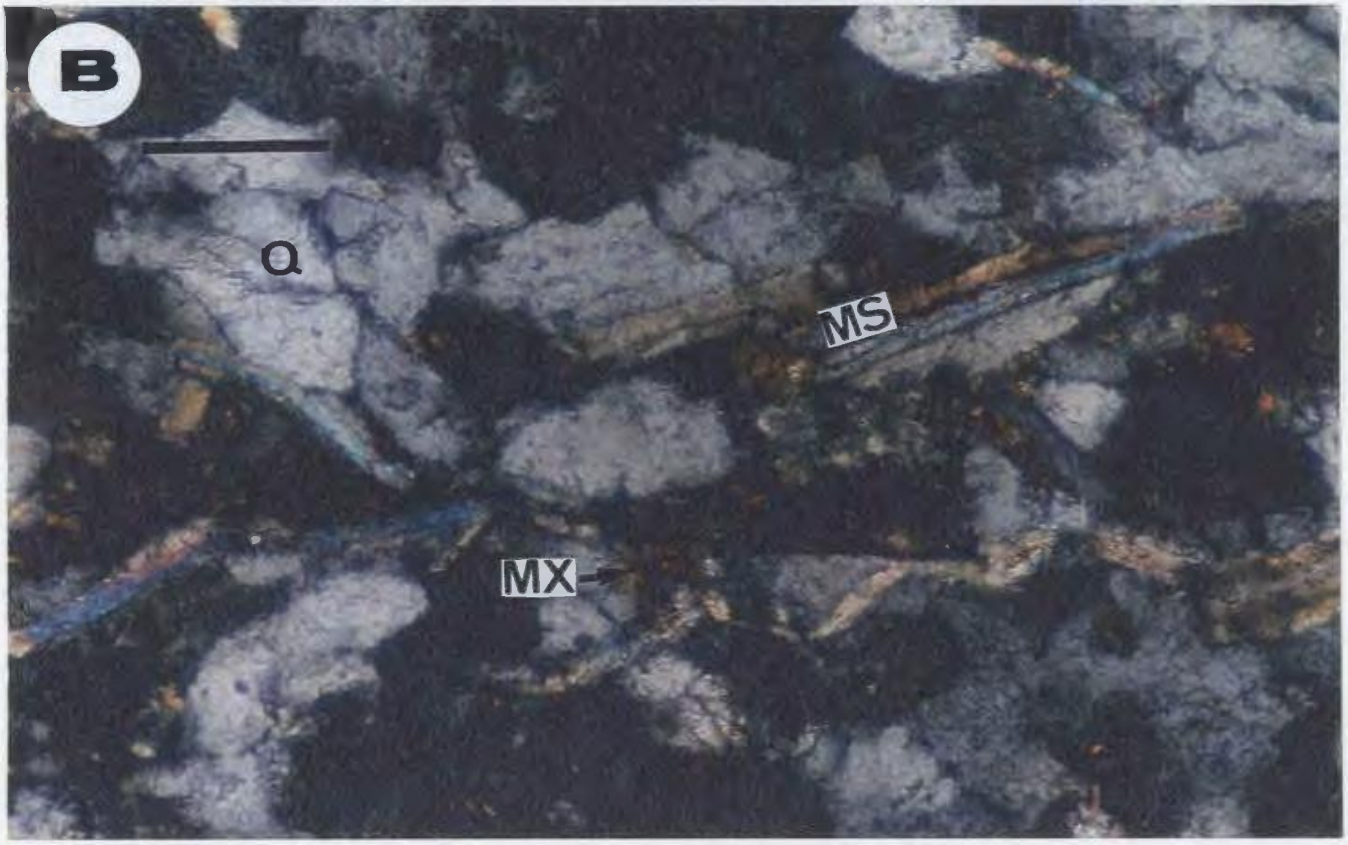

APPENDIX II

THIN-SECTION PHOTOMICROGRAPHS: PLATE 8

A- Shows a number of glauconite pellets (G) in a very fine-fine reworked marine sandstones. The glauconite is easily identified in the photograph taken in plane-polarized light (PPL) by its green occasionally brownish-green colour, and also show some deformation between rigid quartz grains (Q) due to compaction. This sandstone is highly calcite cemented (C). Well Q1-23 @ 2275 m. (7461 ft.). Scale bar= 0.1mm.

(PPL)

B- Detrital chlorite (CH) present as traces in the fine-medium grained sandstone of proximal delta front facies, and it may also shows some deformation due to compaction. Note the presence of plagioclase feldspar (PF) in this sample. Well D1-61 @ 2510 m. (8234 ft.). Scale bar= 0.1mm.

(XPL)

APPENDIX II

THIN-SECTION PHOTOMICROGRAPHS: PLATE 8

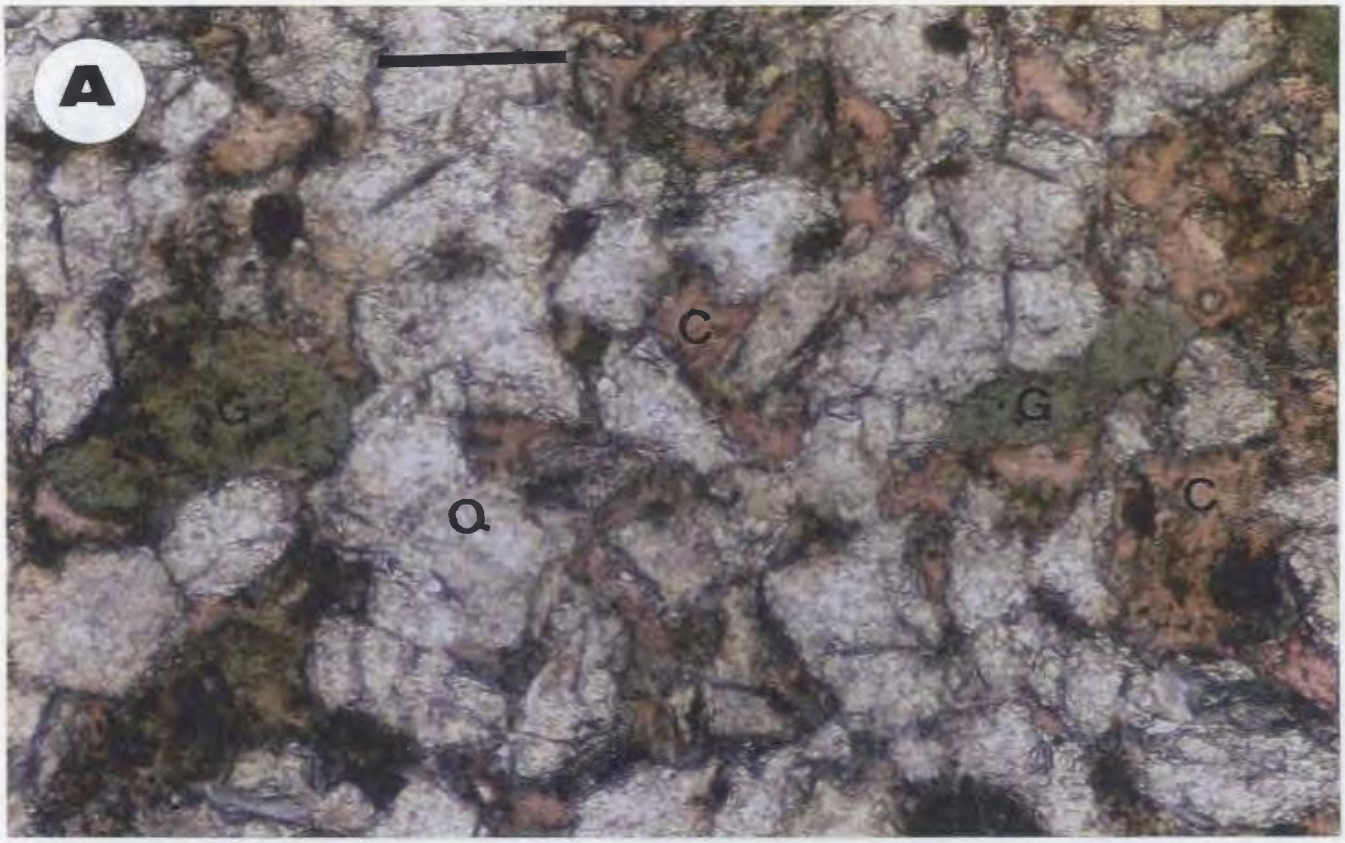

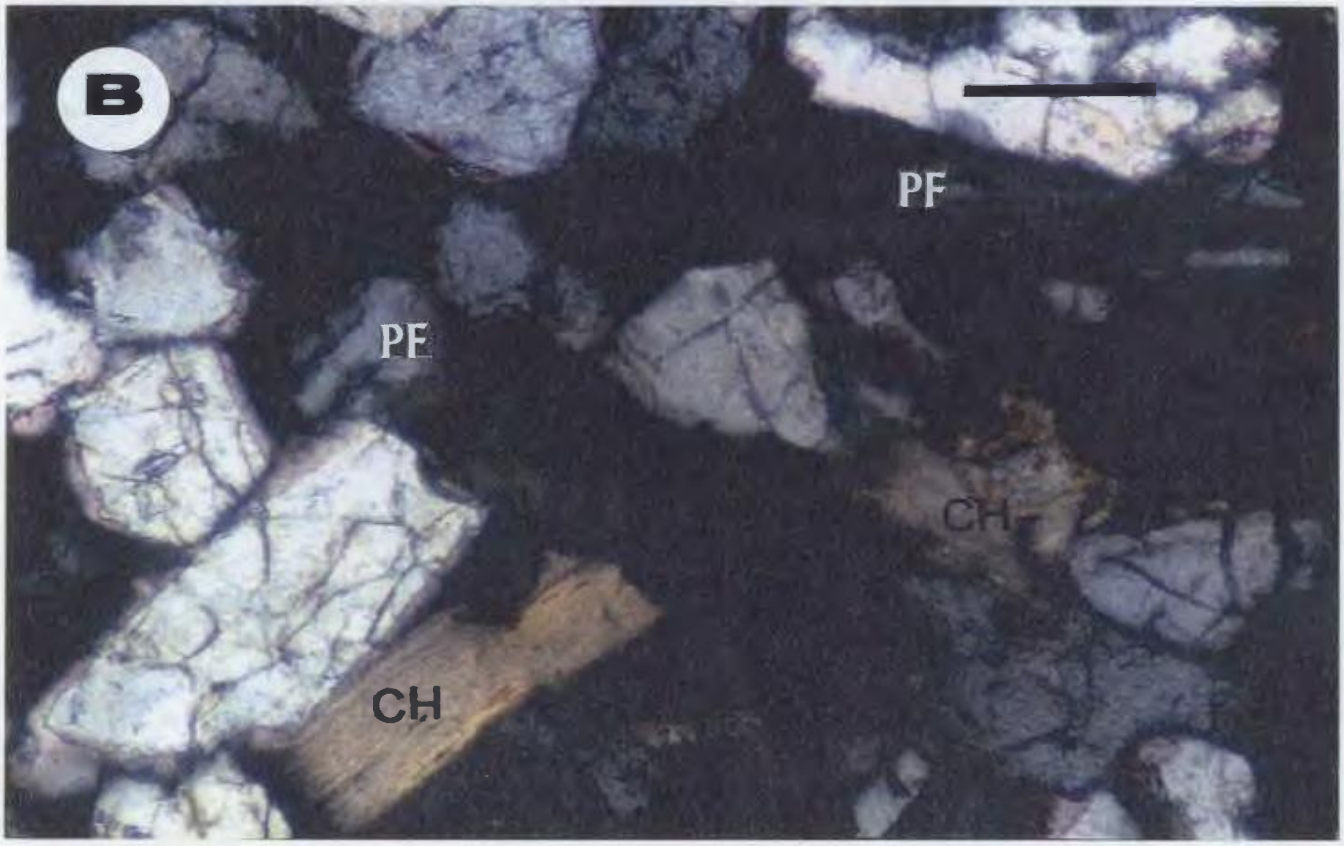

APPENDIX II

THIN-SECTION PHOTOMICROGRAPHS: PLATE 9

A- trace of oolitic chamosite (CHM) between quartz grains (Q) in the fine-medium grained, carbonate cemented sandstones of proximal delta front facies. Well B1-61 @ 2567 m. (8420 ft.). Scale bar= 0.1mm.

(XPL)

B- Same as previous photo but with plane-polarized light (PPL). Note secondary porosity (P) due to mainly partial dissolution of calcite cement (C) in this unit.

(PPL)

APPENDIX II

THIN-SECTION PHOTOMICROGRAPHS: PLATE 9

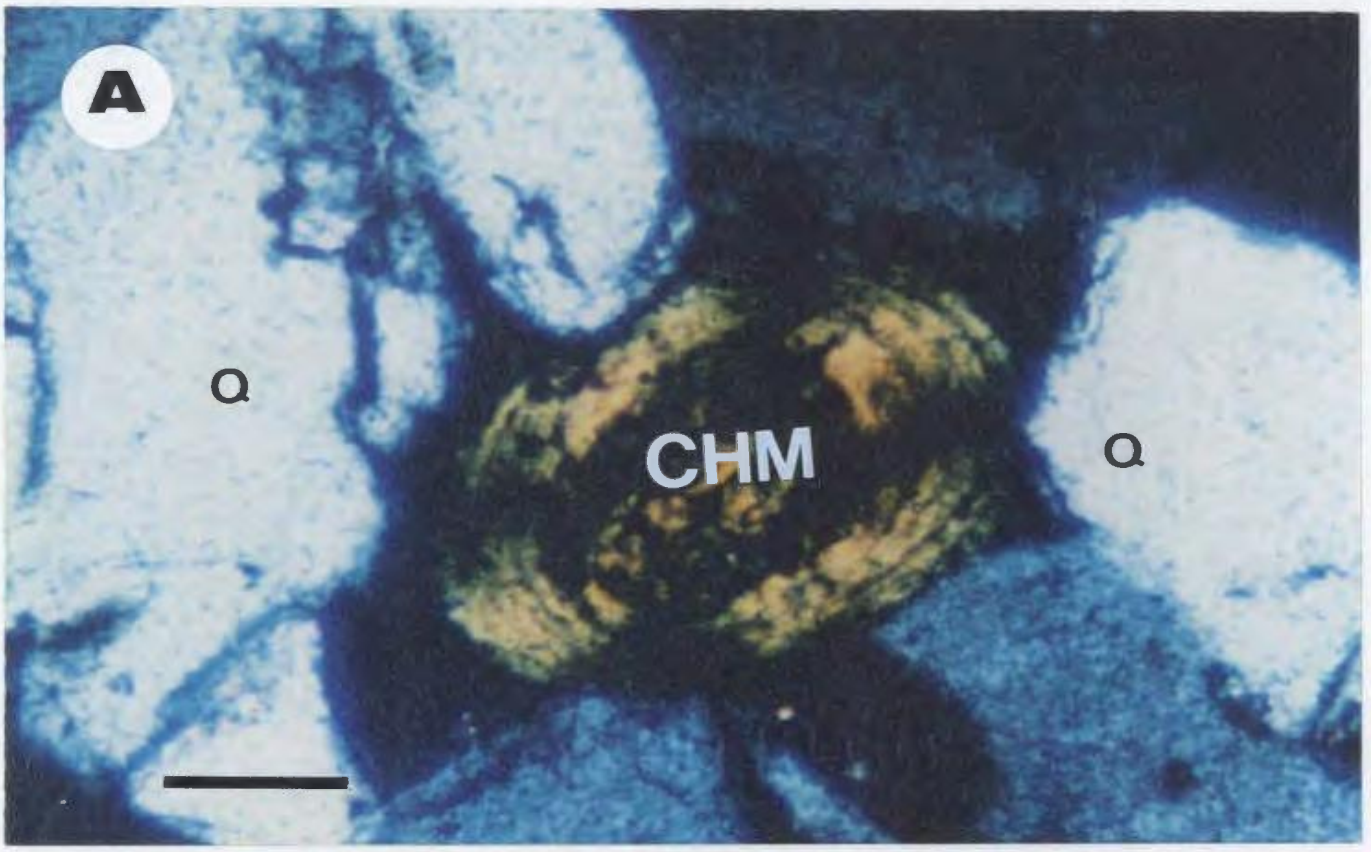

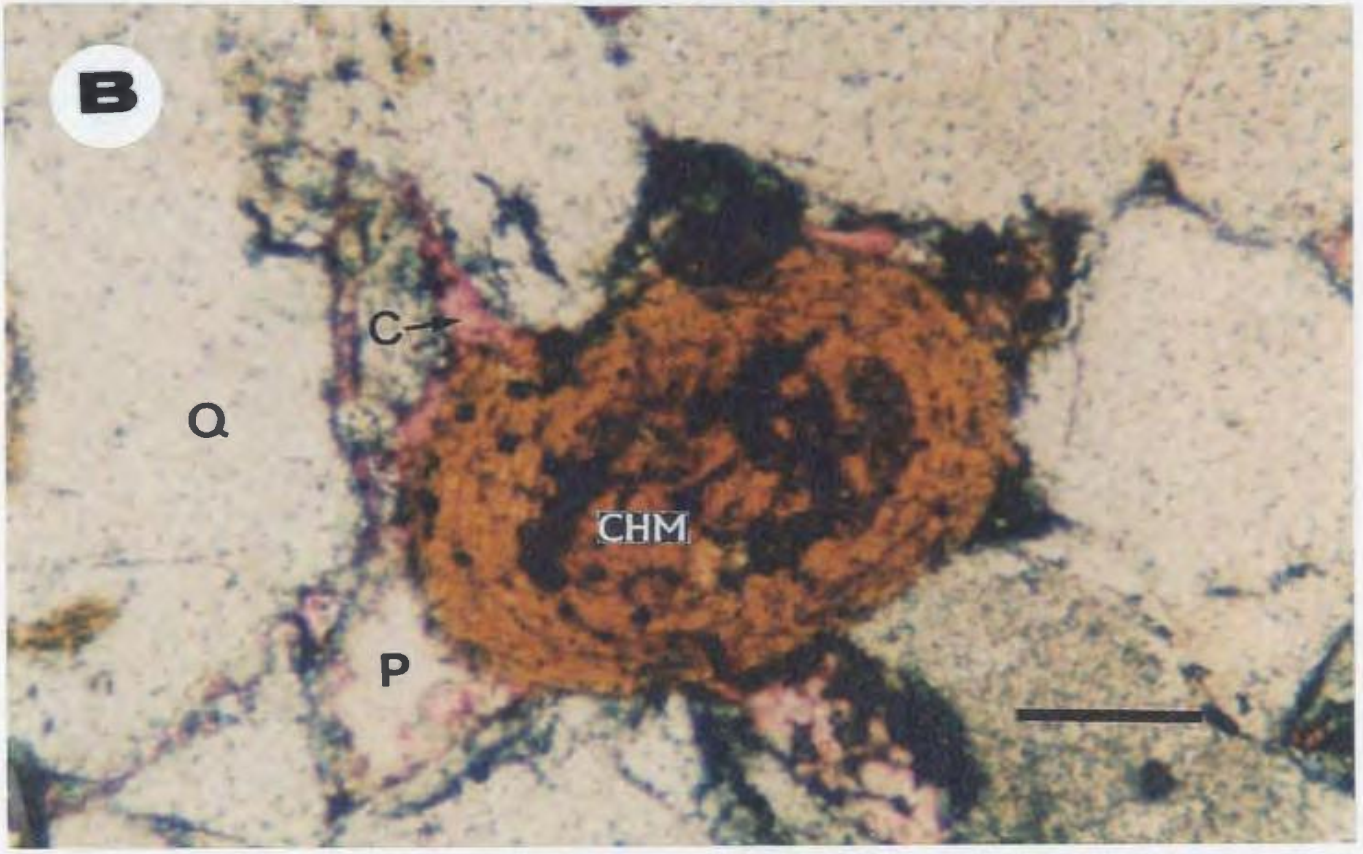

APPENDIX II

THIN-SECTION PHOTOMICROGRAPHS: PLATE 10

A- Trace of euhedral, prismatic zircon crystal (Z) with bipyramidal termination, characterized by high relief, pale-green colour, and with some inclusions. Note primary porosity (P) of uncorroded quartz grains (Q), and the partial shallow calcite cement (C). Fluvial sandstone, well A1-NC118 @ 3061 m. (10040 ft.). Scale bar= 0.1mm.

(PPL)

B- Pore-filling, poikilotopic calcite cement (C) in fine-medium grained sandstone of proximal delta front facies. Note detrital quartz grains (Q) are floating in calcite cement, also the fractured quartz grains, and the corroded nature of their boundaries (arrows). Well B1-NC2 @ 2608 m. (8555 ft.). Scale bar= 0.1mm.

(PPL)

THIN-SECTION PHOTOMICROGRAPHS: PLATE 10

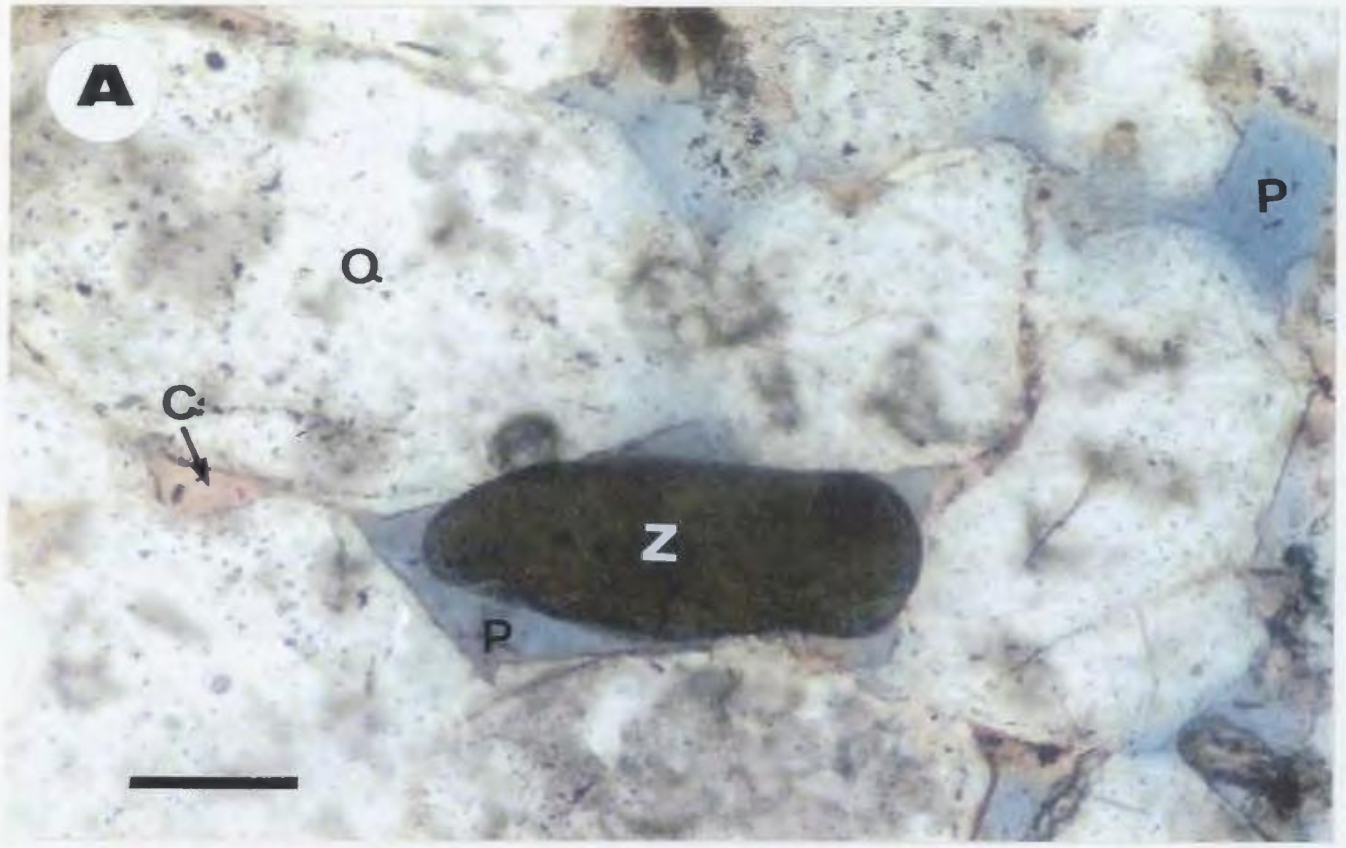

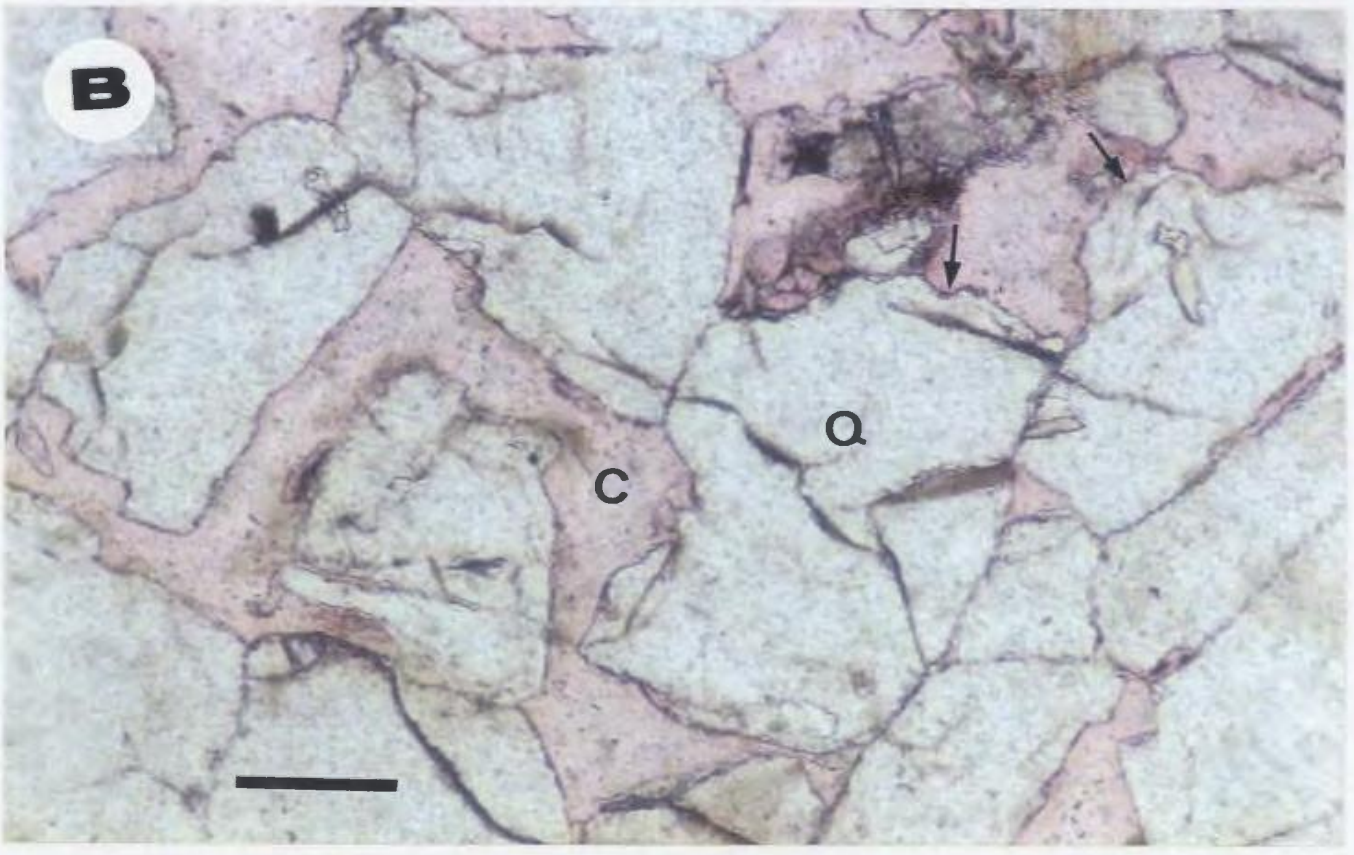

APPENDIX II

THIN-SECTION PHOTOMICROGRAPHS: PLATE 11

A- Abundant calcite (C) and patchy dolomite (D) cements in fine-medium grained of proximal delta front sandstone. Dolomite cement (D) show no response to staining with moderate high relief. Well T1-23 @ 2577 m. (8454 ft.). Scale bar= 0.1mm.

(PPL)

B- Patchy calcite (C) and dolomite (D) cements in the fine grained reworked marine sandstone. The calcite cement has been stained pink by Alizarin Red S., where dolomite cement show no response to staining; with dark grey colour, rhombic outlines, and moderate relief. Note the good grain packing which may suggesting that this stage of cementation followed quartz-overgrowths, and these grains were cemented by carbonate cements (calcite/dolomite) after appreciable compaction. Well B3-61 @ 2670 m. (8756 ft.). Scale bar= 0.1mm.

(PPL)

APPENDIX II
THIN-SECTION PHOTOMICROGRAPHS: PLATE 11

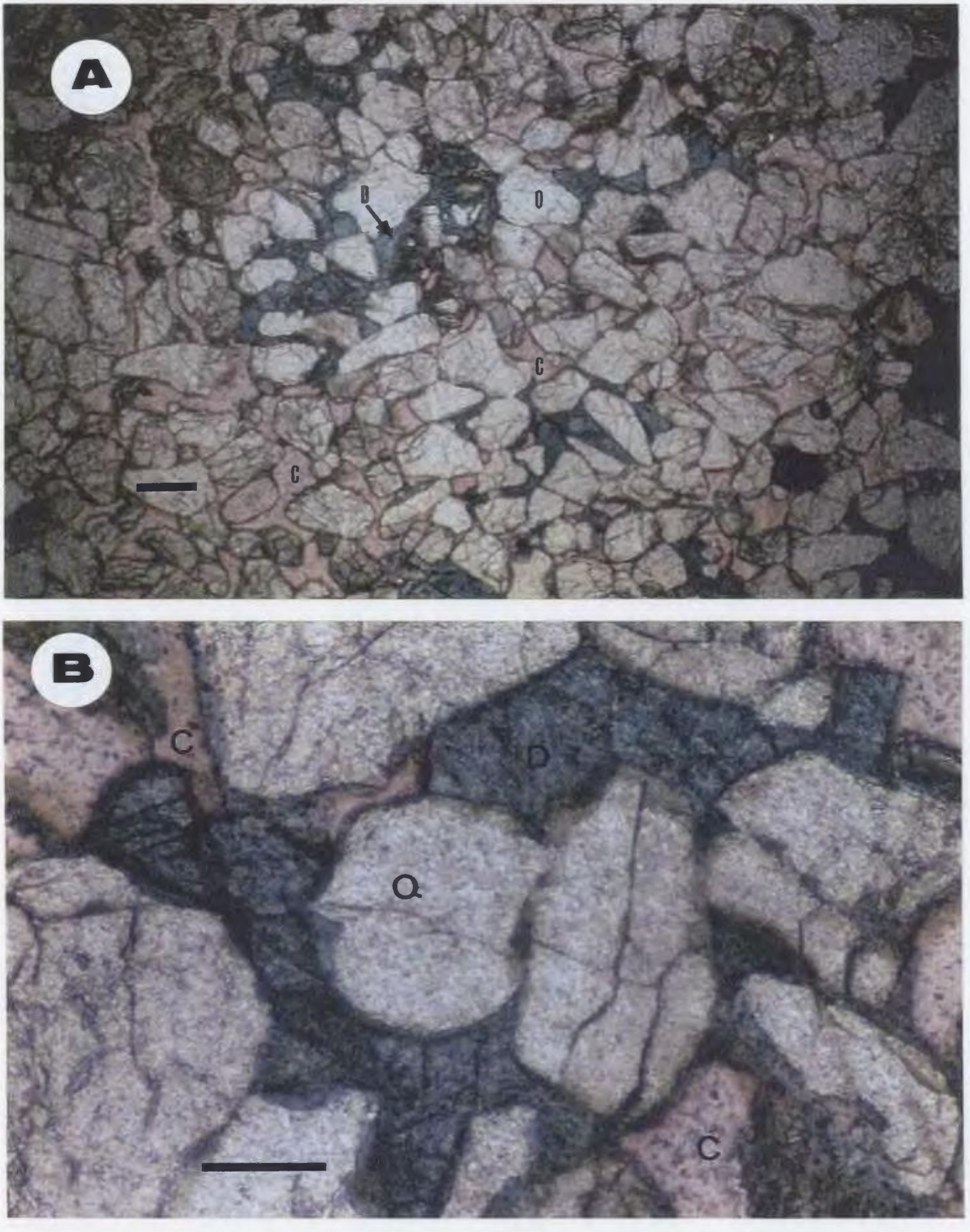

APPENDIX II

THIN-SECTION PHOTOMICROGRAPHS: PLATE 12

A- Patchy calcite (C) cemented, medium-coarse grained fluvial sandstone. Calcite cement filling partially pore-spaces (P) between quartz grains (Q). Note the matrix between these quartz grains contains some opaque iron oxides (I) filling partially pore-spaces. Well EE1-NC7A @ 2686 m. (8810 ft.). Scale bar= 0.1mm.

(PPL)

B- Aggregates of dark brown, rhombic siderite crystals (S) partially filling pores in the fluvial sandstone unit (Af4) in well Z1-66 @ 2768 m. (9080 ft.). Scale bar= 0.1mm.

(PPL)

THIN-SECTION PHOTOMICROGRAPHS: PLATE 12

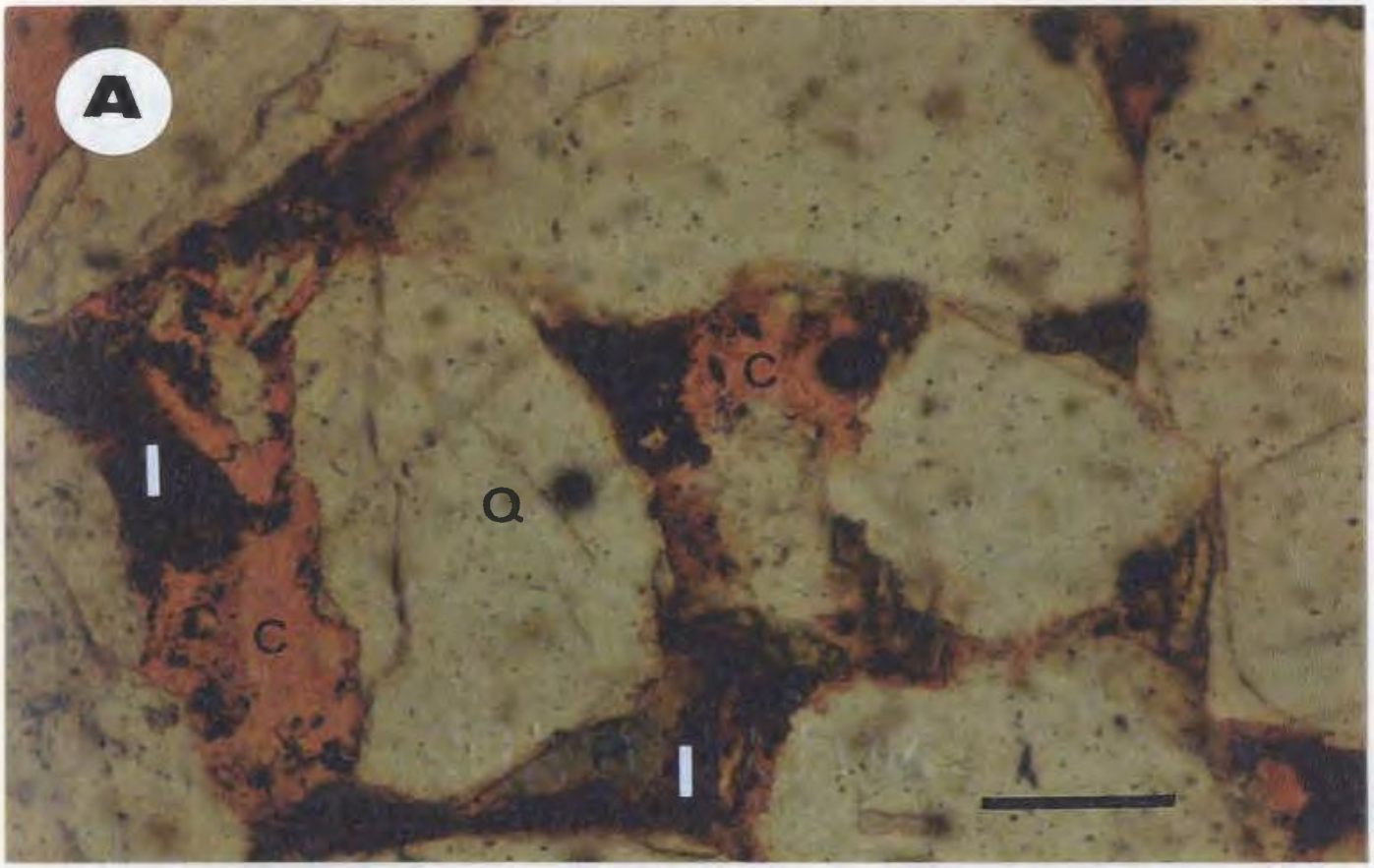

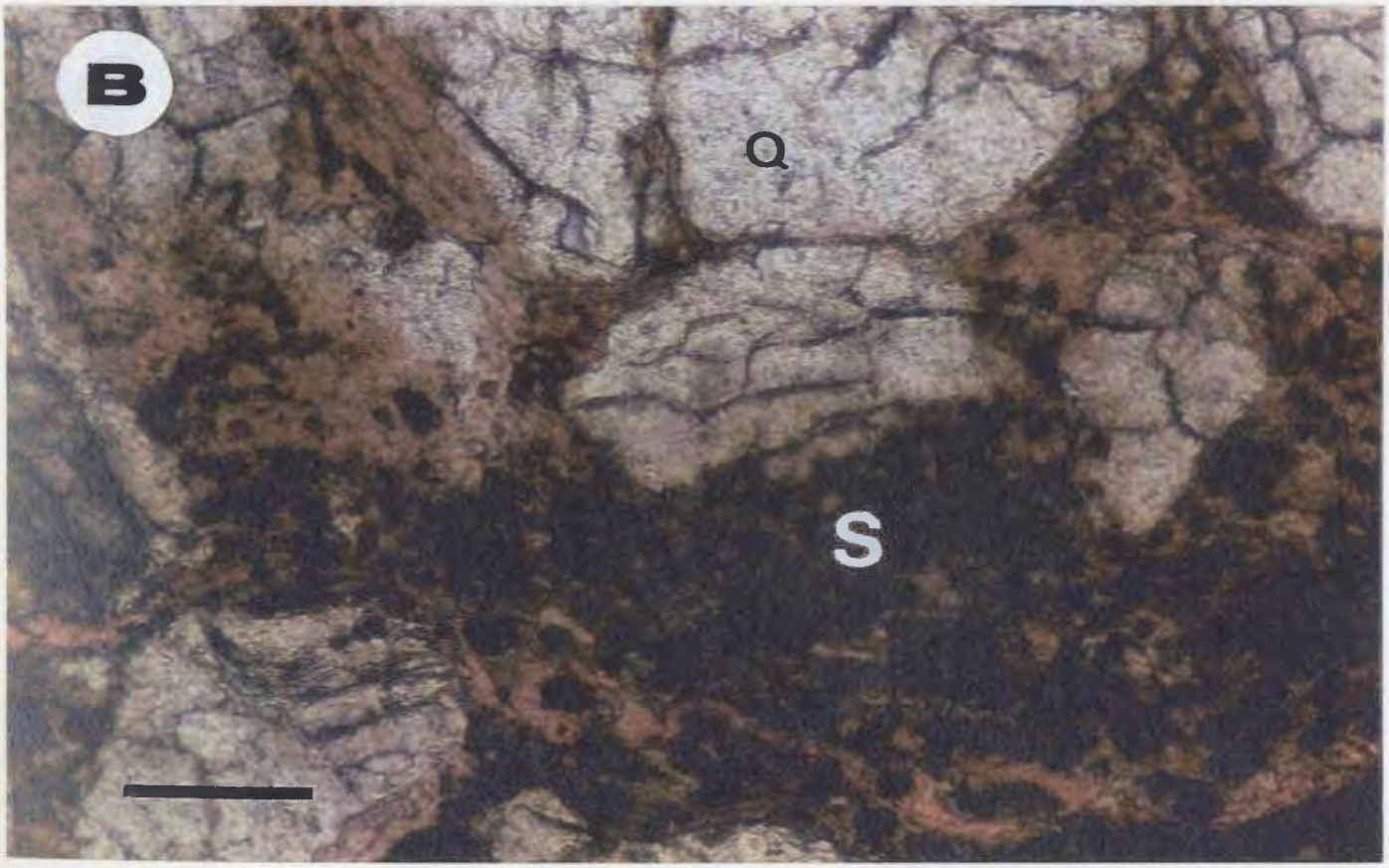

APPENDIX II

THIN-SECTION PHOTOMICROGRAPHS: PLATE 13

A- Shows medium-coarse, highly porous sandstone, with rounded quartz grains (Q). The sandstone is well-cemented partially by authigenic quartz in the form of overgrowths (O) on the detrital grains. Note the welded grains due to quartz-overgrowths (O) interlocking as it is partially filling the primary pores (P) (shown in blue), and the overall shape of the grains has changed from rounded to subhedral. Well CC1-NC7A @ 2750 m. (9020 ft.). Scale bar= 0.1mm.

(PPL)

B- Medium-coarse grained, quartzarenite, with quartz-overgrowths (O) interlocked with other quartz grains (Q). These quartz-overgrowths are readily visible because of abundant inclusions trapped at the boundary (arrows) between the detrital quartz (Q) and the authigenic quartz-overgrowths (O). Note the partial filling of pores with opaque iron oxides (I), and some dolomite cement (D). Fluvial sandstone, well Z1-66 @ 2784 m. (9131 ft.). Scale bar= 0.1mm.

(XPL)

APPENDIX II
THIN-SECTION PHOTOMICROGRAPHS: PLATE 13

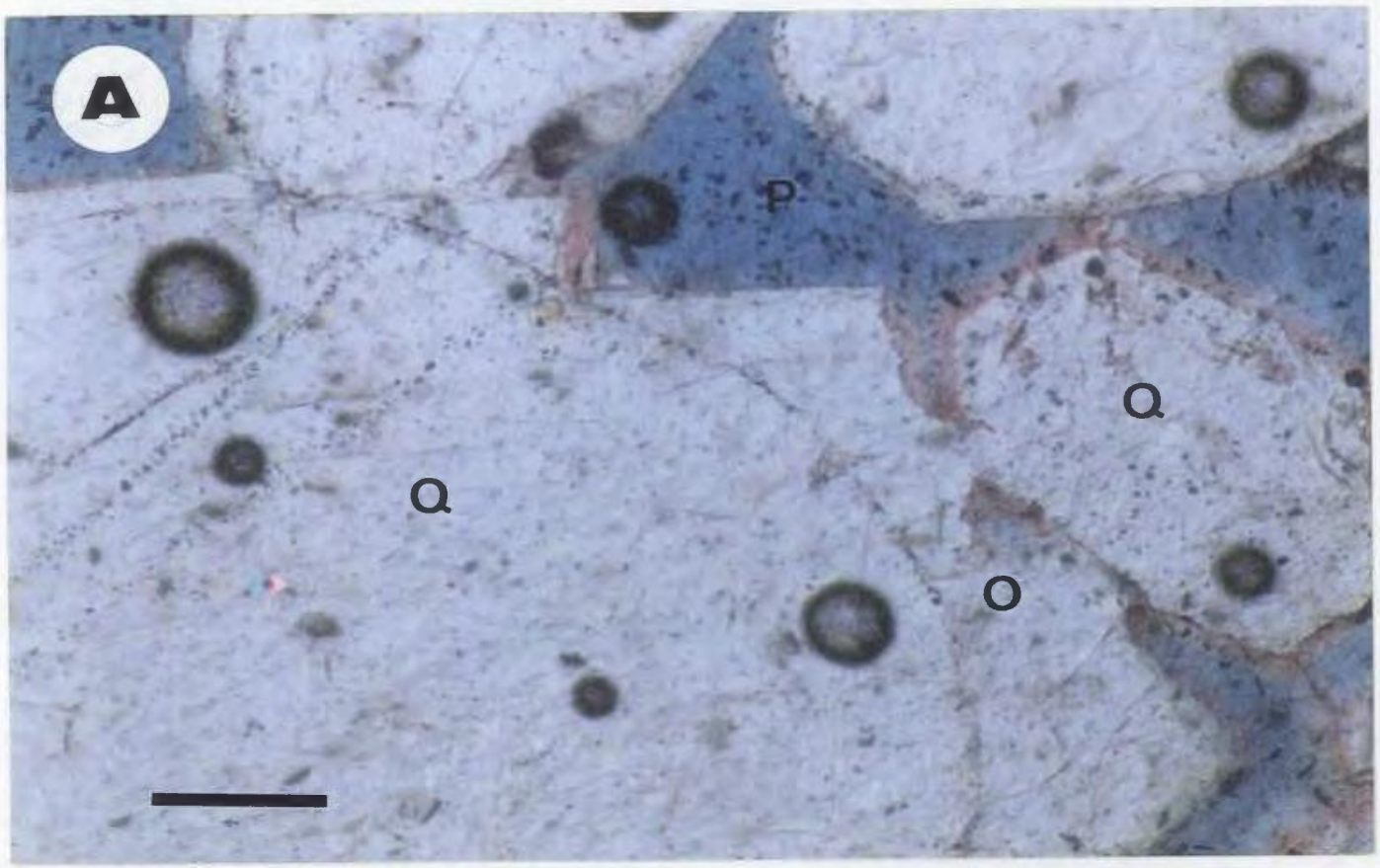

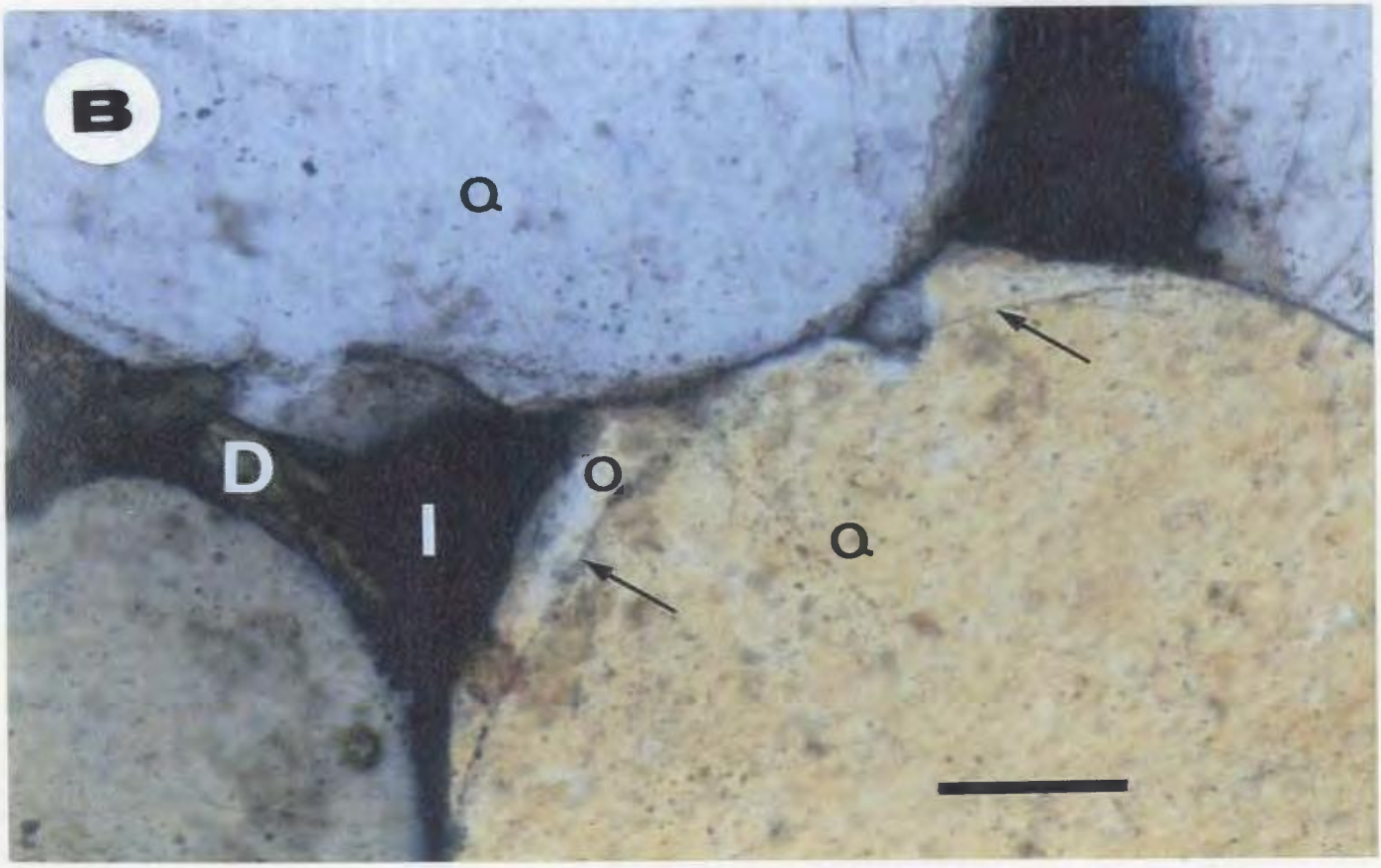

APPENDIX II

THIN-SECTION PHOTOMICROGRAPHS: PLATE 14

A- Kaolinite cement (K) in fine-grained reworked marine sandstones, characterized by low relief, low birefringence fine stacked crystal aggregates. This is best seen in the centre and in the upper right corner of the photograph. Note also in this type of sandstone there are some percentages (8%) of feldspars (plagioclase in this photograph, PF) which may be a major contributor for the formation of kaolinite. Well Q1-23 @ 2580 m. (8461 ft.). Scale bar= 0.1mm.

(XPL)

B- Same photograph but with plane-polarized light (PPL), note hydrocarbon droplets (H) associated partially with kaolinite cement, pores are filled partially with calcite cement (C) also note the highly fractured quartz grains (Q).

(PPL)

THIN-SECTION PHOTOMICROGRAPHS: PLATE 14

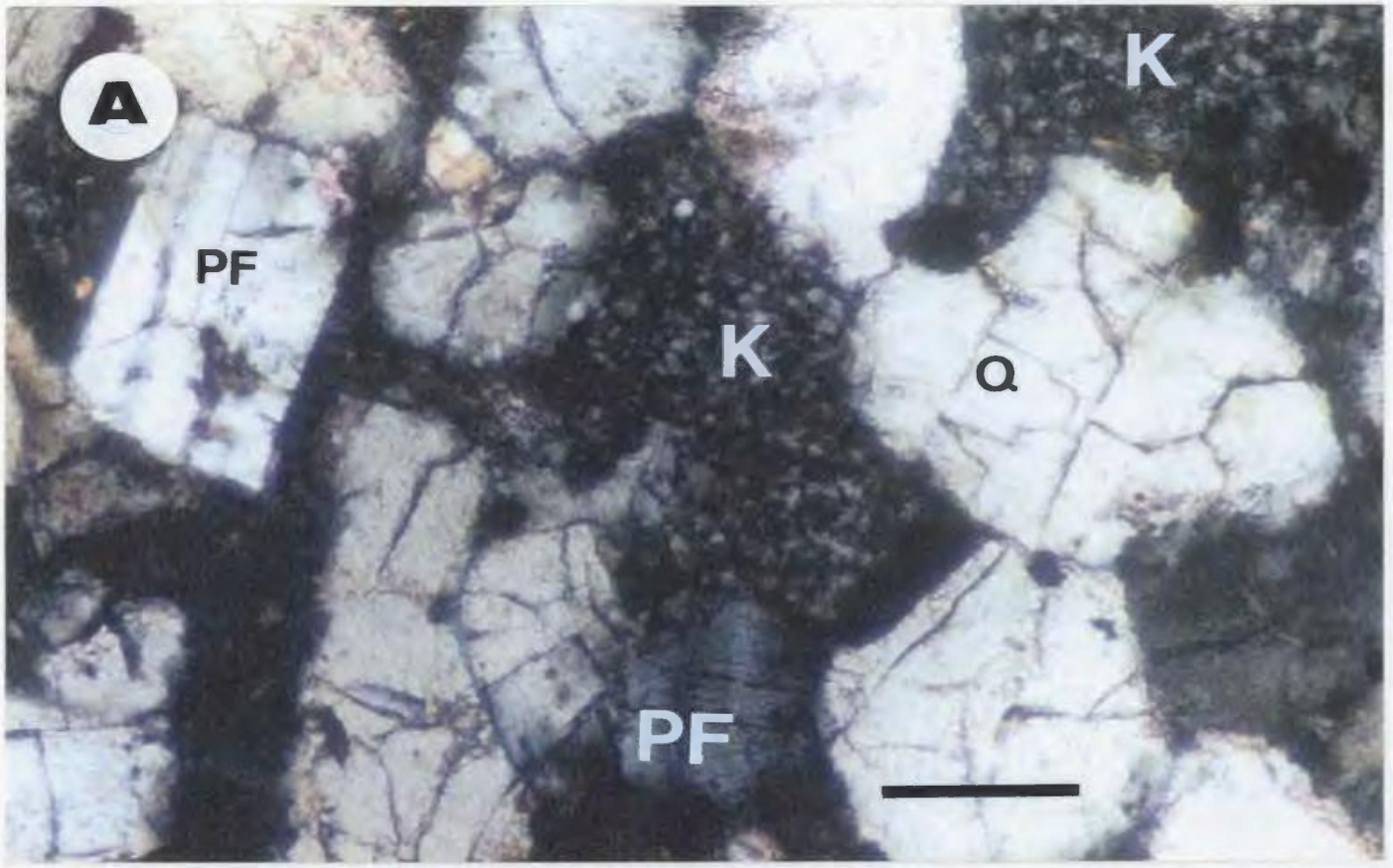

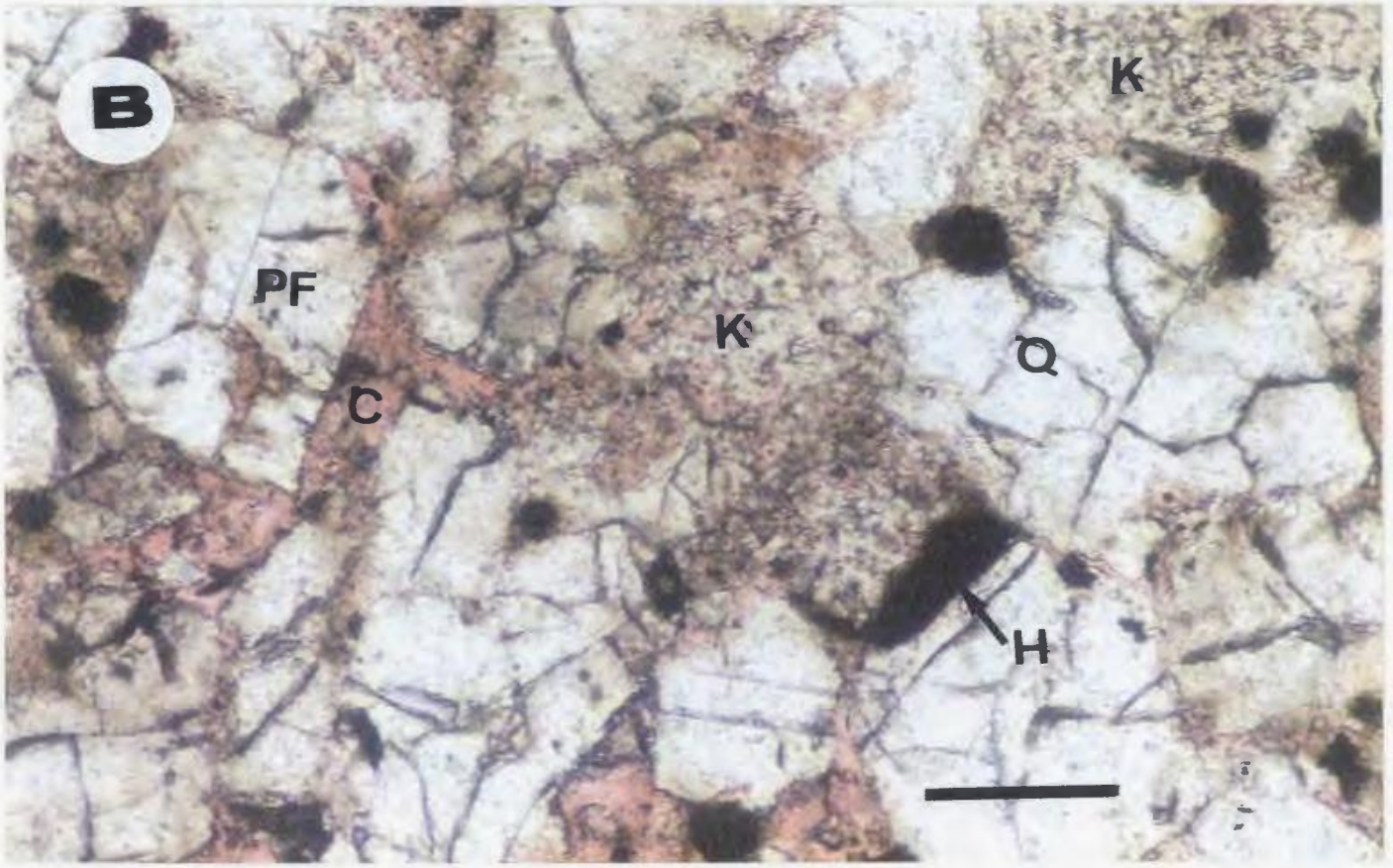

APPENDIX II

THIN-SECTION PHOTOMICROGRAPHS: PLATE 15

A- Shows partial authigenic kaolinite cement (K) with its vermicular texture, coupled with its low birefringence filing pores between quartz grains (Q). Fluvial sandstone, well A1-NC118 @ 3061 m. (10040 ft.). Scale bar= 0.1mm.

(This kaolinite cement was also identified by SEM/EDS analyses and X-ray diffraction).

(XPL)

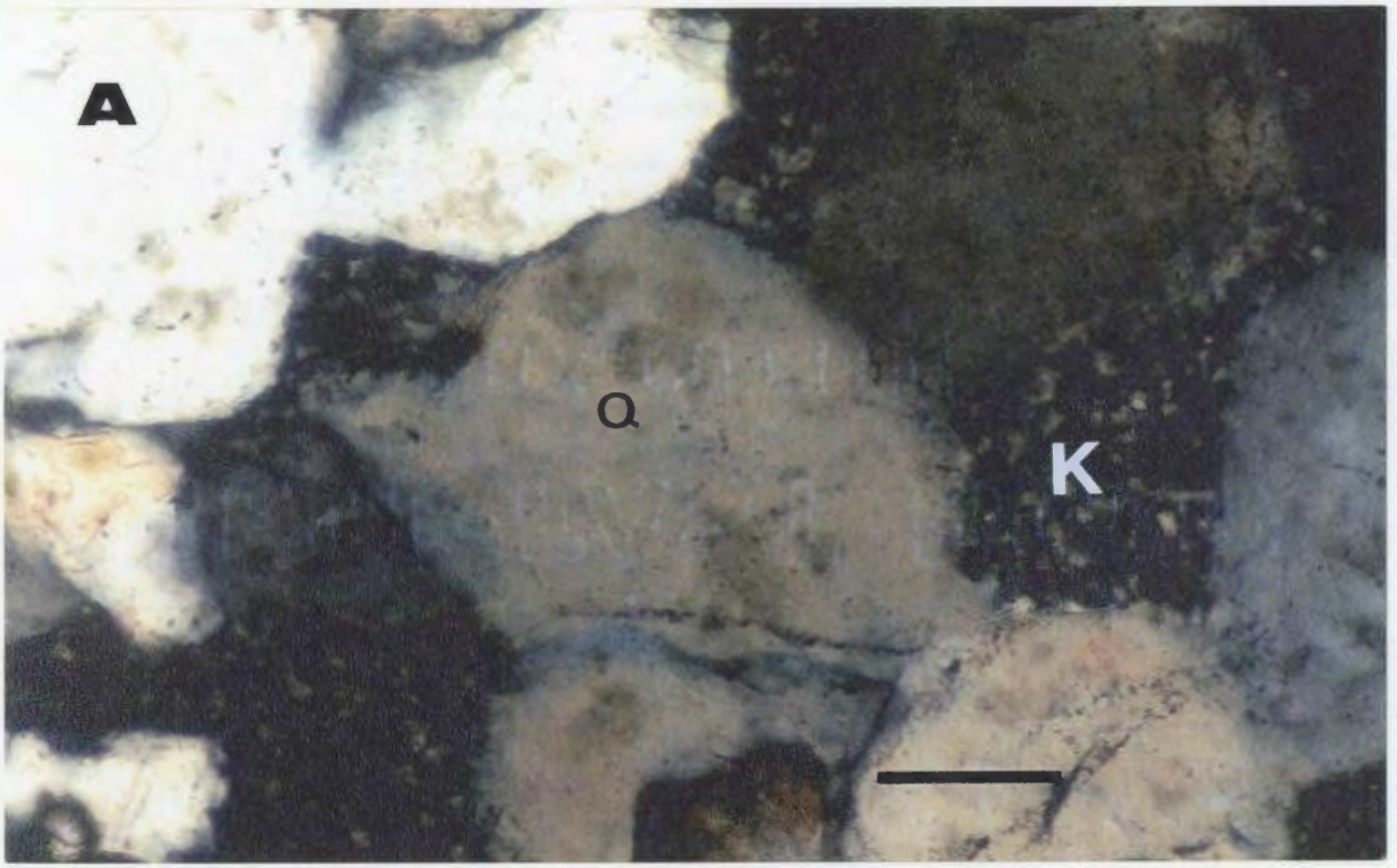
A
Q
K

APPENDIX II

THIN-SECTION PHOTOMICROGRAPHS: PLATE 16

A- Authigenically formed illite clay cement (IL) in fine-medium grained, feldspar-rich (mainly microcline, MF) fluvial sandstone. The occurrence of this clay mineral as of high birefringence, oriented, lining grains and partially filling pores indicating authigenic growth as a pore-filling cement. (Illite cement in this sample was also identified by using SEM/EDS analyses, and X-ray diffraction). Fluvial sandstone, well B3-61 @ 2839 m. (9311 ft.). Scale bar= 0.1mm

(XPL)

B- Same photograph but with plane-polarized light (PPL).

THIN-SECTION PHOTOMICROGRAPHS: PLATE 16

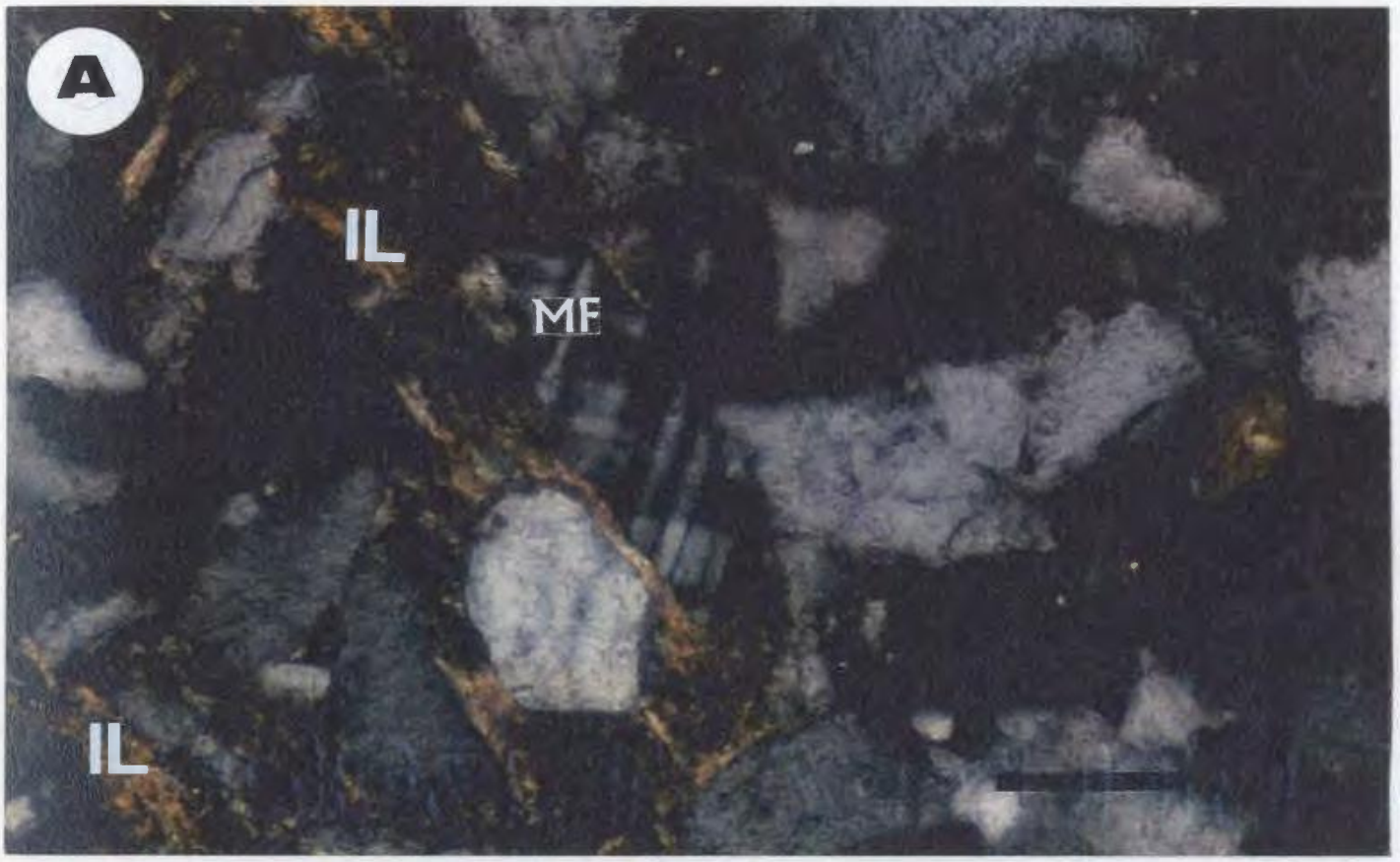

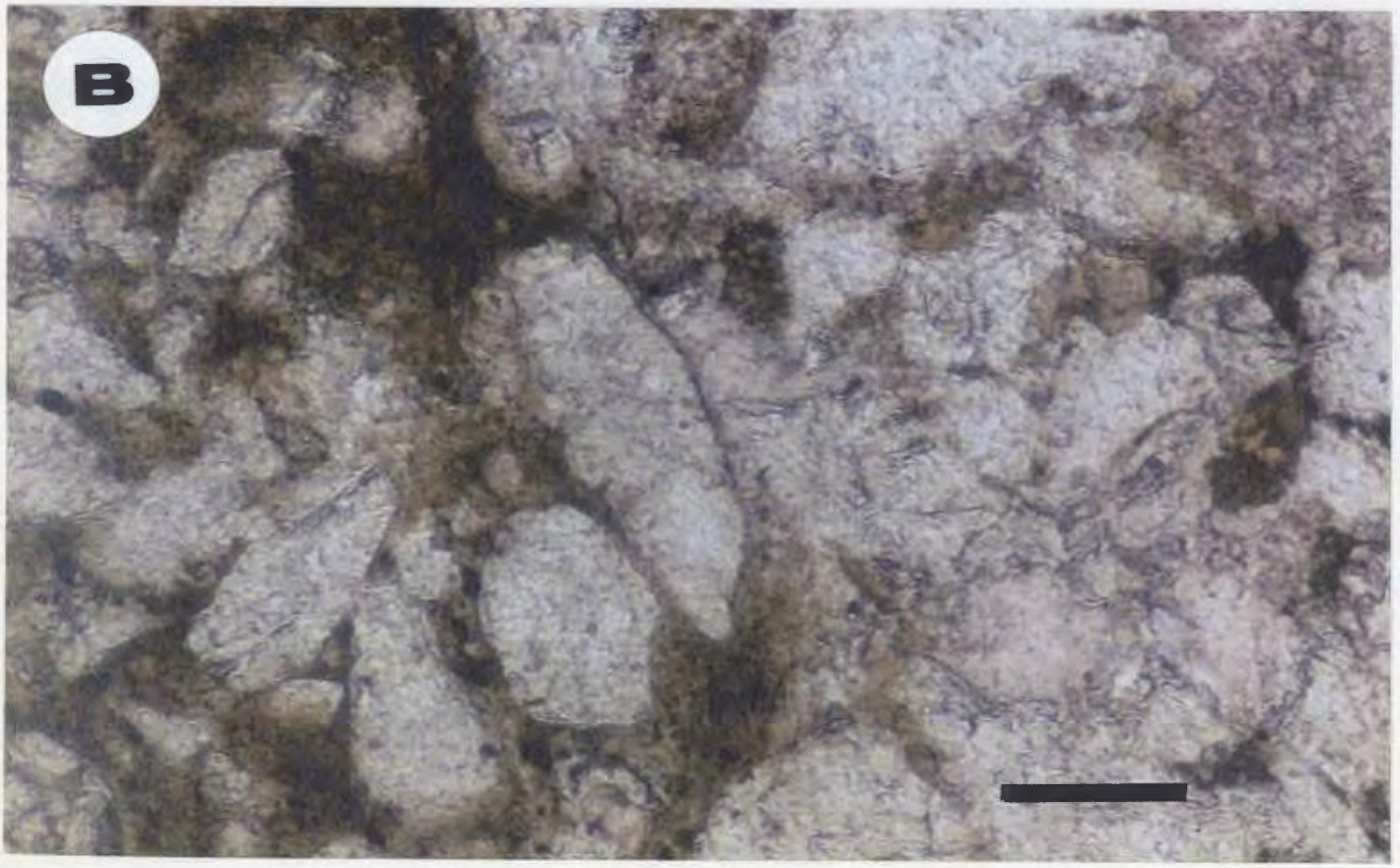

APPENDIX II

THIN-SECTION PHOTOMICROGRAPHS: PLATE 17

A- Dispersed clay coatings (Cly) of generally moderate thickness between the very fine quartz grains (Q) can have a remarkably effect on porosity/permeability reduction in this siltstone of distal delta front facies. Here in this sample the brownish authigenic clay cement can either completely line grains (long arrow) or bridge pores (short arrow). Note the origin of this clay have been detected by SEM/EDS analyses and X-ray diffraction to be illite. Well A1-NC2 @ 2383 m. (7817 ft.). Scale bar= 0.03mm. (XPL)

B- Same as previous photograph but with plane-polarized light (PPL).

APPENDIX II
THIN-SECTION PHOTOMICROGRAPHS: PLATE 17

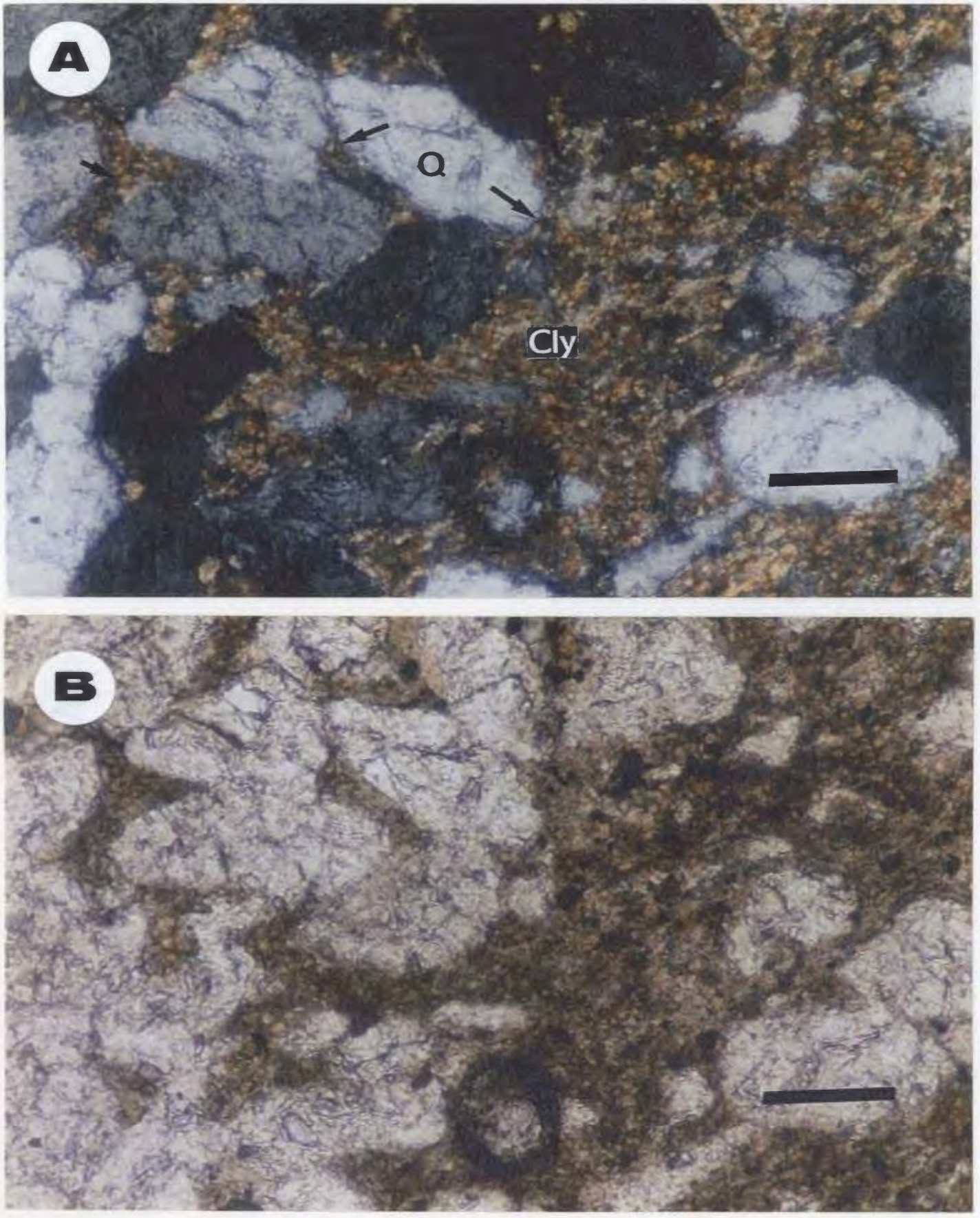

APPENDIX II

THIN-SECTION PHOTOMICROGRAPHS: PLATE 18

A- Authigenic iron oxides (I) coating or film as rimming fractured quartz grains (Q). Note primary pore-spaces (P) are partially filled with iron oxides, and some dolomite cement (D). Medium-coarse grained, fluvial sandstone, well C1-61 @ 2294 m. (7525 ft.). Scale bar= 0.1mm.

(PPL)

B- Shows subrounded-rounded, medium-coarse quartz grains (Q) which are single crystals coated by opaque iron oxides (I). Fluvial sandstone, well CC1-NC7A @ 2749 m. (9017 ft.). Scale bar= 0.1mm.

(PPL)

THIN-SECTION PHOTOMICROGRAPHS: PLATE 18

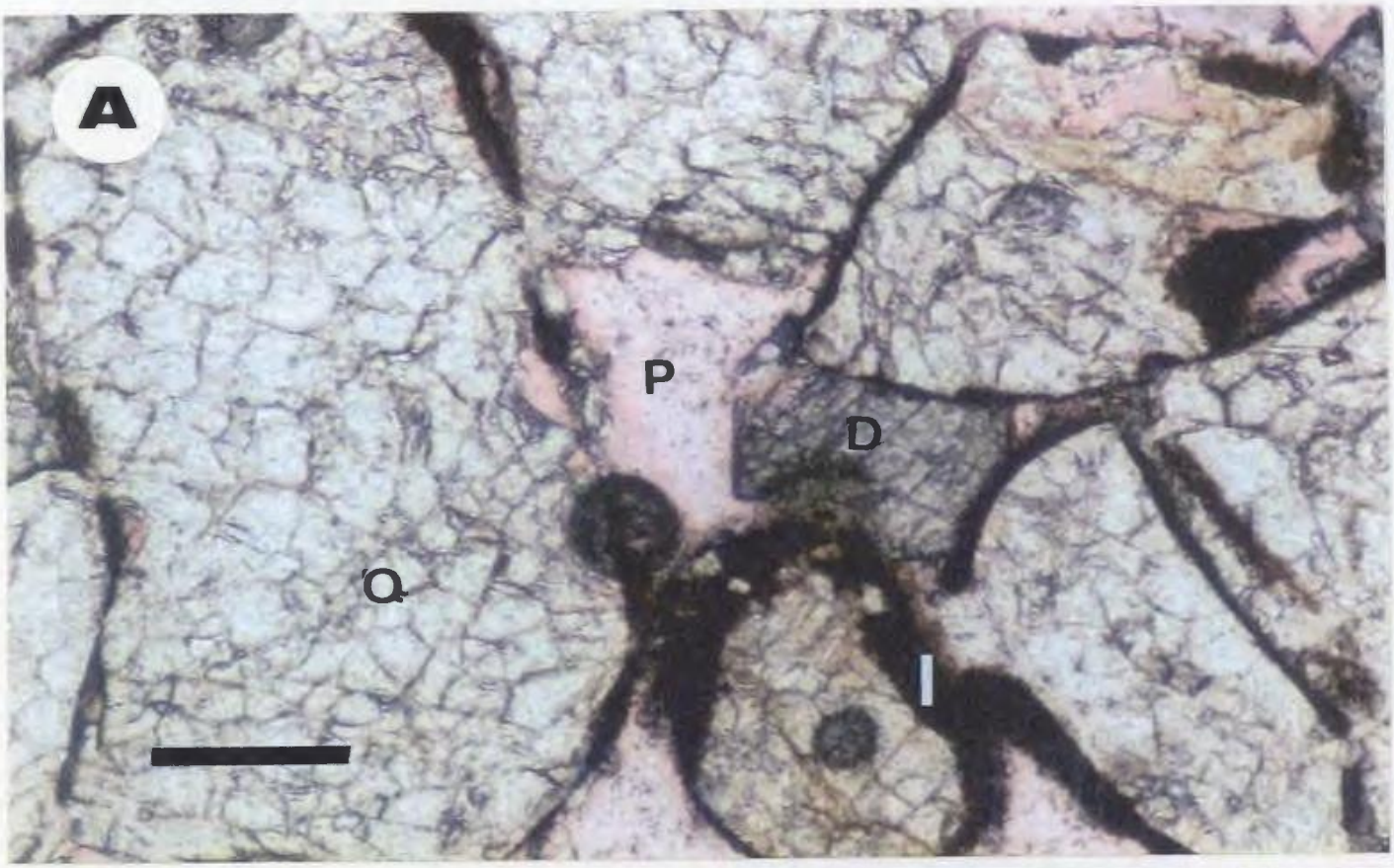

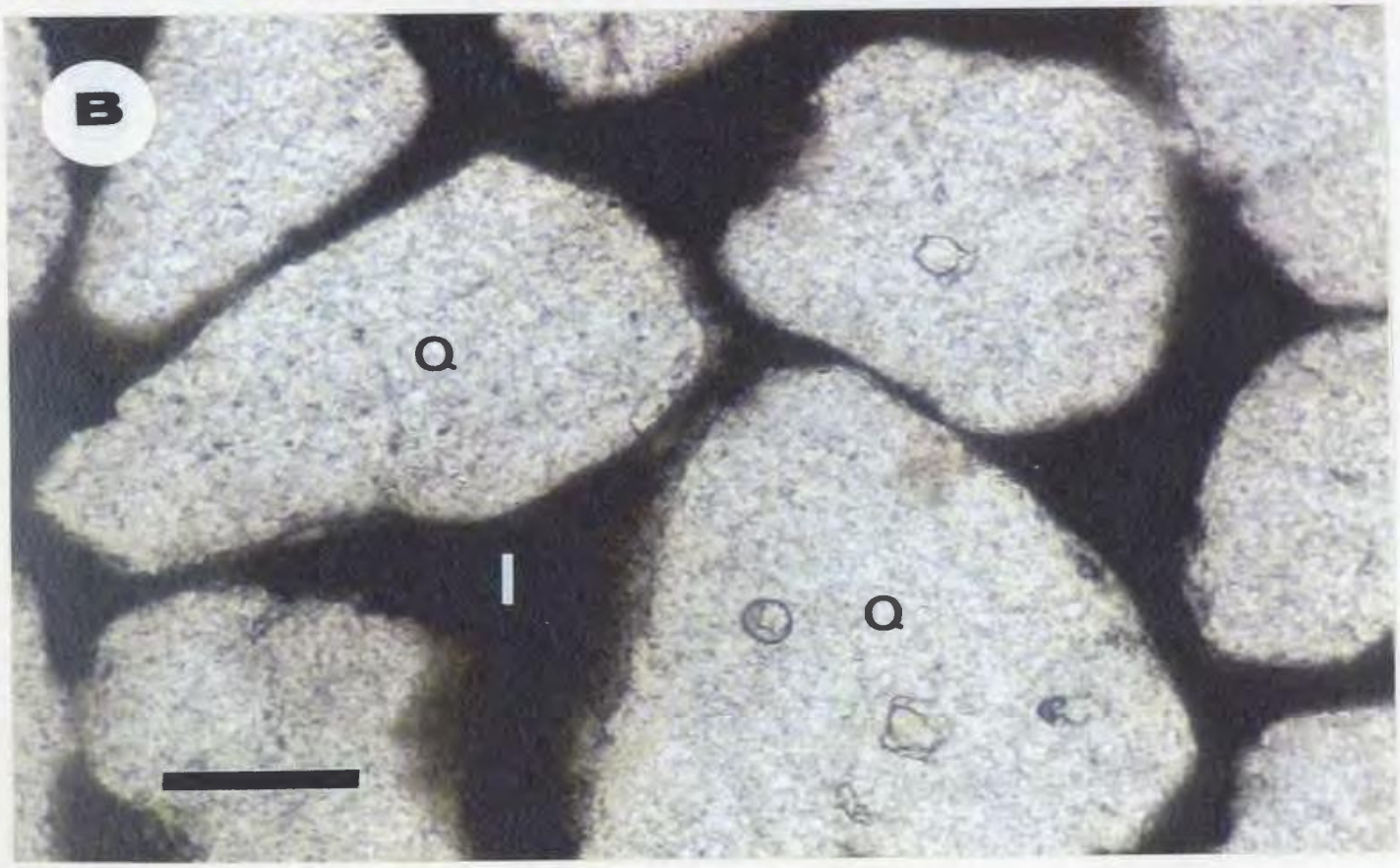

APPENDIX II

THIN-SECTION PHOTOMICROGRAPHS: PLATE 19

A- Iron oxides (I) lining quartz grains (Q) with commonly interspersed clay matrix (MX) which filling either partially or totally some pore-spaces between quartz grains. Note partially filled or unfilled primary pore-spaces (P) which shown in blue. Fluvial sandstone, well EE1-NC7A @ 2687 m. (8812 ft.). Scale bar= 0.1mm.

(PPL)

APPENDIX II
THIN-SECTION PHOTOMICROGRAPHS: PLATE 19

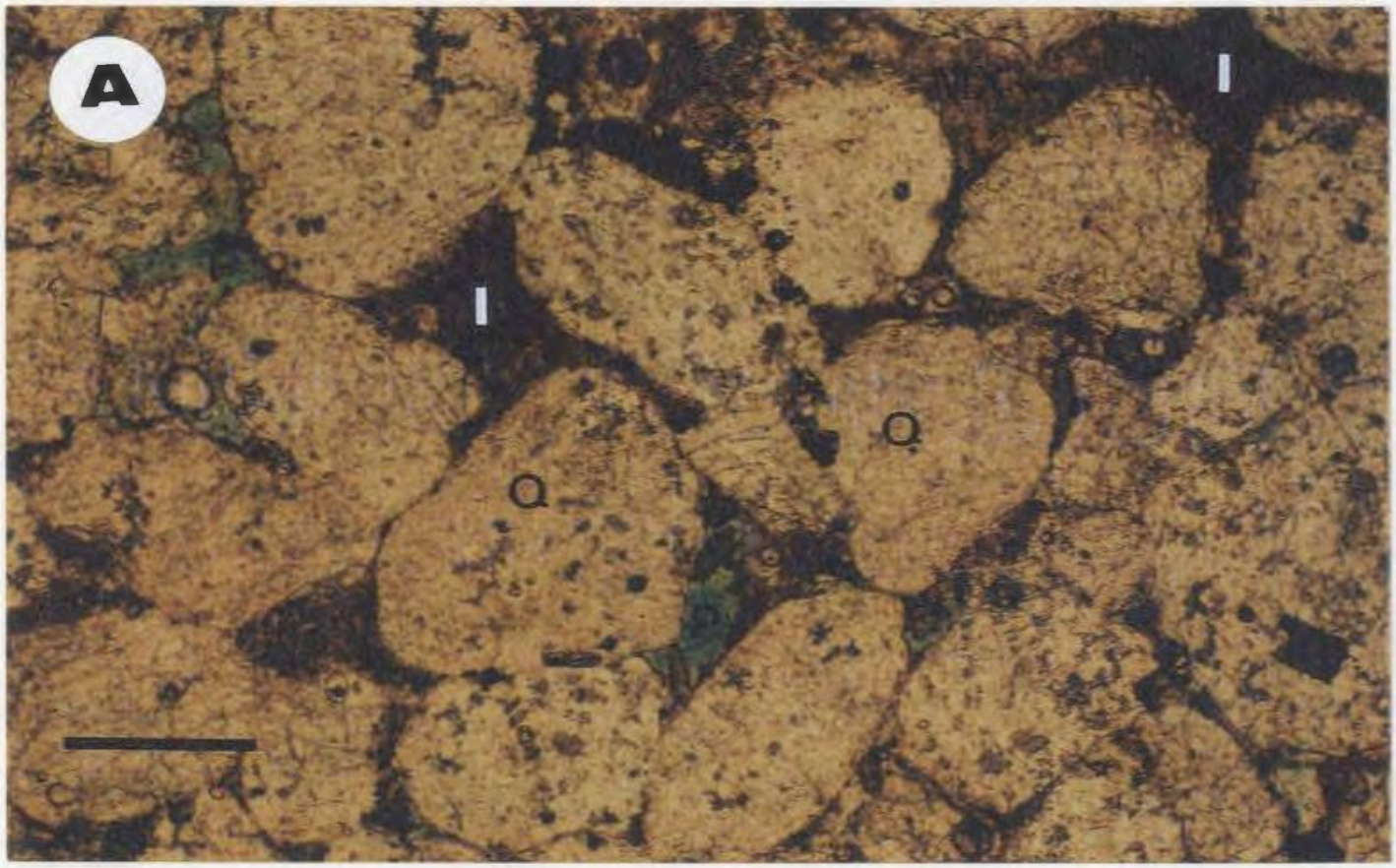

APPENDIX II

THIN-SECTION PHOTOMICROGRAPHS: PLATE 20

A- Quartzarenite-sublitharenite sandstone, with some partial kaolinite cement (K) of vermicular texture filling primary porosity between quartz grains (Q). Fluvial sandstone, well A1-NC118 @ 3061 m. (10040 ft.). Scale bar= 0.1mm.

(XPL)

B- Sublitharenite sandstone of proximal delta front facies showing partial kaolinite cement (K) between quartz grains (Q). Note brown clay clasts (Cly C.) are very common in this sample. Well T1-23 @ 2577 m. (8454 ft.). Scale bar= 0.1mm.

(XPL)

THIN-SECTION PHOTOMICROGRAPHS: PLATE 20

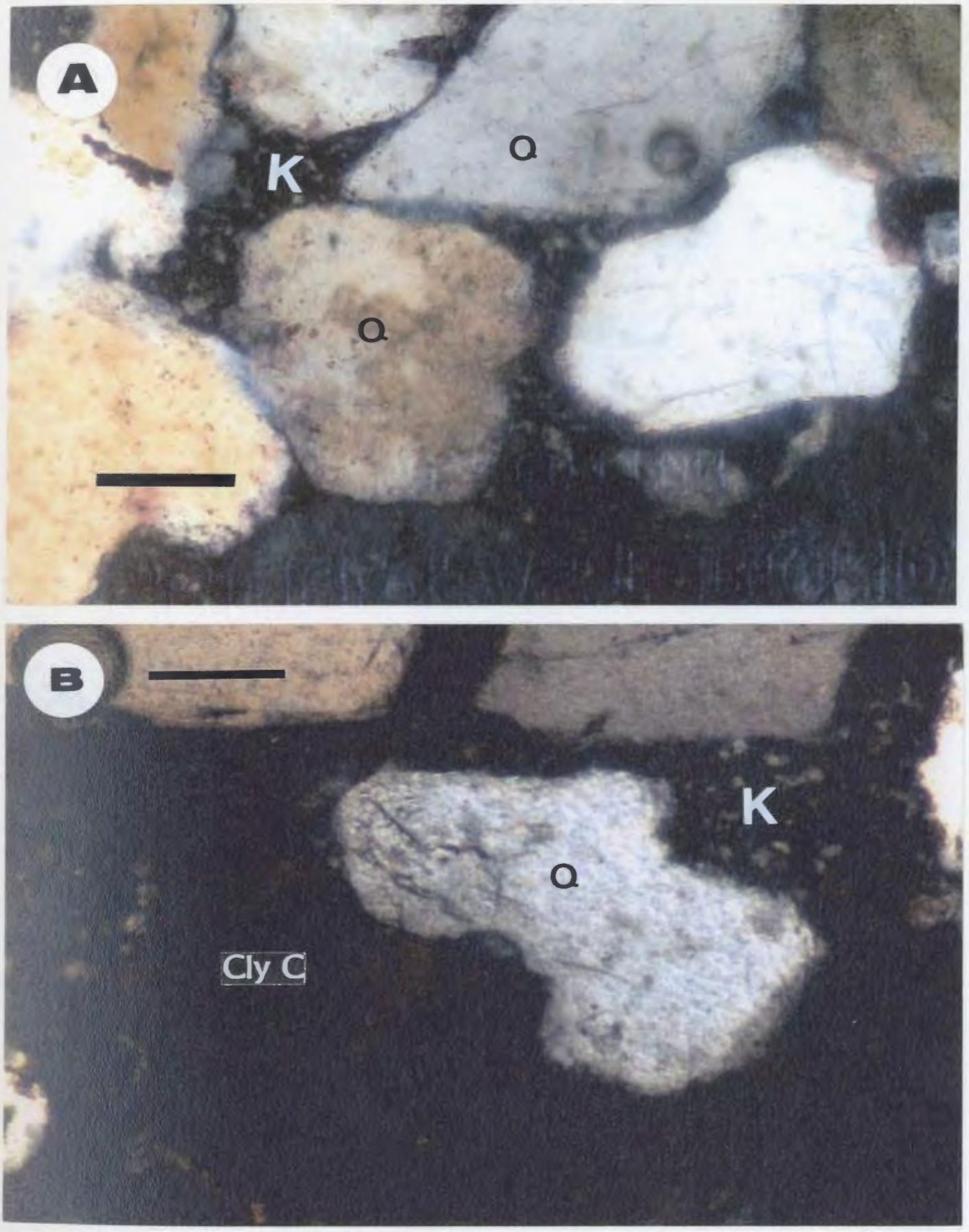

APPENDIX II

THIN-SECTION PHOTOMICROGRAPHS: PLATE 21

A- Kaolinite cement (K)-rich reworked marine sandstone, here in this sample kaolinite cement of vermicular texture completely filling pores and sharply reduced overall permeability. The kaolinite cement of this sandstone was also distinguished by using SEM/EDS analyses and X-ray diffraction. Well Q1-23 @ 2580 m. (8461 ft.). Scale bar = 0.1mm.

(XPL)

B- This photograph shows calcite cement (C) has been dissolved leaving tiny pores which filled partially or totally by authigenic kaolinite (K). Note kaolinite cement (K) occurs in some places as an alteration product of dissolved K-feldspar grains (MF). Some illite (IL) of high birefringence occasionally either lining quartz grains (Q) or grow directly on kaolinite cement. Siltstone of distal delta front facies, well D1-61 @ 2535 m. (8314 ft.). Scale bar = 0.03mm.

(XPL)

THIN-SECTION PHOTOMICROGRAPHS: PLATE 21

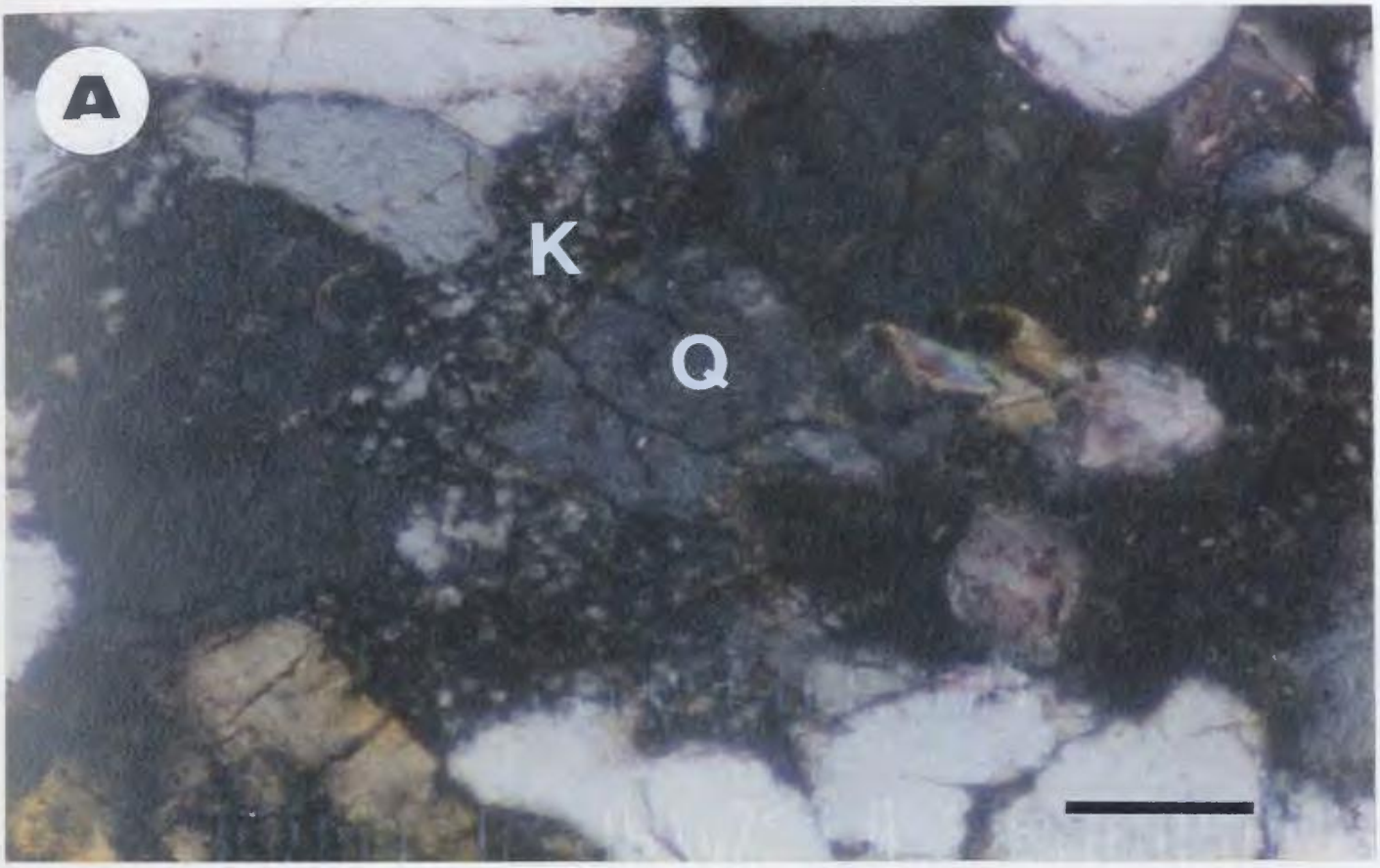

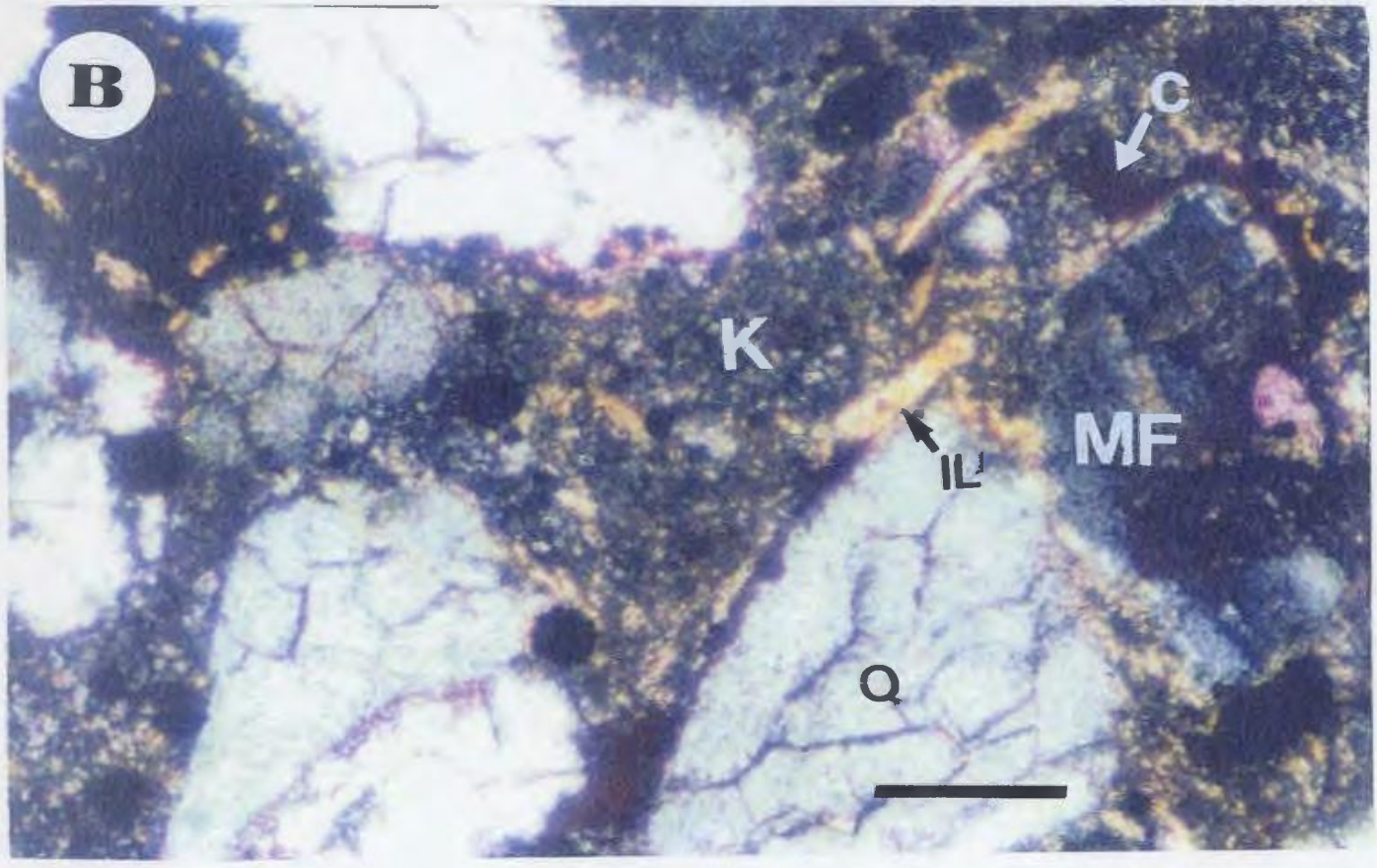

APPENDIX II

THIN-SECTION PHOTOMICROGRAPHS: PLATE 22

A- Enlarged photograph shows authigenic kaolinite cement (K) of low birefringence and of vermicular texture concentrated between the fine-v.fine, fractured quartz grains (Q) and microcline feldspar (MF). Some illite cement (IL) of high birefringence occasionally either lining quartz grains or grow on top of kaolinite cement (both SEM/EDS analyses and X-ray diffraction suggested the presence of kaolinite and illite cements in this sample). Siltstone of distal delta front facies, A1-NC2 @ 2382 m. (7814 ft.). Scale bar = 0.03mm.

(XPL)

B- High magnification photograph shows authigenic kaolinite cement (K) of vermicular texture between quartz grains (Q), and plagioclase feldspar grains (PF). (Kaolinite cement in this sample was identified using X-ray diffraction. Siltstone of distal delta front facies, well A1-NC2 @ 2383 m. (7817 ft.). Scale bar = 0.03mm.

(XPL)

THIN-SECTION PHOTOMICROGRAPHS: PLATE 22

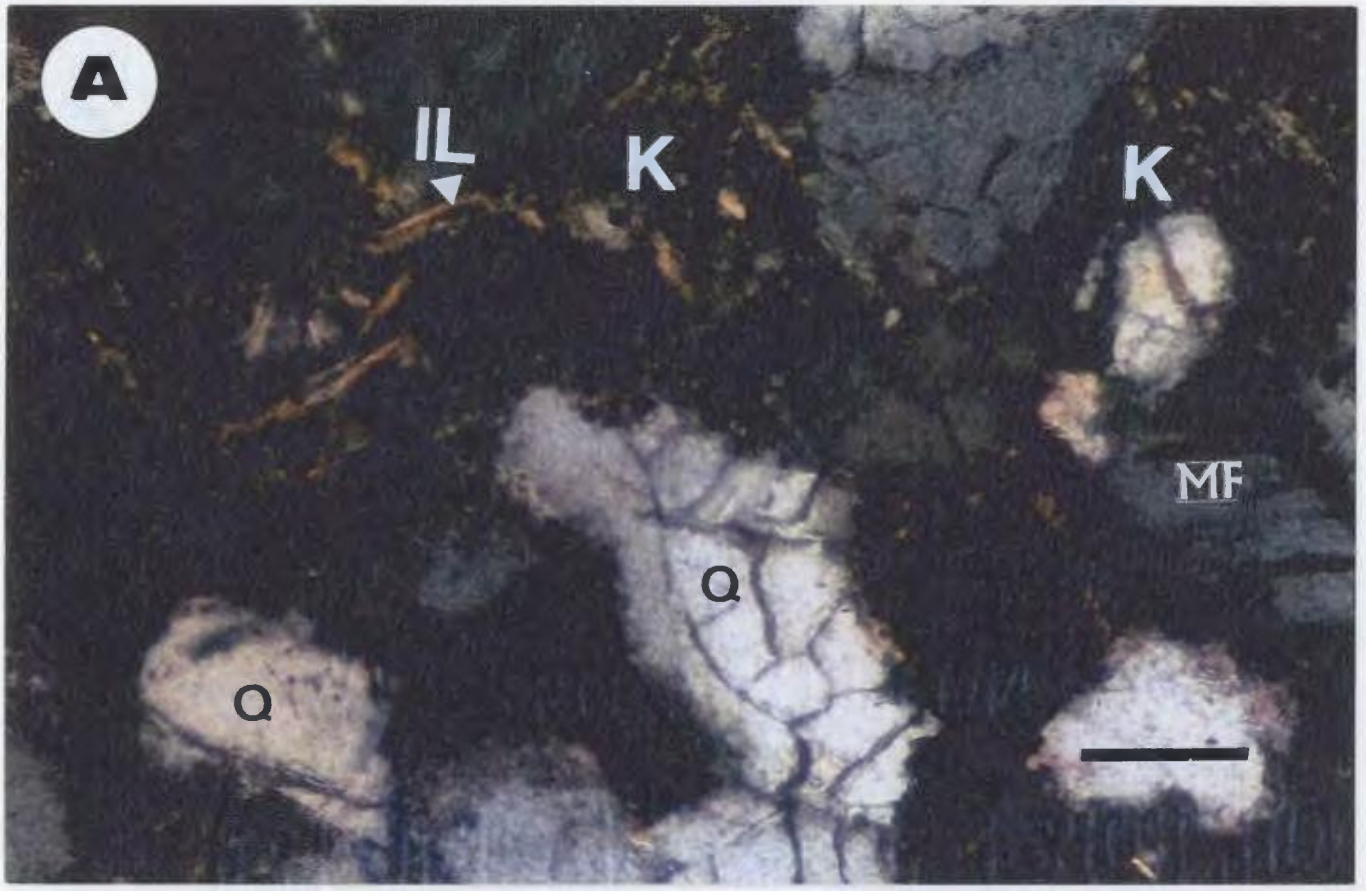

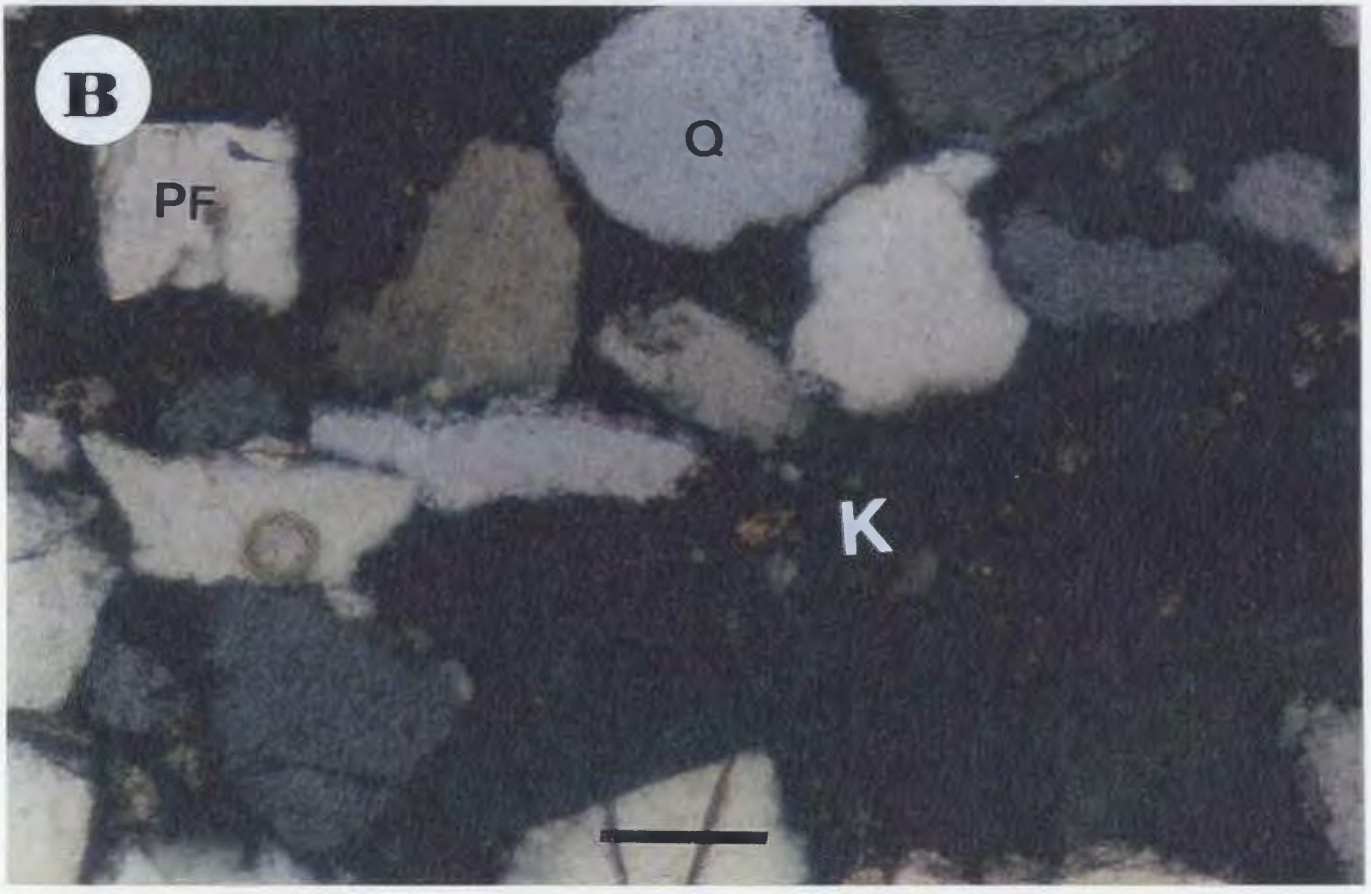

APPENDIX II

THIN-SECTION PHOTOMICROGRAPHS: PLATE 23

A- Authigenic illite cement (IL) partially filling fractures (FR), and in some instances appears to be forming as an alteration of unstable detrital grains (arrows). Note detailed investigation of the origin of this clay cement was conducted on this sample using SEM/EDS analyses and X-ray diffraction. Siltstone of distal delta front facies, well A1-NC2 @ 2383 m. (7817 ft.). Scale bar= 0.03mm.

(XPL)

B- Same as previous photograph but with plane-polarized light (PLL).

THIN-SECTION PHOTOMICROGRAPHS: PLATE 23

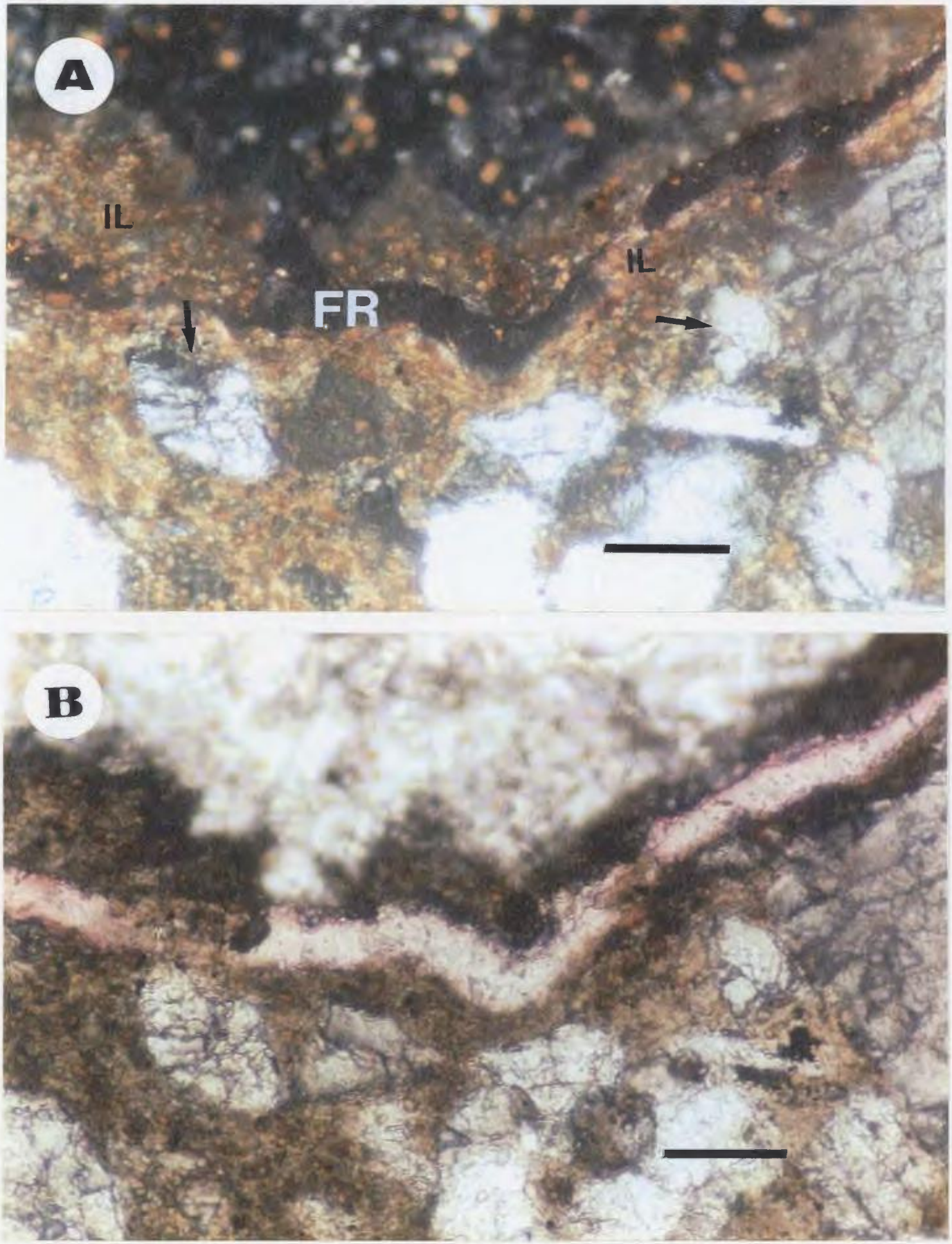

APPENDIX III
CATHODOLUMINESCENT PHOTOMICROGRAPHS

APPENDIX III

CATHODOLUMINESCENT PHOTOMICROGRAPHS: PLATE 24

A- CL photo illustrating one generation of uniformly dull-light brown luminescence quartz-overgrowths (O). Pores between quartz grains (Q) are partially filled with dark brown, non-luminescent iron-oxides (I), and some are filled with navy, blue luminescent kaolinite cement (K). Fluvial sandstone, well EE1-NC7A @ 2686 m. (8810 ft.). Scale bar= 0.1mm.

B- Plane-polarized light photo of the same previous sample showing quartz-grain contact enlargement, which achieved by partial compaction and pressure solution (long white arrows) and interlocking quartz cementation through quartz-overgrowths (short white arrows). Also shows clearly pores filled with iron-oxides (I) mixed with clay matrix.

APPENDIX III
CATHODOLUMINESCENT PHOTOMICROGRAPHS: PLATE 24

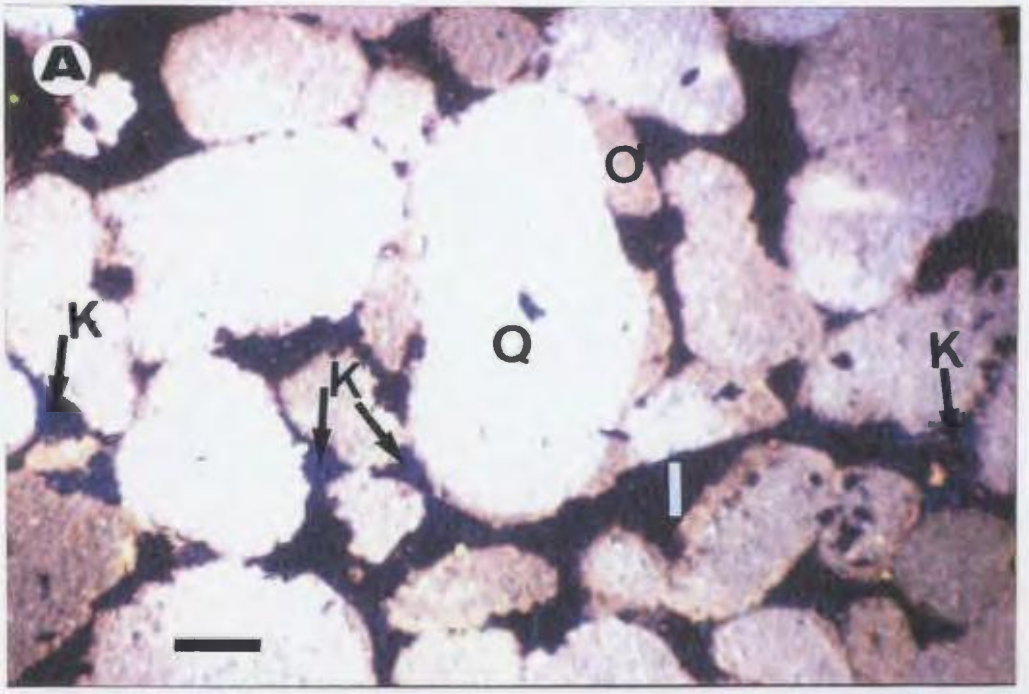

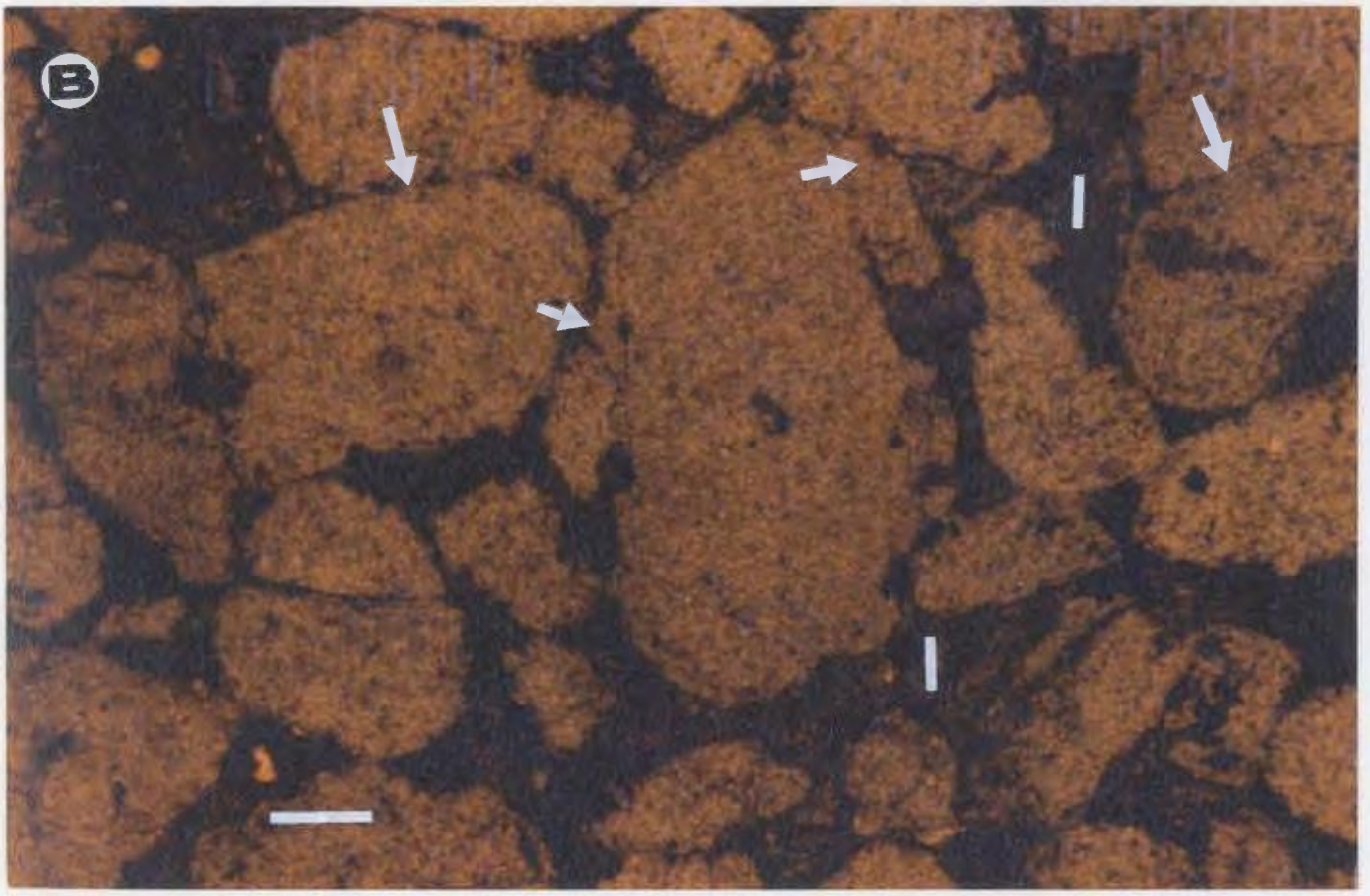

APPENDIX III

CATHODOLUMINESCENT PHOTOMICROGRAPHS: PLATE 25

A- CL photo illustrating quartz-overgrowths (O) which uniformly dull-light brown luminescence and range in thickness from less than 0.05mm to 0.25mm. Some scattered bright-orange to yellow luminescence of calcite cement (C) surrounding quartz grains and filling partially pore-spaces (P). Dark brown-non-luminescence iron-oxides (I) are lining pores at some places. Fluvial sandstone, Z1-66 @ 2769 m. (9081ft.). Scale bar = 0.1mm.

APPENDIX III
CATHODOLUMINESCENT PHOTOMICROGRAPHS: PLATE 25

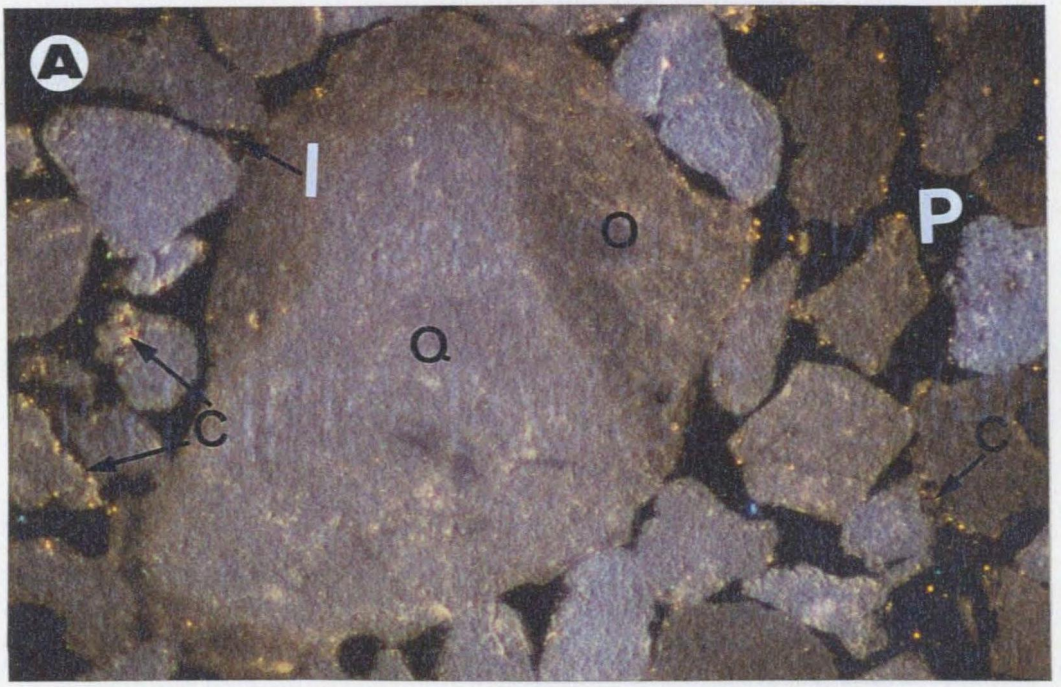

APPENDIX III

CATHODOLUMINESCENT PHOTOMICROGRAPHS: PLATE 26

A- CL photograph illustrating fractured quartz grains (Q) which contribute to mechanical compaction, subsequently healed by quartz cement of brown-yellowish luminescence (arrows), or occasionally filled by some kaolinite cement of navy-blue luminescence (K). Shining, bright-golden luminescence probably zircon crystal (Z). The sample contains some bright-blue luminescent microcline feldspar grains (MF). Fluvial sandstone, C1-61 @ 2294 m. (7525 ft.). Scale bar= 0.1mm.

B- Same photo but in plane-polarized light, showing clearly the highly fractured quartz grains with some straight contacts (arrows).

APPENDIX III
CATHODOLUMINESCENT PHOTOMICROGRAPHS: PLATE 26

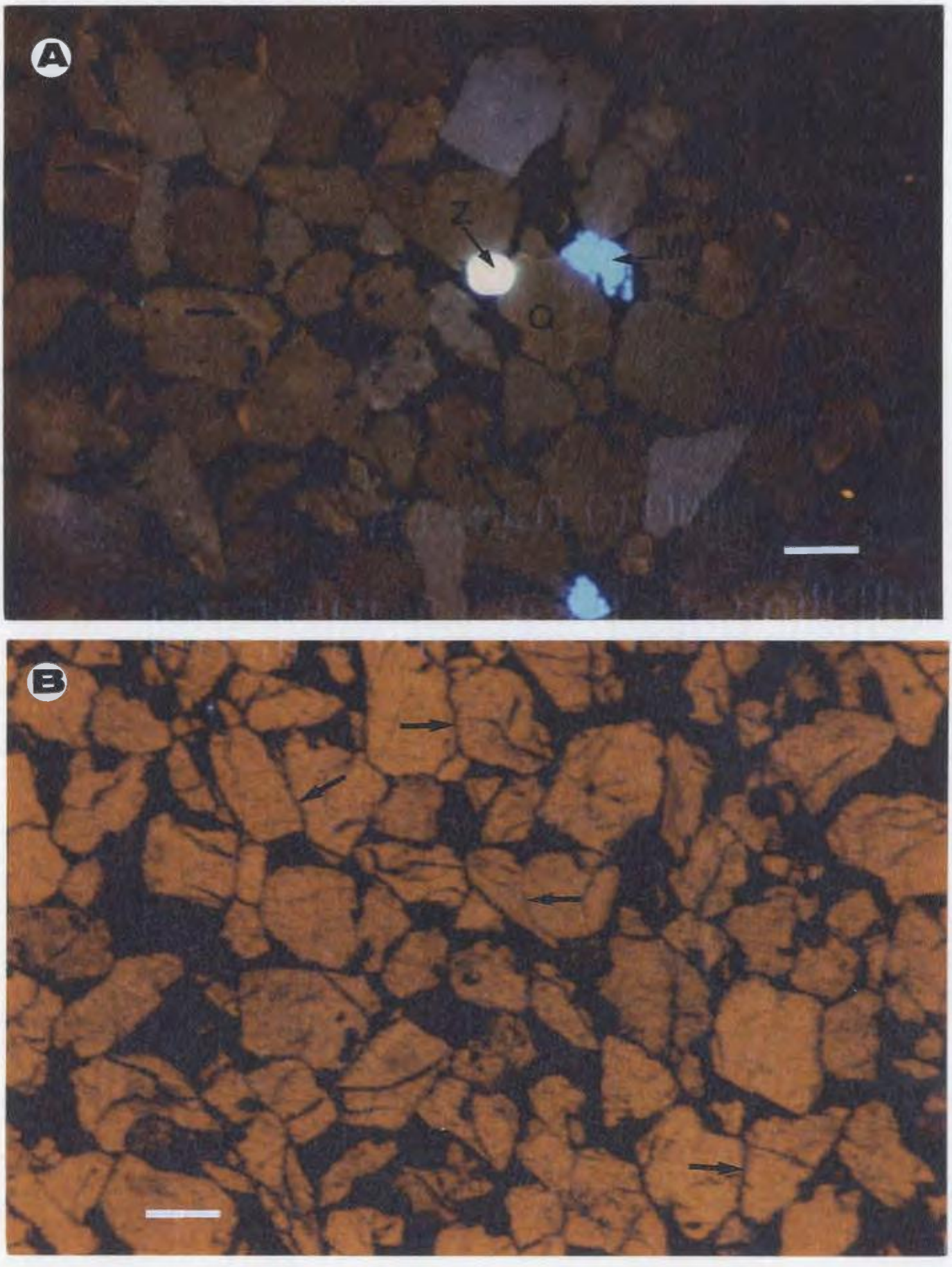

APPENDIX III

CATHODOLUMINESCENT PHOTOMICROGRAPHS: PLATE 27

A- CL enlarged photo shows fractured, fine quartz grains (Q) subsequently healed by dull-brown luminescent authigenic quartz-overgrowths (O). The photo contains also royal-blue (navy) luminescent kaolinite cement (K). Siltstone of distal delta front facies, well A1-NC2 @ 2382 m. (7814 ft.). Scale bar= 0.03mm.

APPENDIX III
CATHODOLUMINESCENT PHOTOMICROGRAPHS: PLATE 27

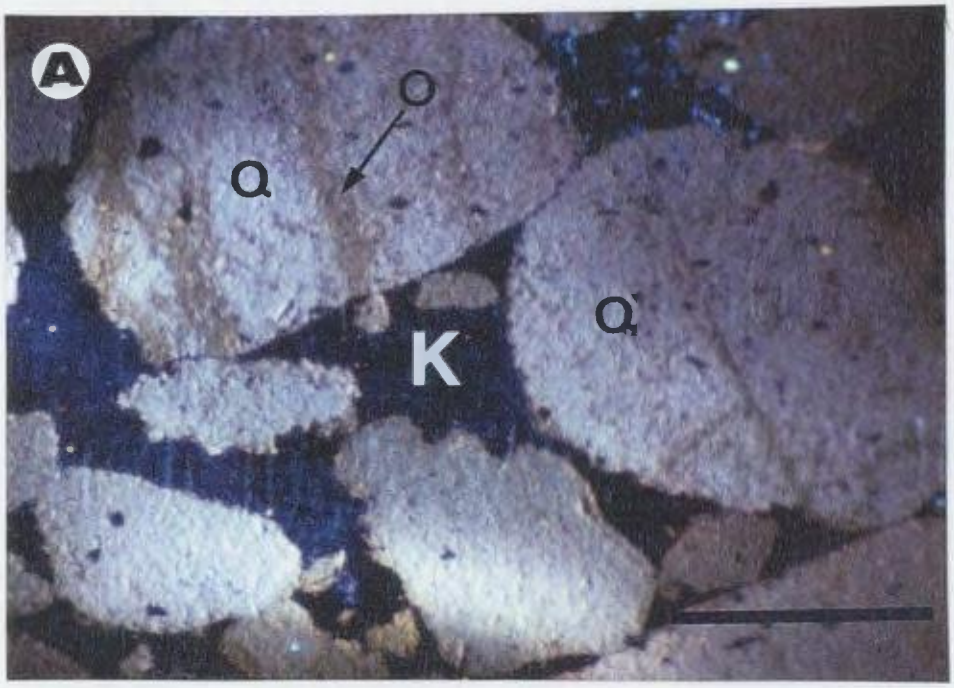

APPENDIX III

CATHODOLUMINSCENT PHOTOMICROGRAPHS: PLATE 28

A- CL photo contains bright-blue luminescent feldspar grains. Pore-spaces (P) are of dark luminescence may also filled with iron-oxides. Fluvial sandstone, well B3-61 @ 2839 m. (9311 ft.). Scale bar= 0.1mm.

B- CL photo in feldspar rich sandstone where the bright-blue luminescent grains are K-feldspar. Pores at the centre of photo contain navy-blue luminescent kaolinite cement (K). Proximal delta front sandstone, well T1-23 @ 2577 m. (8454 ft.).
Scale bar= 0.1mm.

APPENDIX III
CATHODOLUMINESCENT PHOTOMICROGRAPHS: PLATE 28

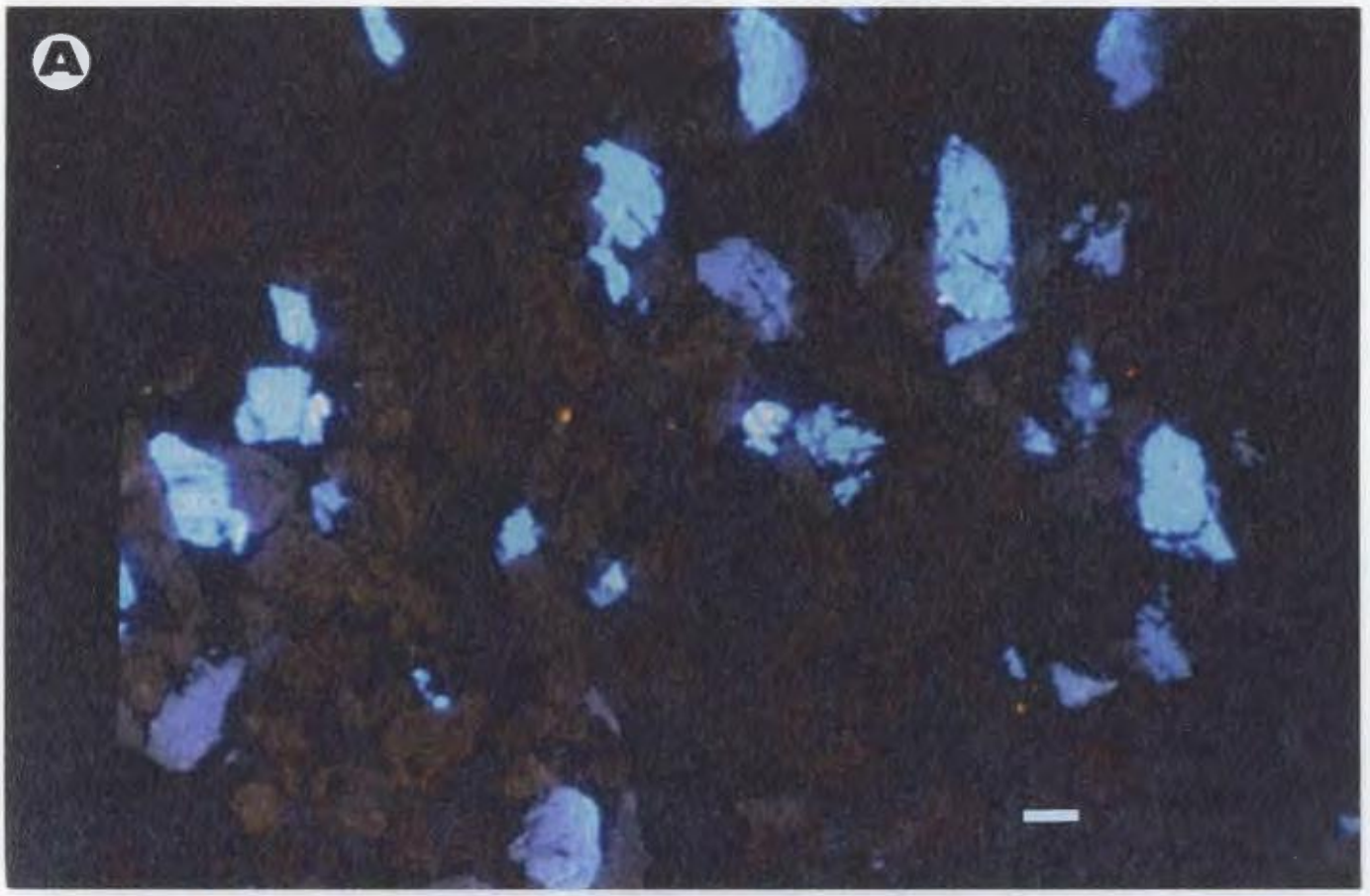

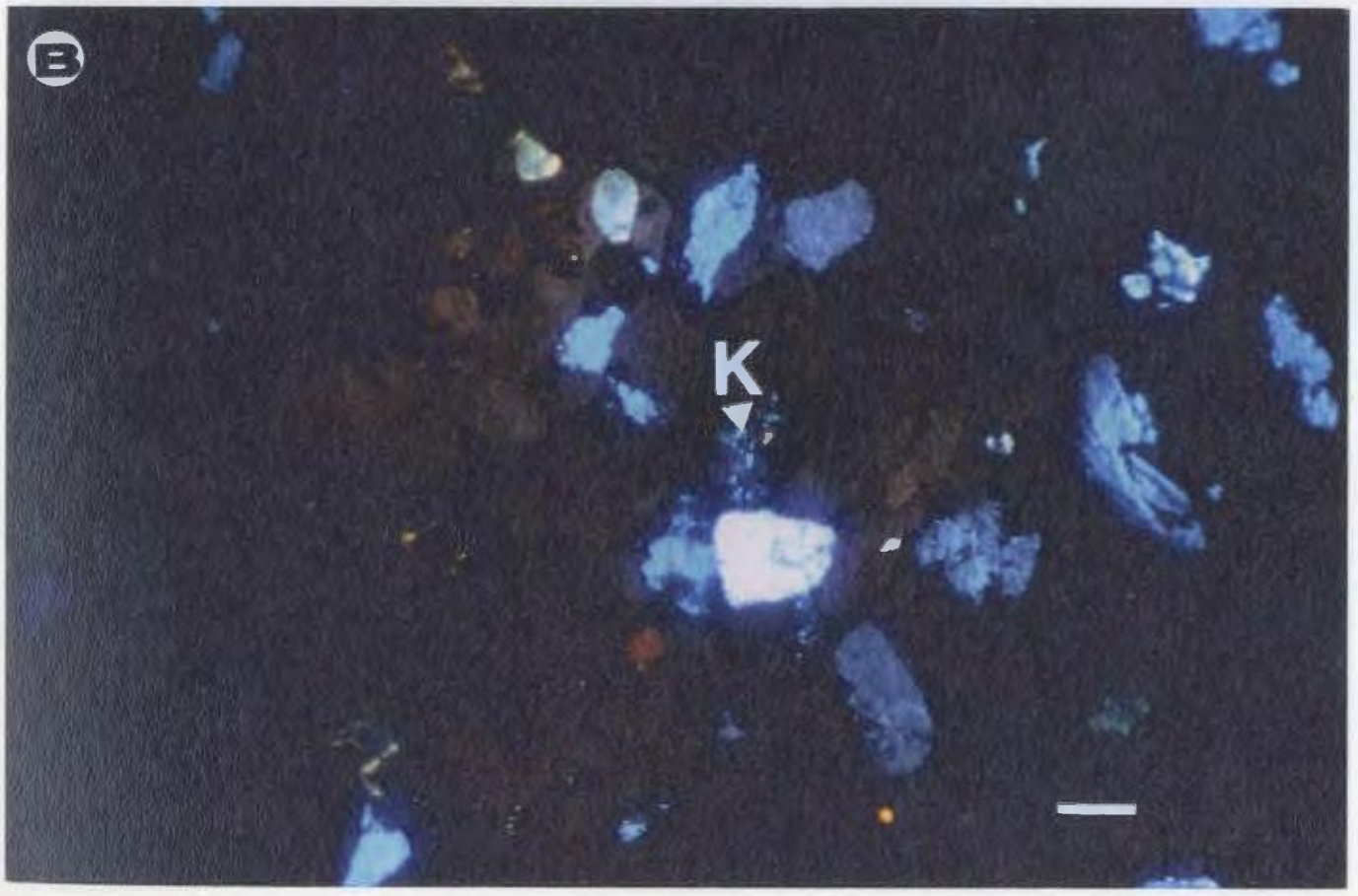

APPENDIX III

CATHODOLUMINESCENT PHOTOMICROGRAPHS: PLATE 29

A- CL photo contains light brown to orange (iron-rich) occasionally yellow luminescent calcite cement (C) which partially filling pores in this fluvial sandstone. Note straight (long arrow) and point (short arrow) silica cement contacts between quartz grains (Q), and the partial filling of primary porosity with dark brown luminescent iron-oxides (I). Pores appear to have black luminescence (P). Fluvial sandstone, well Z1-66 @ 2769 m. (9081 ft.). Scale bar= 0.1mm.

B- CL photo contains yellow-bright orange luminescence of calcite cement (C) which occurs in spary-wide spread crystals to scattered patches and corrodes quartz grains (Q) of whitish-dull brown luminescence. Pores (P) of black luminescence. Proximal delta front sandstone, well C1-NC2 @ 2958 m. (9703 ft.). Scale bar= 0.1mm.

APPENDIX III
CATHODOLUMINESCENT PHOTOMICROGRAPHS: PLATE 29

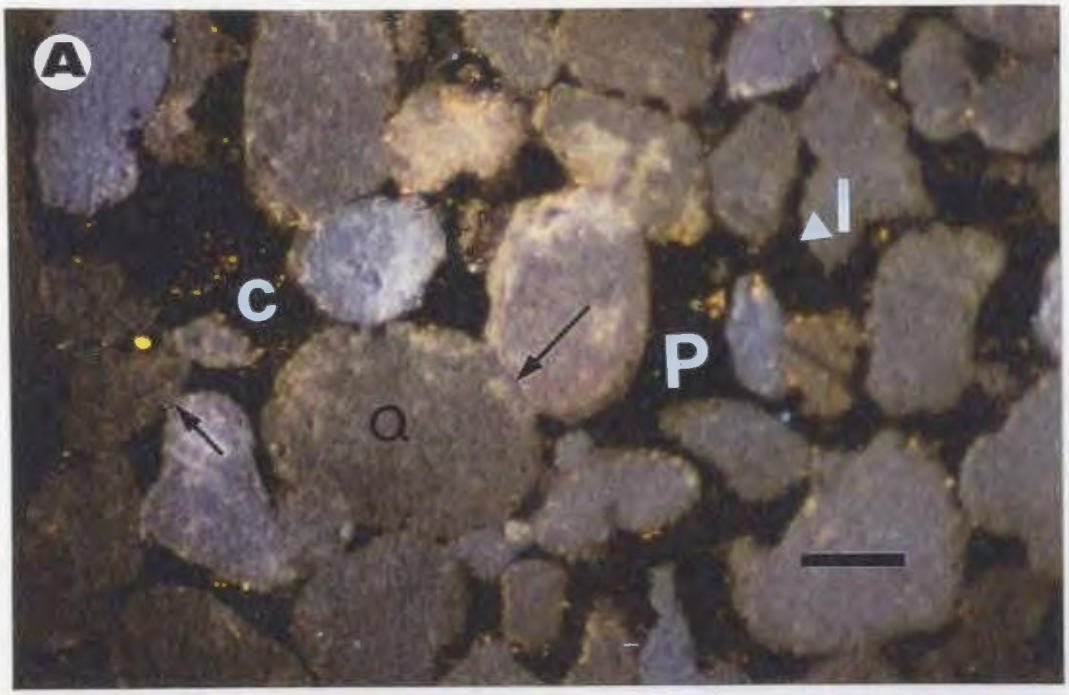

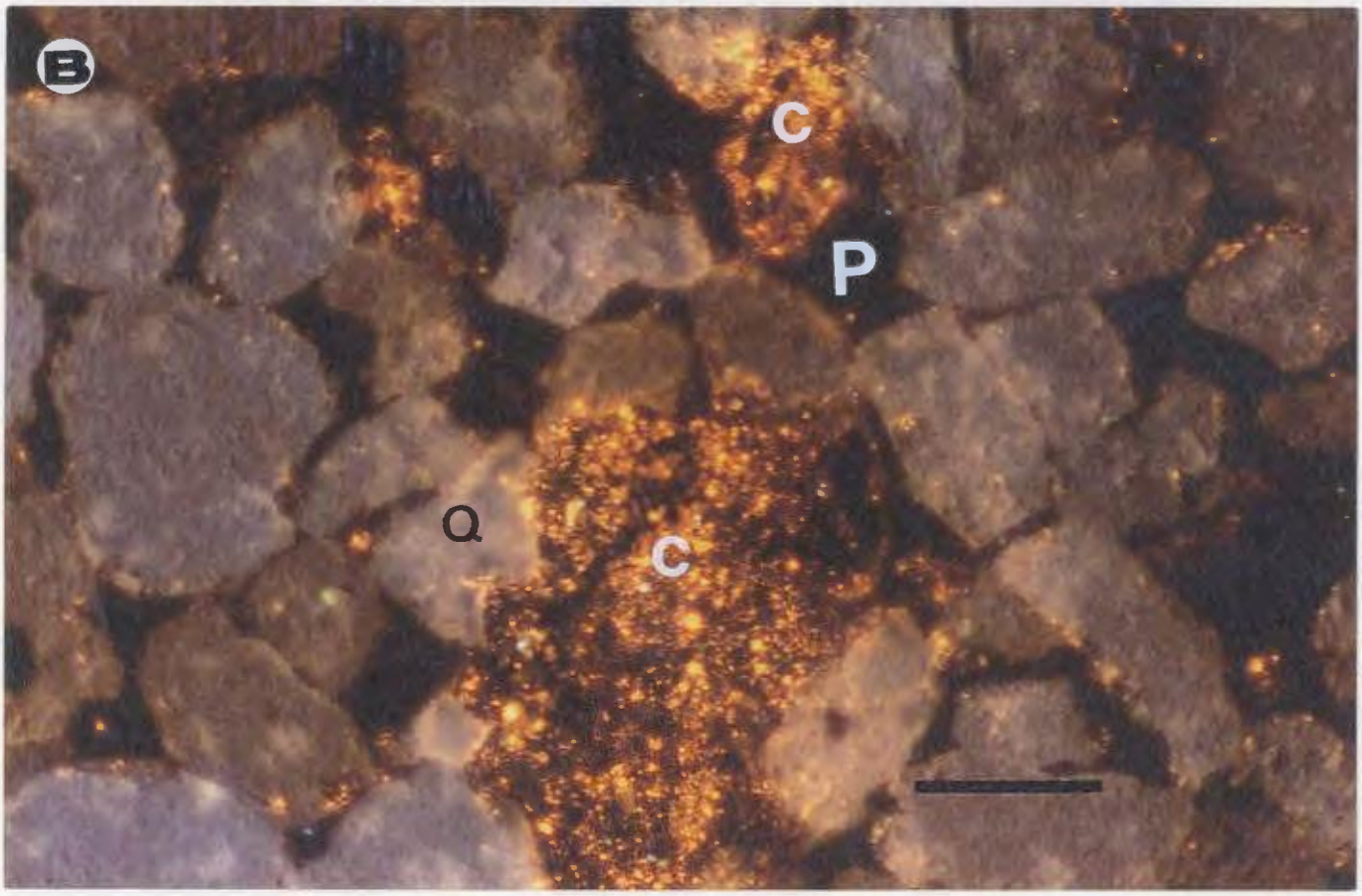

APPENDIX III

CATHODOLUMINESCENT PHOTOMICROGRAPHS: PLATE 30

A- CL photo in siltstone of distal delta front facies, shows authigenic kaolinite cement (K) of royal-blue (navy) luminescence between corroded quartz grains (Q). Note fractures in quartz grains have been healed by dull-brown luminescent quartz-overgrowths (O). Distal delta front, well A1-NC2 @ 2383 m. (7817 ft.). Scale bar= 0.03mm.

B- CL photo illustrating the navy blue-luminescent intergranular kaolinite cement (K) partially filling pores between quartz grains (Q). Pores are partially filled with yellow-orange luminescent calcite cement (C). Note the loose grain packing in this sample suggests early calcite cementation. Fluvial sandstone, well A1-NC118 @ 3084 m. (10115 ft.). Scale bar= 0.1mm.

APPENDIX III
CATHODOLUMINESCENT PHOTOMICROGRAPHS: PLATE 30

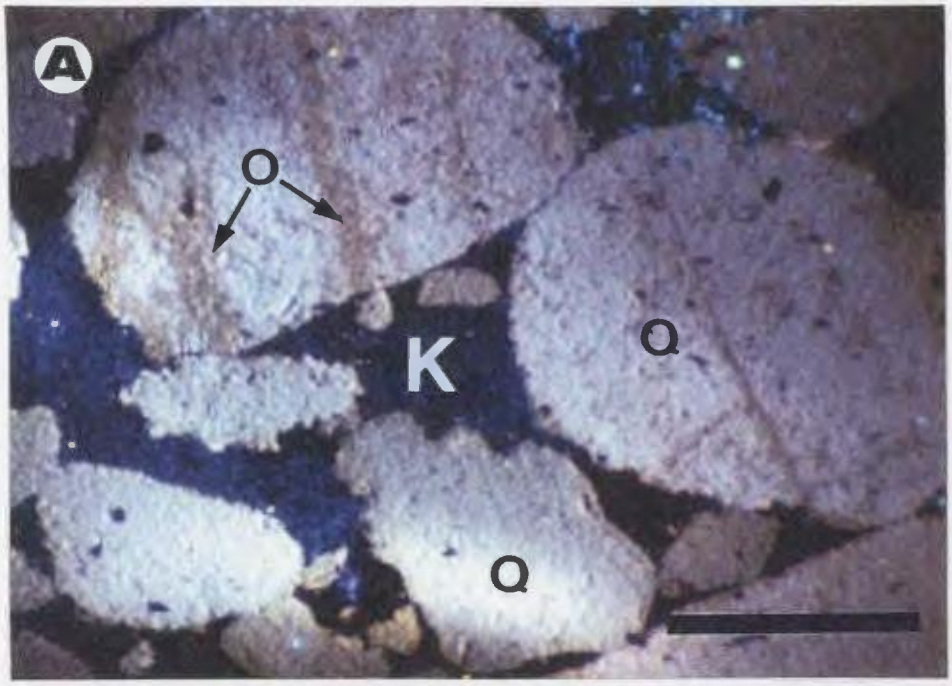

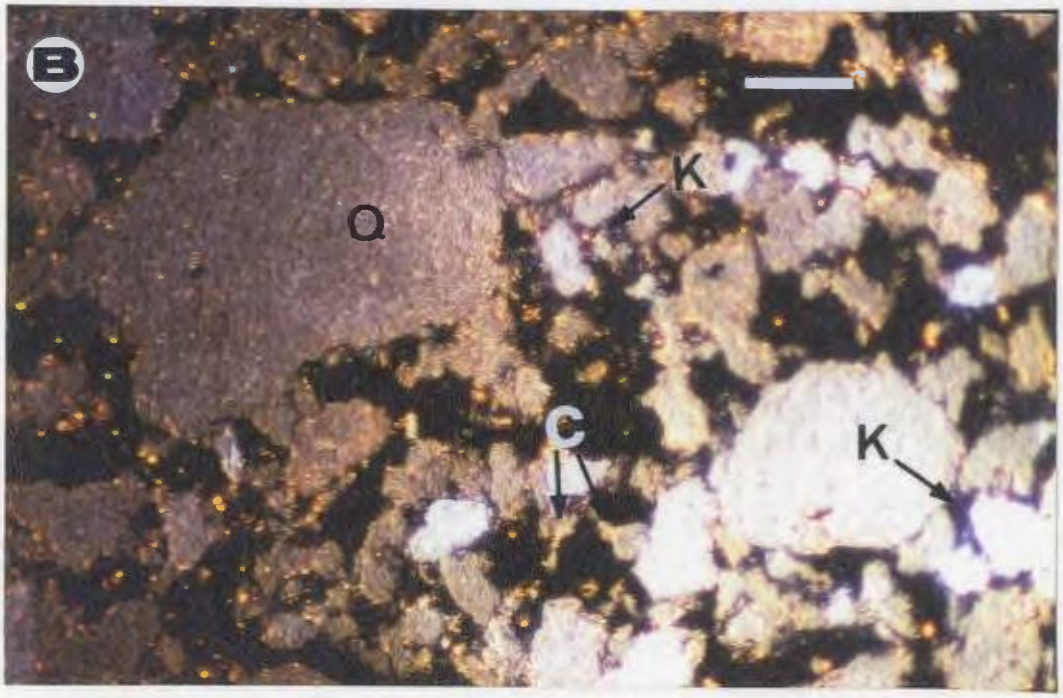

APPENDIX III

CATHODOLUMINESCENT PHOTOMICROGRAPHS: PLATE 31

A- CL photo illustrating the excessively blocking pore-spaces with the dark brown-non-luminescent iron-oxides (I) clay rich coating. Fluvial sandstone, well CC1-NC7A @ 2749 m. (9017 ft.). Scale bar= 0.1mm.

B- Plane-polarized light photo of the previous sample.

APPENDIX III
CATHODOLUMINESCENT PHOTOMICROGRAPHS: PLATE 31

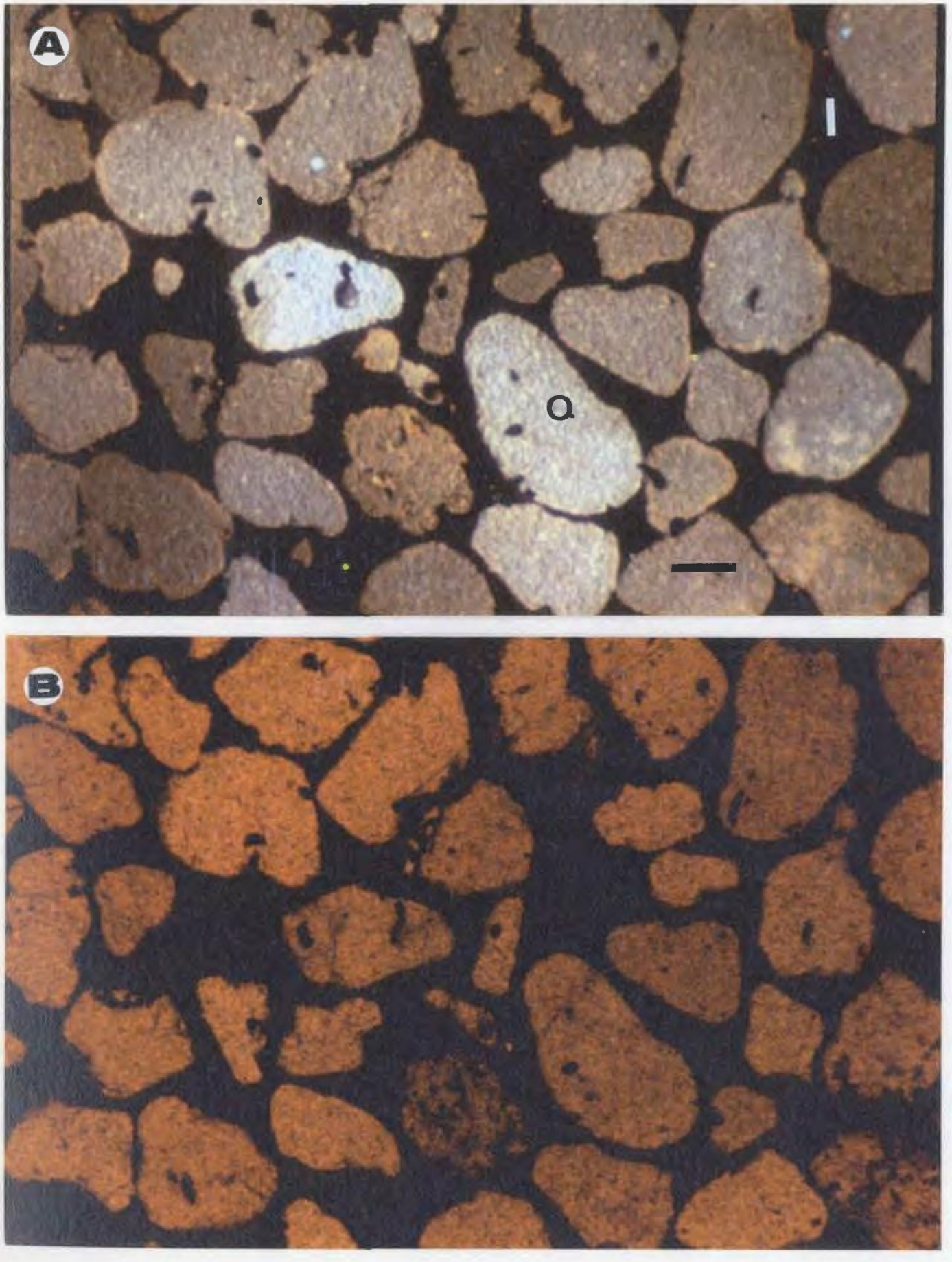

APPENDIX III

CATHODOLUMINESCENT PHOTOMICROGRAPHS: PLATE 32

A- CL photo contains dark brown- non-luminescent pore filling clay-rich iron oxides (I). Fluvial sandstone, well EE1-NC7A @ 2687 m. (8812 ft.). Scale bar= 0.1mm.

B- Plane-polarized light photo of the pervious sample, note the partial filling of primary porosity with clay-iron oxides coating (I). Black areas are unfilled pores (P).

APPENDIX III
CATHODOLUMINESCENT PHOTOMICROGRAPHS: PLATE 32

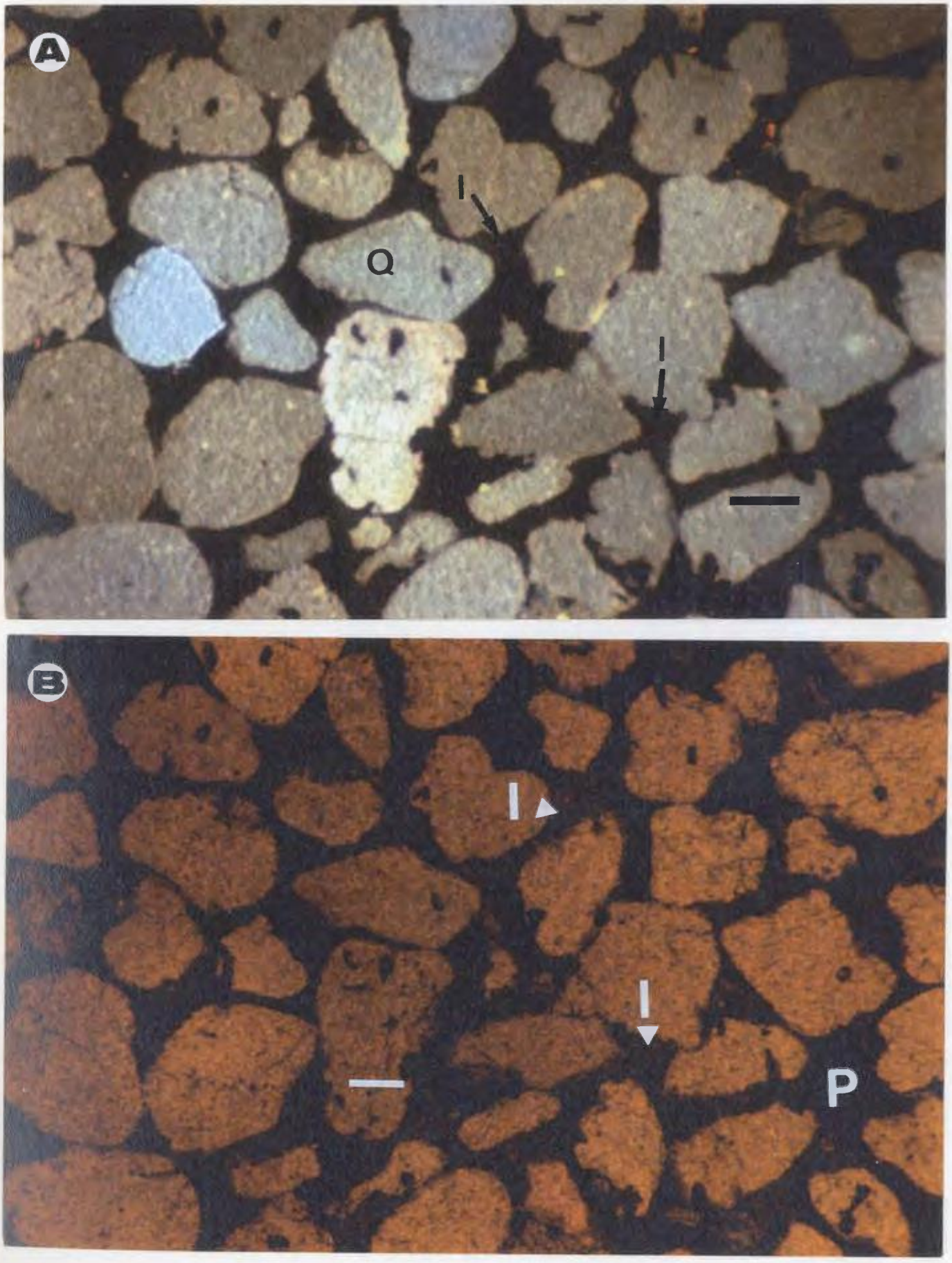

APPENDIX III

CATHODOLUMINESCENT PHOTOMICROGRAPHS: PLATE 33

A- CL photo shows traces of detrital zircon crystal (Z) of bright golden luminescence associated with fluvial sandstone. Note partial filling of pores with dark brown- non-luminescent clay-rich iron oxides (I), also note quartz grain contact enlargement through authigenic quartz-overgrowths (O) of dull-brown luminescence. Fluvial sandstone, well A1-NC118 @ 3061 m. (10040 ft.). Scale bar= 0.1mm.

B- Plane-polarized light photo of the pervious sample in which the partial filling of clay-rich iron oxides (I) can easily be seen. Note black areas are primary porosity (P) between quartz grains (Q).

APPENDIX III
CATHODOLUMINESCENT PHOTOMICROGRAPHS: PLATE 33

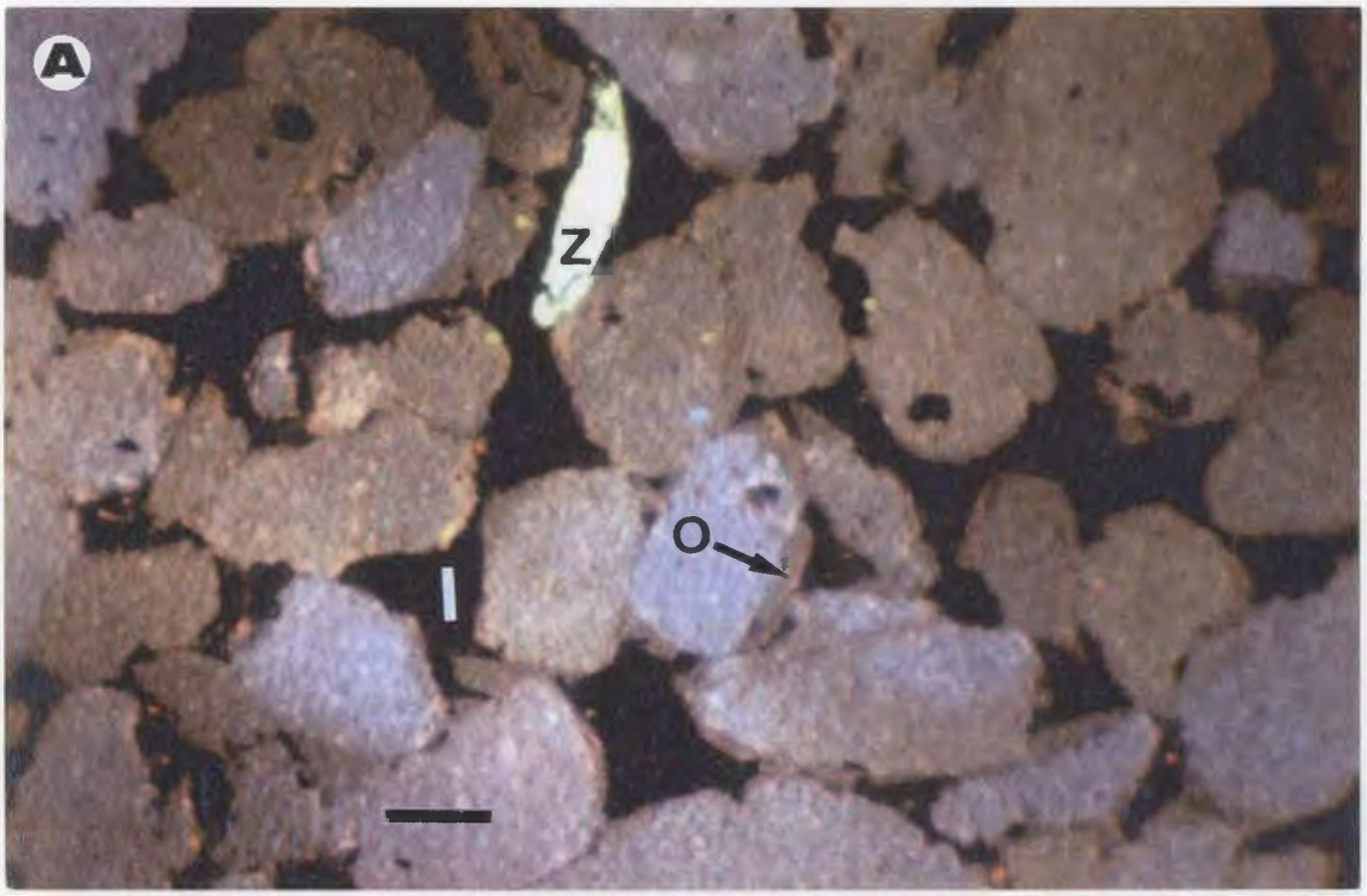

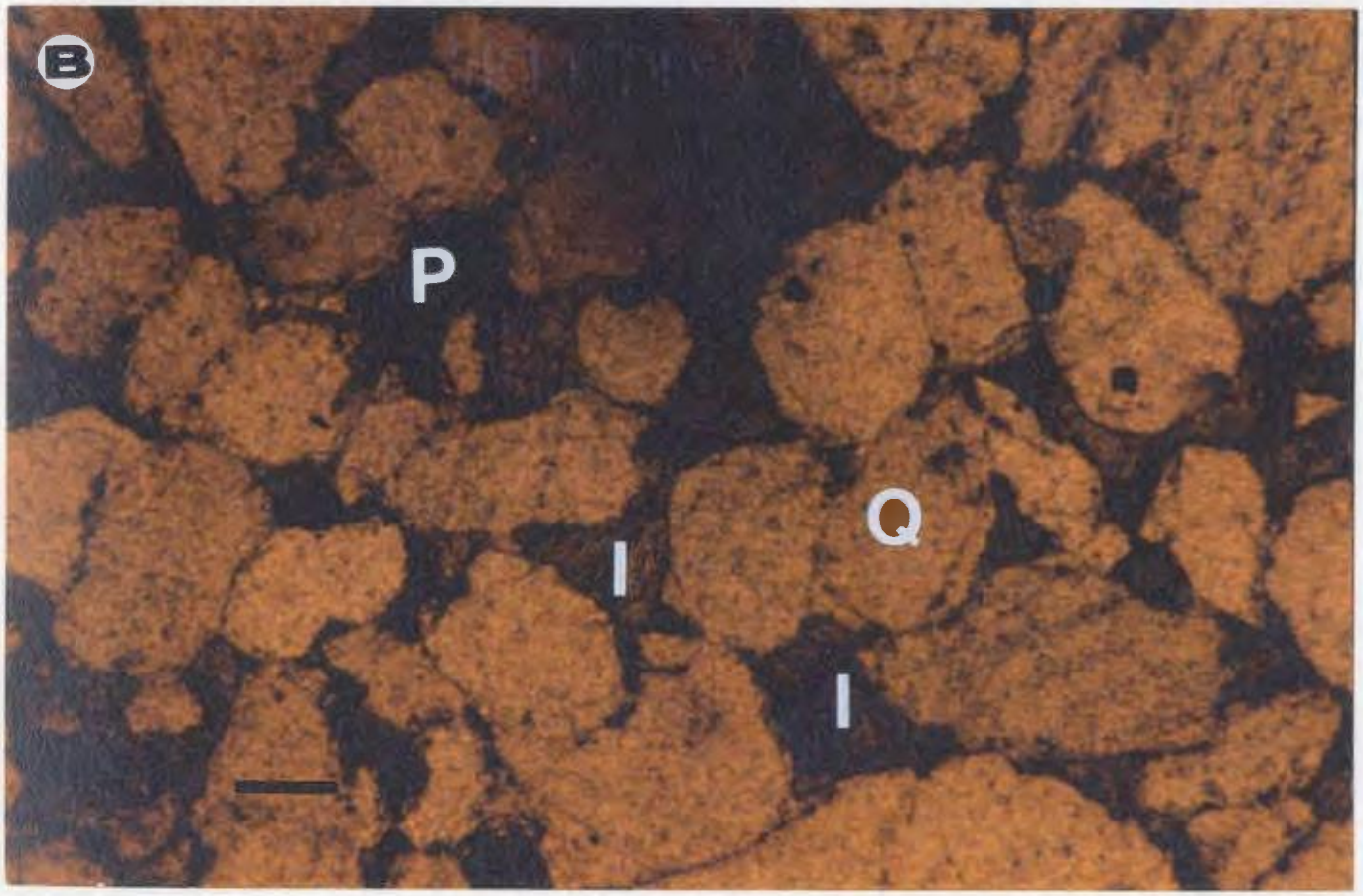

APPENDIX IV
SCANNING ELECTRON PHOTOMICROGRAPHS

APPENDIX IV

SCANNING ELECTRON PHOTOMICROGRAPHS: PLATE 34

A- Scanning electron photomicrograph showing detrital quartz grains (Q), overgrowths (O) and preserved primary porosity (P) in the medium-coarse grained, fluvial sandstone of well EE1-NC7A @ 2686 m. (8810 ft.). (EDS beam spot-mode analyses suggested silica mineralogy).

B- Scanning electron photomicrograph showing rough surface and complex texture of quartz sand grains from fluvial sandstone of Sahara desert. Note the stepped crystal morphology (arrow) may be caused by etching and abrasion. (EDS beam spot-mode analyses indicated its mineralogy). Well EE1-NC7A @ 2687 m. (8812 ft.).

C- Scanning electron photograph showing detrital quartz grains (Q), quartz-overgrowths (O), and pores (P). Note coalescing of quartz-overgrowths (arrow) which reduced pore-spaces. Quartz-rich fluvial sandstone, well CC1-NC7A @ 2750 m. (9020 ft.).

D- Is a higher magnification photo of the area indicated by white arrow in previous photo (C). (EDS beam spot-mode analysis confirms the presence of silica).

APPENDIX IV
SCANNING ELECTRON PHOTOMICROGRAPHS: PLATE 34

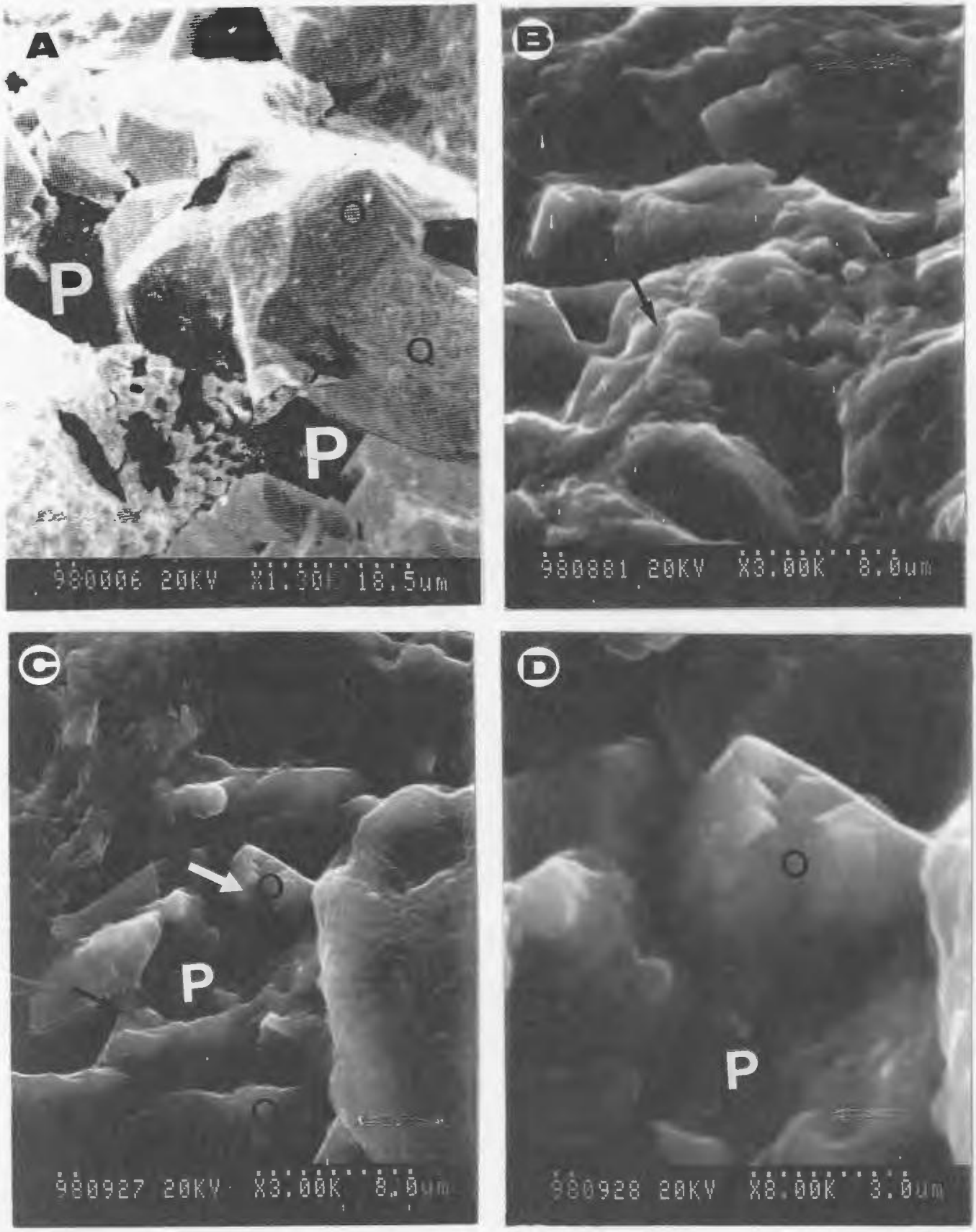

APPENDIX IV

SCANNING ELECTRON PHOTOMICROGRAPHS: PLATE 35

A- scanning electron photograph showing detrital quartz grains (Q), quartz-overgrowths (O), and triangular shape primary pores (P) which is open and not blocked by authigenic cements. Fluvial sandstone, well CC1-NC7A @ 2750 m. (9020 ft.).

B- Scanning electron photomicrograph of platy, coarsely crystalline authigenic iron oxides (I) (hematite) in coarse-grained fluvial sandstone of well CC1-NC7A @ 2749 m. (9017 ft.). (EDS beam spot-mode analysis confirms its mineralogy).

C- Scanning electron photomicrograph of fairly fresh, long-platy feldspar crystals (MF) with remarkable corrosion along crystal faces. This detrital feldspar was found to be associated with the fluvial sandstone of well B3-61 @ 2839 m. (9311 ft.). Note preserved primary porosity (P) between quartz grains (Q) and feldspar grains (MF). (EDS beam-spot-mode analysis confirms the K-feldspar (Microcline) occurrence).

APPENDIX IV
SCANNING ELECTRON PHOTOMICROGRAPHS: PLATE 35

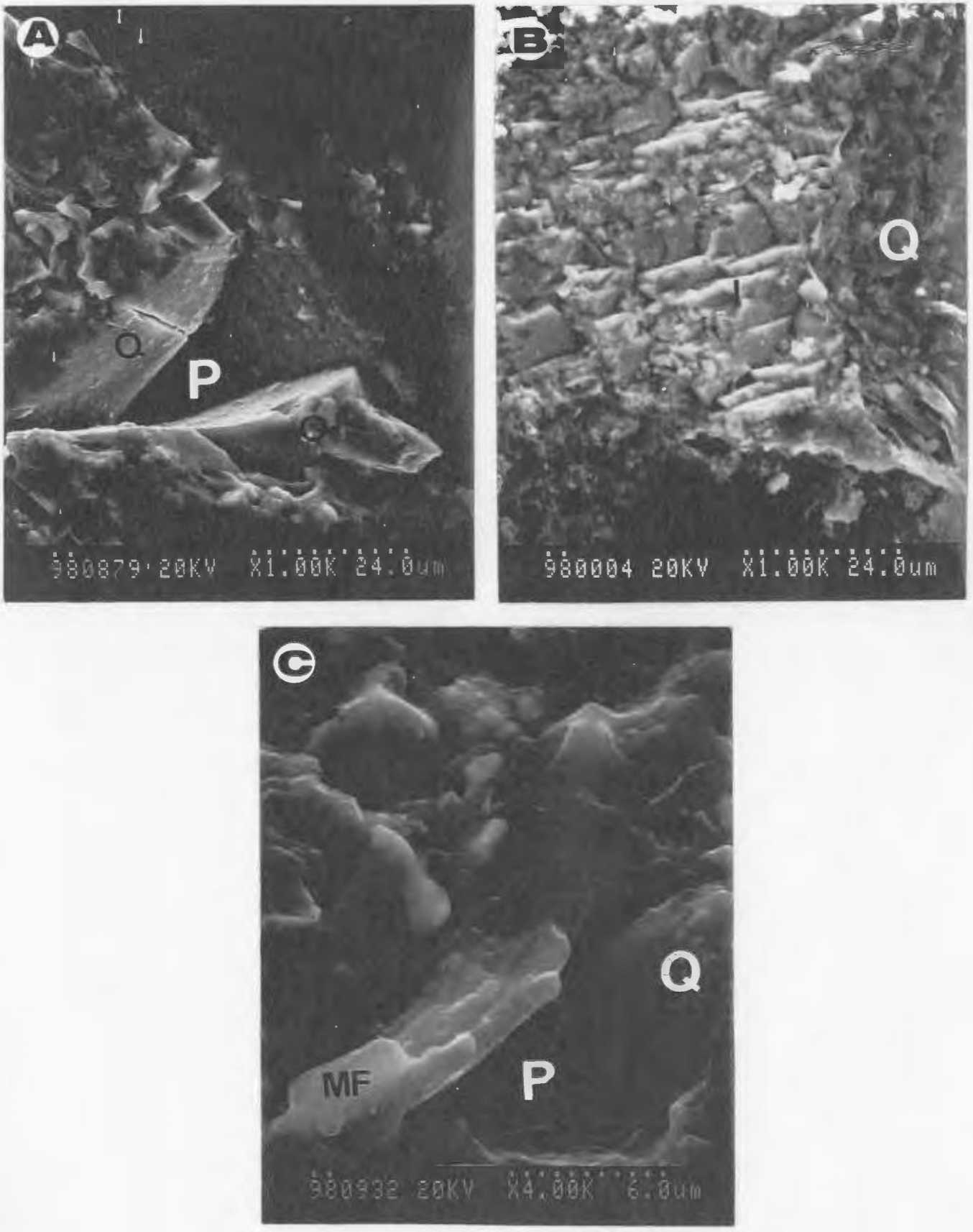

APPENDIX IV

SCANNING ELECTRON PHOTOMICROGRAPHS: PLATE 36

A- Scanning electron photomicrograph showing some calcite crystals (C) filling partially intergranular porosity (P) in fluvial sandstone of well EE1-NC7A @ 2686 m. (8810 ft.).

B- Is a higher magnification photograph of the area indicated by arrow in previous photo, showing cluster of calcite cement crystals.

C- Low magnification scanning electron photomicrograph showing poikilotopic (pervasive) calcite cement (C) in the fine-grained, proximal delta front sandstone of well C1-NC2 @ 2958 m. (9703 ft.).

D- Scanning electron photomicrograph showing leaching of calcite cement (C) and the formation of secondary porosity. Note very corroded quartz grain (Q) boundaries (arrow). Proximal delta front sandstone, well C1-NC2 @ 2965 m. (9725 ft.). (EDS beam spot-mode analyses indicated calcite mineralogy).

APPENDIX IV

SCANNING ELECTRON PHOTOMICROGRAPHS: PLATE 36

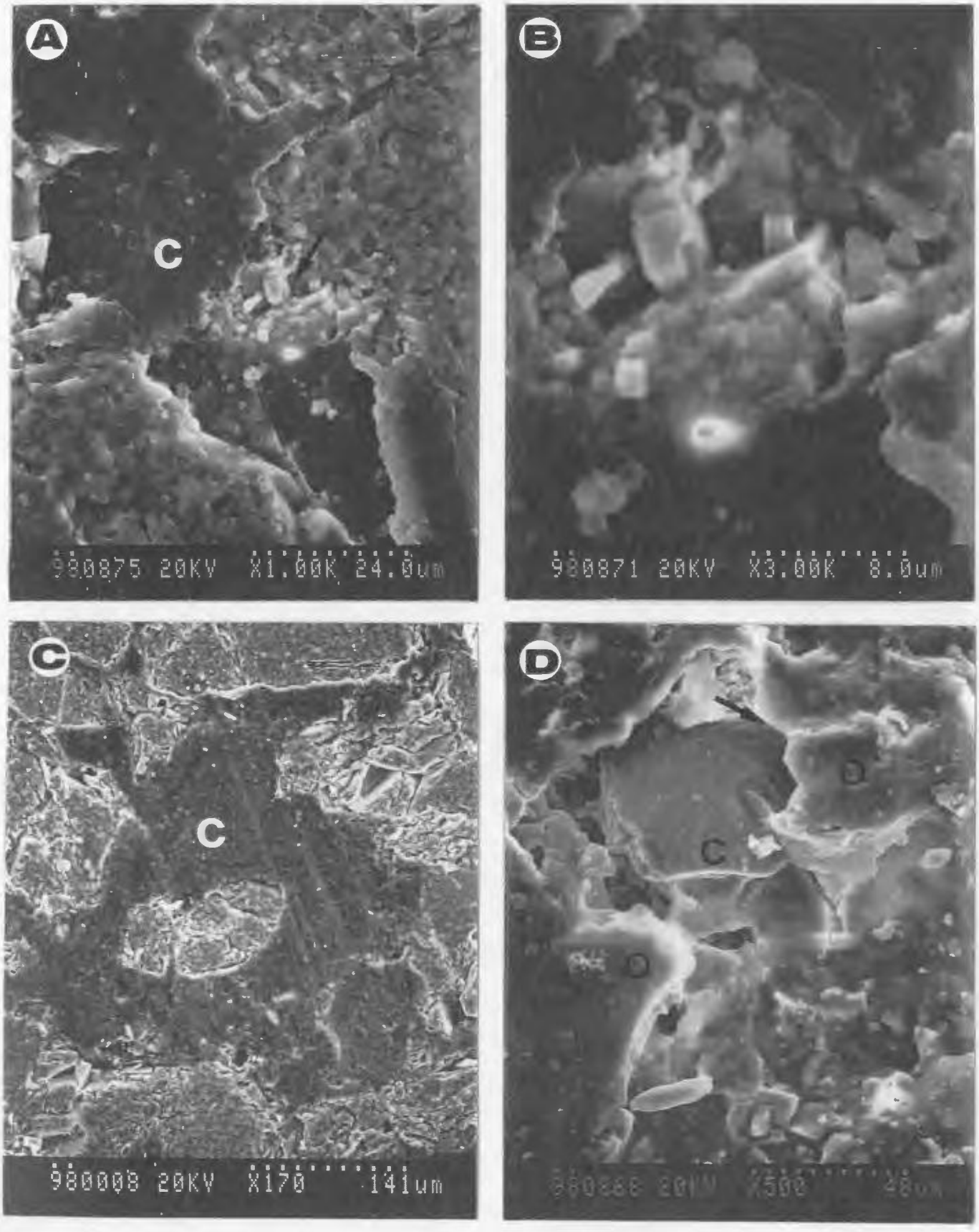

APPENDIX IV

SCANNING ELECTRON PHOTOMICROGRAPHS: PLATE 37

A- Scanning electron photomicrograph showing pore-filling ferroan dolomite cement (D) of rhombic crystals in the fine-medium grained, proximal delta front sandstone of well T1-23 @ 2577 m. (8454 ft.). (EDS beam spot-mode analyses indicated dolomite richness with iron).

B- Scanning electron photomicrograph showing rhombic outlined ferroan dolomite cement (D) filling secondary porosity in reworked marine sandstone of well B3-61 @ 2670 m. (8756 ft.). (EDS beam spot-mode analyses confirmed iron-rich dolomite).

C- Low magnification scanning electron photomicrograph showing partially filled primary porosity with ferroan dolomite (D) in fluvial sandstones of well EE1-NC7A @ 2687 m. (8812 ft.). (EDS beam spot-mode analyses confirmed iron-rich dolomite).

D- Scanning electron photomicrograph showing some minor rhombic crystals of siderite cement (S) occasionally associated with the fluvial sandstone unit (Af4) in well Z1-66 @ 2768 m. (9080 ft.). (EDS beam spot-mode analyses Fig. 21D identify and confirm the mineralogy of siderite in this sample. See also Fig. 12B for petrographic confirmation).

APPENDIX IV
SCANNING ELECTRON PHOTOMICROGRAPHS: PLATE 37

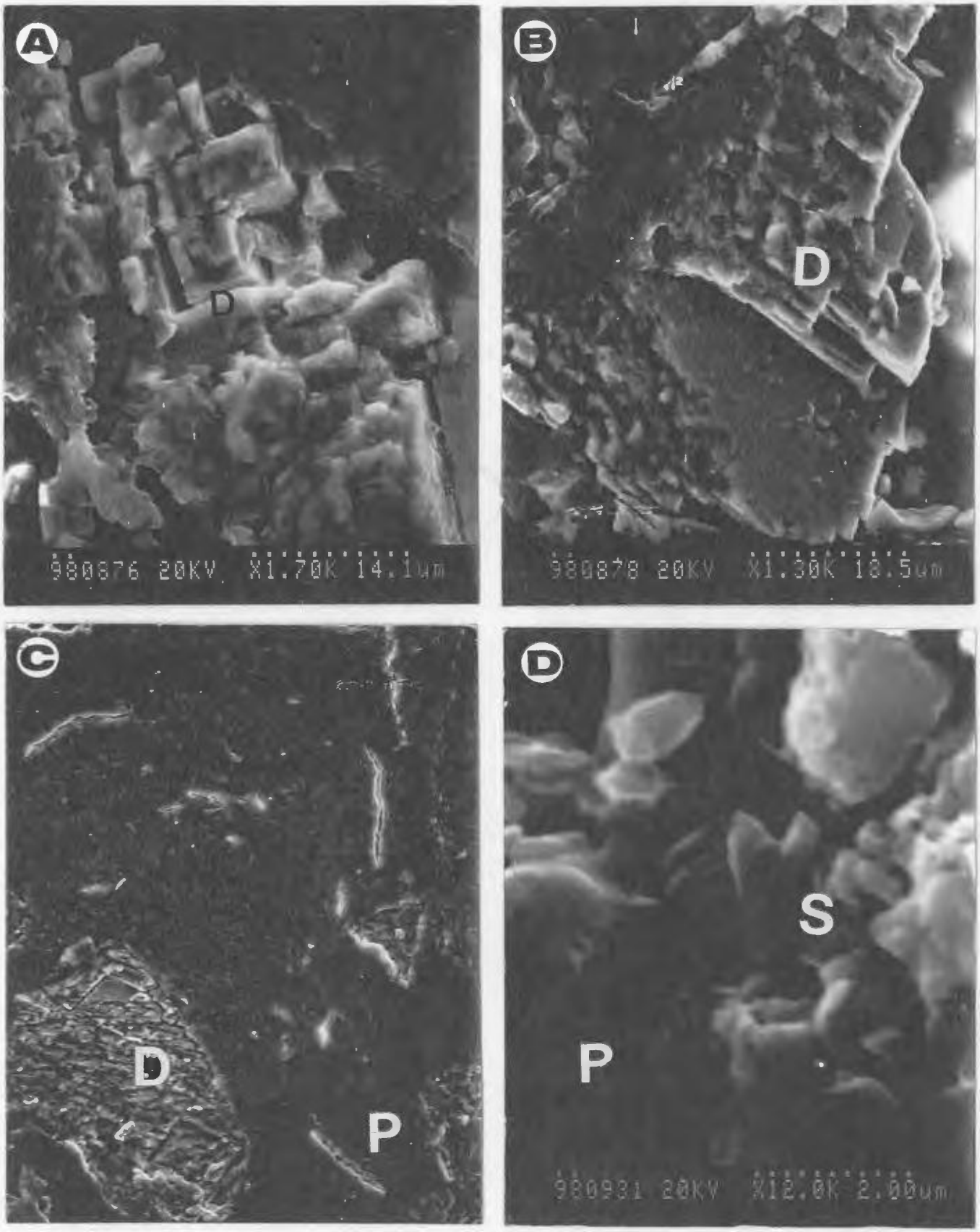

APPENDIX IV

SCANNING ELECTRON PHOTOMICROGRAPHS: PLATE 38

A- Scanning electron photomicrograph showing quartz-overgrowth (O) precipitated onto the detrital quartz grains, where this early precipitation exerted primary control on the pore-space configuration. After precipitation of quartz-overgrowths, kaolinite cement (K) precipitated partially in the remnant pore-spaces (P). Fluvial sandstone, well A1-NC118 @ 3061 m. (10040 ft.). (EDS beam spot-mode analyses confirmed the kaolinite mineralogy).

B- Scanning electron photomicrograph showing aggregates of kaolinite cement booklets (K) partially filling secondary porosity (P) in proximal delta front sandstone of well T1-23 @ 2577 m. (8454 ft.).

C- Scanning electron photomicrograph showing well-crystallized pore-blocking kaolinite books (K), intergrown with quartz (Q). The vermicular kaolinite stacks seen here in this sandstone are characterized with considerable intercrystalline microporosity (P), however, it is presumably of very low permeability. Reworked marine sandstone, well Q1-23 @ 2580 m. (8461 ft.).

D- Scanning electron photomicrograph showing kaolinite cement (K) booklets totally filled microporosity in the distal delta front siltstone of well A1-NC2 @ 2382 m. (7814 ft.). Note late illite cement (IL, arrows) that has grown on top of kaolinite cement (K), which may indicates illite precipitated after kaolinite. (EDS beam spot-mode analyses confirmed the presence of kaolinite and illite cements in this sample).

APPENDIX IV
SCANNING ELECTRON PHOTOMICROGRAPHS: PLATE 38

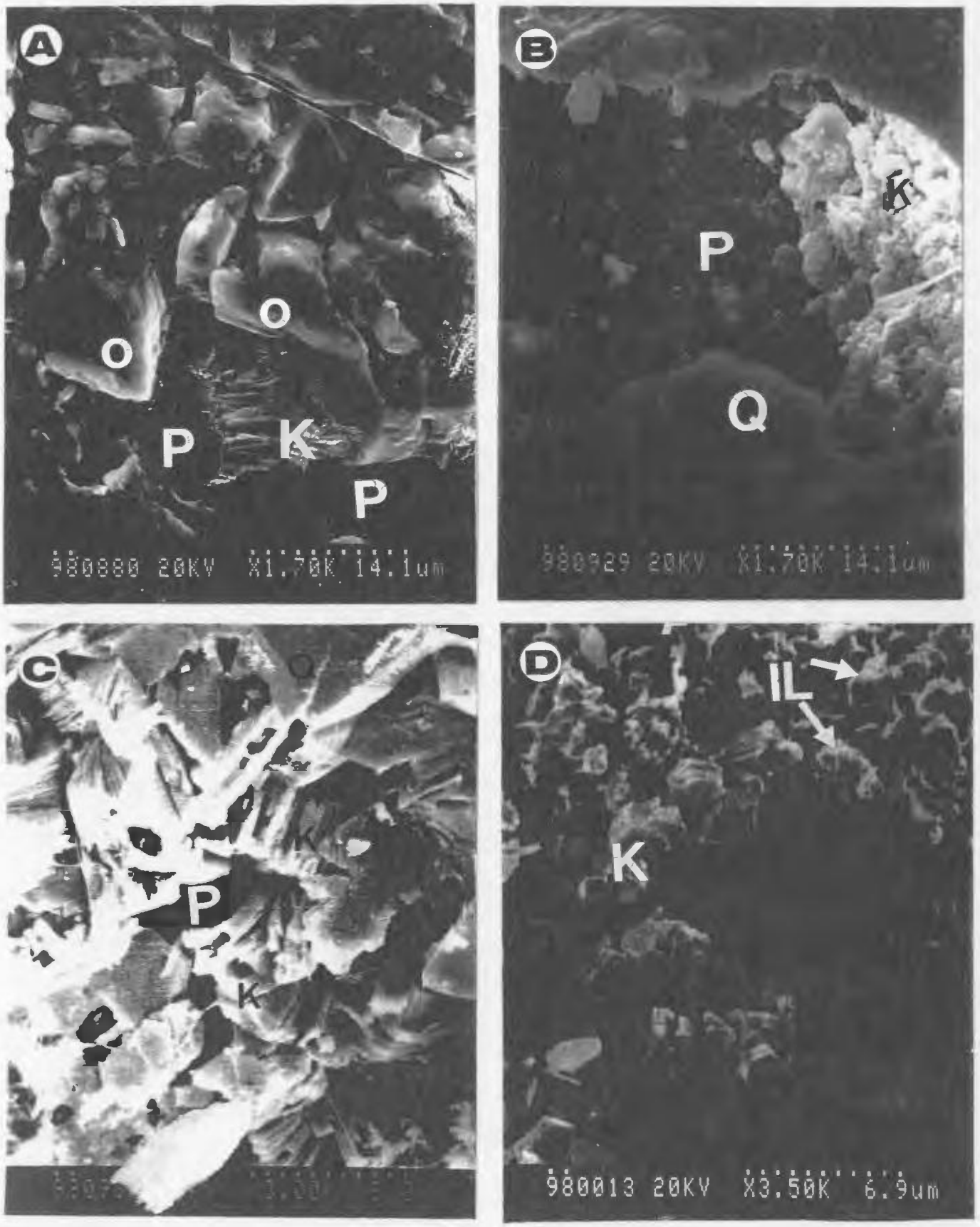

APPENDIX IV

SCANNING ELECTRON PHOTOMICROGRAPHS: PLATE 39

A- Scanning electron photomicrograph of very shaly-siltstone of distal delta front facies, showing detrital quartz grain (Q) supported by densely packed, matted sheet of pasty to ragged authigenic illite (IL). Note authigenic illite forms a meshwork of plates occasionally lining surrounding pore-spaces (P). Well A1-NC2 @ 2383 m. (7817 ft.). (EDS beam spot-mode analyses confirmed illite mineralogy).

B- Scanning electron photomicrograph shows micro-plates of illite cement (IL) and detrital quartz grains (Q) in medium-coarse grained, fluvial sandstone of well B3-61 @ 2839 m. (9311 ft.). Note the late stage precipitation of illite cement flames on top of quartz, and surrounding pores (P), seems to have inhibited development of quartz-overgrowths. (EDS beam spot-mode analyses confirmed the presence of illite cement in this sample).

C- scanning electron photomicrograph of another view in the previous sample under low magnification, in which illite cement (IL) appears to form a pile of plates accumulated directly on quartz grain surface and surrounding pores (P). Fluvial sandstone, well B3-61 @ 2839 m. (9311 ft.).

APPENDIX IV
SCANNING ELECTRON PHOTOMICROGRAPHS: PLATE 39

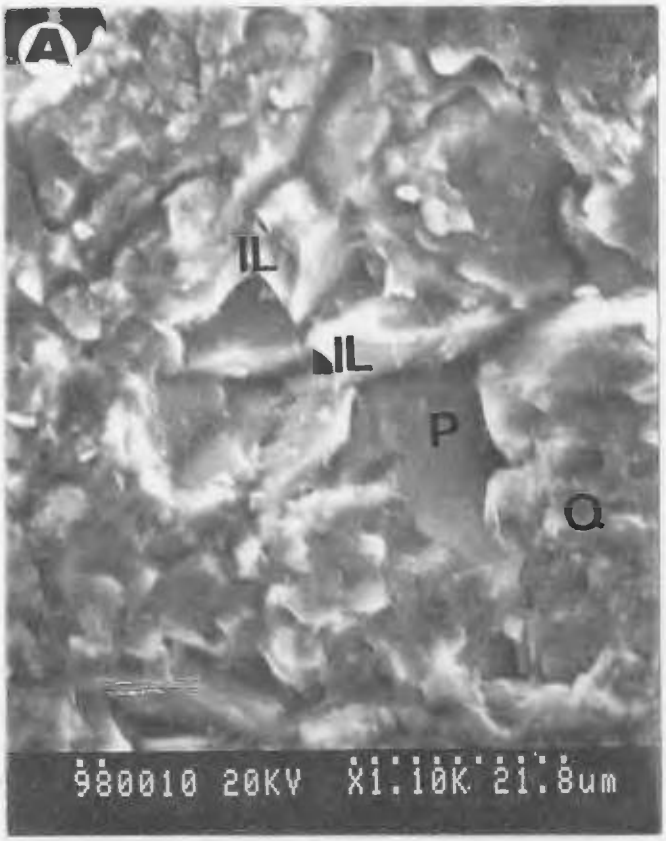

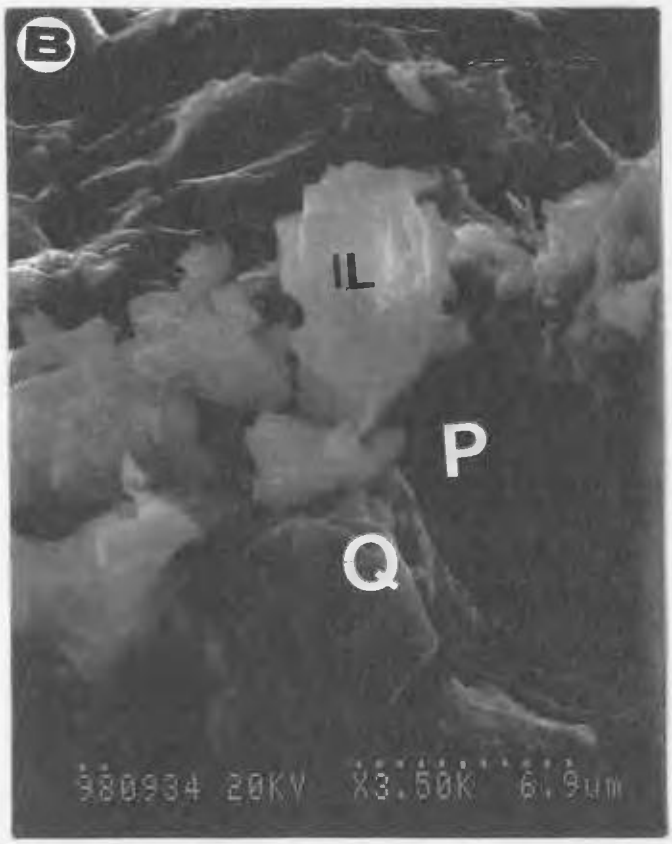

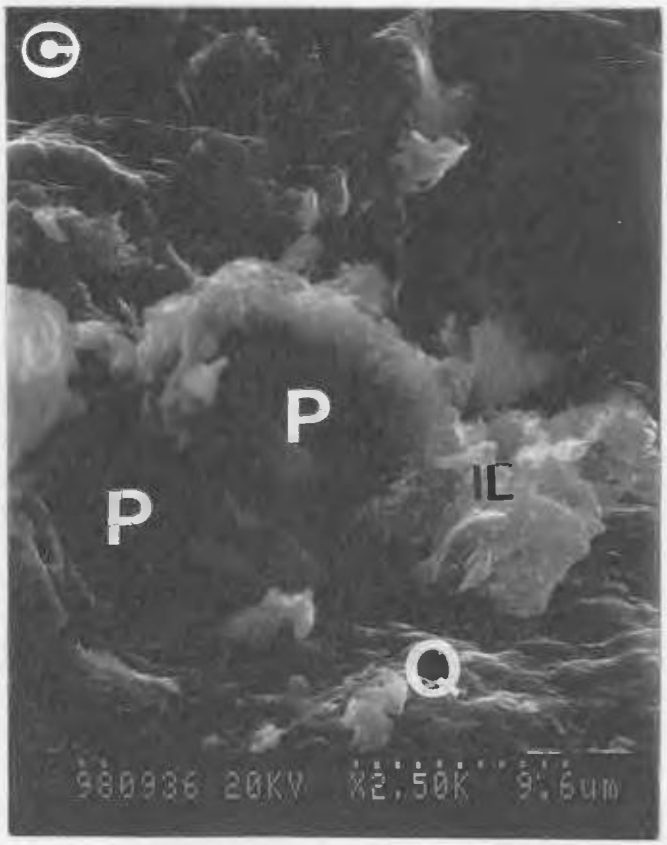

APPENDIX V
THIN-SECTION DIAGENESIS AND POROSITY

APPENDIX V

THIN-SECTION DIAGENESIS AND POROSITY: PLATE 40

A,B- Zones of major iron-oxide (I) coating filled the bottom of primary pores (P), preventing any development of quartz-overgrowths (early stage of diagenesis in this facies), whereas quartz-overgrowths (O) are grown on the top edge of the pores (pendant crystals overgrowth) which indicates growth of quartz crystals in fluid filled pores. Note partial dolomite cement (D) can be seen in sample B. Fluvial sandstone units (Af4, Af3), well Z1-66 @ 2768.5 m. (9081 ft.), 2784 m. (9130 ft.) respectively. Scale bar = 0.1mm.

(PPL)

APPENDIX V
THIN-SECTION DIAGENESIS AND POROSITY: PLATE 40

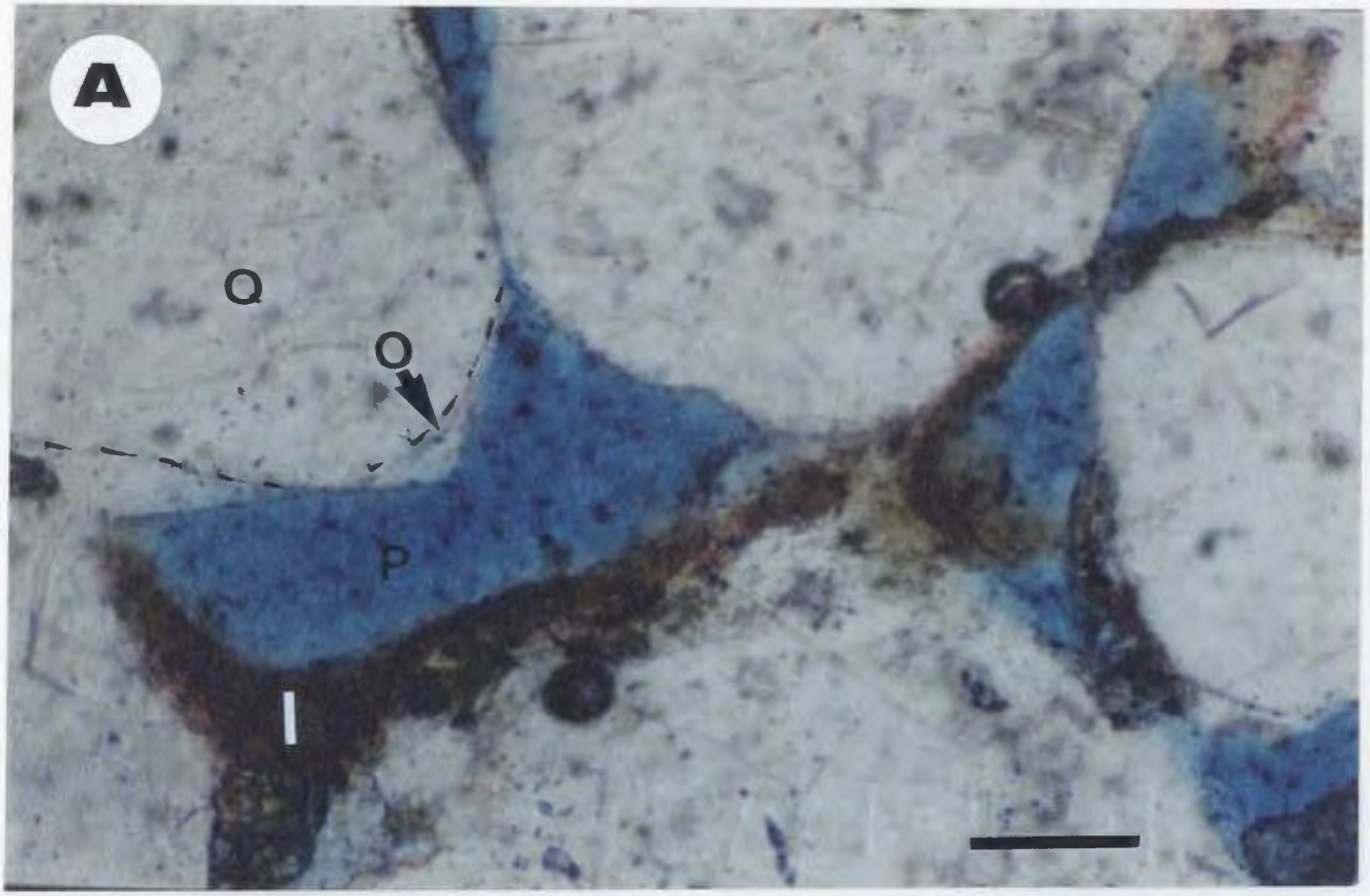

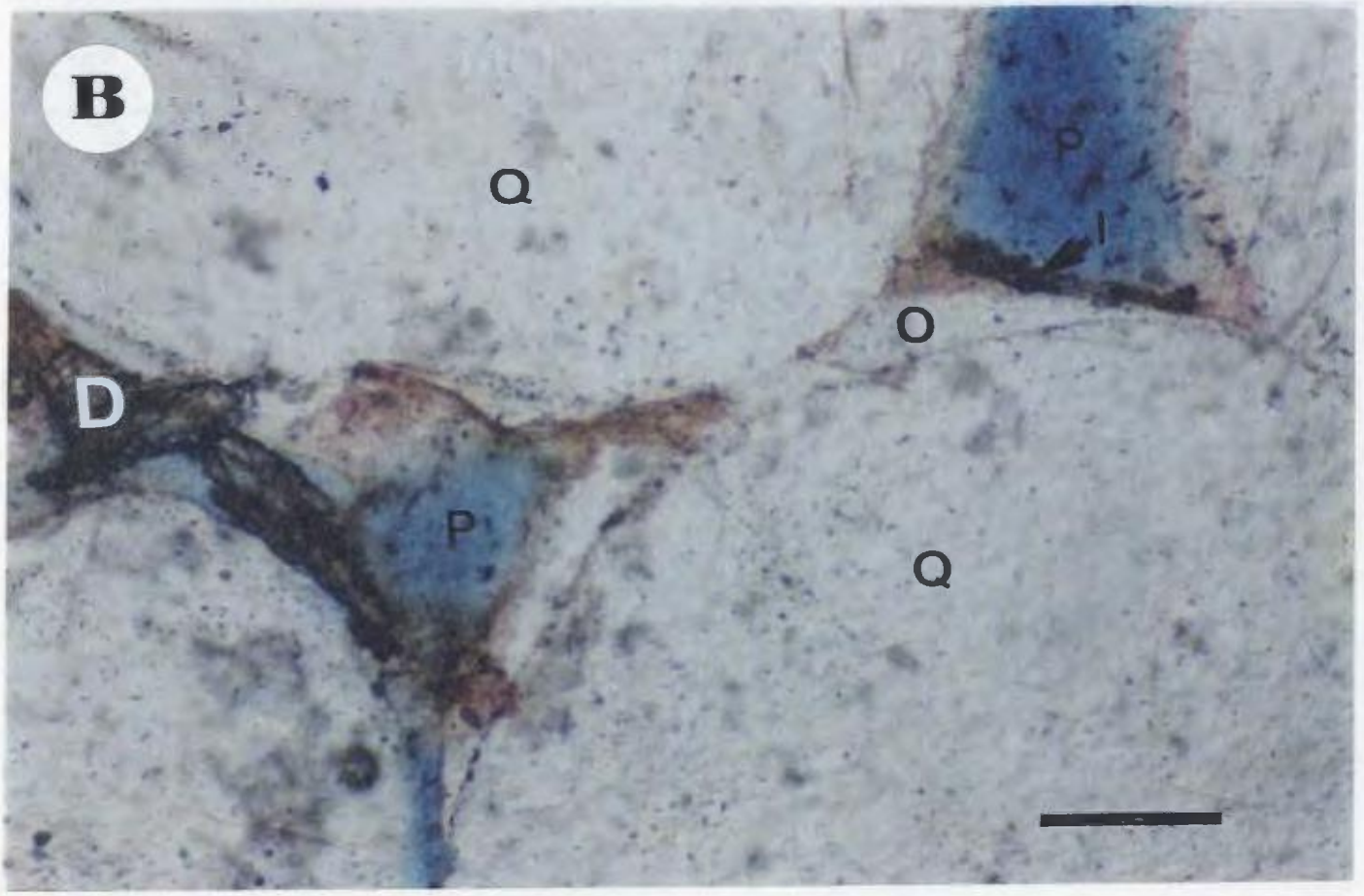

APPENDIX V

THIN-SECTION DIAGENESIS AND POROSITY: PLATE 41

A- Iron-oxides (I) rimming partially quartz grains (Q) and where it was initiated first on grain surfaces (on the bottom of the pores), quartz-overgrowths (O) was apparently inhibited, whereas in other parts of the same grain (the top of the pores) or in other adjacent grains (arrow) the quartz-overgrowths (O) were initiated first and no iron-oxides rim was observed. The two processes appear to have occurred simultaneously until the quartz-overgrowths become dominant and limit development of iron-oxides coatings. Note also dolomite cement (D) is partially filling pore spaces (P). Fluvial sandstone unit (Af3), well EE1-NC7A @ 2686 m. (8810 ft.). Scale bar = 0.1mm.

(PPL)

APPENDIX V
THIN-SECTION DIAGENESIS AND POROSITY: PLATE 41

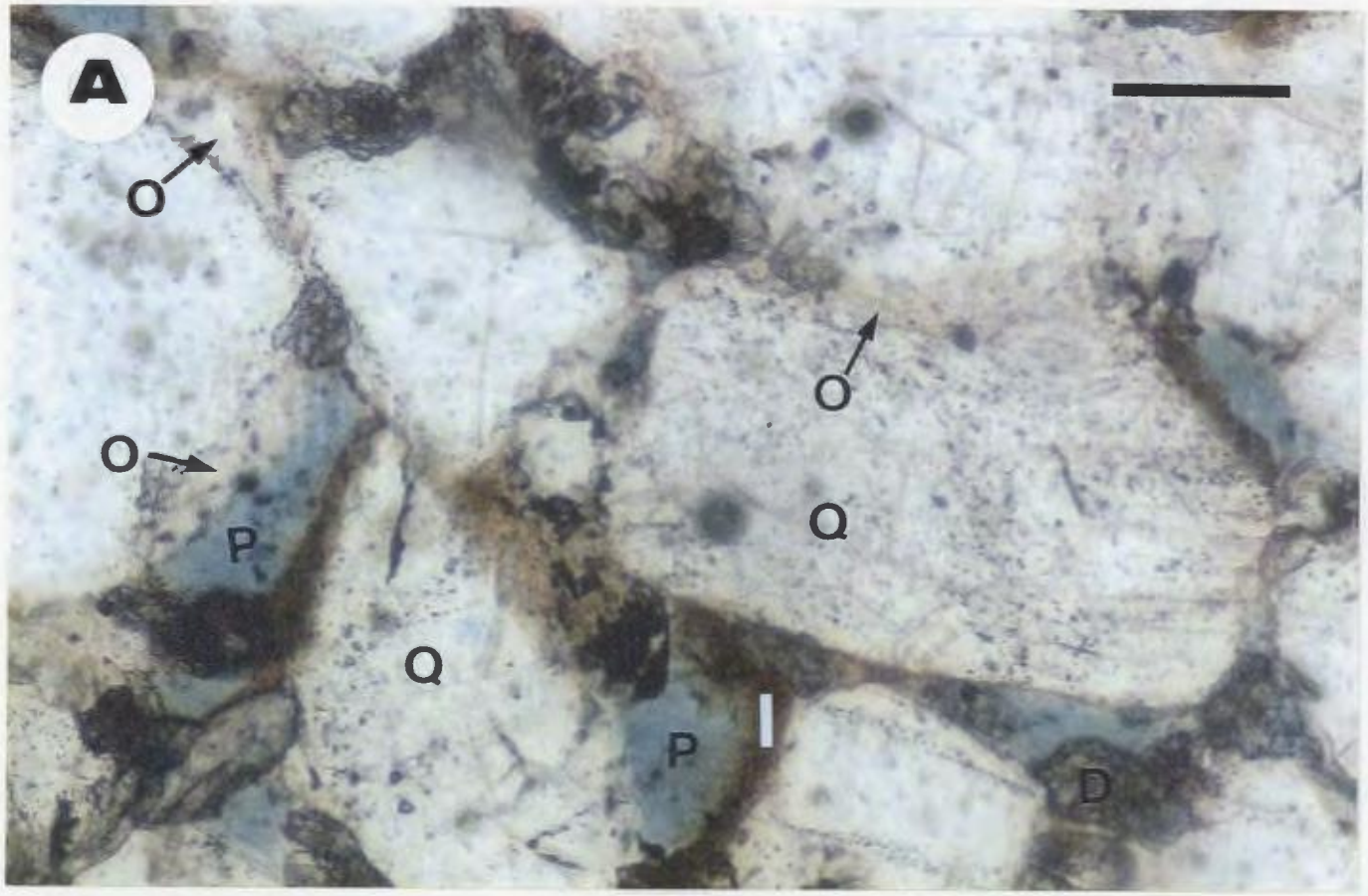

APPENDIX V

THIN-SECTION DIAGENESIS AND POROSITY: PLATE 42

A- Shallow calcite cement (C) in fluvial sandstone unit (Af3), partially filling primary porosity (P), and appears to post-dates quartz-overgrowths (O). Note also iron-oxides (I) occupied partially pore-spaces which may suggests that shallow calcite cement and iron-oxides are overlapping in time. Well EE1-NC7A @ 2686 m. (8810 ft.). Scale bar = 0.1mm.

(PPL)

B- Shallow calcite-cement (C) in fluvial sandstone unite (Af2) filling partially primary porosity (P). Leaching of calcite cement can be quite patchy where it has been dissolved only in certain areas as recognized by the highly corroded quartz grains (arrow). Well CC1-NC7A @ 2750 m. (9020 ft.). Scale bar = 0.1mm.

(PPL)

APPENDIX V
THIN-SECTION DIAGENESIS AND POROSITY: PLATE 42

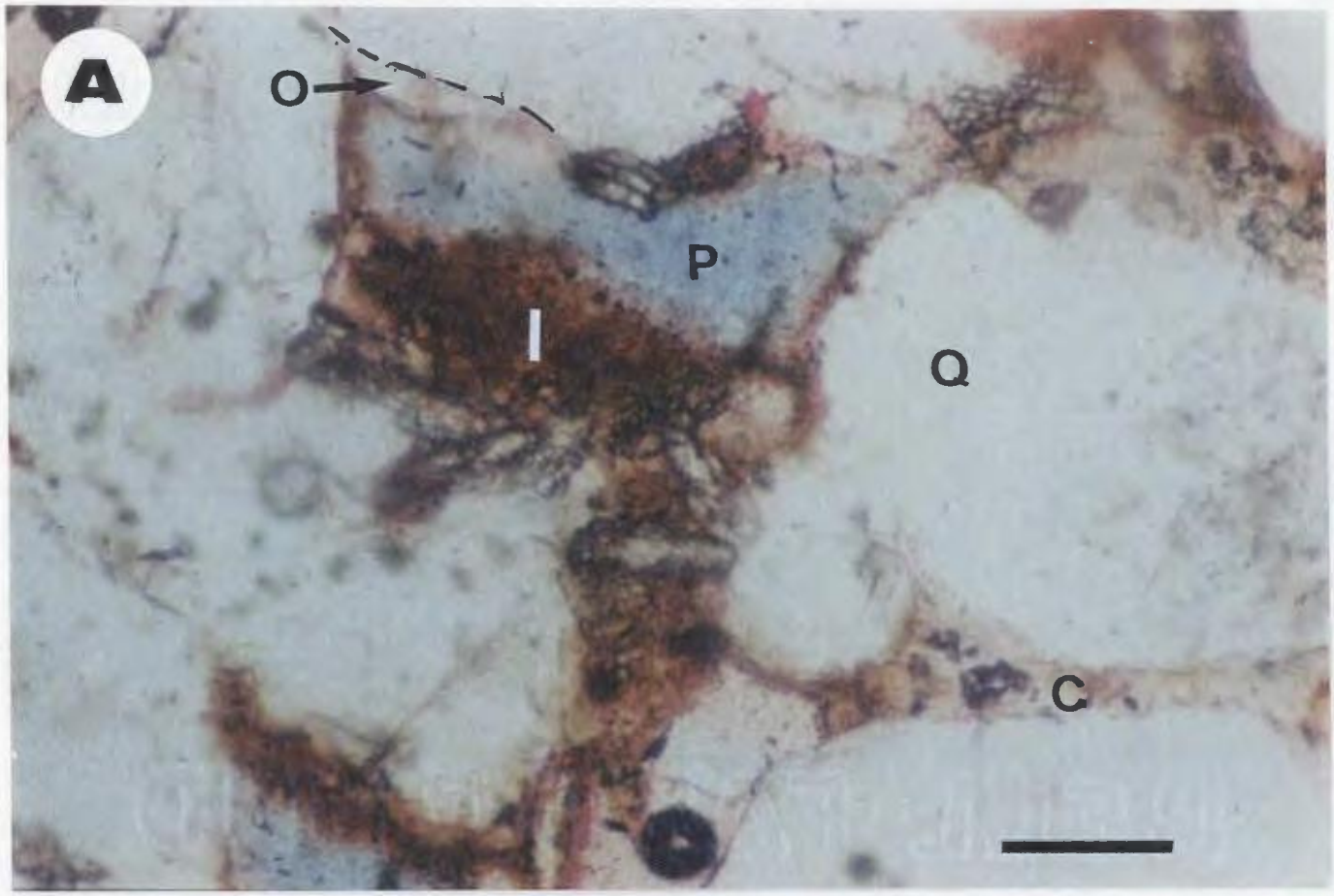

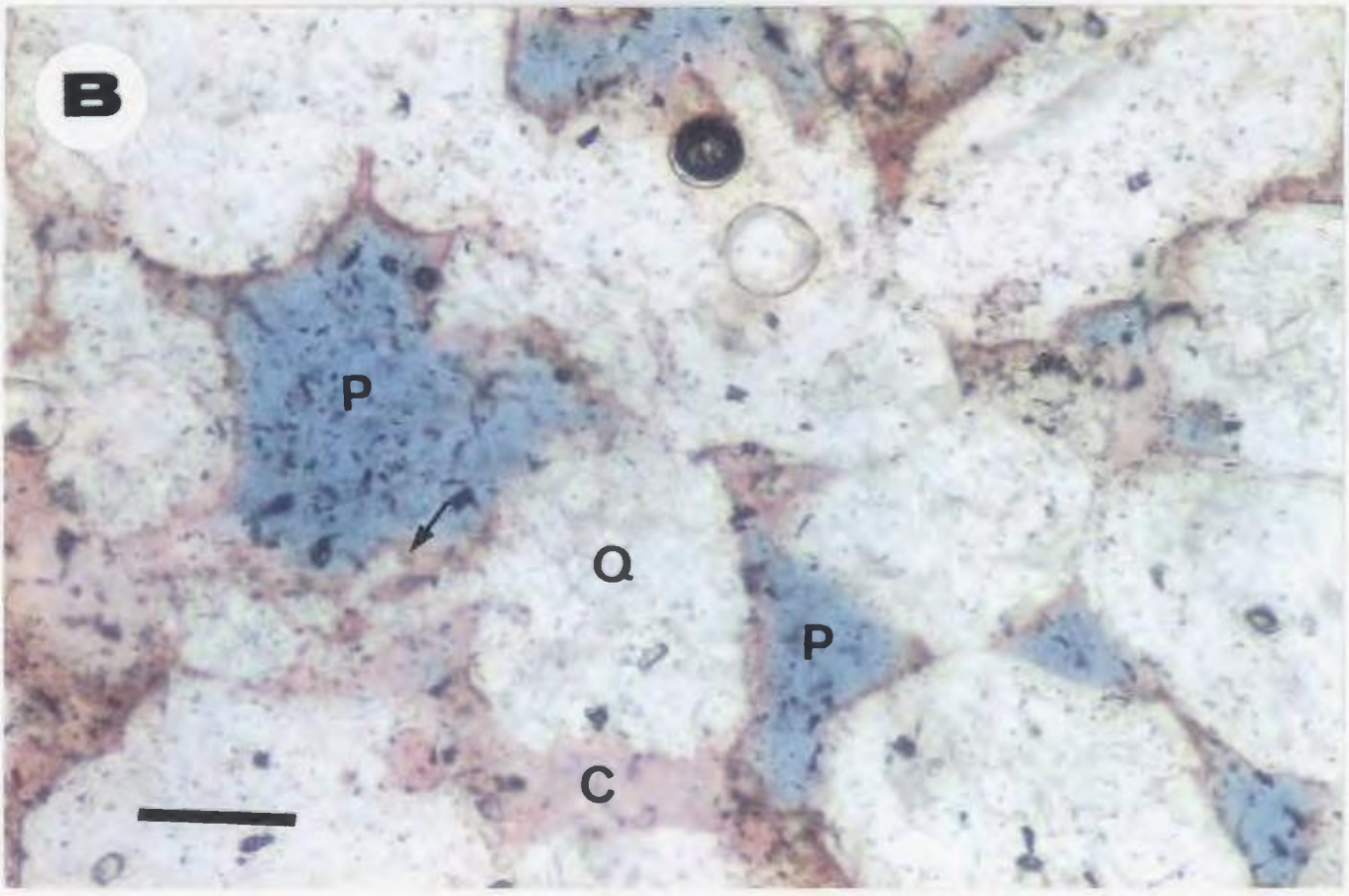

APPENDIX V

THIN-SECTION DIAGENESIS AND POROSITY: PLATE 43

A- Partial iron-oxides coatings (I), and shallow calcite cement (C) filling partially primary pores in fluvial sandstone unit (Af3), well EE1-NC7A @ 2686 m. (8810 ft.). Note the corroded quartz grain (short arrow) and the floating remnants of dissolved framework grains (long arrow) which replaced by shallow calcite latter. Scale bar = 0.1mm.

(PPL)

B- Iron-oxides (I) coatings and shallow calcite cement (C) are partially filling primary pore-spaces (P), in fluvial sandstone unit (Af3), well EE1-NC7A @ 2687 m. (8812 ft.). Note the relatively poor grain packing in this sample which may suggests an early stage of calcite cementation. Scale bar = 0.1mm.

(PPL)

APPENDIX V
THIN-SECTION DIAGENESIS AND POROSITY: PLATE 43

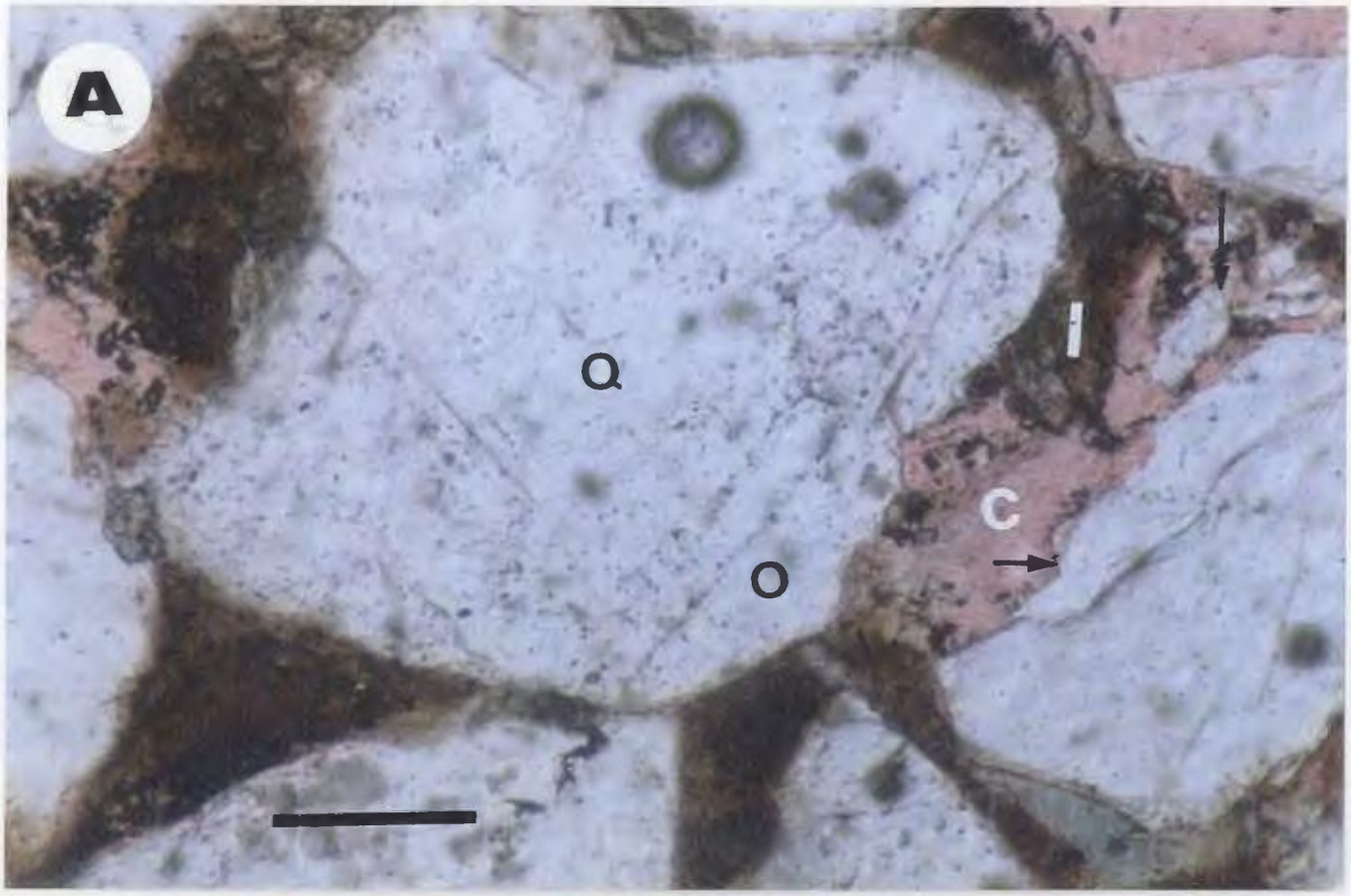

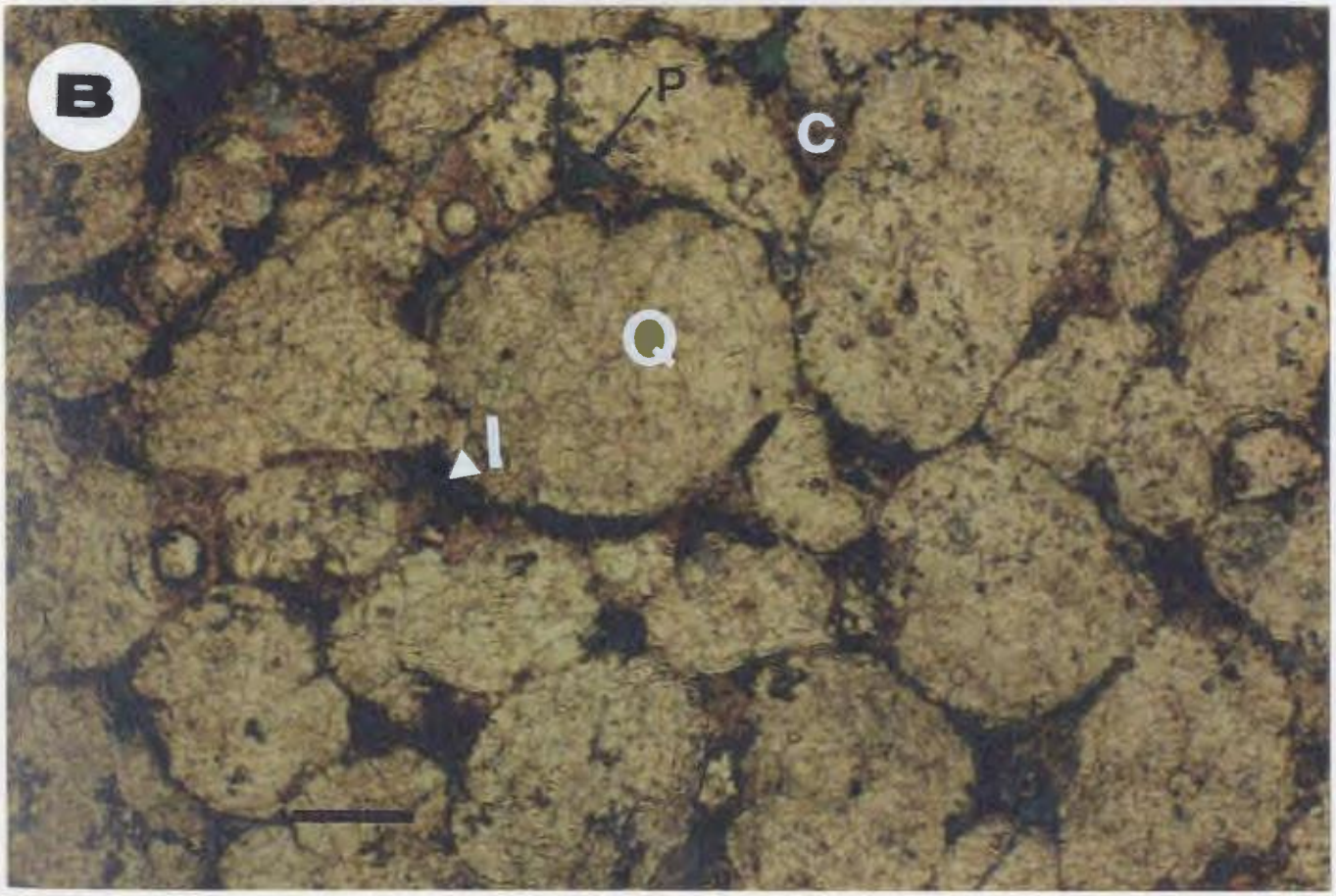

APPENDIX V

THIN-SECTION DIAGENESIS AND POROSITY: PLATE 44

A- Low magnification photograph showing shallow calcite cement (C) filling intergranular pore- spaces (P) in the fluvial sandstone unit (Af3) of well Z1-66 @ 2784 m. (9130 ft.). Note the loose grain packing with pores filling partially with shallow calcite cement which an evidence of early stage of calcite cementation in this rock. Scale bar = 0.1mm.

(PPL)

B- Same as previous photo but with crossed polarized light (XPL), note the shallow calcite cement (C) which shows high-order pink-greenish pink interference colours.

(XPL)

APPENDIX V
THIN-SECTION DIAGENESIS AND POROSITY: PLATE 44

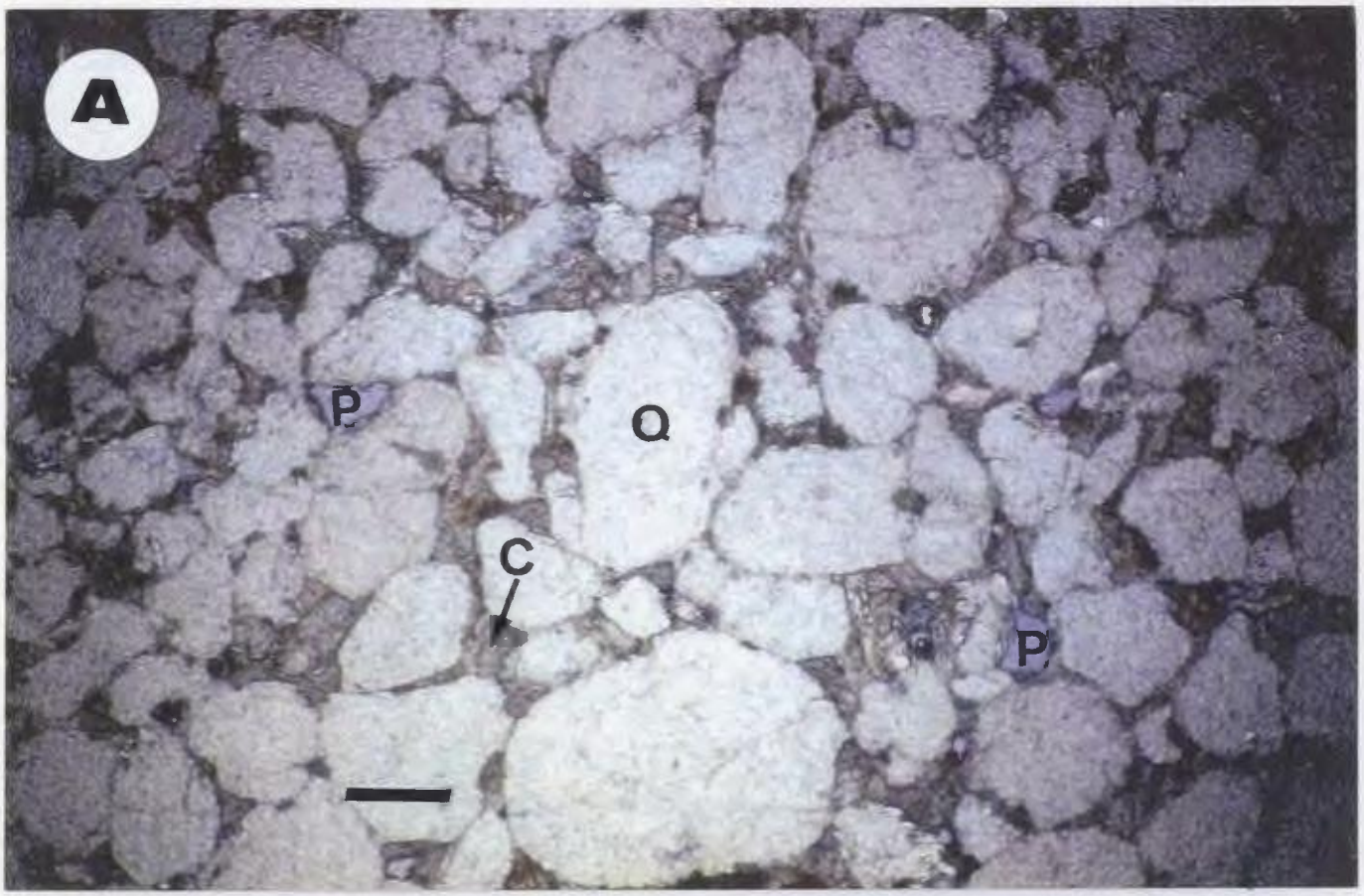

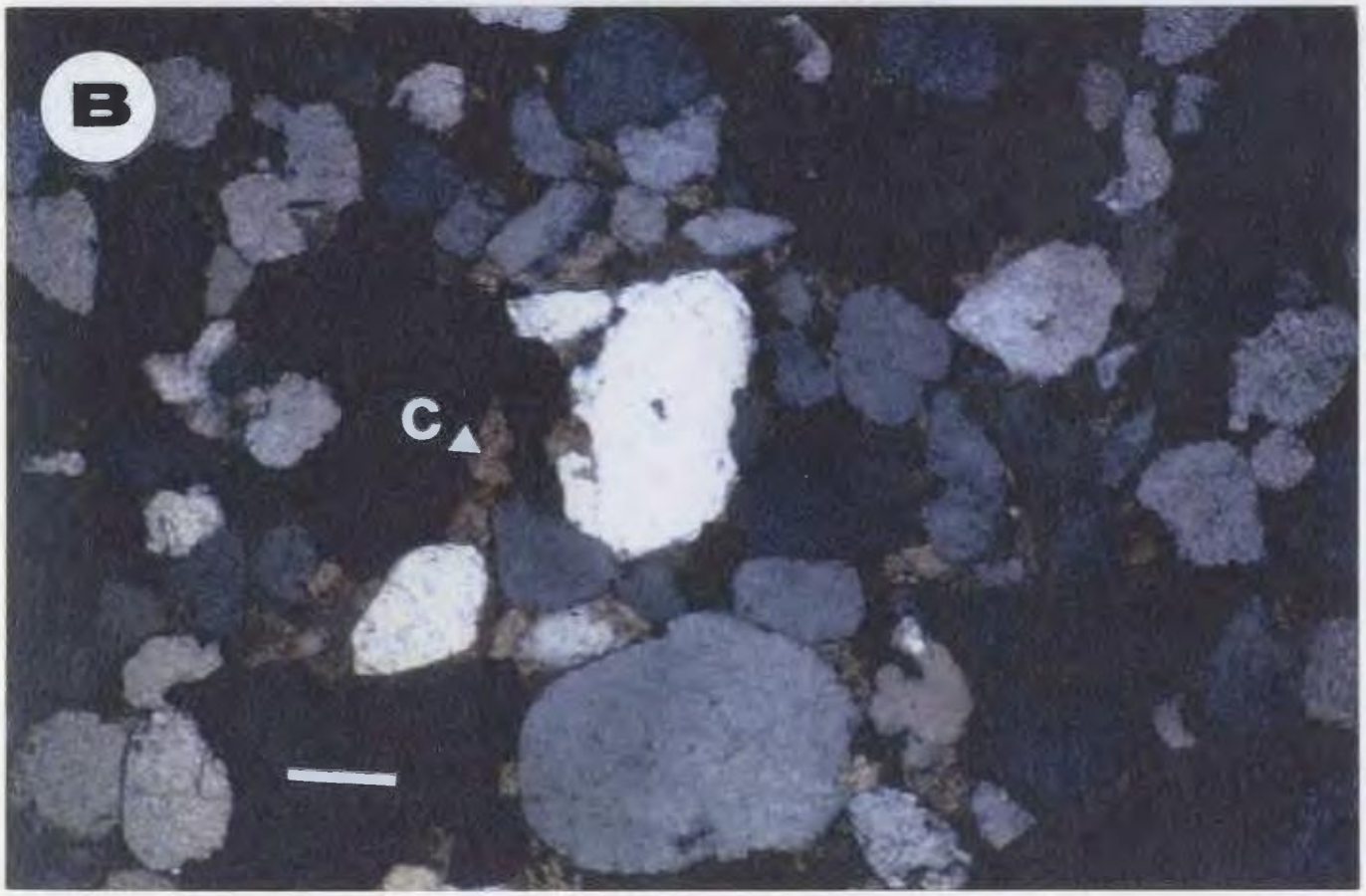

APPENDIX V

THIN-SECTION DIAGENESIS AND POROSITY: PLATE 45

A- Thin-section photograph shows partial dissolution of feldspar grain (possiblyplagioclase feldspar, PF) forming dissolution porosity (P) in the fluvial sandstone unit (Af5), well C1-61 @ 2293 m. (7522 ft.). Note partial shallow calcite cement (C) and iron-oxides remnants occluded pore-spaces. Scale bar = 0.1mm.

(PPL)

B- Same as previous photo but with (XPL).

APPENDIX V
THIN-SECTION DIAGENESIS AND POROSITY: PLATE 45

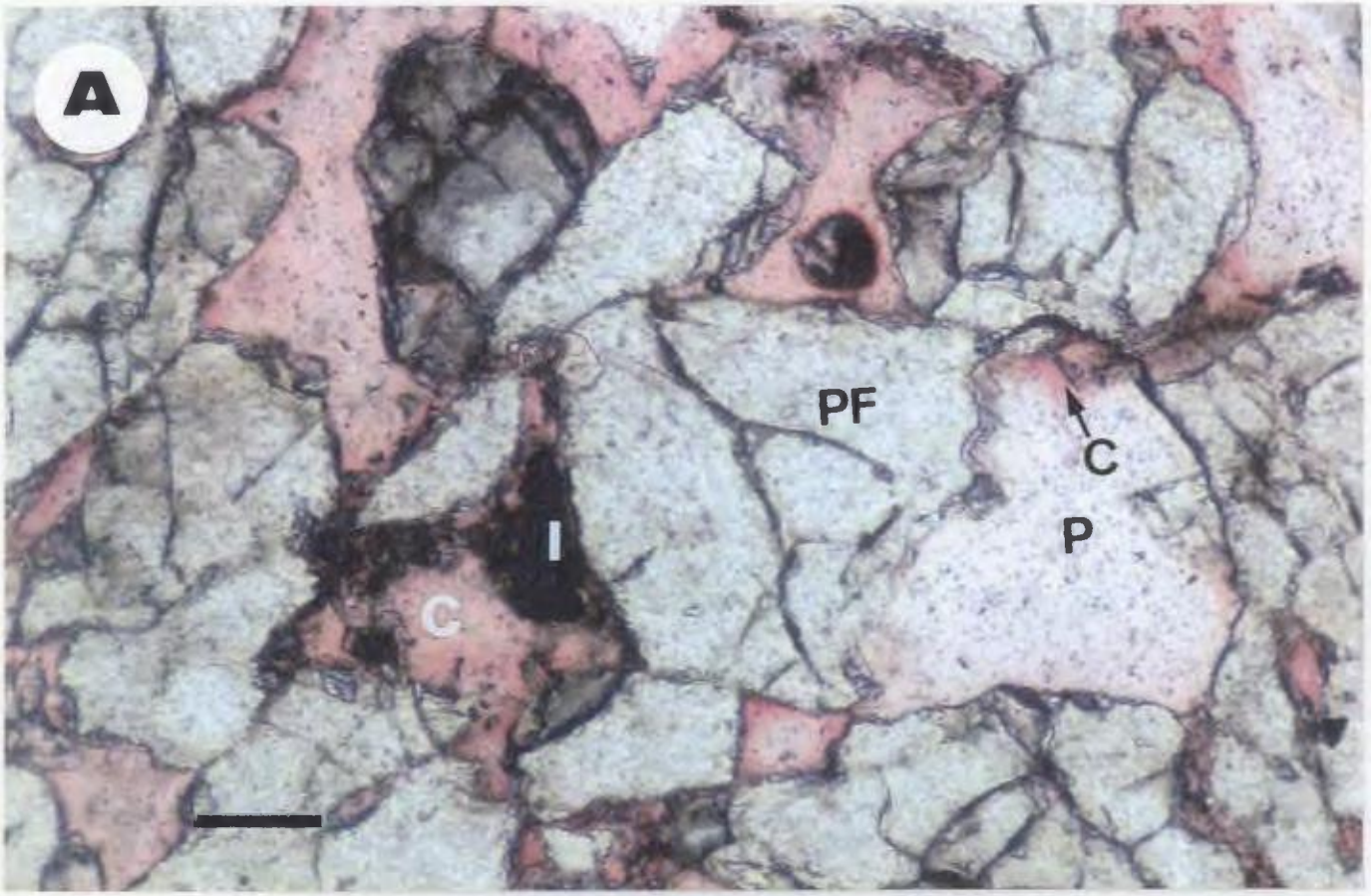

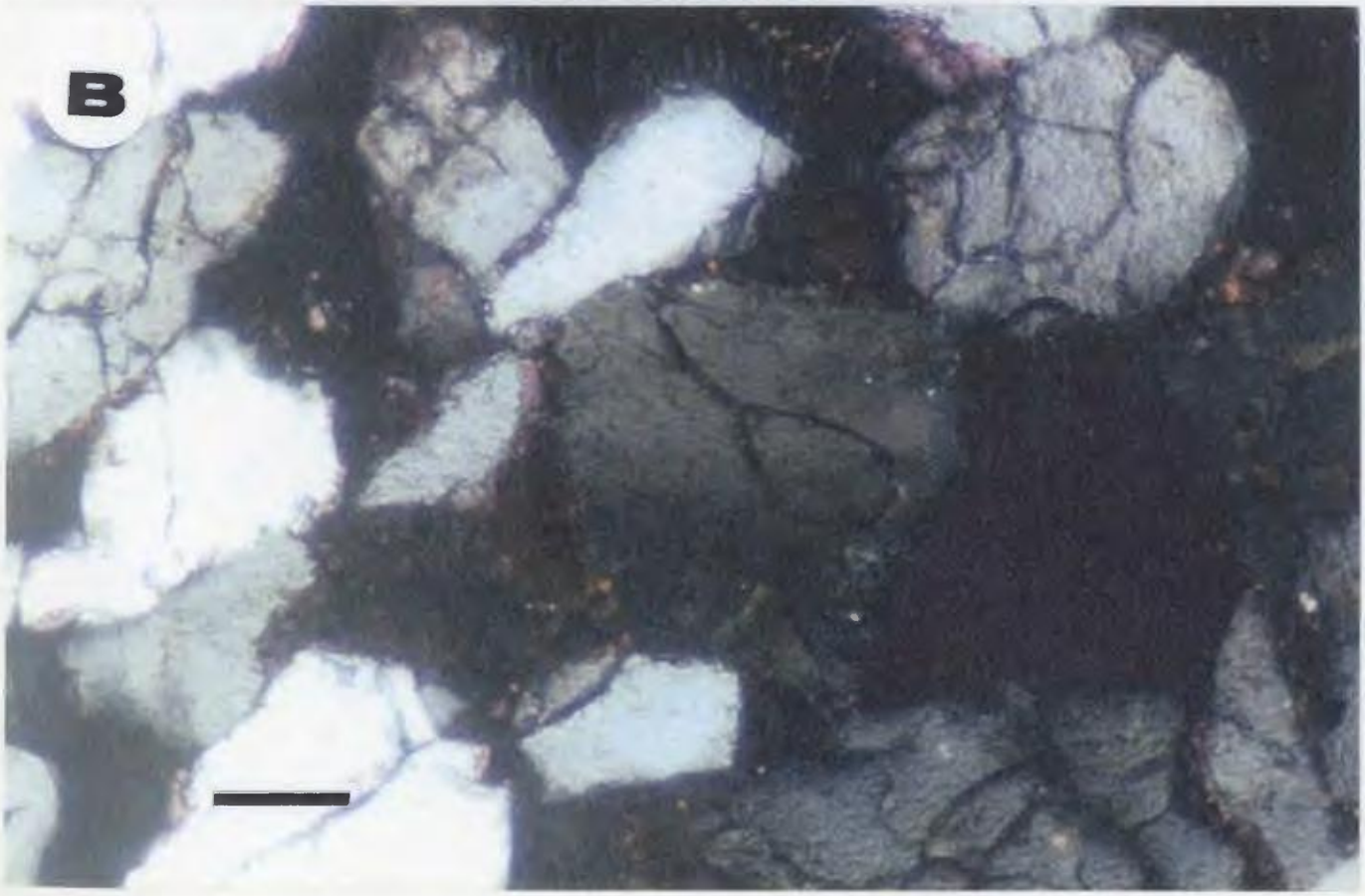

APPENDIX V

THIN-SECTION DIAGENESIS AND POROSITY: PLATE 46

A- Partially hematitic grain coatings (I) surrounding quartz grains (Q) were partially removed by moving fluids at an advanced stage in its diagenetic sequence. Fluvial sandstone unit (Af3), well EE1-NC7A @ 2686 m. (8810 ft.). Note pendant crystals of quartz-overgrowth (O) on top of pore (P). Also note shallow calcite cement (C) and ferroan-dolomite cement (D) are partially filling pore-spaces. Scale bar = 0.1mm.

(PPL)

B- Ferroan-dolomite cement (D) of rhombic outlines and rooted in quartz grain (Q) surfaces and filling partially primary pore-spaces (P). Fluvial sandstone unit (Af3), well EE1-NC7A @ 2687 m. (8812 ft.). Scale bar = 0.1mm.

(PPL)

APPENDIX V
THIN-SECTION DIAGENESIS AND POROSITY: PLATE 46

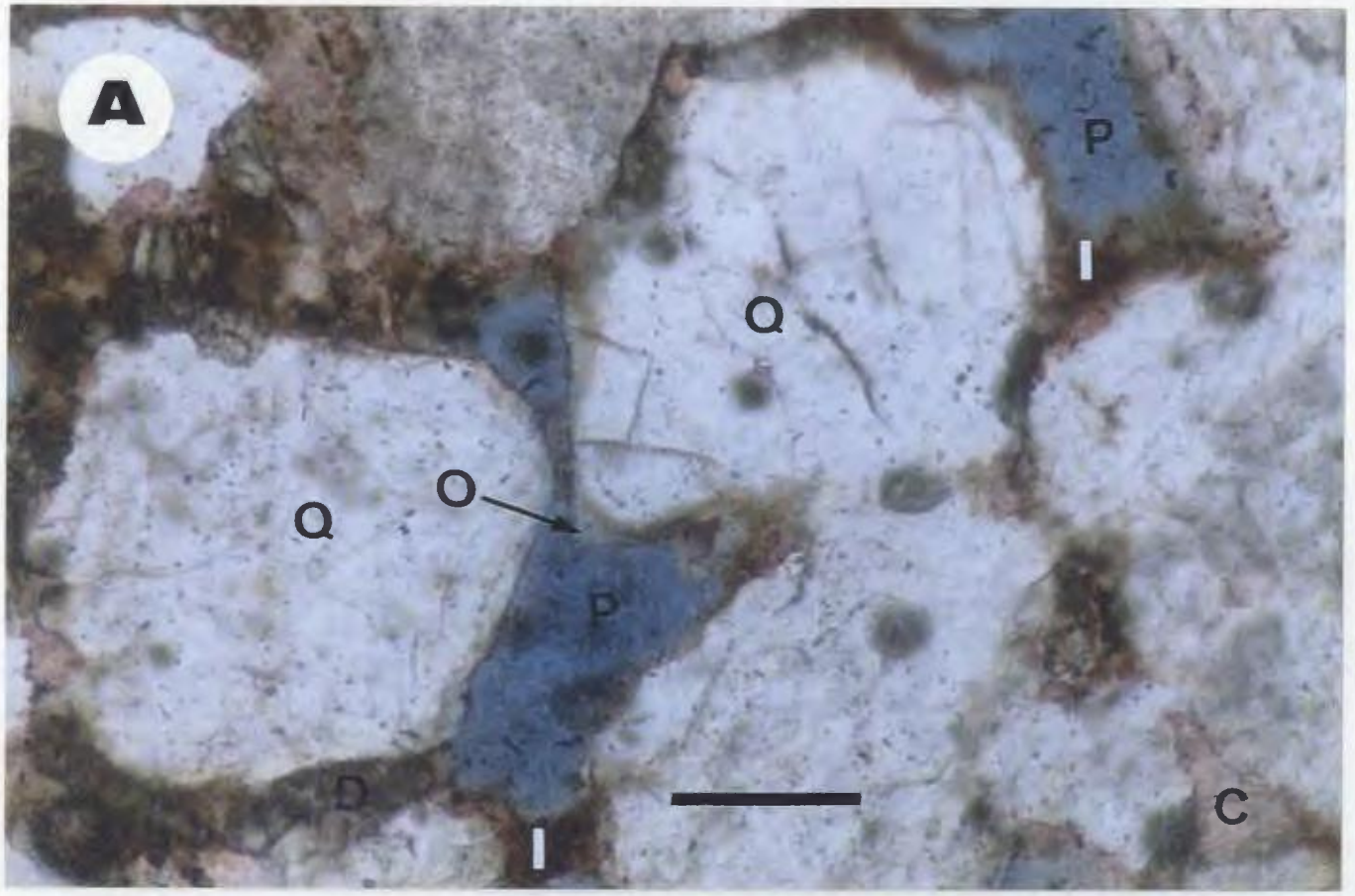

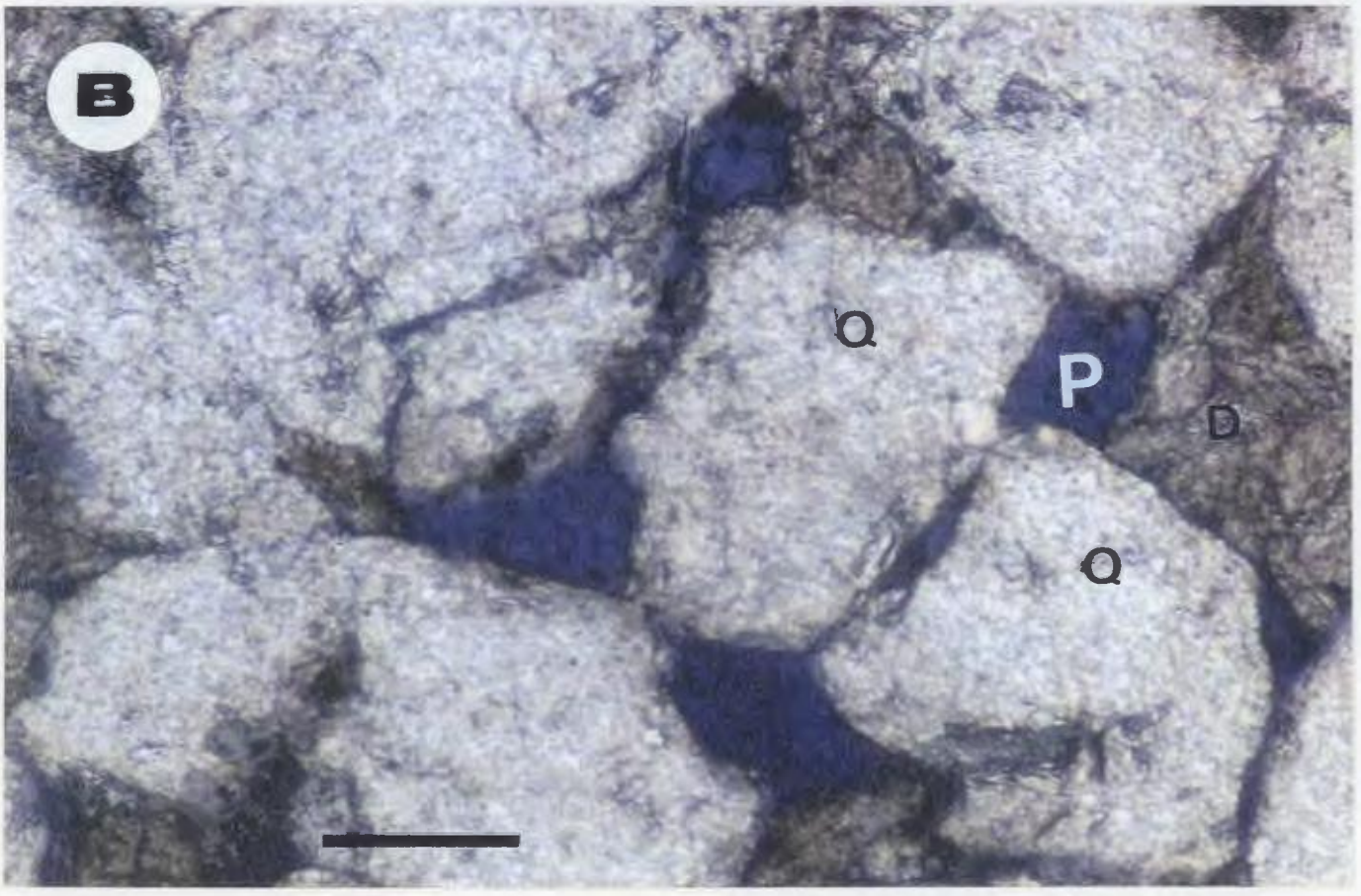

APPENDIX V

THIN-SECTION DIAGENESIS AND POROSITY: PLATE 47

A- Ferroan-dolomite cement (D), unstained, and of high relief rhombic outlines, partially rimming quartz grains (Q, arrows) or replacing calcite cement (C) and filling partially pore-spaces. Note pink stained calcite cement (C) of piokilotopic texture filling totally pore spaces. Reworked marine sandstone unit (Am), well B3-61 @ 2670 m. (8756 ft.). Scale bar = 0.1mm.

(PPL)

APPENDIX V
THIN-SECTION DIAGENESIS AND POROSITY: PLATE 47

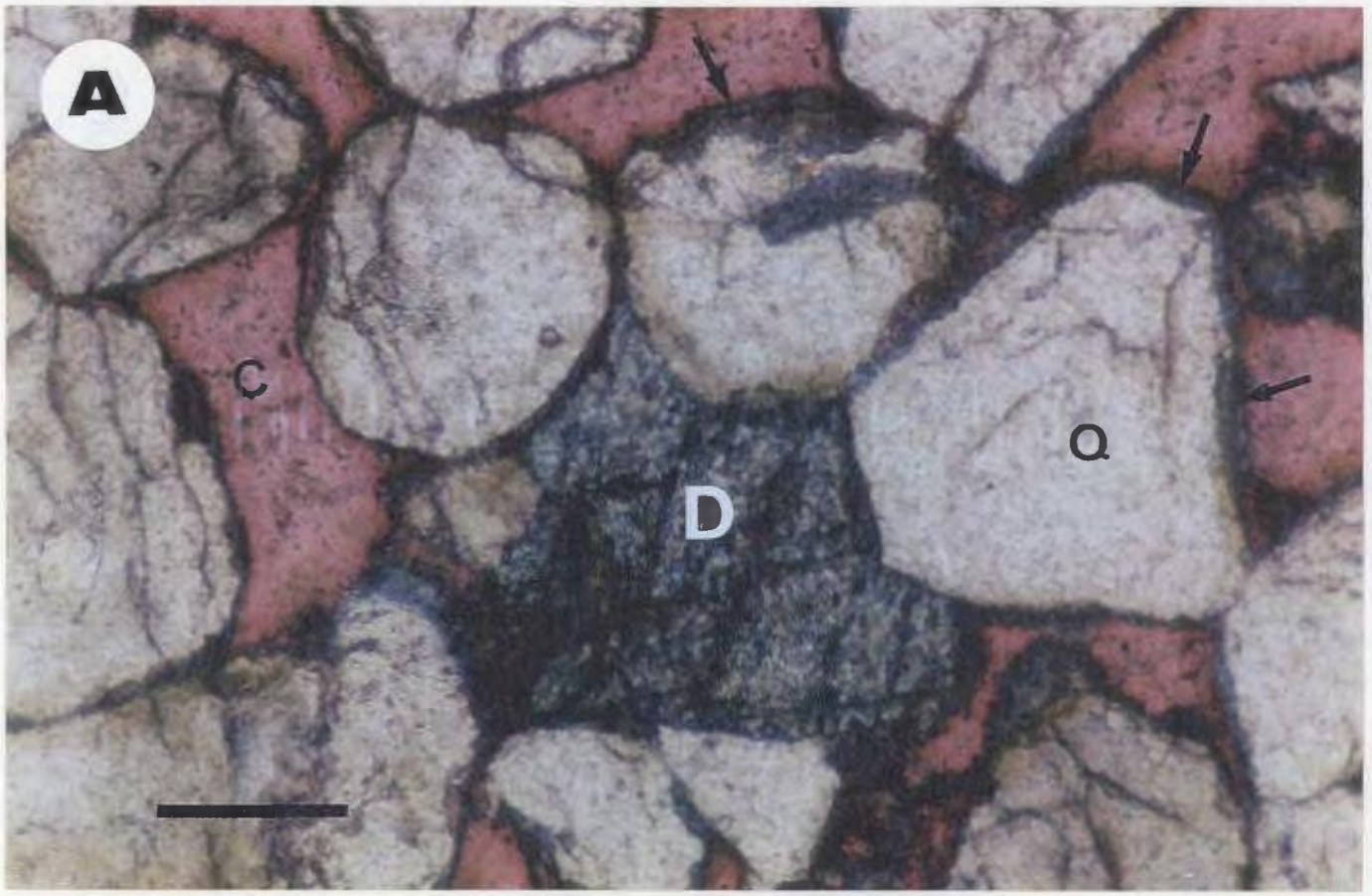

APPENDIX V

THIN-SECTION DIAGENESIS AND POROSITY: PLATE 48

A,B- Triangular shaped primary porosity (P) between uncorroded quartz grains (Q) in fluvial sandstone units (Af3) of well CC1-NC7A @ 2750 m. (9020 ft.), and of well Z1-NC100 @ 3561 m. (11680 ft.) respectively. Scale bar = 0.1mm.

(PPL)

APPENDIX V
THIN-SECTION DIAGENESIS AND POROSITY: PLATE 48

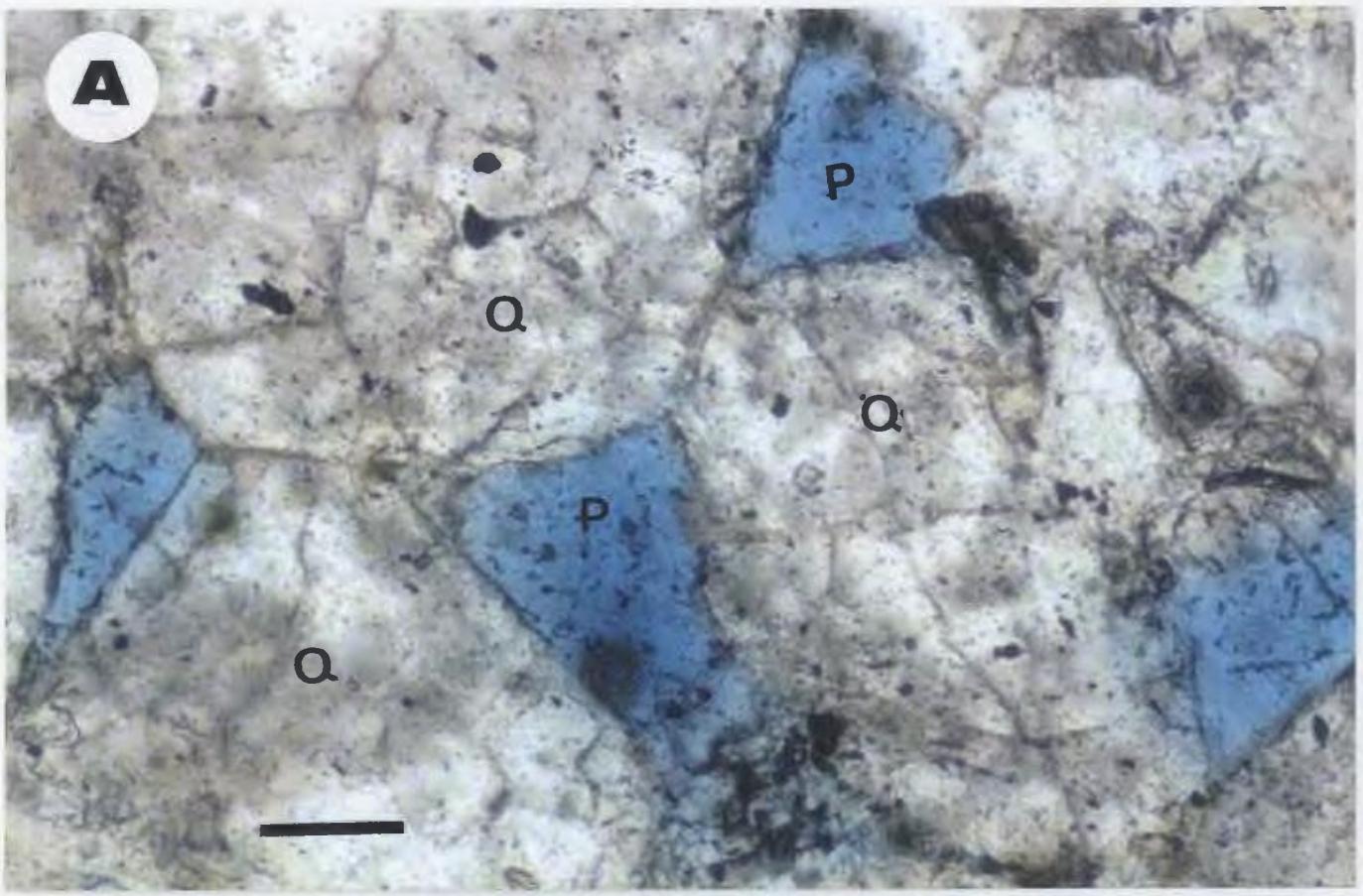

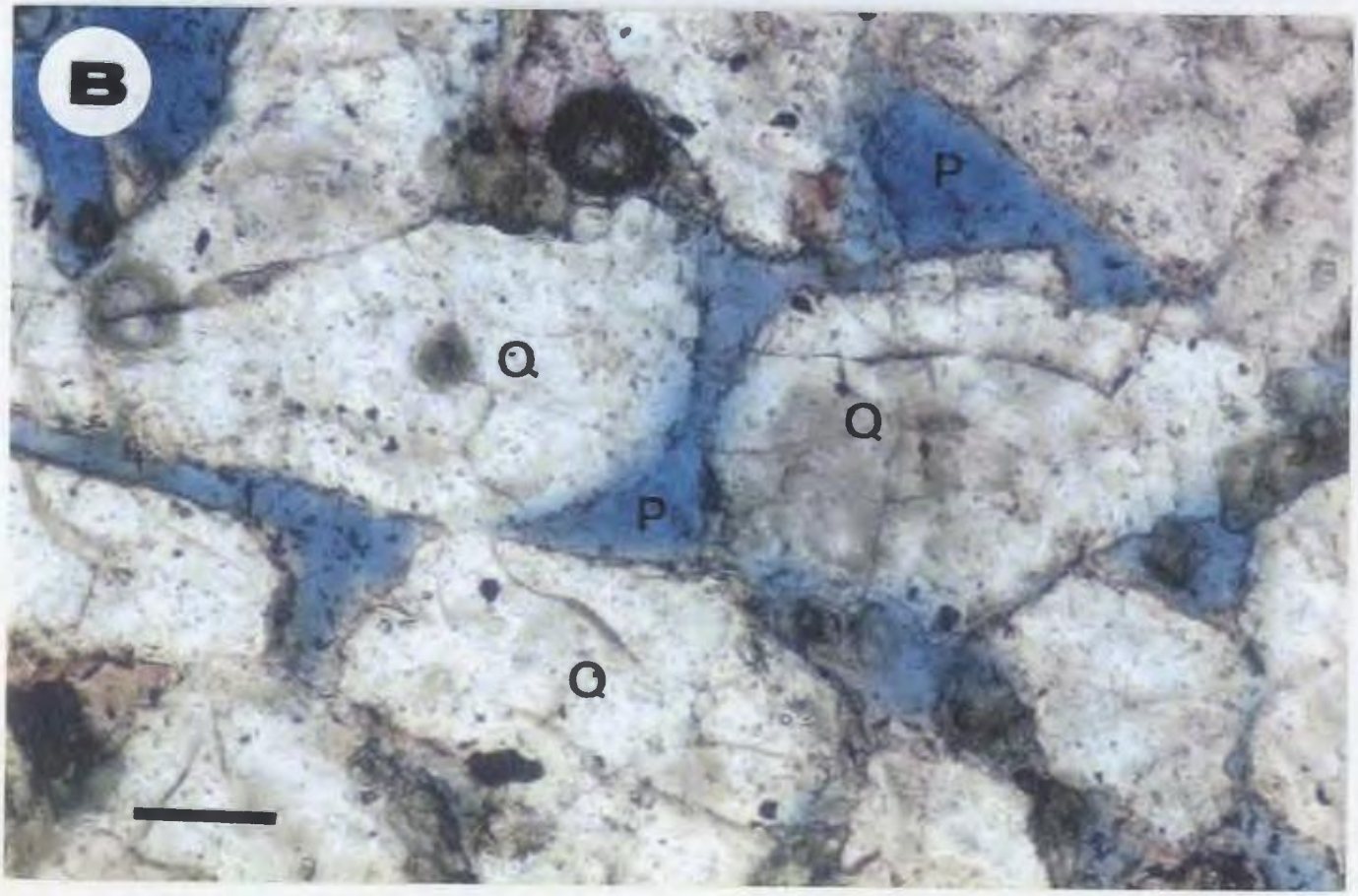

APPENDIX V

THIN-SECTION DIAGENESIS AND POROSITY: PLATE 49

A- Preserved primary porosity (P) of different angular shapes between uncorroded quartz grains (Q). Note the loose of packing in this sample which suggests the early stage of compaction and quartz cementation through grain-to-grain contacts. Thin iron-oxides (I) coatings may some times surrounded pores and prevent further silica-cementation. Fluvial sandstone unit (Af4), well Z1-66 @ 2768.5 m (9081 ft.). Scale bar = 0.1mm.

(PPL)

B- Low magnification photo shows preserved intergranular primary porosity of angular shapes between uncorroded quartz grains (Q), which may suggesting a stage of an open system through which diagenetic fluids may pass easily and contact other sandstone units down-section (measured porosity = 17%). Fluvial sandstone unit (Af3), well Z1-NC100 @ 3561 m. (11680 ft.). Scale bar = 0.1mm.

(PPL)

APPENDIX V
THIN-SECTION DIAGENESIS AND POROSITY: PLATE 49

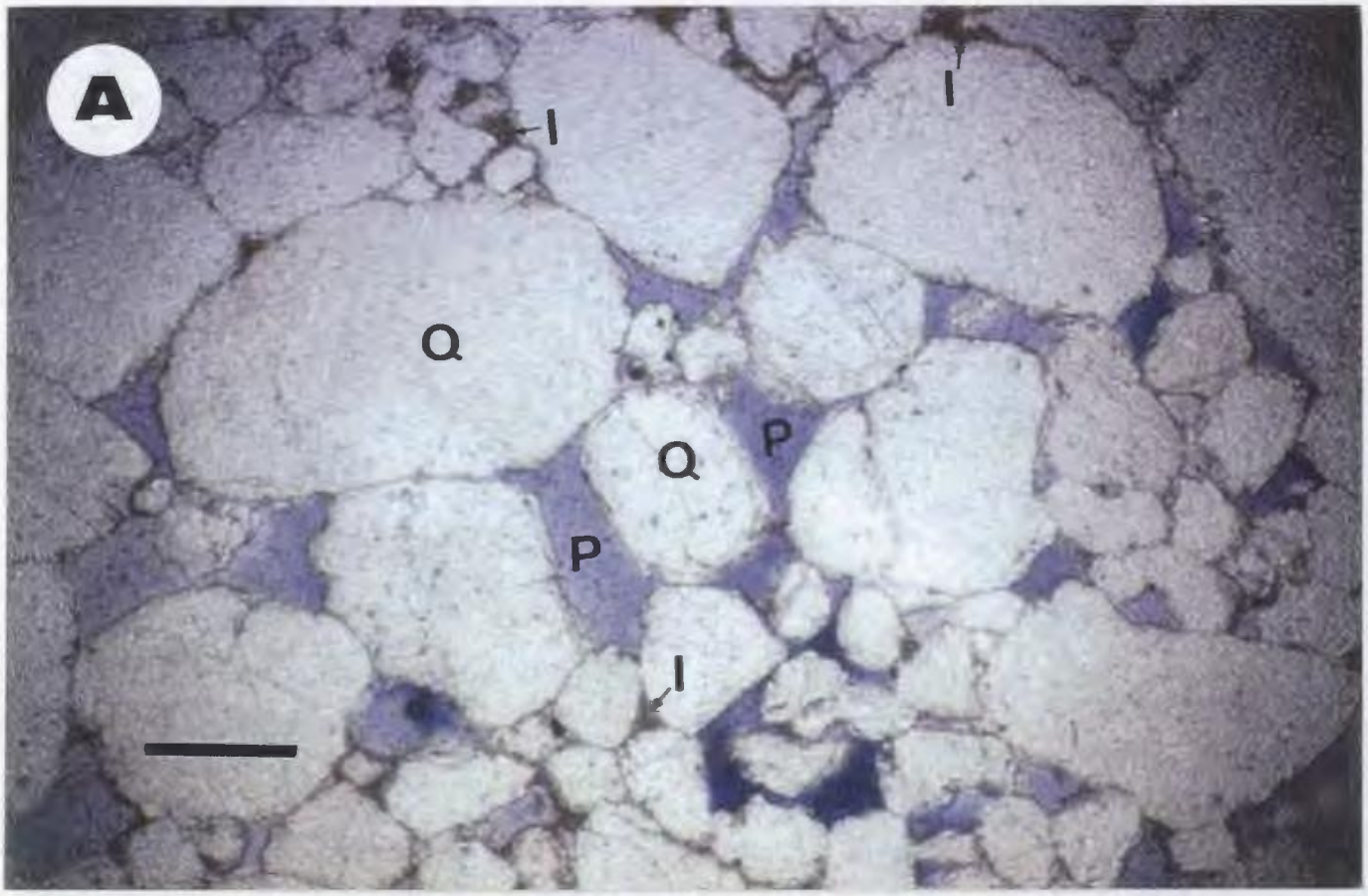

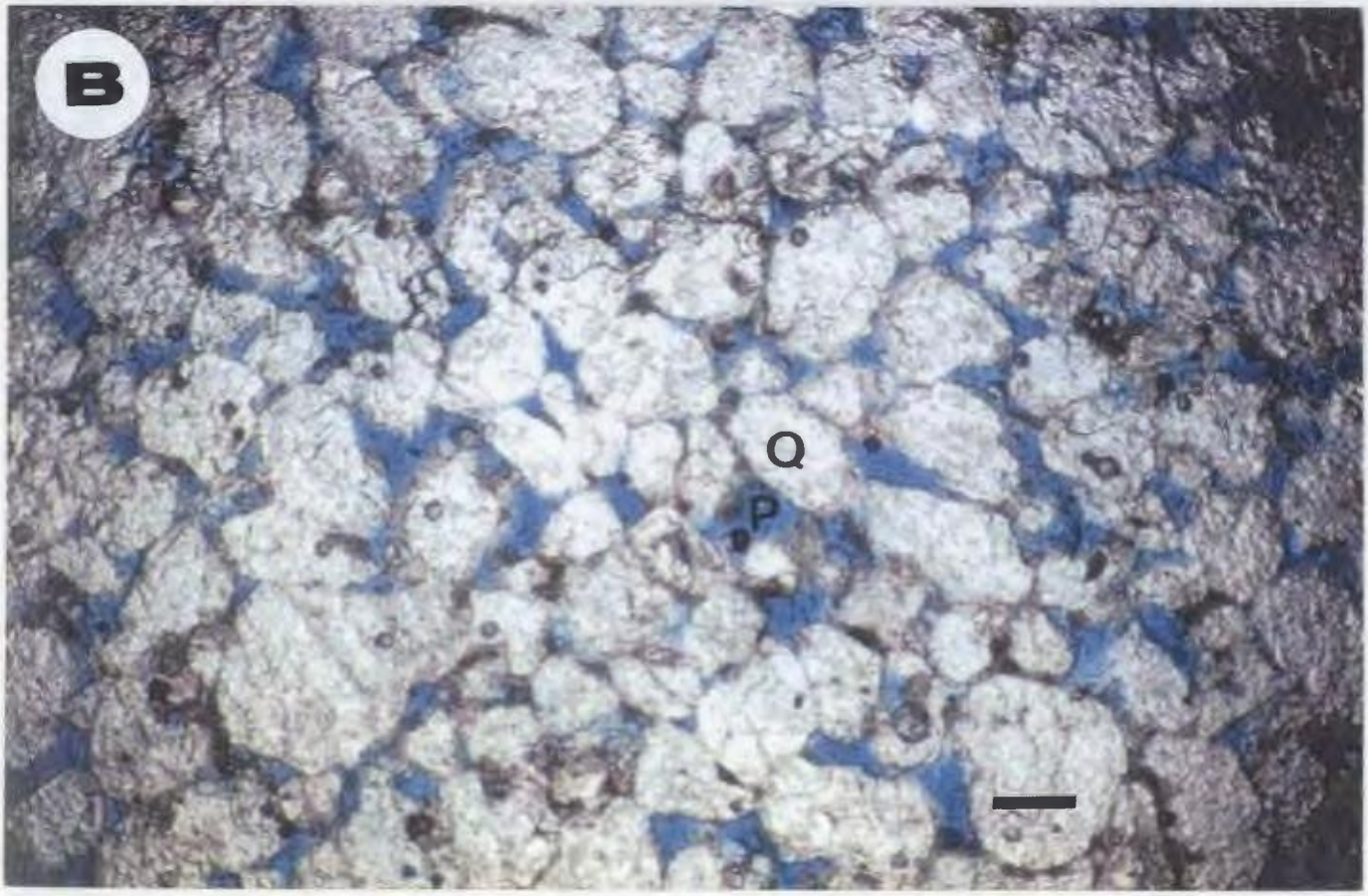

APPENDIX V

THIN-SECTION DIAGENESIS AND POROSITY: PLATE 50

A- Low magnification general view showing primary porosity (P), partial iron-oxides coatings (I), and dolomite cement (D) which may suggesting their time synchronous relationship in this sample. Fluvial sandstone unit (Af3), well EE1-NC7A @ 2687 m. (8812 ft.). Scale bar = 0.1mm.

(PPL)

APPENDIX V
THIN-SECTION DIAGENESIS AND POROSITY: PLATE 50

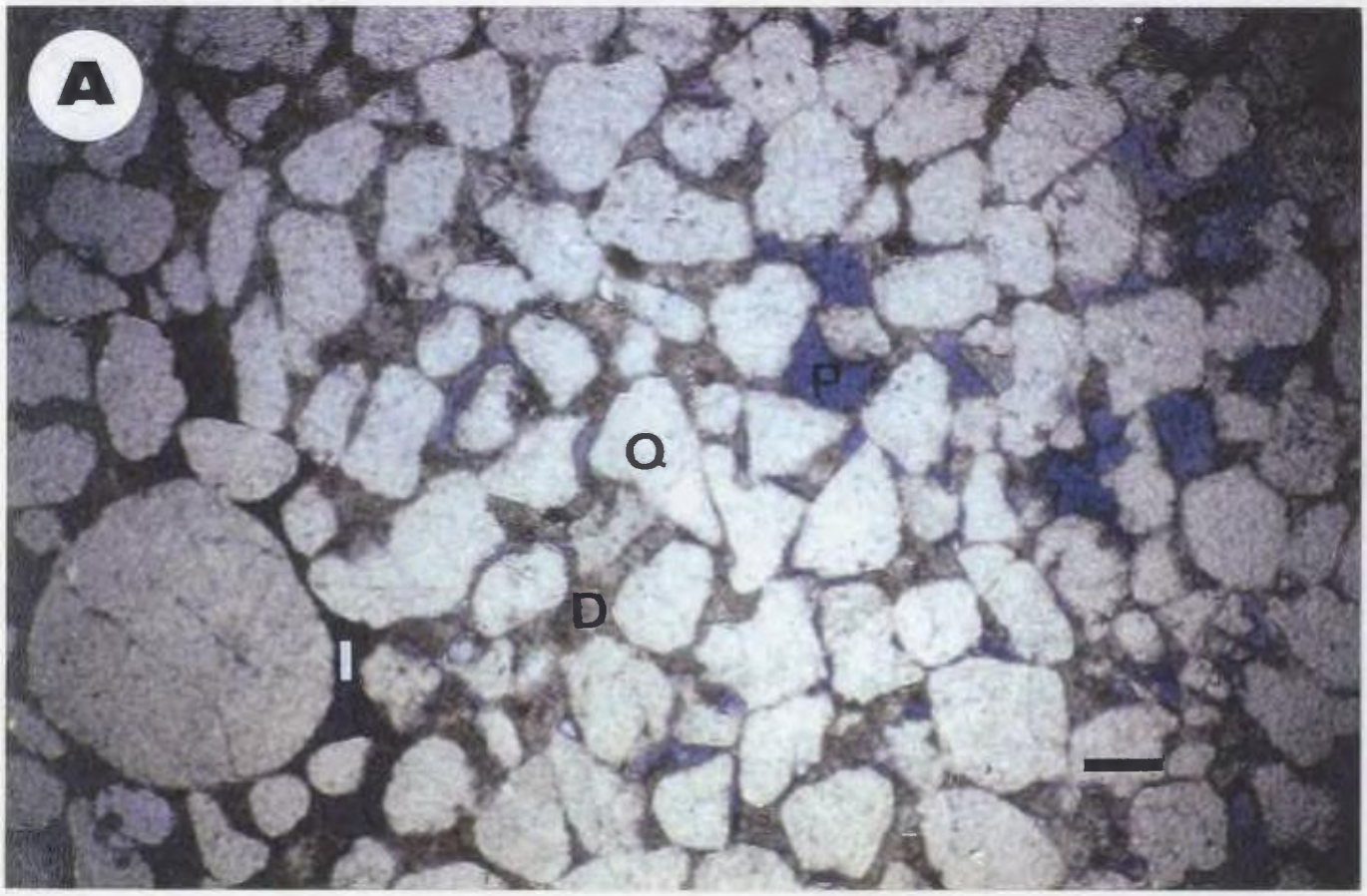

APPENDIX V

THIN-SECTION DIAGENESIS AND POROSITY: PLATE 51

A- Photograph shows oversized pores (P) resulted from total dissolution of calcite cement (remnants of calcite cement, C), and some dissolved grain framework (R). Note the corroded nature of quartz grains (Q) due to leaching calcite cement. Proximal delta front sandstone unit (A8), well C1-NC2 @ 2957 m. (9703 ft.). Scale bar = 0.1mm.

(PPL)

B- This photograph shows oversized pore (P) resulted from near total dissolution of calcite cement (C). Also you can see some floating grain remnants (R) in the pore. Proximal delta front sandstone unit (A12), well B3-61 @ 2711 m. (8893 ft.) (estimated measured porosity in this rock is about 16%). Scale bar = 0.1mm.

(PPL)

APPENDIX V
THIN-SECTION DIAGENESIS AND POROSITY: PLATE 51

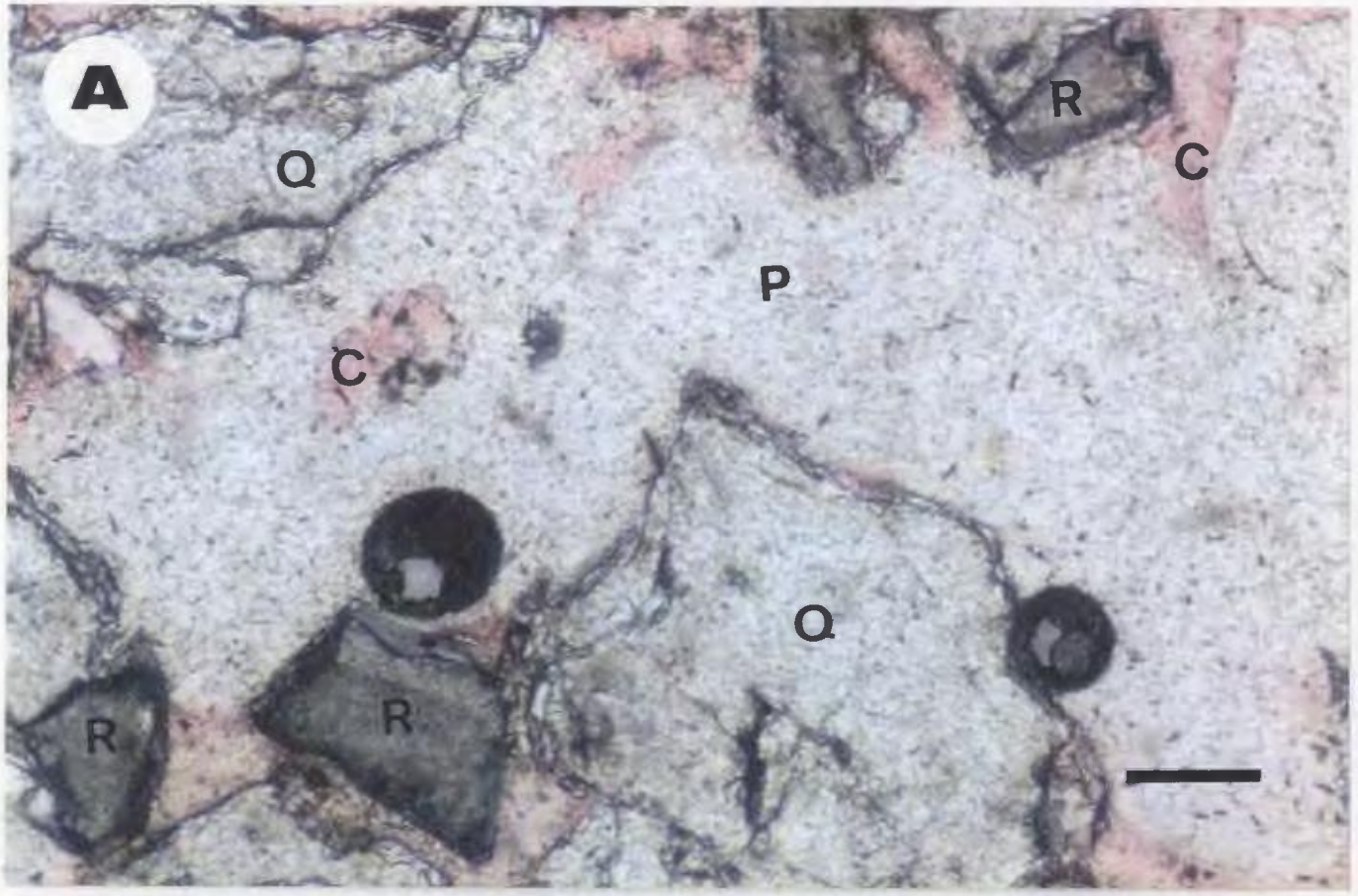

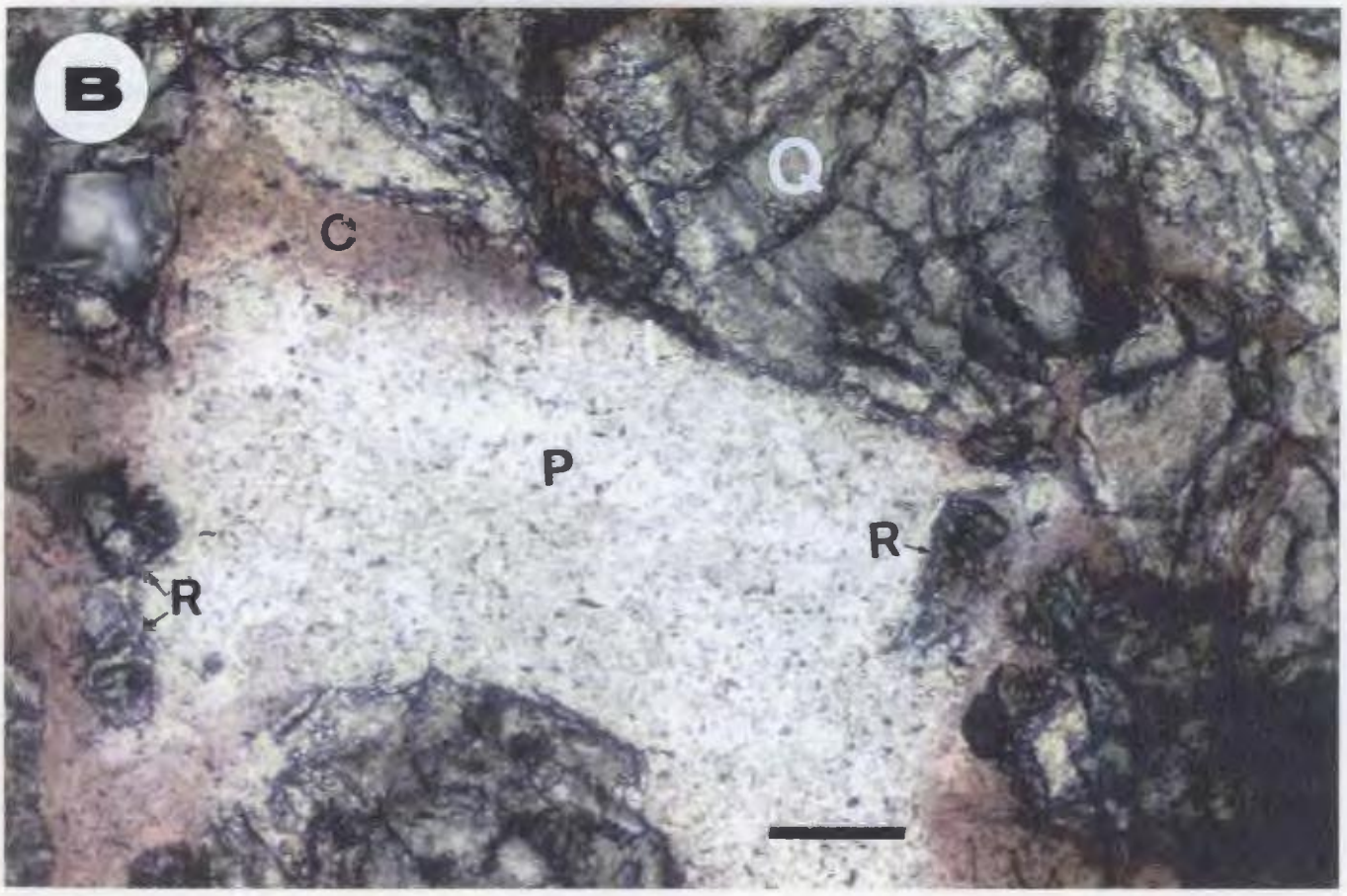

APPENDIX V

THIN-SECTION DIAGENESIS AND POROSITY: PLATE 52

A- Photograph shows oversized secondary pores (P) that may be resulted from total dissolution of unstable grains. Note the dissolved grain remnants (R) in pores, and surrounded quartz grains (Q) are heavily corroded. Proximal delta front sandstone unit (A8), well C1-NC2 @ 2965 m. (9725 ft.). Scale bar = 0.1mm.

(PPL)

APPENDIX V
THIN-SECTION DIAGENESIS AND POROSITY: PLATE 52

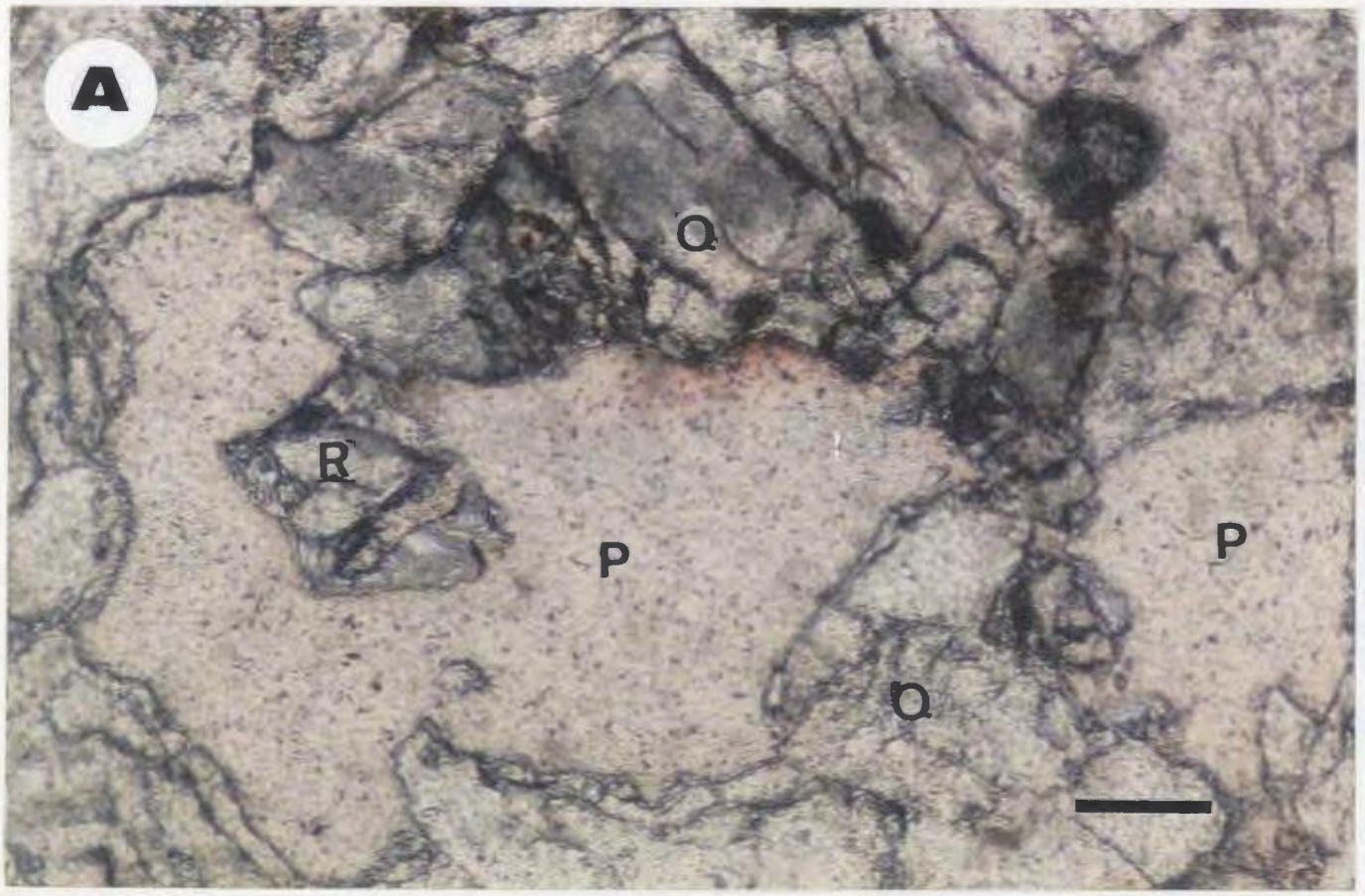

APPENDIX V

THIN-SECTION DIAGENESIS AND POROSITY: PLATE 53

A- Photograph shows secondary porosity (P) that resulted from partial dissolution of unstable plagioclase feldspar grain (PF). Note remnant of non-dissolved parts of feldspar grain can easily be seen inside the pore. Proximal delta front sandstone unit (A12), well B3-61 @ 2711 m. (8893 ft.). Scale bar = 0.1mm.

(PPL)

B- Same view but with (XPL), black area represents pore space (P), with remnants of dolomite cement (D).

APPENDIX V
THIN-SECTION DIAGENESIS AND POROSITY: PLATE 53

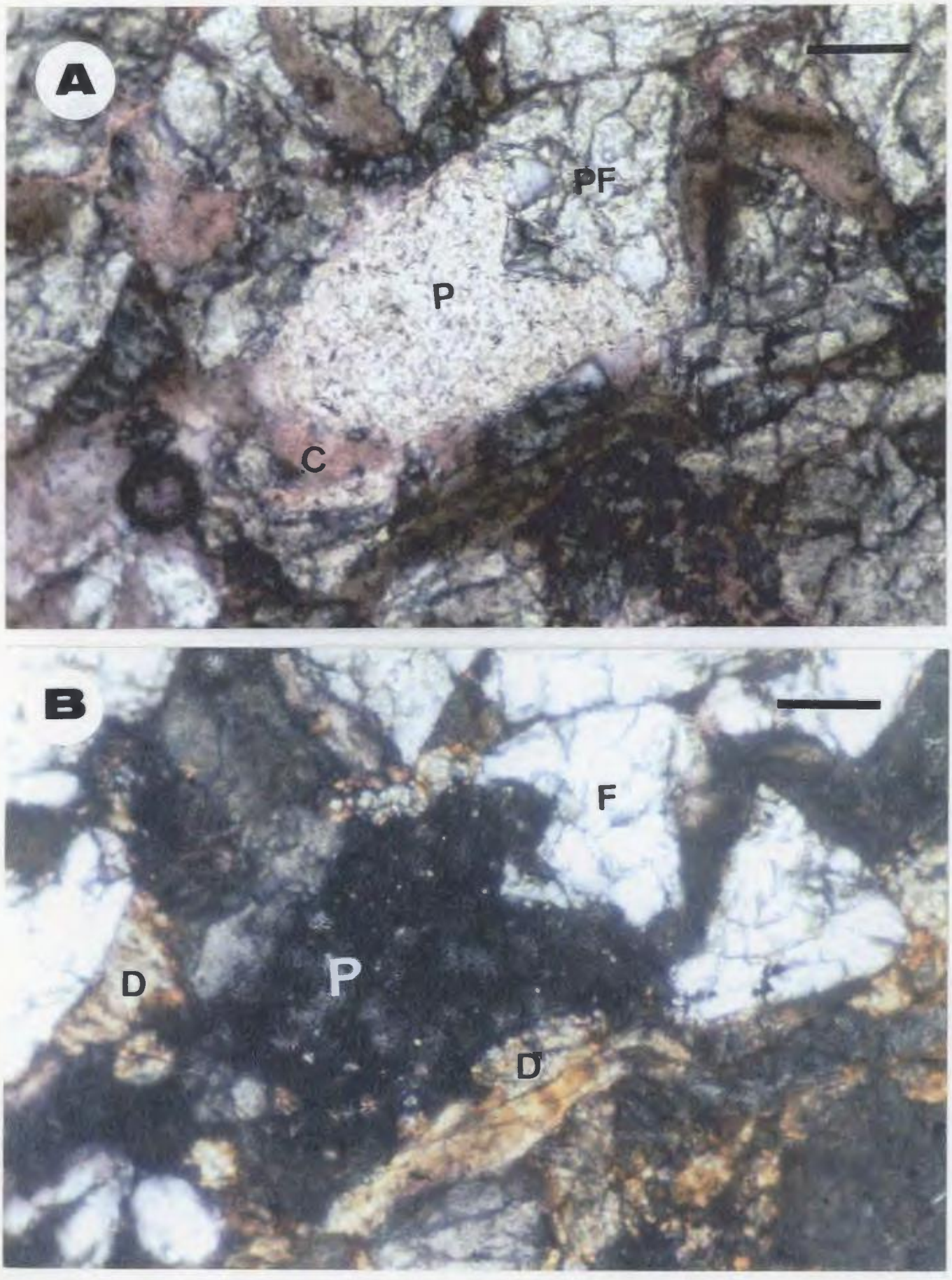

APPENDIX V

THIN-SECTION DIAGENESIS AND POROSITY: PLATE 54

A- Secondary porosity (P) resulted from partial dissolution of feldspar grain (probably plagioclase feldspar, PF). Note the high corroded edges of feldspar grain by calcite cement (C) with its remnant partially filling the pore (also note that partial calcite cement dissolution can also be seen at central top part of the photo and along the left side of the dissolved feldspar grain. Proximal delta front sandstone unit (A8), well C1-NC2 @ 2958 m. (9703 ft.). Scale bar = 0.1mm.

(PPL)

B- Same as previous photo but with (XPL).

APPENDIX V
THIN-SECTION DIAGENESIS AND POROSITY: PLATE 54

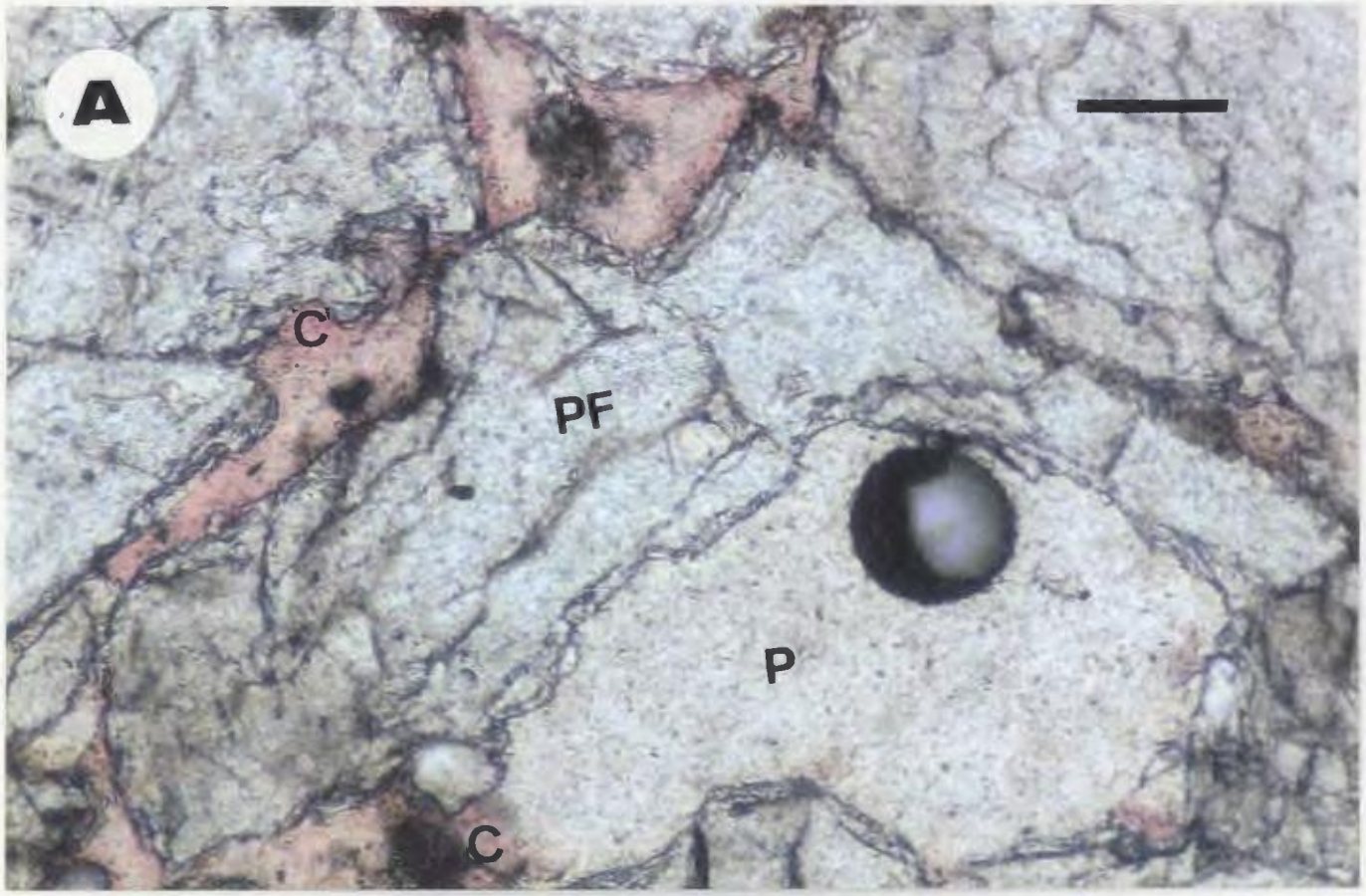

APPENDIX V

THIN-SECTION DIAGENESIS AND POROSITY: PLATE 55

A- Photograph shows elongate to oversized pores (P) resulted from total dissolution of feldspar grain (probably plagioclase feldspar, PF), see also some feldspar grain remnant inside and surrounding the pore (arrow). Proximal delta front sandstone unit (A12), well E1-NC2 @ 2900 m. (9512 ft.). Scale bar = 0.1mm.

(PPL)

B- Same as previous photo but with (XPL). Note speckled areas in (PPL) photo which appear black in this XPL photo are pores probably filled with mounting medium.

APPENDIX V
THIN-SECTION DIAGENESIS AND POROSITY: PLATE 55

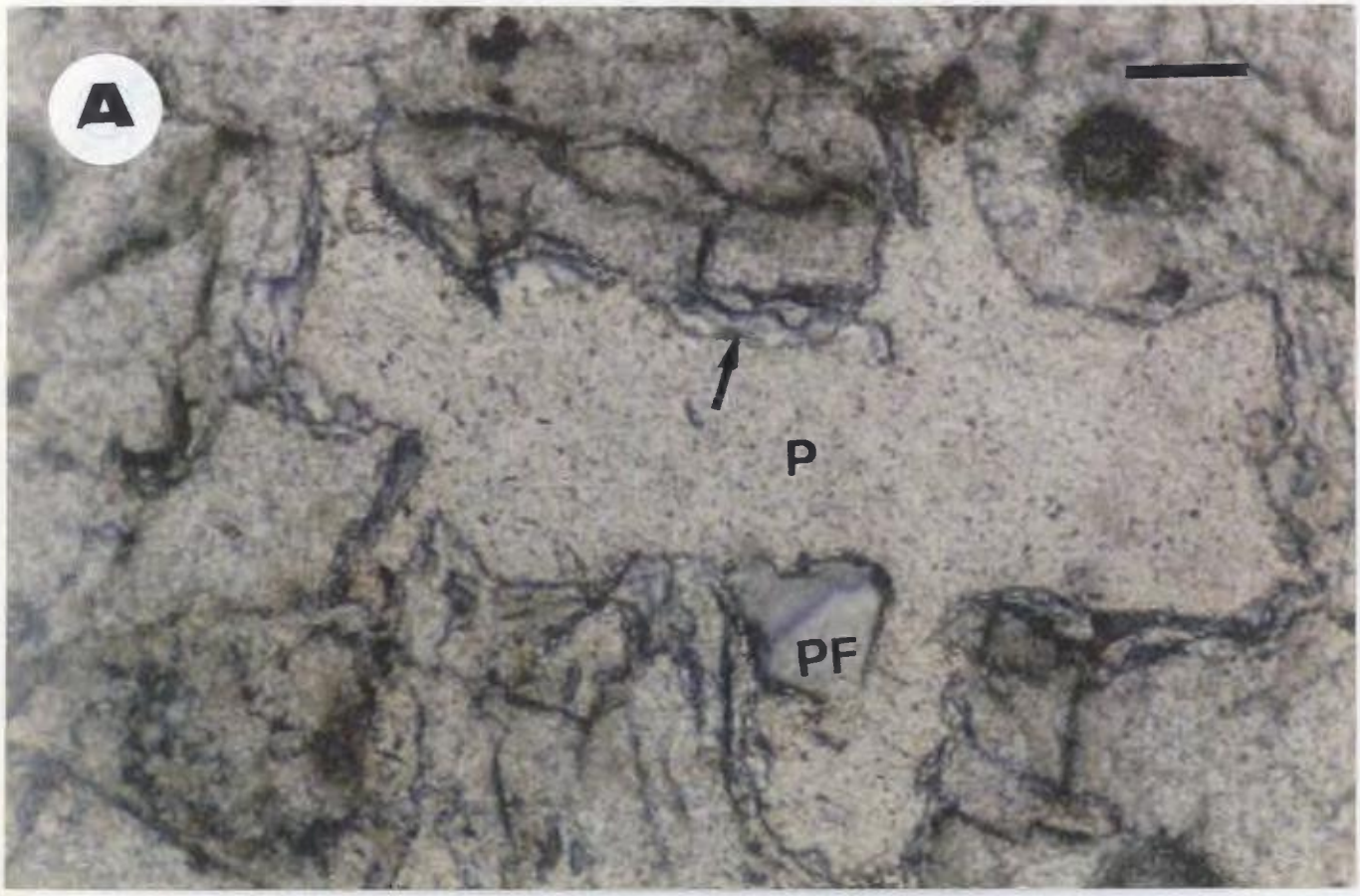

APPENDIX V

THIN-SECTION DIAGENESIS AND POROSITY: PLATE 56

A- Photograph shows elongated pore (P) resulted mainly from total dissolution of calcite cement (C) between quartz grains (Q) (remnant of calcite cement can be seen inside the pore). Proximal delta front sandstone unit (A14), well T1-23 @ 2577 m. (8454 ft.). Scale bar = 0.1mm.

(PPL)

B- Same as previous photo but with (XPL), black area represents pore-space.

APPENDIX V
THIN-SECTION DIAGENESIS AND POROSITY: PLATE 56

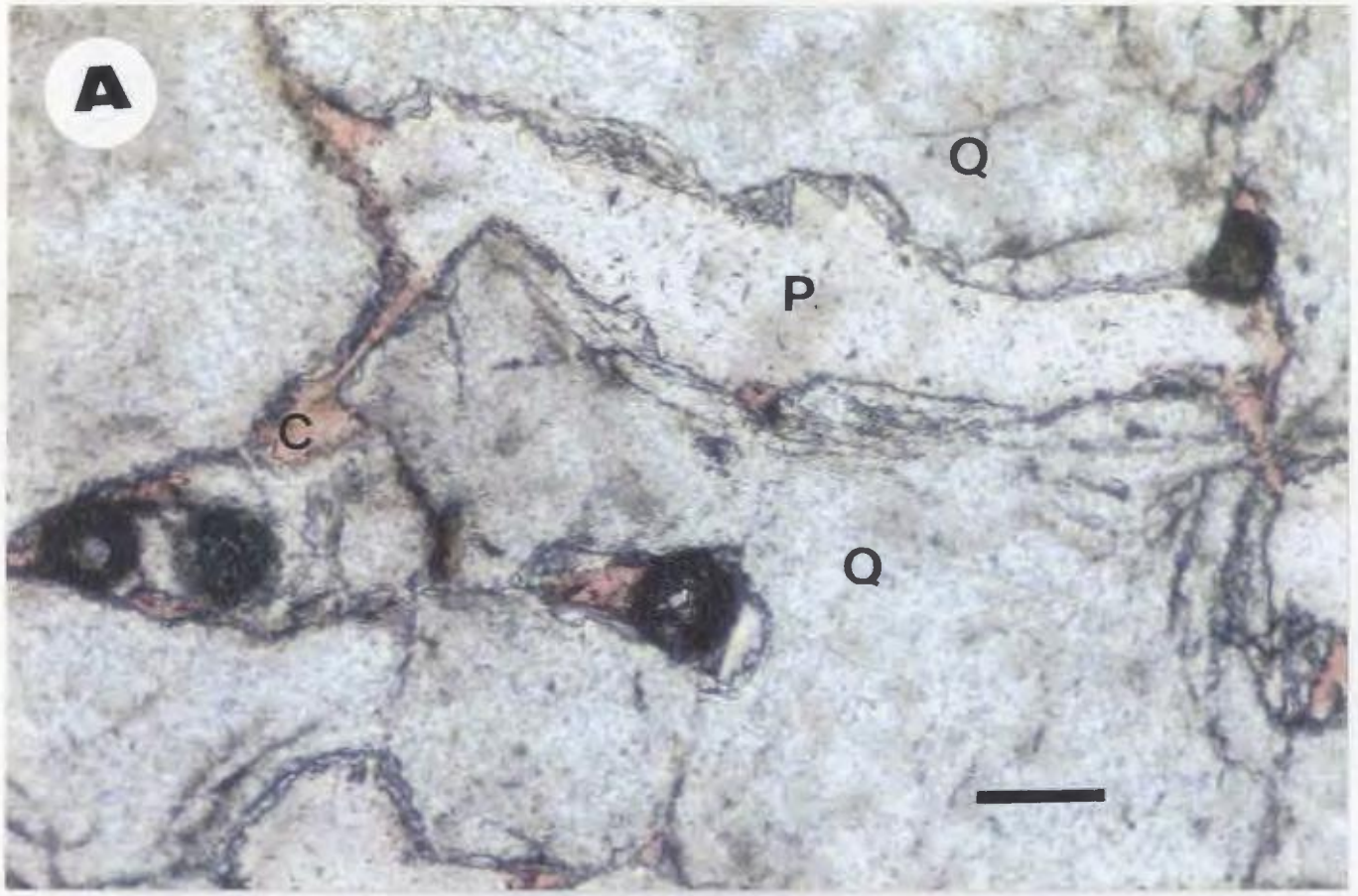

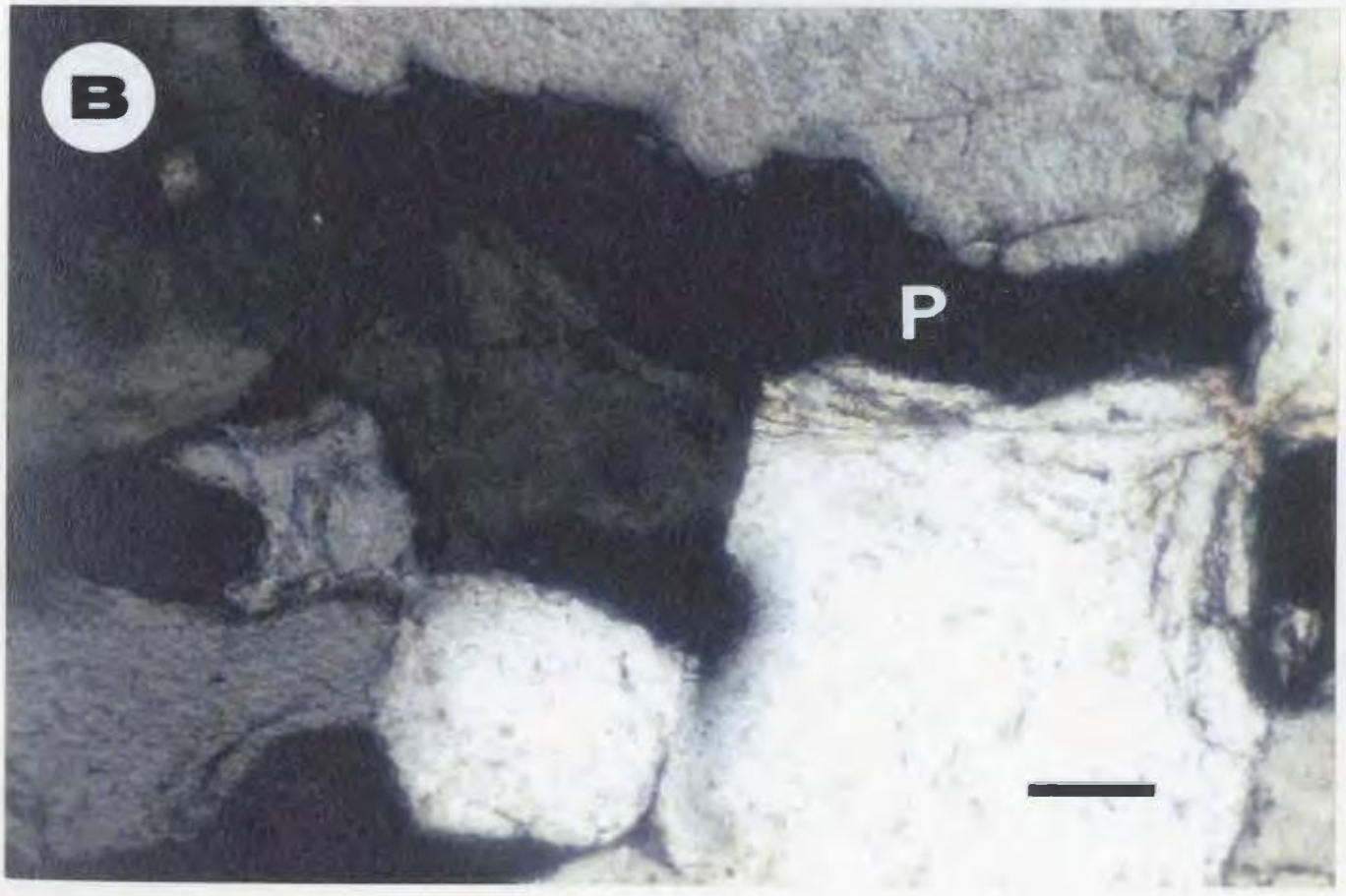

APPENDIX V

THIN-SECTION DIAGENESIS AND POROSITY: PLATE 57

A- Photograph shows elongate pore (P) (> 0.4mm) along the well packed quartz grains (Q). This pore resulted from almost total dissolution of calcite cement between quartz grains (note remnant of calcite cement (C) can easily be seen at some places inside the pore). Proximal delta front sandstone unit (A14), well B1-61 @ 2567 m. (8420 ft.) (estimated measured porosity is about 19%). Scale bar = 0.1mm.

(PPL)

B- Same as previous photo but with (XPL), black area represents secondary porosity.

APPENDIX V
THIN-SECTION DIAGENESIS AND POROSITY: PLATE 57

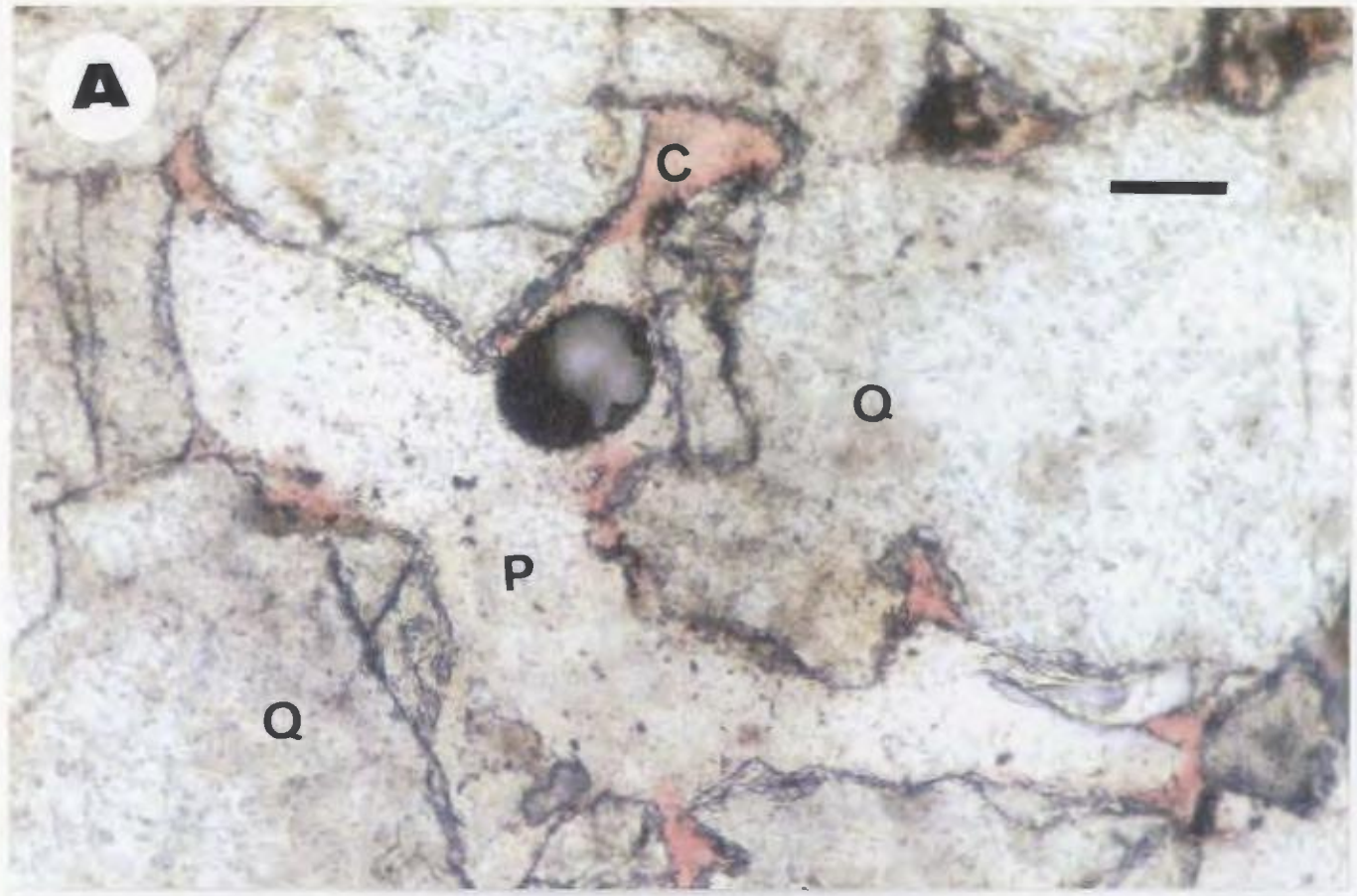

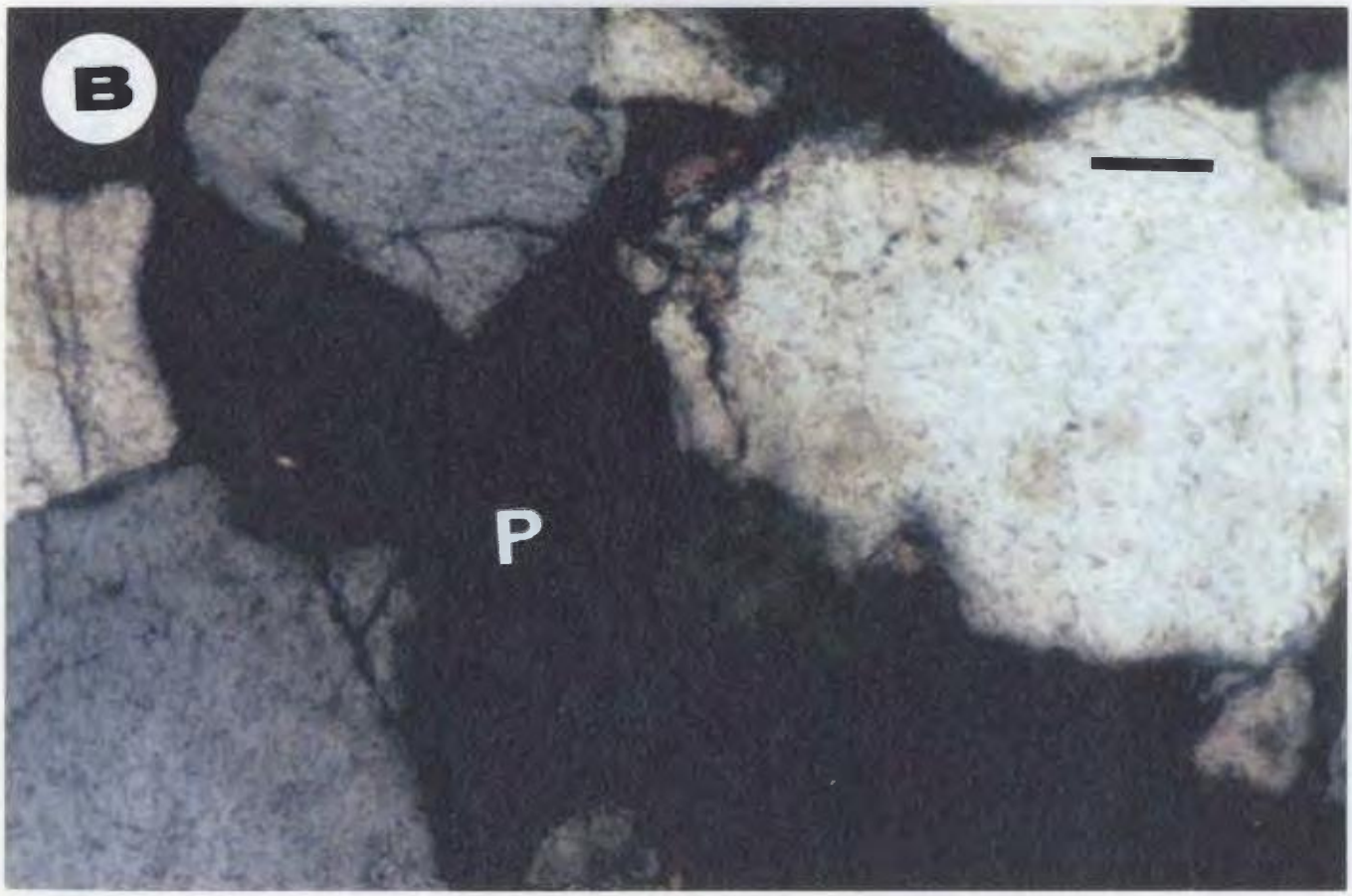

APPENDIX V

THIN-SECTION DIAGENESIS AND POROSITY: PLATE 58

A- Photograph shows recognizable moldic porosity (P) between quartz grains (Q) originated possibly from total dissolved unstable grains (remnant of the dissolved grain can be seen at some places around the pore, arrow), Dolomite cement (D) of rhombic outlines also present in this sample. Estimated measured porosity is about 14%. Proximal delta front sandstone unit (A12), well B3-61 @ 2734 m. (8969 ft.). Scale bar = 0.1mm.

(PPL)

B- Same as previous photo with (XPL). Note speckled area in the (PPL) view which appears to be black in this (XPL) view is pore may be filled with mounting medium.

APPENDIX V
THIN-SECTION DIAGENESIS AND POROSITY: PLATE 58

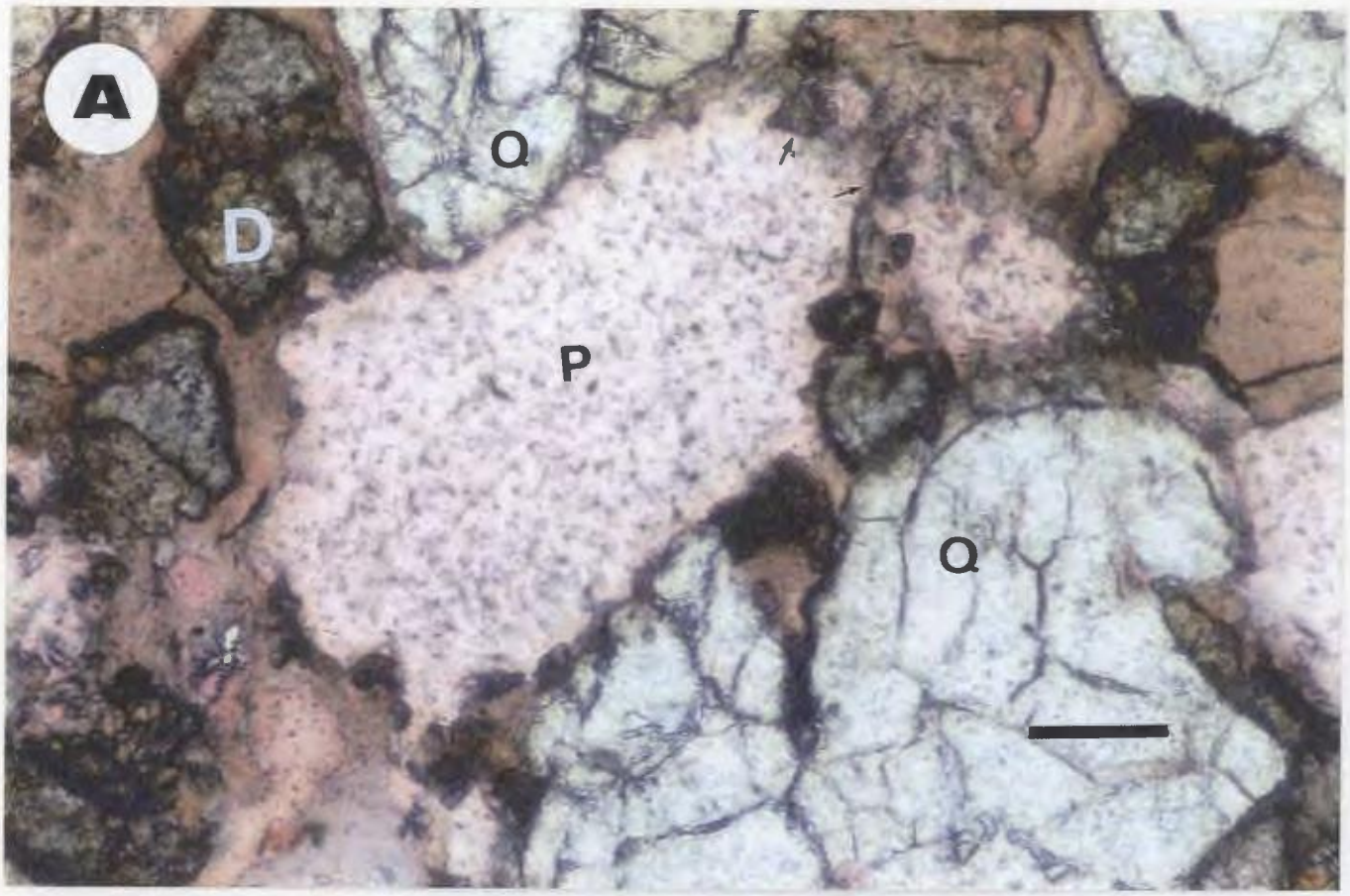

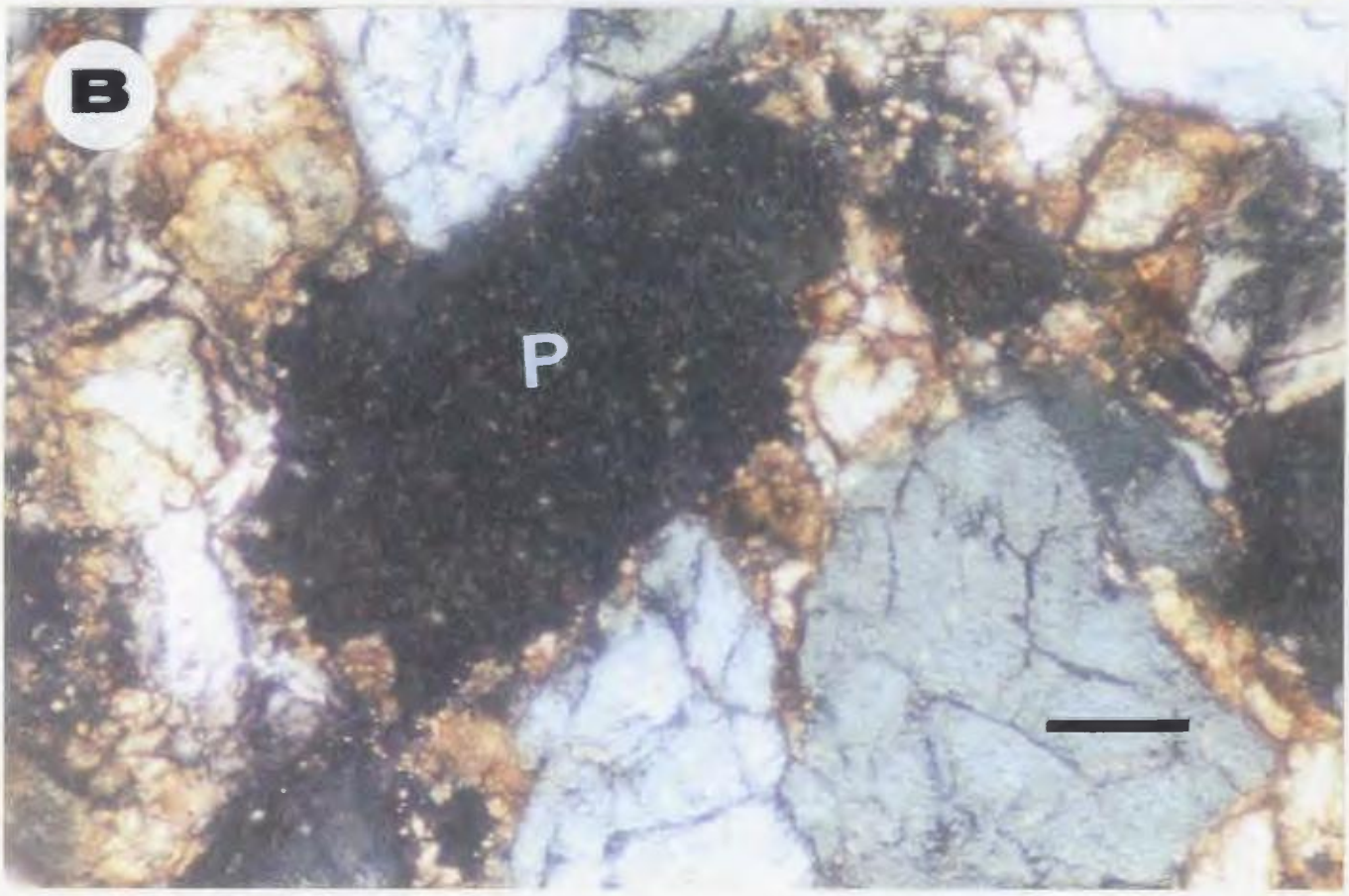

APPENDIX V

THIN-SECTION DIAGENESIS AND POROSITY: PLATE 59

A- Photo shows secondary pore-spaces (P) resulted from partial dissolution of dolomite cement (D), note remnant of non-dissolved dolomite cement can be seen surrounding the pore (P). Proximal delta front sandstone unit (A14), well E1-NC2 @ 2784 m. (9131 ft.) (estimated measured porosity is about 22%). Scale bar = 0.1mm.

(PPL)

B- Same as previous photo but with (XPL) where dark area is secondary porosity (P).

APPENDIX V
THIN-SECTION DIAGENESIS AND POROSITY: PLATE 59

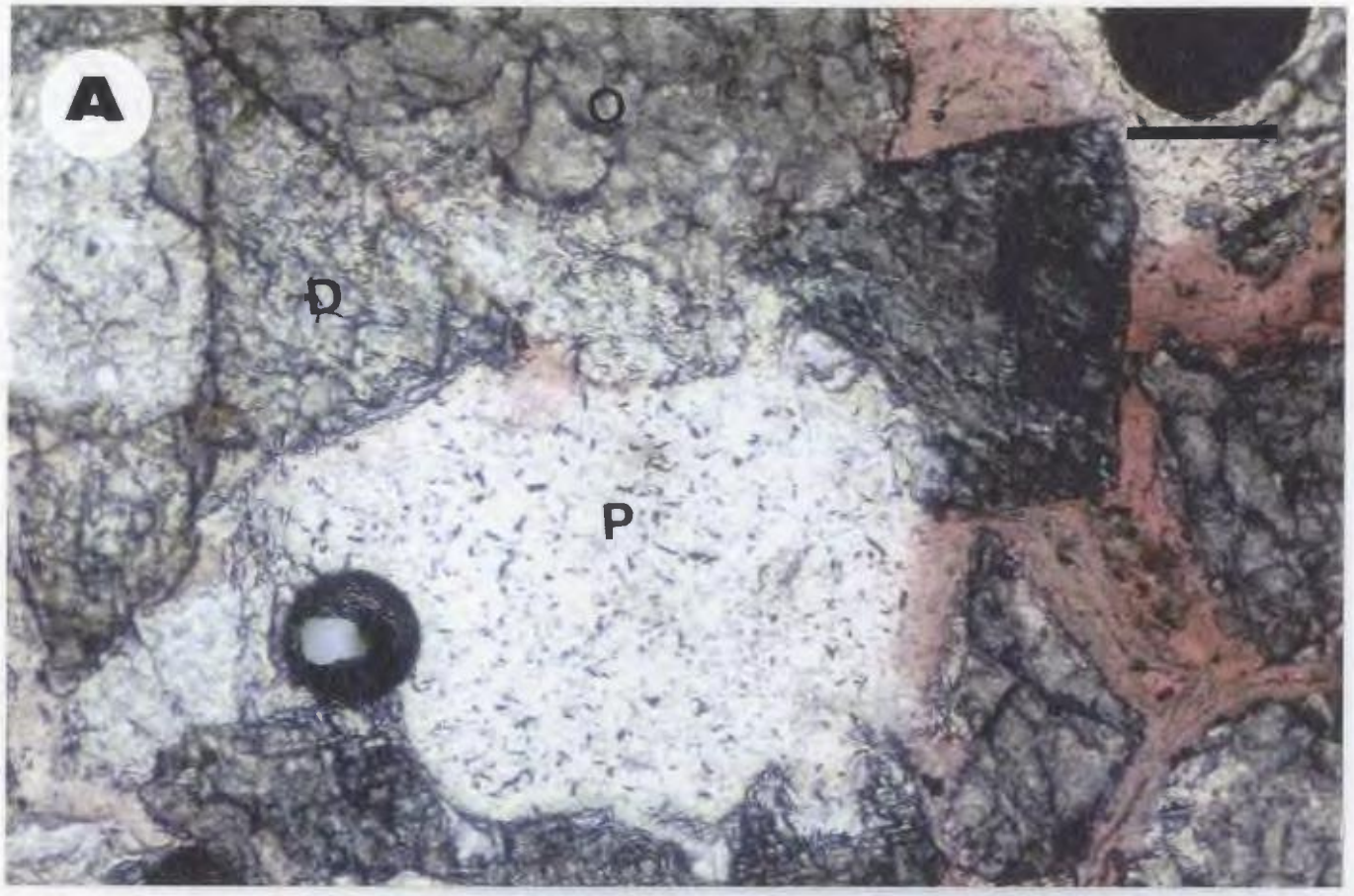

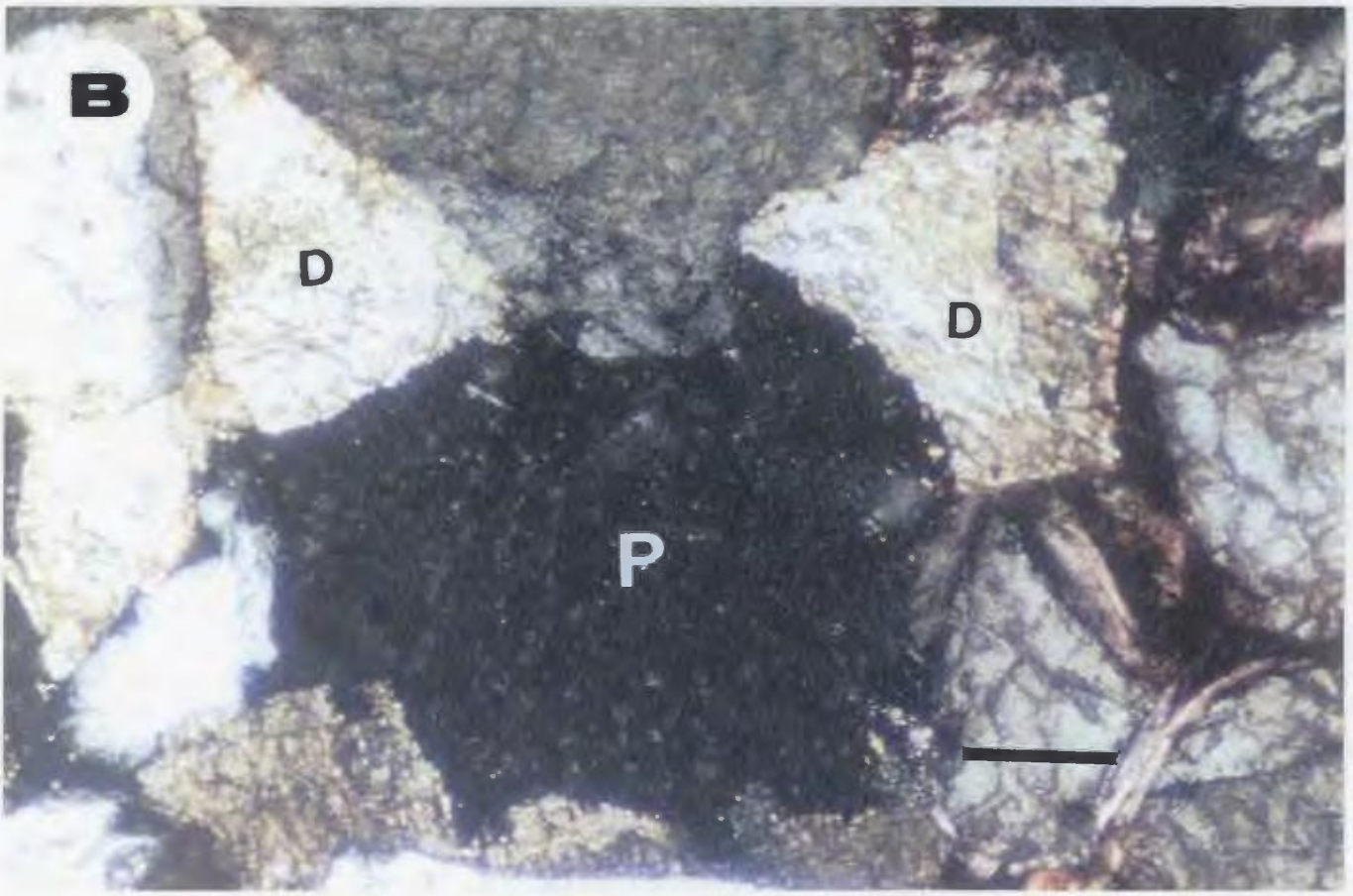

APPENDIX V

THIN-SECTION DIAGENESIS AND POROSITY: PLATE 60

A- Photograph shows the development of secondary porosity (P) from partial dissolution of dolomite cement (D) (rhombic outlines and unstained). Note the corroded edges of dolomite cement. Proximal delta front sandstone unit (A12), well B3-61 @ 2711 m. (8893 ft.). (estimated measured porosity is about 16%). Scale bar = 0.1mm.

(PPL)

B- Same as previous photo but with (XPL), black area is secondary porosity.

APPENDIX V
THIN-SECTION DIAGENESIS AND POROSITY: PLATE 60

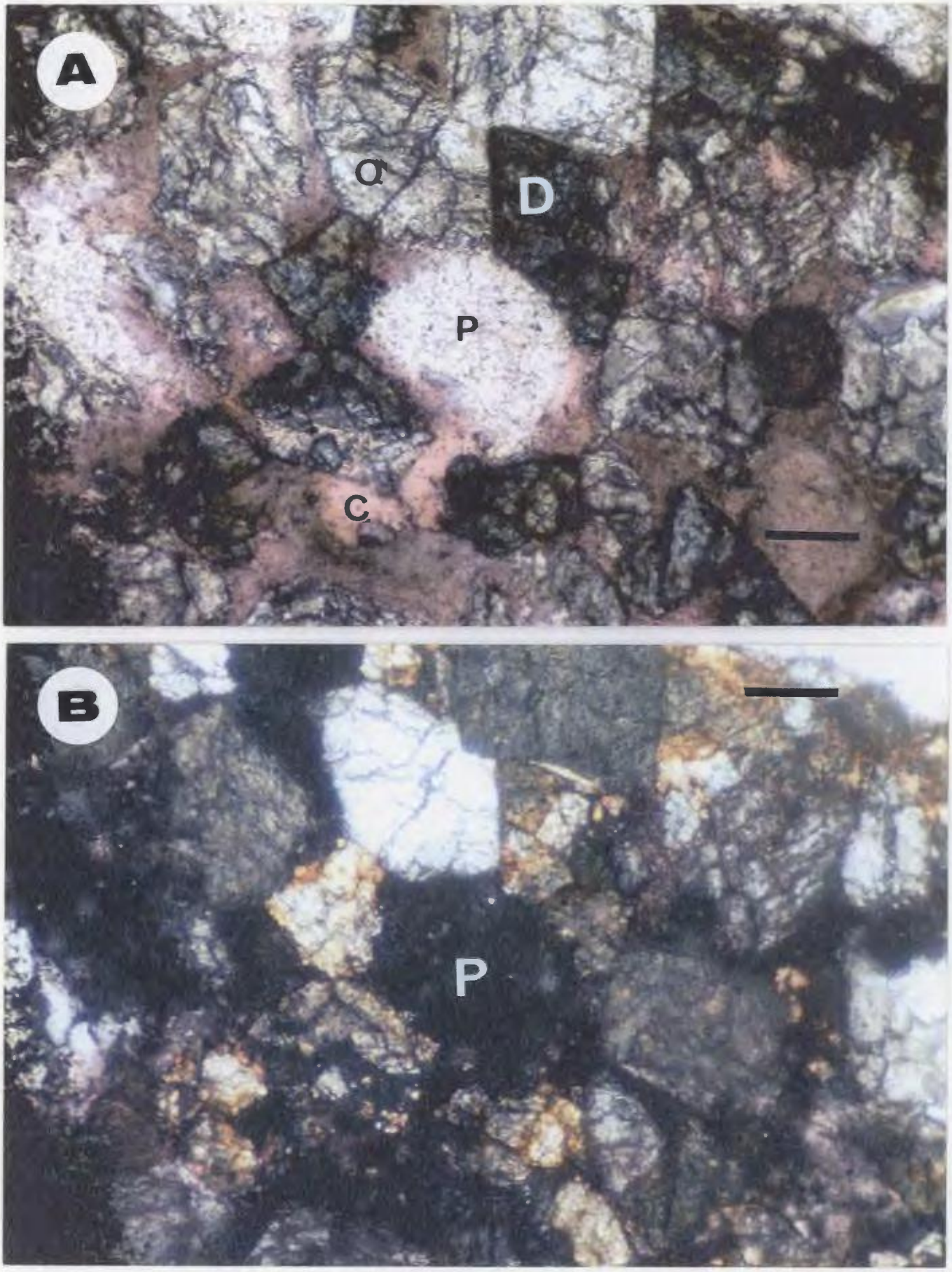

APPENDIX V

THIN-SECTION DIAGENESIS AND POROSITY: PLATE 61

A- Fracture porosity (FR) in clay-rich reworked marine sandstone unit (Am) in well Q1-23 @ 2687 m. (8812 ft.) which partially filled with later diagenetic clay mineral (Cly). The fracture in this sample still open and significantly enhanced porosity (about 27%), and improved overall permeability (about 5202 md) as well. Scale bar = 0.07mm.

(PPL)

B- Same view but with (XPL), note black long, partially open fracture that transects the sample.

APPENDIX V
THIN-SECTION DIAGENESIS AND POROSITY: PLATE 61

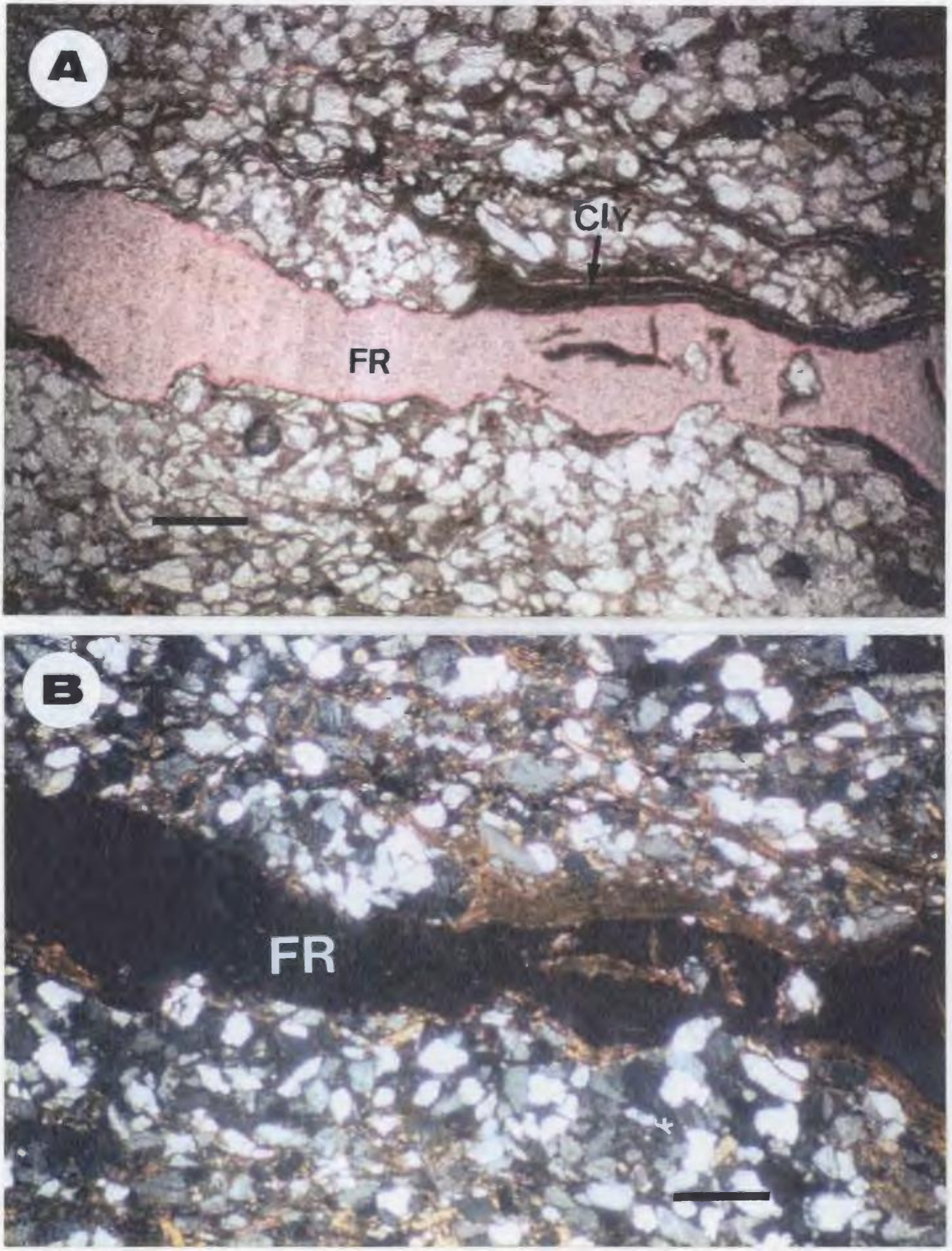

APPENDIX V

THIN-SECTION DIAGENESIS AND POROSITY: PLATE 62

A- Filled secondary (fracture, FR) porosity. The fracture in this sample has been partially cemented or healed by authigenic clay mineral (Cly). It is difficult to prove petrographically whether fractures in this sample are original or were produced during coring or sample processing. However, the presence of oil staining (H) in fracture walls of this sample may indicates that fracture predated drilling at least. Also the presence of some incipient clay cementation along fracture can be used as an evidence of original fracturing. Fractures in this sample may improved overall porosity and permeability (16%, 113 md). Proximal delta front sandstone unit (A12), well B3-61 @ 2711 m. (8893 ft.). Scale bar = 0.1mm.

(PPL)

B- Same as previous photo but with (XPL).

APPENDIX V
THIN-SECTION DIAGENESIS AND POROSITY: PLATE 62

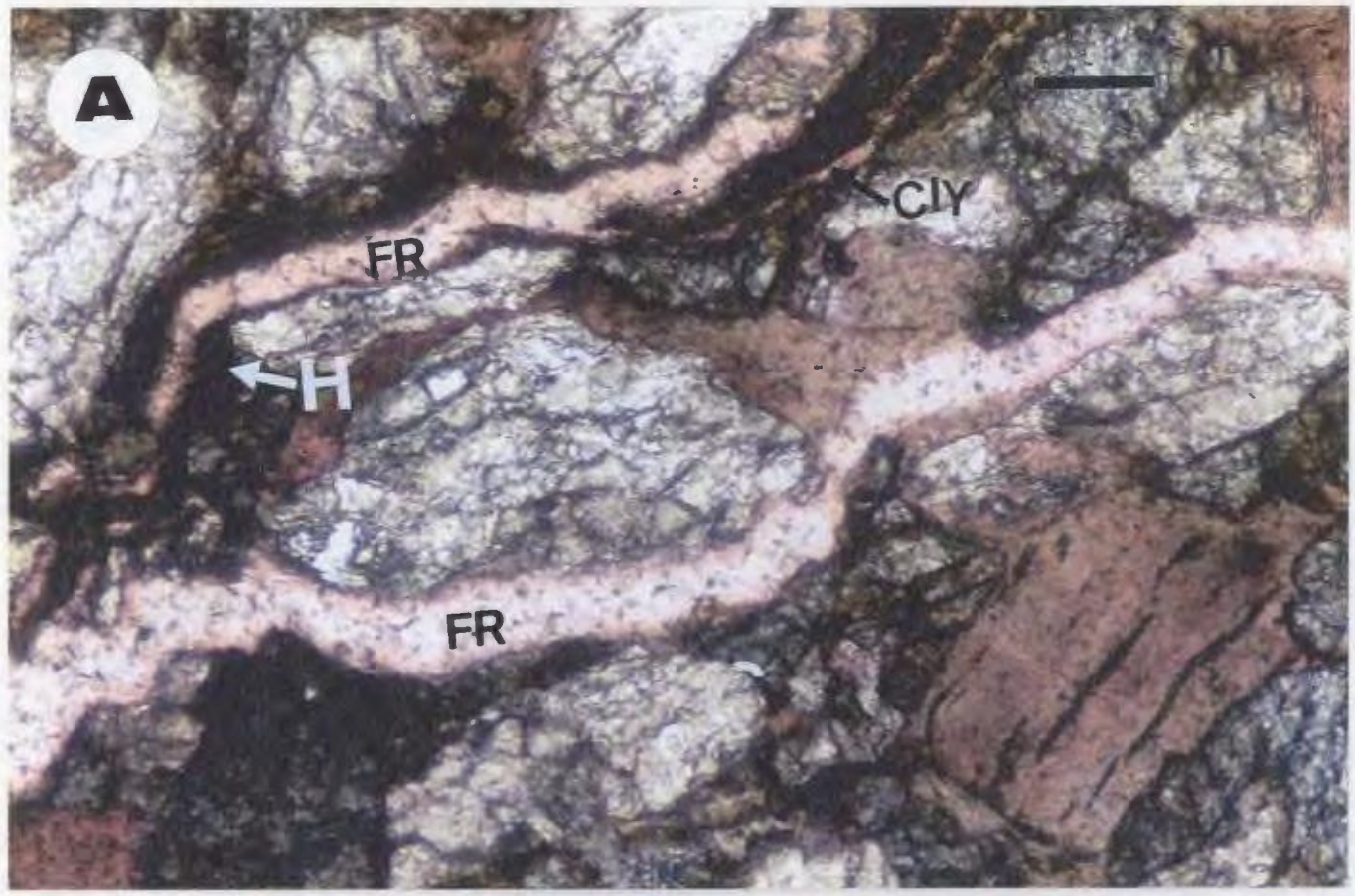

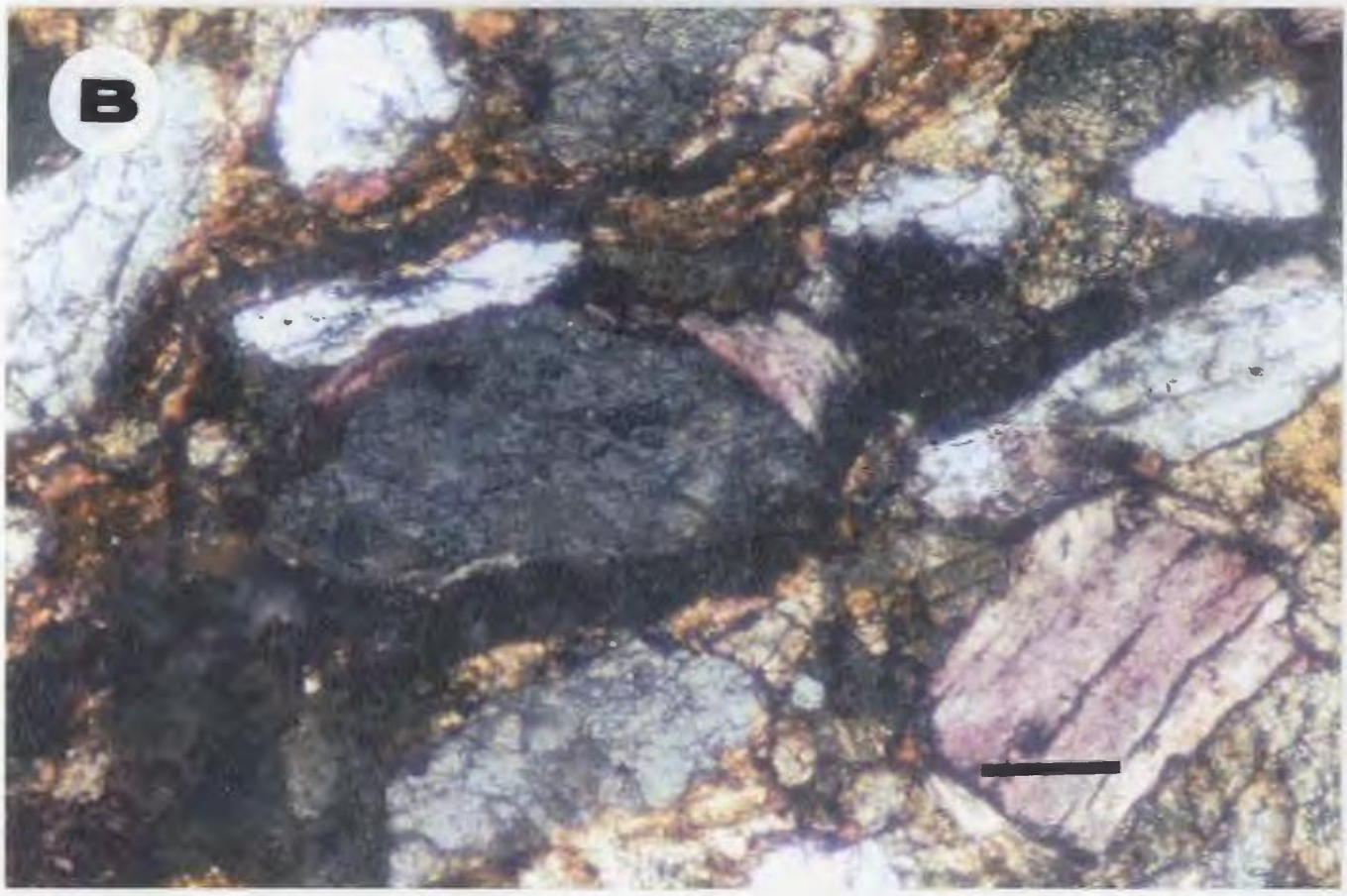

APPENDIX V

THIN-SECTION DIAGENESIS AND POROSITY: PLATE 63

A- Hydrocarbon (H) emplaced in large pore-spaces between quartz grains (Q) that originated by either total leaching of calcite cement or total dissolution of unstable grains in an advanced diagenetic stage, and inhibiting further cementation. Proximal delta front sandstone unit (A8), well C1-NC2 @ 2958 m. (9703 ft.).
Scale bar = 0.1mm.

(PPL)

B- Significant calcite cement leaching porosity in this rock filled with hydrocarbon (H). The rock in general is still highly cemented by calcite cement (C) and in turn reduces its permeability (measured porosity 14.5%, permeability 8.5 md). Reworked marine sandstone unit (Am), well Q1-23 @ 2494 m. (8180 ft.). Scale bar = 0.1mm.

(PPL)

APPENDIX V
THIN-SECTION DIAGENESIS AND POROSITY: PLATE 63

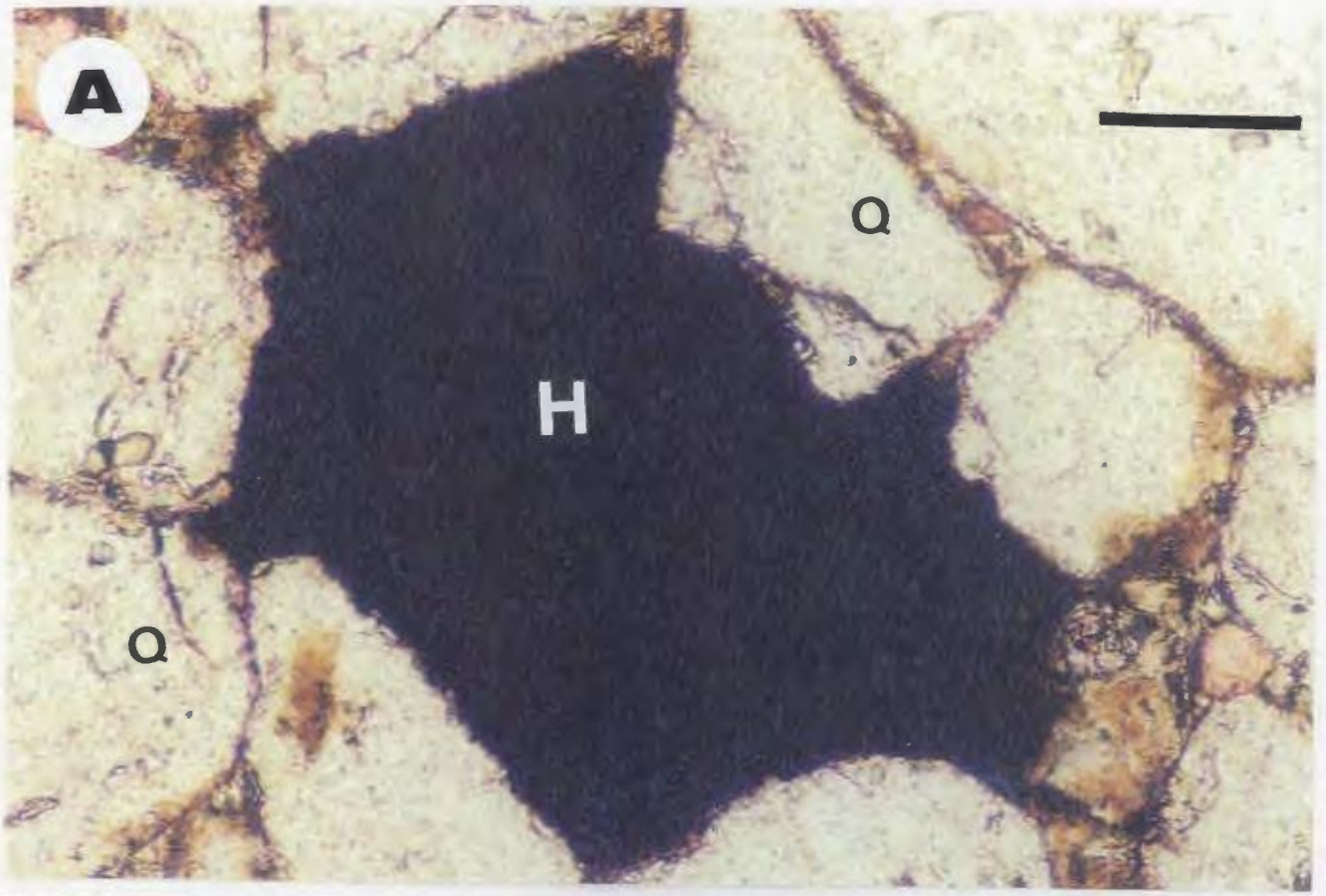

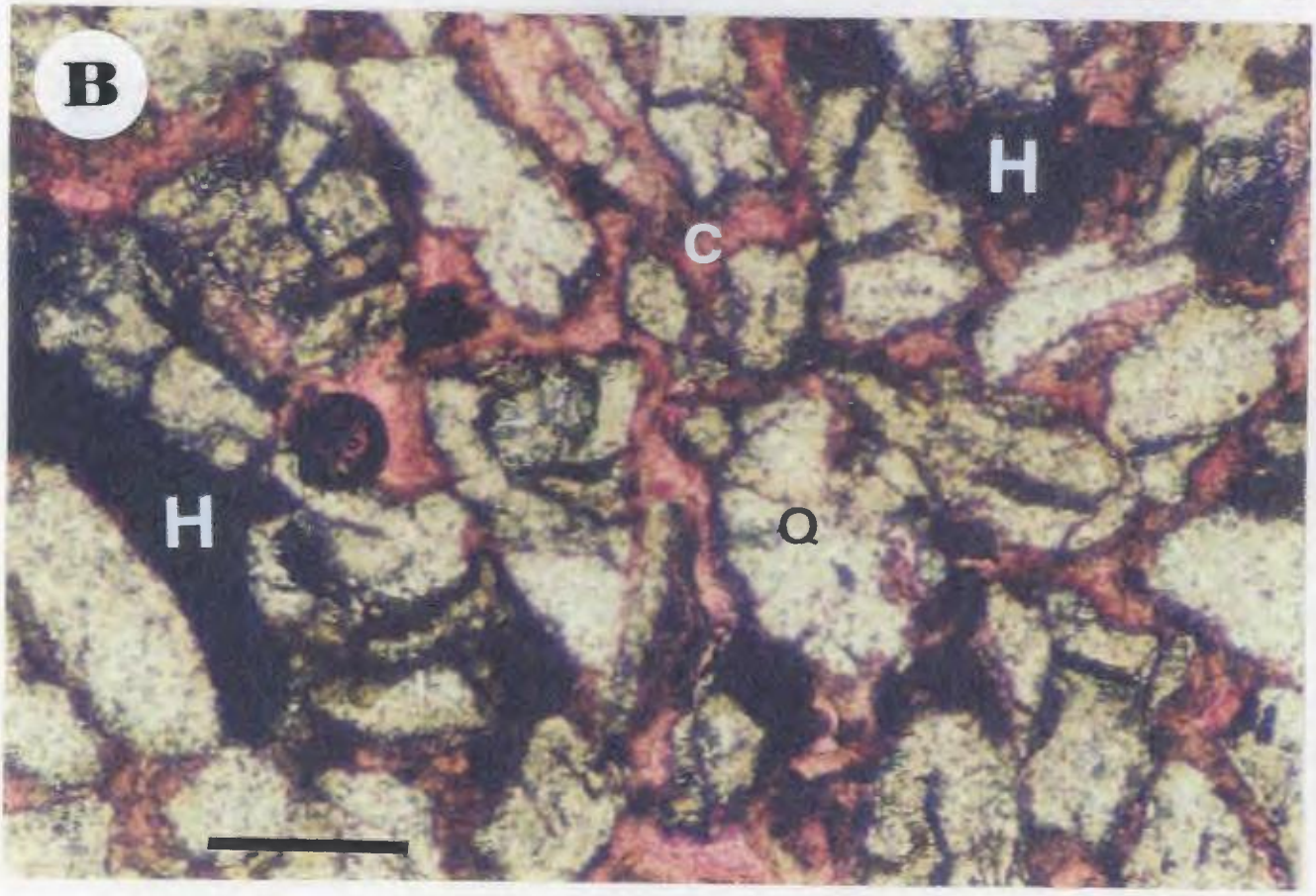

APPENDIX V

THIN-SECTION DIAGENESIS AND POROSITY: PLATE 64

A- Hydrocarbon (H) droplets as filling microporosity associated with kaolinite cement (K) in reworked marine sandstone unit (Am) of well Q1-23 @ 2580 m. (8461 ft.). The nature of hydrocarbon droplets in this cement suggests kaolinite cement predated hydrocarbon migration into this rock.(Measured porosity is about 19.6%, but of very low permeability of only 3 md). Scale bar = 0.1mm.

(PPL)

B- Same as previous photo but with (XPL). Note the aggregates of kaolinite cement (K) crystals of vermicular texture filling pore-spaces between quartz grains (Q). Also note the presence of some plagioclase feldspar (PF) which may be the main contributor to the formation of kaolinite in this rock.

APPENDIX V
THIN-SECTION DIAGENESIS AND POROSITY: PLATE 64

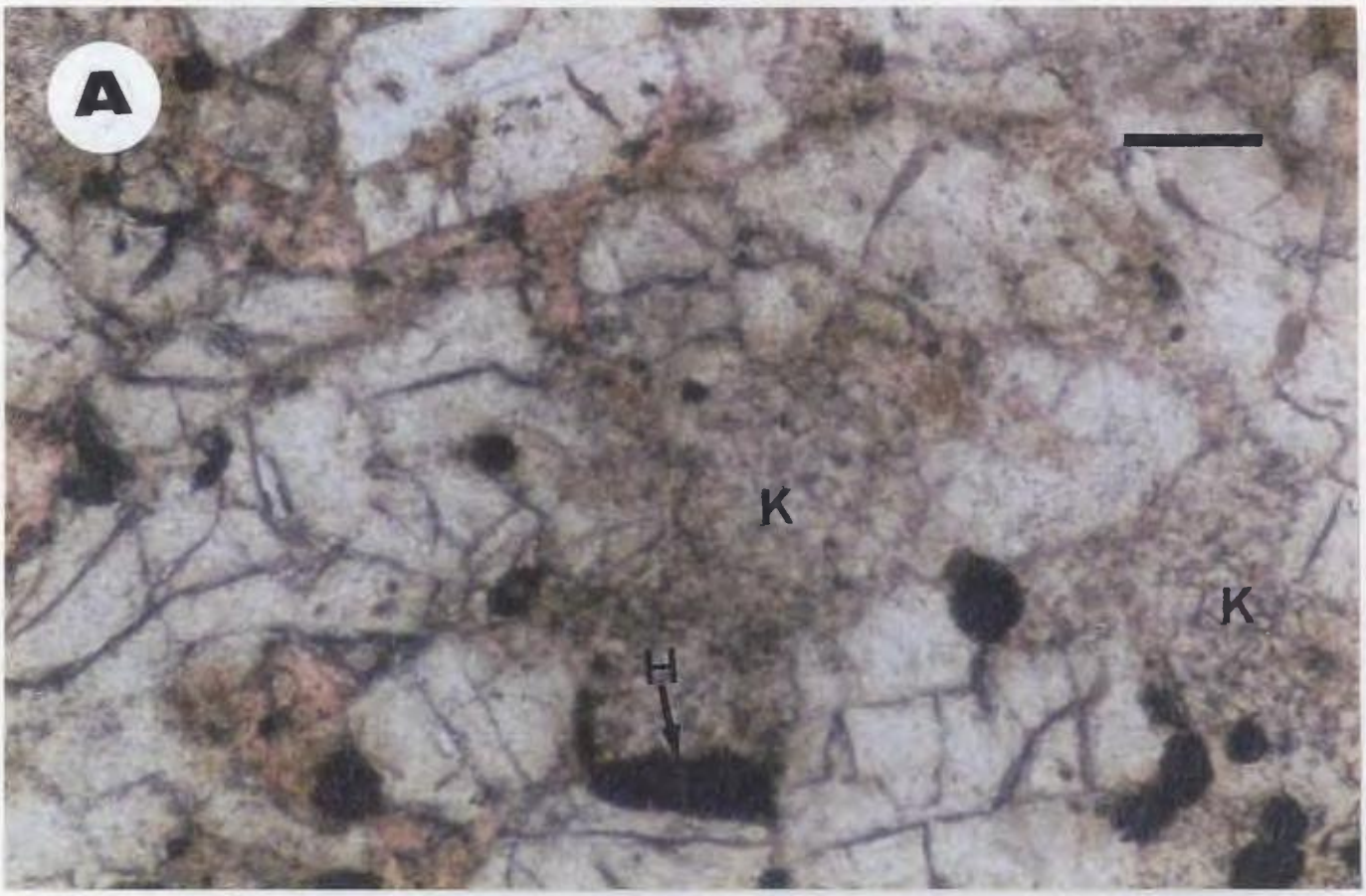

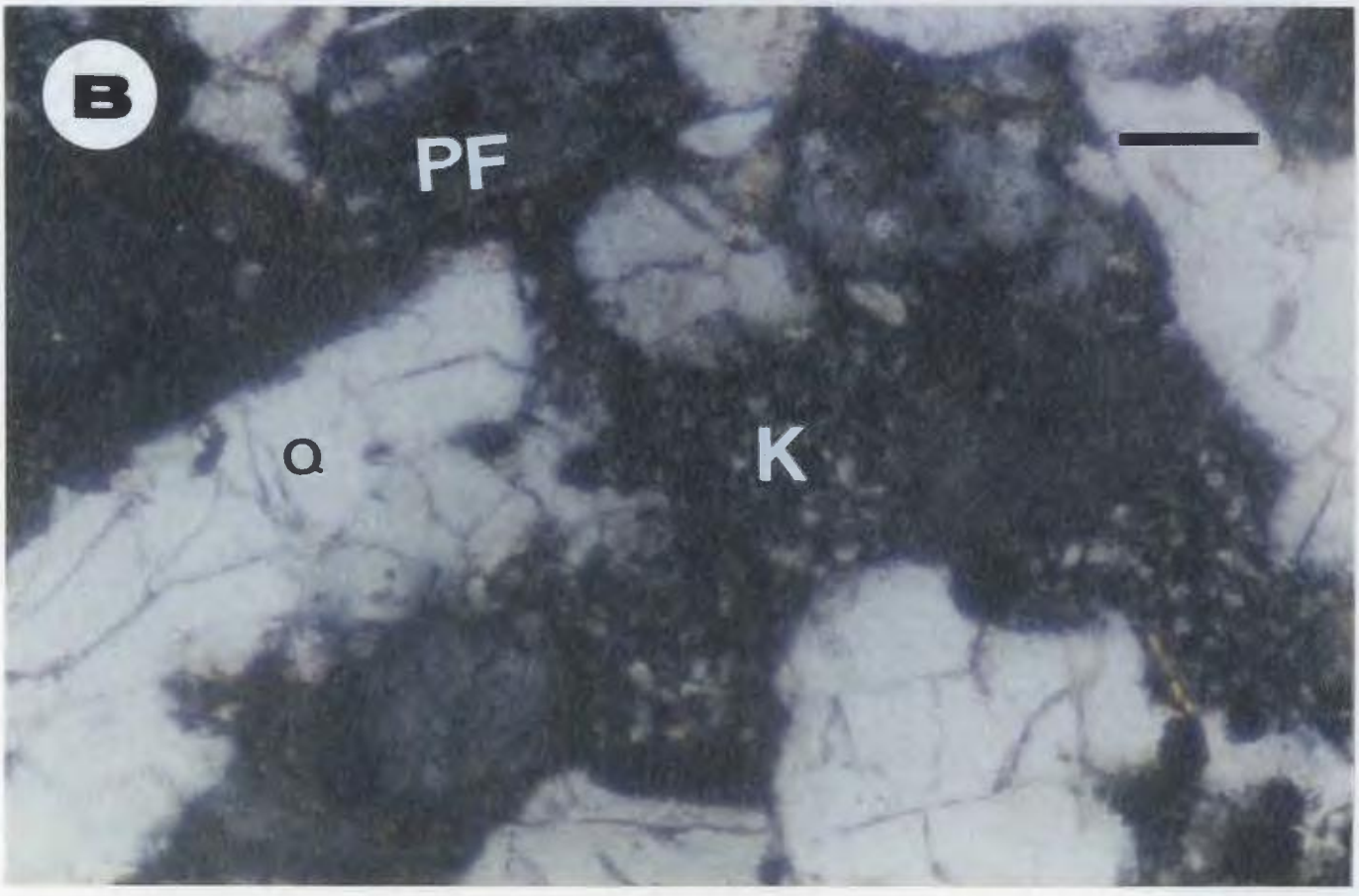

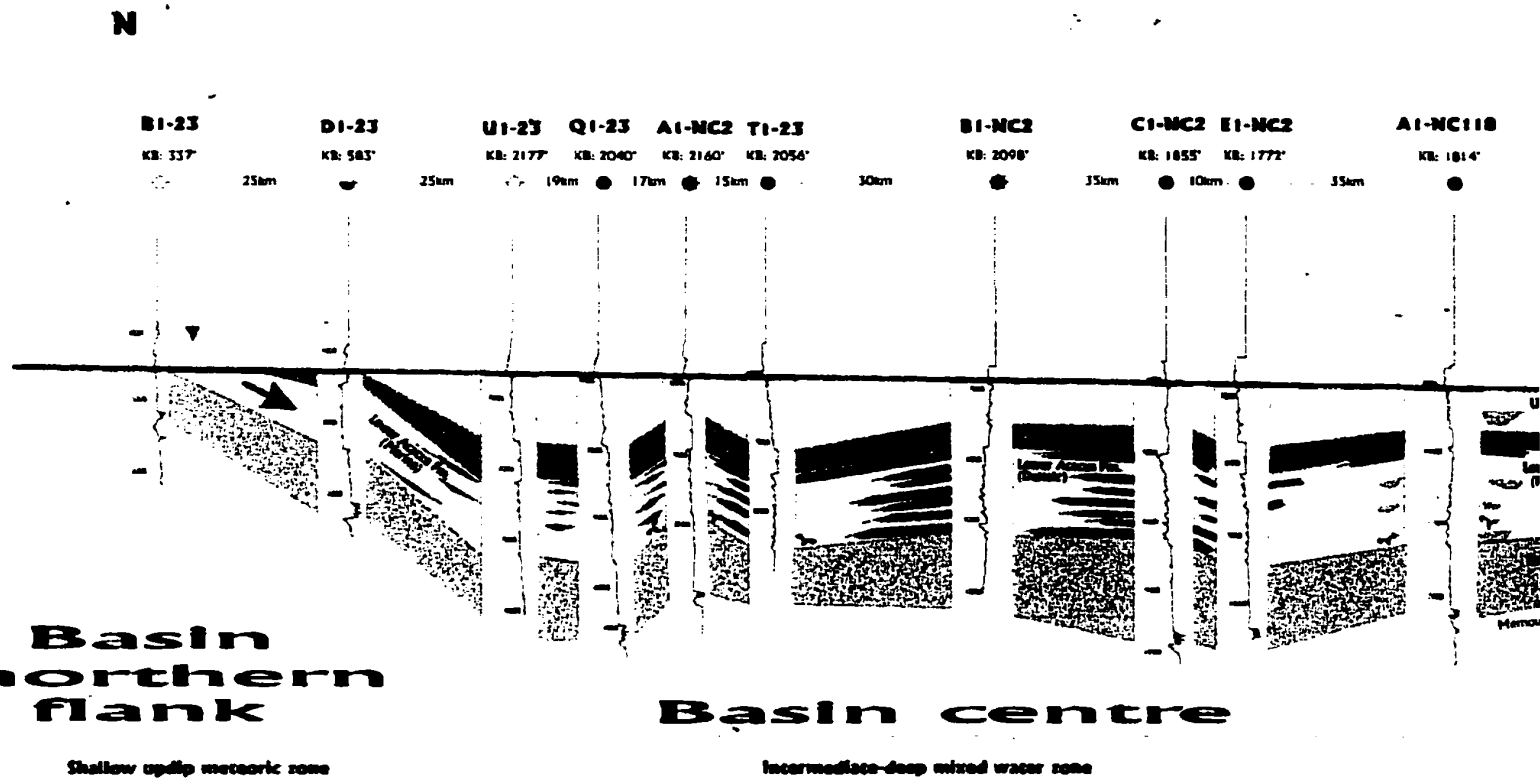

LEGEND

- Fluvial sandstones
- SST. / SLST. — Deltaic sandstones/siltstones
- Reworked marine sandstones
- Possible basement faults
- Meteoric water direction
- Possible fluid pathways from underlying horizones
- Caledonian unconformity

S

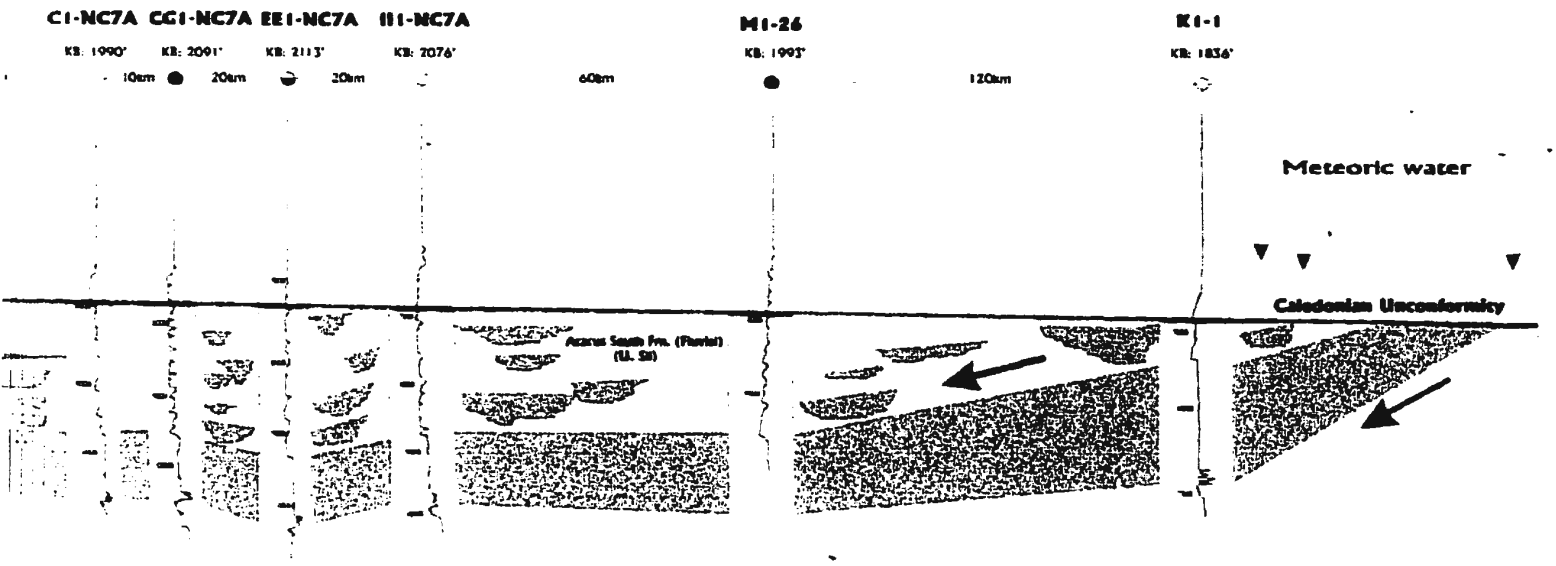

uthern flank

allow updip meteoric zone

tion at the
ework, facies
Formation,

gs).

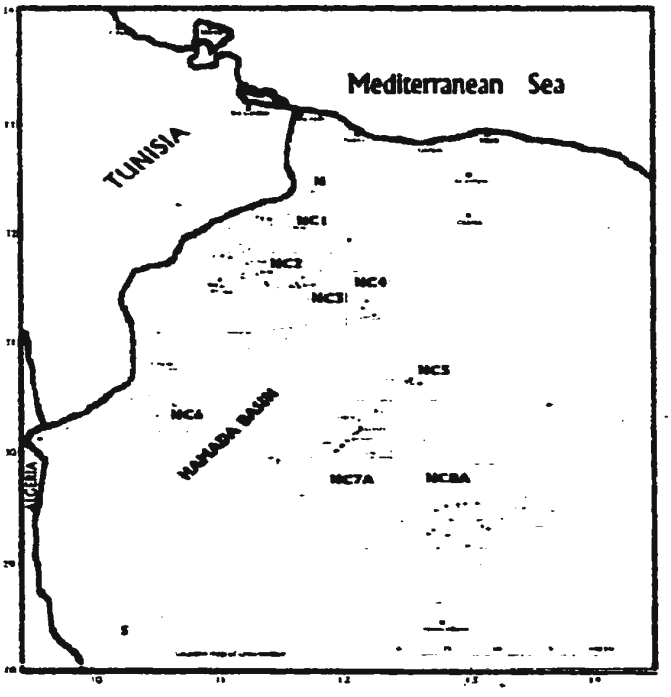

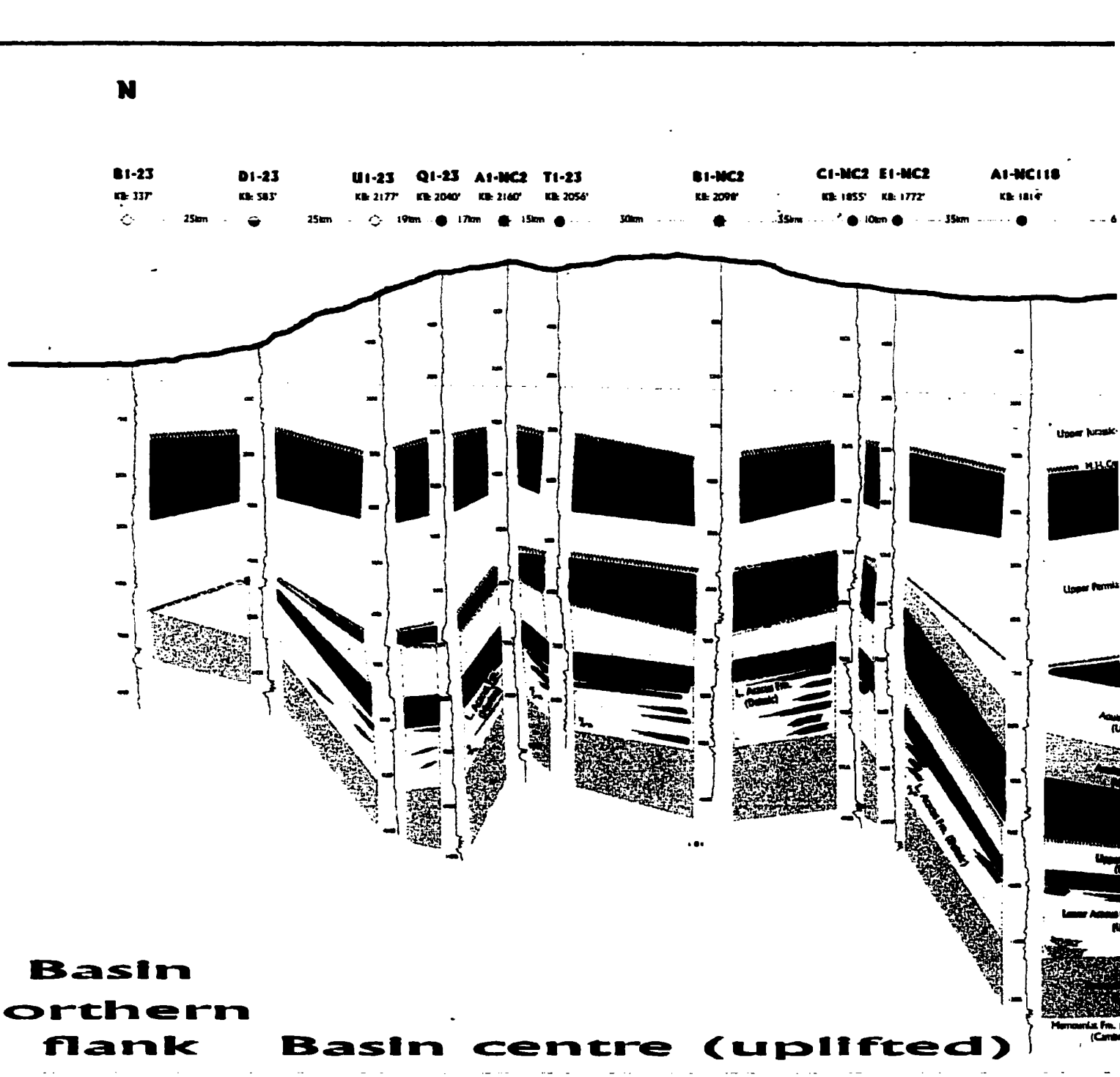
N
B1-23
KB: 337'
D1-23
KB: 583'
U1-23
KB: 2177'
Q1-23
KB: 2040'
A1-NC2
KB: 2160'
T1-23
KB: 2056'
B1-NC2
KB: 2098'
C1-NC2
KB: 1855'
E1-NC2
KB: 1772'
A1-NC118
KB: 1814'
25km
25km
19km
17km
15km
30km
35km
10km
35km
Basin northern flank
Basin centre (uplifted)
Shallow updip meteoric zone
Intermediate-deep mixed water zone
LEGEND
Fluvial sandstones
SST
SLST
Deltaic sandstones/siltstones
Reworked marine sandstones
Possible basement faults
possible fluid pathways from underlying horizones
Meteoric water direction
Caledonian/Hercynian unconformities

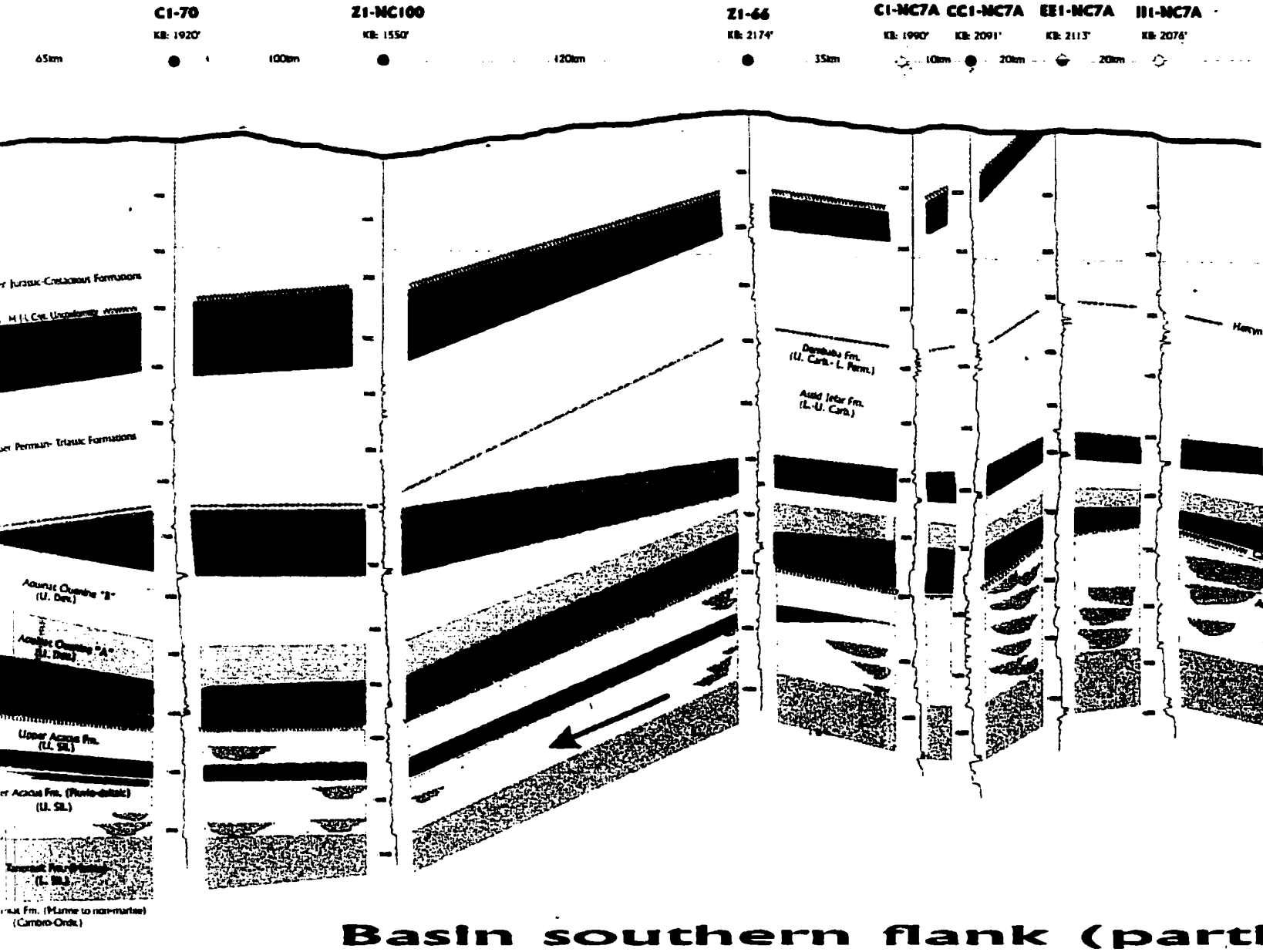

Basin southern flank (parti

Shallow updip meteoric zone

ENCLOSURE No. 2

Regional cross-section illustrating concepts of structural, stratigraphic and hydrological relationships and showing present day picture of the Hamada Basin, NW Libya. Note facies distribution of the Lower Acacus Formation from south to north, and changes in structure as the basin centre area has been uplifted compared with Enclosure No. 3.

(Note: The units of depth are in feet as recorded on well logs).

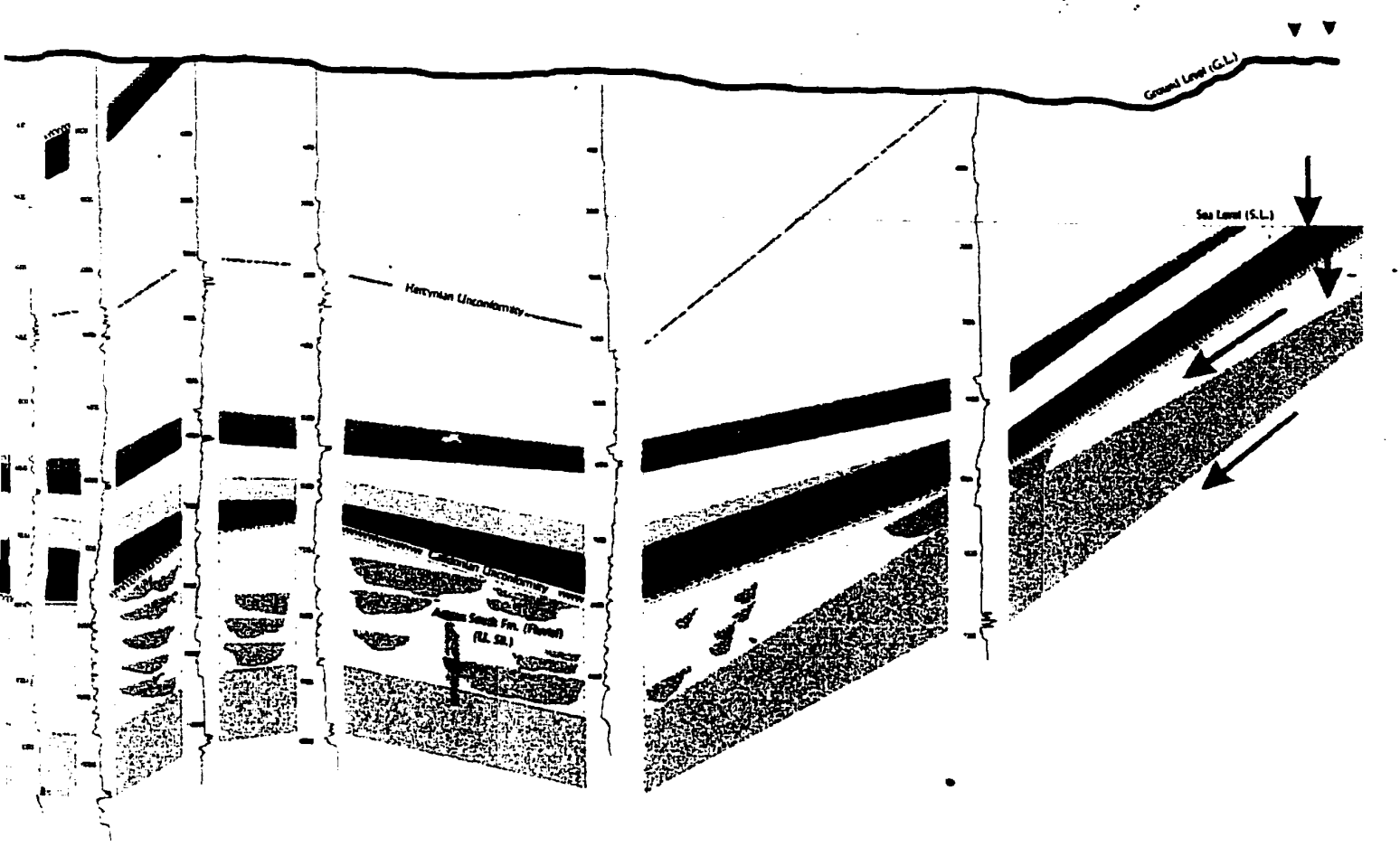

flank (partially subsided)

ow updip meteoric zone

phic and
Hamada
rmation
area has

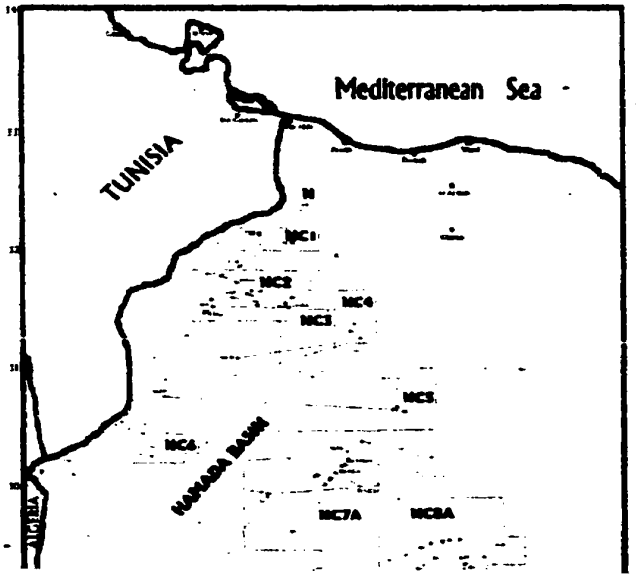

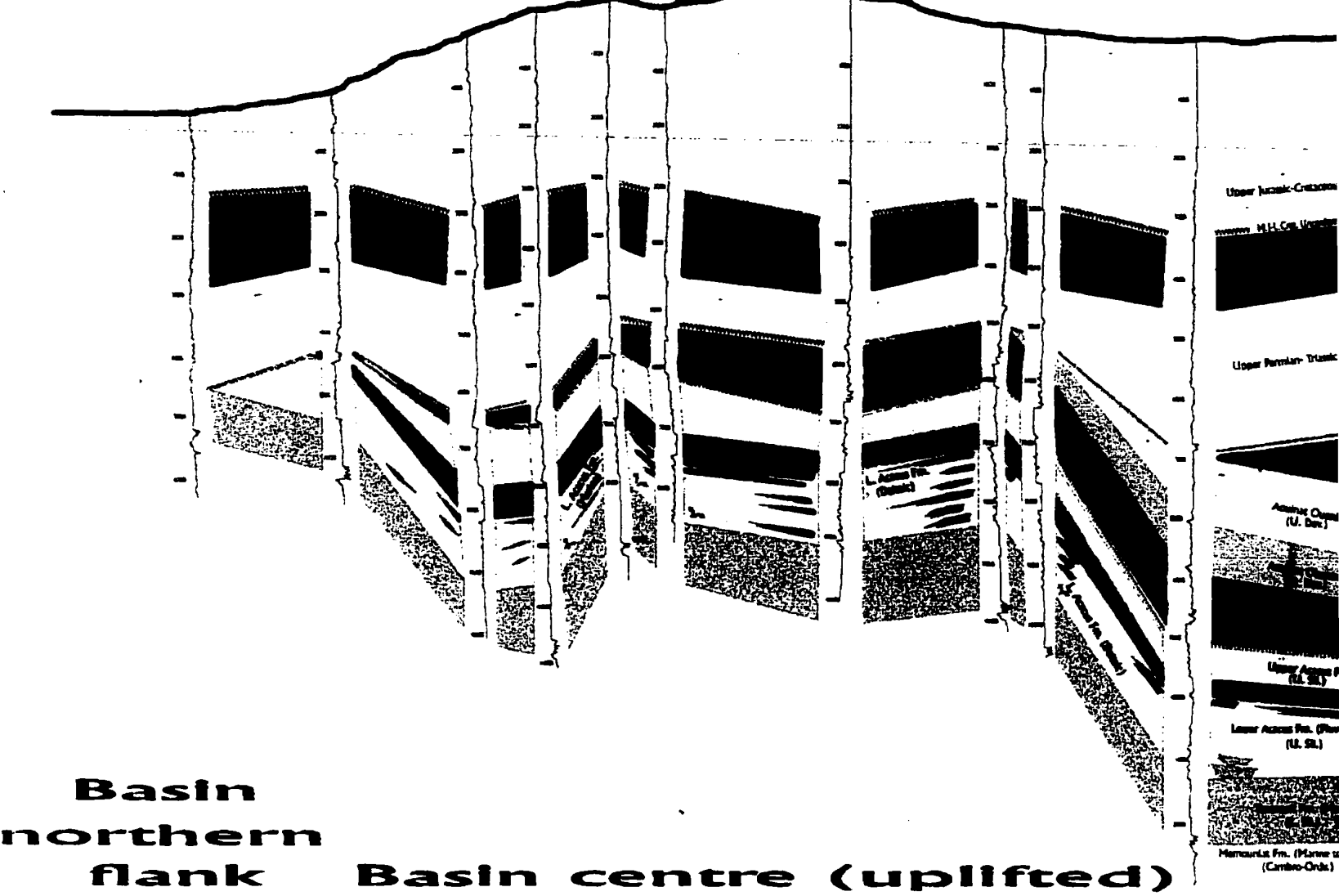
Basin northern flank
Basin centre (uplifted)
Shallow updip meteoric zone
Intermediate-deep mixed water zone
LEGEND
Fluvial sandstones
SLST.
SST.
Deltaic sandstones/siltstones
Reworked marine sandstones
Possible basement faults
possible fluid pathways from underlying horizones
Meteoric water direction
Caledonian/Hercynian unconformities

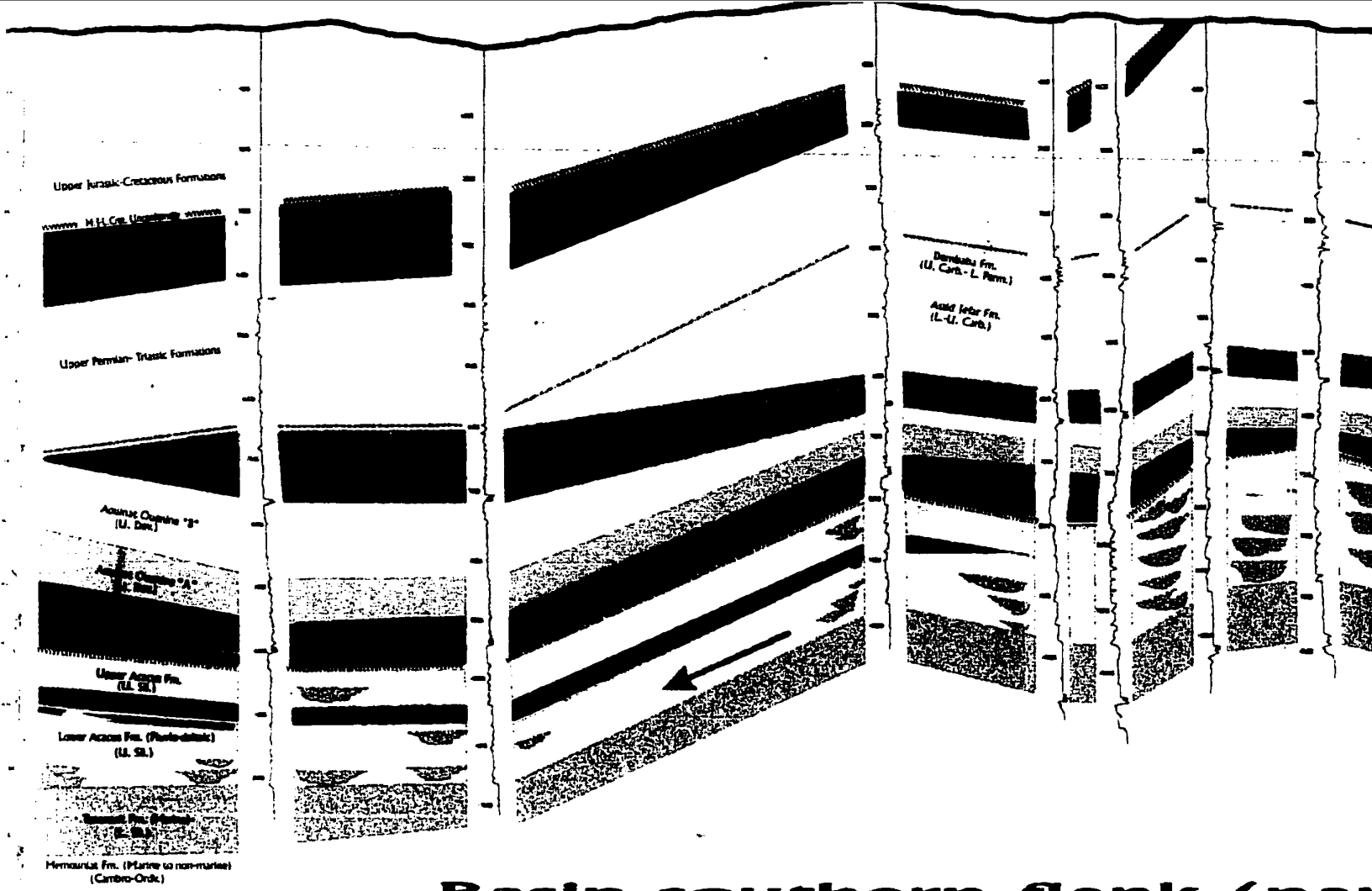

Basin southern flank (par

Shallow updip meteoric zone

ENCLOSURE No. 2

Regional cross-section illustrating concepts of structural, stratigraphic and hydrological relationships and showing present day picture of the Hamada Basin, NW Libya. Note facies distribution of the Lower Acacus Formation from south to north, and changes in structure as the basin centre area has been uplifted compared with Enclosure No. 3.
(Note: The units of depth are in feet as recorded on well logs).

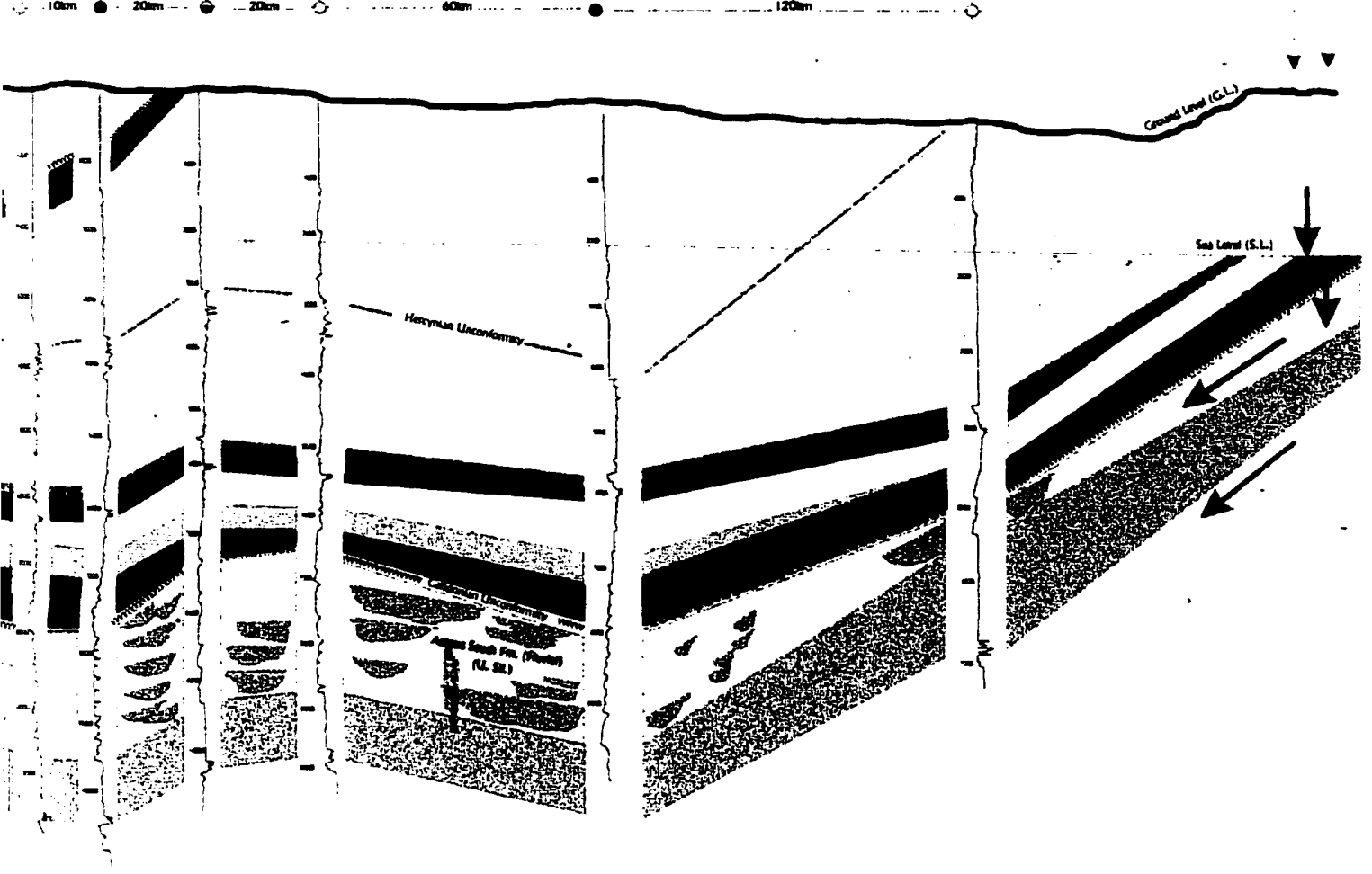

flank (partially subsided)

ow updip meteoric zone

phic and
Hamada
ormation
area has

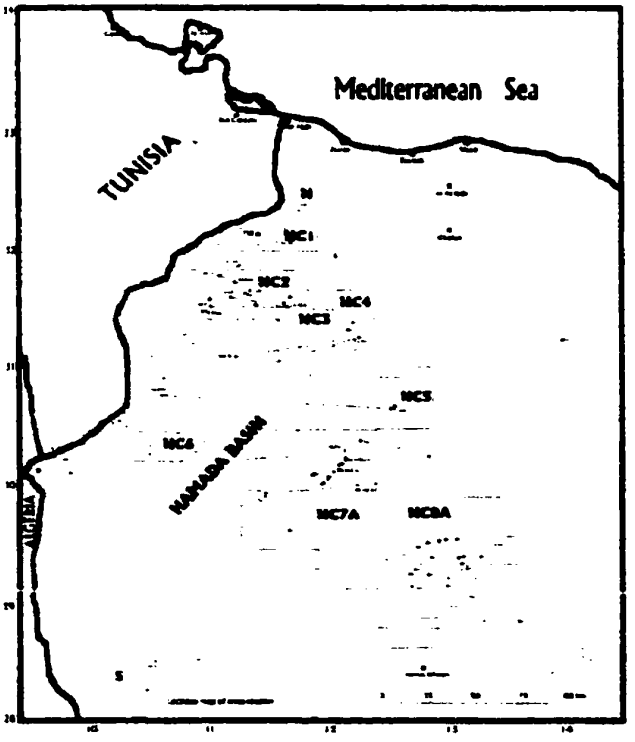

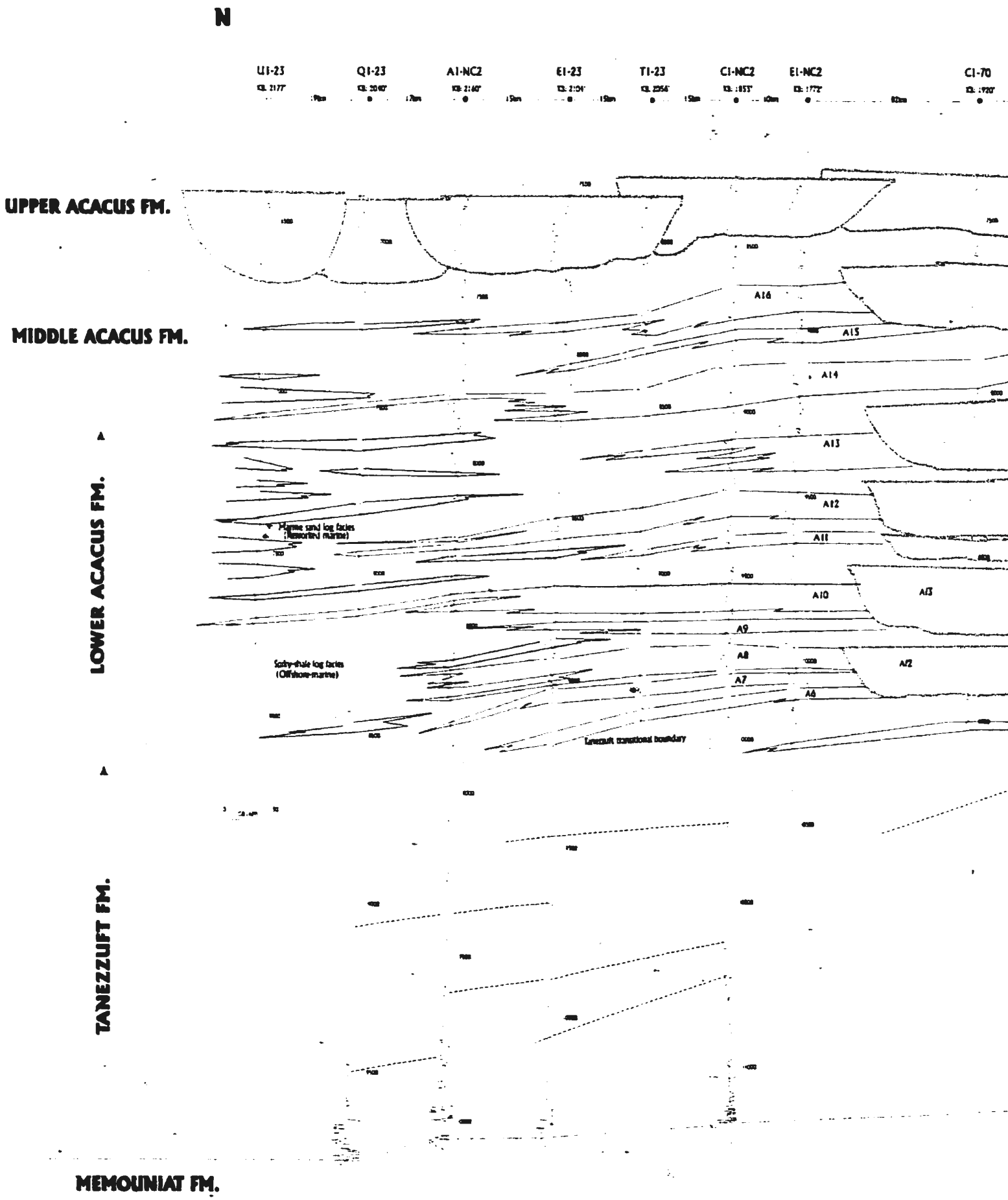
N
UI-23
QI-23
AI-NC2
EI-23
TI-23
CI-NC2
EI-NC2
CI-70
UPPER ACACUS FM.
MIDDLE ACACUS FM.
LOWER ACACUS FM.
TANEZZUFT FM.
MEMOUNIAT FM.
A16
A15
A14
A13
A12
A11
A10
A9
A8
A7
A6
A5
A4
A3
A2
Marine sand log facies
(Nearshore marine)
Silty-shale log facies
(Offshore-marine)
Lowstand transitional boundary

S

Z1-NC100 | Z1-66 | C1-NC7A | CC1-NC7A | EE1-NC7A | II1-NC7A

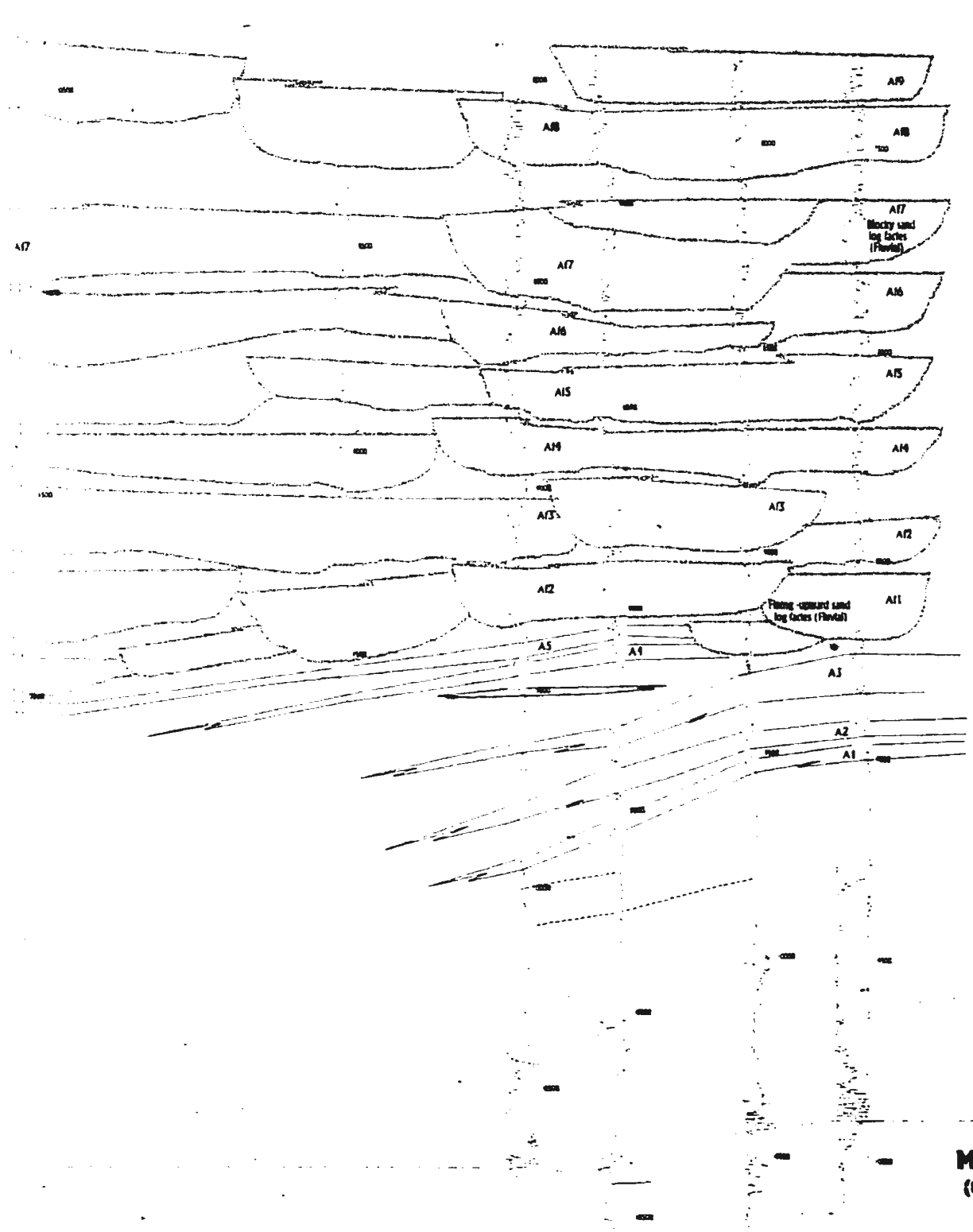

ACACUS SOUTH Fm.
(Upper Silurian)

LOWER ACACUS FM.
(Upper Silurian)

TANEZZUFT FM.
(Lower Silurian)

MEMOUNIAT FM.
(Cambro-Ordovician)

S

CI-NC7A EE1-NC7A III-NC7A

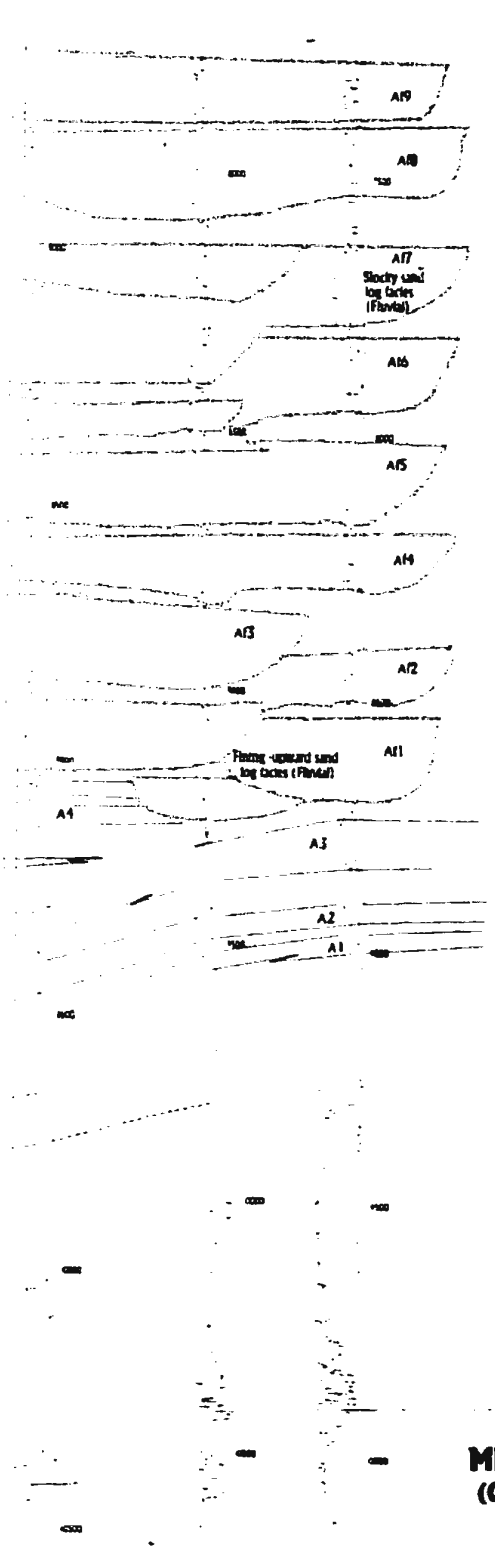

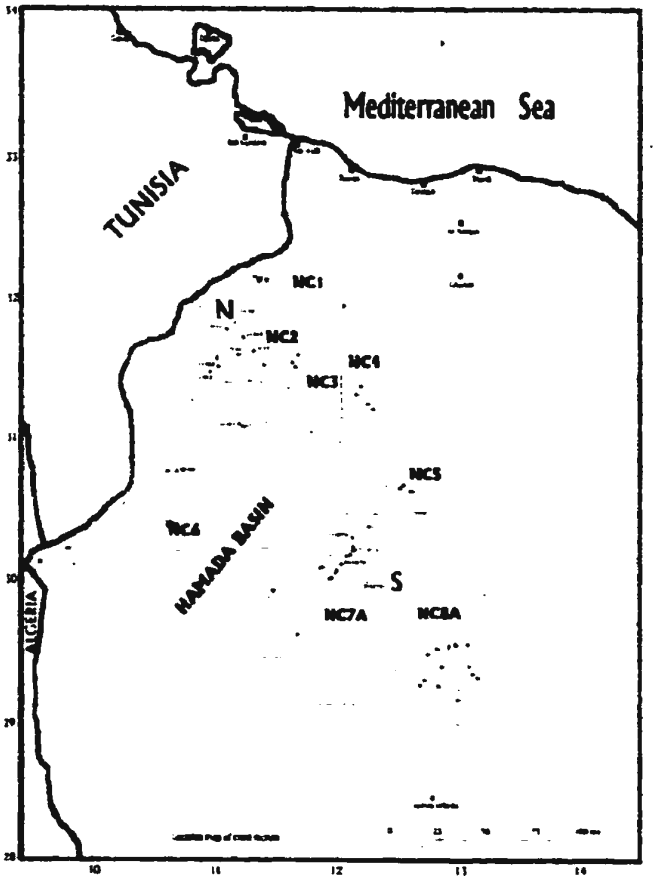

ENCLOSURE No. 3

S-N REGIONAL STRATIGRAPHIC CROSS-SECTION SHOWING FACIES DISTRIBUTION OF THE LOWER ACACUS FORMATION ACROSS THE HAMADA BASIN, NW LIBYA.

(Note: The units of depth are in feet as recorded on well logs).

(M.S. as indicated)

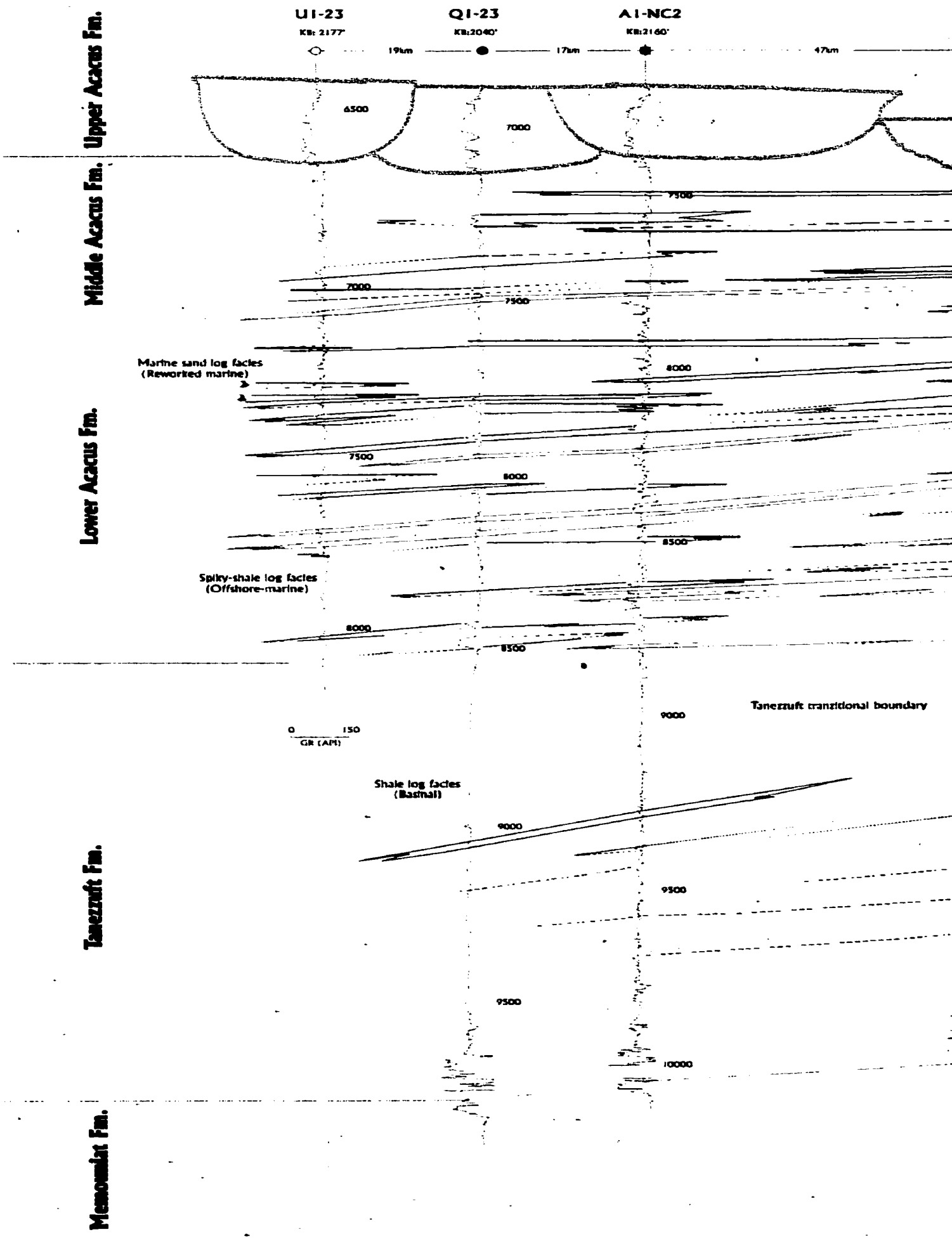
NWN
U1-23
KB: 2177'
Q1-23
KB:2040'
A1-NC2
KB:2160'
19km
17km
47km
Upper Acacus Fm.
Middle Acacus Fm.
Lower Acacus Fm.
Tanezzuft Fm.
Mamoumiat Fm.
6500
7000
7500
7000
7500
8000
Marine sand log facies
(Reworked marine)
7500
8000
8500
Spiky-shale log facies
(Offshore-marine)
8000
8500
9000
Tanezzuft tranzitional boundary
0
150
GR (API)
Shale log facies
(Basinal)
9000
9500
9500
10000

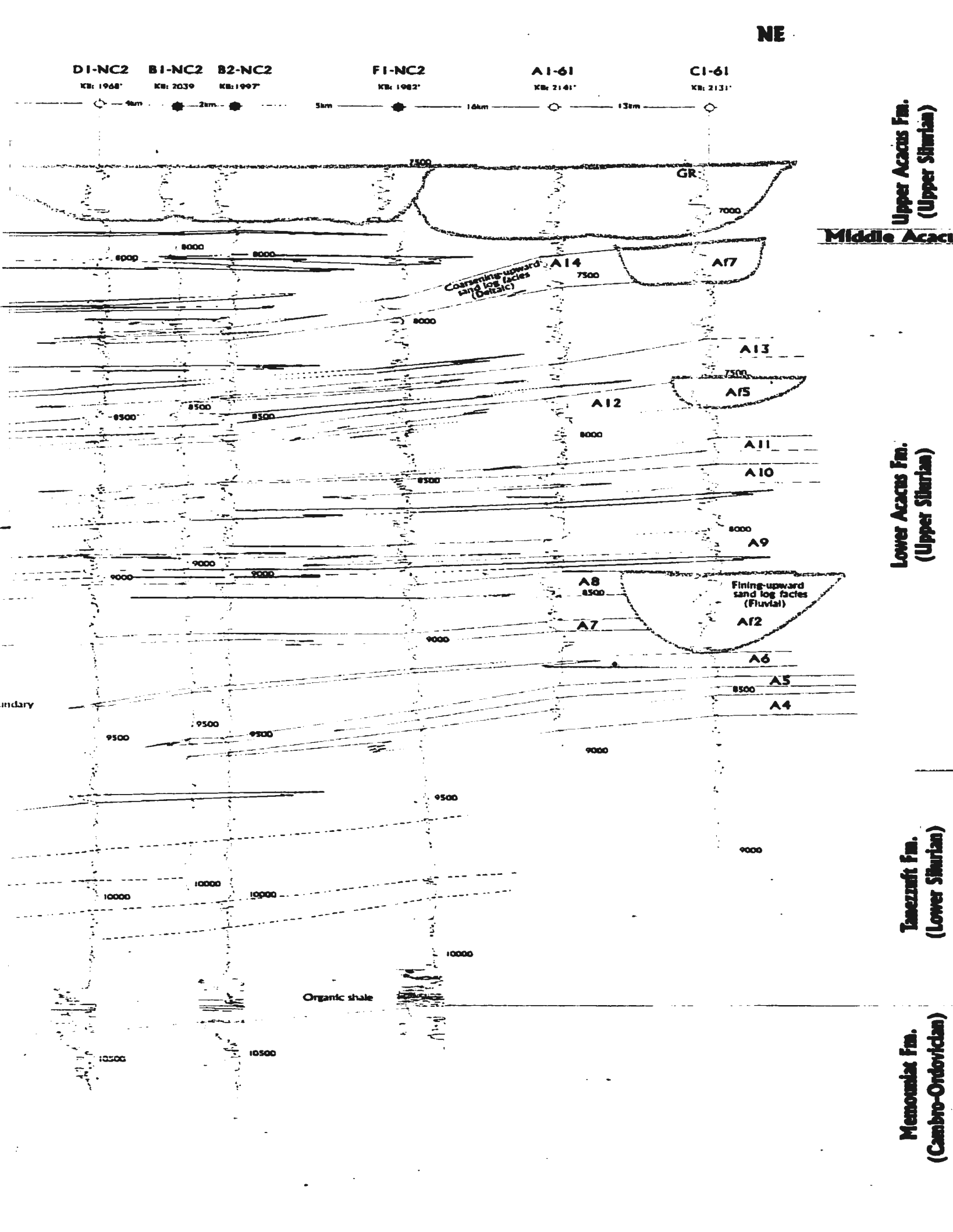
NE
D1-NC2
KB: 1968'
B1-NC2
KB: 2039
B2-NC2
KB: 1997'
F1-NC2
KB: 1982'
A1-61
KB: 2141'
C1-61
KB: 2131'
4km
2km
5km
16km
13km
GR
7500
7000
8000
8000
8000
A14
Af7
7500
Coarsening-upward sand log facies (Deltaic)
8000
A13
7500
Af5
A12
8500
8500
8500
8000
A11
A10
8500
8000
A9
9000
9000
A8
8500
Fining-upward sand log facies (Fluvial)
Af2
A7
9000
A6
A5
8500
A4
9500
9500
9500
9000
9500
10000
10000
10000
10000
Organic shale
10500
10500
Upper Acacus Fm. (Upper Silurian)
Middle Acacu
Lower Acacus Fm. (Upper Silurian)
Tanezzuft Fm. (Lower Silurian)
Memouniat Fm. (Cambro-Ordovician)

NE

C1-61

KB: 2131'

GR

7000

Af7

A13

7500

Af5

A11

A10

8000

A9

Fining-upward sand log facies (Fluvial)

Af2

A6

A5

8500

A4

9000

Upper Acacus Fm. (Upper Silurian)

Middle Acacus Fm.(Upper Silurian)

Lower Acacus Fm. (Upper Silurian)

Tanezzuft Fm. (Lower Silurian)

Memouniat Fm. (Cambro-Ordovician)

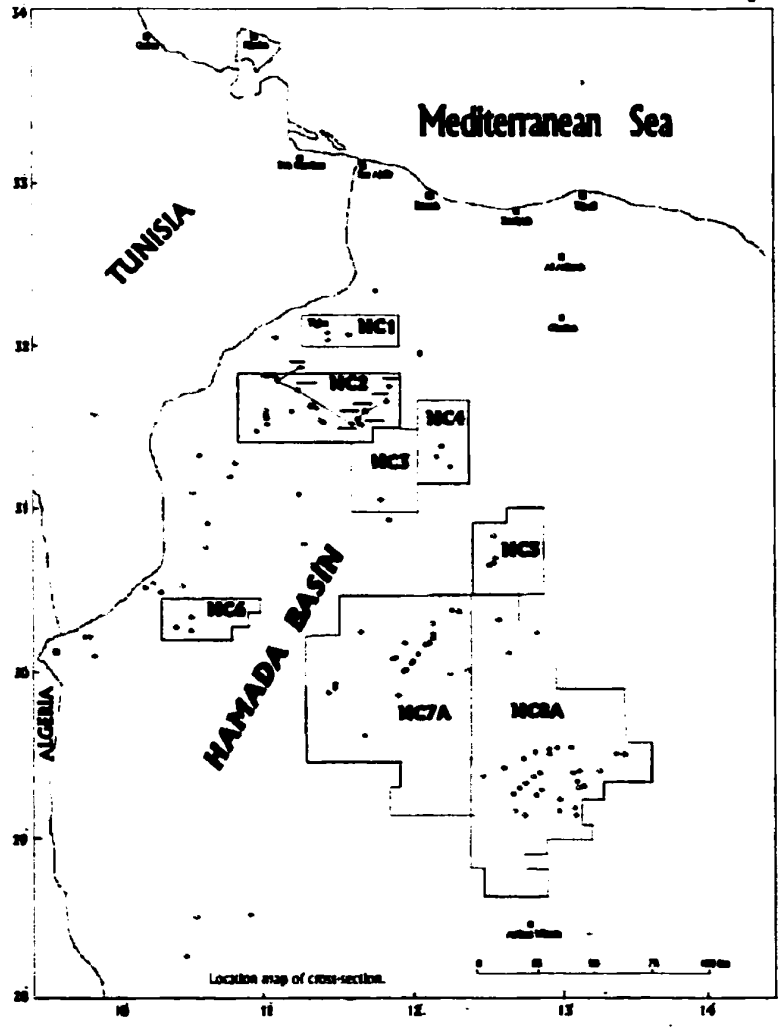

ENCLOSURE No. 4

NE-NWN STRATIGRAPHIC CROSS-SECTION IN THE NORTHERN FLANK OF THE HAMADA BASIN, NW LIBYA (MODIFIED AFTER ELFIGIH, 1991).

(Note: The units of depth are in feet as recorded on well logs).

V.S. 0 ft. 100 200 (H.S. as indicated).

SHALLOW

FLUIDS / DIAGENETIC EVENTS

METEORIC WATER
(Basin Flank, <2439 m. (8000 ft.), 25-60°C)

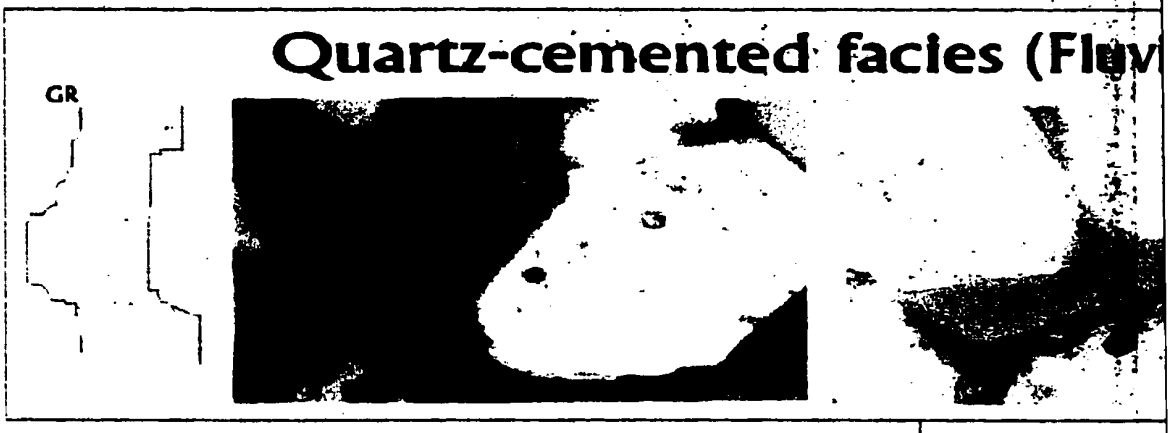

deposition of quartz-rich
in wells

EE1-NC7A CC1-NC7A Z1-66 Z1-NC100 A1-NC1

Iron oxides/ clay matrix

Mechanical compaction

Quartz-overgrowths

Shallow calcite cement

Shallow calcite dissolution

(2439 m. - 30

uvial sandstones, Af units)

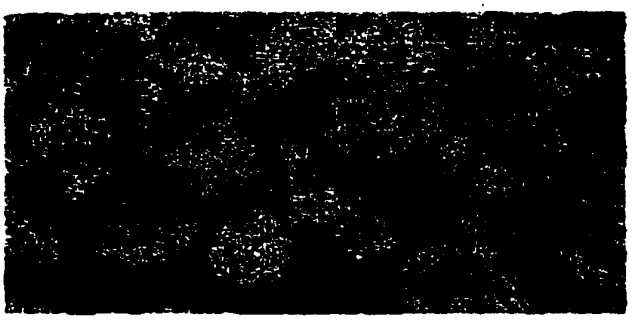

h sediments

C118 B3-61 C1-61

Carbonate

proximal deltaic

GR

deposition of fine-medium quart
in wells

B1-NC2 D1-61 E1-NC2

A10	A12	A10	A14	A12	A1

Deep calcite cement

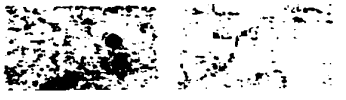

TIC DEPTH

MIXED WATER
n. - 3049 m. (8000 ft.- 10000 ft.), 60-90°C)

nate-cemented facies

nal deltaic sandstones

reworked marine sandstones

um quartz grains, lithic sediments
n wells

glauconitic sediments
in well

E1-NC2		C1-NC2	T1-23	Q1-23
A12	A14	A8	A14	Am

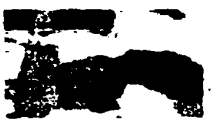

DEEP

SALINE + ACIDIC WATERS
(Basin Centre, > 3049 m. (10000 ft.) , > 90°C)

Clay-cemented facies

distal deltaic siltstones

deposition of very fine quartz grains, and micaceous clay-rich materials in wells

Shallow calcite dissolution

Dissolution of feldspars

Partial kaolinite cement

Partial illite cement

Dissolution of iron-oxides

Partial siderite cement

Partial ferroan dolomite cement

(PRIMARY POROSITY REDUCTIO

Enclosure 5. Distribution of diagenetic sequences

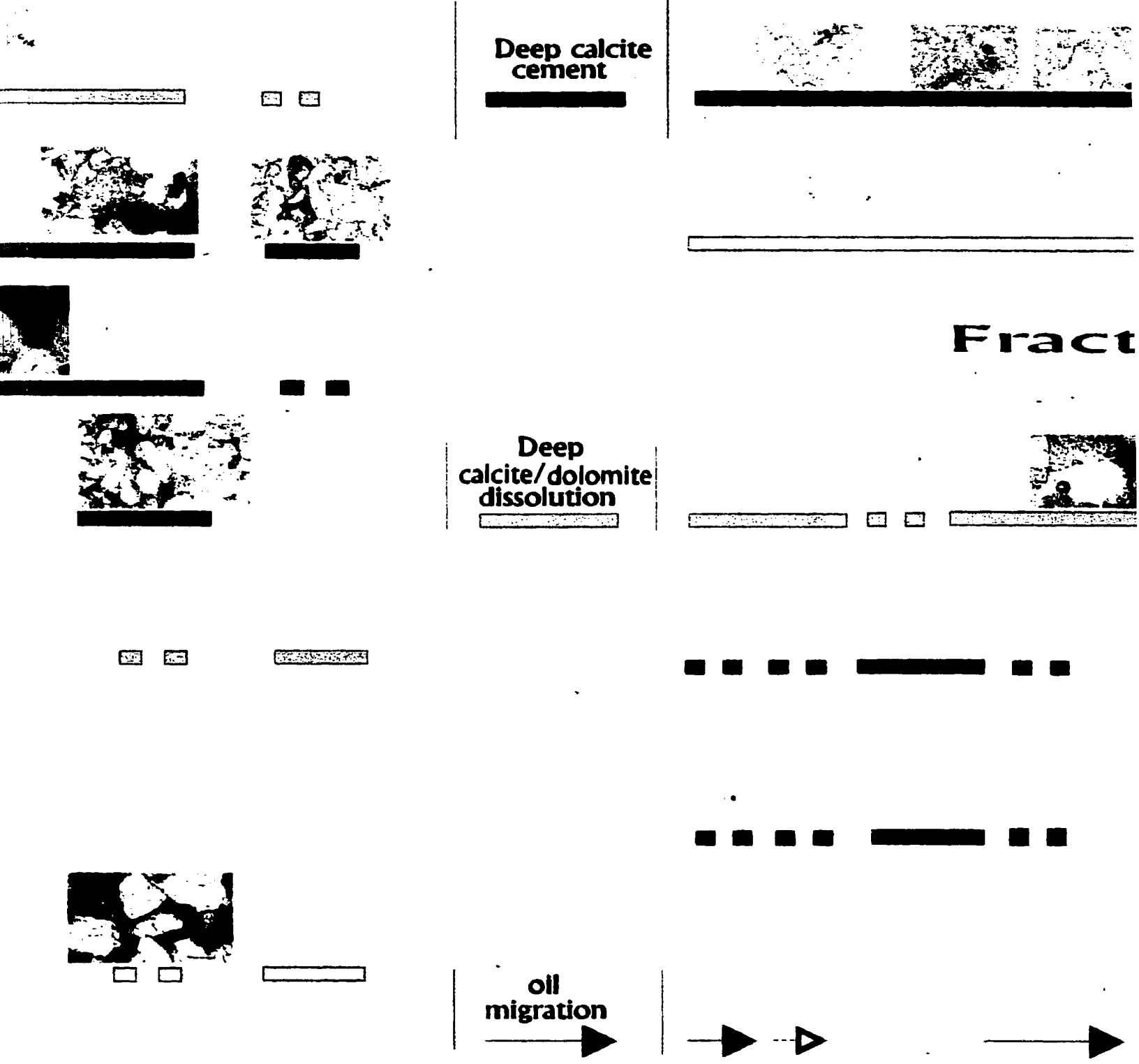

ON PHASE)

(PORE-FORMING AND N

s in the various diagenetic facies of the Lower Aca

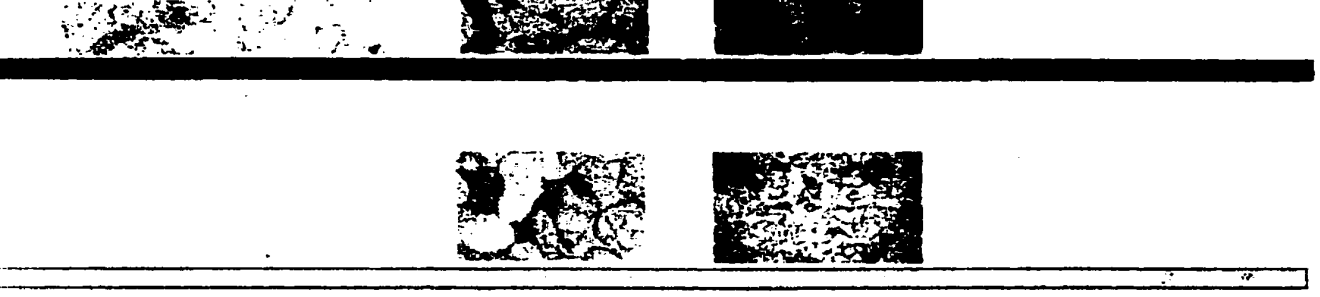

Fracturing

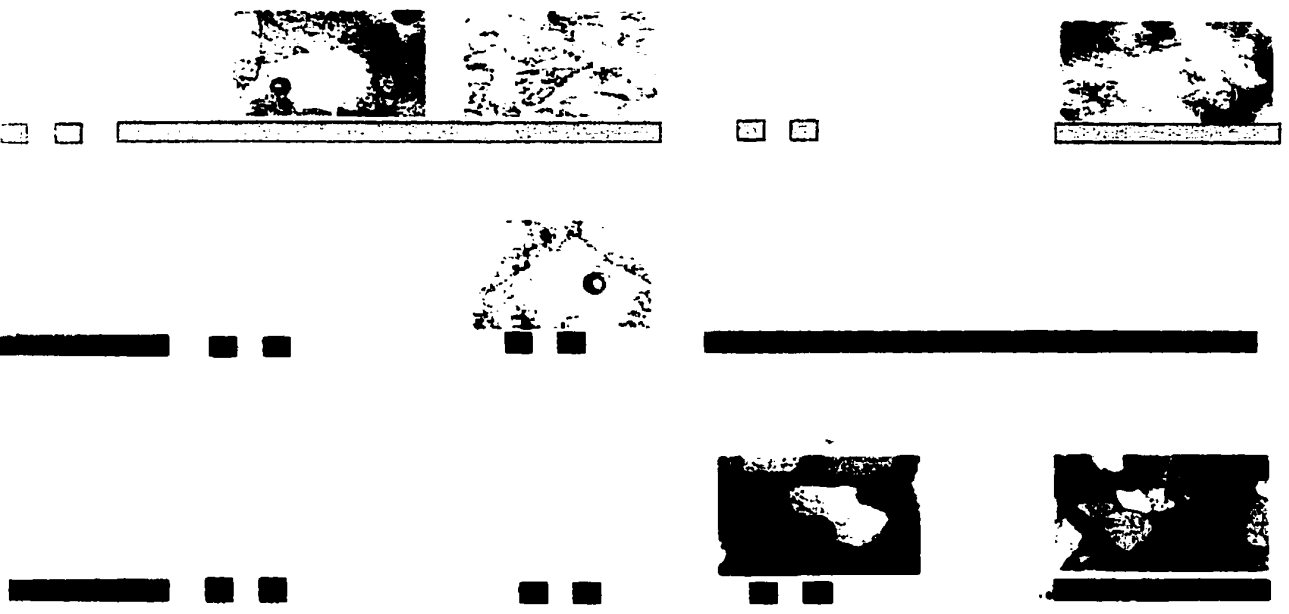

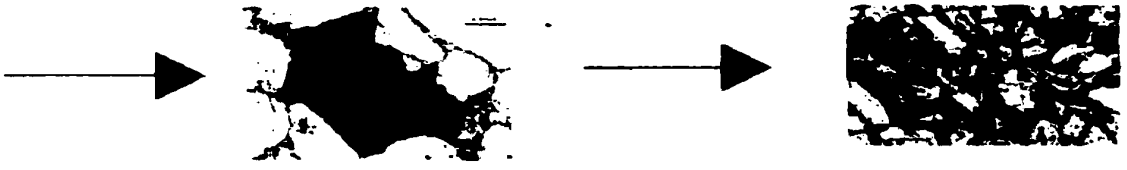

RMING AND MODIFICATION PHASE)

Tota

ne Lower Acacus Formation, Hamada Basin, NW Li

D1-61	E1-NC2	A1-NC2
(Ad) distal A10	(Ad) distal A14	(Ad) distal A14

Fracturing

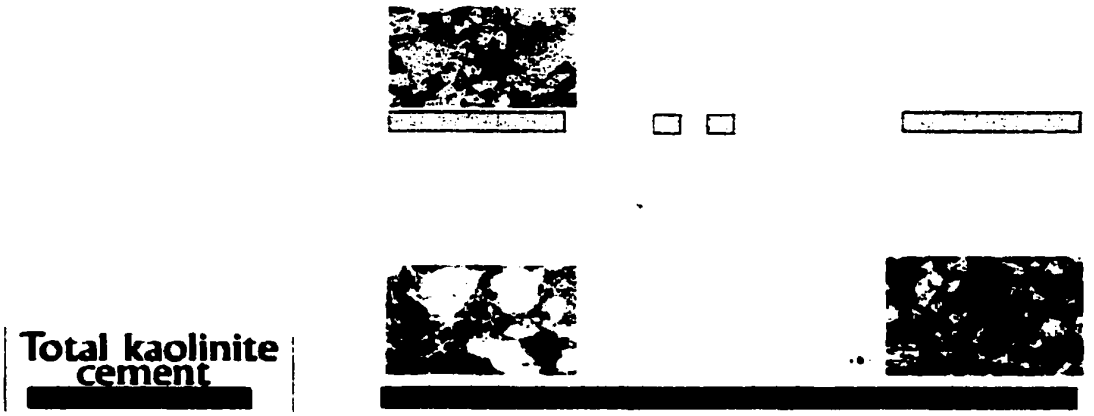

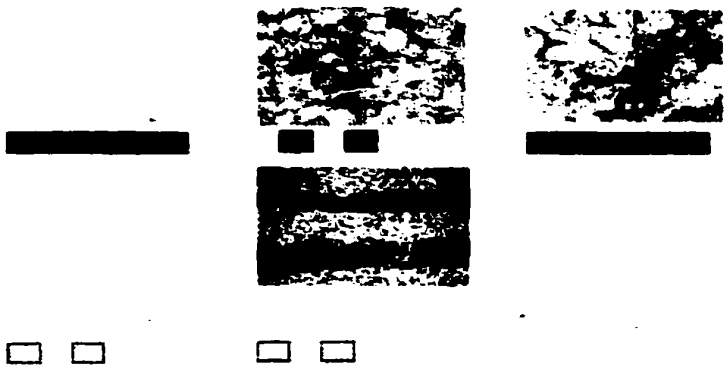

(PORE-FILLING PHASE)

n, NW Libya. (see text for additional discussion)